

EMERGING INFECTIOUS DISEASES[®]



COVID-19

May 2021



AMBIKA DEVI

Ambika Devi (1971), *Handwashing Is Important*, 2020. Natural pigments on handmade paper, 7.5 inches x 7.5 inches/19.1 cm x 19.1 cm. Digital image used with permission from Dastkar, Kisan Haat Andheria Modh, Anurath Marg, New Delhi 110074 India.

EMERGING INFECTIOUS DISEASES®

EDITOR-IN-CHIEF

D. Peter Drotman

ASSOCIATE EDITORS

Charles Ben Beard, Fort Collins, Colorado, USA
 Ermias Belay, Atlanta, Georgia, USA
 David M. Bell, Atlanta, Georgia, USA
 Sharon Bloom, Atlanta, Georgia, USA
 Richard Bradbury, Melbourne, Australia
 Mary Brandt, Atlanta, Georgia, USA
 Corrie Brown, Athens, Georgia, USA
 Benjamin J. Cowling, Hong Kong, China
 Michel Drancourt, Marseille, France
 Paul V. Effler, Perth, Australia
 David O. Freedman, Birmingham, Alabama, USA
 Peter Gerner-Smidt, Atlanta, Georgia, USA
 Stephen Hadler, Atlanta, Georgia, USA
 Matthew J. Kuehnert, Edison, New Jersey, USA
 Nina Marano, Atlanta, Georgia, USA
 Martin I. Meltzer, Atlanta, Georgia, USA
 David Morens, Bethesda, Maryland, USA
 J. Glenn Morris, Jr., Gainesville, Florida, USA
 Patrice Nordmann, Fribourg, Switzerland
 Johann D.D. Pitout, Calgary, Alberta, Canada
 Ann Powers, Fort Collins, Colorado, USA
 Didier Raoult, Marseille, France
 Pierre E. Rollin, Atlanta, Georgia, USA
 Frederic E. Shaw, Atlanta, Georgia, USA
 David H. Walker, Galveston, Texas, USA
 J. Todd Weber, Atlanta, Georgia, USA
 J. Scott Weese, Guelph, Ontario, Canada

Associate Editor Emeritus

Charles H. Calisher, Fort Collins, Colorado, USA

Managing Editor

Byron Breedlove, Atlanta, Georgia, USA

Copy Editors

Deanna Altomara, Dana Dolan, Terie Grant,
 Thomas Gryczan, Amy Guinn, Shannon O'Connor,
 Tony Pearson-Clarke, Jill Russell, Jude Rutledge,
 P. Lynne Stockton, Deborah Wenger

Production

Thomas Ehemann, William Hale, Barbara Segal,
 Reginald Tucker

Journal Administrator

Susan Richardson

Editorial Assistants

J. McLean Boggess, Kaylyssa Quinn

Communications/Social Media

Heidi Floyd,
 Sarah Logan Gregory

Founding Editor

Joseph E. McDade, Rome, Georgia, USA

EDITORIAL BOARD

Barry J. Beaty, Fort Collins, Colorado, USA
 Martin J. Blaser, New York, New York, USA
 Andrea Boggild, Toronto, Ontario, Canada
 Christopher Braden, Atlanta, Georgia, USA
 Arturo Casadevall, New York, New York, USA
 Kenneth G. Castro, Atlanta, Georgia, USA
 Christian Drosten, Charité Berlin, Germany
 Anthony Fiore, Atlanta, Georgia, USA
 Isaac Chun-Hai Fung, Statesboro, Georgia, USA
 Kathleen Gensheimer, College Park, Maryland, USA
 Rachel Gorwitz, Atlanta, Georgia, USA
 Duane J. Gubler, Singapore
 Scott Halstead, Arlington, Virginia, USA
 David L. Heymann, London, UK
 Keith Klugman, Seattle, Washington, USA
 S.K. Lam, Kuala Lumpur, Malaysia
 Shawn Lockhart, Atlanta, Georgia, USA
 John S. Mackenzie, Perth, Australia
 John E. McGowan, Jr., Atlanta, Georgia, USA
 Jennifer H. McQuiston, Atlanta, Georgia, USA
 Tom Marrie, Halifax, Nova Scotia, Canada
 Nkuchia M. M'ikanatha, Harrisburg, Pennsylvania, USA
 Frederick A. Murphy, Bethesda, Maryland, USA
 Barbara E. Murray, Houston, Texas, USA
 Stephen M. Ostroff, Silver Spring, Maryland, USA
 W. Clyde Partin, Jr., Atlanta, Georgia, USA
 Mario Raviglione, Milan, Italy and Geneva, Switzerland
 David Relman, Palo Alto, California, USA
 Connie Schmaljohn, Frederick, Maryland, USA
 Tom Schwan, Hamilton, Montana, USA
 Rosemary Soave, New York, New York, USA
 Robert Swanepoel, Pretoria, South Africa
 David E. Swayne, Athens, Georgia, USA
 Kathrine R. Tan, Atlanta, Georgia, USA
 Phillip Tarr, St. Louis, Missouri, USA
 Duc Vugia, Richmond, California, USA
 Mary Edythe Wilson, Iowa City, Iowa, USA

Emerging Infectious Diseases is published monthly by the Centers for Disease Control and Prevention, 1600 Clifton Rd NE, Mailstop H16-2, Atlanta, GA 30329-4027, USA. Telephone 404-639-1960; email, eideditor@cdc.gov

The conclusions, findings, and opinions expressed by authors contributing to this journal do not necessarily reflect the official position of the U.S. Department of Health and Human Services, the Public Health Service, the Centers for Disease Control and Prevention, or the authors' affiliated institutions. Use of trade names is for identification only and does not imply endorsement by any of the groups named above.

All material published in *Emerging Infectious Diseases* is in the public domain and may be used and reprinted without special permission; proper citation, however, is required.

Use of trade names is for identification only and does not imply endorsement by the Public Health Service or by the U.S. Department of Health and Human Services.

EMERGING INFECTIOUS DISEASES is a registered service mark of the U.S. Department of Health & Human Services (HHS).

EMERGING INFECTIOUS DISEASES[®]

COVID-19

May 2021



On the Cover

Ambika Devi (1971), *Handwashing Is Important*, 2020.

Natural pigments on handmade paper, 7.5 inches x 7.5 inches/19.1cm x 19.1 cm. Digital image used with permission from Dastkar, Kisan Haat Andheria Modh, Anuvrat Marg, New Delhi 110074 India.

About the Cover p. 1547

Perspective

Coordinated Strategy for a Model-Based Decision Support Tool for Coronavirus Disease, Utah, USA

H.R. Meredith et al. 1259

Synopses

Coccidioidomycosis and COVID-19 Co-Infection, United States, 2020

A.K. Heaney et al. 1266

Transmission of Severe Acute Respiratory Syndrome Coronavirus 2 during Border Quarantine and Air Travel, New Zealand (Aotearoa)

N. Eichler et al. 1274

Successful Control of an Onboard COVID-19 Outbreak Using the Cruise Ship as a Quarantine Facility, Western Australia, Australia

T.A. Codreanu et al. 1279

SARS-CoV-2 in Nursing Homes after 3 Months of Serial, Facilitywide Point Prevalence Testing, Connecticut, USA

H.Y. Ehrlich et al. 1288

Case Series of Laboratory-Associated Zika Virus Disease, United States, 2016–2019

S.L. Hills et al. 1296

Epidemiologic Findings from Case Investigations and Contact Tracing for First 200 Cases of Coronavirus Disease, Santa Clara County, California, USA

N. Ortiz et al. 1301

Clinical Laboratory Perspective on *Streptococcus halichoeri*, an Unusual Nonhemolytic, Lancefield Group B Streptococcus Causing Human Infections

S.M. Shakir et al. 1309

Research

Use of Genomics to Track Coronavirus Disease Outbreaks, New Zealand

J.L. Geoghegan et al. 1317

Clinical Evaluation of Roche SD Biosensor Rapid Antigen Test for SARS-CoV-2 in Municipal Health Service Testing Site, the Netherlands

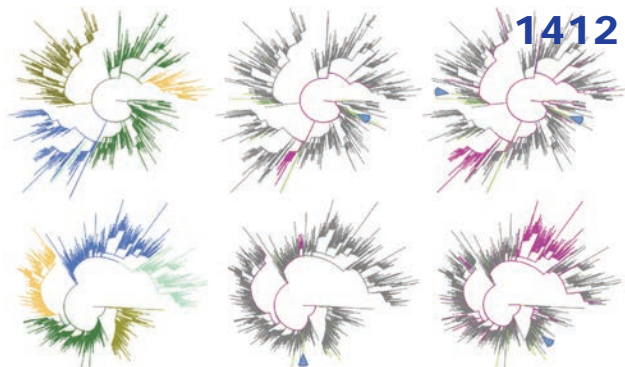
Z. Iglò et al. 1323

Prevalence and Clinical Profile of Severe Acute Respiratory Syndrome Coronavirus 2 Infection among Farmworkers, California, USA, June–November 2020

J.A. Lewnard et al. 1330

Herd Immunity against Severe Acute Respiratory Syndrome Coronavirus 2 Infection in 10 Communities, Qatar

A. Jeremijenko et al. 1343



Dispatches

Symptom Diary–Based Analysis of Disease Course among Patients with Mild Coronavirus Disease, Germany, 2020

P.N. Wiegele et al. 1353

Serologic Screening of Severe Acute Respiratory Syndrome Coronavirus 2 Infection in Cats and Dogs during First Coronavirus Disease Wave, the Netherlands

S. Zhao et al. 1362

Active Case Finding of Current Bornavirus Infections in Human Encephalitis Cases of Unknown Etiology, Germany, 2018–2020

P. Eisermann et al. 1371

Susceptibility to SARS-CoV-2 of Cell Lines and Substrates Commonly Used to Diagnose and Isolate Influenza and Other Viruses

L. Wang et al. 1380

Epidemiologic History and Genetic Diversity Origins of Chikungunya and Dengue Viruses, Paraguay

T. Gräf et al. 1393

Monitoring SARS-CoV-2 Circulation and Diversity through Community Wastewater Sequencing, the Netherlands and Belgium

R. Izquierdo-Lara et al. 1405



Characteristics and Clinical Implications of Carbapenemase-Producing *Klebsiella pneumoniae* Colonization and Infection, Italy

We found 15-day mortality rates were higher for patients with severe infections than for those with mild infections or colonization.

M. Rossi et al. 1416

Engineered NS1 for Sensitive, Specific Zika Virus Diagnosis from Patient Serology

T.L. Yap et al. 1427

Global Trends in Norovirus Genotype Distribution among Children with Acute Gastroenteritis

J.L. Cannon et al. 1438

Genetic Evidence and Host Immune Response in Persons Reinfected with SARS-CoV-2, Brazil

N. Fintelman-Rodrigues et al. 1446

COVID-19–Associated Mold Infection in Critically Ill Patients, Chile

R. Rabagliati et al. 1459

Multisystem Inflammatory Syndrome in Children, Chile, May–August 2020

C. Niño-Taravilla et al. 1457



Prescribing Antimicrobial Drugs for Acute Gastroenteritis, Primary Care, Australia, 2013–2018

W.-Q. He et al. 1462

Prescriptions for 6.8% of cases suggests a need for greater antimicrobial stewardship.

Epidemiology of Confirmed COVID-19 Deaths in Adults, England, March–December 2020

A.E. Brown et al. 1468

Longevity of Middle East Respiratory Syndrome Coronavirus Antibody Responses in Humans, Saudi Arabia

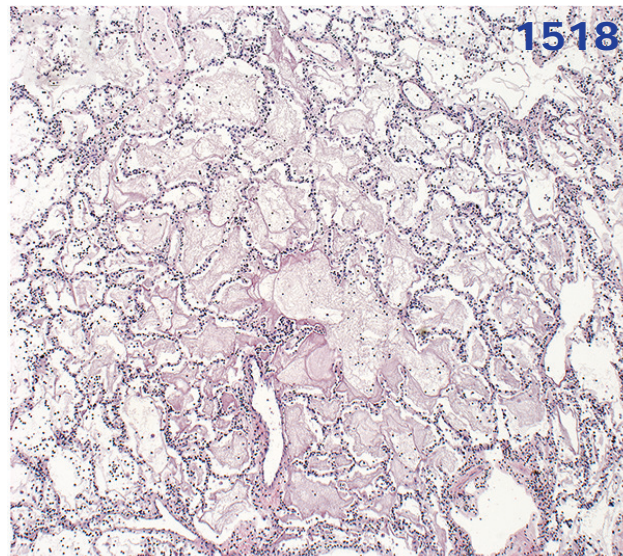
A.N. Alshukairi et al. 1472

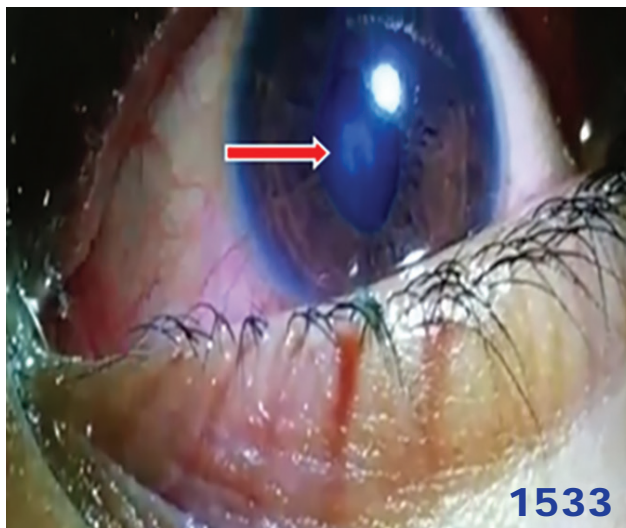
Racial and Ethnic Disparities in Incidence of SARS-CoV-2 Infection, 22 US States and DC, January 1–October 1, 2020

N.D. Hollis et al. 1477

Emergence of Toscana Virus, Romania, 2017–2018

C.P. Popescu et al. 1482





EMERGING INFECTIOUS DISEASES®

May 2021

SARS-CoV-2 Serial Interval Variation, Montana, USA, March 1–July 31, 2020

I.G. Reed et al. 1486

Introduction of ORF3a-Q57H SARS-CoV-2 Variant Causing Fourth Epidemic Wave of COVID-19, Hong Kong, China

D.K.W. Chu et al. 1492

Detecting Rapid Spread of SARS-CoV-2 Variants, France, January 26–February 16, 2021

S. Haim-Boukobza et al. 1496

Detecting COVID-19 Clusters at High Spatiotemporal Resolution, New York City, NY, USA, June–July 2020

S.K. Greene et al. 1500

Evaluating Differences in Whole Blood, Serum, and Urine Screening Tests for Zika Virus, Puerto Rico, USA, 2016

A.Y. Rosinger et al. 1505

Whole-Genome Sequencing of Shiga Toxin–Producing *Escherichia coli* OX18 from a Fatal Hemolytic Uremic Syndrome Case

K. Lee et al. 1509

Coordinated Response to Imported Vaccine-Derived Poliovirus Infection, Barcelona, Spain, 2019–2020

D. Álamo-Junquera et al. 1513

Research Letters

Intersecting Paths of Emerging and Reemerging Infectious Diseases

T.M. Wilson et al. 1517

Novel Mutation of SARS-CoV-2, Vietnam, July 2020

H.V.M. Phuong et al. 1519

Genomic Evidence of SARS-CoV-2 Reinfection Involving E484K Spike Mutation, Brazil

C.K. Vasques Nonaka et al. 1522

Upper Respiratory Infections in Schools and Childcare Centers Reopening after COVID-19 Dismissals, Hong Kong

M.W. Fong et al. 1525

Risk for International Importations of New Variant SARS-CoV-2 Originating in the United Kingdom

Z. Du et al. 1527

Severe Case of Rickettsiosis Identified by Metagenomic Sequencing, China

Z. Teng et al. 1530

Eosinophilic Meningitis and Intraocular Infection Caused by *Dirofilaria* sp. Genotype Hongkong

A.S. Jyotsna et al. 1532

COVID-19 Co-infection with *Legionella pneumophila* in 2 Tertiary-Care Hospitals, Germany

H.L. Verhasselt et al. 1535

Temporal Variations in Respiratory Syncytial Virus Epidemics, by Virus Subtype, 4 Countries

L. Staadegaard et al. 1537

Novel SARS-CoV-2 Variant Derived From Clade 19B, France

S. Fourati et al. 1540

Undocumented Migrants Reintroducing COVID-19, Yunnan Province, China

M.L. Zhang et al. 1543

Books and Media

Apollo's Arrow: The Profound and Enduring Impact of Coronavirus on the Way We Live

N.M. M'ikanatha, C.E. Carr 1546

About the Cover

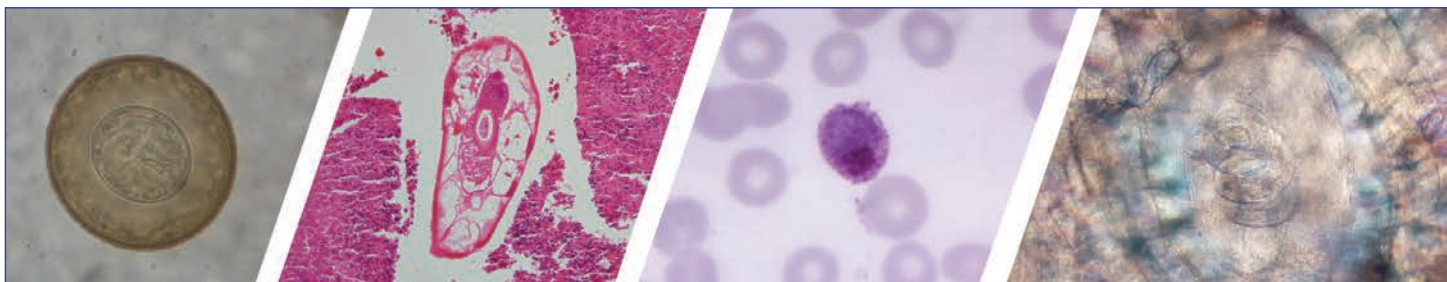
Ancient Methods Deliver a Current Message

B. Breedlove 1547

Correction

Vol. 27, No. 3 1545

The order of the authors was incorrect for Drug-Resistant Tuberculosis in Pet Ring-Tailed Lemur, Madagascar.



Diagnostic Assistance and Training in Laboratory Identification of Parasites

A free service of CDC available to laboratorians, pathologists, and other health professionals in the United States and abroad



Diagnosis from photographs of worms, histological sections, fecal, blood, and other specimen types



Expert diagnostic review



Formal diagnostic laboratory report



Submission of samples via secure file share

Visit the DPDx website for information on laboratory diagnosis, geographic distribution, clinical features, parasite life cycles, and training via Monthly Case Studies of parasitic diseases.

www.cdc.gov/dpdx
dpdx@cdc.gov



U.S. Department of Health and Human Services
Centers for Disease Control and Prevention

Coordinated Strategy for a Model-Based Decision Support Tool for Coronavirus Disease, Utah, USA

Hannah R. Meredith, Emerson Arehart,¹ Kyra H. Grantz,¹ Alexander Beams, Theresa Sheets, Richard Nelson, Yue Zhang, Russell G. Vinik, Darryl Barfuss, Jacob C. Pettit, Keegan McCaffrey, Angela C. Dunn, Michael Good, Shannon Frattaroli, Matthew H. Samore, Justin Lessler, Elizabeth C. Lee, Lindsay T. Keegan

The coronavirus disease pandemic has highlighted the key role epidemiologic models play in supporting public health decision-making. In particular, these models provide estimates of outbreak potential when data are scarce and decision-making is critical and urgent. We document the integrated modeling response used in the US state of Utah early in the coronavirus disease pandemic, which brought together a diverse set of technical experts and public health and healthcare officials and led to an evidence-based response to the pandemic. We describe how we adapted a standard epidemiologic model; harmonized the outputs across modeling groups; and maintained a constant dialogue with policymakers at multiple levels of government to produce timely, evidence-based, and coordinated public health recommendations and interventions during the first wave of the pandemic. This framework continues to support the state's response to ongoing outbreaks and can be applied in other settings to address unique public health challenges.

The emergence of severe acute respiratory syndrome coronavirus 2 (SARS-CoV-2) has demonstrated the need for epidemiologic models in public health decision-making. Modeling has been critical to planning outbreak responses since at least the emergence of HIV 40 years ago (1–3). However, the response to the coronavirus disease (COVID-19) pandemic has highlighted several challenges with incorporating modeling into public health decision-making.

Author affiliations: Johns Hopkins Bloomberg School of Public Health, Baltimore, Maryland, USA (H.R. Meredith, K.H. Grantz, S. Frattaroli, J. Lessler, E.C. Lee); University of Utah, Salt Lake City, Utah, USA (E. Arehart, A. Beams, T. Sheets, R. Nelson, Y. Zhang, R.G. Vinik, D. Barfuss, J.C. Pettit, M. Good, M.H. Samore, L.T. Keegan); Utah Department of Health, Salt Lake City (K. McCaffrey, A.C. Dunn); Veterans Affairs Salt Lake City Health Care System, Salt Lake City (M.H. Samore, L.T. Keegan)

DOI: <https://doi.org/10.3201/eid2705.203075>

The fast-moving operational timescales of public health policy are often at odds with the traditionally slower and iterative science of epidemiologic modeling. When models are effective, they catalyze policies that prevent their sometimes-dire predictions, thus making the initial predictions seem inaccurate. This feedback loop has heightened skepticism, resulting in high-profile controversies around modeling results (4,5).

In the rush to provide evidence-based guidance to policymakers, modeling experts were overwhelmed with requests, leaving little time to respond or to coordinate with broader efforts. Meanwhile, many groups unfamiliar with the nuances of how modeling has evolved through years of infectious disease modeling research were producing models for public policy that failed to reflect state-of-the-art modeling science (6,7). This situation often resulted in conflicting evidence presented to decision-makers tasked with quickly setting up pandemic response plans. As the pandemic has progressed, substantial efforts have been made to help stakeholders interpret the results and assumptions of multiple, often contradictory, modeling efforts for policy decisions. These efforts include proposed frameworks for effectively incorporating multiple models into a structured decision-making process (8) and efforts to assemble forecasts from multiple models to produce unified predictions as is done for many other common forecasting systems, such as weather forecasts (9).

A major challenge in developing evidence-based models for policy is aligning models with policymakers' needs. Models that cannot rapidly provide actionable results, although useful in a basic science context, will not be useful for guiding policy. Likewise, not all models are equally well-equipped to answer every question, and aligning the best model to address a

¹These authors contributed equally to this article.

given policy question is challenging, especially during a rapidly evolving pandemic. This challenge is exacerbated by differing expectations between epidemiologists and policymakers. Epidemiologists often seek to match model assumptions to reality and highlight the resulting uncertainty, whereas policymakers seek a concrete basis for making and defending policy decisions and often need a single number to put the results into use (e.g., order a particular quantity of N95 masks). Developing strong relationships with policymakers is essential for clearly communicating this uncertainty.

As of June 22, 2020, the US state of Utah had a low attack rate (55 infections/10,000 population reported statewide, compared with 70 infections/10,000 population reported nationwide) and few deaths (158 deaths statewide, or 0.5 deaths/10,000 population, compared with 3.7 deaths/10,000 population nationwide), all accomplished with less aggressive mandated social distancing than other states. Utah's success might be attributable to its early adoption of an integrated control strategy that has relied heavily on testing and isolating case-patients, contact tracing, and quarantining case-patient contacts (>300,000

persons tested statewide [936 tests/10,000 population] compared with 828 tests/10,000 population nationally). The decision to take this course, its implementation, and evaluation were informed heavily by an integrated modeling approach that brought together a diverse set of technical experts and public health and healthcare officials. Given the limited data on COVID-19 at the time, our approach was helpful for all involved; however, without a counterfactual scenario, we cannot determine whether our efforts had the intended consequences. With this caveat, we present the approaches taken over 3 different phases and highlight key points in hopes the lessons learned can inform future modeling efforts (Figure 1).

Phase 1: Epidemiologic Model for Public Health Planning

Utah, like other state, local, and national governments, sought epidemiologic modeling estimates to inform their COVID-19 response. Utah public health decision-makers initially engaged with our group, Infectious Disease Dynamics, at the University of Utah to help prepare for and respond to COVID-19. To address their questions, we adapted a metapopulation

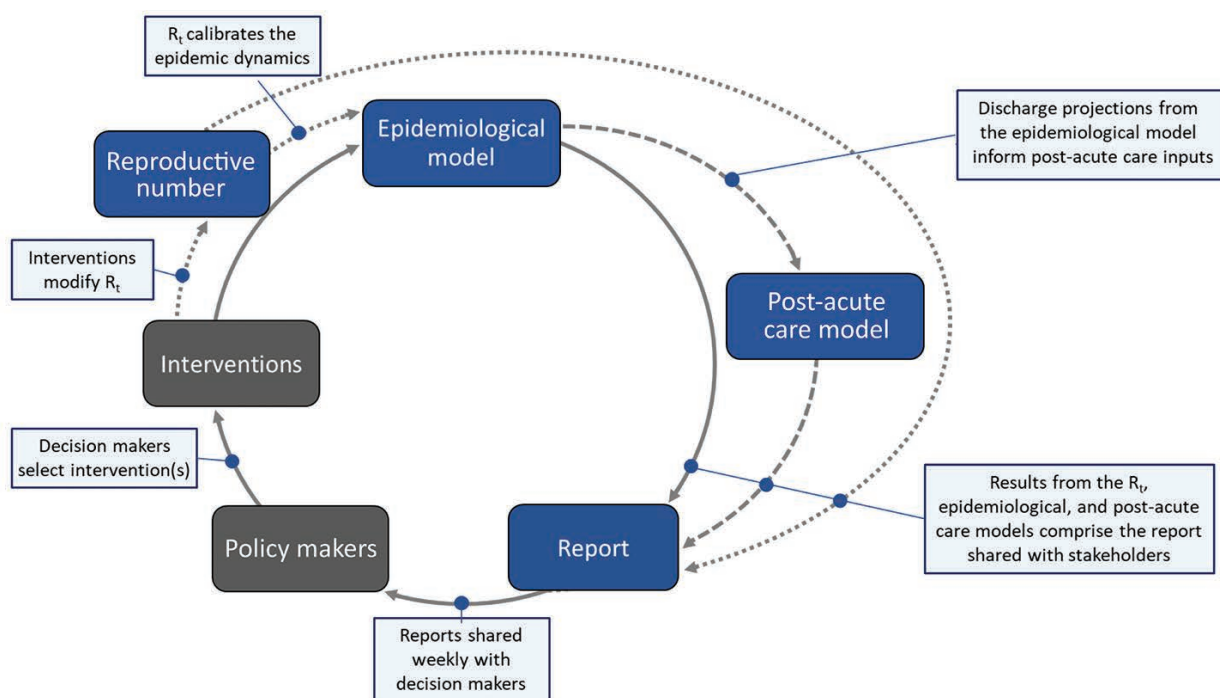


Figure 1. Schematic of the modeling process used as a decision support tool for coronavirus disease, Utah, USA. The epidemiologic model produces outputs of disease impact and key health outcomes that are used by the post-acute-care model. All model results are incorporated into the report, which is generated weekly and shared with policymakers who then make decisions on which interventions to implement. Those interventions impact the reproductive number, which is then used as an input to the epidemiologic model. The color of the box represents the time input was added, with dark blue for earliest and light blue for most recent. Policymakers and interventions are gray to indicate that although they are a critical component of our modeling process, they are external to our inputs to the process. R_t , real-time effective reproduction number.

Susceptible-Exposed-Infectious-Recovered/Removed modeling process to develop planning scenarios for the state (J.C. Lemaitre et al., unpub. data, <https://doi.org/10.1101/2020.06.11.20127894>). We projected infections, deaths, and health system needs under multiple nonpharmaceutical interventions (NPIs) being considered by decision-makers (Figure 2). In particular, we compared the effects of comprehensive testing and isolation strategies on the lockdown measures being implemented by other states (e.g., California). Although testing and isolation strategies were not yet feasible in many states because of slow scale-up of testing capacity, Utah was well positioned to take such an approach. As of March 25, 2020, a national diagnostic medicine laboratory located in Salt Lake City had ample resources to rapidly develop and scale up COVID-19 testing capacity.

We compiled the model-based projections and comparison of NPIs and rapidly shared a report on March 23, 2020, with key leadership at the University of Utah Health, the Utah Department of Health (UDOH), ARUP Laboratories (Salt Lake City), the Governor's Office of Management and Budget, and Intermountain Healthcare, the largest healthcare system in Utah. These stakeholders encompassed the key health decision-makers in the state, including those responsible for $\approx 60\%$ of the state's hospital market share.

On March 24, university leadership coordinated a meeting between scientists and policymakers to discuss this initial report. The goal of the meeting was to review model projections, compare the different NPI scenario

estimates, and discuss the best paths forward for the state. The resulting consensus was that the state should strive to rapidly achieve levels of per-capita testing of symptomatic persons similar to those seen in South Korea, a goal that was achieved in Utah by March 25, 2020. After this meeting, we maintained open lines of communication with health experts and policymakers, soliciting insight into new operational questions (further discussed in phase 3) and distributing weekly scenario-based projections of probable outcomes under different NPIs over the course of the local outbreak.

Phase 2: Establishing Local Model Consensus

The University of Utah model was not the only model used to estimate COVID-19 impact in Utah. In addition to national-level models that included projections for Utah (e.g., projections described in University of Washington Institute for Health Metrics and Evaluation [IHME] COVID-19 Health Service Utilization Forecasting Team et al., unpub. data, <https://doi.org/10.1101/2020.04.21.20074732>), 3 other groups within the state were developing models of COVID-19 to inform policy. Intermountain extended an existing Susceptible-Infected-Recovered (SIR) model to project expected burden on their healthcare facilities statewide, later switching to a timeseries model for short-term forecasting. UDOH used an SIR model, and another group constructed an operational model of COVID-19 that projected forward on the basis of current trends, thereby implicitly projecting the effect of current NPIs at the state level (group 1 in Figure 3), later

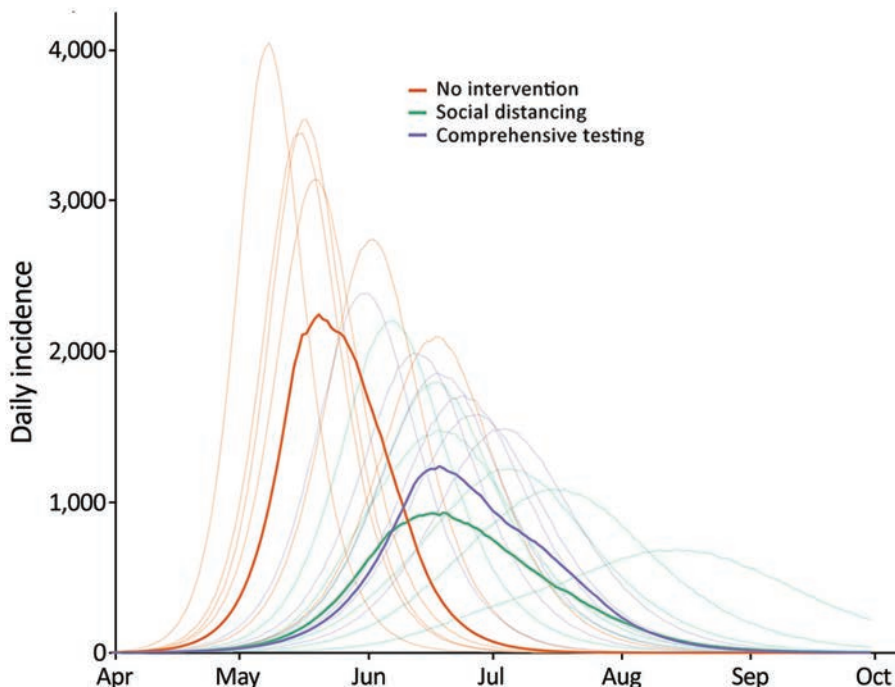


Figure 2. Example epidemiologic model output presented to stakeholders as part of decision support tool for coronavirus disease, Utah, USA. Model results compare daily incidence across 3 planning scenarios: no interventions, social distancing only, and comprehensive testing only. Bold lines represent the median daily incidence (cases/100,000 population) calculated from 1,000 simulations, whereas the lighter lines represent 15 random example simulations.

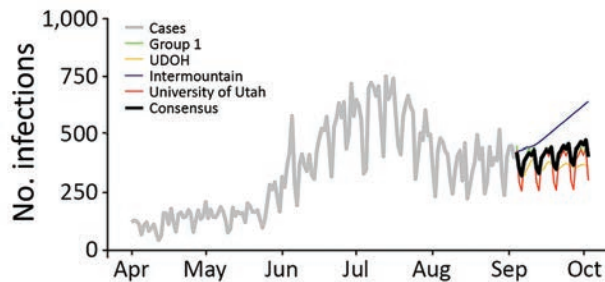


Figure 3. Example of a consensus model figure from a decision support tool for coronavirus disease, Utah, USA. Model results compare the number of new reported infections (daily) across the 4 modeling groups presented to Utah stakeholders on September 9, 2020. Light gray line represents reported infections, black line represents the consensus model (i.e., the average of the 4 individual group models), green line represents the results from modeling group 1, yellow line represents the results from the UDOH, blue line represents the results from the Intermountain Healthcare model, and red line represents the results from the University of Utah model. UDOH, Utah Department of Health.

moving to a timeseries model for short-term forecasting. The different modeling approaches, which often yielded qualitatively different results (Figure 3), were creating uncertainty about the relative strengths and weaknesses of policy options.

To improve consistency in model outputs and communication of results across the 3 modeling groups, we arranged weekly consensus modeling meetings starting on April 8, 2020, that included representatives from all groups and other stakeholders (e.g., UDOH). Those meetings covered evidence-based model parameters, key modeling scenarios (e.g., determining which NPIs to model), data quality, and appropriate interpretation of high-profile models from outside the state. At these meetings, participants learned that the University of Utah was using a Susceptible-Exposed-Infectious-Recovered/Removed model (later changing to a timeseries model for short-term forecasting) with a latent period of 5 days and an average duration of infection of 6 days, whereas Intermountain was using an SIR model with an average duration of infection of 6 days. Likewise, the University of Utah group assumed that 10% of all infections were in hospitalized case-patients and the duration of hospitalization was on average 11.5 days, whereas Intermountain assumed that 2.5% of infections were in hospitalized case-patients and the duration of hospitalization was on average 7 days. Further, the University of Utah assumed that 15% of hospitalized patients required a stay in the intensive-care unit (ICU), whereas Intermountain assumed that 38% of hospitalized patients required an ICU stay. The consensus modeling group also served

as a forum for informal peer review of models from each group. The consensus modeling meetings produced weekly joint reports reflecting the collective research, modeling, and operational efforts of the group, standardizing the outputs (Figure 3) to improve communication. Central to these reports was presenting results from all 3 groups in a format that could enable comparisons, guide public health decision-makers on the strengths and limitations of each model type, and indicate which models were more appropriate for informing certain decisions, such as models that aimed to forecast weekly incidence compared with those aiming to provide big-picture epidemiologic dynamics. To improve communication, these reports began presenting a consensus model, which was calculated as the average of each of the individual group models over the forecast period.

Phase 3: Iterative Modeling and Ongoing Assessment

As the epidemic evolved, new operational questions required new approaches. To address these new questions, we contacted collaborators at the University of Utah to develop new decision support tools that expanded the modeling process. In particular, assessing the efficacy of key interventions in a local context became paramount. Doing so required an increased focus on ensuring the model's assumptions matched the current epidemic situation.

To characterize the effectiveness of the NPIs that were implemented in Utah in March 2020, we estimated the time varying local reproduction number, R_t (the real-time average number of secondary infections from a single infected person), with assistance from the Study Design and Biostatistics Center at the University of Utah (Y. Zhang et al., unpub. data, <https://doi.org/10.1101/2020.05.08.20095703>). Estimates of R_t became a weekly input into the transmission model, and these projections served as a baseline for comparing current and possible interventions (Figure 4, panel A). As the epidemic progressed, local outbreaks sparked concerns of substantial spatial heterogeneity in the impact of interventions across the state. Hence, we began estimating R_t at the county level and capturing this heterogeneity in our wider modeling efforts, as well as including these estimates directly in the report beginning April 13, 2020.

As COVID-19 patients were discharged, public health officials learned that the pandemic would have downstream effects on post-acute-care facilities. These case-patients often require further supportive care after hospitalization; however, they might still be infectious and pose a risk to other long-term care

facility residents and staff (10). One week after we shared model outputs with state decision-makers, the state opened a dedicated long-term care facility to accommodate COVID-19 patients. To help calibrate the appropriate capacity of the center and anticipate the need for expansion, we collaborated with a team of hospitalists (general internists who care for hospitalized patients) to extend the process with a module aimed at projecting post-acute-care flows. This module explicitly models the discharge of case-patients

directly to home, to home healthcare, to skilled nursing facilities, or to hospice (Figure 4, panel B), and was first included in reports on May 18, 2020 (M. Maloney et al., unpub. data, <https://doi.org/10.1101/2020.06.12.20129551>).

Phase 4: Ongoing Activities and Future Directions

Although we have devised a process for responding to the ongoing pandemic, the situation continues to evolve. What appears to be effective now might not

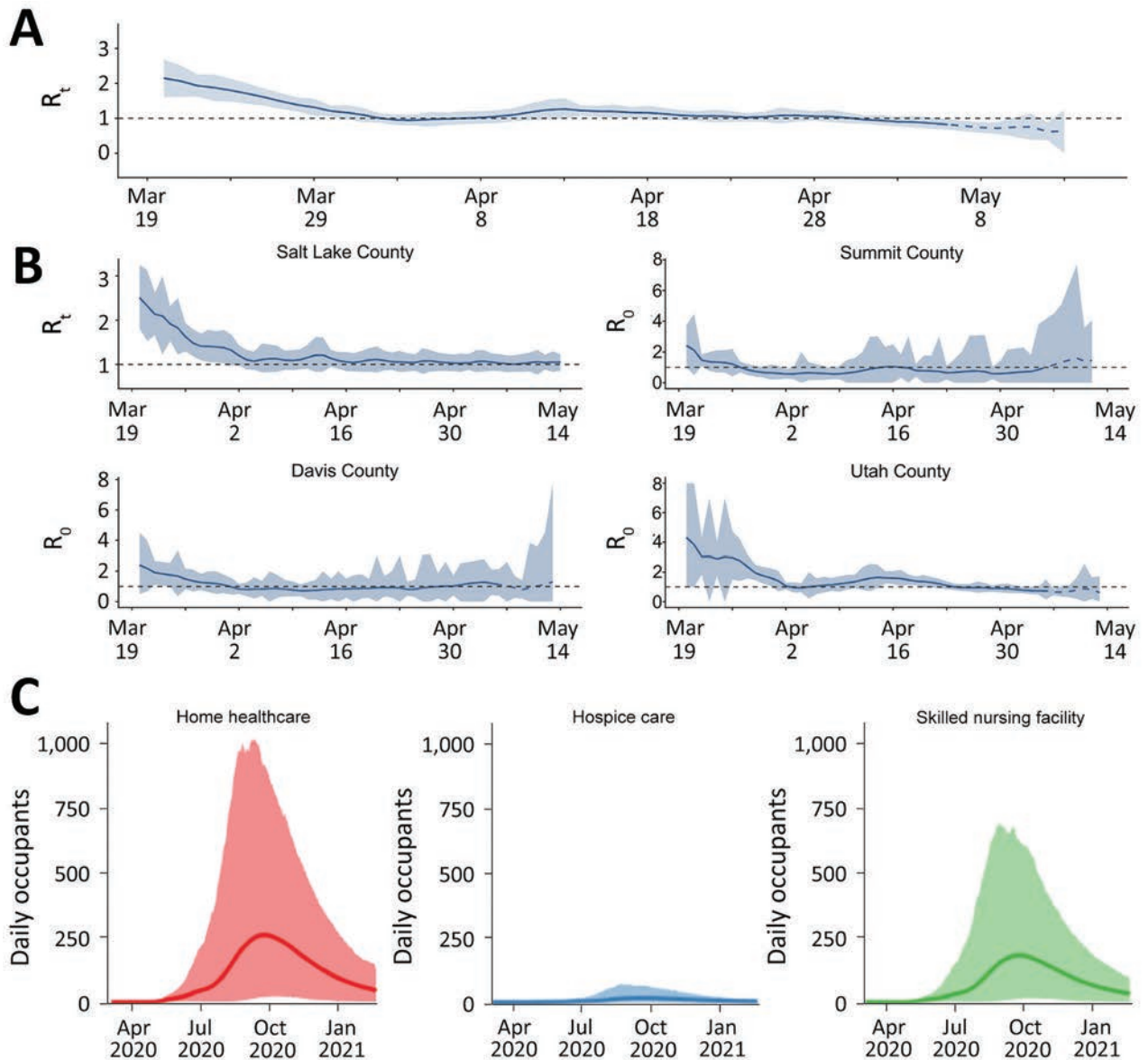


Figure 4. Sample model outputs from additional model components for a decision support tool for coronavirus disease, Utah, USA. Solid lines indicate the average daily occupancy, and shaded areas represent 95% CIs. A, B) Estimates of R_t for the entire state of Utah (A) and for 4 counties (B). The dashed blue line at the end of each time course represents the period within 1 serial interval from the end of the available data, where estimates of R_t are not accurate; dashed black line depicts $R_t = 1$, below which the disease will disappear and above which the disease will spread. C) Post-acute-care occupancy for each of 3 care types: home healthcare, hospice care, and skilled nursing facility. R_t , real-time effective reproduction number.

continue to be fruitful as the outbreak progresses. Likewise, the questions that have arisen thus far represent just a small sample of the potential hurdles that might be faced during a dynamic situation. For instance, we are already working to integrate a health economic model with the post-acute-care components to help guide the development and expansion of additional patient-care resources after hospitalization. In addition, we are beginning to develop collaborations across states with similar experiences, priorities, and concerns to learn from their experiences and further improve pandemic response. Although some future directions are clear, others will emerge as the pandemic evolves. As subsequent outbreaks occur, the response continues to leverage these developed collaborations to provide the state with evidence-based guidance for pandemic response.

Discussion

We identify 3 key points from the process so far. The first is establishing processes for bidirectional communication among stakeholders, the second is promoting communication and consensus among modeling teams, and the third is inviting multidisciplinary perspectives to inform modeling.

First, ongoing iterative communication with public health officials, policymakers, and other stakeholders is key for developing an understanding of policymakers' needs and gaining their trust, thereby creating a bidirectional relationship with effective communication. Through the process of producing and sharing weekly scenario-based projections of outcomes with policymakers and health experts, we demonstrated that we incorporated their feedback into the model, offered new interventions and evaluation criteria to consider, and provided support in interpreting the projections. Regular, open communication between stakeholders and modelers also fostered an environment that facilitated conversation between modeling groups and spurred new modeling developments.

The second key point is that debate and discussion of results between modeling groups increased confidence in model results and overall interpretability by policymakers. Before Utah developed its own models, several high-profile, out-of-state models produced unrealistic projections because they failed to account for the local context. For instance, the IHME model predicted hospital capacity would be exceeded in early April, much earlier than was observed, probably a result of drawing parallels with other COVID-19 epidemics based on little evidence and failing to incorporate important con-

textual details (IHME COVID-19 Health Service Utilization Forecasting Team et al.). The guidance of local models produced a more measured approach to outbreak control (i.e., a rapid scale-up of state testing and isolation), compared with a strict lockdown, which would have been justified to prevent the dire hospital overflow predicted by other models. The interagency collaboration developed through the consensus group helped to draw on diverse perspectives, account for local context, and boost confidence in model projections statewide. Importantly, comparing multiple models helped refute the false narrative that differing models are necessarily in competition. This comparison helped to highlight to both the consumers of the results and the individual modeling teams that each model is a tool optimized for addressing a particular type of policy question by making certain assumptions.

Finally, modeling approaches need to be adaptable and multidisciplinary to address changing policy questions. By using a solution-oriented modular approach, we were able to adjust and expand the initial epidemiologic model to assess how using an NPI affected the number of cases, the number of hospital or ICU beds needed in the short term, and the number of skilled nursing facility beds needed on a longer time scale, as well as, ultimately, the effectiveness of the NPIs used. An additional benefit of incorporating multiple modeling components was the differing perspectives in evaluating model assumptions and interpreting outputs gained by collaborating with experts from a range of disciplines. This collaboration between epidemiologists, health economists, biostatisticians, and hospitalists yielded perspectives beyond any single discipline and enabled groups to focus on modeling within their areas of expertise. Each model component was developed as a separate module, but results were shared regularly to solicit feedback, determine how they would inform the other modules, and formulate a consistent message for stakeholders.

In conclusion, the framework we have described can be applied in other settings to address additional public health challenges. This approach is best used at the level that decisions are being made and policies put into place. Each jurisdiction, whether at the city, county, state, or regional level, has its own particular conditions that affect disease transmission and number of cases (e.g., population density and demographics), and which intervention and treatment options are feasible (e.g., local laboratory capacity to scale up testing). As a result, modeling approaches for the same public health threat are bound to vary. An interdisciplinary modeling hub with university-

level support for these kinds of cross-cutting collaborations, such as the one we created, would enable the kind of inclusive, rigorous exchange that can yield valid models and estimates that multiple modeling groups can support. By enabling sharing of modeling approaches and sustaining dialogue focused on policymakers' questions, the forum would help modelers propose relevant and operationalizable scenarios that will probably resonate with policymakers and result in greater uptake. Another strategy would be to apply this multidisciplinary approach at the national level; however, a continuous dialogue between modelers, experts on the varied local conditions, and local politicians would be integral for the success of a national-level response.

H.R.M., K.H.G., J.L., E.C.L., and L.T.K. were supported by the State of California. J.L. and E.C.L. were supported by the US Department of Homeland Security. This work was also supported with computing service credits from Amazon Web Services and the Johns Hopkins Health System. L.T.K. and M.H.S. were supported by the Centers for Disease Control and Prevention (grant nos. 5U01CK000585-02 and 5U01CK000538-03). L.T.K., E.A., and T.S. were supported by the University of Utah Immunology, Inflammation, and Infectious Disease (3i) Seed Grant (grant no. 26798)

About the Author

Dr. Meredith is a postdoctoral researcher in the Department of Epidemiology at the Johns Hopkins Bloomberg School of Public Health. Her research interests include applying mathematical models to understand the impact of human mobility on disease transmission and to optimize treatment and control strategies for infectious diseases.

References

1. Meltzer MI, Atkins CY, Santibanez S, Knust B, Petersen BW, Ervin ED, et al.; Centers for Disease Control and Prevention. Estimating the future number of cases in the Ebola epidemic – Liberia and Sierra Leone, 2014–2015. *MMWR Suppl.* 2014;63:1–14.
2. Keegan LT, Lessler J, Johansson MA. Quantifying Zika: advancing the epidemiology of Zika with quantitative models. *J Infect Dis.* 2017;216(Suppl 10):S884–90. <https://doi.org/10.1093/infdis/jix437>
3. May RM, Anderson RM. Transmission dynamics of HIV infection. *Nature.* 1987;326:137–42. <https://doi.org/10.1038/326137a0>
4. Jewell NP, Lewnard JA, Jewell BL. Caution warranted: using the Institute for Health Metrics and Evaluation Model for predicting the course of the COVID-19 pandemic. *Ann Intern Med.* 2020;173:226–7. <https://doi.org/10.7326/M20-1565>
5. Boland H, Zolfagharifard E. Coding that led to lockdown was “totally unreliable” and a “buggy mess,” say experts. *The Telegraph.* 2020 May 16 [cited 2020 Nov 23]. <https://www.telegraph.co.uk/technology/2020/05/16/coding-led-lockdown-totally-unreliable-buggy-mess-say-experts>
6. Pueyo T. Coronavirus: why you must act now. *Medium.* 2020 [cited 2021 Mar 13]. <https://tomaspuoyo.medium.com/coronavirus-act-today-or-people-will-die-f4d3d9cd99ca>
7. Kirn J. Bay Area coronavirus – 4/23/20. *Medium.* 2020 [cited 2021 Mar 13]. <https://medium.com/@johnkirn/bay-area-coronavirus-4-23-20-1a81fbc36a91>
8. Shea K, Runge MC, Pannell D, Probert WJM, Li SL, Tildesley M, et al. Harnessing multiple models for outbreak management. *Science.* 2020;368:577–9. <https://doi.org/10.1126/science.abb9934>
9. Gneiting T, Raftery AE. Atmospheric science. Weather forecasting with ensemble methods. *Science.* 2005;310:248–9. <https://doi.org/10.1126/science.1115255>
10. Hu R, Jiang Z, Gao H, Huang D, Jiang D, Chen F, et al. Recurrent Positive Reverse Transcriptase-Polymerase Chain Reaction Results for Coronavirus Disease 2019 in Patients Discharged From a Hospital in China. *JAMA Netw Open.* 2020;3:e2010475. <https://doi.org/10.1001/jamanetworkopen.2020.10475>

Address for correspondence: Lindsay Keegan, Department of Epidemiology, 295 Chipeta Way, Salt Lake City, UT 84102, USA; email: lindsay.keegan@utah.edu

Coccidioidomycosis and COVID-19 Co-Infection, United States, 2020

Alexandra K. Heaney, Jennifer R. Head, Kelly Broen, Karen Click,
John Taylor, John R. Balmes, Jon Zelner, Justin V. Remais

We review the interaction between coronavirus disease (COVID-19) and coccidioidomycosis, a respiratory infection caused by inhalation of *Coccidioides* fungal spores in dust. We examine risk for co-infection among construction and agricultural workers, incarcerated persons, Black and Latino populations, and persons living in high dust areas. We further identify common risk factors for co-infection, including older age, diabetes, immunosuppression, racial or ethnic minority status, and smoking. Because these diseases cause similar symptoms, the COVID-19 pandemic might exacerbate delays in coccidioidomycosis diagnosis, potentially interfering with prompt administration of antifungal therapies. Finally, we examine the clinical implications of co-infection, including severe COVID-19 and reactivation of latent coccidioidomycosis. Physicians should consider coccidioidomycosis as a possible diagnosis when treating patients with respiratory symptoms. Preventive measures such as wearing face masks might mitigate exposure to dust and severe acute respiratory syndrome coronavirus 2, thereby protecting against both infections.

Persons with coronavirus disease (COVID-19) can have a wide range of symptoms, including cough, difficulty breathing, and fatigue (1). These symptoms are also common among patients with coccidioidomycosis (2), a primarily pulmonary disease caused by inhalation of *Coccidioides*, a soil-dwelling dimorphic fungi. These spores spread through the air, especially through wind erosion in dusty environments and dirt disrupting activities such as digging or construction. *Coccidioides* spores are found in hot and arid environments, including much of the southwestern United States, where coccidioidomycosis incidence has been increasing.

Since 2016, California has recorded its highest incidences of coccidioidomycosis (3,4).

We reviewed epidemiologic and clinical literature on coccidioidomycosis and COVID-19 to identify subpopulations that might be at risk for co-infection and severe disease. We discuss how the COVID-19 pandemic might affect coccidioidomycosis diagnosis, surveillance, and clinical management. We also evaluate evidence that co-infection might contribute to severe COVID-19 or reactivation of latent *Coccidioides* infection. Our study informs healthcare providers, policymakers, and populations in regions to which coccidioidomycosis is endemic on potential interactions between this disease and COVID-19, encouraging protective measures and prompt diagnosis.

Methods

We searched peer-reviewed journals on PubMed, Google Scholar, Scopus, and Web of Science; preprints posted on medRxiv and bioRxiv; and reports from state health departments and correctional agencies for articles on risk factors for infection and disease severity, diagnosis, surveillance, and preventive measures for coccidioidomycosis and COVID-19. We assessed titles and abstracts for relevance to the risk factors, diagnostic issues, and complications of coccidioidomycosis and COVID-19 co-infections. We conducted searches published during April–December 2020 and did not exclude articles on the basis of publication date. We identified other relevant publications by backward citation searching. We analyzed 116 peer-reviewed articles, 4 preprints, and 28 reports.

Possible Risk Factors for Coccidioidomycosis and COVID-19

COVID-19 and coccidioidomycosis share certain risk factors for exposure, potentially increasing the risk for co-infection. In California and Arizona, the 2 states with the highest number of reported coccidioidomycosis cases, substantial overlap exists between

Author affiliations: University of California, Berkeley, California, USA (A.K. Heaney, J.R. Head, K. Click, J. Taylor, J.R. Balmes, J.V. Remais); University of Michigan, Ann Arbor, Michigan, USA (K. Broen, J. Zelner); University of California, San Francisco, California, USA (J.R. Balmes)

DOI: <https://doi.org/10.3201/eid2705.204661>

county-level incidence of COVID-19 in 2020 and coccidioidomycosis in 2019 (Figures 1, 2).

Occupational Risks

Certain occupations pose increased risk for coccidioidomycosis. Because soil disruption and dusty environments promote dispersal of *Coccidioides* spores, coccidioidomycosis outbreaks frequently occur among workers in the construction and agricultural sectors (8,9,10). Of 47 coccidioidomycosis outbreaks reported during 1940–2015, a total of 25 (53%) were associated with occupational exposure, including 15 (60%) that were related to construction (11). An analysis of workers' compensation claims found that the incidence of coccidioidomycosis related to occupational exposure nearly quadrupled in California during 2000–2006, the highest rates seen among construction and agricultural workers (12).

Continued in-person work within the construction and agricultural sectors, which are considered essential occupations, also increases risk for COVID-19. In the United States, an estimated 8% of construction workers have had workplace exposure to the causative agent of COVID-19, severe acute respiratory syndrome coronavirus 2 (SARS-CoV-2), at least monthly, and nearly 60% of the construction labor force has ≥ 1 risk factor for severe COVID-19 (13, 14). Agricultural workers might also have heightened risk for COVID-19 because of high workforce turnover, shared transportation, and overcrowded living quarters that are often shared with other workers, multigenerational families, or both (15–19).

Incarcerated Populations

Incarcerated persons have a high risk for exposure to *Coccidioides* spores and SARS-CoV-2. Prisons and other facilities, such as immigration detention centers, are often in isolated areas with high environmental dust concentrations that can place inmates at higher risk for *Coccidioides* infection (Appendix, <https://wwwnc.cdc.gov/EID/article/27/5/20-4661-App1.pdf>). In addition, crowding, unsanitary conditions, and poor ventilation in carceral environments contributes to the rapid spread of communicable respiratory diseases like COVID-19 (20). Researchers have documented COVID-19 outbreaks among fire-fighting crews composed of incarcerated persons (21); similarly, researchers documented 7 coccidioidomycosis outbreaks among such fire-fighting crews during 2000–2017 (22). During 1940–2015, a total of 5 (11%) reported coccidioidomycosis outbreaks were among incarcerated populations (11). During 2007–2011, a total of 19% of coccidioidomycosis cases in California

were among incarcerated persons (23). More than 25% of California Department of Corrections and Rehabilitation facilities, including Lompoc Prison Complex (Lompoc, CA, USA), where a COVID-19 outbreak infected $>1,000$ persons (24), are in regions with high coccidioidomycosis incidence (25).

Researchers have documented several outbreaks of COVID-19 in carceral facilities (Appendix). During January 21–April 21, 2020, a total of 82% of reporting state and territorial health department jurisdictions reported confirmed COVID-19 cases among incarcerated or detained persons (including 4,893 reported

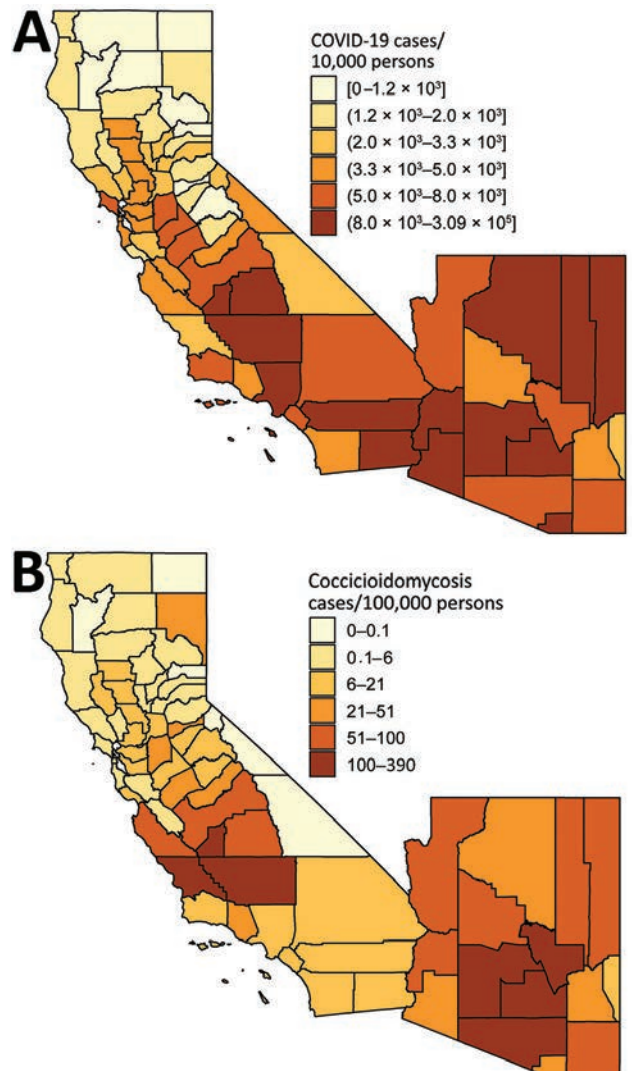


Figure 1. County-level incidence of (A) coronavirus disease (COVID-19) in 2020 and (B) coccidioidomycosis in 2019, California and Arizona. COVID-19 incidence reflects cumulative case count as of August 14, 2020 (5). Coccidioidomycosis incidence reflects annual incidence in 2019 (6,7). Shading indicates levels of incidence. Brackets indicate inclusive bounds; parentheses indicate exclusive bounds.

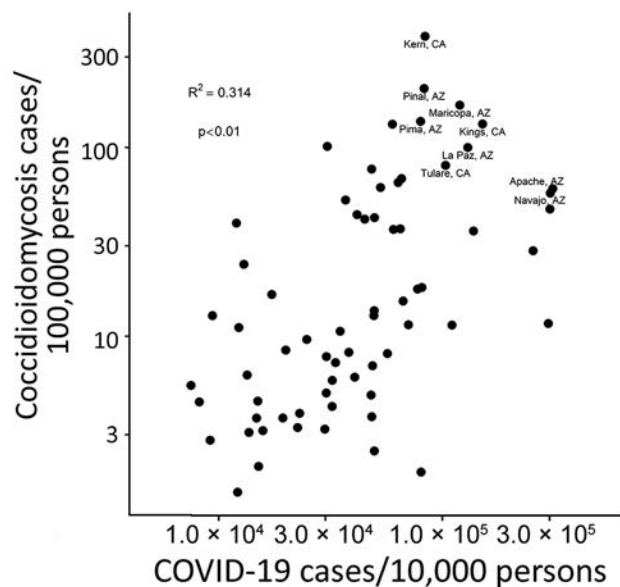


Figure 2. Scatterplot of county-level incidence of COVID-19 in 2020 and coccidioidomycosis in 2019, California and Arizona. $R^2 = 0.259$; $p < 0.01$.

cases and 88 deaths) or staff members (including 2,778 reported cases and 15 deaths) (26). COVID-19 outbreaks affecting $>1,000$ persons have occurred among incarcerated persons and staff working at carceral facilities in states from California to New York (Appendix).

Racial and Ethnic Minorities

Substantial racial and ethnic disparities exist in COVID-19 and coccidioidomycosis infection rates. Persons of Black and Latino heritage are at heightened risk for these infections. In California as of February 2021, Latino persons comprise 39% of the total population but account for 55% of COVID-19 cases (27). In the United States, COVID-19 incidence and death rates in counties with predominantly Black populations are significantly higher than in counties with predominantly white populations (28). In addition, Latino persons comprise 39% of the California population but 47% of its coccidioidomycosis patients; in the same state, non-Hispanic Black persons comprise 6% of the population but 9% of coccidioidomycosis patients (3).

Numerous societal inequities (including racism and discrimination, economic and educational disadvantages, and lack of healthcare access) contribute to higher pathogen exposure and infection rates among Black and Latino populations (29). In the context of the COVID-19 pandemic, social distancing might be more difficult for persons of low socioeconomic status because of their overrepresentation in essential occupations, elevated risk of living in densely

populated homes and neighborhoods, and higher numbers of multigenerational households (15–19). For example, 55% of Latino and 48% of Black persons work in essential jobs, compared with 35% of White persons (30). Disparities in coccidioidomycosis rates might also be caused by the disproportionate numbers of Black and Latino persons who are incarcerated or work in occupations with high exposure risk. More than 50% of farm laborers, agricultural workers, and construction workers in California are Latino (31,32). In addition, Black and Latino persons are overrepresented in carceral facilities: in California, Black persons comprise 27% and Latino persons comprise 41% of jail and prison populations (33).

Exposure to Particulate Matter

Persons living in environments with high concentrations of dust, which is a major constituent of particulate matter $\leq 10 \mu\text{m}$ or $\leq 2.5 \mu\text{m}$ in diameter, might be at elevated risk for infection with *Coccidioides* and SARS-CoV-2 and severe illness from COVID-19. Exposure to particulate matter is a risk factor for illness and death from viral respiratory infections, including COVID-19 (Appendix). Exposure to outdoor particulate air pollution is also associated with *Coccidioides* infection because mineral dust can mobilize airborne spores (34,35). Coccidioidomycosis outbreaks have been linked to dust plumes generated by military exercises, agriculture, construction, archeology excavations, windstorms, and landslides (36–43). For example, in an outbreak affecting 89 persons at a solar farm, persons who reported being in a dust cloud had ≈ 6 times the odds of symptomatic coccidioidomycosis than those who were not in the dust cloud. Wetting the dirt before soil-disrupting activities, a common practice to reduce dust, decreased the odds of symptomatic infection by 58% (44). Because COVID-19 control measures encourage the use of outdoor spaces, persons might have increased exposures to mineral dust and other air pollutants during the pandemic.

Co-Circulation with SARS-CoV-2 Hampering Coccidioidomycosis Diagnosis

The diagnosis of coccidioidomycosis in areas with community transmission of COVID-19 might be challenging because the diseases cause similar symptoms, which might exacerbate existing delays in coccidioidomycosis diagnosis and treatment. Without antifungal treatment, coccidioidomycosis patients are at risk for severe illness, including disseminated disease, and for death (45). Promptly administering antifungal treatments reduces unnecessary use of antimicrobial drugs

and resolves symptoms more effectively (45). In addition, early case management, including assessing risk factors for severity, regular follow-up visits to monitor symptoms, regular testing to check antibody titer levels, and physical therapy, is crucial to mitigating severe disease (46).

One reason for the underdiagnosis of coccidioidomycosis is low testing rates. For instance, a study in Tucson, Arizona, estimated that 15%–44% of community-acquired pneumonia cases could be attributed to coccidioidomycosis (47), but only 2%–13% of community-acquired pneumonia cases were tested for coccidioidomycosis (48). Valdivia et al. (47) found that half of patients had ≥ 2 clinic visits before being tested for coccidioidomycosis. Low sensitivities of coccidioidomycosis tests might further contribute to delays in diagnosis (Appendix). Given such diagnostic constraints, the median time between seeking healthcare and coccidioidomycosis diagnosis was estimated to be 23 days in Arizona (49).

The COVID-19 pandemic might contribute to further delays in coccidioidomycosis diagnosis. Both diseases can cause dry cough, muscle aches, headache, fatigue, and difficulty breathing; however, patients with COVID-19 tend to have a more acute progression of symptoms than those with coccidioidomycosis (50; Appendix references 51–54). Although pulmonary specialists and primary care physicians in regions to which coccidioidomycosis is endemic are probably aware of the diagnosis and treatment of this fungal infection, physicians in other regions might be less familiar with the diagnosis. Attributing coccidioidomycosis symptoms to COVID-19, whether presumed or laboratory-confirmed, might preclude coccidioidomycosis diagnosis in patients with monoinfections or co-infections. In addition, underutilization of healthcare services during the COVID-19 pandemic might result in further delays in the testing and diagnosis of coccidioidomycosis (Appendix reference 55).

Risk Factors for Severe Disease

Although most cases of coccidioidomycosis or COVID-19 are mild respiratory illnesses, either infection can cause severe disease and death (Appendix). Risk factors associated with severe coccidioidomycosis or COVID-19 often overlap, prompting concerns of elevated death rates associated with co-infections or serial infections. Patients with SARS-CoV-2 and *Coccidioides* co-infection might be at higher risk for severe disease; however, whether synergistic effects might exist requires further data. Overlapping risk factors associated with severe disease caused by coccidioidomycosis or COVID-19 include older age, diabetes

mellitus, immunosuppression, Black/African American ancestry, and smoking (Appendix references 56–70). Although the long-term pulmonary effects of COVID-19 remain unknown, early data suggest that the virus might cause lung damage (Appendix reference 71), resulting in elevated long-term risk for severe coccidioidomycosis.

Age

Older persons have heightened risk for severe disease caused by either infection. In the United States, 62% of COVID-19 hospitalizations and 80% of deaths were among patients >65 years of age (Appendix reference 72). Similarly, older persons, especially those >65 years of age, with coccidioidomycosis have higher risk for severe pulmonary disease. Rates of coccidioidomycosis-associated death increase with age. These trends might be partially explained by the higher prevalence among older adults of preexisting conditions and immunosuppression, which are risk factors for severe COVID-19 and coccidioidomycosis (Appendix references 56–64).

Diabetes

Diabetes is also associated with severe progression of either disease (Appendix references 56,63–68). A study of COVID-19 patients found that those with diabetes had a higher risk for severe pneumonia and organ damage (Appendix reference 73). The study also showed that patients with diabetes were more susceptible to a SARS-CoV-2-induced cytokine storm, which can cause rapid deterioration and death (Appendix reference 73). In addition, patients with diabetes are more likely to have relapsing coccidioidomycosis (risk ratio [RR] 3.39, 95% CI 1.65–6.46) or cavitary lung disease (RR 2.94, 95% CI 1.63–4.90) than those without diabetes (Appendix reference 74). Furthermore, among coccidioidomycosis patients with diabetes, those with higher serum glucose levels are more likely to have disseminated coccidioidomycosis, the most severe form of the disease, than those with lower levels (Appendix reference 74). The exact mechanisms through which diabetes influences the progression of coccidioidomycosis and COVID-19 are not well understood but might be related to impaired innate and adaptive cellular immunity (especially T-cell function) or the effects of a hyperglycemic environment on microorganism virulence (Appendix reference 75).

Immunosuppression

Although immunosuppressive steroids such as dexamethasone have reduced inflammatory lung

damage in patients with severe COVID-19 (Appendix reference 76), emerging evidence suggests that persons with a history of prolonged immunosuppression might be at higher risk for severe COVID-19. A study of 17 million adults in the United Kingdom found higher risks for death among COVID-19 patients who have hematologic malignancies, who are taking immunosuppressant drugs for organ transplants, or who have other causes of immunosuppression (Appendix reference 77). Immunosuppressed patients with cancer or solid organ transplants might be at higher risk for severe COVID-19 (Appendix reference 78). Coccidioidomycosis patients with suppressed immune responses, such as patients with hematologic malignancies, HIV, or organ transplants, also have higher risk for disseminated disease (Appendix references 61–63).

Black/African American Ancestry

Black persons have higher rates of severe COVID-19 and disseminated coccidioidomycosis than do White persons. Growing evidence indicates higher risk for severe COVID-19–associated disease and death among Black than White persons living in the United States (Appendix). A study of coccidioidomycosis in military personnel found dissemination rates to be 10 times higher among Black than White persons (Appendix reference 79). Similarly, a study in Kern County, California, found that patients with disseminated coccidioidomycosis were 4.6 times more likely to be Black than patients with mild disease (Appendix reference 56). The observed racial and ethnic disparities in severe COVID-19 and coccidioidomycosis are probably driven by structural inequities that systematically disadvantage persons of color in the forms of reduced healthcare access and exposure to environmental stressors that increase risk for conditions such as diabetes, obesity, and hypertension, which are associated with severe disease (29). For coccidioidomycosis, whether any biological basis for this association exists is unclear but might be related to immunogenic differences in T-cell function (Appendix references 56,69,70).

Smoking

Recent history of cigarette smoking has been linked to higher risk for severe disease from either infection. A systematic review and meta-analysis found that smokers with COVID-19 were significantly more likely (RR 2.4, 95% CI 1.43–4.04) to be admitted to an intensive care unit, need mechanical ventilation, or die compared with nonsmokers (Appendix reference 80). A case-control study in Kern County found that

patients with severe or disseminated coccidioidomycosis were more likely to have smoked cigarettes in the previous 6 months compared with patients with mild coccidioidomycosis (Appendix reference 56).

Possible Effects of Co-Infection on Disease Progression

Severe COVID-19

Underlying respiratory illness is a major risk factor for severe COVID-19 (Appendix references 60,64). The Centers for Disease Control and Prevention reported that among COVID-19 patients in the United States with available data on concurrent conditions, 9.2% had a chronic lung disease such as chronic obstructive pulmonary disease, asthma, or emphysema; chronic lung disease was the most common concurrent condition after diabetes (Appendix reference 81). The prevalence of chronic lung disease is higher among hospitalized patients (15%) and highest among patients in the intensive care unit (21%) (Appendix reference 81). Several studies of COVID-19 patients in China have also shown elevated rates of death and severe disease among those with underlying chronic respiratory conditions (Appendix references 64,82,83). Acute coccidioidomycosis is often self-limiting, but ≈3%–5% of patients have a chronic pulmonary form of the illness (Appendix references 84,85). The evidence that chronic lung disease increases risk for severe COVID-19 suggests that patients with chronic pulmonary coccidioidomycosis might be predisposed to severe COVID-19.

Coccidioidomycosis Reactivation

Infection with COVID-19 might reactivate disease in a coccidioidomycosis patient whose illness has progressed to a chronic but inactive state. After an initial *Coccidioides* infection resolves, the fungus can remain in the lungs in a latent state and become reactivated under certain conditions (Appendix references 86–93). Coccidioidomycosis reactivation has been reported among pregnant women, especially those who previously had disseminated coccidioidomycosis (Appendix reference 94). Patients with organ transplants, which usually require immunosuppressive medications, also have higher rates of coccidioidomycosis reactivation (Appendix references 87–92). SARS-CoV-2 infection has been associated with immune dysregulation, including lymphopenia (Appendix reference 95), which might lower the host's ability to regulate *Coccidioides* infection (Appendix reference 96). Although no studies have reported coccidioidomycosis reactivation in COVID-19 patients

as of February 2021, emerging evidence suggests that COVID-19 infection might accelerate the reactivation of latent tuberculosis (L. Pathak, unpub. data, <https://www.biorxiv.org/content/10.1101/2020.05.06.077883v2>). In addition, dexamethasone, a medication recommended for patients with severe COVID-19, increases the risk for severe coccidioidomycosis (Appendix references 97,98).

Areas for Future Research

Cloth Masks

Although cloth masks are a critical control method for COVID-19 (Appendix), studies have not examined the efficacy of cloth masks for filtering *Coccidioides* arthroconidia. At 2–5 μm in diameter, *Coccidioides* arthroconidia are substantially larger than SARS-CoV-2; this size difference might lead to differing levels of filtration effectiveness (Appendix references 99,100). One study found that cloth masks containing tightly woven cottons can filter 98% of particles in the 300 nm–6 μm range (Appendix reference 101), yet such results are difficult to extrapolate to specific particles such as *Coccidioides* arthroconidia (Appendix reference 102). It is also difficult to extrapolate results to other cloth masks, which vary widely in their filtration properties. Furthermore, leakage from improperly fitting masks can reduce efficacy of particle filtration by up to 50% (Appendix reference 101). The effects of leakage on disease prevention might differ on the basis of infectious dose; although a single *Coccidioides* spore might confer infection, the infectious dose of SARS-CoV-2 is probably higher. California therefore requires employers with worksites in regions to which coccidioidomycosis is endemic to provide respiratory protection filters rated at least N95 to workers if dust cannot be controlled; no mask recommendation exists for the general public (Appendix reference 103).

Climate

Transmission of SARS-CoV-2 and *Coccidioides* spores might be influenced by climatic conditions, such as temperature and humidity, that can affect pathogen survival and transport. For example, high humidity can suppress aerosol transmission of respiratory pathogens such as influenza and respiratory syncytial virus (Appendix references 104–110). Early research in Wuhan, China, suggested that SARS-CoV-2 might be transmitted more efficiently in less humid environments (Appendix references 111–113; W. Luo, unpub. data, <https://www.medrxiv.org/content/10.1101/2020.02.12.20022467v1>). Although the influence of temperature and other climatic conditions on transmission and

seasonality of SARS-CoV-2 currently might be outweighed by the large size of the susceptible population, the introduction of a vaccine could result in patterns of population immunity that enable climate to play a larger moderating role (Appendix reference 114). Because relative humidity plays a major role in regulating atmospheric dust concentrations, high atmospheric moisture can limit the dispersal of *Coccidioides* spores, potentially suppressing coccidioidomycosis transmission. For example, under wind conditions strong enough to mobilize dust, increases in relative humidity were associated with decreasing atmospheric dust concentrations (Appendix reference 115).

Disparities in Surveillance

The extent of socioeconomic, demographic, racial, and other disparities in COVID-19 and coccidioidomycosis is probably greater than reflected in administrative data sources. For example, analyses from hard-hit regions have indicated that high rates of excess death probably reflect a large burden of unreported SARS-CoV-2 infection (Appendix reference 116; J. Felix-Cardoso, unpub. data, <https://www.medrxiv.org/content/10.1101/2020.04.28.20083147v1>). Although testing coverage for SARS-CoV-2 is increasing, infections will probably continue to be undercounted in certain regions and populations because of factors such as disparate healthcare access, reagent shortages, and varied willingness to get tested. Undocumented or migrant farmworkers at high risk for exposure to *Coccidioides* spores are mostly uninsured, ineligible for healthcare benefits, or unable to afford healthcare (Appendix reference 117,118). The disparities seen in rates of illness and death caused by COVID-19 and coccidioidomycosis might have many contributing factors, including barriers to affordable, high-quality, and accessible healthcare; occupational exposures; mass incarceration; residential segregation; discrimination; and differential rates of concurrent conditions. Understanding these disparities is critical for attracting the attention and resources needed to remedy inequities in exposures, care-seeking, and illness and death caused by coccidioidomycosis and COVID-19.

Conclusions

Public health professionals, healthcare providers, and populations in areas to which coccidioidomycosis is endemic should be aware of the overlap in risk factors for coccidioidomycosis and COVID-19. Because prompt diagnosis is critical for effective management of coccidioidomycosis and the COVID-19 pandemic might exacerbate existing delays,

healthcare professionals should know how to identify these diseases and potential co-infection. Agricultural and construction workers, firefighters, Black and Latino persons, persons with diabetes, elderly persons, incarcerated persons, and migrant or undocumented farmworkers might be at increased risk for coccidioidomycosis and COVID-19. Employers and public health officials should mitigate exposure to dust and SARS-CoV-2 by promoting the use of face masks and social distancing practices.

This research was supported in part by the National Science Foundation (grant no. 2032210), the National Institutes of Health (grant nos. R01AI125842 and R01AI148336), and the University of California Multicampus Research Programs and Initiatives (award no. 17-446315). About the Author

Dr. Heaney is a postdoctoral scholar at the University of California, Berkeley, California, USA. Her research interests include the epidemiology and environmental determinants of infectious diseases.

References

- Goyal P, Choi JJ, Pinheiro LC, Schenck EJ, Chen R, Jabri A, et al. Clinical characteristics of Covid-19 in New York City. *N Engl J Med*. 2020;382:2372–4. <https://doi.org/10.1056/NEJMc2010419>
- Blair JE, Chang YHH, Cheng MR, Vaszar LT, Vikram HR, Orenstein R, et al. Characteristics of patients with mild to moderate primary pulmonary coccidioidomycosis. *Emerg Infect Dis*. 2014;20:983–90. <https://doi.org/10.3201/eid2006.131842>
- California Department of Public Health. Epidemiological summary of coccidioidomycosis in California, 2018. 2019 [cited 2020 May 18]. <https://www.cdph.ca.gov/Programs/CID/DCDC/CDPH%20Document%20Library/CocciEpiSummary2018.pdf>
- Centers for Disease Control and Prevention. Valley fever (coccidioidomycosis) statistics. 2020 [cited 2020 May 14]. <https://www.cdc.gov/fungal/diseases/coccidioidomycosis/statistics.html>
- USAFacts. US coronavirus cases and deaths by state. 2020 [cited 2020 May 21]. <https://usafacts.org/visualizations/coronavirus-covid-19-spread-map>
- California Department of Public Health. Coccidioidomycosis in California provisional monthly report: January–April 2020. 2020 [cited 2020 May 28]. <https://www.cdph.ca.gov/Programs/CID/DCDC/CDPH%20Document%20Library/CocciinCAProvisionalMonthlyReport.pdf>
- Arizona Department of Health Services. Valley fever 2019 annual report. 2021 [cited 2021 Feb 24]. <https://www.azdhs.gov/documents/preparedness/epidemiology-disease-control/valley-fever/reports/valley-fever-2019.pdf>
- Levan NE, Huntington RW. Primary cutaneous coccidioidomycosis in agricultural workers. *Arch Dermatol*. 1965;92:215–20. <https://doi.org/10.1001/archderm.1965.01600150005001>
- Schmelzer LL, Tabershaw IR. Exposure factors in occupational coccidioidomycosis. *Am J Public Health Nations Health*. 1968;58:107–13. <https://doi.org/10.2105/AJPH.58.1.107>
- Johnson WM. Occupational factors in coccidioidomycosis. *J Occup Med*. 1981;23:367–74.
- Freedman M, Jackson BR, McCotter O, Benedict K. Coccidioidomycosis outbreaks, United States and worldwide, 1940–2015. *Emerg Infect Dis*. 2018;24:417–23. <https://doi.org/10.3201/eid2403.170623>
- Das R, McNary J, Fitzsimmons K, Dobraca D, Cummings K, Mohle-Boetani J, et al. Occupational coccidioidomycosis in California: outbreak investigation, respirator recommendations, and surveillance findings. *J Occup Environ Med*. 2012;54:564–71. <https://doi.org/10.1097/JOM.0b013e3182480556>
- Baker MG, Peckham TK, Seixas NS. Estimating the burden of United States workers exposed to infection or disease: a key factor in containing risk of COVID-19 infection. *PLoS One*. 2020;15:e0232452. <https://doi.org/10.1371/journal.pone.0232452>
- Brown S, Brooks R, Dong XS. Coronavirus and health disparities in construction. The Center for Construction Research and Training. 2020 [cited 2020 Oct 16]. <https://www.cpwr.com/wp-content/uploads/publications/DataBulletin-May2020.pdf>
- Acs G, Loprest PJ. Job differences by race and ethnicity in the low-skill job market. The Urban Institute. 2009 [cited 2020 Jun 15]. <https://www.urban.org/sites/default/files/publication/30146/411841-Job-Differences-by-Race-and-Ethnicity-in-the-Low-Skill-Job-Market.PDF>
- Murray CJL, Kulkarni SC, Michaud C, Tomijima N, Bulzacchelli MT, Iandiorio TJ, et al. Eight Americas: investigating mortality disparities across races, counties, and race-counties in the United States [Erratum in: *PLoS Med*. 2006 Dec;3:e545]. *PLoS Med*. 2006;3:e260. <https://doi.org/10.1371/journal.pmed.0030260>
- Centers for Disease Control and Prevention. Communities, schools, workplaces, and events. 2020 [cited 2020 Oct 16]. <https://www.cdc.gov/coronavirus/2019-ncov/community/guidance-agricultural-workers.html>
- Arcury TA, Weir M, Chen H, Summers P, Pelletier LE, Galván L, et al. Migrant farmworker housing regulation violations in North Carolina. *Am J Ind Med*. 2012;55:191–204. <https://doi.org/10.1002/ajim.22011>
- Quandt SA, Brooke C, Fagan K, Howe A, Thornburg TK, McCurdy SA. Farmworker housing in the United States and its impact on health. *New Solut*. 2015;25:263–86. <https://doi.org/10.1177/1048291115601053>
- Simpson PL, Simpson M, Adily A, Grant L, Butler T. Prison cell spatial density and infectious and communicable diseases: a systematic review [Erratum in: *BMJ Open*. 2020;10:e026806corr1]. *BMJ Open*. 2019;9:e026806. <https://doi.org/10.1136/bmjopen-2018-026806>
- Sabalow R, Pohl J. California severely short on firefighting crews after COVID-19 lockdown at prison camps. *The Sacramento Bee*. 2020 [cited 2020 Aug 18]. <https://www.sacbee.com/news/california/fires/article243977827.html>
- Lucas KD, Wheeler C, Mohle-Boetani JC. Coccidioidomycosis outbreaks among inmate wildland firefighters in California. Proceedings of the 63rd Coccidioidomycosis Study Group Annual Meeting; 2019 Apr 5–6. Sacramento, CA, USA.
- MacLean M. Epidemiology of coccidioidomycosis – 15 California counties, 2007–2011. 2014 [cited 2020 May 28]. https://www.vfce.arizona.edu/sites/vfce/files/the_epidemiology_of_coccidioidomycosis_collaborative_county_report.pdf
- The New York Times. Coronavirus in the U.S.: latest map and case count. 2020 [cited 2020 May 28]. <https://www.nytimes.com/2020/05/28/us/coronavirus-map.html>

- nytimes.com/interactive/2020/us/coronavirus-us-cases.html?auth=login-email&login=email
25. Prison Law Office. Valley fever and CDCR housing. 2019 [cited 2020 May 28]. <https://prisonlaw.com/wp-content/uploads/2019/04/Valley-Fever-info-April-2019.pdf>
 26. Wallace M, Hagan L, Curran KG, Williams SP, Handanagic S, Bjork A, et al. COVID-19 in correctional and detention facilities – United States, February–April 2020. *MMWR Morb Mortal Wkly Rep.* 2020;69:587–90. <https://doi.org/10.15585/mmwr.mm6919e1>
 27. California Department of Public Health. COVID-19 race and ethnicity data. 2020 [cited 2020 Jun 15]. <https://www.cdph.ca.gov/Programs/CID/DCDC/Pages/COVID-19/Race-Ethnicity.aspx>
 28. Moore JT, Ricaldi JN, Rose CE, Fuld J, Parise M, Kang GJ, et al. Disparities in incidence of COVID-19 among underrepresented racial/ethnic groups in counties identified as hotspots during June 5–18, 2020 – 22 states, February–June 2020. *MMWR Morb Mortal Wkly Rep.* 2020;69:1122–6. <https://dx.doi.org/10.15585/mmwr.mm6933>
 29. Zelner J, Trangucci R, Narahariseti R, Cao A, Malosh R, Broen K, et al. Racial disparities in COVID-19 mortality are driven by unequal infection risks. *Clin Infect Dis.* 2020;72:e88–95. <https://doi.org/10.1093/cid/ciaa1723>
 30. Thomason S, Bernhardt A. Front-line essential jobs in California: a profile of job and worker characteristics. UC Berkeley Labor Center. 2020 [cited 2020 Aug 18]. <https://laborcenter.berkeley.edu/front-line-essential-jobs-in-california-a-profile-of-job-and-worker-characteristics/>
 31. United States Department of Agriculture. Farm labor. 2020 [cited 2020 Jun 15]. <https://www.ers.usda.gov/topics/farm-economy/farm-labor/#demographic>
 32. United States Census Bureau. Five-year public use microdata sample (PUMS), 2014–2018. 2020 [cited 2020 Jun 15]. <https://www.census.gov/programs-surveys/acs/technical-documentation/pums/documentation.html>
 33. United States Census Bureau. 2010 census summary file 1. 2016 [cited 2020 Jun 5]. <https://www.census.gov/data/datasets/2010/dec/summary-file-1.html>
 34. Chow NA, Griffin DW, Barker BM, Loparev VN, Litvintseva AP. Molecular detection of airborne *Coccidioides* in Tucson, Arizona. *Med Mycol.* 2016;54:584–92. <https://doi.org/10.1093/mmy/myw022>
 35. Pappagianis D, Einstein H. Tempest from Tehachapi takes toll or *Coccidioides* conveyed aloft and afar. *West J Med.* 1978; 129:527–30.
 36. Das R, McNary J, Fitzsimmons K, Dobraca D, Cummings K, Mohle-Boetani J, et al. Occupational coccidioidomycosis in California: outbreak investigation, respirator recommendations, and surveillance findings. *J Occup Environ Med.* 2012;54:564–71. <https://doi.org/10.1097/JOM.0b013e3182480556>
 37. Cummings KC, McDowell A, Wheeler C, McNary J, Das R, Vugia DJ, et al. Point-source outbreak of coccidioidomycosis in construction workers. *Epidemiol Infect.* 2010;138:507–11. <https://doi.org/10.1017/S0950268809990999>
 38. Petersen LR, Marshall SL, Barton C, Hajjeh RA, Lindsley MD, Warnock DW, et al. Coccidioidomycosis among workers at an archeological site, northeastern Utah. *Emerg Infect Dis.* 2004;10:637–42. <https://doi.org/10.3201/eid1004.030446>
 39. Standaert SM, Schaffner W, Galgiani JN, Pinner RW, Kaufman L, Durry E, et al. Coccidioidomycosis among visitors to a *Coccidioides immitis*-endemic area: an outbreak in a military reserve unit. *J Infect Dis.* 1995;171:1672–5. <https://doi.org/10.1093/infdis/171.6.1672>
 40. Wilken JA, Sondermeyer G, Shusterman D, McNary J, Vugia DJ, McDowell A, et al. Coccidioidomycosis among workers constructing solar power farms, California, USA, 2011–2014. *Emerg Infect Dis.* 2015;21:1997–2005. <https://doi.org/10.3201/eid2111.150129>
 41. de Perio MA, Materna BL, Sondermeyer Cooksey GL, Vugia DJ, Su CP, Luckhaupt SE, et al. Occupational coccidioidomycosis surveillance and recent outbreaks in California. *Med Mycol.* 2019;57:S41–5. <https://doi.org/10.1093/mmy/myy031>
 42. Gorris ME, Cat LA, Zender CS, Treseder KK, Randerson JT. Coccidioidomycosis dynamics in relation to climate in the southwestern United States. *Geohealth.* 2018;2:6–24. <https://doi.org/10.1002/2017GH000095>
 43. Schneider E, Hajjeh RA, Spiegel RA, Jibson RW, Harp EL, Marshall GA, et al. A coccidioidomycosis outbreak following the Northridge, Calif, earthquake. *JAMA.* 1997;277:904–8. <https://doi.org/10.1001/jama.1997.03540350054033>
 44. Sondermeyer Cooksey GL, Wilken JA, McNary J, Gilliss D, Shusterman D, Materna BL, et al. Dust exposure and coccidioidomycosis prevention among solar power farm construction workers in California. *Am J Public Health.* 2017;107:1296–303. <https://doi.org/10.2105/AJPH.2017.303820>
 45. Galgiani JN, Ampel NM, Blair JE, Catanzaro A, Johnson RH, Stevens DA, et al. Coccidioidomycosis. *Clin Infect Dis.* 2005;41:1217–23. <https://doi.org/10.1086/496991>
 46. Galgiani JN, Blair JE, Ampel NM, Thompson GR. Treatment for early, uncomplicated coccidioidomycosis: what is success? *Clin Infect Dis.* 2020;70:2008–12. <https://doi.org/10.1093/cid/ciz933>
 47. Valdivia L, Nix D, Wright M, Lindberg E, Fagan T, Lieberman D, et al. Coccidioidomycosis as a common cause of community-acquired pneumonia. *Emerg Infect Dis.* 2006;12:958–62. <https://doi.org/10.3201/eid1206.060028>
 48. Chang DC, Anderson S, Wannemuehler K, Engelthaler DM, Erhart L, Sunenshine RH, et al. Testing for coccidioidomycosis among patients with community-acquired pneumonia. *Emerg Infect Dis.* 2008;14:1053–9. <https://doi.org/10.3201/eid1407.070832>
 49. Tsang CA, Anderson SM, Imholte SB, Erhart LM, Chen S, Park BJ, et al. Enhanced surveillance of coccidioidomycosis, Arizona, USA, 2007–2008. *Emerg Infect Dis.* 2010;16:1738–44. <https://doi.org/10.3201/eid1611.100475>
 50. Fu L, Wang B, Yuan T, Chen X, Ao Y, Fitzpatrick T, et al. Clinical characteristics of coronavirus disease 2019 (COVID-19) in China: a systematic review and meta-analysis. *J Infect.* 2020;80:656–65. <https://doi.org/10.1016/j.jinf.2020.03.041>
 51. Goyal P, Choi JJ, Pinheiro LC, Schenck EJ, Chen R, Jabri A, et al. Clinical characteristics of Covid-19 in New York City. *N Engl J Med.* 2020;382:2372–4. <https://doi.org/10.1056/NEJMc2010419>

Address for correspondence: Justin Remais, University of California, Berkeley, 2121 Berkeley Way, Rm no 5302, Berkeley, CA 94720-7360, USA; email: jvr@berkeley.edu

Transmission of Severe Acute Respiratory Syndrome Coronavirus 2 during Border Quarantine and Air Travel, New Zealand (Aotearoa)

Nick Eichler, Craig Thornley, Tara Swadi, Tom Devine, Caroline McElnay, Jillian Sherwood, Cheryl Brunton, Felicity Williamson, Josh Freeman, Sarah Berger, Xiaoyun Ren, Matt Storey, Joep de Ligt, Jemma L. Geoghegan

The strategy in New Zealand (Aotearoa) to eliminate coronavirus disease requires that international arrivals undergo managed isolation and quarantine and mandatory testing for severe acute respiratory syndrome coronavirus 2. Combining genomic and epidemiologic data, we investigated the origin of an acute case of coronavirus disease identified in the community after the patient had spent 14 days in managed isolation and quarantine and had 2 negative test results. By combining genomic sequence analysis and epidemiologic investigations, we identified a multibranching chain of transmission of this virus, including on international and domestic flights, as well as a probable case of aerosol transmission without direct person-to-person contact. These findings show the power of integrating genomic and epidemiologic data to inform outbreak investigations.

New Zealand (Aotearoa in Māori) has a goal of eliminating coronavirus disease (COVID-19), which has resulted in a low incidence of this disease in this country (1-3). Managed isolation and quarantine (MIQ) is the mainstay of postborder controls to minimize importation risk. With few exceptions, international arrivals to New Zealand undergo a mandatory 14-day period of MIQ in designated facilities before entering the community. MIQ facilities are

repurposed commercial hotels used exclusively for isolation and quarantine of returnees.

During the MIQ period, regular health monitoring, as well as PCR testing on days 3 and 12, is undertaken to identify persons with COVID-19, whether symptomatic or asymptomatic, and measures are taken to control transmission. Subsequent to this study, a day 1 test has also been put in place, as have pre-departure tests. Persons who complete their 14-day period, show negative PCR results for severe acute respiratory syndrome coronavirus 2 (SARS-CoV-2), and remain asymptomatic are cleared to be released. We report a case of COVID-19 in a recent arrival to New Zealand in September 2020.

Human Ethics

A review by the New Zealand Health and Disability Ethics Committees advised that its approval was not required for this study. Nasopharyngeal samples that had positive results for SARS-CoV-2 by real-time reverse transcription PCR were obtained from public health medical diagnostics laboratories located throughout New Zealand. Under contract for the Ministry of Health, the Institute of Environmental Science and Research has approval to conduct genomic sequencing for surveillance of notifiable diseases.

Index Case-Patient

On September 18, 2020, a COVID-19 case was identified in New Zealand. The case was in a person who was a recent international arrival from India who had completed 14 days in MIQ in Christchurch, New Zealand, had shown negative results twice for SARS-CoV-2 on days 3 and 12, and had subsequently been released. This case-patient is denoted as case-patient G.

Author affiliations: Auckland District Health Board, Auckland, New Zealand (N. Eichler, F. Williamson); Hutt Valley District Health Board, Lower Hutt, New Zealand (C. Thornley); New Zealand Ministry of Health, Wellington, New Zealand (T. Swadi, T. Devine, C. McElnay); Institute of Environmental Science and Research, Porirua, New Zealand (J. Sherwood, X. Ren, M. Storey, J. de Ligt, J.L. Geoghegan); Canterbury District Health Board, Christchurch, New Zealand (C. Brunton, J. Freeman, S. Berger); University of Otago, Dunedin, New Zealand (J.L. Geoghegan)

DOI: <https://doi.org/10.3201/eid2705.210514>

Case-patient G flew from Christchurch to Auckland, New Zealand, on the day of release on a government-chartered flight with several other persons released from MIQ. This case-patient subsequently showed development of symptoms and showed positive results for SARS-CoV-2 four days later. Persons who had close contact with case-patient G were subsequently monitored and tested (Table). All persons who were positive for SARS-CoV-2 as a result of this investigation have provided verbal consent to be included in this study.

Travel from India to New Zealand

Case-patient G had been part of a cohort of 149 repatriated New Zealand citizens or permanent residents who had returned from India to New Zealand on August 27, 2020. The entire cohort who arrived in Christchurch had traveled on the same chartered flight (a Boeing 747) from Delhi, India, through Nadi, Fiji; all passengers disembarked from the flight in Fiji. Several passengers remained in Fiji, 3 of whom later showed positive results for SARS-CoV-2 during their quarantine period but who were not included in this investigation. Predeparture testing for SARS-CoV-2

was not mandatory at the time and no passengers reported having been tested.

Of the persons who arrived in Christchurch on this flight, 8 showed positive results for SARS-CoV-2 while in MIQ. Of these 8 case-patients, 3 were shown to be genomically linked and are denoted as case-patients A, B, and C (Figure 1). During the first (\approx 18 hour) flight from New Delhi to Nadi, case-patients A, B, and C sat within 2 rows of each other; all other case-patients observed physical distancing (Table). The flight was at \approx 35% occupancy, and passengers were evenly spaced throughout the aircraft.

The timing at which case-patient C experienced symptoms was consistent with transmission during the flight from India to New Zealand by case-patient A or B. Case-patients A or B might have been infected during or before the flight from a common source. All passengers were required to wear facemasks for the duration of the flight, and the flight crew followed infection prevention measures. The passengers in question did not travel together and did not know each other. On arrival in Christchurch, passengers were disembarked in groups of 10 to enable physical distancing to be maintained in the terminal, and each

Table. Characteristics for 9 case-patients tested for transmission of severe acute respiratory syndrome coronavirus 2 during border quarantine and air travel, New Zealand, September, 2020*

Case-patient	Symptom onset date	Positive sample date	Probable source of infection	Place of probable acquisition	GISAID accession no.	Flight seating details		
						India to Fiji: Aug 26	Fiji to Christchurch: Aug 27	Christchurch to Auckland: Sep 11
A	Asymptomatic	Aug 30	Residence overseas	India	EPI_ISL_548116	Row 50–55	7D	19A
B	Aug 29	Aug 30	Case-patient A or same source as case-patient A	In India or during travel to New Zealand	EPI_ISL_548118	53A	19D	Not on flight
C	Sep 6	Sep 8	Case-patients A or B	During travel to New Zealand	EPI_ISL_579092	49D	10F	Not on flight
D	Asymptomatic	Sep 21	Case-patient C	MIQ	EPI_ISL_579108	NR	17C	5A
E	Asymptomatic	Sep 21	Case-patient D	MIQ	EPI_ISL_579105	NR	17C	5A
F	Sep 22	Sep 21	Case-patient E	(child of case-patient D) Household (parent of case-patient E)	EPI_ISL_579107	Not on flight	Not on flight	Not on flight
G	Sep 15	Sep 17	Case-patient D	Domestic flight from Christchurch to Auckland	EPI_ISL_579103	55G	18F	4A
H	Sep 17	Sep 19	Case-patient G	Household (partner of case-patient G)	EPI_ISL_579104	Not on flight	Not on flight	Not on flight
I	Asymptomatic	Sep 19	Case-patient D	Household (child of case-patients G and H)	EPI_ISL_579099	Not on flight	Not on flight	Not on flight

*MIQ, managed isolation and quarantine; NR, not reported.

case-patient was provided with a fresh surgical mask. The cohort was transferred by bus to MIQ upon arrival in Christchurch. Physical distancing and surgical mask use were used while boarding and on board, but seating was not preallocated to specific passengers.

Evidence of Transmission in Hotel-Managed Isolation and Quarantine

The MIQ facility was a repurposed commercial hotel, in which each room had its own bathroom and no balconies. Case-patient C was positive on day 12 and was relocated to the isolation section of the facility. Before their relocation, an adult and infant child, both of whom had returned from India on the same flight, were in the adjacent room (Figure 1). Both the adult and child completed their 14-day quarantine. Each person had 2 negative test results and no reported symptoms but later showed positive results for SARS-CoV-2 while in the community (these 2 case-patients are denoted as case-patients D and E). We consider that these 2 case-patients were infected while in MIQ.

Closed-circuit television review of the period between the arrival of case-patients C, D, and E and the transfer of case-patient C to the isolation section of MIQ showed that there were no instances where the 3 persons were outside of their rooms at the same time. Nevertheless, footage showed that during routine testing on day 12, which took place within the doorway of the hotel rooms, there was a 50-second window between closing the door to the room of case-patient C and opening the door to the room of case-patients D and E. Therefore, we hypothesized that suspended aerosol particles were the probable mode of transmission in this instance, and that the enclosed and unventilated space in the hotel corridor probably facilitated this event (4). A commissioned review of the ventilation system found that the rooms in question had a net positive pressure compared with the corridor. Fomite transmission through use of

communal bins in the corridor was considered to be a less probable route of transmission because contact with the bin lid by case-patient D was >20 hours after it was touched by case-patient C.

Domestic In-Flight and Household Transmission

Following their 14-day completion of MIQ, case-patients A (who was deemed to be recovered), D, E, and G boarded an 85-min government-chartered domestic flight (on a Boeing 737) from Christchurch to Auckland. All passengers were required to wear masks, and the flight was at ≈50% occupancy. Case-patient G sat directly in front of case-patients D and E, and case-patient A sat at a distance (Figure 1). On arrival at Auckland airport, case-patients D and E were met by a household contact, denoted as case-patient F, and case-patient G was met by household contacts (case-patients H and I). These household contacts had not been in MIQ because they had no recent history of travel outside New Zealand. However, both contacts subsequently tested positive for SARS-CoV-2 (Figure 1).

Genome Sequencing of SARS-CoV-2

We generated the genomes of the 9 positive SARS-CoV-2 samples from case-patients A–I according to reported sequencing protocols (5–7) (https://github.com/ESR-NZ/NZ_SARS-CoV-2_genomics). These genomes were classified within the (now ancestral) PANGO (8) genomic lineage B.1.36.17. Because of the dynamic nature of this genomic nomenclature, this cluster from New Zealand is now classified as lineage F.1, which is now extinct (Figure 2).

We compared these data to virus genomes sequenced from New Zealand and those B.1.36.17 genomes from the global dataset that were available on GISAID (<https://www.gisaid.org>) as of February 2021 (n = 1,994) (9). The 9 SARS-CoV-2 sequences from New Zealand, together with 500 B.1.36.17

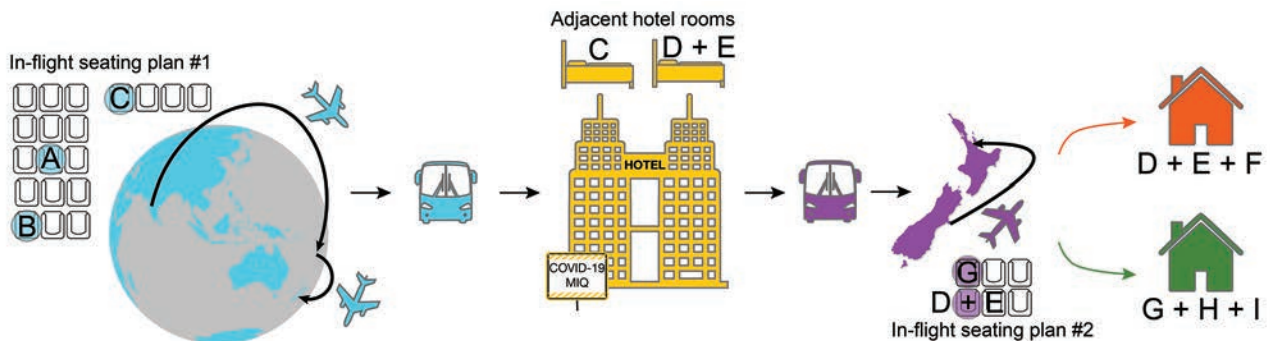


Figure 1. Sequence of probable transmission events and associated relevant locations in-flight and MIQ for severe acute respiratory syndrome coronavirus 2 during border quarantine and air travel, New Zealand, September 2020. Location of case A is approximate (Table). COVID-19, coronavirus disease; MIQ, managed isolation and quarantine.

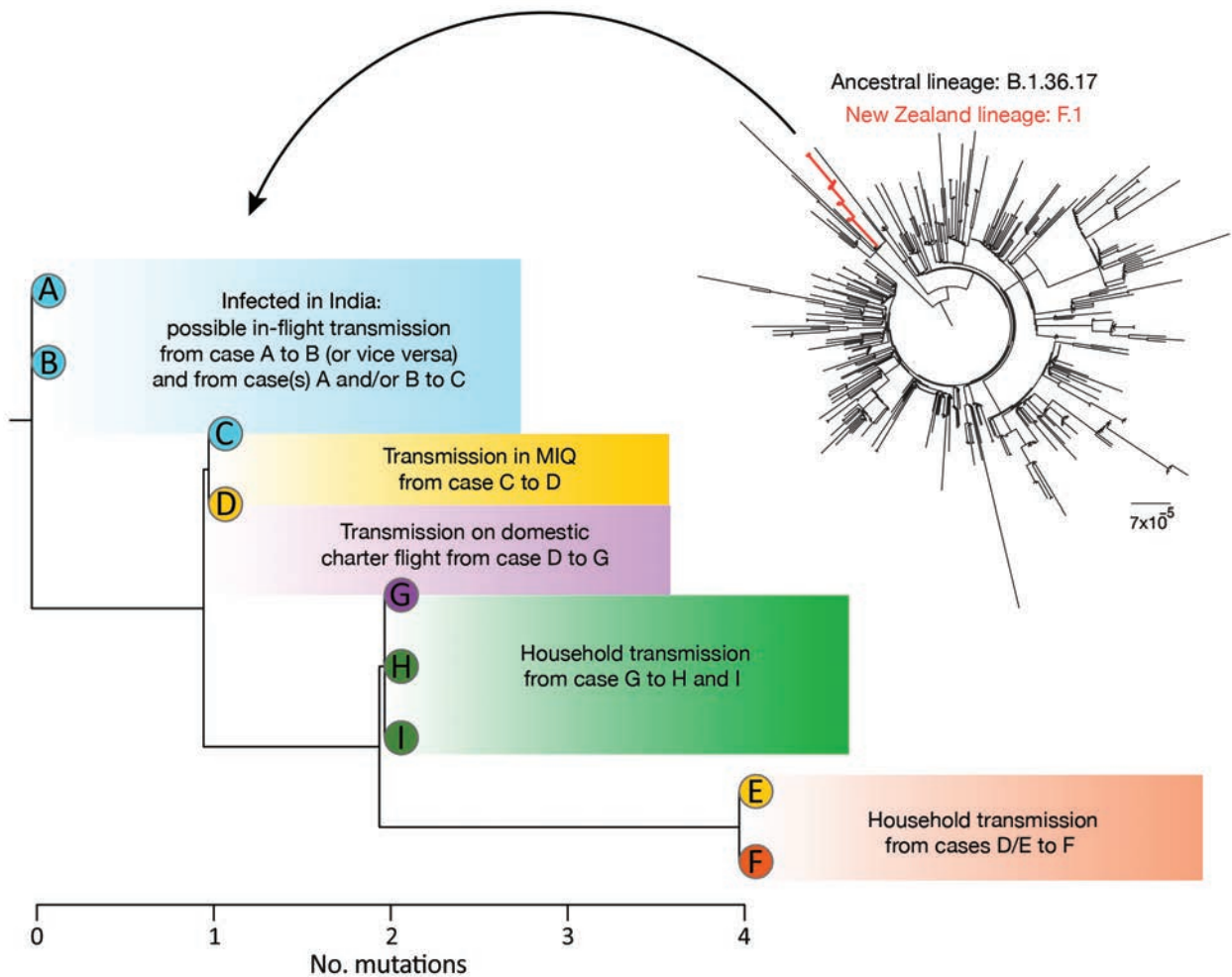


Figure 2. Phylogenetic trees showing genomic relationship of severe acute respiratory syndrome coronavirus 2 genomes generated for 9 case-patients, New Zealand, September 2020. Shown are number of mutations, as well as the F.1 cluster (red) within the context of the closest ancestral B.1.36.17 lineage (black). Scale bar indicates nucleotide substitutions per site. MIQ, managed isolation and quarantine.

genomes, uniformly sampled at random from the global population (Appendix, <https://wwwnc.cdc.gov/EID/article/27/5/21-0514-App1.xlsx>), were aligned by using MAFFT version 7 and the FFT-NS-2 algorithm (10). Ambiguous sites that have been flagged as potential sequencing errors were masked. We created a maximum-likelihood phylogenetic tree by using IQ-TREE version 1.6.8 (11) and the Hasegawa-Kishino-Yano (12) nucleotide substitution model with a gamma-distributed rate variation among sites. We determined the best fit model by using ModelFinder (13). We assessed branch support by using the ultrafast bootstrap method (14).

We found a genomic link between virus isolated from all 9 case-patients and a maximum genomic distance of 4 single-nucleotide polymorphisms (Figure 2). Placing this cluster within the global context

provides high confidence (100% bootstrap node support of 1,000 iterations) that it was a single introduction of the virus into New Zealand (Figure 2). Of the other 5 case-patients who were positive for SARS-CoV-2 and arrived on the same flight from India, 1 case-patient was definitively excluded from the cluster on the basis of virus genome being within a different (non-F.1) genomic PANGO lineage (Appendix). Four samples did not contain adequate RNA for genomic sequencing.

Conclusions

This case study of COVID-19 transmission demonstrates a multibranch chain of transmission involving numerous settings, supported by closed-circuit television observations, genomic sequence analyses, and epidemiologic investigations. Major aspects included

a probable case of transmission without direct person-to-person contact by aerosol within MIQ; transmission in-flight, as well as within households; and use of genomic sequence analysis to confirm probable direction of transmission between cases. These findings reinforce the need for rigorous border control processes for countries pursuing COVID-19 elimination, as well as real-time integration of genomic and epidemiologic data to inform outbreak investigations.

Acknowledgments

We thank the ARTIC network for making their protocols and tools openly available, diagnostic laboratories that performed the initial RT-PCRs and referred samples for sequencing, public health units for providing epidemiologic data; and all those who have contributed SARS-CoV-2 sequences to the GISAID database.

Genomic sequencing was supported by the Ministry of Health of New Zealand, the New Zealand Ministry of Business, the Innovation and Employment COVID-19 Innovation Acceleration Fund (CIAF-0470), and the Institute of Environmental Science and Research Strategic Science Investment Fund.

About the Author

Dr. Eichler is a medical officer of health at the Auckland Regional Public Office Service, Auckland, New Zealand. His research interests are prevention of childhood bacterial infections and COVID-19 control.

References

1. Jefferies S, French N, Gilkison C, Graham G, Hope V, Marshall J, et al. COVID-19 in New Zealand and the impact of the national response: a descriptive epidemiological study. *Lancet Public Health*. 2020;5:e612–23. [https://doi.org/10.1016/S2468-2667\(20\)30225-5](https://doi.org/10.1016/S2468-2667(20)30225-5)
2. Baker MG, Wilson N, Anglemeyer A. Successful elimination of COVID-19 transmission in New Zealand. *N Engl J Med*. 2020;383:e56. <https://doi.org/10.1056/NEJMc2025203>
3. Geoghegan JL, Moreland NJ, Le Gros G, Ussher JE. New Zealand's science-led response to the SARS-CoV-2 pandemic. *Nat Immunol*. 2021;22:262–3. <https://doi.org/10.1038/s41590-021-00872-x>
4. COVID-19 transmission – up in the air [editorial]. *Lancet Respir Med*. 2020;8:1159. [https://doi.org/10.1016/S2213-2600\(20\)30514-2](https://doi.org/10.1016/S2213-2600(20)30514-2)
5. Geoghegan JL, Douglas J, Ren X, Storey M, Hadfield J, Silander OK, et al. Use of genomics to track coronavirus disease outbreaks, New Zealand. *Emerg Infect Dis*. 2021;27:xxxx–xxxx.
6. Geoghegan JL, Ren X, Storey M, Hadfield J, Jelley L, Jefferies S, et al. Genomic epidemiology reveals transmission patterns and dynamics of SARS-CoV-2 in Aotearoa New Zealand. *Nat Commun*. 2020;11:6351. <https://doi.org/10.1038/s41467-020-20235-8>
7. Swadi T, Geoghegan JL, Devine T, McElnay C, Sherwood J, Shoemack P, et al. Genomic evidence supports in-flight transmission of SARS-CoV-2 despite pre-departure testing. *Emerg Infect Dis*. 2021;27:687–93. <https://doi.org/10.3201/eid2703.204714>
8. Rambaut A, Holmes EC, O'Toole Á, Hill V, McCrone JT, Ruis C, et al. A dynamic nomenclature proposal for SARS-CoV-2 lineages to assist genomic epidemiology. *Nat Microbiol*. 2020;5:1403–7. <https://doi.org/10.1038/s41564-020-0770-5>
9. Elbe S, Buckland-Merrett G. Data, disease and diplomacy: GISAID's innovative contribution to global health. *Glob Chall*. 2017;1:33–46. <https://doi.org/10.1002/gch2.1018>
10. Katoh K, Standley DM. MAFFT multiple sequence alignment software version 7: improvements in performance and usability. *Mol Biol Evol*. 2013;30:772–80. <https://doi.org/10.1093/molbev/mst010>
11. Nguyen L-T, Schmidt HA, von Haeseler A, Minh BQ. IQ-TREE: a fast and effective stochastic algorithm for estimating maximum-likelihood phylogenies. *Mol Biol Evol*. 2015;32:268–74. <https://doi.org/10.1093/molbev/msu300>
12. Hasegawa M, Kishino H, Yano T. Dating of the human-ape splitting by a molecular clock of mitochondrial DNA. *J Mol Evol*. 1985;22:160–74. <https://doi.org/10.1007/BF02101694>
13. Kalyaanamoorthy S, Minh BQ, Wong TK, von Haeseler A, Jermini LS. ModelFinder: fast model selection for accurate phylogenetic estimates. *Nat Methods*. 2017;14:587–9. <https://doi.org/10.1038/nmeth.4285>
14. Hoang DT, Chernomor O, von Haeseler A, Minh BQ, Vinh LS. UFBoot2: improving the ultrafast bootstrap approximation. *Mol Biol Evol*. 2018;35:518–22. <https://doi.org/10.1093/molbev/msx281>

Address for correspondence: Jemma L. Geoghegan, Department of Microbiology and Immunology, University of Otago Division of Health Sciences, 720 Cumberland St, Dunedin, Otago 9054, New Zealand; email: jemma.geoghegan@otago.ac.nz

Successful Control of an Onboard COVID-19 Outbreak Using the Cruise Ship as a Quarantine Facility, Western Australia, Australia

Tudor A. Codreanu, Sera Ngeh, Abigail Trewin, Paul K. Armstrong

Onboard quarantining has been only partially effective to control outbreaks of coronavirus disease on cruise ships. We describe the successful use of the ship as a quarantine facility during the response to the outbreak on the MS Artania, which docked in Western Australia, Australia. The health-led 14-day quarantine regime was based on established principles of outbreak management and experiences of coronavirus disease outbreaks on cruise ships elsewhere. The attack rate in the crew was 3.3% (28/832) before quarantine commencement and 4.8% (21/441) during quarantine on board. No crew members became symptomatic after completion of quarantine. Infection surveillance involved telephone correspondence, face-to-face visits, and testing for severe acute respiratory syndrome coronavirus 2. No serious health issues were reported, no response staff became infected, and only 1 quarantine breach occurred among crew. Onboard quarantine could offer financial and operational advantages in outbreak response and provide reassurance to the shore-based wider community regarding risk for infection.

Cruise ships are a highly susceptible environment for the rapid spread of infectious diseases because of high population density, encouragement of social interaction, and common food and water sources. A variety of pathogens have been implicated, including norovirus (1), influenza virus (2), *Legionella pneumophila* (3), *Cyclospora* (4), *Salmonella enterica* serotype Enteritidis (5), and measles (6). Passengers are often elderly and have underlying conditions that put them at higher risk for health complications after infection.

The use of quarantine (i.e., “the restriction of activities of or the separation of persons who are not

ill but who may have been exposed to an infectious agent or disease” [7]) has been a cornerstone of infectious disease control for centuries. Quarantine ensures the early detection of cases by monitoring for illness onset and isolating infected persons from others until they are no longer infectious (8). In modern times, the period of quarantine is normally set at the maximum incubation period of the disease of interest (9). Quarantine has been used, in conjunction with other measures, to control infectious disease outbreaks on cruise ships (10–12).

On January 7, 2020, severe acute respiratory syndrome coronavirus 2 (SARS-CoV-2) was identified as the causative organism of an infectious respiratory disease affecting residents of Wuhan, China. Coronavirus disease (COVID-19) rapidly spread around the world and was declared a pandemic on March 12, 2020 (13). Outbreaks of COVID-19 on cruise ships were an early feature of the pandemic, and quarantine was used to varying degrees as a control measure. One of the earliest and largest outbreaks of COVID-19 on a cruise ship was reported aboard the Diamond Princess, which arrived in Yokohama, Japan, on February 3, 2020; ultimately, 712 of 3,711 (19.2%) passengers and crew contracted the infection, and 13 persons died (14). On February 5, the government of Japan instituted a 14-day quarantine period on board the Diamond Princess (15,16). Quarantined passengers were allowed periods outside their cabins for health and well-being, and crew continued their usual duties after quarantine began (14,15,17). SARS-CoV-2 continued to be transmitted on board within passenger cabins and by infected food service workers (15,17–19). This quarantine measure proved effective in decreasing transmission; however, it did not completely control the outbreak, and further cases occurred after release from quarantine (14,17–20).

Author affiliations: Department of Health Western Australia, Perth, Western Australia, Australia (T.A. Codreanu, S. Ngeh, P.K. Armstrong); National Critical Care and Trauma Response Centre, Darwin, Northern Territory, Australia (A. Trewin)

DOI: <https://doi.org/10.3201/eid2705.204142>

The cruise ship MS Artania, which is 230 meters long, 9 decks, and built in 1984, can carry $\leq 1,260$ passengers in 594 cabins and 537 crew members in 321 cabins. Departing Hamburg, Germany, on December 21, 2019, for a 6-month world tour, the ship arrived in Fremantle Port, Western Australia (WA), on March 25, 2020, carrying 832 passengers (age range 7–89 years) of 12 nationalities and 503 crew members (age range 23–61 years) of 30 nationalities.

On arrival, the ship's medical team reported to WA health authorities that 2 passengers had tested positive for SARS-CoV-2 upon their return to Germany after disembarking the ship in Sydney, Australia, on March 14, 2020, and that a further 15 passengers and 10 crew had reported fever, mild respiratory symptoms, or both during March 21–25. Point-of-care test kits for influenza A and B were not available on board. According to standard ship protocols, these persons were immediately isolated in their cabins and released 48 hours after symptoms resolved. On March 25, specimens were collected from 9 persons who remained in isolation; 7 (5 passengers and 2 crew members) tested positive for SARS-CoV-2 by reverse transcription PCR (RT-PCR). On the same day, 2 further persons evacuated for non-COVID-19 medical reasons also tested positive for SARS-CoV-2, and an outbreak was declared.

Methods

Command and Coordination

The government of Australia has legislated responsibility for human biosecurity for international maritime arrivals and took the lead role in a multiagency response to the outbreak. It tasked an Australian Medical Assistance Team (AUSMAT) to coordinate the operational aspects of managing the outbreak. The AUSMAT team worked closely with federal agencies involved in biosecurity and border control, the state health department and law enforcement agency, and the local port authority.

Onboard Population Density Reduction

Vessel command divided the crew remaining on board into 2 groups, determined by the Minimum Safe Manning Certificate of the vessel: essential crew (EC), whose role was to maintain the safety (fire-fighting capacity, mooring lines) and vital functions (power supply and remote or direct systems monitoring) of the ship, and nonessential crew (nEC). Before quarantine began, all known SARS-CoV-2-positive case-patients (7 passengers and 2 crew members), along with their cabin-sharing contacts (7 passengers and 2 crew members) disembarked and were transferred to a hospital

or hotel, depending on their clinical condition. An additional 2 passengers disembarked for other medical reasons and tested positive for SARS-CoV-2 upon hospital admission. Once they disembarked, no passengers or crew members returned to the ship, even if cleared of SARS-CoV-2 infection. Asymptomatic persons from Europe (791 passengers and 23 nEC) who were medically fit-to-fly (not tested for SARS-CoV-2 infection) repatriated to Germany on March 29, 2020, aboard 4 Condor Flugdienst charter flights.

Case Identification and Management

We defined a case according to Australia's public health guidelines for COVID-19 (21): a suspected case required symptoms of acute respiratory infection or a temperature of $\geq 38.0^{\circ}\text{C}$, and a confirmed case required a positive test result by RT-PCR on an oropharyngeal and bilateral deep nasal specimen. After commencement of quarantine, a health questionnaire based on the same guidelines was used for daily screening of nEC by using a cloud-based short message service (SMS) system or fixed telephone lines in cabins. Any health screening failure prompted a face-to-face interview and temperature measurement; otherwise, a face-to-face interview was conducted every 3 days. EC were monitored by daily face-to-face health screening and temperature measurement. The ship's doctor (also in quarantine on board) provided additional information daily because crew reported symptoms directly. We collated and analyzed data pertaining to demographics, symptomatology, temperature recording, and laboratory results in Excel (Microsoft, <https://www.microsoft.com>).

Laboratory Methods

Oropharyngeal and bilateral deep nasal swab samples were obtained from any crew member with symptoms, either self-reported or elicited during health screening, for SARS-CoV-2 testing. The swabs were placed in viral transport medium and stored at 4°C – 8°C before testing. Testing was conducted at PathWest Laboratory Medicine WA by using a combined in-house RT-PCR directed at envelope and spike protein gene targets. This work was deemed a routine public health investigation and response, and no ethics approval was required.

Operational Aspects of the Outbreak Response

Vessel Cleaning and Disinfection

Before quarantine began, a 30-person commercial cleaning team conducted a hospital-grade (22,23) environmental disinfection. The common areas of

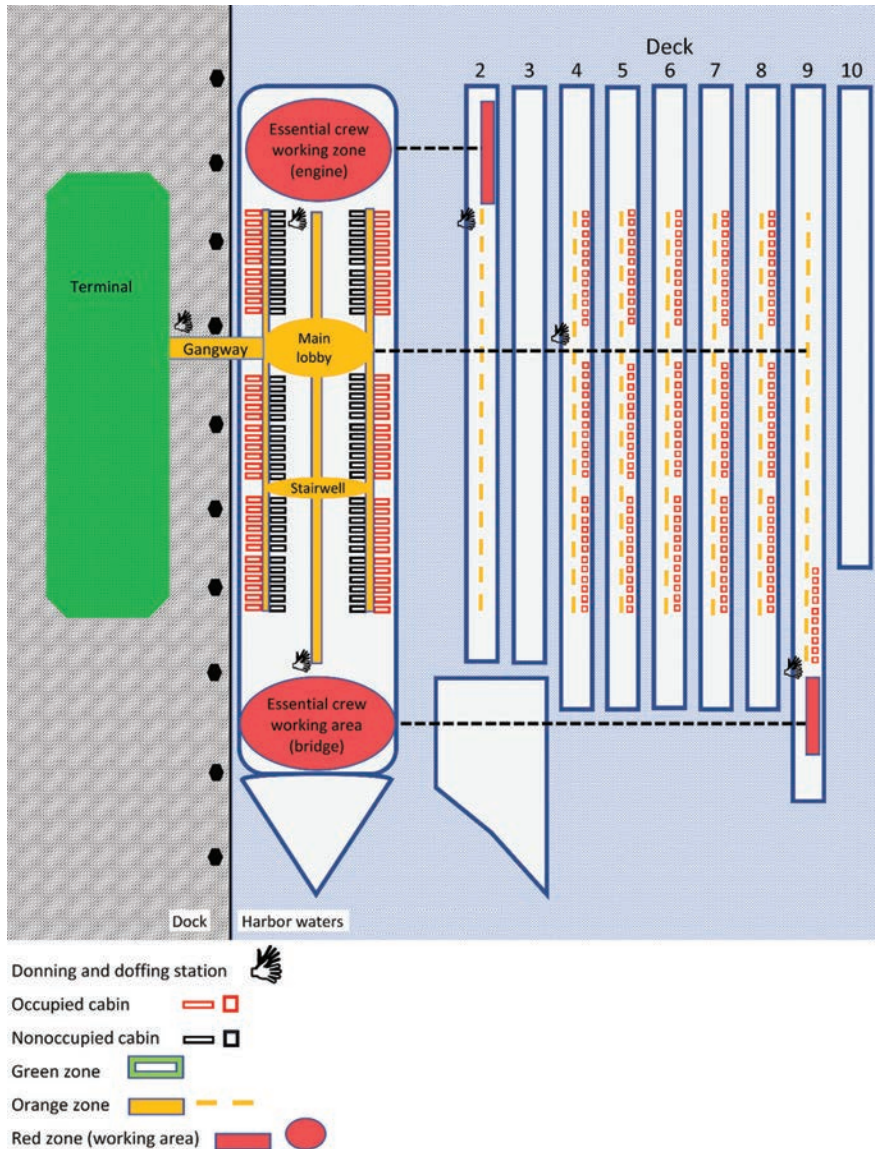


Figure 1. Layout of control zones for quarantine management aboard cruise ship used as quarantine facility to control onboard coronavirus disease outbreak, Western Australia, Australia. The terminal and dock were considered decontaminated (green zones); occupied cabins and work areas were considered contaminated (red zones); accessways from the shore to contaminated areas were considered buffer zones (yellow zones). Donning and doffing stations were placed at transition points between each zone.

decks 4–9 were targeted first (Figure 1). The aim was to create decontaminated access areas that would be used by external medical, catering, and security personnel. Frequently touched surfaces and floors in common areas were cleaned daily. Cabins where the nEC were to be quarantined were decontaminated the next night, after which EC work areas were cleaned. EC work areas were cleaned to environmental standards but were considered contaminated because of ongoing work traffic from potentially infected EC during quarantine. Cleaning equipment was disinfected daily.

Crew Segregation

EC were accommodated in their own cabins and allowed to go to their designated work areas (bridge

and engine room) and to respond to vessel emergencies. All nEC were accommodated individually in a separate area of the vessel in either unused or decontaminated cabins vacated by the disembarked passengers. They remained in strict quarantine for 14 days. EC and nEC could disembark, under escort, only if they tested positive for SARS-CoV-2, for other medical reasons, or because of a vessel emergency. The doors of all occupied cabins were marked to identify crew and food drop locations and for emergency evacuation purposes.

Infection Zones

The dock alongside the vessel and the adjacent terminal building were considered free of SARS-CoV-2 contamination (green zone). The access gangway,

Table. PPE requirements in control zones on cruise ship used as a quarantine facility to control onboard COVID-19 outbreak, Western Australia, Australia*

Cohort	Location or activity	PPE requirement
All crew	Own cabin	Not required
	Own cabin balcony	Surgical mask
	Food collection and cabin waste removal	Surgical mask, gloves, distancing of 2 m
Essential crew	Routine duties in normal work zones	Surgical mask, gloves, and distancing of 2 m unless impossible because of the nature of the work carried out
	Emergency duties outside normal work zones	Tyvek suit, surgical mask, gloves, distancing of 2 m unless impossible because of the nature of the work carried out
Health team	Vessel-based telephone health screening	Surgical mask, gloves, distancing of 2 m
	Face-to-face cabin visit	N95 mask, protective eyewear, impervious gown and gloves
External contractors	CCTV monitoring desk, roving security,	Surgical mask, gloves, distancing of 2 m
	food delivery	Impervious protective Level C suits, respirator masks, and protective eyewear
	Waste removal	

*CCTV, closed-circuit television; COVID-19, coronavirus disease; PPE, personal protective equipment.

stairwells, and corridors to cabins were considered at low risk for contamination (yellow zone) and functioned as buffer zones. Contaminated areas (red zones) consisted of EC work areas and all occupied cabins (Figure 1).

Personal Protective Equipment Requirements

Entry to the green zone did not require personal protective equipment (PPE), but surgical masks and gloves were required for entry to the yellow zone. Within the red zone, different levels of PPE were mandated (Table). All external contractors were trained in PPE procedures, and AUSMAT monitored compliance at entry and exit points.

Health and Well-being

Access to interpreter services was available, but because the official language on board was English, all crew had a reasonably good command of the language. All could communicate by using their own mobile phones (top-up credit vouchers were provided) and fixed-line telephones in cabins. AUSMAT also received, attended, and assessed health-related calls from crew. Initial contact was by telephone and escalated to a cabin visit or engagement of onshore WA health emergency resources, if required. Medical facilities on board were not used.

Efforts to minimize psychological stress and feelings of isolation and improve compliance included encouraging communication by individual 2-way and mass-SMS messaging systems, by using daily health checks as opportunities for high-quality contact time, and by using the public address and closed-circuit television (CCTV) systems to keep crew accurately informed. Other measures included acknowledging special events (birthdays and religious days), daily brain teaser exercises, and unsolicited local community support (handwritten postcards from primary school students).

Food Preparation, Supply, and Delivery

Before quarantine began, refrigerators in each cabin were stocked with several days’ supply of bottled water and long-life food and beverage items. To limit potential fomite spread, kitchen and catering facilities on board were not used. A 15-person external catering company prepared and delivered food for all persons on board, under direct supervision of AUSMAT. No food allergies were declared and meals consisted of culturally appropriate dish options not dissimilar to those normally available on board.

Food delivery was conducted through evening-only food-drops, consisting of a cold breakfast and lunch and hot dinner. Food was dropped in front of each cabin, and the bridge informed the relevant nEC by public address to open the door and collect the food package after delivery.

Waste Collection and Removal

Waste bags were prelocated in each cabin, collected from the front of each cabin, and disposed of by the nightly cleaning team. Judicious food packaging resulted in minimal waste.

Laundry and Linen

To minimize traffic, 2 sets of bed linens were placed in each occupied cabin; a contingency procedure for special circumstances was available through an external contractor. At the end of the quarantine period, all laundry and linen were collected in plastic bags and heat-cleaned at 60°C by using the washing facilities aboard the vessel.

Security

A comprehensive brief detailing the quarantine process, requirements, and restrictions was communicated to the crew. Compliance was continuously monitored by a temporary 16-camera internal CCTV

system, supplemented by 5 security guards whose responsibilities included immediately reporting any breaches of quarantine protocols.

Results

Description of the Outbreak

Before quarantine began on April 3, a total of 28 of 832 passengers and 30 of 503 crew members experienced symptoms and tested positive for SARS-CoV-2. The earliest symptoms in crew were recorded on March 21 in a motorman who later tested positive for SARS-CoV-2. We identified 2 distinct crew clusters: 5 security guards in whom symptom onset occurred during March 25–April 2, and 9 food service staff (6 wait staff and 3 food preparation staff) in whom symptom onset occurred during March 22–30.

During quarantine, 39 nEC disembarked: 21 (4.8%) symptomatic and SARS-CoV-2–positive persons (18 men and 3 women; mean age 41 years), and 18 close contacts, none of whom tested positive. After clearance testing on day 13 of quarantine, 2 asymptomatic EC tested positive, which resulted in all EC disembarking for a further 14-day onshore quarantine. All close contacts remained negative for SARS-CoV-2. A previously identified EC backup team from nEC subsequently managed the vessel.

The attack rate in crew before quarantine was 6.0% (30/503); during quarantine, the rate was 4.8% (21/441) (4.2% [18/427] in nEC and 21.4% [3/14] in EC). We recorded 1 COVID-19–related death in a male crew member 42 years of age. By the end of quarantine, 81 persons (30 passengers and 51 crew members) tested positive for SARS-CoV-2 (Figure 2); of those, 3 passengers and 1 crew member died (Figure 3).

Management of Health and Well-being Aspects during Quarantine

We performed health screening through 2,934 SMS messages, 3,339 telephone calls, and 1,033 face-to-face visits; we also reviewed 13 medical calls made by crew to the onboard doctor. A total of 245 RT-PCR tests were performed, including those used for clearance testing. No serious mental or physical health issues were reported; the main complaints conveyed by crew were constipation, lack of access to exercise, and lack of fresh air in some cabins.

A breach of quarantine was reported on day 5 when 3 nEC shared a kettle between adjacent rooms. Subsequently, 1 nEC became symptomatic and tested positive for SARS-CoV-2. A member of the external catering staff reported headache and fever (38°C) on day 7 of quarantine. She tested negative for SARS-CoV-2 and quarantined at home until symptoms resolved.

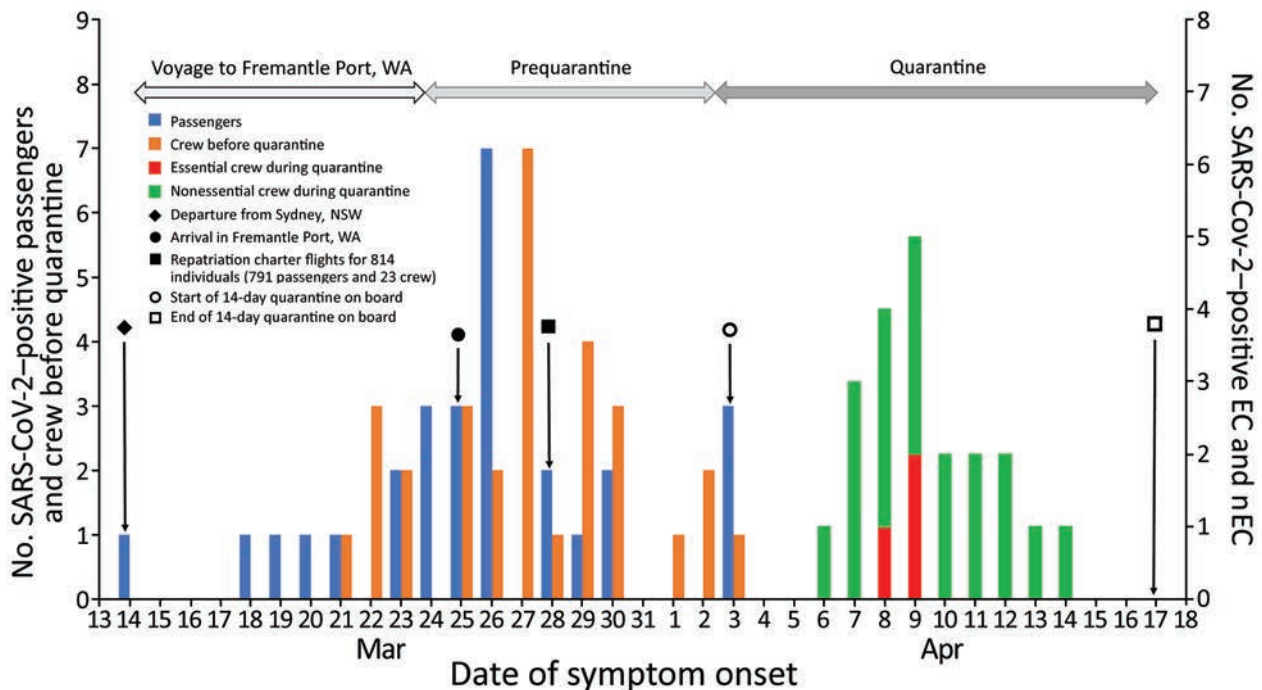


Figure 2. Epidemic curve of passenger and crew coronavirus disease cases by date of symptom onset aboard the MS Artania, WA, Australia, March 14–April 17, 2020. EC, essential crew; nEC, nonessential crew; NSW, New South Wales; SARS-CoV-2, severe acute respiratory syndrome coronavirus 2; WA, Western Australia.

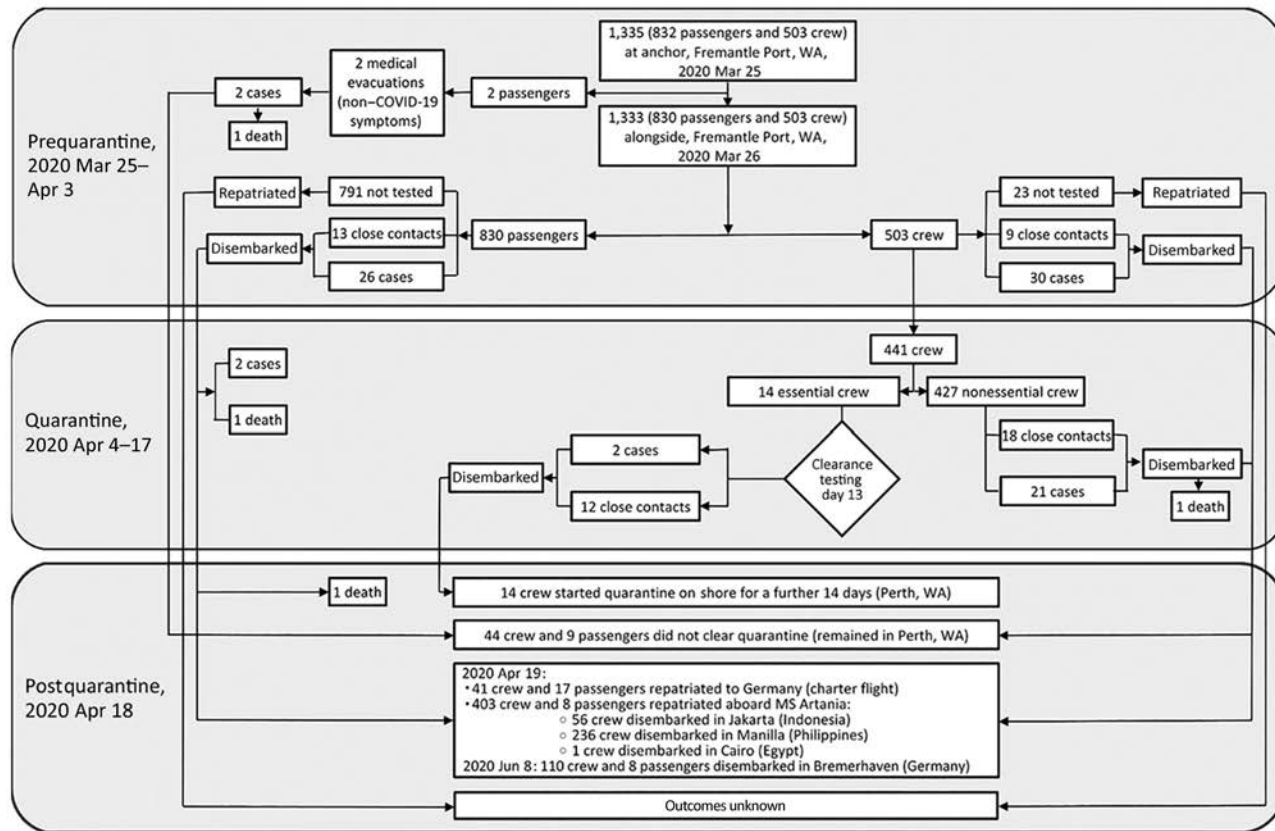


Figure 3. Flowchart of coronavirus disease outbreak outcomes of passengers and crew of the MS Artania, WA, Australia, March 14–April 18, 2020. WA, Western Australia.

Postquarantine Period

MS Artania departed Fremantle on April 18, 2020, carrying 403 crew and 8 passengers to return to its home port in Bremerhaven, Germany. During the voyage, crew were repatriated in Jakarta, Indonesia (56 crew members); Manila, Philippines (236 crew members); and Cairo, Egypt (1 crew member). Because of the possibility of asymptomatic infection and transmission during the 51-day voyage, the vessel command continued to impose AUSMAT recommendations for social distancing and mask-wearing in communal areas. The medical team continued rigorous COVID-19 symptom screening and temperature measurement of all persons. No crew members demonstrated elevated temperature or symptoms of acute respiratory infection before arrival in Germany on June 8, 2020 (W. Roeske, MS Artania Medical Team, pers. comm., 2020 May 31).

Discussion

Outbreaks of infectious diseases on cruise ships are a known risk, and cruise companies are well-versed in managing outbreaks of various types. However, SARS-CoV-2 poses a new and more severe threat, for which established prevention and response methods

are inadequate. Early in the pandemic, several COVID-19 outbreaks on cruise ships drew global attention, and the level of risk and complexities involved in their control led to a shutdown of the cruise industry. We demonstrate that under certain circumstances, a COVID-19 outbreak aboard a cruise ship can be successfully controlled by using the vessel as a quarantine facility, which can have substantial financial, operational, and safety advantages.

The outbreak aboard the MS Artania occurred in a setting of low prevalence of the disease in the WA community but intense political and community concern about the risk of importing the virus into the state (24,25). Strong economic, political, and health and welfare imperatives existed to end the outbreak safely, effectively, and as quickly as possible, to enable the vessel to leave Australia’s waters and return to Germany. These conditions required that we establish minimum requirements to main the function and safety of the vessel while we enacted a stringent quarantine process using a holistic approach guided by established infection prevention and control (IPC) principles and in consideration of the welfare of all persons on board (16,18,26–30).

In many ways, a cruise ship is an appropriate environment to conduct a large-scale quarantine operation. Its many well-appointed accommodation spaces enable the isolation of a large number of persons comfortably and with good communication options. The main alternative—removing crew and passengers and housing them onshore—introduces sizeable cost and additional risk for infection transmission in the transfer process.

This outbreak resulted in 51 known cases and 1 death in crew members and 30 cases and 3 deaths in passengers. Isolation of case-patients, quarantining of exposed persons, and segregating onboard crew into EC and nEC groups were key response measures. To maximize the number of noninfected crew available to sail the vessel at the end of quarantine, and to reduce the quarantine duration, crew members were confined to their own cabins with nonshared facilities. EC, however, were required to perform their essential duties on board and thus were not in strict isolation. EC were not permitted to share food and were always requested to observe infection-prevention measures, but their entire working area could not be monitored by CCTV. The detection of 2 cases on day 13 might have been the result of a breach in infection-prevention measures during quarantine.

One key factor in determining the feasibility of using a ship as a quarantine facility is the number of cabins required to quarantine persons separately. In this outbreak, we achieved appropriate cabin numbers by disembarking passengers for repatriation or hospitalization before quarantine began, enabling the shortest possible time to prepare and conduct the quarantine: 20 days from the decision to quarantine to the ship's departure from Fremantle Port. If there had been too few cabins to accommodate individual quarantine, regular RT-PCR testing of those who were sharing cabins would have enabled an early separation of discordant cabin mates, minimizing the overall period of quarantine.

Strict adherence to IPC was another tenet of our quarantine operation. The ship was separated into areas that reflected the level of risk for contamination and infection. Thorough daily cleaning maintained the status of these zones, and PPE requirements for each zone were rigidly enforced. Strict control of food preparation and delivery was a key component of the quarantine process. The use of external caterers mitigated the risk for fomite transmission through food prepared by potentially infected crew. The food-drop system essentially eliminated direct contact between catering staff and crew, negating the need for high-level PPE.

The presence of roving security personnel and the installation of CCTV cameras to monitor adherence to quarantine proved useful in 2 ways. These measures acted as incentives for quarantined crew to remain secluded in their rooms and ensured that any breaches were recognized and infection risk managed. The swift alert to the quarantine breach among 3 nEC enabled immediate review of events and decisive action.

The low level of SARS-CoV-2 activity in the WA community at the time of the operation, coupled with temperature and symptom screening of all responders (AUSMAT and contractors), gave us a high level of confidence that the WA responders were not themselves a risk vector for infection. In geographic locations where SARS-CoV-2 activity is higher, introduction of the virus on board by infected responders would need to be mitigated by regular symptom and temperature checks, SARS-CoV-2 testing, or both.

Solitary quarantine is challenging and potentially detrimental to physical and mental health. We focused on minimizing the length of quarantine through strict adherence to its principles and excellent communication by using a variety of technologies. Daily health checks provided the opportunity to build rapport and support and to reinforce and encourage compliance with quarantine requirements, and efforts were made to acknowledge special events. This approach might have contributed to a lack of reported serious mental or physical issues. The ultimate measure of success of this operation was that no symptoms consistent with SARS-CoV-2 infection were detected in any crew member after the 14-day quarantine period on board ended.

The first limitation of our study is that it does not provide a complete description of the outbreak on board the MS Artania. Whereas no passengers or crew had to quarantine or be tested upon arrival in Bremerhaven, some crew who disembarked in other countries had to quarantine or be tested upon arrival home. None of these crew were symptomatic, but we could not obtain further details after their arrival. Our attempts to identify other cases from the cohort of repatriated passengers and crew before the start of quarantine have not been successful. Second, we could not be certain that all asymptomatic nEC were not infected and infectious during quarantine and at its conclusion because we did not test asymptomatic nEC as a condition of release. However, none subsequently experienced symptoms of COVID-19, and ongoing IPC measures for the duration of the voyage back to Germany mitigated this small risk even further. The guidelines for screening and testing for SARS-CoV-2 are constantly evolving. Our screening and testing protocols reflected

best practices in Australia at that time, and a similar vessel outbreak would now be managed under a more rigorous testing regime.

Although the international cruise industry was effectively halted because of the COVID-19 pandemic, some cruises have restarted and the risk for COVID-19 outbreaks will endure. The severe consequences of such outbreaks to human life and to the viability of the cruise industry necessitate a precautionary approach, including the ability to manage outbreaks effectively and efficiently.

In conclusion, use of the ship itself as a quarantine facility during an onboard outbreak offers financial and operational advantages, and we have demonstrated its feasibility under certain circumstances. Onboard quarantine should be considered as an option in COVID-19 outbreak response plans for cruise ships.

Acknowledgments

The authors would like to acknowledge the significant contribution of those who made possible the implementation of the response plan for the COVID-19 outbreak onboard the MS Artania: from the Australian Medical Assistance Team, Abigail Trewin, Karen Were, Merrilyn Diveral, Trista Barbarino, Christopher Lack, Rhys Gloury, Richelle Stannard, Davianne Munro, Sarah Singh, Matthew Cowie, Philippa Rokkas, Kelly Sauvarin, Peter Petilla, Benjamin Schmidt, Alex Swann, Matthew McLaughlin, Jason Paul, Chris Bertram, Allan Anderson, Roslyn Smith, Patrick Armour, Conrad Ng, Toby Gwynne, Dee Gunn, Elizabeth Marrack, Paul Rogers, Rebecca Gillespie, and Edmond O'Loughlin; from the Western Australian Medical Assistance Team, Debbie Gibbins; Australian Government Deputy Secretary of Health Lisa Studdert; PathWest Laboratories, Head of Microbiology David Speers; Superintendent BSM Cruise Services Sinah Lucius; and from the MS Artania, Bernhard Schulte Cruise Services GmbH & Co. (Technical), Phoenix Reisen GmbH (Charterer), and Wolfgang Roeske, Aileen Fritz, and Miriam Turbanisch (Medical Team).

About the Author

Dr. Codreanu is the medical advisor to the WA State Health Incident Coordination Centre and the WA Medical Assistance Team Divisional Commander for complex medical deployments, and Clinical Team Lead for the Australian Medical Assistance Team, in addition to teaching Disaster Medicine in Italy and Belgium (Faculty of the European Master of Disaster Medicine) and Romania (University of Medicine Cluj). He is passionate about the disaster preparedness of vulnerable populations, especially adolescents.

References

1. Isakbaeva ET, Widdowson M-A, Beard RS, Bulens SN, Mullins J, Monroe SS, et al. Norovirus transmission on cruise ship. *Emerg Infect Dis*. 2005;11:154–8. <https://doi.org/10.3201/eid1101.040434>
2. Brotherton JML, Delpech VC, Gilbert GL, Hatzi S, Paraskevopoulos PD, McAnulty JM; Cruise Ship Outbreak Investigation Team. A large outbreak of influenza A and B on a cruise ship causing widespread morbidity. *Epidemiol Infect*. 2003;130:263–71. <https://doi.org/10.1017/S0950268802008166>
3. Mouchtouri VA, Rudge JW. Legionnaires' disease in hotels and passenger ships: a systematic review of evidence, sources, and contributing factors. *J Travel Med*. 2015; 22:325–37. <https://doi.org/10.1111/jtm.12225>
4. Minooee A, Rickman LS. Infectious diseases on cruise ships. *Clin Infect Dis*. 1999;29:737–43, quiz 744. <https://doi.org/10.1086/520426>
5. Rooney RM, Cramer EH, Mantha S, Nichols G, Bartram JK, Farber JM, et al. A review of outbreaks of foodborne disease associated with passenger ships: evidence for risk management. *Public Health Rep*. 2004;119:427–34. <https://doi.org/10.1016/j.phr.2004.05.007>
6. Lanini S, Capobianchi MR, Puro V, Filia A, Del Manso M, Karki T, et al. Central task force for measles outbreak. Measles outbreak on a cruise ship in the western Mediterranean, February 2014, preliminary report. *Euro Surveill*. 2014;19:10. <https://doi.org/10.2807/1560-7917.ES2014.19.10.20735>
7. World Health Organization. Considerations for quarantine of contacts of COVID-19 cases, 2020 [cited 2020 Mar 26]. [https://www.who.int/publications/i/item/considerations-for-quarantine-of-individuals-in-the-context-of-containment-for-coronavirus-disease-\(covid-19\)](https://www.who.int/publications/i/item/considerations-for-quarantine-of-individuals-in-the-context-of-containment-for-coronavirus-disease-(covid-19))
8. World Health Organization. Operational considerations for managing COVID-19 cases/outbreak on board ships. 2020 [cited 2020 May 1]. <https://www.who.int/publications-detail/operational-considerations-for-managing-covid-19-cases-outbreak-on-board-ships>
9. Sehdev PS. The origin of quarantine. *Clin Infect Dis*. 2002;35:1071–2. <https://doi.org/10.1086/344062>
10. Chimonas MA, Vaughan GH, Andre Z, Ames JT, Tarling GA, Beard S, et al. Passenger behaviors associated with norovirus infection on board a cruise ship – Alaska, May to June 2004. *J Travel Med*. 2008;15:177–83. <https://doi.org/10.1111/j.1708-8305.2008.00200.x>
11. Millman AJ, Kornlyo Duong K, Lafond K, Green NM, Lippold SA, Jhung MA. Influenza outbreaks among passengers and crew on two cruise ships: A recent account of preparedness and response to an ever-present challenge. *J Travel Med*. 2015;22:306–11. <https://doi.org/10.1111/jtm.12215>
12. Ward KA, Armstrong P, McAnulty JM, Iwasenko JM, Dwyer DE. Outbreaks of pandemic (H1N1) 2009 and seasonal influenza A (H3N2) on cruise ship. *Emerg Infect Dis*. 2010;16:1731–7. <https://doi.org/10.3201/eid1611.100477>
13. World Health Organization. WHO announces COVID-19 outbreak a pandemic. 2020 [cited 2020 Apr 12]. <https://www.euro.who.int/en/health-topics/health-emergencies/coronavirus-covid-19/news/news/2020/3/who-announces-covid-19-outbreak-a-pandemic>
14. Moriarty LF, Plucinski MM, Marston BJ, Kurbatova EV, Knust B, Murray EL, et al.; CDC Cruise Ship Response Team; California Department of Public Health COVID-19 Team; Solano County COVID-19 Team. Public health responses to

- COVID-19 outbreaks on cruise ships – worldwide, February–March 2020. *MMWR Morb Mortal Wkly Rep.* 2020;69:347–52. <https://doi.org/10.15585/mmwr.mm6912e3>
15. Mizumoto K, Chowell G. Transmission potential of the novel coronavirus (COVID-19) onboard the diamond Princess Cruises Ship, 2020. *Infect Dis Model.* 2020;5:264–70. <https://doi.org/10.1016/j.idm.2020.02.003>
 16. Rocklöv J, Sjödin H, Wilder-Smith A. COVID-19 outbreak on the Diamond Princess cruise ship: estimating the epidemic potential and effectiveness of public health countermeasures. *J Travel Med.* 2020;27:taaa030.
 17. Kakimoto K, Kamiya H, Yamagishi T, Matsui T, Suzuki M, Wakita T. Initial investigation of transmission of COVID-19 among crew members during quarantine of a cruise ship – Yokohama, Japan, February 2020. *MMWR Morb Mortal Wkly Rep.* 2020;69:312–3. <https://doi.org/10.15585/mmwr.mm6911e2>
 18. Dahl E. Coronavirus (Covid-19) outbreak on the cruise ship Diamond Princess. *Int Marit Health.* 2020;71:5–8. <https://doi.org/10.5603/MH.2020.0003>
 19. Japanese National Institute of Infectious Disease. Field briefing: Diamond Princess COVID-19 cases. 2020 Feb 20 [cited 2020 Mar 1]. <https://www.niid.go.jp/niid/en/2019-ncov-e/9407-covid-dp-fe-01.html>
 20. Centers for Disease Control and Prevention. Coronavirus disease 2019. 2020 [cited 2020 Mar 2]. <https://www.cdc.gov/coronavirus/2019-ncov/index.html>
 21. Communicable Diseases Network Australia. Coronavirus Disease 2019 (COVID-19): CDNA National Guidelines for Public Health Units [cited 2020 Mar 24]. <https://www1.health.gov.au/internet/main/publishing.nsf/Content/cdna-song-novel-coronavirus.htm>
 22. Australian Government Department of Health. Public Summary: Diversey Australia Pty Ltd – Oxivir FIVE16 – disinfectant, hospital grade. 2017 [cited 2020 Apr 24]. <http://www.diverseyvericlean.com/images/DiverseyHumming/TGA/PublicSummary/Oxivir-Five-16-JF-SD-3.78L---AUST-R-286618---Public-Summary.pdf>
 23. Australian Government Department of Health. Coronavirus disease (COVID-19): environmental cleaning and disinfection principles for COVID-19. 2020 [cited 2020 May 13]. <https://www.health.gov.au/sites/default/files/documents/2020/03/environmental-cleaning-and-disinfection-principles-for-covid-19.pdf>
 24. Hedley KWA. Premier blindsided by news sick passengers still on cruise ship refusing to leave Freo. *WA Today.* 2020 Apr 1 [cited 2020 Apr 23]. <https://www.watoday.com.au/national/western-australia/wa-premier-blindsided-by-news-sick-passengers-still-on-cruise-ship-refusing-to-leave-freo-20200401-p54g2k.html>
 25. Western Australia Government. Emergency management act 2005 (WA) section 67: MS Artania Directions. 2020 [cited 2020 Apr 23]. https://www.wa.gov.au/sites/default/files/2020-03/Ms%20Artania%20Directions_0.pdf
 26. Boyce JM. Modern technologies for improving cleaning and disinfection of environmental surfaces in hospitals. *Antimicrob Resist Infect Control.* 2016;5:10. <https://doi.org/10.1186/s13756-016-0111-x>
 27. Rutala WA, Weber DJ. Disinfectants used for environmental disinfection and new room decontamination technology. *Am J Infect Control.* 2013;41(Suppl):S36–41. <https://doi.org/10.1016/j.ajic.2012.11.006>
 28. Dancer SJ. Controlling hospital-acquired infection: focus on the role of the environment and new technologies for decontamination. *Clin Microbiol Rev.* 2014;27:665–90. <https://doi.org/10.1128/CMR.00020-14>
 29. van Doremalen N, Bushmaker T, Morris DH, Holbrook MG, Gamble A, Williamson BN, et al. Aerosol and surface stability of SARS-CoV-2 as compared with SARS-CoV-1. *N Engl J Med.* 2020;382:1564–7. <https://doi.org/10.1056/NEJMc2004973>
 30. Triandis CH. *Interpersonal behaviour.* Monterey (CA): Brooks/Cole Publishing Company; 1977.

Address for correspondence: Tudor A. Codreanu, State Health Incident Coordination Centre, Department of Health, 189 Royal St, 6000 Perth, Western Australia, Australia; email: Tudor.Codreanu@health.wa.gov.au

SARS-CoV-2 in Nursing Homes after 3 Months of Serial, Facilitywide Point Prevalence Testing, Connecticut, USA

Hanna Y. Ehrlich, Adora Harizaj, Lauren Campbell, McKenzie Colt, Karen Yuan, Therese Rabatsky-Ehr, Daniel M. Weinberger, Vivian Leung, Linda M. Niccolai, Sunil Parikh

Nursing homes house populations that are highly vulnerable to coronavirus disease. Point prevalence surveys (PPSs) provide information on the severe acute respiratory syndrome coronavirus 2 infection status of staff and residents in nursing homes and enable isolation of infectious persons to halt disease spread. We collected 16 weeks of public health surveillance data on a subset of nursing homes (34/212) in Connecticut, USA. We fit a Poisson regression model to evaluate the association between incidence and time since serial PPS onset, adjusting for decreasing community incidence and other factors. Nursing homes conducted a combined total of 205 PPSs in staff and 232 PPSs in residents. PPS was associated with 41%–80% reduction in incidence rate in nursing homes. Our findings provide support for the use of repeated PPSs in nursing home staff and residents, combined with strong infection prevention measures such as cohorting, in contributing to outbreak control.

Nursing home residents represent a population highly vulnerable to the spread of severe acute respiratory syndrome coronavirus 2 (SARS-CoV-2). In the midst of the coronavirus disease (COVID-19) pandemic, nursing homes account for a substantial proportion of total deaths attributed to the virus in the United States and globally (1–3). The high proportion of asymptomatic, presymptomatic, and atypical manifestations of COVID-19 in staff and elderly residents is a critical driver of widespread and rapid transmission of the virus (4–6). Facilitywide testing is a critical tool to identify such infections, particularly

in lieu of effective vaccines or treatments early in a novel viral outbreak (7–10). Point prevalence surveys (PPSs) enable testing of populations at a specific point with the goal of isolating both infectious and exposed persons from unexposed, uninfected persons to prevent ongoing transmission.

Nursing homes in the state of Connecticut experienced a high burden of COVID-19 during the first surge of the pandemic. The first COVID-19 case was reported in a nursing home in Connecticut on March 15, 2020. Over the next 2 months, nursing homes accounted for 61.6% deaths in the state (6). After an increase in testing resources and evidence of asymptomatic transmission, the Connecticut Department of Public Health (CT DPH) began PPS testing in early May, and PPS testing was formally recommended on May 11 and mandated weekly in staff effective June 14 (11,12). Facility staff were trained by public health practitioners to ensure proper separation (hereafter, cohorting) of infected, exposed, and uninfected unexposed persons after receiving PPS results and temporary exclusion of staff from the workplace (13,14). Because data were collected for public health surveillance, not research, institutional review board evaluation was not required.

We previously reported the results of the first round of PPS testing in a subset of Connecticut nursing homes, in which a high number and proportion of asymptomatic infections were detected (6). We also discussed the rapid turnaround time from conduct of PPS and institution of cohorting in those initial PPSs, factors that probably contributed to the positive effect of PPSs in reducing transmission. In this observational study, we followed the same nursing homes as they conducted serial PPS testing. We describe 4 weeks of incidence data before initial PPSs and 12 weeks of follow-up data in which facilities underwent 1–11

Author affiliations: Yale University, New Haven, Connecticut, USA (H.Y. Ehrlich, L. Campbell, M. Colt, K. Yuan, D.M. Weinberger, L.M. Niccolai, S. Parikh); Connecticut Department of Public Health, Hartford, Connecticut, USA (A. Harizaj, T. Rabatsky-Ehr, V. Leung)

DOI: <https://doi.org/10.3201/eid2705.204936>

additional PPSs. We also present the results of PPSs conducted in staff in the selected subset of nursing homes as well as from the first round of PPSs in nearly all ($n = 196/212$) nursing homes in the state.

Methods

Nursing Home Selection

Due to limitations in testing resources at the start of PPS rollout, CT DPH prioritized specific nursing homes to receive test kits based on the size of their outbreaks and potential immediate effect of control measures. Of 212 nursing homes in the state, 34 conducted the first round of PPS testing on or before May 20, 2020, and were selected for extended follow-up in this study; 1 of these homes was COVID-19-naïve and excluded from our previous study (6). The homes selected for inclusion in this study were of average size and quality of nursing homes in the state, with an average of 135 licensed beds and quality rating of 3.58/5 stars (6). By June 25, a total of 196 (92.5%) of 212 nursing homes throughout Connecticut had conducted ≥ 1 round of resident PPS testing and were included for reporting of initial results.

PPS Testing, Cohorting, and Simultaneous Interventions

PPS involved molecular SARS-CoV-2 testing by nasopharyngeal swabs of all residents or staff in a facility within a short time period, in general 1 day (6). The state of Connecticut mandated weekly PPS testing in staff to begin in the latter half of June. In mid-May, CT DPH recommended but did not mandate weekly PPS testing of residents after identification of a new nursing home-onset case until no new cases were detected in residents or staff for 14 days (11,12). These recommendations remained effective through the duration of the study period. Nursing homes were paired with affiliate hospitals or laboratories to help conduct PPS testing and ensure fast turnaround of results.

A primary goal of PPSs was to ensure rapid and comprehensive isolation and cohorting of infected persons and to enact other infection prevention and control (IPC) measures, such as contact tracing to identify exposures and temporary exclusion of infected staff from the workplace. We did not collect data on adherence to these measures in nursing homes.

COVID-19 cases were also detected between PPSs, primarily through selective screening of residents leaving or entering the facility, visiting health-care settings, or experiencing relevant symptoms, and also through limited contact tracing. Many other IPC policies for nursing homes were enacted during the study period federally and in the state of Connecticut,

which can be found in Appendix C of the CT DPH contracted report by Mathematica, Inc. (15).

Data Extraction

Nursing home staff answered daily questionnaires in a web-based COVID-19 database maintained by CT DPH, through which we extracted data on daily case counts, deaths, and censuses. PPS results were confirmed with study investigators by telephone: nursing directors reported the results of tests given to residents or staff who did not have a prior diagnosis of COVID-19. Case dates correspond to the date of specimen collection. We were unable to follow up on how each lab and nursing home responded to inconclusive results: whether they repeated the test, acquired a new sample, or treated the result as positive. New cases excluded residents transferred in with a known SARS-CoV-2 infection. Case counts by town were obtained from the Connecticut COVID-19 portal (16).

Incidence Rates Relative to First PPS

COVID-19 incidence rates were calculated for 3 time periods respective to each nursing home: 4 weeks before first PPS, day of first PPS ("day 0"), and 12 weeks after the first PPS. For each respective time period X and nursing home i , we used the following equation:

$$IR_{i,X} = \left(\frac{\sum_{t_1 \text{ in } X}^{t_n \text{ in } X} \text{new cases}}{\sum_{t_1 \text{ in } X}^{t_n \text{ in } X} \text{person days at risk}} \right) \times 1,000$$

where person-days at risk on day t was calculated as the resident census reported on day t , subtracting the number of previous COVID-19 case-patients who had not died from complications of the disease by day t . The total number of cases and person-days at risk in nursing home i was summed for all days within each time period X . Because we could not follow individual persons over time, we used census data to account for the dynamic nature of nursing home populations. We compared the incidence rates in PPS in individual nursing homes in the 4 weeks prior and 12 weeks following first using the 2-sample Z-test for equality of proportions with Yates' continuity correction.

Poisson Regression Model

We investigated the association between PPS and the trajectory of nursing home outbreaks while accounting for concomitant changes in community incidence and intrinsic variability between nursing homes. The number of new cases y in nursing home i on calendar day t offset by person-days at risk on day t was modeled as a Poisson regression:

$$\begin{aligned}
 Y_{it} &\sim \text{Poisson}(\lambda_{it}) \\
 \log\left(\frac{\lambda_{it}}{\text{person_days}_{it}}\right) &= \alpha_0 + \alpha_i + \beta_1 \log(\text{sum}_{\text{community}_{IR}_t}) \\
 &+ \beta_2 \text{day_of_first_PPS}_i \\
 &+ \sum_{p=2}^4 \gamma_p 1\{\text{time}_{\text{interval since first PPS}_i} = c_p\} \\
 &+ \sum_{d=2}^7 \delta_d 1\{\text{day_of_week}_t = d\}
 \end{aligned}$$

where *person_days_{it}* is as described previously; *sum_{community_IR_{it}}* is the incidence rate per 100,000 population in the town in which nursing home *i* is located over the past 14 days relative to day *t* (17); *day_of_first_PPS_i* is the date of the first PPS, included as a dummy variable to account for the substantial change in screening practices; and *time_interval_since_first_PPS_i* is treated as a categorical variable divided into 1–15, 16–30, 31–60, and 60–90 days. Categorical variables for day of the week and nursing home ID (*a_i*) were also included). The model did not exhibit evidence of overdispersion (deviance/degrees of freedom = 0.8), indicating that the Poisson model was appropriate. We conducted a sensitivity analysis to determine the impact of different lags of community incidence (0, 3, 7, 14, and 28 days) on model results; the sum of incidence over the previous 14 days was found to minimize the Akaike information criterion. Risk ratios were calculated by exponentiation of the relevant regression coefficients. Analyses and figures were executed in R version 3.5.1 (<https://www.r-project.org>).

Results

PPS Implementation

In the 12 weeks of follow-up after initial PPSs, an average of 6.0 (range 1–10) follow-up PPSs in residents and 6.2 (range 2–10) total PPSs in staff were administered

per nursing home, for a total of 198 follow-up surveys in residents and 205 surveys in staff in all 34 nursing homes (Table 1). The average time between the first and second round of resident PPS testing was 30 days; average time between all subsequent PPSs was 9 days. Periods between staff PPSs were shorter than between resident PPSs (Appendix Figure 1, <https://wwwnc.cdc.gov/EID/article/27/5/20-4936-App1.pdf>). The period between resident PPSs decreased over time, in part, because of additional state requirements and recommendations to conduct weekly resident testing in mid-July. Most (31/34) nursing homes in this study conducted ≥1 PPS beyond the recommended threshold of 14 days after a positive case was detected. The total number of PPSs in residents and staff in each nursing home was not statistically associated with the nursing home quality rating.

Resident Cases Detected in Follow-Up Period

Before the first PPS, nursing homes had experienced an average of 36 COVID-19 cases (27.7% infected; range 0–81 cases, 0%–86.1% infected). A total of 601 cases were detected in these facilities during the first PPS, as previously described (6). Approximately 1,775 (55.8%) of all residents in the study were assumed to be susceptible to infection after the first round of testing was complete.

After the initial round of PPS, a total of 44 resident cases were identified in all subsequent rounds of PPS testing, of which 9 (20.4%) were symptomatic at the time of testing (Table 1). The probability of identifying additional cases through PPSs decreased significantly over subsequent PPSs: the second PPS identified 20 cases (n = 34 nursing homes), and subsequent PPSs identified an additional 8 (n = 33), 6 (n = 31), 4 (n = 28), 3 (n = 25), 2 (n = 22), 0 (n = 18), 0 (n = 9), 0 (n = 4), and 0 (n = 1) cases in residents (Figure 1).

In between PPSs, 93 additional resident cases were also detected, of which 70 (75.3%) were symptomatic at the time of testing. Most (85, 90.3%) cases were identified during the longer period between the first and second round of PPS testing. More than half (60.2%) of cases were detected within 1 incubation

Table 1. Summary of point prevalence survey results of severe acute respiratory syndrome coronavirus 2 infection in 34 nursing homes, Connecticut, USA*

Category	Residents					Staff	
	No. follow-up PPS	Positive test results from PPSs†	No. symptomatic at PPS testing	No. cases detected between PPSs†	No. symptomatic at time of non-PPS testing	No. PPS	Positive test results from staff PPSs
Total	198	44	11	93	70	205	87
Average (SD)	6.0 (2.3)	1.3 (1.5)	0.6 (0.9)	2.7 (7.6)	4.1 (9.1)	6.2 (2.0)	2.6 (4.9)

*Results of the first PPS in residents in (6); results displayed here are those of subsequent surveys only. In brief, 601 cases were detected in the first PPS (average 16.8, SD 13.5). One additional facility, coronavirus disease naive at the time of the initial PPS and therefore not included in the original study, detected 0 cases in its first PPS. PPS, point prevalence survey.

†Excludes residents transferred into facilities with known coronavirus infection.

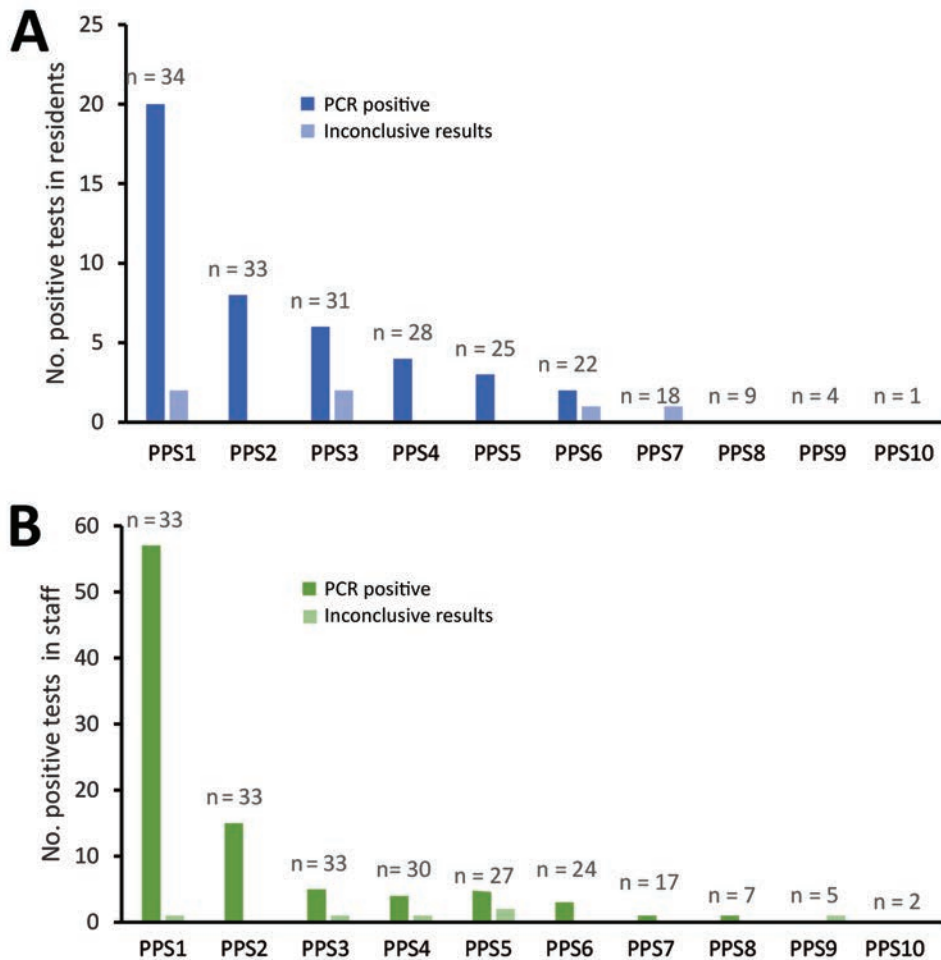


Figure 1. Coronavirus disease cases detected in consecutive PPSs in residents (A) and staff (B) in nursing homes, Connecticut, USA. The number of participating nursing homes for each survey is listed above each bar. One facility was excluded from staff testing data due to lack of verifiable testing results during PPS surveys. The results of the first PPS in residents, in which 601 cases were detected, were previously reported in (6). The probability of detecting a positive case decreased significantly ($p < 0.05$) through PPS7 for residents and PPS8 for staff, compared with the first PPS, using logistic regression for comparisons. PPS, point prevalence survey.

period following the first PPS, when exposure in those persons had likely already occurred; that exposure rendered cohorting measures less effective. Further, there was a positive but nonsignificant correlation ($p = 0.09$) between the number of days between PPS and the number of cases identified in a nursing home (Appendix Figure 2). Two nursing homes contained most of these cases, reporting 38 and 20 cases in the 44 days between their first and second PPS (Figure 2; Appendix Figures 2, 3).

Temporal Patterns of Resident Infections

Nursing homes underwent initial PPS at different stages of outbreak severity (Figure 2). After initial PPS, the proportion of residents infected in each nursing home plateaued for most facilities. In 41.2% of nursing homes, fewer than half of all residents were infected with SARS-CoV-2 by the end of the study period.

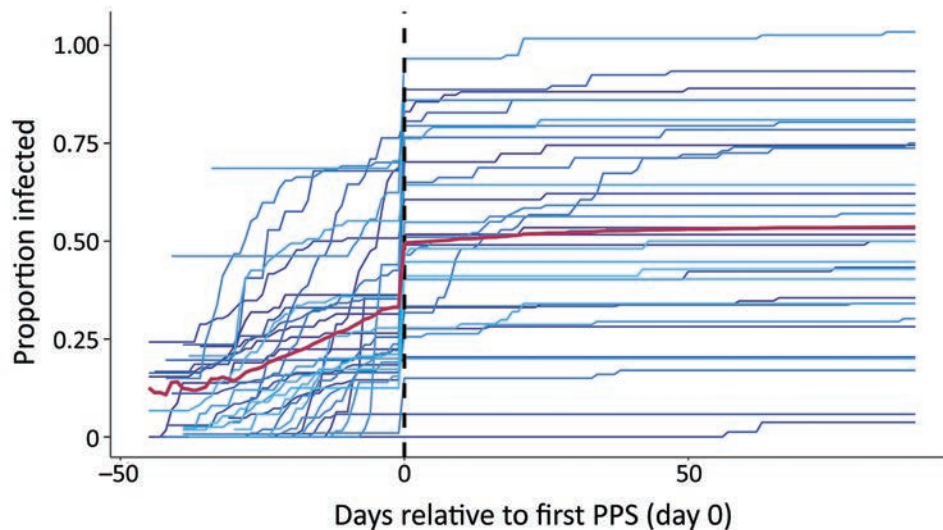
The median incidence rates in nursing homes were 9.3 (95% CI 0.2–49.2) cases/1,000 at-risk person-days before the first PPS; 267.8 (95% CI 0–861.5) cases/1,000 person-days on the day of the first PPS, and

0.54 (95% CI 0–18.4) cases/1,000 person-days in the period after the first PPS. Incidence rates decreased ($p < 0.05$) in 85% (29/34) of facilities following the implementation of PPSs (Figure 2). Of the 4 nursing homes that experienced no significant change, 2 had <10 residents remaining susceptible to SARS-CoV-2 and 1 had not experienced any cases before the first PPS. Meanwhile, 2 nursing homes experienced large outbreaks of >10 cases after the first PPS, 1 of which experienced an increase in incidence rate of 8.3 cases/1,000 person-days (Figure 3; Appendix Figure 3).

Accounting for Concurrent Changes in Community Incidence

The population of the towns and cities in which the nursing homes were located experienced a contemporaneous decrease in community incidence during the study period (Figure 4). Community incidence over the previous 2 weeks was associated with proportional changes in incidence in nursing homes ($\beta_1 = 0.98$, 95% CI 0.84–1.11). After adjusting for community incidence and the change in screening practices,

Figure 2. Cumulative proportion of severe acute respiratory syndrome coronavirus 2 (SARS-CoV-2) infections in individual nursing homes over a 16-week study period relative to the first PPS, Connecticut, USA. Each colored line represents a single nursing home in the ≈4 weeks before first PPS and 12 weeks following first PPS. Data were centered for all nursing homes by the date of receipt of results for the first PPS, signified by the dashed vertical line on day 0. Red line indicates average proportion infected of the total study population on each day. The number of residents infected in each nursing home is based on cumulative case counts out



of the number ever susceptible to SARS-CoV-2 in the nursing home, or the maximum census value in the study period, to account for resident deaths and transfers since the start of reporting. PPS, point prevalence survey.

the implementation of serial PPSs was associated with a significant decrease in nursing home incidence rates of 77% (95% CI 71%–83%) in the first 15 days after the first PPS, 49% (95% CI 31%–63%) from days 16–30, 41% (95% CI 12%–60%) from days 31–60, and 80% (95% CI 64%–89%) reduction from days 61–90, compared with the pre-PPS period.

Staff Cases Detected in Follow-Up Period

Nursing homes identified 87 staff cases (6 inconclusive) or an average of 2.6 cases (SD 4.9) per facility in the follow-up period (Table 1). The first PPS in 34 nursing homes identified 57 total staff cases, and subsequent PPSs ($n = 33$ nursing homes) identified an additional 15 ($n = 34$ nursing home's staff tested), 5 ($n = 33$), 4 ($n = 30$), 5 ($n = 27$), 3 ($n = 24$), 1 ($n = 17$), 1 ($n = 7$), 0 ($n = 5$), and 0 ($n = 2$) staff cases (Figure). Symptomatic status and cases counts identified outside of weekly PPSs were not ascertained. One nursing home was removed from staff testing results beyond the first PPS due to lack of verifiable data.

Statewide Initial PPS Testing

In the state of Connecticut, as of June 25, 2020, a total of 196 nursing homes had completed 1 round of PPS testing. In these initial single round of surveys, 12,336 residents were tested. A total of 1,733 tests (14.0%) were SARS-CoV-2 positive and an additional 70 tests were inconclusive. Of those with positive results, 1,537 (88.7%) were reported by facilities as having been asymptomatic at the time of testing. Follow-up

for symptomatic status beyond the day of testing was not conducted.

Discussion

We compiled a large dataset covering 16 weeks of public health surveillance data in nursing homes, documenting COVID-19 outbreaks in the 4 weeks before and 12 weeks after the start of repeated facility-wide PPSs. Several previous studies have also documented the successful implementation of PPS testing in multiple congregate living facilities in the context of COVID-19 outbreak control (4,7,8,18–26). We describe a study of 34 facilities conducting 437 surveys in residents and staff and 35,133 nasopharyngeal swab tests, or an average of 13 PPSs per nursing home in residents and staff combined, in a 12-week period. Selected nursing homes experienced a range of outbreak severities at the time of initial PPSs, yet all nursing homes experienced 1 or 0 cases in the final 4 weeks of follow-up. In addition, 29/34 (85%) nursing homes exhibited significant ($p < 0.05$) decreases in incidence rates of SARS-CoV-2 infection in the 12-week follow-up period compared with the 4-week period before any PPS.

The initial round of PPS testing likely captured asymptomatic cases and residents with protracted viral shedding that had been missed in the pre-PPS period (and who may have been symptomatic at that time), as well as presymptomatic cases that would have been captured in the post-PPS period in lieu of PPSs (6,27,28). To account for the change in screening practices, we compared trends in incidence rates

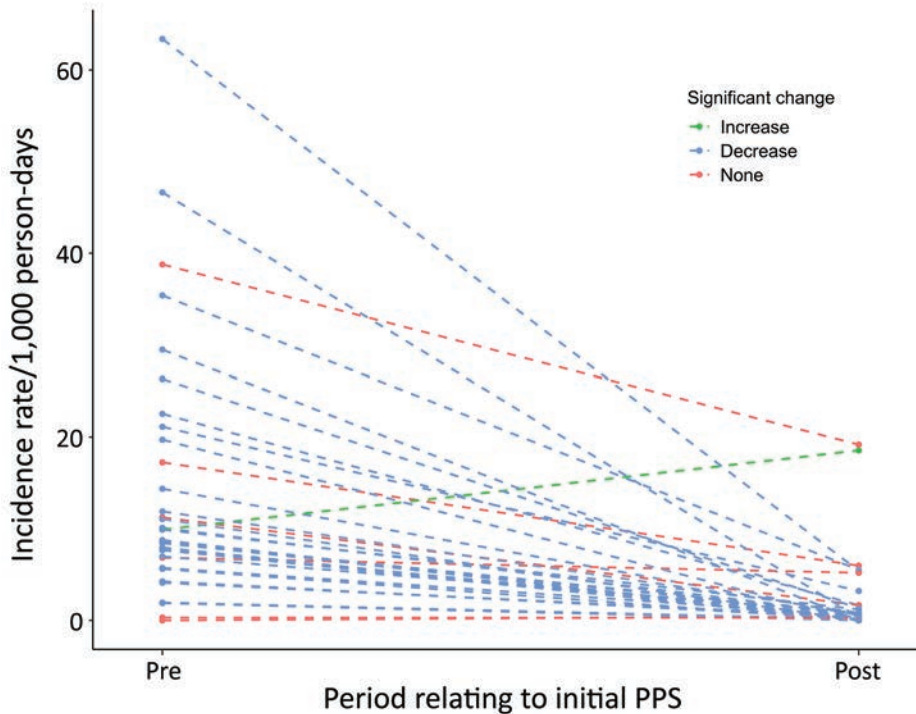


Figure 3. Paired coronavirus disease incidence rate estimates relative to first PPS, Connecticut, USA. Dashed lines represent single nursing homes included in the study. Points represent the incidence in the 4 weeks before the first PPS and 12 weeks following the first PPS, during which additional PPSs were also conducted. Blue indicates significant decreases in incidence for each nursing home over the 2 time periods ($\alpha = 0.05$); green indicates significant increases; red indicates nonsignificant changes in incidence. PPS, point prevalence survey.

before and after initial PPSs. The change in incidence rates of COVID-19 cases in nursing homes over the study period, especially in the period following the first round of PPS, coincided with a decrease in community cases. However, we found that, even after adjusting for community incidence and the change in screening practice, the decrease in incidence rates in nursing homes was significantly associated with the onset of PPSs ($p < 0.05$ for all subsequent time divisions).

Most COVID-19 cases detected in the 12-week follow-up period were identified in the extended period, on average 30 days, between the first and second PPS. These cases were identified primarily through symptom screening; limited contact

tracing; and other types of selective testing, including at the time of resident hospitalization or hemodialysis. We postulate that more frequent PPSs, especially between the first and second rounds of testing, may have improved outbreak control by enabling earlier cohorting and that the extended time period between PPS may have decreased the efficacy of this intervention overall. Our results also suggest that although introductions of the virus from staff, visitors, and patients undergoing outside procedures pose a substantial risk of seeding new outbreaks, nursing homes may be able to alter the trajectory of their outbreaks by rigorous case surveillance once an outbreak occurs, despite ongoing community transmission.

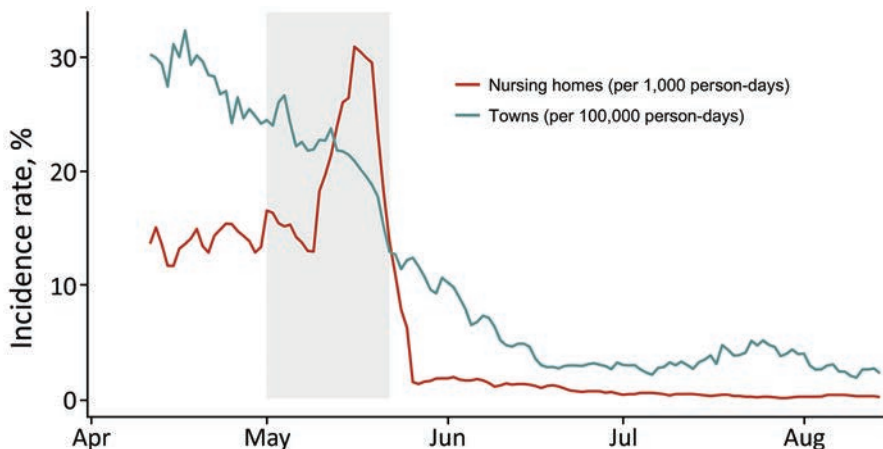


Figure 4. Coronavirus disease incidence rates in nursing homes (cases/1,000 person-days, red) and in towns and cities (cases/100,000 person-days, blue), Connecticut, USA. Incidence rates are aggregated for the 34 nursing homes in this study and 26 towns and cities in which the nursing homes are located; incidence is presented as rolling weekly averages to account for differences in day-of-week reporting. The shaded rectangle shows the time period in which all 34 nursing homes conducted initial PPSs.

Our study's limitations include that we were not able to incorporate a control group in this analysis because this work was done in the context of outbreak control, in which nearly all nursing homes in the state received PPSs over the follow-up period. Furthermore, we were not able to follow individual participants over time due to the dynamic nature of nursing home populations and limitations in public health surveillance capacity. Similarly, we were unable to collect data to track the implementation of cohorting and other behavioral and physical interventions after receiving test results from PPSs. Nonetheless, CT DPH staff called all facilities before the first PPS to assess knowledge of cohorting and train staff on appropriate cohorting; they also followed up on homes with continued transmission after the first PPS to evaluate adherence. Finally, we could not account for all concurrent interventions, including changes in visitation policies, staff cohorting practices, and PPE abundance, limiting the interpretability of the usefulness of repeated PPSs (15).

We described the successful implementation of hundreds of repeated facilitywide PPSs in nursing homes. Although our findings cannot inform policies of asymptomatic testing of staff and residents as a preventive strategy, they suggest that PPSs is one of several effective tools in outbreak management, particularly in the context of low COVID-19 incidence in the general population. In addition to testing, outbreak control relied on use of PPE and other protective behaviors such as social distancing and limitations to visitation, successful cohorting of infected and exposed residents, exclusion of infected staff from the workplace, environmental modifications, and sustained IPC training (18). Our work may motivate states to reserve financial resources for sustained, serial PPS testing in the context of outbreak control and other forms of IPC planning in long-term care. We urge policymakers to continue serial testing in congregate living facilities during the period of vaccine rollout because acquisition of immunity will take time and coverage rates may vary in facilities (9,29,30). Optimal serial testing strategies in the post-vaccine rollout period will require additional study.

Acknowledgments

We thank Barbara Cass, Anu Paranandi, Erin Grogan, Naissa Piverger, Meghan Maloney, Ellen Neuhaus, Surjit Sethuraman, Kim Hriceniak, Kristin Soto, Terry Rabatsky-Ehr, and others at the CT DPH for building and maintaining a nursing home surveillance system for COVID-19. We also thank Kevin O'Laughlin for coordinating initial data collection, Ben Gagne and members of the Connecticut

National Guard for assisting in the deployment of PPS test kits, and Forrest Crawford for helping with statistical models. No individuals listed received compensation for their contributions to this work.

S.P. and V.L. had full access to all the data in the study and take responsibility for the integrity of the data and the accuracy of the data analysis. The data were collected in the setting of a public health response, and there was no specific funder involved in the design and conduct of the study; collection, management, analysis, and interpretation of the data; preparation, review, or approval of the manuscript; and decision to submit the manuscript for publication.

About the Author

Hanna Y. Ehrlich is a PhD candidate at the Yale School of Public Health. Primary research interests include public health surveillance, public health policy, and the epidemiology of vectorborne and emerging diseases.

References

1. Ouslander JG, Grabowski DC. COVID-19 in nursing homes: calming the perfect storm. *J Am Geriatr Soc.* 2020;68:2153–62. <https://doi.org/10.1111/jgs.16784>
2. Barnett ML, Grabowski DC. Nursing homes are ground zero for COVID-19 pandemic. *JAMA Health Forum.* 2020;1:e200369. <https://doi.org/10.1001/jamahealthforum.2020.0369>
3. Danis K, Fonteneau L, Georges S, Daniau C, Bernard-Stoecklin S, Domegan L, et al; ECDC Public Health Emergency Team. High impact of COVID-19 in long-term care facilities, suggestion for monitoring in the EU/EEA, May 2020. *Euro Surveill.* 2020;25:2000956.
4. Louie JK, Scott HM, DuBois A, Sturtz N, Lu W, Stoltey J, et al; San Francisco Department of Public Health COVID-19 Skilled Nursing Facility Outbreak Response Team. Lessons from mass-testing for COVID-19 in long term-care facilities for the elderly in San Francisco. *Clin Infect Dis.* 2020;ciaa1020. <https://doi.org/10.1093/cid/ciaa1020>
5. Marossy A, Rakowicz S, Bhan A, Noon S, Rees A, Virk M, et al. A study of universal severe acute respiratory syndrome coronavirus 2 RNA testing of residents and staff in a large group of care homes in South London. *J Infect Dis.* 2020;223:381–8. <https://doi.org/10.1093/infdis/jiaa565>
6. Parikh S, O'Laughlin K, Ehrlich HY, Campbell L, Harizaj A, Durante A, et al. Point prevalence testing of residents for SARS-CoV-2 in a subset of Connecticut nursing homes. *JAMA.* 2020;324:1101–3. <https://doi.org/10.1001/jama.2020.14984>
7. Dora AV, Winnett A, Jatt LP, Davar K, Watanabe M, Sohn L, et al. Universal and serial laboratory testing for SARS-CoV-2 at a long-term care skilled nursing facility for veterans – Los Angeles, California, 2020. *MMWR Morb Mortal Wkly Rep.* 2020;69:651–5. <https://doi.org/10.15585/mmwr.mm6921e1>
8. Hatfield KM, Reddy SC, Forsberg K, Korhonen L, Garner K, Gulley T, et al. Facility-wide testing for SARS-CoV-2 in nursing homes – seven US jurisdictions, March–June 2020. *MMWR Morb Mortal Wkly Rep.* 2020;69:1095–9. <https://doi.org/10.15585/mmwr.mm6932e5>

9. Njuguna H, Wallace M, Simonson S, Tobolowsky FA, James AE, Bordelon K, et al. Serial laboratory testing for SARS-CoV-2 infection among incarcerated and detained persons in a correctional and detention facility – Louisiana, April–May 2020. *MMWR Morb Mortal Wkly Rep.* 2020;69:836–40. <https://doi.org/10.15585/mmwr.mm6926e2>
10. Birgand G, Blanckaert K, Deschanvres C, Vaudron A, Loury P, King L. Testing strategies for the control of COVID-19 in nursing homes: universal or targeted screening? *J Infect.* 2020;82:159–98. <https://doi.org/10.1016/j.jinf.2020.08.002>
11. Lamont N. Executive order No. 7UU:protection of public health and safety during COVID-19 pandemic and response – staff testing for nursing homes and assisted living; definition of suitable work. June 1, 2020 [cited 2020 Aug 11]. <https://portal.ct.gov/-/media/Office-of-the-Governor/Executive-Orders/Lamont-Executive-Orders/Executive-Order-No-7UU.pdf>
12. Coleman-Mitchell RD. COVID-19 point prevalence survey testing and cohorting in nursing homes [interim guidance – May 11, 2020]. State of Connecticut Department of Public Health. May 11, 2020 [cited 2020 Aug 11]. <http://www.mutualaidplan.org/Common/Document.aspx?DDID=17279&klv=1&key=uMyL4RqHDPX56fClceBfiW4N5MY%3D>
13. Centers for Disease Control and Prevention. Testing guidelines for nursing homes: interim SARS-CoV-2 testing guidelines for nursing home residents and healthcare personnel. Oct. 16, 2020 [cited 2020 Oct 20]. <https://www.cdc.gov/coronavirus/2019-ncov/hcp/nursing-homes-testing.html>
14. Centers for Disease Control and Prevention. Return to work criteria for healthcare personnel with SARS-CoV-2 infection (interim guidance). August 10, 2020 [cited 2020 Aug 11]. <https://www.cdc.gov/coronavirus/2019-ncov/hcp/return-to-work.html>
15. Mathematica Policy Research. A study of the COVID-19 outbreak and response in Connecticut long-term care facilities: final report. September 30, 2020 [cited 2020 Oct 20]. <https://portal.ct.gov/Coronavirus/Long-Term-Care-Facility-review>
16. State of Connecticut. Connecticut COVID-19 data tracker. 2020 [cited 2020 Oct 20]. <https://portal.ct.gov/coronavirus/covid-19-data-tracker>
17. Connecticut Department of Public Health Annual town and county population for Connecticut. 2020 [cited 2020 Oct 20]. <https://portal.ct.gov/DPH/Health-Information-Systems-Reporting/Population/Annual-Town-and-County-Population-for-Connecticut>
18. Eckardt P, Guran R, Hennemyre J, Arikupurathu R, Poveda J, Miller N, et al. Hospital affiliated long-term care facility COVID-19 containment strategy by using prevalence testing and infection control best practices. *Am J Infect Control.* 2020;48:1552–55. <https://doi.org/10.1016/j.ajic.2020.06.215>
19. McBee SM, Thomasson ED, Scott MA, Reed CL, Epstein L, Atkins A, et al. Notes from the field: universal statewide laboratory testing for SARS-CoV-2 in nursing homes – West Virginia, April 21–May 8, 2020. *MMWR Morb Mortal Wkly Rep.* 2020;69:1177–9. <https://doi.org/10.15585/mmwr.mm6934a4>
20. Bigelow BF, Tang O, Barshick B, Peters M, Sisson SD, Peairs K, et al. Outcomes of universal COVID-19 testing following detection of incident cases in 11 long-term care facilities. *JAMA Intern Med.* 2021;181:127–9. <https://doi.org/10.1001/jamainternmed.2020.3738>
21. Escobar DJ, Lanzi M, Saberi P, Love R, Linkin DR, Kelly JJ, et al. Mitigation of a coronavirus disease 2019 outbreak in a nursing home through serial testing of residents and staff. *Clin Infect Dis.* 2020 Jul 20 [Epub ahead of print]. <https://doi.org/10.1093/cid/ciaa1021>
22. Taylor J, Carter RJ, Lehnertz N, Kazazian L, Sullivan M, Wang X, et al.; Minnesota Long-Term Care COVID-19 Response Group. Serial testing for SARS-CoV-2 and virus whole genome sequencing inform infection risk at two skilled nursing facilities with COVID-19 outbreaks – Minnesota, April–June 2020. *MMWR Morb Mortal Wkly Rep.* 2020;69:1288–95. <https://doi.org/10.15585/mmwr.mm6937a3>
23. Telford CT, Onwubiko U, Holland DP, Turner K, Prieto J, Smith S, et al. Preventing COVID-19 outbreaks in long-term care facilities through preemptive testing of residents and staff members – Fulton County, Georgia, March–May 2020. *MMWR Morb Mortal Wkly Rep.* 2020;69:1296–9. <https://doi.org/10.15585/mmwr.mm6937a4>
24. Sanchez GV, Biedron C, Fink LR, Hatfield KM, Polistico JMF, Meyer MP, et al. Initial and repeated point prevalence surveys to inform SARS-CoV-2 infection prevention in 26 skilled nursing facilities – Detroit, Michigan, March–May 2020. *MMWR Morb Mortal Wkly Rep.* 2020;69:882–6. <https://doi.org/10.15585/mmwr.mm6927e1>
25. Montoya A, Jenq G, Mills JP, Beal J, Divinye Chun E, Newton D, et al. Partnering with local hospitals and public health to manage COVID-19 outbreaks in nursing homes. *J Am Geriatr Soc.* 2020;69:30–36. <https://doi.org/10.1111/jgs.16869>
26. Borrás-Bermejo B, Martínez-Gómez X, San Miguel MG, Esparalba J, Antón A, Martín E, et al. Asymptomatic SARS-CoV-2 infection in nursing homes, Barcelona, Spain, April 2020. *Emerg Infect Dis.* 2020;26:2281–3. <https://doi.org/10.3201/eid2609.202603>
27. He X, Lau EHY, Wu P, Deng X, Wang J, Hao X, et al. Temporal dynamics in viral shedding and transmissibility of COVID-19. *Nature Medicine.* 2020;26:672–675.
28. Cevik M, Tate M, Lloyd O, Maraolo AE, Schafers J, Ho A. SARS-CoV-2, SARS-CoV, and MERS-CoV viral load dynamics, duration of viral shedding, and infectiousness: a systematic review and meta-analysis. *Lancet Microbe.* 2021;2:E13–3E22. [https://doi.org/10.1016/S2666-5247\(20\)30172-5](https://doi.org/10.1016/S2666-5247(20)30172-5)
29. Tavoschi L, Vroling H, Madeddu G, Babudieri S, Monarca R, Vonk Noordegraaf-Schouten M, et al. Active case finding for communicable diseases in prison settings: increasing testing coverage and uptake among the prison population in the European Union/European Economic Area. *Epidemiol Rev.* 2018;40:105–20. <https://doi.org/10.1093/epirev/mxy001>
30. Paltiel AD, Schwartz JL, Zheng A, Walensky RP. Clinical outcomes of a COVID-19 vaccine: implementation over efficacy. *Health Aff (Millwood).* 2021;40:42–52. <https://doi.org/10.1377/hlthaff.2020.02054>

Address for correspondence: Sunil Parikh, Department of Epidemiology of Microbial Diseases, Yale School of Public Health, 60 College St, New Haven, CT 06510, USA; email: sunil.parikh@yale.edu

Case Series of Laboratory-Associated Zika Virus Disease, United States, 2016–2019

Susan L. Hills, Andrea Morrison, Shawna Stuck, Kayleigh Sandhu, Krystal L. Mason, Danielle Stanek, Julie Gabel, Matthew A. Osborne, Betsy A. Schroeder, Edhelene Rico, Cherie L. Drenzek, Glen R. Gallagher, Jennifer Fiddner, Lea A. Heberlein-Larson, Catherine M. Brown, Marc Fischer

Zika virus diagnostic testing and laboratory research increased considerably when Zika virus began spreading through the Americas in 2015, increasing the risk for potential Zika virus exposure of laboratory workers and biomedical researchers. We report 4 cases of laboratory-associated Zika virus disease in the United States during 2016–2019. Of these, 2 were associated with needlestick injuries; for the other 2 cases, the route of transmission was undetermined. In laboratories in which work with Zika virus is performed, good laboratory biosafety practices must be implemented and practiced to reduce the risk for infection among laboratory personnel.

Zika virus is a flavivirus that was first isolated in 1947 from a rhesus macaque in the Zika Forest in Uganda. Zika virus is primarily transmitted to humans by infected mosquitoes, but other confirmed transmission modes include intrauterine, sexual, and intrapartum transmission, and probable modes include transmission through blood transfusion and breastfeeding (1). Laboratory-associated infection also has been reported in a small number of cases; one of the earliest reports of human Zika virus infection

was possibly laboratory-acquired (2). A researcher was working in a Uganda laboratory in 1963 with Zika virus strains isolated from mosquitoes. After he experienced fever and rash, laboratory testing indicated Zika virus infection. However, no apparent breakdown in biosafety procedures was identified, and mosquito-borne transmission could not be excluded. In 1972, Zika virus infection in another laboratory worker occurred, this time in the absence of a potential mosquito-borne route of transmission (3). The person was symptomatic, and infection was confirmed by virus isolation. He worked in an arboviral laboratory but no exposure that might have led to infection was reported. A 1980 report by the American Committee on Arthropod-borne Viruses, which documented results of global laboratory surveys conducted in 1976 and 1978, noted an additional 3 Zika virus disease cases in laboratory workers. The suspected sources of these infections were through the aerosol route or unknown, and further details were not provided (4). Finally, a laboratory-acquired Zika virus infection occurred in 2017 in Brazil after an infected mouse bit a researcher's finger (5).

Zika virus diagnostic testing and laboratory research increased considerably beginning in 2015 when Zika virus began spreading through the Americas, increasing the risk for potential Zika virus exposure for laboratory workers and researchers. We report 4 cases of laboratory-associated Zika virus disease in the United States during 2016–2019.

Case Reports

Exposure to Zika Virus through Needlestick Injury

Case 1

In May 2016, a female researcher who worked in a Biosafety Level (BSL) 3 microbiology laboratory sustained

Author affiliations: Centers for Disease Control and Prevention, Fort Collins, Colorado, USA (S.L. Hills, M. Fischer); Florida Department of Health, Tallahassee, Florida, USA (A. Morrison, D. Stanek); Georgia Department of Public Health, Atlanta, Georgia, USA (S. Stuck, J. Gabel, C.L. Drenzek); Massachusetts Department of Public Health, Jamaica Plain, Massachusetts, USA (K. Sandhu, M.A. Osborne, G.R. Gallagher, C.M. Brown); Pennsylvania Department of Health, Harrisburg, Pennsylvania, USA (K.L. Mason, B.A. Schroeder); Florida Department of Health in Miami-Dade County, Miami, Florida, USA (E. Rico); Allegheny County Health Department, Pittsburgh, Pennsylvania, USA (J. Fiddner); Florida Department of Health Bureau of Public Health Laboratories, Tampa, Florida, USA (L.A. Heberlein-Larson)

DOI: <https://doi.org/10.3201/eid2705.203602>

a needlestick injury with a bifurcated needle; information on whether the skin was punctured was not available. The incident occurred during in vitro inoculation of human skin cells with wild-type Zika virus for vaccine research purposes. She was wearing 2 pairs of nitrile gloves and working in a biosafety cabinet. She immediately used a surgical sponge and chlorohexidine to scrub the wound for 15 minutes, then washed her hands with soap and water. After 9 days, she experienced a low-grade fever, generalized maculopapular rash, headache, myalgia, and fatigue; mild unilateral conjunctivitis occurred the next day. She did not live in an area with local Zika virus transmission, and in the month before illness onset she had no other risk factors for acquisition of Zika virus infection (i.e., no history of travel, no sexual contact with a traveler, and no history of blood transfusion or organ transplantation). She reported full resolution of her symptoms within 5 days. Zika virus infection was confirmed through the detection of Zika virus RNA in serum and urine and Zika virus IgM and neutralizing antibodies in serum (Table).

Case 2

In July 2018, a female researcher received an accidental needlestick injury while recapping a needle after inoculating a mouse with the Uganda Zika virus strain

MR766 at a concentration of 10^7 PFU/mL (6). At the time of the incident, she was working in a biosafety cabinet and was double gloved. She felt the stick from the needle on her left middle finger but did not see any blood. She immediately removed her gloves, washed her hands with soap and water, and applied alcohol. After 10 days, she became symptomatic with a pruritic maculopapular rash, arthralgia, and myalgia. Zika virus infection was confirmed on the basis of the detection of Zika virus RNA in urine and serologic testing (Table). There was no reported local Zika virus transmission where she lived, and apart from the needlestick injury she had no other risk factors for acquisition of Zika virus infection. She recovered completely within \approx 2 weeks of symptom onset.

Other Laboratory-Associated Zika Virus Exposures

Case 3

In November 2017, a male worker in a BSL-2 virology laboratory had onset of symptoms (day 0) of headache, arthralgia, myalgia, fatigue, and a rash that initially appeared on his face and spread to his whole body during the next 2 days. The arthralgia and myalgia became progressively more severe and debilitating through day 5, but recovery occurred by day 13. Zika virus infection was confirmed

Table. Laboratory results from 4 patients with laboratory-associated Zika virus disease, United States, 2016–2019*

Case no.	Days after onset of collection†	Sample type	Test conducted‡	Result
1	1	Serum	RT-PCR	Zika virus RNA detected
	2	Serum	RT-PCR	Zika virus RNA detected
	2	Urine	RT-PCR	Zika virus RNA detected
	2	Serum	IgM ELISA	Zika virus IgM equivocal
	2	Serum	PRNT	Zika virus titer >20, DENV titer <10
2	4	Serum	RT-PCR	Negative
	4	Urine	RT-PCR	Zika virus RNA detected
	4	Serum	IgM ELISA	Zika virus IgM positive
	4	Serum	PRNT	Zika virus titer <10, DENV titer <10
	20	Serum	RT-PCR	Negative
	20	Urine	RT-PCR	Negative
	20	Serum	IgM ELISA	Zika virus IgM positive
	20	Serum	PRNT	Zika virus titer 320, DENV titer 20
3	2	Serum	RT-PCR	Zika virus RNA detected
	2	Serum	IgM ELISA	Negative
	20	Serum	RT-PCR	Negative
	20	Serum	IgM ELISA	Zika virus IgM positive
	20	Serum	PRNT	Zika virus titer >1,280, DENV titer <10
	\approx 120	Semen	RT-PCR	Zika virus RNA detected
4	5	Serum	RT-PCR	Negative
	5	Urine	RT-PCR	Zika virus RNA detected
	5	Serum	PRNT	Zika virus titer 160
	10	Urine	RT-PCR	Zika virus RNA detected
	10	Serum	RT-PCR	Negative
	10	Serum	IgM ELISA	Zika virus IgM positive
	10	Serum	PRNT	Zika virus titer 1280

*DENV, dengue virus; PRNT, plaque-reduction neutralization test; RT-PCR, reverse transcription PCR.

†Day 0 equals day of illness onset.

‡Tests conducted at state public health laboratories, commercial laboratories, and the Centers for Disease Control and Prevention.

through detection of Zika virus RNA in serum and semen and with serologic methods (Table). He had no other risk factors for acquisition of infection and there was no local Zika virus transmission where he lived.

The patient reported that he typically worked with large quantities (4–100 L) of Zika virus in the laboratory but did not recall any specific exposure or incident of concern within the 2 weeks before illness onset. His activities included clarifying Zika virus materials through filters, performing pump-driven chromatography, using buffers to dilute concentrated Zika virus, and adding formaldehyde to initiate Zika virus inactivation. The recommended personal protective equipment (PPE) he routinely wore included a first PPE layer, donned in an external area, of disposable laboratory coat or coverall, booties, a hairnet, goggles, and 1 pair of gloves and a second PPE layer of a second coverall, hairnet, pair of gloves, and disposable face shield donned once inside the laboratory; no mask was used. He performed his work inside a biosafety cabinet when possible but could not do so when using larger containers (e.g., the biosafety cabinet could not accommodate the large vessels used for pouring liquid live virus through a funnel). The liquid could sometimes potentially splash. On 1 occasion during the probable exposure period, while he was working in a biosafety cabinet, a large droplet of live virus dripped onto his glove; he immediately changed the outer glove. He reported it was possible he might have rubbed his face with the back of a gloved hand; however, no confirmed mucus membrane exposure could be identified. An additional 12 employees working with Zika virus in the same laboratory were subsequently tested and showed no serologic evidence of recent or past Zika virus infection.

Case 4

In October 2019, a male researcher in a vaccine research laboratory experienced fever, rash, arthralgia, and conjunctival injection. His laboratory activities sometimes involved working with Zika virus, including performing serum neutralization testing, and he had worked with Zika virus 8 and 10 days before symptom onset. He routinely wore gloves in the laboratory, but more detailed PPE information was unavailable. An investigation did not identify any specific exposure or reported breach in biosafety procedures, and no sharps were used in the laboratory. He did not live in an area with a history of Zika virus transmission and he had no other risk factors for Zika virus infection. Confirmation of infection was by

detection of Zika virus RNA in urine and by serologic methods (Table). Symptoms resolved within 8 days.

Discussion

During the 4-year period from 2016–2019, 4 cases of laboratory-acquired Zika virus infection were reported in the United States: 2 associated with needlestick injuries and 2 in which the means of exposure was undetermined. In laboratories where work with Zika virus is performed, good laboratory safety practices are critical to reduce the risk to personnel of Zika virus exposure and disease.

Many factors affect the likelihood of Zika virus infection following exposure, including the type and severity of any injury or exposure, route of exposure, viral concentration and dose, transmissibility of the strain, immediate management of any recognized exposure, and the worker's health status. At least 3 other potential occupational exposures to Zika virus have occurred among researchers without subsequent Zika virus infection: a bite from an infected mouse that punctured the skin of a gloved researcher's finger (7), a puncture wound from a needle that occurred when a double-gloved researcher was collecting a blood sample from a Zika virus-infected ferret (M. Sauri, Occupational Health Consultants, pers. comm., 2017 Jan 30), and a thumb laceration from a scalpel contaminated with chicken blood in a researcher harvesting chickens inoculated with Zika virus (7). Other exposures or infections might have occurred and remained unreported or been undetected if appropriate testing was not completed.

A limitation of this report is that viral sequencing could not be done to provide supporting evidence that the Zika virus infections were laboratory-acquired. However, the patients lived in areas without endemic Zika virus disease and patient investigations revealed no other risk factors for acquisition of Zika virus infection (i.e., no patients had traveled, had sexual contact with a traveler, or received a blood transfusion or organ transplant). Therefore, the infections were likely laboratory-acquired.

The Biosafety in Microbiological and Biomedical Laboratories guidelines recommend BSL-2 practices, safety equipment, and facilities for working with Zika virus (8). Similarly, recommendations exist for animal BSL-2 practices, equipment, and facility requirements when animal studies involving Zika virus are conducted (8). In addition, laboratories should perform a risk assessment to determine whether certain procedures or specimens might require higher levels of biocontainment (9). For example, manipulating large quantities of virus or high titer preparations might

warrant a shift to BSL-3 practices, including additional respiratory protection (8). Altering practices might be particularly critical when working outside a biosafety cabinet or when not wearing adequate PPE to protect against aerosol or droplet transfer of infectious material.

Laboratory personnel should have appropriate training regarding precautions to prevent exposures associated with the tasks they perform (8). Institutional policies also should be in place and accessible. Because careful management of needles and other sharps is vital, policies should include recommendations for the safe handling of sharps; for needles, actions that involve manipulation by hand before disposal, including bending, recapping, or removing from the syringe, are not advised (8). Biosafety in Microbiological and Biomedical Laboratories guidelines provide comprehensive information on recommended practices, safety equipment, and laboratory facilities (8). Broader guidance for protecting workers from occupational exposure to Zika virus also is available from the Occupational Safety and Health Administration and from the Centers for Disease Control and Prevention National Institute for Occupational Safety and Health (10).

Appropriate evaluation and management of occupational Zika virus exposures is crucial. If an incident occurs, established workplace procedures for initial wound management or mucous membrane exposures should be followed and the event immediately reported to a supervisor. No specific Zika virus post-exposure prophylaxis exists; however, as soon as possible after the incident, a baseline serum sample should be obtained and stored in case comparison with a convalescent serum sample is needed. Persons should be advised to take steps to prevent potential sexual transmission of Zika virus and to avoid mosquito bites if in a geographic area with risk for mosquito-borne transmission of Zika virus. These measures should be continued until laboratory testing excludes infection; if Zika virus infection is confirmed, additional counseling should be provided. If symptoms consistent with Zika virus disease occur within 2 weeks of the exposure, serum and urine should be collected and tested by using appropriate molecular and serologic methods. For an exposed person who remains asymptomatic, a serum sample should be obtained ≥ 2 weeks postexposure. This serum sample should be tested for Zika virus IgM and if positive, tested by plaque-reduction neutralization test, and results compared with those from the baseline sample to assess for asymptomatic infection. Similarly, if a person is symptomatic within 2 weeks of exposure and test results on collected samples are negative,

indicating the illness is unrelated to Zika virus infection, consideration should be given to obtaining an additional serum sample at ≥ 2 weeks postexposure and similarly evaluating for asymptomatic infection.

Although Zika virus transmission has declined substantially in recent years, research using Zika virus is ongoing. Exposure and infection are occupational risks for laboratory and biomedical research workers who work with live virus. Strong infection prevention practices are essential for reducing this risk (11). Establishing and implementing appropriate policies and procedures, providing adequate training, making available and ensuring proper use of PPE and other safety equipment, and confirming facilities are suitable for the type of work being conducted are all required to protect personnel from any adverse health outcomes.

Acknowledgments

We thank Heather Forbes, Alana Sulka, Brittany Carter, Samir Gunjan, and Tamara Simmons for their contributions to the investigation and laboratory expertise. We thank Ann Powers for her review of the manuscript and Ingrid Rabe for assistance with case investigation.

About the Author

Dr. Hills is a medical epidemiologist in the Arboviral Diseases Branch, Division of Vector-Borne Diseases, National Center for Emerging and Zoonotic Infectious Diseases, Centers for Disease Control and Prevention, Fort Collins, Colorado, USA. She has worked for more than 20 years on the epidemiology, prevention, and control of arboviral diseases in domestic and international settings.

References

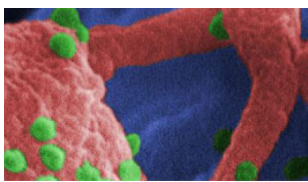
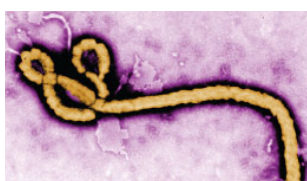
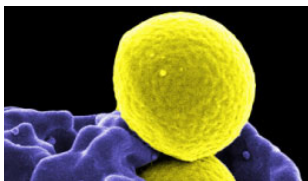
1. Gregory CJ, Oduyebo T, Brault AC, Brooks JT, Chung KW, Hills S, et al. Modes of transmission of Zika virus. *J Infect Dis.* 2017;216(suppl_10):S875–83. <https://doi.org/10.1093/infdis/jix396>
2. Simpson DI. Zika virus infection in man. *Trans R Soc Trop Med Hyg.* 1964;58:335–8. [https://doi.org/10.1016/0035-9203\(64\)90201-9](https://doi.org/10.1016/0035-9203(64)90201-9)
3. Filipe AR, Martins CMV, Rocha H. Laboratory infection with Zika virus after vaccination against yellow fever. *Arch Gesamte Virusforsch.* 1973;43:315–9. <https://doi.org/10.1007/BF01556147>
4. The Subcommittee on Arbovirus Laboratory Safety of the American Committee on Arthropod-Borne Viruses. Laboratory safety for arboviruses and certain other viruses of vertebrates. *Am J Trop Med Hyg.* 1980;29:1359–81. <https://doi.org/10.4269/ajtmh.1980.29.1359>
5. Talon de Menezes M, Rilo Christoff R, Higa LM, Pezzuto P, Rabello Moreira FR, Ribeiro LJ, et al. Laboratory acquired Zika virus infection through mouse bite: a case report. *Open Forum Infect Dis.* 2020;7:ofaa259.

SYNOPSIS

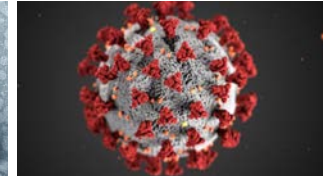
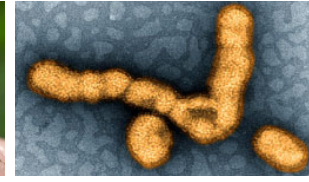
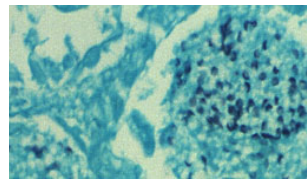
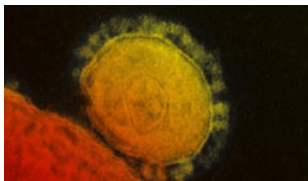
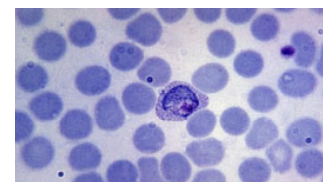
- Lichtenberger PN, Ricciardi MJ, Solorzano D, Raccamarich P, Leda A, Sharkey M, et al. Occupational exposure to the Ugandan research strain (MR766) of Zika virus. *Open Forum Infect Dis*. 2019;6:ofz420. <https://doi.org/10.1093/ofid/ofz420>
- Shugart JM, Brown CK. Zika virus presents an ongoing occupational health hazard for laboratory and biomedical research workers. *J ABSA Int*. 2019;24:8–9. <https://doi.org/10.1177/1535676018818562>
- US Department of Health and Human Services. Biosafety in microbiological and biomedical laboratories. 5th edition. 2009 [cited 2020 Feb 5]. <https://www.cdc.gov/labs/pdf/CDC-BiosafetyMicrobiologicalBiomedicalLaboratories-2009-P.PDF>
- Centers for Disease Control and Prevention. Laboratory safety when working with Zika virus [cited 2020 Feb 5]. <https://www.cdc.gov/zika/laboratories/lab-safety.html>
- Occupational Safety and Health Administration, National Institute for Occupational Safety and Health. Interim guidance for protecting workers from occupational exposure to Zika virus [cited 2020 Feb 5]. <https://www.osha.gov/zika>
- Brown CK, Shugart JM. Zika virus in workers: Considerations for ongoing exposure prevention. *Am J Ind Med*. 2019;62:455–9. <https://doi.org/10.1002/ajim.22978>

Address for correspondence: Susan Hills, Arboviral Diseases Branch, Centers for Disease Control and Prevention, 3156 Rampart Road, Fort Collins, CO 80521, USA; email: shills@cdc.gov

Emerging Infectious Diseases Spotlight Topics



**Antimicrobial resistance • Ebola
Etymologia Food safety • HIV-AIDS
Influenza • Lyme disease • Malaria
MERS • Pneumonia • Rabies • Ticks
Tuberculosis • Coronaviru • Zika**



EID's spotlight topics highlight the latest articles and information on emerging infectious disease topics in our global community

<https://wwwnc.cdc.gov/eid/page/spotlight-topics>

Epidemiologic Findings from Case Investigations and Contact Tracing for First 200 Cases of Coronavirus Disease, Santa Clara County, California, USA

Nancy Ortiz, Elsa Villarino, James T. Lee, Kristina L. Bajema, Jessica N. Ricaldi, Shanon Smith, Wen Lin, Margaret Cortese, Albert E. Barskey, Juliana F. Da Silva, Brandon J. Bonin, Sarah L. Rudman, George S. Han, Marc Fischer, Shua J. Chai, Sara H. Cody, for the Santa Clara County COVID-19 Case Investigation Team¹

In January 2020, Santa Clara County, California, USA, began identifying laboratory-confirmed coronavirus disease among residents. County staff conducted case and contact investigations focused on households and collected detailed case demographic, occupation, exposure, and outcome information. We describe the first 200 test-positive cases during January 31–March 20, 2020, to inform future case and contact investigations. Probable infection sources included community transmission (104 cases), known close contact with a confirmed case-patient (66 cases), and travel (30 cases). Disease patterns across race and ethnicity, occupational, and household factors suggested multiple infection risk factors. Disproportionately high percentages of case-patients from racial and ethnic subgroups worked outside the home (Hispanic [86%] and Filipino [100%]); household transmission was more common among persons from Vietnam (53%). Even with the few initial cases, detailed case and contact investigations of household contacts capturing occupational and disaggregated race and ethnicity data helped identify at-risk groups and focused solutions for disease control.

On January 31, 2020, the Santa Clara County Department of Public Health (SCCDPH) in San Jose, California, USA, identified its first case of coronavirus disease (COVID-19) in a resident who had recently returned from Wuhan, China (1). On February

28, the county reported its first case of COVID-19 associated with probable community transmission, 48 hours after the first presumed community-acquired case in the United States was identified 91 miles north in Solano County (2). Staff of the SCCDPH, the California Department of Public Health, and the Centers for Disease Control and Prevention (CDC) began conducting detailed interviews with each case-patient or their surrogate to identify, quarantine, and monitor close contacts, and isolate and test those who were symptomatic. Santa Clara initiated a series of community mitigation strategies to slow the spread of the virus that causes COVID-19, severe acute respiratory syndrome coronavirus 2 (SARS-CoV-2), including canceling large gatherings (3,4). On March 16, Santa Clara and 5 adjacent San Francisco Bay Area counties became the first US region to implement shelter-in-place orders requiring all residents to limit activity outside of their home and to order nonessential businesses and operations to close (5). SCCPHD collected detailed information on demographic characteristics to help identify communities at risk and those disproportionately affected by COVID-19. Since the initial identification of cases, surges in COVID-19 incidence have often constrained public health and community capacity to respond, including overwhelming case and contact investigation efforts. We describe the epidemiology of the first 200 COVID-19 cases reported to SCCPHD to identify key transmission factors that could already be identified early in the COVID-19 pandemic through detailed case investigation and

Author affiliations: Centers for Disease Control and Prevention, Atlanta, Georgia, USA (N. Ortiz, J.T. Lee, K.L. Bajema, J.N. Ricaldi, M. Cortese, A.E. Barskey, J.F. Da Silva, M. Fischer, S.J. Chai); County of Santa Clara Public Health Department, San Jose, California, USA (E. Villarino, S. Smith, W. Lin, B.J. Bonin, S.L. Rudman, G.S. Han, S.H. Cody)

DOI: <https://doi.org/10.3201/eid2705.204876>

¹Members of the Santa Clara County COVID-19 Case Investigation Team are listed at the end of this article.

contact tracing focused on households and to demonstrate the utility of focusing these efforts throughout the pandemic response.

Methods

Case Identification and Testing

We defined a confirmed COVID-19 case as an illness in a resident of Santa Clara County with SARS-CoV-2 detected by reverse transcription PCR (RT-PCR) on a nasopharyngeal or oropharyngeal swab specimen by a public health, hospital, or reference clinical microbiology laboratory or CDC. Testing was recommended in line with the following evolving CDC Person Under Investigation case definition: clinical findings of lower respiratory illness and travel to Wuhan, China (later expanded to all of China) or an epidemiologic link to a laboratory-confirmed COVID-19 case (6,7); hospitalization for severe respiratory disease and no alternative diagnosis (8); and clinically compatible illness regardless of travel or known contact with a confirmed case-patient. Included COVID-19 case-patients comprised those reported to SCCDPH and those identified by a community-based sentinel surveillance project for COVID-19 conducted during March 5–14, 2020, among clinic patients with respiratory illness who tested negative for influenza virus (9). This activity was reviewed by CDC and was conducted consistent with applicable federal law and CDC policy.

Case Investigation and Contact Tracing

SCCDPH, California Department of Public Health, and CDC staff identified cases reported to California's electronic reportable disease system. Staff interviewed COVID-19 cases or their surrogates for information on case age, sex, race, ethnicity, address, occupation, travel history, known contact with another confirmed case-patient, symptom onset (earliest of any symptoms listed on CDC's standardized case report form) (10), and hospitalization. Investigators collected detailed race and ethnicity data, including racial subgroup among case-patients reporting Asian ancestry.

Case-patients with no recent travel and no known close contact with another confirmed case-patient in the 2 weeks before symptom onset were classified as probable community transmission. Known close contact was defined as living with, caring for, working with, transporting, or prolonged exposure (close contact <6 feet for ≥ 30 minutes) to a person with confirmed COVID-19. Case-patients with any travel outside of Santa Clara County in the

2 weeks before their symptom onset were considered travel-associated cases.

SCCPHD's contact tracing involved identifying persons with close contact with the case-patient 2 weeks after the case-patient's symptom onset and notifying contacts of their exposure. Owing to the rapid rise in case counts and limited personnel capacity, the team focused on following up with household contacts. In-hospital outcomes were collected from review of medical records and case-patient interviews. Deaths through May 20, 2020 (60 days after the 200th case was reported), were defined as COVID-19-associated if the cause or other contributing cause on the death certificate was listed as COVID-19.

Data Analysis

We collected data using standard forms and open-ended case-patient interviews and entered results into Excel 365 (Microsoft, <https://www.microsoft.com>) and California's electronic reportable disease system. Categorical variables were described as counts and percentages, and continuous variables were described using median and range. We estimated associations between illness severity measures (hospitalization defined as admission for ≥ 1 night in an inpatient acute-care facility [including intensive-care unit (ICU) stay and mechanical intubation with ventilation]; ICU stay [including mechanical ventilation]; mechanical ventilation; and death) as the dependent variables, and age and sex as independent variables with odds ratios (ORs) and 95% CIs using bivariate logistic regression. Because of the limited number of cases, to avoid invalid results or unstable models, measurements were not adjusted. We analyzed data using Stata 14 (StataCorp, <https://www.stata.com>) and Epi Info version 7 (Epi Info, <https://www.cdc.gov/epiinfo>) and generated maps using Excel 365 (Microsoft, <https://www.microsoft.com>).

Results

Case Description

Of the 200 cases with laboratory confirmation of SARS-CoV-2 positivity during January 31–March 20, 2020, a total of 191 (96%) were identified through routine surveillance and contact tracing and 9 (4%) were identified through clinic-based sentinel surveillance. Onset of illness ranged from January 24 through March 18; these case-patients were exposed before shelter-in-place orders were invoked (Figure 1). Among the first cases identified during January 31–February 2, travel accounted for the largest reported source of exposure. Over subsequent weeks, case-patients reported

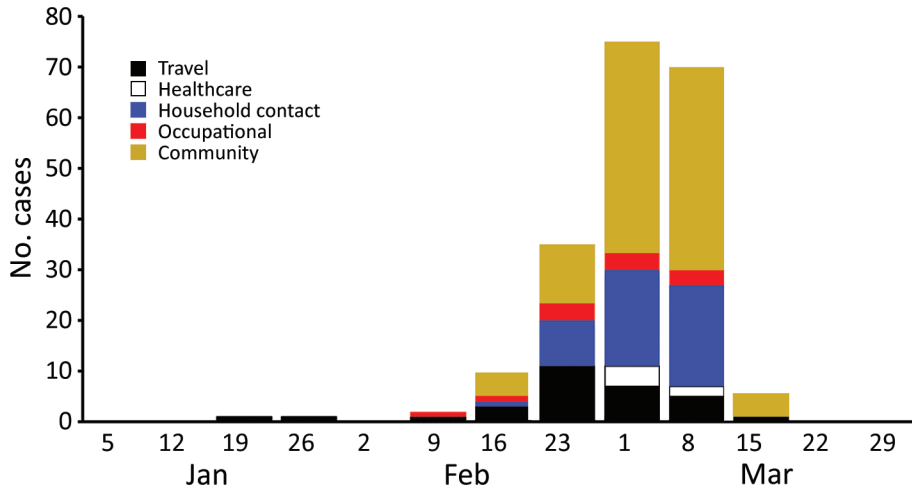


Figure 1. Week of symptom onset, for first 200 confirmed coronavirus disease cases, by exposure source, Santa Clara County, California, USA, January 31–March 20, 2020.

unknown and household exposure at higher frequencies than other exposures. The percentage of case-patients who were hospitalized decreased over time as testing availability increased and focus of testing broadened to include additional populations, including symptomatic contacts.

Among the 200 case-patients, 112 (56%) were male, and the median age was 50 years (range 6 months–94 years); only 10 (5%) case-patients were <20 years of age, whereas 71 (36%) were ≥60 years of age (Table, <https://wwwncdc.gov/EID/article/27/5/20-4876-T1.htm>). The racial and ethnic distribution of case-patients was similar to that of the county population overall: 70 (35%) reported as Asian, 52 (26%) Hispanic, 52 (26%) White non-Hispanic, 4 (2%) Black non-Hispanic, and 3 (1%) Pacific Islander; race or ethnicity was unknown for 19 (9%) case-patients. Although Asian-identifying persons comprised a similar proportion of case-patients as that of Santa Clara County, a higher proportion of case-patients identified as Filipino (10% vs. 5%), a similar proportion as Vietnamese (7% vs. 7%), and a lower proportion as Indian (4% vs. 9%) or Chinese (4% vs. 10%) than among the general population of Santa Clara County (11,12). Of the 200 case-patients, 89 (44%) were hospitalized (Table); 45 (23%) were on a general ward, 18 (9%) were admitted to an ICU without requiring mechanical ventilation, and 26 (13%) required mechanical ventilation in an ICU. The proportion of case-patients hospitalized, admitted to the ICU, requiring mechanical ventilation, and who died each increased with increasing age (Figure 2). Compared with case-patients <60 years of age, case-patients ≥60 years of age had higher odds of hospitalization (OR 4.4 [95% CI 2.4–8.3]), ICU stay (OR 10.9 [95% CI 4.9–24.2]), mechanical ventilation (OR 6.3 [95% CI 2.5–16.0]), and death (OR 9.0 [95% CI 2.9–28.4]). No statistically

significant association was observed between clinical outcomes and sex.

Among the 200 case-patients, 20 (10%) had a matching death certificate. The median age of deceased case-patients was 70.5 years (range 42–87 years), and 15 (75%) were male. Among the 20 case-patients who died, 9 (45%) were Asian, 5 (25%) were White non-Hispanic, 2 (10%) were Hispanic, and 4 (20%) had unknown race or ethnicity. Five (25%) of the 20 deaths occurred among persons of Filipino ethnicity; these case-patients did not have a known close contact to one another.

Case-patient residences were distributed among 47 (79%) of the 59 ZIP codes in the county; 18 (30%) ZIP codes had 1–2 cases, 13 (22%) had 3–4 cases, and 16 (8%) had ≥5 cases (Figure 3, panel A). Case-patient residences clustered in the northeastern part of the county, where 2 adjacent ZIP codes accounted for 36 (18%) of the 200 case-patients; in the ZIP code with the most cases, 9 were associated with a single household. COVID-19 incidence rates by ZIP code ranged from 0–113 cases/100,000 persons; rates were generally highest in eastern ZIP codes in the county (Figure 3, panel B).

Exposure Type and Setting

Of the 200 case-patients, 66 (33%) had known close contact with another confirmed case-patient, 30 (15%) were considered travel-associated cases (Table), and 104 (52%) were attributable to probable community transmission. Among the 66 case-patients with known close contact with another confirmed case-patient, 49 (74%) were exposed to a household member, and 17 (26%) had occupational exposures. Most households with evidence of transmission (13/15 [86%]) had 2–3 confirmed case-patients identified. However, 2

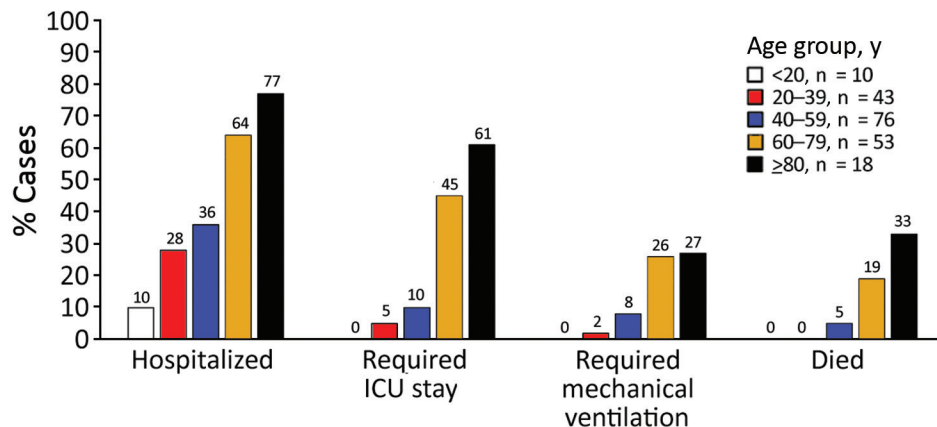


Figure 2. Hospitalization status and outcomes, for first 200 confirmed coronavirus disease cases, by age group, Santa Clara County, California, USA, January 31–March 20, 2020. Outcomes are classified by most severe status at time of case investigation. Deaths are as of May 20, 2020. ICU, intensive-care unit.

multigenerational households each had 9 and 4 case-patients; the cluster of 4 case-patients was only identified as a result of contact tracing.

Of the 200 case-patients, 159 (79%) were adults with reported occupation. Of these, 111 (69%) were actively employed (not retired and reported employment), and of these, 82 (73%) reported jobs requiring work outside the home, which included healthcare workers, firefighters, food service workers, retail employees, construction workers, housekeepers, and other workers. Among these 82 case-patients reporting jobs requiring work outside the home, 46% of exposures were attributable to probable community transmission, followed by 22% household and 21% occupational exposures.

Type and location of exposure, as well as having an occupation that requires work outside the home, varied by race and ethnicity. Among 49 cases in Hispanic adults, occupation was known for 44 (89%); of the 38 actively employed, 89% held occupations that required them to work outside of the home. Occupation was known for 16 of 20 Filipino case-patients; for the 9 case-patients who were actively employed, all had jobs outside the home. Occupational exposure to a confirmed case-patient, including in a healthcare setting, accounted for 5 (25%) of 20 cases in Filipino persons, compared with 12 (7%) of all other cases with reported race and ethnicity. Household transmission accounted for exposures in 53% of Vietnamese case-patients and 32% of Hispanic case-patients, compared with 23% of all other case-patients with known race/ethnicity. Among case-patients of Indian and Chinese ethnicity, >50% had travel-related exposures.

Among the 17 case-patients with an occupational exposure to a confirmed case-patient, 11 (64%) exposures occurred in a nonhealthcare setting. Of these 11, all were employed as essential workers in occupations or settings in which they had frequent

contact with many persons in the community. Occupational clusters and groupings included 6 airport employees, 4 employees at a supermarket, 3 child-care workers who shared a classroom and bathroom, and 2 firefighters who worked at the same station. At least 3 additional cases were identified among other firefighters who worked at the same station or attended a common function but were not Santa Clara County residents.

Of the 200 case-patients, 16 (8%) were healthcare workers with jobs that provided direct patient care or were first responders with direct patient exposure, of whom 8 (50%) were nurses. Only 6 transported, cared for, or had other known close contact with a confirmed case-patient in a healthcare setting. Of the other 10 cases in healthcare workers, 1 case-patient had travel-related exposure, 3 had known close contact with a case-patient in their household, and 6 did not have exposure to a known COVID-19 case-patient and were categorized as attributable to probable community transmission.

Discussion

Detailed case investigations and household contact tracing of the first 200 case-patients of COVID-19 in Santa Clara County were able to help elucidate factors associated with being a COVID-19 case-patient and identify populations at risk for infection early in the response, including possible racial and ethnic disparities, elevated risks within households, and high-risk occupational groups. Many of these factors and populations at risk were subsequently confirmed by studies later in the pandemic (13,14). Case investigations identified possible sources of transmission in 96 (48%) of cases, and for those case-patients with known exposure, household transmission was the most commonly reported source, especially in Vietnamese and Hispanic communities. Work outside the

home was commonly reported by Hispanic case-patients. Case-patients ≥ 60 years of age had significantly higher odds of being hospitalized, being admitted to the ICU, requiring mechanical ventilation, and dying; these findings are consistent with reports from China, Italy, and other parts of the United States (15–17).

Because SCCPHD conducted contact tracing and monitoring specifically among household contacts of case-patients, the finding that approximately one quarter of the first 200 case-patients were household contacts of a confirmed case-patient is not surprising. However, SCCPHD's prioritization of contact tracing and monitoring contacts within households early in the pandemic was high-yield, and findings were consistent with disease transmission factors for COVID-19 reported in subsequent studies (18,19). Investigations identified not only that older persons had increased odds of poor outcomes from COVID-19 but also that case-patients with multiple factors potentially increased risk. For example, several large clusters were identified within families that consisted of members of multiple generations, and several individuals >80 years of age might have been exposed. In 2 of these clusters, the index case-patient was a nonelderly household member who presumably transmitted SARS-CoV-2 to elderly household members. Anecdotally, several of these households also reported crowding and inability to self-isolate from other members within the home (Santa Clara COVID-19 Case Investigation Team, pers. comm., group discussion during case review, March 2020). Households have been identified as a high-risk

setting for SARS-CoV-2 transmission (20–22), and household crowding is a risk factor for COVID-19 (23). In the ZIP code with the highest case rate in northeast Santa Clara, 14% of households are overcrowded (>1.0 persons/room), as measured by the American Community Survey, compared with the median of 6% of households in Santa Clara County as a whole (24). Although information on an individual case-patient's household density was not collected as part of case and contact investigations, 4 (33%) of 12 ZIP codes where household transmission was identified reported $>10\%$ frequency of overcrowded households, compared with 7 (20%) of 35 ZIP codes where cases were identified but no household transmission was noted. Household density might be associated with other factors, such as high-risk occupations of household members (25,26), to increased risk for COVID-19 within households. Case investigators collecting information regarding household density during interviews can help not only to elucidate transmission risk in a particular household, but also link persons at high risk for poor outcomes to resources to prevent household transmission. One example of a solution to prevent household transmission is The NYC Test and Trace Corps, a collaborative public health program led by NYC Health + Hospitals in collaboration with the New York City Department of Public Health and Mental Hygiene, which offers hotel stays for persons who have COVID-19, exhibit COVID-19 symptoms, or are contacts of a known COVID-19 case-patient and who need to isolate or quarantine from household members (27).

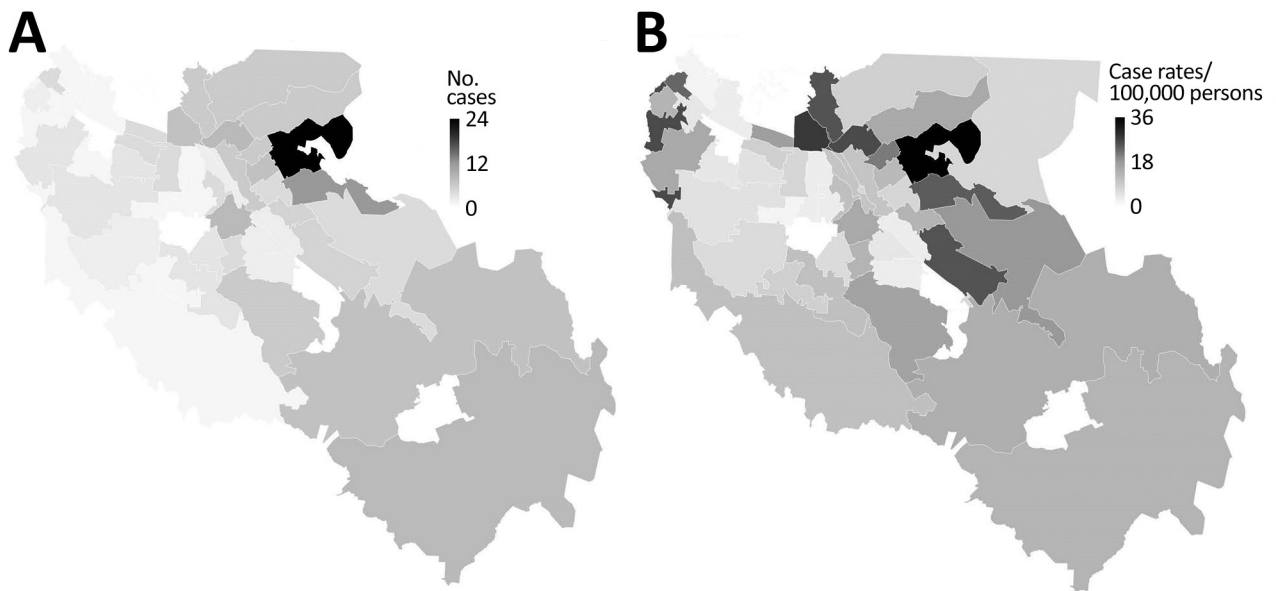


Figure 3. Geographic location of first 200 confirmed coronavirus disease cases, by case-patient's ZIP code area of residence (for those areas with $>2,000$ residents), Santa Clara County, California, USA, January 31–March 20, 2020. A) No. cases; B) case rate (cases/100,000 population).

Working outside the home, especially with public-facing duties (e.g., airport workers), was especially common in this early cohort; >40% of case-patients reported an occupation that did not allow them to work from home. A large frequency of case-patients who performed work outside the home did not report a known exposure or travel, suggesting that difficult-to-trace exposures, such as exposure to someone the case-patient did not know or did not know was infected, probably occurred (28). Moreover, occupational exposures were probably more common than we reported, because case-patients who did not have known exposure to a person with confirmed COVID-19 and had not traveled were classified as having community exposure. Identifying the source of exposure for case-patients with occupations that interact with the public might prove to be very labor-intensive or impossible, given the number of potential contacts involved. However, case and contact investigations, at a minimum, should include notifying co-workers and alerting employers to a positive case in a workplace (29) and collecting occupation data to help identify occupational subgroups at risk.

Occupational exposures probably differed by racial and ethnic groups among the first 200 case-patients in Santa Clara County. Among employed Filipino case-patients, all held jobs that required work outside the home. Although few Hispanic case-patients reported an occupational exposure with a confirmed COVID-19 case-patient, a greater percentage of Hispanic case-patients (89%) had occupations that required them to work outside the home than did White non-Hispanic case-patients (56%). Many of the Hispanic case-patients in Santa Clara County communicated that they could not afford the lost wages that would result from staying home from work (Santa Clara COVID-19 Case Investigation Team, pers. comm., group discussion during case review, March 2020). Hispanic persons nationwide have reported higher frequencies of job loss and wage reduction because of the COVID-19 pandemic compared with persons from other racial and ethnic minority groups, and less than one third of Hispanic persons surveyed reported that they could weather a financial emergency (30). These financial and occupational factors together might be critical drivers for transmission within the Hispanic population in Santa Clara County and perhaps statewide, where Hispanic persons have accounted for a disproportionately high number of cases (31). A disproportionately high percentage of COVID-19 cases and deaths occurred in Filipino

persons; cases among Filipino persons associated with occupational exposures involved providing direct patient care to known COVID-19 patients or contact with a person with confirmed COVID-19 in public-facing service jobs.

Household exposures also differed by racial and ethnic groups. Vietnamese and Hispanic case-patients more frequently reported exposure to a person with confirmed COVID-19 in their household compared with case-patients from other race and ethnicity groups. Anecdotally, among Vietnamese and Hispanic case-patients, ≥ 3 reported living in multigenerational households with high densities of persons and an inability to self-isolate within the home, posing a serious risk to older adults residing in these households. Household case clusters occurred in eastern ZIP codes that had high percentages of Hispanic persons (58% of the population in the ZIP code with the most cases and highest rates) and Vietnamese persons (22%), compared with 26% of Hispanic and 7% of Vietnamese persons in the county as a whole (32–37). Together, these findings suggest that household crowding might be an especially important driver of household transmission in traditionally underserved communities.

Few of the first 200 COVID-19 cases in Santa Clara County occurred in healthcare workers or persons in institutional or congregate living settings. Although more than one third of infected healthcare workers reported an occupational exposure and a quarter traveled or had a nonoccupational close-contact exposure, none of these exposures was identified for 40% of them. Evidence to date does not support substantial occupational transmission of SARS-CoV-2 to healthcare workers (38). Community transmission could have been an important source of exposure for healthcare workers, given the widespread community transmission occurring simultaneously in Santa Clara County.

One limitation of this analysis is, as with most reports on COVID-19, case identification was largely dictated by testing practices. At the start of the outbreak, the number of persons eligible for testing according to CDC criteria and testing capacity were limited, biasing these initial findings to case-patients with higher disease and mortality rates and to persons with recent travel or known contact with a confirmed case-patient. Had testing been more widely available and criteria included milder symptoms or risk for exposure regardless of symptoms, broader or earlier detection of community transmission might have occurred. This

investigation occurred when information was limited for this new and emerging disease. The definition of prolonged COVID-19 exposure and guidance for case and contact investigations has been updated since this investigation concluded (39). Although we observed differences in sources of exposure by race and ethnicity, data on race were missing for 19 (9%) cases and racial subgroup for 16 (23%) of 70 cases among Asian persons; therefore, these data should be interpreted with caution. Our data reflect the epidemiology of COVID-19 in Santa Clara early in the pandemic among those with clinical manifestations that were eligible for testing and probably are not reflective of the current epidemiology (40).

Even with results from only the first 200 case-patients, detailed case investigation and contact tracing focused on households revealed patterns of at-risk populations, including older age adults, racial and ethnic subgroups, occupational categories, and potentially crowded households. Detailed case reviews, including disaggregation of race and ethnicity data, helped identify local factors of transmission and disparities important for public health intervention. Importantly, occupational exposures continue to be a source of infection (41), and understanding transmission risk within specific occupational settings, especially among professions that require persons to work outside their homes, is important to ensure safe workplaces and reopening of economies as the pandemic continues to evolve. As mitigation measures to suppress community transmission evolve throughout the pandemic response, novel preventive measures (e.g., temporary housing) might continue to be necessary to protect disproportionately affected subpopulations and older adults.

Members of the Santa Clara County COVID-19 Case Investigation Team: Nora Chea, Calin Chiribau, Lindsey Duca, Joseph Hicks, Jimmie Hwang, Jessica Leung, Joel London, Huong Pham, Matthew Stuckey, Diya Surie, Kathleen Thurman, and Douglas Trout.

Acknowledgments

We thank the Case Investigation Team for their support in the field.

About the Author

Dr. Ortiz is an Epidemic Intelligence Service Officer in the Division of Scientific Education And Professional Development, Center For Surveillance, Epidemiology, and Laboratory Services, Centers for Disease Control and Prevention. Her research interests include infectious diseases, emerging infections, and applied epidemiology.

References

1. Santa Clara County Public Health Department. Letter from the Health Officer. February 3, 2020 [cited 2021 Jan 28]. <https://www.sccgov.org/sites/covid19/Pages/health-officer-letter-2-3-2020.aspx>
2. Santa Clara County Public Health Department. County of Santa Clara Public Health Department reports third case of COVID-19. February 28, 2020 [cited 2021 Jan 28]. <https://www.sccgov.org/sites/phd/news/Pages/third-novel-coronavirus-case-02-2020.aspx>
3. Santa Clara County Public Health Department. County of Santa Clara issues order to cancel mass gatherings due to increasing rates of COVID-19. March 9, 2020 [cited 2021 Jan 28]. <https://www.sccgov.org/sites/phd/news/Pages/order-health-officer-03092020.aspx>
4. Santa Clara County Public Health Department. Due to increasing rates of COVID-19, County Public Health issues new order cancelling gatherings of more than 100 people and restricting gatherings of more than 35 people. March 13, 2020 [cited 2021 Jan 28]. <https://www.sccgov.org/sites/phd/news/Pages/press-release-03-13-20.aspx>
5. Santa Clara County Public Health Department. Seven bay area jurisdictions order residents to stay home. March 16, 2020 [cited 2021 Jan 28]. <https://www.sccgov.org/sites/phd/news/Pages/press-release-03-16-20.aspx>
6. Centers for Disease Control and Prevention. Health alert network: update and interim guidance on outbreak of 2019 novel coronavirus (2019-nCoV) in Wuhan, China. 2020 [cited 2021 Jan 28]. <https://emergency.cdc.gov/han/han00427.asp>
7. Centers for Disease Control and Prevention. Health alert network: update and interim guidance on outbreak of 2019 novel coronavirus (2019-nCoV) in Wuhan, China. 2020 [cited 2021 Jan 28]. <https://emergency.cdc.gov/han/han00426.asp>
8. Centers for Disease Control and Prevention. Update and interim guidance on outbreak of coronavirus disease 2019 (COVID-19). February 28, 2020 [cited 2021 Jan 28]. <https://emergency.cdc.gov/han/2020/han00428.asp>
9. Zwald ML, Lin W, Sondermeyer Cooksey GL, Weiss C, Suarez A, Fischer M, et al. Rapid sentinel surveillance for COVID-19—Santa Clara County, California, March 2020. *MMWR Morb Mortal Wkly Rep.* 2020;69:419–21. <https://doi.org/10.15585/mmwr.mm6914e3>
10. Centers for Disease Control and Prevention. Human infection with 2019 novel coronavirus case report form [cited 2021 Jan 29]. <https://www.cdc.gov/coronavirus/2019-ncov/downloads/pui-form.pdf>
11. US Census Bureau. United States Census. Quick facts: Santa Clara County, California. July 1, 2019 [cited 2021 Jan 28]. <https://www.census.gov/quickfacts/santaclaracountycalifornia>
12. US Census Bureau. 2018 American Community Survey 5-year estimates, demographic and housing estimates, Table DP05 [cited 2021 Jan 28]. https://data.census.gov/cedsci/table?g=0400000US06_0500000US06085&d=ACS%205-Year%20Estimates%20Data%20Profiles&tid=ACSDP5Y2018.DP05
13. Figueroa JF, Wadhwa RK, Lee D, Yeh RW, Sommers BD. Community-level factors associated with racial and ethnic disparities in COVID-19 rates in Massachusetts. *Health Aff (Millwood)*. 2020;39:1984–92. <https://doi.org/10.1377/hlthaff.2020.01040>
14. Grijalva CG, Rolfes MA, Zhu Y, McLean HQ, Hanson KE, Belongia EA, et al. Transmission of SARS-COV-2 infections in households—Tennessee and Wisconsin, April–September 2020. *MMWR Morb Mortal Wkly Rep.* 2020;69:1631–4. <https://doi.org/10.15585/mmwr.mm6944e1>

15. Grasselli G, Zangrillo A, Zanella A, Antonelli M, Cabrini L, Castelli A, et al.; COVID-19 Lombardy ICU Network. Baseline characteristics and outcomes of 1591 cases infected with SARS-CoV-2 admitted to ICUs of the Lombardy Region, Italy. *JAMA*. 2020;323:1574–81. <https://doi.org/10.1001/jama.2020.5394>
16. Garg S, Kim L, Whitaker M, O'Halloran A, Cummings C, Holstein R, et al. Hospitalization rates and characteristics of cases hospitalized with laboratory-confirmed coronavirus disease 2019 – COVID-NET, 14 states, March 1–30, 2020. *MMWR Morb Mortal Wkly Rep*. 2020;69:458–64. <https://doi.org/10.15585/mmwr.mm6915e3>
17. Bialek S, Boundy E, Bowen V, Chow N, Cohn A, Dowling N, et al.; CDC COVID-19 Response Team. Severe outcomes among cases with coronavirus disease 2019 (COVID-19) – United States, February 12–March 16, 2020. *MMWR Morb Mortal Wkly Rep*. 2020;69:343–6. <https://doi.org/10.15585/mmwr.mm6912e2>
18. Qian G, Yang N, Ma AHY, Wang L, Li G, Chen X, et al. COVID-19 transmission within a family cluster by presymptomatic carriers in China. *Clin Infect Dis*. 2020;71:861–2.
19. Chan JF-W, Yuan S, Kok K-H, To KK, Chu H, Yang J, et al. A familial cluster of pneumonia associated with the 2019 novel coronavirus indicating person-to-person transmission: a study of a family cluster. *Lancet*. 2020;395:514–23. [https://doi.org/10.1016/S0140-6736\(20\)30154-9](https://doi.org/10.1016/S0140-6736(20)30154-9)
20. Wang Z, Ma W, Zheng X, Wu G, Zhang R. Household transmission of SARS-CoV-2. *J Infect*. 2020;81:179–82. <https://doi.org/10.1016/j.jinf.2020.03.040>
21. Haroon S, Chandan JS, Middleton J, Cheng KK. Covid-19: breaking the chain of household transmission. *BMJ*. 2020;370:m3181.
22. Lei H, Xu X, Xiao S, Wu X, Shu Y. Household transmission of COVID-19—a systematic review and meta-analysis. *J Infect*. 2020;81:979–97. <https://doi.org/10.1016/j.jinf.2020.08.033>
23. Emeruwa UN, Ona S, Shaman JL, Turitz A, Wright JD, Gyamfi-Bannerman C, et al. Associations between built environment, neighborhood socioeconomic status, and SARS-CoV-2 infections among pregnant women in New York City. *JAMA*. 2020;324:390–2. <https://doi.org/10.1001/jama.2020.11370>
24. US Census Bureau. Percentage of overcrowded housing units, 2014–2018 American Community Survey 5-year estimates. Table B25014 [cited 2021 Jan 30]. <https://data.census.gov/cedsci/table?q=B25014&tid=ACSDT5Y2018.B25014&hidePreview=false>
25. Ghinai I, Woods S, Ritger KA, McPherson TD, Black SR, Sparrow L, et al. Community transmission of SARS-CoV-2 at two family gatherings – Chicago, Illinois, February–March 2020. *MMWR Morb Mortal Wkly Rep*. 2020;69:446–50. <https://doi.org/10.15585/mmwr.mm6915e1>
26. Centers for Disease Control and Prevention. Households living in close quarters. April 18, 2020 [cited 2021 Jan 29]. <https://www.cdc.gov/coronavirus/2019-ncov/daily-life-coping/living-in-close-quarters.html>
27. Test & Trace Corps. NYC Health + Health Hospitals. Take care [cited 2021 Jan 29]. <https://www.nychealthand-hospitals.org/test-and-trace/take-care>
28. US Department of Labor, Occupational Safety and Health Administration. Safety and Health Topics. COVID-19. Hazard recognition [cited 2020 Jul 13]. <https://www.osha.gov/coronavirus/hazards>
29. Council of State and Territorial Epidemiologists Occupational Health Subcommittee. Recommended interim guidance for collecting employment information about COVID-19 cases [cited 2021 Jan 28]. https://cdn.ymaws.com/www.cste.org/resource/resmgr/publications/Guidance_collecting_io_covid.pdf
30. Pew Research Center. About half of lower-income Americans report household job or wage loss due to COVID-19. April 21, 2020 [cited 2021 Jan 28]. <https://www.pewsocialtrends.org/2020/04/21/about-half-of-lower-income-americans-report-household-job-or-wage-loss-due-to-covid-19>
31. California Department of Public Health. COVID-19 race and ethnicity data. June 7, 2020 [cited 2021 Jan 28]. <https://www.cdph.ca.gov/Programs/CID/DCDC/Pages/COVID-19/Race-Ethnicity.aspx>
32. Census Reporter. 95127. ZIP code tabulation area in: Santa Clara County, CA, San Jose-Sunnyvale-Santa Clara, CA Metro Area, California, United States [cited 2021 Jan 28]. <https://censusreporter.org/profiles/86000US95127-95127>
33. Census Reporter. 95148. ZIP code tabulation area in: Santa Clara County, CA, San Jose-Sunnyvale-Santa Clara, CA Metro Area, California, United States [cited 2021 Jan 28]. <https://censusreporter.org/profiles/86000US95148-95148>
34. Census Reporter. Santa Clara County. CA [cited 2021 Jan 28]. <https://censusreporter.org/profiles/05000US06085-santa-clara-county-ca>
35. Census Reporter. Race. American Community Survey 2018 5-year estimates. Table B02001 [cited 2021 Jan 28]. https://censusreporter.org/data/table/?table=B02001&geo_ids=86000US95148&primary_geo_id=86000US95148#valueType|estimate
36. US Census Bureau. Asian alone by selected groups. American Community Survey 2018 5-year estimates. Table B02015 [cited 2021 Jan 28]. <https://data.census.gov/cedsci/table?q=B02015&g=8600000US95148&tid=ACSDT5Y2018.B02015&hidePreview=false>
37. US Census Bureau. Hispanic or Latino origin by specific origin. American Community Survey 2018 5-year estimates. Table B03001 [cited 2021 Jan 29]. <https://data.census.gov/cedsci/table?q=Table%20B03001&tid=ACSDT5Y2018.B03001&hidePreview=false>
38. Kambhampati AK, O'Halloran AC, Whitaker M, Magill SS, Chea N, Chai SJ, et al.; COVID-NET Surveillance Team. COVID-19-associated hospitalizations among health care personnel – COVID-NET, 13 states, March 1–May 31, 2020. *MMWR Morb Mortal Wkly Rep*. 2020;69:1576–83. <https://doi.org/10.15585/mmwr.mm6943e3>
39. Centers for Disease Control and Prevention. Investigating a COVID-19 case [cited 2021 Jan 29]. <https://www.cdc.gov/coronavirus/2019-ncov/php/contact-tracing/contact-tracing-plan/investigating-covid-19-case.html>
40. Santa Clara County Public Health. County of Santa Clara Emergency Operations Center COVID-19 dashboards [cited 2021 Jan 29]. <https://www.sccgov.org/sites/covid19/Pages/dashboard-demographics-of-cases-and-deaths.aspx>
41. Fisher KA, Olson SM, Tenforde MW, Feldstein LR, Lindsell CJ, Shapiro NI, et al.; IVY Network Investigators; CDC COVID-19 Response Team. Telework before illness onset among symptomatic adults aged ≥18 years with and without COVID-19 in 11 outpatient health care facilities – United States, July 2020. *MMWR Morb Mortal Wkly Rep*. 2020; 69:1648–53. <https://doi.org/10.15585/mmwr.mm6944a4>

Address for correspondence: Nancy Ortiz, Centers for Disease Control and Prevention, 1600 Clifton Rd NE, Mailstop V25-1, Atlanta, GA 30329-4027, USA; email: hqo5@cdc.gov

Clinical Laboratory Perspective on *Streptococcus halichoeri*, an Unusual Nonhemolytic, Lancefield Group B Streptococcus Causing Human Infections

Salika M. Shakir,¹ Rahul Gill,¹ Jonathan Salberg, E. Susan Slechta, Mark Feldman, Thomas Fritsche, Jill Clarridge, Susan E. Sharp, Mark A. Fisher

Streptococcus halichoeri is a relatively newly identified species of pyogenic streptococci that causes zoonotic infection in humans. *S. halichoeri* was first described in 2004 as indigenous to seals, and only 8 reports of human *S. halichoeri* infection have been published. *S. halichoeri* grows as small, white, nonhemolytic colonies and may be strongly catalase-positive on routine blood agar media, which can lead to isolates being misidentified as coagulase-negative staphylococci. *S. halichoeri* is positive for Lancefield group B antigen, like *S. agalactiae*, but can be correctly identified with matrix-assisted laser desorption/ionization time of flight mass spectrometry or partial 16S rRNA sequencing. We describe 3 cases of *S. halichoeri* bone and joint infections in patients in the United States with underlying health conditions. In addition, we examine the microbiologic characteristics of *S. halichoeri* and discuss the importance of fully identifying this organism that might otherwise be disregarded as a skin commensal.

Streptococcus halichoeri is a recently identified member of the genus *Streptococcus* capable of causing pyogenic human infections. It was first isolated from gray seals (*Halichoerus grypus*) and formally described

in 2004 (1). In 2013, it was reported as the causative organism of empyema in a patient with diabetes (2). *S. halichoeri* differs from other pyogenic streptococci in that it is nonhemolytic and may exhibit strong catalase activity when grown in blood-containing media such as chocolate and sheep blood agar (SBA). These phenotypic characteristics, along with its colony and Gram-stain morphology, may lead to its misidentification as a coagulase-negative *Staphylococcus*. In addition, *S. halichoeri* is positive by Lancefield group B-typing assays but can be distinguished from *S. agalactiae* by its gamma hemolysis and negative hippurate hydrolysis results (2). A 2016 study described distinct phenotypic and genetic differences between 6 human clinical isolates and the type strain from a gray seal. The authors proposed distinct subspecies for human (*S. halichoeri* subspecies *hominis*) and grey seal isolates (*S. halichoeri* subsp. *halichoeri*) (3). Our study examined recent clinical experience with *S. halichoeri* as a cause of bone and joint infections in patients in the United States with underlying health conditions. We describe phenotypic, genetic, and antimicrobial susceptibility characteristics of *S. halichoeri* recovered from clinical specimens.

Author affiliations: University of Utah/ARUP Laboratories, Salt Lake City, Utah, USA (S.M. Shakir, M.A. Fisher); Texas Health Presbyterian Hospital of Dallas, Dallas, Texas, USA (R. Gill, M. Feldman); Kaiser Permanente Regional Microbiology and Molecular Infectious Diseases Laboratories, Portland, Oregon, USA (J. Salberg, S.E. Sharp); ARUP Institute for Clinical and Experimental Pathology, Salt Lake City (E.S. Slechta); Marshfield Clinic Health System, Marshfield, Wisconsin, USA (T. Fritsche); University of Washington, Seattle, Washington, USA (J. Clarridge); Copan Diagnostics, Murrieta, California, USA (S.E. Sharp)

Materials and Methods

Bacterial Isolates

We included in this study 45 *S. halichoeri* isolates from 39 patients identified during 2010–2018 at ARUP Laboratories, a national clinical reference laboratory. Sixteen isolates were identified by DNA sequencing and 39 by matrix-assisted laser desorption/ionization time of flight (MALDI-TOF) mass spectrometry. We selected 5

isolates available in the strain repository for further characterization with traditional biochemical tests including pyrrolidonyl arylamidase (PYR), hippurate hydrolysis, and bile-esculin growth/hydrolysis (4). We determined Lancefield type using the Hardy StrepPro Grouping kit (<https://hardydiagnostics.com>). This study was approved by the University of Utah Institutional Review Board (no. 24431).

Antimicrobial Susceptibility Testing

Antimicrobial susceptibility testing (AST) results were available for 22 clinical isolates. We tested the isolates using Sensititer custom broth microdilution panels (<https://www.thermofisher.com>) in cation-adjusted Mueller-Hinton broth supplemented with 5% lysed horse blood. We determined MIC values for penicillin, ceftriaxone, daptomycin, vancomycin, clindamycin, erythromycin, levofloxacin, meropenem, doxycycline, and quinupristin/dalfopristin and interpreted results according to Clinical and Laboratory Standards Institute (CLSI; <https://clsi.org>) guidelines for viridans group *Streptococcus* species (CLSI M100 2019A). We performed quality control using *S. pneumoniae* ATCC 49619 according to CLSI guidelines (5).

MALDI-TOF Mass Spectrometry

We performed MALDI-TOF mass spectrometry as described elsewhere (6). Isolated colonies from Hardy Columbia sheep blood agar incubated at 35°C and 5% CO₂ were spread evenly on a polished steel target and overlaid with 1 µL of matrix (α -cyano-4-hydroxycinnamic acid in 50% acetonitrile, 47.5% water, and 2.5% trifluoroacetic acid) and air dried. We collected mass spectra as described elsewhere (6); each spectrum was a sum of 240 shots collected in increments of 40. We analyzed spectra using the Bruker Biotyper commercial database (<https://www.bruker.com>) and used scores of ≥ 1.9 for identification to the species level (6). Custom mass spectral profiles (main spectra, or MSPs) were created according to manufacturer's recommendations. In brief, we prepared extracts from 5–10 mg of cells using the standard formic acid-acetonitrile method; 10 replicate 1 µL aliquots were air dried on a polished steel target, then overlaid with 1 µL α -cyano-4-hydroxycinnamic acid and air dried. We collected spectra from each spot in triplicate and reviewed them in Bruker FlexAnalysis, then processed 24 spectra for MSP generation in Bruker CompassExplorer using default settings.

16S rRNA Gene Sequencing

We extracted bacterial DNA from 3 McFarland standard suspensions with the PerkinElmer Chemagig

MSM-automated extraction platform (<https://chemagen.com>), according to the manufacturer's instructions. Initially, we generated the first 500 bp of the 16S rRNA gene using 5F-T and 534R-T primers and subsequently generated nearly full-length 16S sequences with 5F, 357F, 534R, 806F, 1053R, and 1492R primers (7). We analyzed sequences using Pathogenomix RipSeq (<https://www.pathogenomix.com>) and BLAST (<https://blast.ncbi.nlm.nih.gov>). We performed phylogenetic analyses and generated neighbor-joining trees on partial and full-length sequences using MEGA version X software (<https://www.megasoftware.net>) (8).

S. halichoeri Clinical Context

We describe 3 representative clinical cases of *S. halichoeri* bone and joint infection to highlight the clinical disease progression and microbiological characteristics of this unusual organism. The first case-patient was a 43-year-old man with poorly controlled type 2 diabetes mellitus, hypertension, and stage 3 chronic kidney disease who sought treatment for a 7-week history of low back pain radiating to his legs. Spinal magnetic resonance imaging (MRI) revealed diffuse edema of the fourth lumbar vertebral body with a possible fracture. Results from fluoroscopy-guided vertebral biopsy were unremarkable. He was discharged with plans for a follow-up MRI in 1 month but was readmitted 2 weeks later with worsening low back pain. Leukocyte count was within reference range; erythrocyte sedimentation rate (110 mm/h; reference <20 mm/h) and C-reactive protein level (CRP; 5.79 mg/dL; reference <0.5 mg/dL) were elevated. MRI results suggested L3 and L4 vertebral osteomyelitis and diskitis. Fluoroscopy-guided L4 vertebral biopsy had negative stains and cultures for bacteria, mycobacteria, and fungi. Additional biopsies from L4 bone, L3–4 disk, and both posterior paraspinal areas were negative by Gram stain, but cultures from all 4 yielded gram-positive cocci in clusters that grew as tiny, whitish-gray, nonhemolytic colonies on SBA. The isolate was initially reported as coagulase-negative Staphylococci on the basis of phenotypic testing but later identified as *S. halichoeri* by MALDI-TOF mass spectrometry (Bruker Biotyper 5627 database) at ARUP Laboratories. The isolate (229 in this study) was catalase-positive when grown in SBA, PYR-positive, weakly positive for Lancefield B antigen, and hippurate hydrolysis negative. Gram stain from SBA showed cocci, mostly in clusters with a few small chains, but revealed substantial chaining when grown in broth, and catalase testing from Mueller-Hinton agar was negative, consistent with the genus *Streptococcus* (Table 1). The isolate was sensitive to all antimicrobials tested, including penicillin, vancomycin, levofloxacin, and

Table 1. Phenotypic characteristics of 5 *Streptococcus halichoeri* human clinical isolates, United States*

Isolate	Hemolysis	Catalase-SBA	Catalase-MHA	PYR	Esculin	Bile-esculin	Hippurate	Lancefield B antigen
018	Negative	Positive	Negative	Positive	Positive	Positive	Negative	Weak positive
116	Negative	Negative	Negative	Positive	Positive	Positive	Negative	Weak positive
076	Negative	Weak positive	Negative	Positive	Positive	Positive	Negative	Weak positive
229†	Negative	Positive	Negative	Positive	Positive	Positive	Negative	Weak positive
853‡	Negative	Positive	Negative	Positive	Positive	Positive	Negative	Weak positive

*MHA, Mueller-Hinton agar; PYR, pyrrolidonyl arylamidase; SBA, sheep blood agar.

†Isolate from patient described in case 1.

‡Isolate from patient described in case 2.

linezolid. Because of a penicillin allergy, the patient was treated with renally adjusted vancomycin (1,500 mg/18 h), but he continued to have back pain, and new weakness developed in his legs after 5 weeks of therapy. Subsequent MRI revealed disease progression with diffuse marrow edema and end-plate disruption of the L3–4 vertebrae along with phlegmon formation and myositis of both psoas muscles, prompting addition of meropenem to his treatment. Needle biopsy of L4 vertebrae revealed reactive bone with degenerative changes and chronic inflammation, but routine bacterial cultures were negative. The patient's symptoms improved after 7 additional weeks of intravenous vancomycin and meropenem. This treatment was followed by 6 weeks of oral minocycline and cefuroxime, during which time his back pain was alleviated and inflammatory markers normalized.

The second case-patient was a 68-year-old man admitted for planned removal of his infected left knee arthroplasty and left knee fusion. The patient had a history of hypertension and giant cell tumor of the left knee 3 years earlier; at that time, left total knee arthroplasty, curettage, and polymethylmethacrylate packing of the left tibia were performed without complications. Three months before his admission for the removal, the patient noted purulent draining lesions around the surgical site for which he was prescribed amoxicillin/clavulanate. Initial radiographs showed no evidence of tumor recurrence and stable-appearing changes of the left proximal tibia and left total knee arthroplasty. Chronic prosthetic joint infection was suspected, as well as left knee arthrofibrosis. Because of a rash attributed to amoxicillin/clavulanate, the patient was switched to trimethoprim/sulfamethoxazole, which was stopped ≈2 weeks before the planned second left knee arthroplasty. During the prosthetic joint removal procedure, knee fluid and resected tissue sent for culture grew 3 organisms: methicillin-susceptible *Staphylococcus aureus* and *S. epidermidis*, both identified by conventional phenotypic methods, and a third organism from thioglycolate broth that stained as gram-positive cocci in chains. This organism, which grew as white, nonhemolytic colonies on SBA and chocolate agar at 48 hours, was positive for catalase, PYR, leucine aminopeptidase, and bile-esculin

and negative for growth in media with 6.5% salt. The organism (isolate 853 in this study) was sent to ARUP laboratories, where it was identified as *S. halichoeri* by 16S rRNA sequencing. Eight separate cultures of the knee tissue grew *S. halichoeri*, methicillin-susceptible *S. aureus*, and *Fingoldia magna*. AAST of *S. halichoeri* by broth microdilution revealed susceptibility to all drugs tested for viridians group streptococci. The patient received treatment for the polymicrobial infection with intravenous ceftriaxone and oral rifampin for 6 weeks.

The third case-patient was a 68-year-old man with a pertinent history of poorly controlled type 2 diabetes mellitus with peripheral neuropathy and suspected arterial insufficiency, seeking treatment for a severe diabetic foot infection and altered mental status. The patient fulfilled 3 of 4 criteria for systemic inflammatory response syndrome: fever of 101.2°F, tachycardia (112 bpm), and leukocytosis (leukocytes 18 k/μL). He had elevated CRP (77 mg/L), erythrocyte sediment rate within reference range (21 mm/h), and elevated blood glucose (248 mg/dL; reference fasting glucose <100 mg/dL). Aside from confusion, the patient had edema, erythema, and pain of the right second toe. No previous history of chronic wound or drainage in this area was noted and the wound was provisionally attributed to a nail grinder. Radiographs showed no signs of osteomyelitis. The patient was started on broad-spectrum intravenous therapy with vancomycin and ampicillin/sulbactam, and he showed marked improvement in the edema and erythema of the toe. Blood cultures collected at the time of examination were negative, however cultures of a right second-toe abscess were positive for gram-positive cocci in chains. The organism grew as small, white, nonhemolytic colonies that were weakly positive for slide coagulase but tube coagulase negative. Catalase-positivity was observed when the organism grew on SBA and chocolate agar but not when grown on tryptic soy agar. The organism was typed as Lancefield group B by latex agglutination and was initially identified by the VITEK 2 system (bioMérieux, <https://www.biomerieux.com>) as *Streptococcus suis*. Because of the discrepancy between the Lancefield typing and VITEK 2 results, we performed 16S rRNA

sequencing, which identified the organism as *S. halichoeri*. Unfortunately, the isolate was not available for further testing in this study. The patient was transitioned to a 14-day course of oral trimethoprim/sulfamethoxazole and amoxicillin/clavulanate, and by 4 months after debridement, the patient's wound had healed.

S. halichoeri Infection Sites

We analyzed 45 *S. halichoeri* isolates from 39 patients identified during 2010–2018 at ARUP Laboratories. Most (n = 28, 71%) isolates were from male patients; 18 isolates (40%) were from wound infections, 9 (20%) from blood specimens, 7 (16%) from tissue, and 4 (9%) each from normally sterile body fluids (1 peritoneal fluid, 2 knee fluid, and 1 unspecified) and urine (9%). Of the 9 patients with positive blood cultures, 3 were also positive for the organism in urine, foot wound, or knee fluid cultures.

Microbiologic Characteristics of S. halichoeri Isolates

We performed a retrospective review of the microbiology results from the laboratory information system on 45 isolates of *S. halichoeri*. The laboratory performed Gram stains on all isolates, which were reported as gram-positive cocci in chains or clusters. All but 1 isolate failed to exhibit hemolysis on SBA plates. Most isolates (n = 29, 64%) were identified by MALDI-TOF mass spectrometry with the remainder (n = 18, 40%) by partial 16S rRNA gene sequencing. We selected 5 isolates available in our strain repository (including isolates from case-patients 1 and 2) for further characterization with biochemical and molecular methods (Table 1). Four of these isolates were catalase-positive when grown on SBA, but all 5 isolates were catalase-negative when grown on Mueller-Hinton agar lacking blood supplementation. All 5 isolates were PYR-positive, bile-esculin and esculin positive, hippurate-negative, and weakly reactive with Lancefield group B antiserum.

Antimicrobial susceptibility testing results were available for 22 clinical isolates (Table 2). All isolates were susceptible to ceftriaxone, daptomycin, levofloxacin, linezolid, meropenem, penicillin, and vancomycin. Six isolates (28%) were resistant to clindamycin and nonsusceptible to erythromycin (5 resistant, 1 intermediate).

16S rRNA Gene Sequence Analysis of S. halichoeri Isolates

We performed partial and near full-length 16S ribosomal RNA gene sequencing on the 5 selected clinical isolates. Partial 16S sequences of all isolates shared 97% identity with *Streptococcus canis* (ATCC 43496)

and 96% identity to *Streptococcus ictaluri* (ATCC BAA-1300) and *Streptococcus iniae* (ATCC 29178). Four isolates (018, 116, 076, and 229) were 99% identical to the partial 16S rRNA sequence of *S. halichoeri* strain M512/02/1 (type strain, CCUG 48324), however, isolate 853 was only 98% identical. With near full-length 16S rRNA sequence analysis, we observed the subspecies distinction proposed in a 2016 study (3). Isolates 018, 116 (GenBank accession no. MT771643), 229, and 853 were 98.5%–98.6% identical to the *S. halichoeri* subsp. *halichoeri*-type strain (GenBank accession no. KP851851) but were more closely related to clinical isolates characterized as *S. halichoeri* subsp. *hominis* (3). Phylogenetic analysis showed the tight clustering (99.9%–100% identity) of isolates 018, 116, 229, and 853 with the proposed *S. halichoeri* subsp. *hominis*-type strain (KP851845) and the 5 isolates from patients in the 2016 study (3) (Figure 1). In contrast, isolate 076 was more closely related to the *S. halichoeri* subsp. *halichoeri*-type strain (CCUG 48324, 99.7% sequence identity) and a *S. halichoeri* isolate from a badger with pyogranulomatous pleuropneumonia (GenBank accession no. KF021280, 99.9%) (9). Isolate 076 (GenBank accession no. MT771642) had 19–20 base substitutions distinct from the previously described *S. halichoeri* subsp. *hominis* isolates and isolates 018, 116, 229, and 853 (98.6%–98.7% identity), suggesting it is more closely related to animal than human strains.

Mass Spectra of S. halichoeri Isolates

We generated MALDI-TOF MSPs from the 5 selected *S. halichoeri* isolates and compared them with Bruker Biotyper database entries from related streptococcal species. The MSP dendrogram (Figure 2) shows that the *S. halichoeri* clinical isolates are readily distinguishable from other streptococci and cluster closely together with the *S. halichoeri* subsp. *halichoeri*-type strain. This suggests that the proposed subspecies are not currently distinguishable by MALDI-TOF mass spectrometry.

Discussion

The genus *Streptococcus* is composed of >130 species of gram-positive, catalase-negative bacteria that are found in a variety of environments. Several streptococcal species cause zoonotic infections in humans, including *S. canis*, *Streptococcus equi* subsp. *zooepidemicus*, *S. iniae*, and *S. suis* (10–13). *S. halichoeri* is one of the more recently identified zoonotic streptococci, first described in 2004 after isolation from gray seals (*H. grypus*) (1). It was originally described as a gram-positive, catalase-negative, nonhemolytic organism, occurring in pairs or short chains, and expressing Lancefield

group B antigen; this combination did not correspond to any previously identified *Streptococcus* species. 16S rRNA gene sequencing confirmed its placement in the genus *Streptococcus*, but the >3% divergence from described taxa suggested it was a novel species (1). *S. halichoeri* was also isolated from a European badger with pyogranulomatous pleuropneumonia (9) and from several canine and fur-producing animal species, including companion animals (14,15). These observations indicate a much broader host range than originally described for this organism.

The clinical laboratories at the Marshfield Clinic in Wisconsin have isolated this organism from both canine (n = 5) and feline (n = 1) clinical specimens (16). All isolates were nonhemolytic, had streptococcal morphology on Gram stain, were catalase and PYR-positive, and typed as Lancefield group B. Although initially reported as "*Streptococcus* species, unable to identify further," they were subsequently identified as *S. halichoeri* by MALDI-TOF mass spectrometry and 16S rRNA gene sequencing.

The first reported human infection with *S. halichoeri* was in a man with diabetes who sought treatment for an empyema; he reported handling fish before his illness (2). *S. halichoeri* was isolated from pleural fluid cultures as tiny, white, nonhemolytic colonies of gram-positive cocci in chains that could not be identified by standard phenotypic methods or 16S rRNA sequencing. The organism was positive for Lancefield group B antigen and was ultimately identified as *S. halichoeri* by MALDI-TOF mass spectrometry. The isolate was sensitive to penicillin and levofloxacin, and the patient's condition was successfully treated with 4 weeks of intravenous ceftriaxone after 10 days of levofloxacin.

Another reported human case was of an 84-year-old man with a history of diabetes who sought treatment for bacterial cellulitis of the left thigh following prior treatment for left-sided endocarditis and cellulitis at the same site due to *S. agalactiae* (17). Blood and wound culture isolates were initially identified as *S. pyogenes* by VITEK 2 and *S. agalactiae* by API 20 STREP (bioMérieux). The discordance in identification necessitated analysis at a reference laboratory where the isolates were identified as *S. halichoeri* by MALDI-TOF mass spectrometry but as *S. suis* by VITEK 2. Ultimately, both were confirmed as *S. halichoeri* by *sodA* and 16S rRNA gene sequencing. The isolates were sensitive to penicillin, levofloxacin, and linezolid but resistant to erythromycin, clindamycin, and tetracycline. The patient's condition was successfully treated with 15 days of amoxicillin.

Finally, a 2016 publication with limited clinical information highlighted 6 additional isolates recov-

Table 2. Antimicrobial susceptibility profiles for 22 human clinical isolates of *Streptococcus halichoeri*, United States*

Antimicrobial agent	MIC values, µg/mL			
	% Susceptible	Range	MIC ₅₀	MIC ₉₀
CRO	100	≤0.06–0.25	0.12	0.25
CLI	77.3	≤0.03 to ≥4	0.03	≥4
DAP	100	≤0.12–0.5	0.25	0.25
DOX†	NA‡	≤0.25–16	0.25	0.5
ERY	72.7	≤0.12 to ≥8	0.12	2
LVX	100	≤0.25–2	1	1
LZD	100	0.5–1	1	1
MEM	100	≤0.06–0.25	0.06	0.06
PEN	100	≤0.03–0.06	0.03	0.03
Q/D‡	94.7	≤0.25 to ≥4	0.25	0.25
VAN	100	≤0.5–1	0.5	0.5

*CLI, clindamycin; CRO, ceftriaxone; DAP, daptomycin; DOX, doxycycline; ERY, erythromycin; LVX, levofloxacin; LZD, linezolid; MEM, meropenem; MIC₅₀, MIC value at which ≥50% of the isolates in a test population are inhibited; MIC₉₀, MIC value at which ≥90% of the isolates in a test population are inhibited; NA, not available; PEN, penicillin; Q/D, quinupristin/dalfopristin; VAN, vancomycin.

†Clinical and Laboratory Standards Institute interpretive breakpoints for doxycycline were not available for viridans group *Streptococcus* spp. If breakpoints for *S. pneumoniae* were applied, 82% would be susceptible (5). ‡n = 19 isolates.

ered from human specimens (3). Most (4/6) isolates were from blood and were shown to have homogeneous phenotypes, sequence at multiple loci, and genomic similarities consistent with a difference at the subspecies level from the originally described *S. halichoeri* isolate, leading to proposal of the new taxon, *S. halichoeri* subsp. *hominis*. AST data on the 6 human isolates revealed susceptibility to most drugs tested, although 1 isolate was erythromycin resistant and 2 were tetracycline resistant.

It is unclear if *S. halichoeri* represents an emerging zoonosis, a rare but still underdiagnosed infection, or if it is simply being recognized only now because of improved identification methods (e.g., MALDI-TOF mass spectrometry). The source for infection with *S. halichoeri* is certainly not limited to marine life, because the organism has been isolated from both domestic and wild terrestrial mammals (14). Patients in the cases presented here had no known exposures to animals; therefore, reservoirs for infection by *S. halichoeri* might be more widespread than once thought.

S. halichoeri was originally described as catalase-negative, but our testing confirmed reports that it can be catalase-positive when grown on blood-supplemented media. This observation is not unprecedented for *Streptococcus*-like organisms; some streptococci and enterococci can be weakly catalase-positive when grown on media containing blood (4). However, some *S. halichoeri* isolates are strongly catalase-positive under these conditions, leading to the risk of misidentification (Table 1). A 2020 study identified genes in some *S. halichoeri* isolates highly similar to known catalase genes, potentially

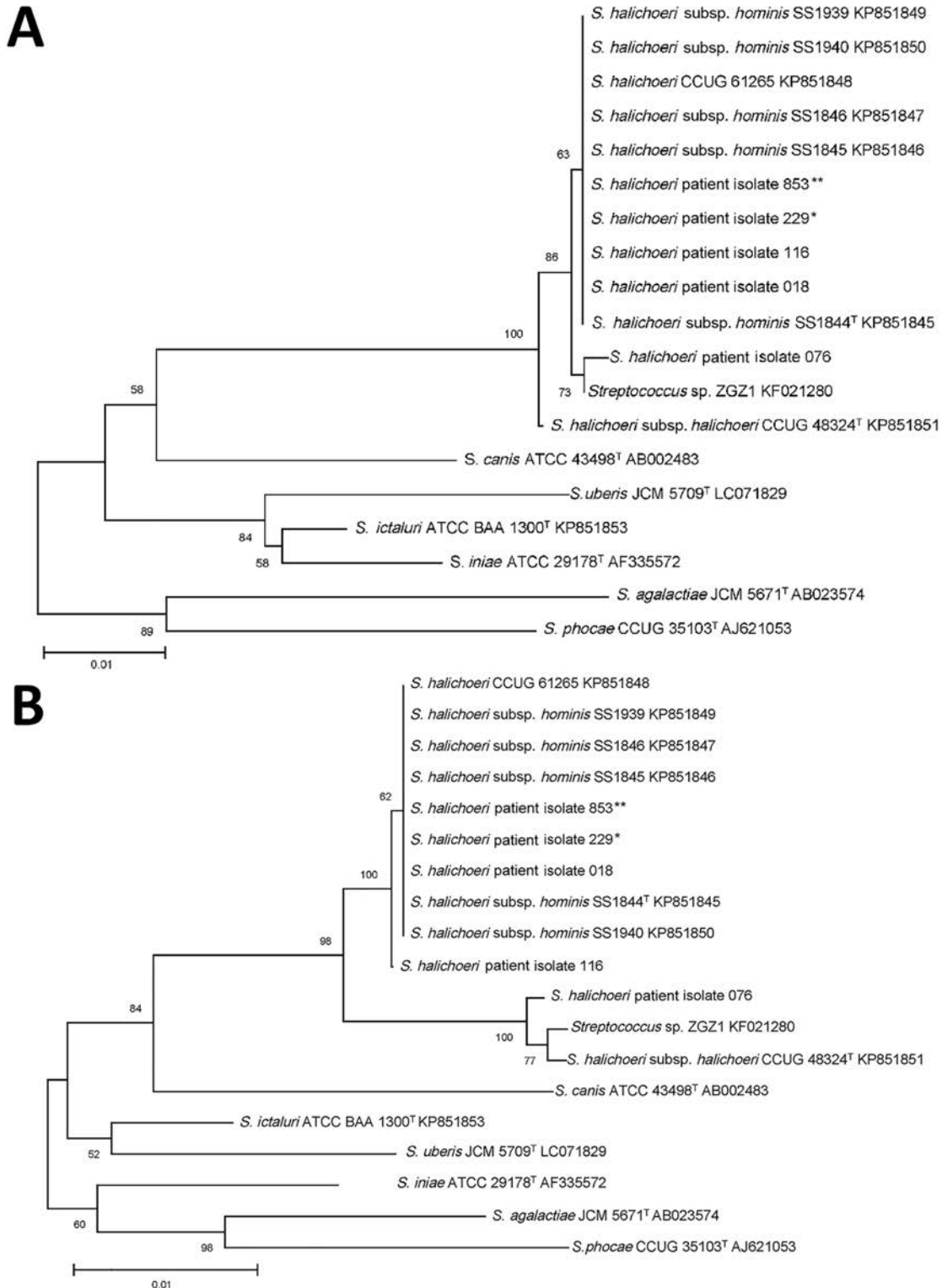


Figure 1. Phylogenetic trees based on 16S sequences of clinical and type strains of *Streptococcus halichoeri* and related taxa used in study of human infections caused by unusual strains of *S. halichoeri*, United States. A) Partial sequences (496 nt); B) full-length sequences (1,434 nt). We generated alignments using ClustalW (<http://www.clustal.org>), trimmed them to the length of the shortest sequence, and computed neighbor-joining trees with bootstrap analysis with 1,000 replicates using MEGA X (<https://www.megasoftware.net>). Isolates from case-patients are represented with asterisks (*patient 1; **patient 2). [†] indicates type strains.

explaining these phenotypic observations (14). Whereas phenotypic methods may be misleading, MALDI-TOF mass spectrometry is a rapid and reliable method for identifying *S. halichoeri* (Figure 2). As the MALDI-TOF mass spectrometry method becomes more widely available, we may begin to identify more infections caused by *S. halichoeri* and other underrecognized bacteria (6). In the absence of MALDI-TOF mass spectrometry, laboratories should consider further testing on atypical isolates from deep wound and sterile body sites when they are phenotypically identified as coagulase-negative staphylococci but morphologically consistent with streptococci.

S. halichoeri subsp. *hominis* isolates were described as positive for bile-esculin, esculin, and acid from sucrose fermentation, but *S. halichoeri* subsp. *halichoeri* was negative for all 3 tests (3), suggesting possible phenotypic distinction of the subspecies. The 5 clinical isolates we characterized were positive for bile-esculin and esculin; 4 of them (isolates 018, 116, 229, and 583) were most closely related to *S. halichoeri* subsp. *hominis* by full-length 16S sequencing. Surprisingly, isolate 076 was positive for bile-esculin and esculin, like *S. halichoeri* subsp. *hominis*, but was nearly identical to the full-length 16S rRNA sequences from *S. halichoeri* subsp. *halichoeri* from both gray seals and badgers. This apparent discrepancy suggests that isolate 076 was a phenotypic variant of the *S. halichoeri* subsp. *halichoeri*. However, because of

limited published data, the reliability of esculin or other phenotypic tests for distinguishing these proposed subspecies is unknown. Unfortunately, we do not have information on recent zoonotic exposures for isolate 076.

There are several parallels between the patients reported in our study, 2 of whom had diabetes, and the patients from the 2 previously published cases, both of whom also had diabetes (2,17). These similarities may indicate an opportunistic nature of this organism, in which establishing infection requires diabetes or an immunocompromised state. A similar association with diabetes mellitus has been observed among fishmongers who have contracted zoonotic infections through occupational exposures (13). Diabetes mellitus is also one of the most common coexisting health conditions associated with group B *Streptococcus* infection (18,19). One patient from this study and 1 from another study (2) had purulent infections, which may indicate pathogenic potential similar to the pyogenic streptococci, to which *S. halichoeri* is closely related (20).

All isolates in this study, as well as those in previous reports, were susceptible to β -lactams and levofloxacin, which may be considered antimicrobials of choice; daptomycin, linezolid, and vancomycin also showed very good antimicrobial activity. Our AST analysis showed that 5 (23%) of 22 isolates were resistant to erythromycin and 4 (18%) were nonsusceptible to doxycycline (when CLSI

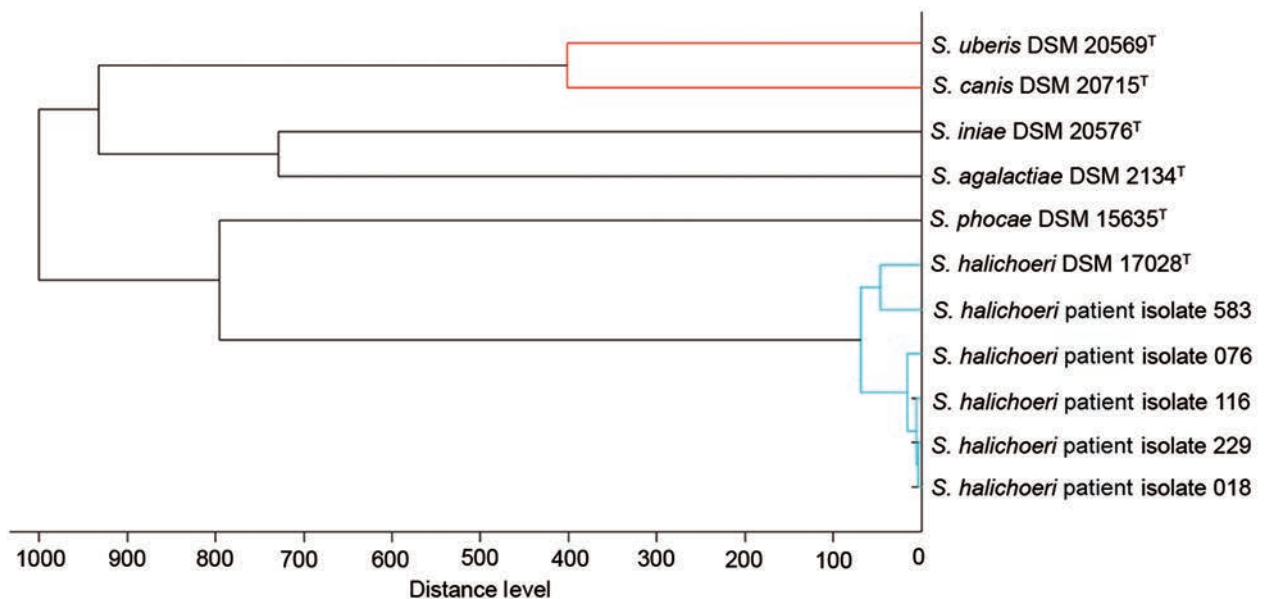


Figure 2. Matrix-assisted laser desorption/ionization time of flight mass spectrometry profile dendrogram of selected pyogenic and zoonotic streptococci used in study of human infections caused by unusual strains of *Streptococcus halichoeri*, United States. We compared main spectra from *S. halichoeri* isolates to Bruker Biotyper (<https://www.bruker.com>) database entries from related streptococcal species. Distance level indicates relative similarity of mass spectral profiles. ^T indicates type strains.

breakpoints for *S. pneumoniae* were applied) (5), similar to observations made elsewhere (3). This analysis highlights the relative antimicrobial susceptibility of *S. halichoeri* isolates, but the exceptions point out the need to monitor the susceptibility patterns of this emerging pathogen. Given its phenotypic similarities with coagulase-negative staphylococci and the viridans group streptococci, it is likely that *S. halichoeri* continues to be disregarded by some as a skin commensal rather than a true cause of infection. In addition, our study highlights the importance of recognizing *S. halichoeri* infections and the role of MALDI-TOF mass spectrometry and 16S rRNA gene sequencing in accurately identifying this pathogen.

About the Author

Dr. Shakir is the medical director of the Microbial Amplified Detection Laboratory at ARUP Laboratories and assistant professor of pathology at the University of Utah School of Medicine in Salt Lake City. Her research interests include implementation and effective use of molecular assays for sexually transmitted diseases and women's health. Dr. Gill is a full-time hospitalist and associate program director of the internal medicine residency program at Texas Health Presbyterian Hospital in Dallas.

References

1. Lawson PA, Foster G, Falsen E, Davison N, Collins MD. *Streptococcus halichoeri* sp. nov., isolated from grey seals (*Halichoerus grypus*). *Int J Syst Evol Microbiol*. 2004;54:1753–6. <https://doi.org/10.1099/ijms.0.63082-0>
2. Foo RM, Chan D, Doern GV. A fishy tale: a man with empyema caused by *Streptococcus halichoeri*. *J Clin Microbiol*. 2014;52:681–2. <https://doi.org/10.1128/JCM.03055-13>
3. Shewmaker PL, Whitney AM, Humrighouse BW. Phenotypic, genotypic, and antimicrobial characteristics of *Streptococcus halichoeri* isolates from humans, proposal to rename *Streptococcus halichoeri* as *Streptococcus halichoeri* subsp. *halichoeri*, and description of *Streptococcus halichoeri* subsp. *hominis* subsp. nov., a bacterium associated with human clinical infections. *J Clin Microbiol*. 2016;54:739–44. <https://doi.org/10.1128/JCM.03214-15>
4. Jorgensen JH, Pfaller MA, Carroll KC, Funke G, Landry ML, Richter SS, et al. *Manual of clinical microbiology*. 11th ed. Washington: American Society of Microbiology; 2015.
5. Clinical and Laboratory Standards Institute. *Performance standards for antimicrobial susceptibility testing*. 29th ed. CLSI supplement M100. Wayne (PA): Clinical and Laboratory Standards Institute; 2019.
6. Khot PD, Couturier MR, Wilson A, Croft A, Fisher MA. Optimization of matrix-assisted laser desorption ionization-time of flight mass spectrometry analysis for bacterial identification. *J Clin Microbiol*. 2012;50:3845–52. <https://doi.org/10.1128/JCM.00626-12>
7. Kallstrom G, Chang T, Albertson M, Morilla D, Fisher MA, Eberly B. Recovery of a catalase-negative *Staphylococcus epidermidis* strain in blood and urine cultures from a patient with pyelonephritis. *J Clin Microbiol*. 2011;49:4018–9. <https://doi.org/10.1128/JCM.01031-11>
8. Kumar S, Stecher G, Li M, Knyaz C, Tamura K. MEGA X: Molecular Evolutionary Genetics Analysis across computing platforms. *Mol Biol Evol*. 2018;35:1547–9. <https://doi.org/10.1093/molbev/msy096>
9. Moreno B, Bolea R, Morales M, Martín-Burriel I, González C, Badiola JJ. Isolation and phylogenetic characterization of *Streptococcus halichoeri* from a European badger (*Meles meles*) with pyogranulomatous pleuropneumonia. *J Comp Pathol*. 2015;152:269–73. <https://doi.org/10.1016/j.jcpa.2014.12.012>
10. Eisenberg T, Hudemann C, Hossain HM, Hewer A, Tello K, Bandorski D, et al. Characterization of five zoonotic *Streptococcus suis* strains from Germany, including one isolate from a recent fatal case of streptococcal toxic shock-like syndrome in a hunter. *J Clin Microbiol*. 2015;53:3912–5. <https://doi.org/10.1128/JCM.02578-15>
11. Fulde M, Valentin-Weigand P. Epidemiology and pathogenicity of zoonotic streptococci. *Curr Top Microbiol Immunol*. 2013;368:49–81. https://doi.org/10.1007/82_2012_277
12. Weinstein MR, Litt M, Kertesz DA, Wyper P, Rose D, Coulter M, et al.; S. iniae Study Group. Invasive infections due to a fish pathogen, *Streptococcus iniae*. *N Engl J Med*. 1997; 337:589–94. <https://doi.org/10.1056/NEJM199708283370902>
13. Yacoub A, Janz T, Mojica L, Jones L, Greene JN. A fish-monger's tale: a case report and review of literature. *Infect Dis Clin Pract*. 2015;23:248–53. <https://doi.org/10.1097/IPC.0000000000000234>
14. Aaltonen K, Kant R, Eklund M, Raunio-Saarnisto M, Paulin L, Vapalahti O, et al. *Streptococcus halichoeri*: comparative genomics of an emerging pathogen. *Int J Genomics*. 2020;2020:8708305. <https://doi.org/10.1155/2020/8708305>
15. Eklund M, Aaltonen K, Sironen T, Raunio-Saarnisto M, Grönthal T, Nordgren H, et al. Comparison of *Streptococcus halichoeri* isolates from canine and fur animal infections: biochemical patterns, molecular characteristics and genetic relatedness. *Acta Vet Scand*. 2020;62:26. <https://doi.org/10.1186/s13028-020-00525-3>
16. Bulgrin BM, Stemper ME, Rentschler AE, Novicki TJ, Moore FM, Fritsche TR. Utilization of MALDI-TOF mass spectrometry for the rapid identification of *Streptococcus halichoeri* infections in canines: a novel pathogen and host range expansion. American Society of Microbiology 112th General Meeting; 2012 June 16–19; San Francisco, CA, USA.
17. Del Giudice P, Plainvert C, Hubiche T, Tazi A, Fribourg A, Poyart C. Infectious cellulitis caused by *Streptococcus halichoeri*. *Acta Derm Venereol*. 2018;98:378–9. <https://doi.org/10.2340/00015555-2837>
18. Farley MM, Strasbaugh LJ, Group B. Group B streptococcal disease in nonpregnant adults. *Clin Infect Dis*. 2001;33:556–61. <https://doi.org/10.1086/322696>
19. Jackson LA, Hilsdon R, Farley MM, Harrison LH, Reingold AL, Plikaytis BD, et al. Risk factors for group B streptococcal disease in adults. *Ann Intern Med*. 1995;123:415–20. <https://doi.org/10.7326/0003-4819-123-6-199509150-00003>
20. Köhler W. The present state of species within the genera *Streptococcus* and *Enterococcus*. *Int J Med Microbiol*. 2007;297:133–50. <https://doi.org/10.1016/j.jimm.2006.11.008>

Address for correspondence: Salika M. Shakir, University of Utah, Department of Pathology, ARUP Laboratories, 500 Chipeta Way, Salt Lake City, UT 84108, USA; email: salika.shakir@aruplab.com

Use of Genomics to Track Coronavirus Disease Outbreaks, New Zealand

Jemma L. Geoghegan,¹ Jordan Douglas,¹ Xiaoyun Ren, Matthew Storey, James Hadfield, Olin K. Silander, Nikki E. Freed, Lauren Jelley, Sarah Jefferies, Jillian Sherwood, Shevaun Paine, Sue Huang, Andrew Sporle, Michael G. Baker, David R. Murdoch, Alexei J. Drummond, David Welch, Colin R. Simpson, Nigel French, Edward C. Holmes, Joep de Lig

Real-time genomic sequencing has played a major role in tracking the global spread of severe acute respiratory syndrome coronavirus 2 (SARS-CoV-2), contributing greatly to disease mitigation strategies. In August 2020, after having eliminated the virus, New Zealand experienced a second outbreak. During that outbreak, New Zealand used genomic sequencing in a primary role, leading to a second elimination of the virus. We generated genomes from 78% of the laboratory-confirmed samples of SARS-CoV-2 from the second outbreak and compared them with the available global genomic data. Genomic sequencing rapidly identified that virus causing the second outbreak in New Zealand belonged to a single cluster, thus resulting from a single introduction. However, successful identification of the origin of this outbreak was impeded by substantial biases and gaps in global sequencing data. Access to a broader and more heterogeneous sample of global genomic data would strengthen efforts to locate the source of any new outbreaks.

A genome of the novel severe acute respiratory syndrome coronavirus 2 (SARS-CoV-2) was published only 12 days after the virus was identified

Author affiliations: University of Otago, Dunedin, New Zealand (J.L. Geoghegan); Institute of Environmental Science and Research, Wellington, New Zealand (J.L. Geoghegan, X. Ren, M. Storey, L. Jelley, S. Jefferies, J. Sherwood, S. Paine, S. Huang, J. de Lig); University of Auckland, Auckland, New Zealand (J. Douglas, A. Sporle, A.J. Drummond, D. Welch); Fred Hutchinson Cancer Research Centre, Seattle, Washington, USA (J. Hadfield); Massey University, Auckland (O.K. Silander, N.E. Freed); iNZight Analytics Ltd., Auckland (A. Sporle); University of Otago, Wellington (M.G. Baker); University of Otago, Christchurch, New Zealand (D.R. Murdoch); Victoria University of Wellington, Wellington (C.R. Simpson); University of Edinburgh, Edinburgh, Scotland, UK (C.R. Simpson); Massey University, Palmerston North, New Zealand (N. French); The University of Sydney, Sydney, New South Wales, Australia (E.C. Holmes)

DOI: <https://doi.org/10.3201/eid2705.204579>

(1). This information was pivotal to the subsequent rapid development of diagnostic tests and identification of potential treatments (2,3). As of January 2021, ≈400,000 genomes of SARS-CoV-2 had been shared publicly (4). The underlying genome sequencing was performed so rapidly that during this infectious disease outbreak, virologic and epidemiologic data could be integrated in real time (5). Analysis of these data also played a role in informing the coronavirus disease (COVID-19) response by tracking the global spread and evolution of SARS-CoV-2, including identification of the number, source, and timing of introductions into individual countries, leading to a greater understanding of COVID-19 outbreaks around the world (6–9; A.D.S. Filipe et al., unpub. data, <https://www.medrxiv.org/content/10.1101/2020.06.08.20124834v1>; T. Seemann et al., unpub. data, <https://www.medrxiv.org/content/10.1101/2020.05.12.20099929v1>; L. Zhang et al., unpub. data, <https://www.biorxiv.org/content/10.1101/2020.06.12.148726v1>; J. Douglas et al., unpub. data, <https://www.medrxiv.org/content/10.1101/2020.08.04.20168518v1>).

As of January 2021, of the 219 countries that had reported positive cases of COVID-19 to the World Health Organization (WHO) (10), 65% (n = 142) had sequenced and shared SARS-CoV-2 genomes on the GISAID database (<https://www.gisaid.org>) (4). This immense global sequencing effort has enhanced ongoing genomic surveillance of the pandemic, including the monitoring of viral genetic changes of interest (L. Zhang et al., unpub. data, <https://www.biorxiv.org/content/10.1101/2020.06.12.148726v1>) and informing public health responses (11–14). Nevertheless, the number and proportion of SARS-CoV-2 genomes from COVID-19 case-patients that were sequenced, and genomes published, varies dramatically between

¹These authors contributed equally to this article.

countries and over time (Figure 1). For example, the COVID-19 Genomics UK Consortium (<https://www.cogconsortium.uk>) has led to the United Kingdom being the most represented sampling location, totaling $\approx 180,000$ genomes and comprising 44% of the global dataset despite recording only $\approx 4\%$ of the world's positive cases ($n = 3,669,658$). Conversely, SARS-CoV-2 genomes sequenced in India represent just 1% of the global dataset but 11% of the world's total reported cases ($n = 10,677,710$).

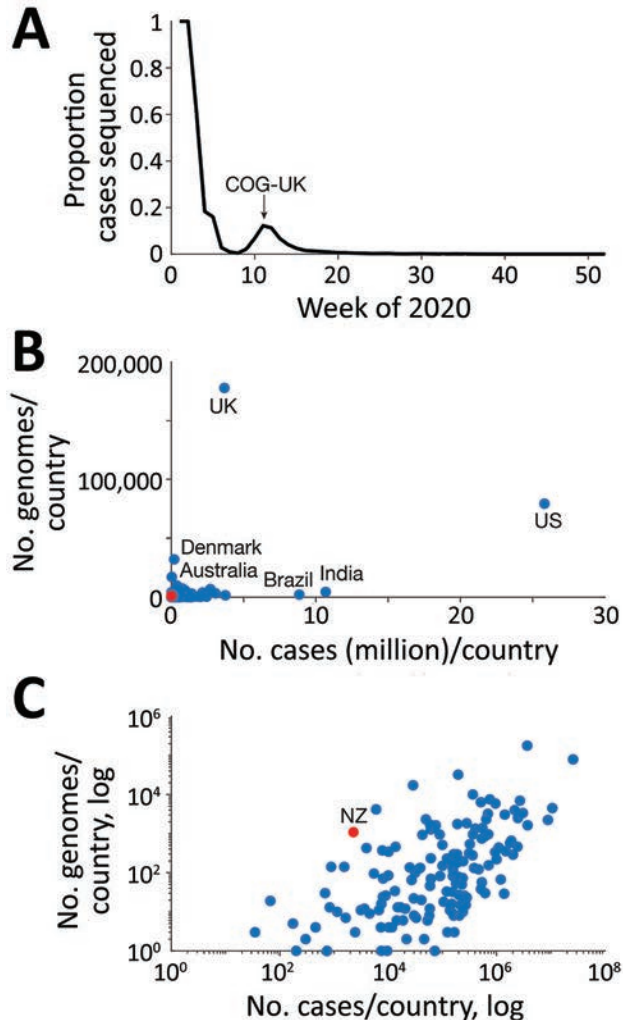


Figure 1. Sequenced and published genomes of global severe acute respiratory syndrome coronavirus 2 isolates. A) Proportion of global cases sequenced and shared on GISAID (<https://www.gisaid.org>) from December 2019 through January 2021, for which the second mode was largely driven by COG-UK as illustrated. B) Number of genomes sequenced and number of reported cases per country on a linear scale. Red, New Zealand (NZ); blue, other countries. C) Number of genomes sequenced and number of reported cases per country on a logarithmic scale. COG-UK, COVID-19 Genomics UK Consortium (<https://www.cogconsortium.uk>); UK, United Kingdom; US, United States.

Such disparate sequencing efforts can have major implications for data interpretation and must be carefully considered. Real-time sequencing of SARS-CoV-2 genomes has, however, been particularly useful for tracking the re-emergence of the virus in New Zealand. By June 2020, New Zealand had effectively eliminated COVID-19 in the community and positive cases were limited to those linked to managed quarantine facilities at the border (7,15; J. Douglas et al., unpub. data, <https://www.medrxiv.org/content/10.1101/2020.08.04.20168518v1>). After ≈ 100 days with no detected community transmission of COVID-19, on August 11, 2020, four new cases emerged with no apparent epidemiologic link to any known case. We used genomic sequencing of SARS-CoV-2 cases to investigate the probable origins of this outbreak, generating genomes for 78% ($n = 140$) of the 179 laboratory-confirmed samples from this outbreak.

We obtained nasopharyngeal samples positive for SARS-CoV-2 by real-time reverse transcription PCR (rRT-PCR) from public health medical diagnostics laboratories located throughout New Zealand. All samples had been de-identified before receipt. Under contract for the New Zealand Ministry of Health, the Institute of Environmental Science and Research (ESR) has approval to conduct genomic sequencing for surveillance of notifiable diseases.

Methods

Genomic Sequencing

Of 179 laboratory-confirmed samples of SARS-CoV-2 from the August 2020 outbreak in New Zealand, 172 were received by ESR for whole-genome sequencing. Genome sequencing of SARS-CoV-2 samples was performed as before (7). In brief, viral extracts were prepared from respiratory tract samples in which SARS-CoV-2 was detected by rRT-PCR by using World Health Organization–recommended primers and probes targeting the envelope and nucleocapsid genes. Extracted RNA from SARS-CoV-2–positive samples was subjected to whole-genome sequencing by following the ARTIC network protocol version 3 (<https://www.protocols.io/view/ncov-2019-sequencing-protocol-v3-locost-bh42j8ye>) and using the Massey University 1200-bp primer set (<https://www.protocols.io/view/ncov-2019-sequencing-protocol-rapid-barcoding-1200-bh7hj9j6>) (16).

We used 1 of the tiling amplicon designs to amplify viral cDNA prepared with SuperScript IV (ThermoFisher Scientific, <https://www.thermofisher.com>). Sequence libraries were then constructed by using Oxford Nanopore Ligation Sequencing and Native

Barcoding Expansion kits for samples amplified with the ARTIC version 3 primer sets and the Oxford Nanopore Rapid Barcoding Kit for samples amplified with the 1,200-bp primer sets (<https://nanoporetech.com>). We used the 1,200-bp primers and rapid barcoding when genomes were required urgently. Libraries were sequenced by using R9.4.1 MinION flow cells (Oxford Nanopore). Near-complete (>90% recovered) viral genomes were subsequently assembled through reference mapping. Steps included in the pipeline are described in detail at https://github.com/ESR-NZ/NZ_SARS-CoV-2_genomics. The reads generated with Nanopore sequencing using ARTIC primer sets (version 3) were mapped and assembled by using the ARTIC bioinformatics Medaka pipeline version 1.1.0. In total, 140 of 172 genomes from the August 2020 outbreak passed quality control. All data are available on GISAID (<https://www.gisaid.org>).

Phylogenetic Analysis

All SARS-CoV-2 genomes from humans, assigned to the B.1.1.1. lineage in the pangolin nomenclature (17), were obtained from GISAID (4) ($n = 7,363$ as of January 26, 2021) and subsampled to include 1,996 most recent-in-time sequences to the August 2020 New Zealand outbreak along with 4 outgroup (non-B.1.1.1.) sequences. Sequences were aligned with those from the August 2020 outbreak ($n = 140$) by using MAFFT version 7 (18) and the FFT-NS-2 progressive alignment algorithm (Appendix 1, <https://wwwnc.cdc.gov/EID/article/27/5/20-4579-App1.xlsx>). Bayesian phylogenetic analyses were performed by using BEAST 2.5 (19). We used a strict clock model with an HKY (Hasegawa, Kishino, and Yano) substitution model (estimated frequencies) for each codon position and 1 for noncoding positions. We used the Bayesian skyline model (20) as a tree to allow effective population sizes to change over time intervals. These components of the model and their prior distributions have been previously used (J. Douglas et al., unpub. data, <https://www.medrxiv.org/content/10.1101/2020.08.04.20168518v1>). Phylogenetic trees were annotated by using FigTree version 1.4 (<http://tree.bio.ed.ac.uk/software/figtree>) and Tree of Life version 4 (21).

Results

Of the virus genomes generated in real time for 78% of cases in this cluster, from August 11 through September 14, 2020, when the last case in this outbreak was reported, the maximum distance among the genome was 5 single-nucleotide polymorphisms. When we compared the genomes from patients in the

August 2020 New Zealand outbreak with sequenced genomes from patients affected by the first COVID-19 wave in New Zealand and those in quarantine facilities, we found no link. Most available sequence data from case-patients in New Zealand quarantine facilities indicated virus lineages different from those of the August 2020 outbreak. However, this observation was of limited value given that only 42% of case-patients in those quarantine facilities had adequate viral RNA for successful genomic sequencing. To determine the likely origins of this outbreak, we compared genomes from the new community outbreak to the global dataset.

An initial genomic sequence analysis found that the reemergence of COVID-19 in New Zealand was caused by a SARS-CoV-2 from the (now ancestral) lineage B.1.1.1 of the pangolin nomenclature (17). Of the countries that have contributed SARS-CoV-2 data, 30% had genomes of this lineage. Remarkably, 80% of B.1.1.1. genomes were from the United Kingdom and were generated during March 2020–January 2021; however, most samples were collected during the first wave of disease in the United Kingdom (Figure 2). Phylogenetic analysis of the most recently sampled B.1.1.1. genomes identified genomes from South Africa, England, and Switzerland in August as the most likely to be contained within the sister clade (Figure 2); these genomes were the closest sampled genomic relatives of the viruses associated with the August 2020 outbreak in New Zealand (Appendix 2, <https://wwwnc.cdc.gov/EID/article/27/5/20-4579-App2.pdf>). Because of the dynamic nature of the pangolin lineage nomenclature, genomes sampled from the August 2020 outbreak in New Zealand are now distinctly classified as lineage C.12, which is now extinct.

Additional Bayesian analysis estimated that the outbreak originated 10 days before the first transmission event; the 95% highest posterior density was 0–25 days. We also estimated that the first transmission event in the outbreak occurred during July 22–August 13, 2020 (95% highest posterior density mean date of August 2). Epidemiologic data showed that 2 confirmed case-patients linked to the outbreak had a symptom onset date of July 31, although the most probable sampled genomes within the sister clade were sampled later, August 6–28. Hence, it is unlikely that the currently available global genomic dataset contains the source of this outbreak.

Discussion

Genomic epidemiologic analysis of the possible origins of the COVID-19 re-emergence in New Zealand

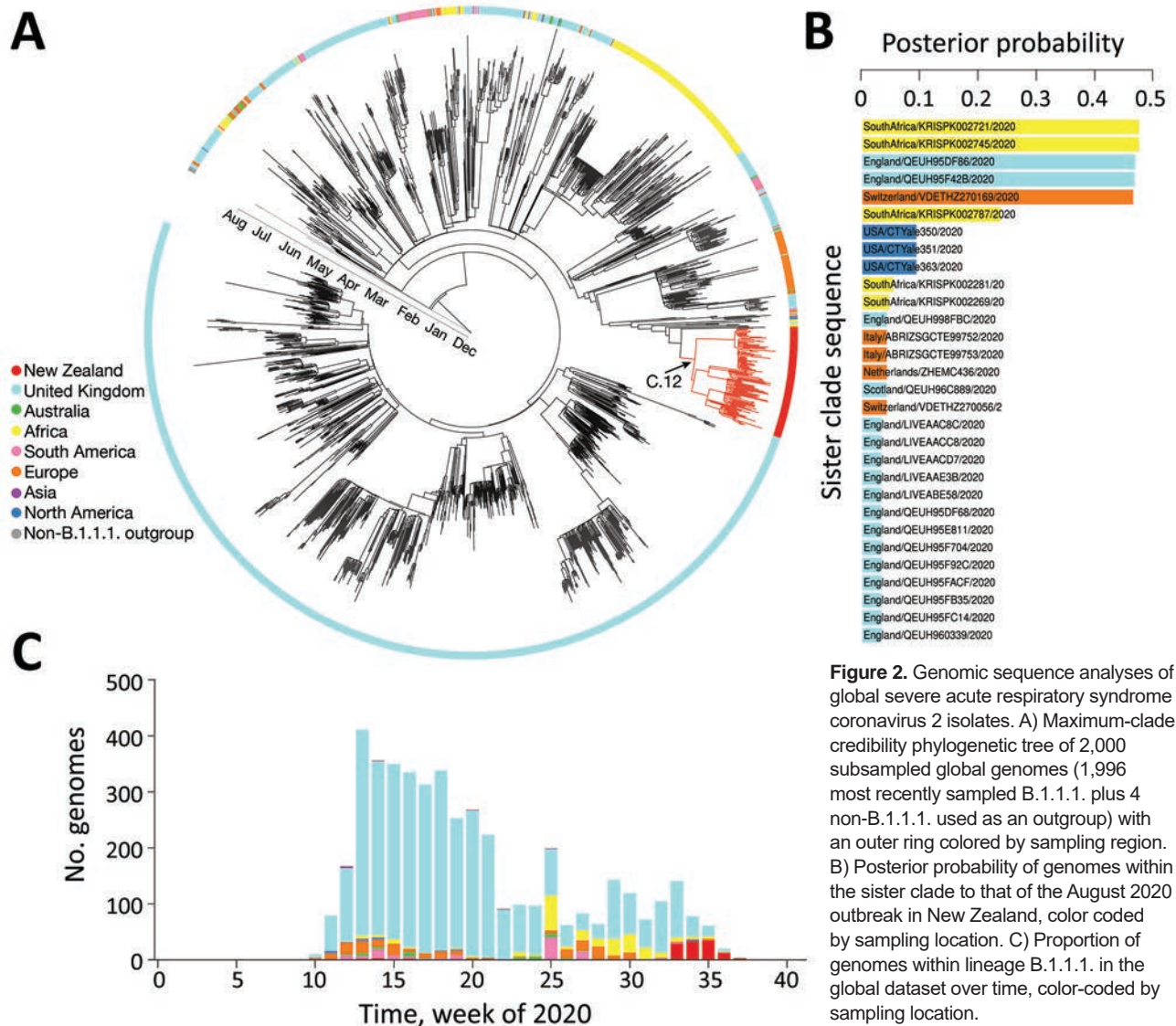


Figure 2. Genomic sequence analyses of global severe acute respiratory syndrome coronavirus 2 isolates. A) Maximum-clade credibility phylogenetic tree of 2,000 subsampled global genomes (1,996 most recently sampled B.1.1.1. plus 4 non-B.1.1.1. used as an outgroup) with an outer ring colored by sampling region. B) Posterior probability of genomes within the sister clade to that of the August 2020 outbreak in New Zealand, color coded by sampling location. C) Proportion of genomes within lineage B.1.1.1. in the global dataset over time, color-coded by sampling location.

in August 2020 was inconclusive, probably because of missing genomic data within the quarantine border facilities and in the global dataset. A glimpse into the genomic diversity probably omitted from the global dataset can be seen in the genomes sequenced in New Zealand from SARS-CoV-2-positive quarantined case-patients, comprising citizens and residents returning from across the globe. For example, 12 SARS-CoV-2 genomes from persons returning to New Zealand from India who arrived on the same flight fell across at least 4 genomic lineages and comprised sequence divergence of up to 34 single-nucleotide polymorphisms (<https://www.nextstrain.org>). This divergence represented far more genomic mutations than was observed in New Zealand during the first outbreak in March–May 2020 (7). Such a high level of

diversity in just a small sample of SARS-CoV-2-positive case-patients from India suggests that the currently available genomic data fail to encompass the true diversity that existed locally, let alone globally.

The genome sequences identified after the re-emergence of SARS-CoV-2 in New Zealand in August 2020 exemplified one of the most complete genomic datasets for a specific outbreak compiled to date, comprising 78% of positive case-patients (140 of 179 total case-patients SARS-CoV-2 positive by PCR). Real-time genomic sequencing quickly informed track-and-trace efforts to control the outbreak, setting New Zealand on track to eliminate the virus from the community for the second time. The rapid genome sequencing of positive samples provided confidence to public health teams regarding links to the outbreak and identified that

cases and subclusters were linked to a single genomic lineage, resulting from a single introduction event. Indeed, the timing and length of lockdown measures were partly informed on the basis of these data. Overall, real-time viral genomics has played a pivotal role in eliminating COVID-19 from New Zealand and has since helped prevent additional regional lockdowns, leading to substantial economic savings.

Nevertheless, the biased nature of global sampling, including the contribution of very few genome sequences from certain geographic locations, clearly limited the power of genomics to attribute the geographic origin of the August 2020 outbreak in New Zealand. We therefore advocate that potential sampling biases and gaps in available genomic data be carefully considered whenever attempting to determine the geographic origins of a specific SARS-CoV-2 outbreak. Analyses should consider all available evidence, including that from genomic and epidemiologic sources.

This article was preprinted at <https://www.medrxiv.org/content/10.1101/2020.10.28.20221853v1>.

Acknowledgments

We thank the ARTIC network for making their protocols and tools openly available and specifically Josh Quick for sending the initial V1 and V3 amplification primers. We thank the diagnostic laboratories that performed the initial rRT-PCRs and referred samples for sequencing as well as the public health units for providing epidemiologic data. We thank Genomics Aotearoa for their support, the NextStrain team for their support and timely global and local analysis, and all those who have contributed SARS-CoV-2 sequences to the GenBank and GISAID databases. We also acknowledge the use of New Zealand eScience Infrastructure (NeSI) high-performance computing facilities.

This work was funded by the Ministry of Health of New Zealand, New Zealand Ministry of Business, Innovation and Employment COVID-19 Innovation Acceleration Fund (CIAF-0470), ESR Strategic Innovation Fund, and the New Zealand Health Research Council (20/1018 and 20/1041). New Zealand's national facilities are provided by NeSI and funded jointly by NeSI's collaborator institutions and through the Ministry of Business, Innovation and Employment's Research Infrastructure program.

About the Author

Dr. Geoghegan is an evolutionary virologist at the University of Otago, Dunedin, New Zealand, and the Institute of Environmental Science and Research, Wellington, New Zealand. Her research focus is understanding how viruses emerge and spread in new populations.

References

1. Holmes EC. Novel 2019 coronavirus genome [cited 2021 Jan 20]. <https://virological.org/t/novel-2019-coronavirus-genome/319>
2. Shin MD, Shukla S, Chung YH, Beiss V, Chan SK, Ortega-Rivera OA, et al. COVID-19 vaccine development and a potential nanomaterial path forward. *Nat Nanotechnol.* 2020;15:646–55. <https://doi.org/10.1038/s41565-020-0737-y>
3. Stebbing J, Phelan A, Griffin I, Tucker C, Oechsle O, Smith D, et al. COVID-19: combining antiviral and anti-inflammatory treatments. *Lancet Infect Dis.* 2020;20:400–2. [https://doi.org/10.1016/S1473-3099\(20\)30132-8](https://doi.org/10.1016/S1473-3099(20)30132-8)
4. Elbe S, Buckland-Merrett G. Data, disease and diplomacy: GISAID's innovative contribution to global health. *Glob Chall.* 2017;1:33–46. <https://doi.org/10.1002/gch2.1018>
5. Hadfield J, Megill C, Bell SM, Huddleston J, Potter B, Callender C, et al. Nextstrain: real-time tracking of pathogen evolution. *Bioinformatics.* 2018;34:4121–3. <https://doi.org/10.1093/bioinformatics/bty407>
6. Bedford T, Greninger AL, Roychoudhury P, Starita LM, Famulare M, Huang M-L, et al.; Seattle Flu Study Investigators. Cryptic transmission of SARS-CoV-2 in Washington state. *Science.* 2020;370:571–5. <https://doi.org/10.1126/science.abc0523>
7. Geoghegan JL, Ren X, Storey M, Hadfield J, Jelley L, Jefferies S, et al. Genomic epidemiology reveals transmission patterns and dynamics of SARS-CoV-2 in Aotearoa New Zealand. *Nat Commun.* 2020;11:6351. <https://doi.org/10.1038/s41467-020-20235-8>
8. Candido DS, Claro IM, de Jesus JG, Souza WM, Moreira FRR, Dellicour S, et al.; Brazil-UK Centre for Arbovirus Discovery, Diagnosis, Genomics and Epidemiology (CADDE) Genomic Network. Evolution and epidemic spread of SARS-CoV-2 in Brazil. *Science.* 2020;369:1255–60. <https://doi.org/10.1126/science.abd2161>
9. Eden J-S, Rockett R, Carter I, Rahman H, de Ligt J, Hadfield J, et al.; 2019-nCoV Study Group. An emergent clade of SARS-CoV-2 linked to returned travellers from Iran. *Virus Evol.* 2020;6:a027. <https://doi.org/10.1093/ve/veaa027>
10. Dong E, Du H, Gardner L. An interactive web-based dashboard to track COVID-19 in real time. *Lancet Infect Dis.* 2020;20:533–4. [https://doi.org/10.1016/S1473-3099\(20\)30120-1](https://doi.org/10.1016/S1473-3099(20)30120-1)
11. Oude Munnink BB, Nieuwenhuijse DF, Stein M, O'Toole Á, Haverkate M, Mollers M, et al.; Dutch-Covid-19 response team. Rapid SARS-CoV-2 whole-genome sequencing and analysis for informed public health decision-making in the Netherlands. *Nat Med.* 2020;26:1405–10. <https://doi.org/10.1038/s41591-020-0997-y>
12. Kalinich CC, Jensen CG, Neugebauer P, Petrone ME, Peña-Hernández M, Ott IM, et al. Real-time public health communication of local SARS-CoV-2 genomic epidemiology. *PLoS Biol.* 2020;18:e3000869. <https://doi.org/10.1371/journal.pbio.3000869>
13. Rockett RJ, Arnott A, Lam C, Sadsad R, Timms V, Gray K-A, et al. Revealing COVID-19 transmission in Australia by SARS-CoV-2 genome sequencing and agent-based modeling. *Nat Med.* 2020;26:1398–404. <https://doi.org/10.1038/s41591-020-1000-7>
14. Bauer DC, Tay AP, Wilson LOW, Reti D, Hosking C, McAuley AJ, et al. Supporting pandemic response using genomics and bioinformatics: a case study on the emergent SARS-CoV-2 outbreak. *Transbound Emerg Dis.* 2020;67:1453–62. <https://doi.org/10.1111/tbed.13588>
15. Jefferies S, French N, Gilkison C, Graham G, Hope V, Marshall J, et al. COVID-19 in New Zealand and the impact

- of the national response: a descriptive epidemiological study. *Lancet Public Health*. 2020;5:e612–23. [https://doi.org/10.1016/S2468-2667\(20\)30225-5](https://doi.org/10.1016/S2468-2667(20)30225-5)
16. Freed NE, Vlková M, Faisal MB, Silander OK. Rapid and inexpensive whole-genome sequencing of SARS-CoV-2 using 1200 bp tiled amplicons and Oxford Nanopore Rapid Barcoding. *Biol Methods Protoc*. 2020;5:a014. <https://doi.org/10.1093/biomethods/bpaa014>
 17. Rambaut A, Holmes EC, O’Toole Á, Hill V, McCrone JT, Ruis C, et al. A dynamic nomenclature proposal for SARS-CoV-2 lineages to assist genomic epidemiology. *Nat Microbiol*. 2020;5:1403–7. <https://doi.org/10.1038/s41564-020-0770-5>
 18. Katoh K, Standley DM. MAFFT multiple sequence alignment software version 7: improvements in performance and usability. *Mol Biol Evol*. 2013;30:772–80. <https://doi.org/10.1093/molbev/mst010>
 19. Bouckaert R, Vaughan TG, Barido-Sottani J, Duchêne S, Fourment M, Gavryushkina A, et al. BEAST 2.5: an advanced software platform for Bayesian evolutionary analysis. *PLoS Comput Biol*. 2019;15:e1006650. <https://doi.org/10.1371/journal.pcbi.1006650>
 20. Drummond AJ, Rambaut A, Shapiro B, Pybus OG. Bayesian coalescent inference of past population dynamics from molecular sequences. *Mol Biol Evol*. 2005;22:1185–92. <https://doi.org/10.1093/molbev/msi103>
 21. Letunic I, Bork P. Interactive Tree Of Life (iTOL) v4: recent updates and new developments. *Nucleic Acids Res*. 2019;47:W256–9. <https://doi.org/10.1093/nar/gkz239>

Address for correspondence: Jemma L. Geoghegan, University of Otago Division of Health Sciences, Microbiology and Immunology, 720 Cumberland St, Dunedin, Otago 9054, New Zealand; email: jemma.geoghegan@otago.ac.nz

The Public Health Image Library (PHIL)



The Public Health Image Library (PHIL), Centers for Disease Control and Prevention, contains thousands of public health-related images, including high-resolution (print quality) photographs, illustrations, and videos.

PHIL collections illustrate current events and articles, supply visual content for health promotion brochures, document the effects of disease, and enhance instructional media.

PHIL images, accessible to PC and Macintosh users, are in the public domain and available without charge.

Visit PHIL at: <http://phil.cdc.gov/phil>

Clinical Evaluation of Roche SD Biosensor Rapid Antigen Test for SARS-CoV-2 in Municipal Health Service Testing Site, the Netherlands

Zsófia Iglói, Jans Velzing, Janko van Beek, David van de Vijver, Georgina Aron, Roel Ensing, Kimberley Benschop, Wanda Han, Timo Boelsums, Marion Koopmans, Corine Geurtsvankessel, Richard Molenkamp

Rapid detection of infection is essential for stopping the spread of severe acute respiratory syndrome coronavirus 2 (SARS-CoV-2). The Roche SD Biosensor rapid antigen test for SARS-CoV-2 was evaluated in a nonhospitalized symptomatic population. We rapid-tested a sample onsite and compared results with those from reverse transcription PCR and virus culture. We analyzed date of onset and symptoms using data from a clinical questionnaire. Overall test sensitivity was 84.9% (95% CI 79.1–89.4) and specificity was 99.5% (95% CI 98.7–99.8). Sensitivity increased to 95.8% (95% CI 90.5–98.2) for persons who sought care within 7 days of symptom onset. Test band intensity and time to result correlated strongly with viral load; thus, strong positive results could be read before the recommended time. Approximately 98% of all viable specimens with cycle threshold <30 were detected. Rapid antigen tests can detect symptomatic SARS-CoV-2 infections in the early phase of disease, thereby identifying the most infectious persons.

Severe acute respiratory syndrome coronavirus 2 (SARS-CoV-2) emerged >1 year ago (1) but still keeps a strong grip not only on daily life but also on diagnostic capacities. Reverse transcription PCR (RT-PCR) has been the standard for diagnosis of acute infection (2) but has several limitations, such as the requirement for specialized laboratory infrastructure, trained personnel, and reagents that

have been in shortage globally (3). In addition, the current turnaround time from sample collection to reporting of the result may take >48 hours (J. van Beek et al., unpub. data, <https://doi.org/10.1101/2020.10.13.20211524>), compromising effectiveness of triage, isolation, and contact tracing strategies. Rapid antigen detection tests (Ag RDT) for SARS-CoV-2 appeared on the market in early 2020, but initial reports of poor performance and the lack of independent evaluation results made governments reluctant to invest and consider inclusion into testing algorithms. As of February 2021, more than 140 assays are on the market (5), but relatively few have been extensively validated (5–6; V.M. Corman et al., unpub. data. <https://doi.org/10.1101/2020.11.12.20230292>). Initial results show that these tests are suitable for detecting early-onset cases with high viral load. As expected, the sensitivity of the tests is lower than that of RT-PCR, but in patients in the early phase of illness who have high viral load, performance meets World Health Organization-set criteria of $\geq 80\%$ sensitivity and $\geq 97\%$ specificity compared with nucleic acid detection methods (8). Thus, these tests could be useful in identifying the most infectious persons (4). In an outbreak scenario, diagnostics with lower sensitivity but a faster result can render interventions more effective than standard tests (9). Implementation of Ag RDT into testing algorithms would enable rapid detection and isolation of new cases and thereby support the test, trace, and isolate strategy with the intent to stop transmission chains and reduce the impact of coronavirus disease (COVID-19).

In this study, we assessed the performance of the Roche SD Biosensor SARS-CoV-2 rapid antigen

Author affiliations: Erasmus MC, Rotterdam, the Netherlands (Z. Iglói, J. Velzing, J. van Beek, D. van de Vijver, G. Aron, M. Koopmans, C. Geurtsvankessel, R. Molenkamp); Public Health Service Rotterdam-Rijnmond, Rotterdam (R. Ensing, T. Boelsums); National Public Health Institute (RIVM), Bilthoven, the Netherlands (K. Benschop, W. Han)

DOI: <https://doi.org/10.3201/eid2705.204688>

test (Roche Diagnostics, <https://www.roche.com>) compared with both RT-PCR and virus culture. We conducted the field evaluation study at a large public health service testing facility in Rotterdam-Rijnmond, the Netherlands, where most visitors sought care for COVID-19 symptoms. Every person >18 years of age who had an appointment for SARS-CoV-2 RT-PCR testing was invited to participate. An additional nasopharyngeal swab specimen was obtained for the Ag RDT in parallel and processed onsite to compare sensitivity and specificity to RT-PCR. All samples positive by Ag RDT and PCR were cultured to correlate results with infectivity. The medical research ethics committee of Utrecht decided the study was not subject to the Medical Research Involving Human Subjects Act and did not require full review by an accredited committee (protocol no. 20-606/C).

Materials and Methods

Testing Population, Setup and Patient Recruitment

The study was conducted at the largest drive-through testing location in Rotterdam-Rijnmond, at which testing is by appointment only. Eligibility for a free-of-charge test included either presence of symptoms or close contact with a confirmed SARS-CoV-2-infected person. Most persons who requested testing had symptoms. At the entrance of the testing site, we approached all persons >18 years of age; after providing written informed consent, they were enrolled in the study and directed to one of the dedicated testing posts for sampling. Enrolled persons were also asked to fill in a clinical questionnaire stating the reason for appointment, date of onset or end date of symptoms, and a list of symptoms (fever, sore throat, coughing, shortness of breath/tightness, runny nose, diarrhea, eye complaints, nausea, rash, chills, headache, pain when breathing, coughing phlegm, muscle pain, painful/swollen lymph nodes, fatigue, vomiting, joint pain, loss of appetite, nosebleed, other). The study was conducted for 5 days to achieve the target of 800–1,000 participants. The SARS-CoV-2 rapid antigen test distributed by Roche SD Biosensor was provided by the Ministry of Health, Welfare, and Sport.

Testing Site Setup and the Mobile Laboratory

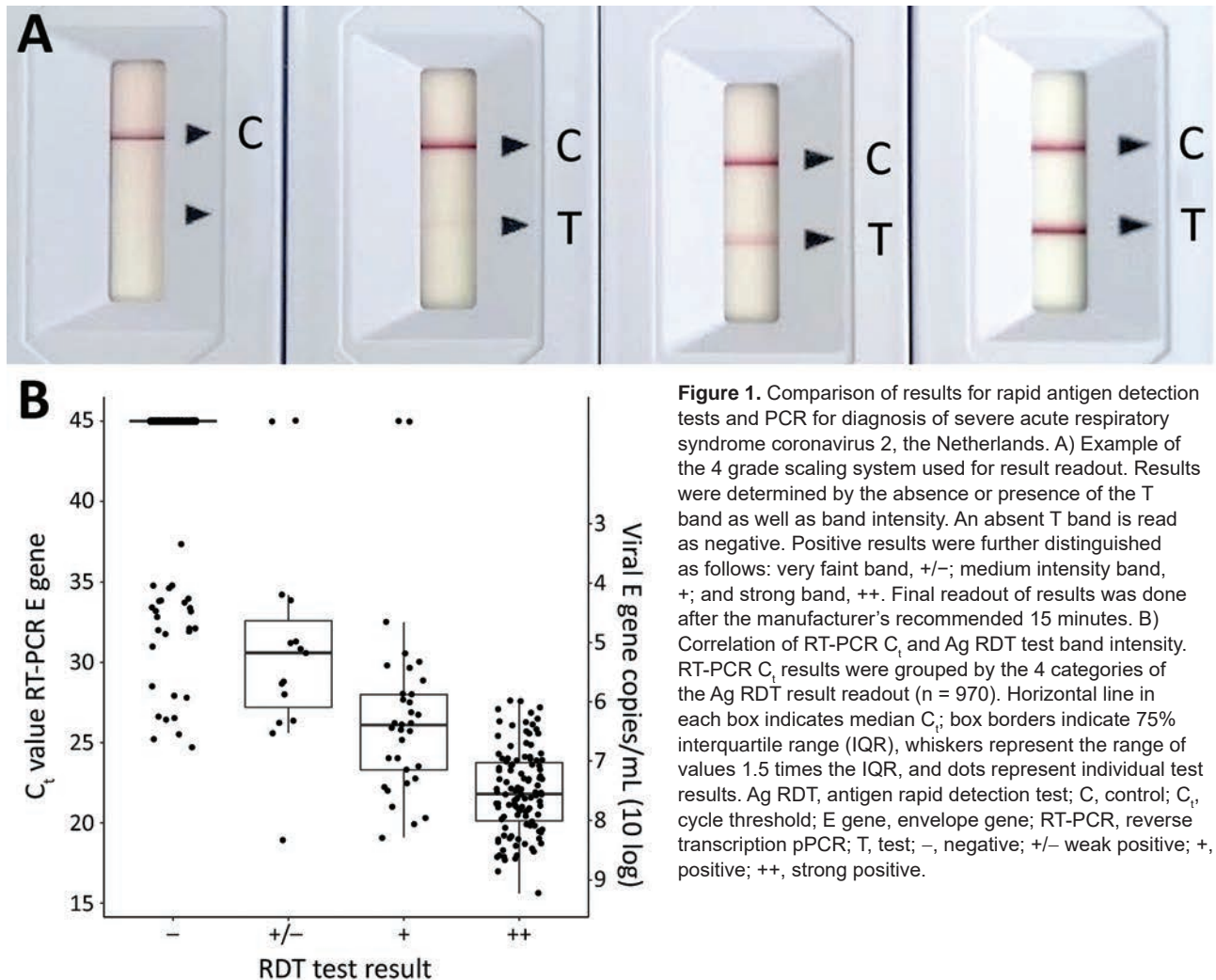
From the 6 available testing posts, we designated 2 posts for sample collection from study participant on the basis of 3 factors: maximum number of subjects per test post (≈ 150 /day); known number of appointments per day; and expected enrollment

rate based on initial results from other study sites in the Netherlands. We expected to include a maximum of 300 persons/day. The site's regular trained personnel performed swabbing to avoid variations to the process. Testing was done on benchtop, in a mobile laboratory unit by trained staff dressed in full personal protective equipment (goggles, FFP3 mask, gloves, and disposable gown). Samples for the Ag RDT were collected at regular intervals and processed as soon as possible within 30 mins in convenient batches (5–10 tests at a time). Swab specimens and RDT devices were inactivated in chlorine and disposed of as biohazard material. Results were recorded in a Microsoft Access database (<https://www.microsoft.com>) designated for this study.

Specimen Collection, Testing and Culture Procedures

Standard method for SARS-CoV-2 testing was by RT-PCR, which was conducted in parallel with the Ag RDT on separate swab specimens. Two swab specimens (1 oropharyngeal and 1 nasopharyngeal swab) were taken for RT-PCR and virus culture, placed directly in 3 mL universal transport media (HiViral; HiMedia Laboratories PVT, Ltd., <https://www.himedialabs.com>) and shipped to the Erasmus MC viroscience diagnostic laboratory (Rotterdam, the Netherlands). For the Ag RDT evaluation, a second nasopharyngeal swab specimen was taken from the same nostril, using the swab included in the kits, to directly compare RT-PCR results with Ag RDT results. Swabs were placed into empty tubes to transport to the mobile laboratory onsite. Routine RT-PCR testing was performed on combined oropharyngeal and one nasopharyngeal swabs in virus transport medium using the cobas SARS-CoV-2 test on the COBAS6800 (Roche Diagnostics). Because cycle threshold (C_t) values differ between PCR methods, genome copies per milliliter were calculated based on an in-house established standard curve. The leftover virus transport medium from the oropharyngeal and nasopharyngeal swabs was directly inoculated onto Vero cells clone 118 without freezing or extended storage. Samples were cultured for 7 days; once cytopathic effect was visible, the presence of SARS-CoV-2 was confirmed with immunofluorescent detection of SARS CoV-2 nucleocapsid protein (rabbit polyclonal antibody; Sino Biologic Inc., <https://www.sinobiological.com>).

For the Ag RDT, the SD Biosensor SARS-CoV-2 rapid antigen test distributed by Roche (reference no. 9901-NCOV-01G; lot no. QCO3020079/Sub:A-2) was



performed immediately onsite following manufacturer's instructions. A 4-grade scaling readout (-; +/-, +; ++) representing the strength of the test band was used (Figure 1, panel A). Time until positive results was logged as <5 min, <10 min (not part of the manufacturer's instructions for use), or 15 min; recommended readout was 15–30 min. When results were dubious (i.e., test line barely visible or labeled as +/- but regarded as positive test result), 2 persons performed the readout.

Data Analysis

We merged data from the Ag RDT, RT-PCR, virus culture, and clinical questionnaire using Microsoft Access and data performed analysis using R version 4.0.2 (The R Project for Statistical Computing, <https://www.r-project.org>). Sensitivity and specificity of Ag RDT were calculated in relation to the RT-PCR results. Wilcoxon score interval was used to determine CIs of proportions.

Results

Characteristics of Study Population

During the study period of October 9–15, 2020, a total of 970 (26.8%) of 3,615 persons visiting the testing site were included in the study; inclusion was put on hold occasionally during the day when testing posts became crowded. The average age of study participants was 42 years (range 18–86 years); most were female ($n = 525$, 54.7%). Among the participants manifesting symptoms, 73.4% had symptom onset ≤ 7 days ($n = 650/886$). Most (84.9%) of the samples had high viral load (PCR $C_t \leq 30$, envelope gene (E gene) 2.17×10^5 copies/mL) (Table 1). The age and sex distribution of study participants was representative of the tested population in general: average age 38.4 years, 57% female (data not shown). We did not record reasons for not participating.

At the time of requesting the appointment, most participants (91.3%) had symptoms; most frequently

Table 1. Characteristics of the population of study comparing rapid antigen test and PCR for severe acute respiratory syndrome coronavirus 2, the Netherlands*

Characteristic	Value
Total	970
Median age, y (range)	42 (18–86)
Sex	
M	435 (44.8)
F	525 (54.1)
Unknown	10 (1.1)
Symptoms reported	886 (91.3)
Days after symptom onset, median (no. cases/total no. tested)	4 (725/970)
0–3	319 (44.0)
4–7	331 (45.7)
≥8	75 (10.3)
Positivity by PCR	186 (19.2)
PCR C _t E gene, median (range)	23.6 (15.6–37.4)
C _t ≥35	1 (0.5)
C _t ≥30	28 (15.1)
C _t ≤30	159 (85.5)
C _t ≤25	113 (60.8)
C _t ≤20	31 (16.7)

*Values are no. (%) except as indicated. E gene, envelope gene; C_t, cycle threshold.

reported were common cold symptoms, such as runny nose (64.5%), sore throat (57%), coughing (55%), headache (48%), tiredness (38%), muscle pain (27%), shortness of breath (21%), and chills (21%). Some of the more typical and serious symptoms such as fever and reproductive cough were reported by 17% of participants. A very small percentage (1.5%) reported loss of taste and smell.

Performance of the Ag RDT

The overall sensitivity of the Ag RDT was 84.9% (95% CI 79.1%–89.4%) (Tables 2, 3). Positive predictive value was 97.5% (95% CI 93.8%–99.0%) under an average of 19.2% current prevalence in the region calculated by PCR positivity rate. Sensitivity improved considerably when analyzed by various PCR C_t intervals showing highest sensitivity for C_t ≤25 (4.87 × 10⁶ E gene copies/mL); sensitivity was 99.1% (95% CI 95.2%–100%). For C_t ≤30 (2.17 × 10⁵ E gene copies/mL), sensitivity was 94.3% (95% CI 89.6%–97.0%). Sensitivity among participants that sought care within 3 days after disease onset was higher (94.9%) than for

Table 2. Overview of results of comparison of rapid antigen test and PCR for severe acute respiratory syndrome coronavirus 2, the Netherlands*

Ag RDT result	PCR result		Total
	Positive	Negative	
Positive	158	4	162
Negative	28	780	808
Total	186	784	970

*Ag RDT, rapid antigen detection test.

participants who came later in their disease progression (90.6%) (Table 3). Hence, sensitivity was strongly associated with viral load. PCR-positive samples that were not positive by Ag RDT (n = 28) showed a mixed distribution of viral load (C_t <30 for 10/28 samples). Date of onset was available for 16/28 patients; 12/28 tested ≤7 days after onset. Of the 28 samples, 5 were cultivable (2 samples were not cultured); all 5 had C_t <30 and onset ≤7 days. Only 2/28 had no symptoms but had contact with a confirmed case (average C_t 33).

The overall specificity of Ag RDT was 99.5% (95% CI 98.7%–99.8%); negative predictive value was 96.5% (95% CI 95.0%–97.6%), which increased with shorter time after symptom onset (Table 3). Three of 4 samples negative by PCR (and culture) that were positive by Ag RDT were negative by RT-PCR for other respiratory viruses; 1 was weakly positive for rhinovirus (C_t >35). Metagenomic sequencing confirmed rhinovirus B.

Association of Ag RDT Results with Infectivity

A total of 176/186 specimens that tested positive by Ag RDT, RT-PCR, or both were inoculated on Vero cells; 140 (79.5%) were culture positive after 7 days of cell culture. We observed cytopathic effect 2–5 days after inoculation. The culture-positive specimens were obtained from persons at a median of 4 days post onset of disease (range 1–12 days) and high viral load (average C_t 22.8, viral load 6.99 × 10⁷ E gene copies/mL). Median days past symptom onset did not differ between Ag RDT and PCR positive samples independently of successful culture (Table 4).

Of the 140 cultured specimens, 5 (3.6%) were Ag RDT negative. These specimens were collected a median of 6 days after onset of disease (range 5–7 days;

Table 3. Characteristics of rapid antigen detection test compared with reverse transcription PCR stratified by days after symptom onset, the Netherlands*

Characteristic	0–3 d past onset		0–7 d past onset		All	
	No.	% (95% CI)	No.	% (95% CI)	No.	% (95% CI)
Clinical sensitivity	319	94.9 (86.1–98.3)	650	90.6 (84.3–94.6)	970	84.9 (79.1–89.4)
Sensitivity C _t ≤30	316	98.2 (90.6–99.9)	640	95.8 (90.5–98.2)	943	94.3 (89.6–97.0)
Sensitivity C _t ≤25	305	100 (92.1–100)	608	98.8 (93.7–99.9)	897	99.1 (95.2–100)
Clinical specificity	319	99.6 (97.9–100)	650	99.6 (98.6–99.9)	970	99.5 (98.7–99.8)
Positive predictive value	NA	98.2 (90.7–99.9)	NA	98.3 (94.0–99.5)	NA	97.5 (93.8–99.0)
Negative predictive value	NA	98.9 (96.7–99.6)	NA	97.7 (96.1–98.7)	NA	96.5 (95.0–97.6)

*Sensitivity and specificity of Ag RDT was calculated based on reverse transcription PCR results and days since symptoms onset. Positive and negative predictive values were calculated using 19.2% prevalence setting. Ag RDT, rapid antigen detection test; C_t, cycle threshold; NA, not applicable.

Table 4. Comparison of rapid test, PCR, and culture results for severe acute respiratory syndrome coronavirus 2, the Netherlands*
PCR C_t

RDT result	Culture result	PCR C _t								Total
		<20		20–25		25–30		>30		
		No.	Median days after onset (range)†	No.	Median days after onset (range)‡	No.	Median days after onset (range)§	No.	Median days after onset (range)¶	
+	NA	1	2	4	3.5	4	6.5	0	NA	9
+	+	30	3	74	4	30	4	1	9	135
+	–	0	NA	3	5	4	5.5	7	7	14
–	NA	0	NA	0	NA	1	3	0	NA	1
–	+	0	NA	1	7	4	5.5	0	NA	5
–	–	0	NA	0	NA	3	NA	19	6.5	22
Total		31	3 (1–9)	82	4 (1–12)	46	4 (1–9)	27	7 (2–15)	186

*No. indicates no. participants. C_t, cycle threshold; NA, not applicable.

†Unknown for 9 participants.

‡Unknown for 16 participants.

§Unknown for 12 participants.

¶Unknown for 9 participants.

2 values missing) and had high viral loads (average C_t 25.7, viral load 3.15 × 10⁶ E gene copies/mL). In samples with C_t <30 (<2.17 × 10⁵ E gene copies/mL), 10/176 (6%) could not be cultured and 4/176 (2%) were not detectable by Ag RDT. For samples with C_t >30, 1/27 (4%) could be cultured and 8/27 (30%) were Ag RDT positive. These data indicate that for C_t >30 (2.17 × 10⁵ E gene copies/mL), most samples are not cultivable, which is in agreement with previously published data (10,11) (Table 4; Figure 2).

Significance of Time to Result

We logged results at 3 time points: 5 minutes, 10 minutes, and the recommended readout time of 15

minutes; we recorded intensity of the test band. In general, most (95%) strong positive samples appeared <5 min after sample addition. Test bands showing medium intensity had a more equal distribution of time to results in the 3 timeframes, whereas most (73%) weak positive bands required the recommended 15-minute readout (Table 5). Band intensity correlated with viral load (Figure 1).

Discussion

We describe the results of a large clinical evaluation study using an antigen rapid test in a medium-high prevalence setting in a symptomatic, nonhospitalized population to detect SARS-CoV-2 infections.

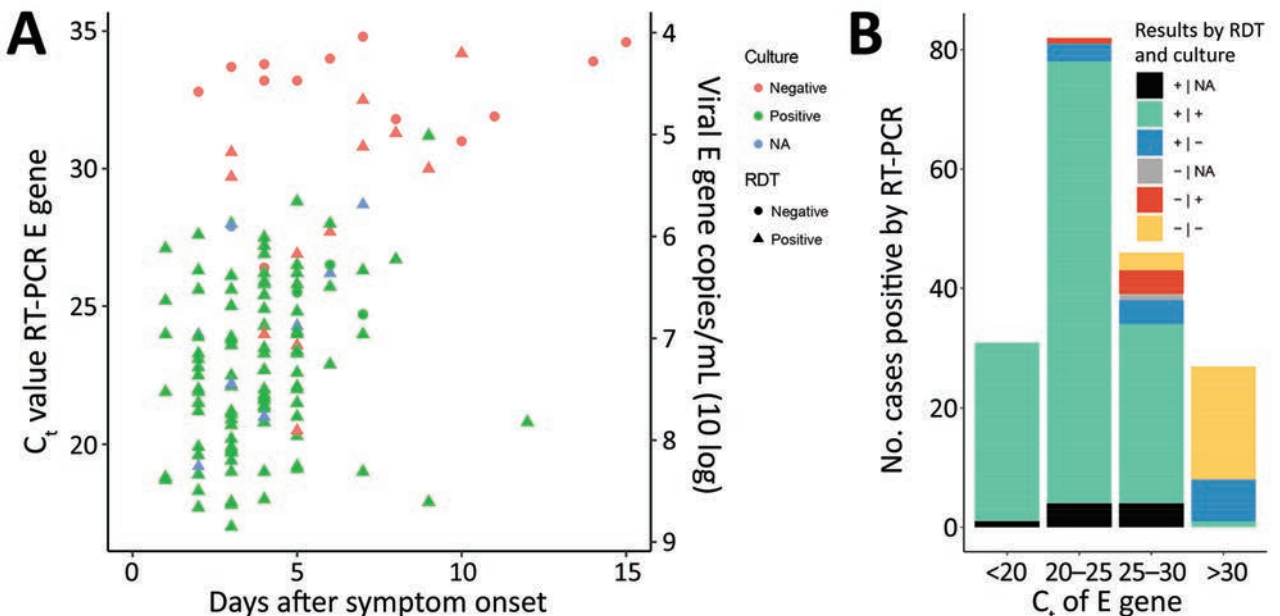


Figure 2. Relationships of time from symptom onset to testing and cycle threshold values to results for rapid antigen detection tests and PCR for diagnosis of severe acute respiratory syndrome coronavirus 2, the Netherlands. A) Cycle thresholds of positive samples in relation to days since symptom onset, Ag RDT positivity, and culture outcomes of participation with known disease onset date (n = 140). B) PCR-positive samples by cycle threshold (n = 186) in relation to Ag RDT and culture test results. Ag RDT, antigen rapid detection test; C_t, cycle threshold; E gene, envelope gene; NA, not available; RT-PCR, reverse transcription PCR.

Table 5. Results of rapid antigen detection test for severe acute respiratory syndrome coronavirus 2, the Netherlands*

Time to result	Result, no. (%)				Total
	-	+/-	+	++	
5 min	NA	1 (7)	8 (24)	108 (95)	117
10 min	NA	3 (20)	12 (36)	4 (4)	19
15 min	NA	11 (73)	13 (39)	2 (1)	26
Total tests	808	15	33	114	970

*Results of the Ag RDT were recorded at 3 time points: 5 min, 10 min, and the manufacturer-recommended 15 min. If result between first and last readout did not change, the first was registered as final result. Ag RDT, rapid antigen detection test; NA, not applicable; -, negative; +/- weak positive; +, positive; ++, strong positive.

Overall, the test performed well, detecting 84.9% of all cases with RT-PCR as reference. Our results align well with data from other independent evaluations, including low rate of false positivity (5). A question to address is if and how Ag RDT can identify infectious persons and support the test, trace, and isolate strategy employed worldwide to control the COVID-19 pandemic. In our evaluation, we have identified $\approx 97\%$ of persons with sufficient viral load to enable virus culture; this finding suggests that Ag RDT alone in this population would have a high sensitivity for identifying infectious persons. On the basis of its performance in our study, the test would fulfill World Health Organization criteria until the prevalence of SARS-CoV-2 drops below 2.5% based on positive predictive value.

One of the unique strengths of this study is the correlation of results with infectivity. Most PCR positive samples with high viral load could be cultured successfully; however, a fraction of a potentially infectious group was not detected by the Ag RDT. These patients were generally tested in the later phase of the infection but still had a high viral load and positive virus cultures. Although the presence of antibodies in patients after the first week of onset could reduce the sensitivity of Ag RDT, this possibility does not explain the discrepancy in the samples that were negative by the RDT and positive by virus culture; we previously demonstrated that the presence of neutralizing antibodies does inversely correlate with virus culture (11). One possible explanation is the use of different swabs, causing discrepancy in viral load in the RT-PCR and culture versus Ag RDT samples. However small the proportion, missing infectious persons can have serious consequences in specific populations. Testing algorithms should therefore be carefully aligned to high-risk and high-priority groups. On the other hand, Ag RDT could detect cases with relatively low viral load with high sensitivity, thereby providing a safety margin around the suggested threshold of infectiousness.

In asymptomatic persons, the absence of symptoms might make them less cautious, whereby they do contribute to the spread of the virus. Previous reports have shown that asymptomatic persons have similar viral loads to symptomatic persons (11,12); therefore, the Ag RDT could be used in this population. Because performance data of Ag RDT in this specific population is scarce as of March 2021, additional validation of the Ag RDT test is recommended. Repeated testing following the calculated incubation time will provide more test certainty.

Several Ag RDTs are on the market; most use nasopharyngeal swabs for sampling. Oropharyngeal and nasopharyngeal swabs are considered the best sample types for detecting SARS-CoV-2 especially in the early phase (2,12). However, the swabbing requires trained personnel and causes discomfort to the patient. Only a few Ag RDTs are marketed directly with a less invasive sample, the nasal swab. The available performance data indicates no notable difference between Ag RDT and RT-PCR in detecting symptomatic cases, and the use of the more superficially collected nasal swab specimens seems to be a good alternative (N. Van der Moeren et al., unpub. data, <https://doi.org/10.1101/2020.10.19.20215202>). Investigators can further explore the use of self-sampling, which is one of the potential directions Ag RDT testing will take because it does not require trained personnel, reduces infection risk for the healthcare worker who takes the swab sample, and enables testing for a wider population. Studies indicate that self-sampling is somewhat less precise than sampling by trained professionals, further lowering detection rate (11); evaluation studies are ongoing.

One limitation of our study is that, in our setting, we compared results of RT-PCR and Ag RDT; however, in contrast to the instructions for 1 swab specimen for the Ag RDT, 2 swab specimens were taken for RT-PCR and virus culture, which probably resulted in a higher amount of viral material collected. This difference might explain some of the discrepancies between Ag RDT and PCR or culture. Furthermore, the same nostril was used to take the second swab for the Ag RDT, which was meant to grant comparability between the 2 tests but might have resulted in lower viral load in the second sample. We used culture as a correlate of infectivity, which has certain limitations but is the best available technique to measure infectivity. Recall bias by the study enrollees when filling out the questionnaires could have affected the data provided. Furthermore, testing is free of charge only for persons who had either relevant symptoms or notified contact with an infected person; therefore, some

persons might have provided symptoms falsely to be tested for other reasons.

We conclude that the use of Ag RDT in our drive-through test stations would provide a good method to identify most infectious patients. The logistics of implementation crucial for further rollout include a safe working environment for personnel performing the assays if implemented onsite and a system that enables follow-up testing by PCR for risk groups. The national outbreak management team of the Netherlands recommends using Ag RDT for rapid screening but cautions against sole use of Ag RDTs in vulnerable persons, such as those at risk for severe illness and those living or working in long-term care facilities, because of the potential of false negative cases. Whereas a positive Ag RDT can be used to trigger contact tracing and isolation, it is imperative to inform patients about the potential for false negative testing, and the need for continued behavioral measures. A slightly higher risk for missed cases is debatable in patients who have little contact with high-risk persons, although the identification of these cases will be challenging. Ideally, rapid antigen testing should be secured through a triage system that guides patients to the proper testing algorithm and includes repeated testing.

This article was preprinted at <https://www.medrxiv.org/content/10.1101/2020.11.18.20234104v1>.

Acknowledgments

Testing was carried out at the Schiedam Testing Centre, at which numerous people contributed to the success of this project; therefore, we thank all involved employees of the GGD Rotterdam-Rijmond and the Schiedam Testing Centre. We are grateful for the vital involvement of the following volunteers who supported patient inclusion and administrative tasks: Pauline de Best, Loubna Bouzyd, Vera Mols, Jasmijn de Rooij, Louella Kasbergen, Axel Bonacic Marinovic, Maarten Hoek, Kamelia Stanoeva, and Nadya Velikova.

This work was partly supported by H2020 project RECoVer (grant no. 101003589).

About the Author

Dr. Iglò is a virologist and public health microbiologist working at the Erasmus Medical Centre viroscience

department. Her primary research interests are arboviruses and emerging viruses, diagnostics, and public health implications.

References

1. World Health Organization. Listings of WHO's response to COVID-19. 29 June 2020 [cited 2021 Mar 8]. <https://www.who.int/news/item/29-06-2020-covid-timeline>
2. World Health Organization. Laboratory testing for 2019 novel coronavirus (2019-nCoV) in suspected human cases. 2020 [cited 2021 Mar 8]. <https://www.who.int/publications/i/item/10665-331501>
3. Beetz C, Skrahina V, Förster TM, Gaber H, Paul JJ, Curado F, et al. Rapid large-scale COVID-19 testing during shortages. *Diagnostics (Basel)*. 2020;10:464. <https://doi.org/10.3390/diagnostics10070464>
4. (FINDdx) FIND. SARS-COV-2 diagnostic pipeline. 2020 [cited 2021 Mar 8]. <https://www.finddx.org/covid-19/pipeline/>
5. Dinnes J, Deeks JJ, Adriano A, Berhane S, Davenport C, Dittrich S, et al.; Cochrane COVID-19 Diagnostic Test Accuracy Group. Rapid, point-of-care antigen and molecular-based tests for diagnosis of SARS-CoV-2 infection. *Cochrane Database Syst Rev*. 2020;8:CD013705.
6. World Health Organization (WHO). Antigen-detection in the diagnosis of SARS-CoV-2 infection using rapid immunoassays. 2020 [cited 2021 Mar 8]. <https://www.who.int/publications/i/item/antigen-detection-in-the-diagnosis-of-sars-cov-2-infection-using-rapid-immunoassays>
7. Bonačić Marinović AA, Koopmans M, Dittrich S, Teunis P, Swaan C, van Steenberghe J, et al. Speed versus coverage trade off in targeted interventions during an outbreak. *Epidemics*. 2014;8:28–40. <https://doi.org/10.1016/j.epidem.2014.05.003>
8. Wölfel R, Corman VM, Guggemos W, Seilmaier M, Zange S, Müller MA, et al. Virological assessment of hospitalized patients with COVID-2019. *Nature*. 2020;581:465–9. <https://doi.org/10.1038/s41586-020-2196-x>
9. van Kampen JJA, van de Vijver DAMC, Fraaij PLA, Haagmans BL, Lamers MM, Okba N, et al. Duration and key determinants of infectious virus shedding in hospitalized patients with coronavirus disease-2019 (COVID-19). *Nat Commun*. 2021;12:267. <https://doi.org/10.1038/s41467-020-20568-4>
10. Walsh KA, Jordan K, Clyne B, Rohde D, Drummond L, Byrne P, et al. SARS-CoV-2 detection, viral load, and infectivity over the course of an infection. *J Infect*. 2020;81:357–71. <https://doi.org/10.1016/j.jinf.2020.06.067>
11. Lindner AK, Nikolai O, Kausch F, Wintel M, Hommes F, Gertler M, et al. Head-to-head comparison of SARS-CoV-2 antigen-detecting rapid test with self-collected nasal swab versus professional-collected nasopharyngeal swab. *Eur Respir J*. 2021 Feb 25 [Epub ahead of print]. <https://doi.org/10.1183/13993003.03961-2020>

Address for correspondence: Zsófia Iglói, Nb1052 Clinical virology, Erasmus MC, Doctor Molewaterplein 40, 3015 GD Rotterdam, the Netherlands; email: z.igloi@erasmusmc.nl

Prevalence and Clinical Profile of Severe Acute Respiratory Syndrome Coronavirus 2 Infection among Farmworkers, California, USA, June–November 2020

Joseph A. Lewnard,¹ Ana M. Mora,¹ Oguchi Nkwocha, Katherine Kogut, Stephen A. Rauch, Norma Morga, Samantha Hernandez, Marcus P. Wong, Karen Huen, Kristin Andrejko, Nicholas P. Jewell, Kimberly L. Parra, Nina Holland, Eva Harris, Maximiliano Cuevas, Brenda Eskenazi, on behalf of the CHAMACOS-Project-19 Study Team²

During the ongoing coronavirus disease (COVID-19) pandemic, farmworkers in the United States are considered essential personnel and continue in-person work. We conducted prospective surveillance for severe acute respiratory syndrome coronavirus 2 (SARS-CoV-2) infection and antibody prevalence among farmworkers in Salinas Valley, California, during June 15–November 30, 2020. We observed 22.1% (1,514/6,864) positivity for SARS-CoV-2 infection among farmworkers compared with 17.2% (1,255/7,305) among other adults from the same communities (risk ratio 1.29, 95% CI 1.20–1.37). In a nested study enrolling 1,115 farmworkers, prevalence of current infection was 27.7% among farmworkers reporting ≥ 1 COVID-19 symptom and 7.2% among farmworkers without symptoms (adjusted odds ratio 4.16, 95% CI 2.85–6.06). Prevalence of SARS-CoV-2 antibodies increased from 10.5% (95% CI 6.0%–18.4%) during July 16–August 31 to 21.2% (95% CI 16.6%–27.4%) during November 1–30. High SARS-CoV-2 infection prevalence among farmworkers underscores the need for vaccination and other preventive interventions.

Author affiliations: University of California, Berkeley, Berkeley, California, USA (J.A. Lewnard, A.M. Mora, K. Kogut, S.A. Rauch, S. Hernandez, M.P. Wong, K. Huen, K. Andrejko, N.P. Jewell, N. Holland, E. Harris, B. Eskenazi); Universidad Nacional, Heredia, Costa Rica (A.M. Mora); Clínica de Salud del Valle de Salinas, Salinas, California, USA (O. Nkwocha, N. Morga, M. Cuevas); London School of Hygiene and Tropical Medicine, London, UK (N.P. Jewell); University of Arizona, Tucson, Arizona, USA (K.L. Parra)

DOI: <https://doi.org/10.3201/eid2705.204949>

In response to the ongoing coronavirus disease (COVID-19) pandemic, the United States and other countries have implemented broad interventions to mitigate community transmission of severe acute respiratory syndrome coronavirus 2 (SARS-CoV-2) (1). Workers in food supply and other industries deemed essential to continuity of public health and safety have continued in-person work (2). COVID-19 outbreaks have been reported among various essential workforce groups, including employees in food processing facilities (3,4), but studies prospectively assessing risk for infection among essential workers involved in food production are lacking.

Agriculture and related food production industries comprise one of the lowest-paid sectors of the US economy; 29% of full-time workers earn an annual individual income of <\$12,760 or \$26,200 for a family of 4 (5). Agriculture in particular draws on a predominantly Latino immigrant workforce (6), who work longer hours, receive lower wages, and experience higher levels of household poverty than their US-born counterparts (7). Among immigrant farmworkers, $\approx 54\%$ are undocumented and thus have reduced access to federal benefits under the Coronavirus Aid, Relief, and Economic Security Act (8). Working conditions, poverty, and immigration status have compounded legal and economic challenges faced by farmworkers during the COVID-19 pandemic (9,10).

¹These authors contributed equally to this article.

²Members of the CHAMACOS-Project-19 Study Team are listed at the end of this article.

We initiated surveillance of SARS-CoV-2 infection among farmworkers in Salinas Valley, California, to monitor the COVID-19 epidemic. We previously described impacts of the pandemic on economic well-being, mental health, and food insecurity within this population (A.M. Mora, unpub. data, <https://doi.org/10.1101/2020.12.18.20248518>). Here, we report on the prevalence of SARS-CoV-2 infection among farmworkers tested during June–November 2020 and on symptoms and antibody responses within a subset of farmworkers enrolled in a cross-sectional study.

Methods

Study Setting

The Salinas Valley is a 90-mile stretch of agricultural land in Monterey County, California; prominent farmed crops include leafy greens, berries, broccoli, artichokes, and wine grapes. The agricultural workforce comprises $\approx 50,000$ resident farmworkers, and an additional $\approx 40,000$ seasonal workers support the peak summer and fall seasons (11). The overall population of Salinas Valley is 75% Latino, and 30%–60% of the region's farmworkers are believed to be undocumented (12). Severe overcrowding and household disrepair are common among farmworkers (13), and many live in multigenerational households (14) or in labor camps, vehicles, and informal dwellings (15). Many farmworkers travel long distances to work, often in shared trucks or buses, and might work in close proximity to one another. The living and working conditions of farmworkers have led to concern about the difficulty of preventing SARS-CoV-2 transmission among farmworkers and in their communities (16).

We undertook this study in partnership with Clínica de Salud del Valle de Salinas (CSVs), a federally qualified community and migrant health center in Monterey County. As the main healthcare provider for the region's farmworkers and their families, CSVs operates a network of 12 comprehensive primary care centers serving $>52,000$ low-income, primarily Spanish-speaking patients. The study was reviewed and approved by the Committee for Protection of Human Subjects at University of California, Berkeley.

SARS-CoV-2 Testing

Testing for SARS-CoV-2 infection at CSVs clinics began on June 15, 2020, and was offered to all persons at clinics during weekday business hours. Medical personnel collected oropharyngeal specimens for detection of SARS-CoV-2 RNA via the qualitative Aptima SARS-CoV-2 Assay (Hologic, <https://www.hologic.com>), a nucleic acid transcription-mediated

amplification (TMA) assay with an analytical sensitivity of 62.5 RNA transcript copies/mL (17) and clinical specificity of 99.9% (18). Patients receiving care from CSVs for any reason were encouraged by their healthcare providers to receive SARS-CoV-2 testing, regardless of symptoms; testing also was made available to persons who were not CSVs patients. No-cost testing for persons without insurance was supported by funding from the US Department of Health and Human Services Health Resources and Services Administration. In addition, CSVs conducted outreach testing via mobile testing facilities at community sites including low-income and employer-provided housing, agricultural fields, homeless shelters, food banks, and CSVs-run health fairs where free SARS-CoV-2 testing was offered alongside seasonal influenza vaccination and food donations.

Clinical Surveillance Study

As part of routine clinical intake, all patients ≥ 18 years of age were asked about employment. We considered farmworkers to include all persons engaged in work in agriculture, including crop, nursery, and greenhouse laborers; agricultural equipment operators; workers in packing sheds and other food processing facilities; and farm and ranch animal workers and breeders.

Cross-Sectional Study

Enrollment

To determine the distribution, dynamics, and clinical profile of infection among farmworkers, we invited farmworkers who were receiving a SARS-CoV-2 TMA test at CSVs to participate in a more in-depth cross-sectional study during July 16–November 30, 2020. This study included SARS-CoV-2 antibody testing and a detailed questionnaire. To advertise the study, Spanish- and English-language fliers were designed describing the opportunity to receive free SARS-CoV-2 testing from CSVs and participate in the study. The fliers were hung in CSVs clinics and distributed in the community and to area growers. We stationed the study team at CSVs testing facilities and aimed to approach all patients receiving SARS-CoV-2 TMA tests to screen for study eligibility and invite them to participate in the cross-sectional study. When time allowed, study personnel called patients who had scheduled SARS-CoV-2 testing appointments at CSVs on the day before their visit to advertise the study and screen for eligibility. Participants in an ongoing longitudinal study of farmworker families (12) and those living in housing for

farmworkers also were invited to participate and to bring other farmworkers.

Eligible participants were nonpregnant adult farmworkers ≥ 18 years of age receiving SARS-CoV-2 TMA testing at CSVS. Participants were eligible if they had conducted farm work ≤ 14 days before their testing date, had not participated previously, and spoke sufficient English or Spanish to give consent and complete study procedures. To accommodate the end of the growing season, from October 5 onward we enrolled persons who had engaged in farm work any time since March 2020.

Study Procedures

The study team obtained a blood sample from each participant by venipuncture, measured participants' height by using large-print tape measurers adhered to a post or wall, and measured their weight by using digital scales. The study team administered a 45-minute computer-guided questionnaire by telephone in Spanish or English within 48 hours of the enrollment visit and before SARS-CoV-2 testing results were available. Questionnaire items addressed participant demographics, socioeconomic status, symptoms since December 2019 and in the 2 weeks preceding enrollment, COVID-19 risk factors and exposures, and impacts of the pandemic on daily life and wellbeing (A.M. Mora et al., unpub. data, <https://doi.org/10.1101/2020.12.18.20248518>; A.M. Mora et al., unpub. data, <https://doi.org/10.1101/2021.02.01.2125096>). After participants completed all components of the study, the study team provided a \$50 incentive via prepaid gift cards.

Blood specimens were stored immediately at 4°C–7°C and centrifuged ≤ 48 hours after collection. After centrifugation, plasma aliquots were heat-inactivated at 56°C for 30 minutes and stored at –80°C, then used for assessment of IgG reactivity against the SARS-CoV-2 spike protein via in-house ELISAs (19). In brief, recombinant full-length SARS-CoV-2 spike protein (courtesy of John Pak, Chan Zuckerberg Biohub, San Francisco, California) was coated on Nunc Maxi-sorp ELISA plates (Thermo Fisher Scientific, <https://www.thermofisher.com>) at 1.5 $\mu\text{g}/\text{mL}$. Plates were blocked with 2.5% nonfat dry milk in 1 \times phosphate-buffered saline (PBS) for 2 hours at 37°C. Plates were then washed 3 times in 1 \times PBS. Plasma samples diluted 1:100 in 1% nonfat dry milk in 1 \times PBS were added to the plate in duplicate wells. After a 1-hour incubation at 37°C, plates were washed 5 times in 1 \times PBS with 0.05% Tween-20 (Millipore Sigma, <https://www.sigmaaldrich.com>). Bound antispikes IgG was detected by using horseradish peroxidase-conjugated goat anti-human

IgG (Thermo Fisher Scientific). Plates were developed by using a 3,3',5,5'-tetramethylbenzidine solution, and the reaction was stopped with 2 mol sulfuric acid after 6 minutes. We performed prior assay validation using convalescent serum samples collected ≥ 8 days post symptom onset from 60 hospitalized, PCR-confirmed COVID-19 cases, 57 of which were mild or subclinical and serum samples collected before 2020 from 131 unexposed persons.

We considered specimens positive for anti-SARS-CoV-2 spike IgG if the ELISA optical density (OD) value was >0.096 . This cutoff maximized area under the receiver operating characteristic curve, yielding 94.0% sensitivity and 98.5% specificity. We processed all specimens in duplicate; conducted reflex testing if ≥ 1 OD measurement fell in the borderline range of 0.07–0.3 or if the coefficient of variation between replicates was $\geq 30\%$ and ≥ 1 OD measure was ≥ 0.07 . We confirmed positive specimens by noting presence of IgG against the receptor-binding domain (RBD) of SARS-CoV-2 spike protein (courtesy of John Pak, Chan Zuckerberg Biohub) using the protocol described above and substituting the coating antigen with RBD at 3 $\mu\text{g}/\text{mL}$. We considered specimens positive when RBD ELISA OD values were >0.205 , determined via a similar validation process as described above for spike protein.

Statistical Analyses

Clinical Surveillance Study

We tabulated results for all patients tested at CSVS during June 15–November 30, 2020, by age, sex, and farmworker status. We also computed 2-week moving averages in the daily proportion of tests yielding positive results and estimates of the final proportion of positive tests by patient age, sex, and farmworker status. We used beta distribution to define 2.5% and 97.5% quantiles for the proportion positive.

Cross-Sectional Study

We computed adjusted odds ratios (aORs) using logistic regression models accounting for age, sex, and venue to determine the association of symptoms experienced in the previous 2 weeks with a positive test result. We used the same logistic regression framework to estimate aORs for the association of each symptom experienced in the prior 2 weeks or at any time since December 2019 with continuous SARS-CoV-2 antibody OD measures.

We computed stabilized sampling weights (20) to correct for differences in the population enrolled in the study over time when estimating prevalence

of infection to generate weights for each recruitment period, July 16–August 31, September 1–30, October 1–31, or November 1–30. We fit a multinomial logistic regression model that included a list of possible exposures (Table 1), the number of symptoms participants reported in the preceding 2 weeks, and the recruitment venue as predictors.

We estimated period-specific prevalence of SARS-CoV-2 infection and seropositivity, accounting for inverse sampling weights, by using a generalized

linear model with a log-binomial link function. Models accounted for the 4 recruitment periods, presence of any symptoms, and recruitment venue. We used the model parameter estimates to summarize period-specific prevalence of TMA-positive and seropositive status for persons with and without symptoms whom we would expect to reach via community outreach. To account for missing data (1.1% of observations across all outcome and predictor variables), we sampled estimates from 5

Table 1. Place of residence, living conditions, and working and transportation conditions that could lead to SARS-CoV-2 exposure among farmworkers enrolled in a cross-sectional study, Monterey County, California, USA, July 16–November 30, 2020*

Characteristics	Enrollees, no. (%)		
	All, n = 1,115	Clinic, n = 565	Outreach, n = 550
Community of residence			
Salinas	492 (44.1)	263 (46.5)	229 (41.6)
Northern Monterey County	73 (6.5)	18 (3.2)	55 (10.0)
Southern Monterey County	539 (48.3)	284 (50.3)	255 (46.4)
Outside Monterey County	11 (1.0)	0	11
Household size	n = 1,115	n = 565	n = 550
0 others	12 (1.1)	8 (1.4)	4 (0.7)
1–3 others	399 (35.8)	187 (33.1)	212 (38.6)
4–6 others	515 (46.2)	259 (45.8)	256 (46.5)
≥7 others	189 (17.0)	111 (19.7)	78 (14.2)
Children in household	n = 1,114	n = 565	n = 549
Any children	836 (75.0)	440 (77.9)	396 (72.1)
Children attending school or daycare	n = 1,111	n = 562	n = 549
Any children	85 (7.7)	57 (10.1)	28 (5.1)
Residential overcrowding	n = 1,115	n = 565	n = 550
<2 persons/bedroom	490 (44.0)	224 (39.7)	266 (48.4)
≥2 to <4 persons/bedroom	510 (45.7)	289 (51.2)	221 (40.2)
≥4 persons/bedroom	115 (10.3)	52 (9.2)	63 (11.5)
Ability to isolate at home if infected	n = 1,115	n = 565	n = 550
Live alone or have >1 bedroom and bathroom	643 (57.7)	330 (58.4)	313 (56.9)
Size of company	n = 939	n = 574	n = 456
<25 workers	108 (11.5)	49 (10.1)	59 (12.9)
25–49 workers	132 (14.1)	67 (13.9)	65 (14.3)
50–499 workers	447 (47.6)	229 (47.4)	218 (47.8)
>500 workers	252 (26.8)	138 (28.9)	114 (25.0)
Work setting	n = 1,114	n = 564	n = 550
Indoors only	192 (17.2)	103 (18.3)	89 (16.2)
Outdoors only	849 (76.2)	425 (75.4)	424 (77.1)
Indoor and outdoor	73 (6.6)	36 (6.4)	37 (6.7)
Type of agricultural work	n = 1,105	n = 555	n = 550
Working in the fields	830 (74.4)	416 (73.6)	414 (75.3)
Packing shed	133 (11.9)	65 (11.5)	68 (12.4)
Processing facility	64 (5.74)	34 (6.0)	30 (5.5)
Nursery	40 (3.6)	18 (3.2)	22 (4.0)
Truck driver	38 (3.4)	19 (3.4)	19 (3.5)
Packing truck	22 (1.97)	15 (2.7)	7 (1.3)
Other	21 (1.88)	12 (2.1)	9 (1.6)
Commute to work	n = 1,088	n = 554	n = 534
Alone or with household members only	714 (65.6)	341 (61.6)	373 (69.9)
With nonhousehold members	374 (34.4)	213 (38.4)	161 (30.1)
Contact with acute respiratory illness cases	n = 1,087	n = 547	n = 540
None	971 (89.3)	449 (82.1)	522 (96.7)
At work only	66 (6.1)	54 (9.9)	12 (2.2)
At home only	44 (4.0)	38 (6.9)	6 (1.1)
At home and work	6 (0.6)	6 (1.1)	0
Attended gatherings	n = 1,113	n = 564	n = 549
Attended in preceding 2 weeks	113 (10.2)	50 (8.9)	63 (11.5)

*Clinic participants are those recruited on clinic premises, where they might have been seeking care for COVID-19 or any other illness. Outreach participants are those recruited at mobile testing operations in the community, who were not seeking medical care. SARS-CoV-2, severe acute respiratory syndrome coronavirus 2.

independent iterations of the analysis carried out on multiple-imputed datasets. We conducted analyses in R version 4.0.3 (R Foundation for Statistical Computing, <https://www.r-project.org>); we used the Amelia II package (21) for multiple imputation and fit the multinomial logistic model using the nnet package (22).

Results

Clinical Surveillance Study

During June 15–November 30, CSVS administered 14,169 SARS-CoV-2 TMA tests to adults, including 6,864 tests among farmworkers and 7,305 among other adults living in the same communities (Figure 1, panel A). In total, 1,514 (22.1%) tests among farmworkers had positive results, compared with 1,255 (17.2%) among other adults in the same communities, which corresponds to a 28.5% (95% CI 20.1%–37.4%) higher probability of positive test results among farmworkers (Figure 1, panels B, C). The test-positive fraction was similarly higher among men than among women, for both farmworkers (men 23.7% vs. women 20.5%; risk ratio [RR] 1.16, 95% CI 1.06–1.27) and

nonfarmworkers (men 21.7% vs. women 18.8%; RR 1.15, 95% CI 1.09–1.23). Point estimates of the test-positive fraction were consistent with equal or higher prevalence of infection among farmworkers across all age and sex strata (Figure 1, panels D, E).

Among farmworkers, multiple peaks in the proportion of TMA tests yielding positive results were evident, with the moving average of the test-positive fraction reaching 32.0% (95% CI 27.2%–37.0%) over the period of June 23–July 7 and 30.4% (95% CI 27.0%–34.0%) over the period of August 7–21 (Figure 1, panel C). After declining from mid-September to early October, both the number of tests and the proportion yielding positive results increased through the remainder of the study period. During October 10–November 23, the 2-week moving average of the number of tests conducted daily increased from 35.5 to 69.5 among farmworkers and from 38.7 to 104.5 among other adults. The proportion positive tests increased from 15.4% (95% CI 12.2%–18.8%) to 22.7% (95% CI 20.0%–25.5%) among farmworkers and from 12.1% (95% CI 9.4%–15.1%) to 19.9% (95% CI 17.9%–22.1%) among other adults. This increase in case volume among nonfarmworker adults in November, without a commensurate rise among

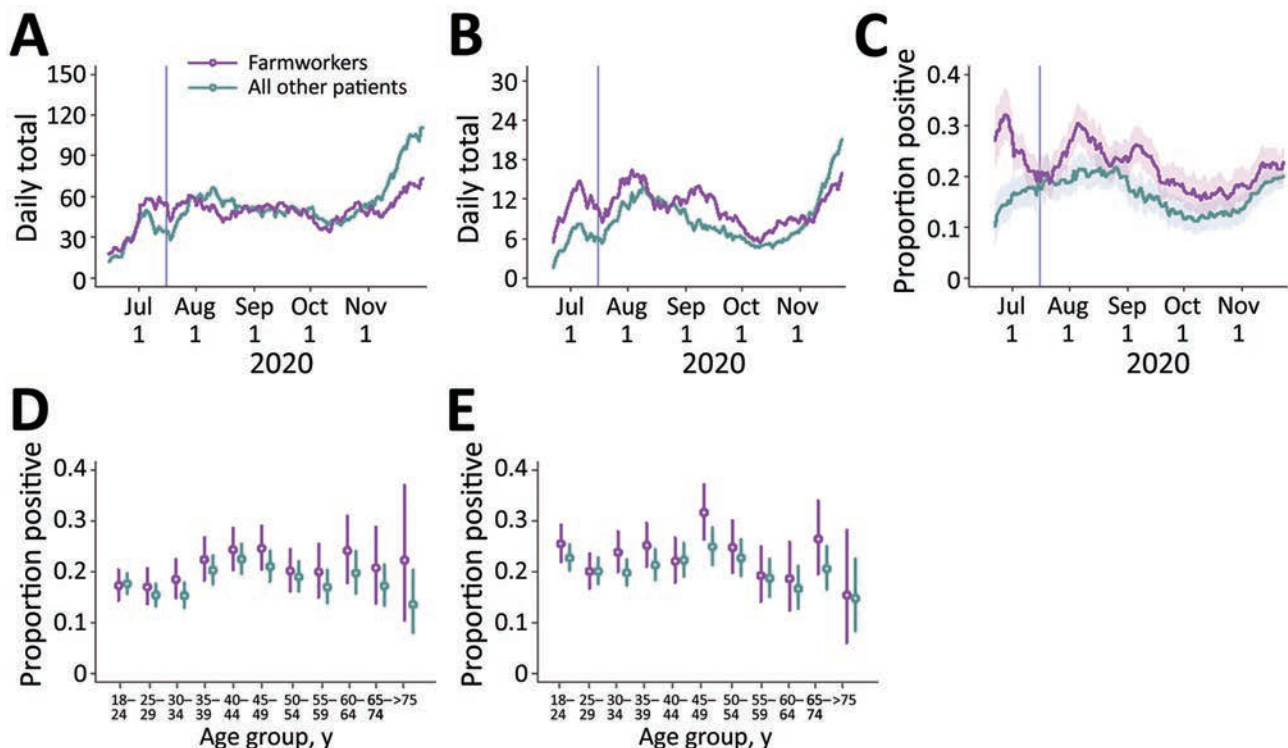


Figure 1. Cases of severe acute respiratory syndrome coronavirus 2 (SARS-CoV-2) diagnosed at Clínica de Salud del Valle de Salinas (CSVs), Monterey County, California, USA, June 15–November 30, 2020. We plotted the 2-week moving averages of the number of patients tested by CSVs (A); the number of SARS-CoV-2 infections diagnosed (B); and the proportion of tests yielding positive results (C). Shading indicates 95% CIs. Vertical lines indicate the date the cross-sectional study began, July 16. We also plotted age- and sex-stratified test-positive fractions for female (D) and male (E) patients. Bars indicate ranges; circles indicate medians.

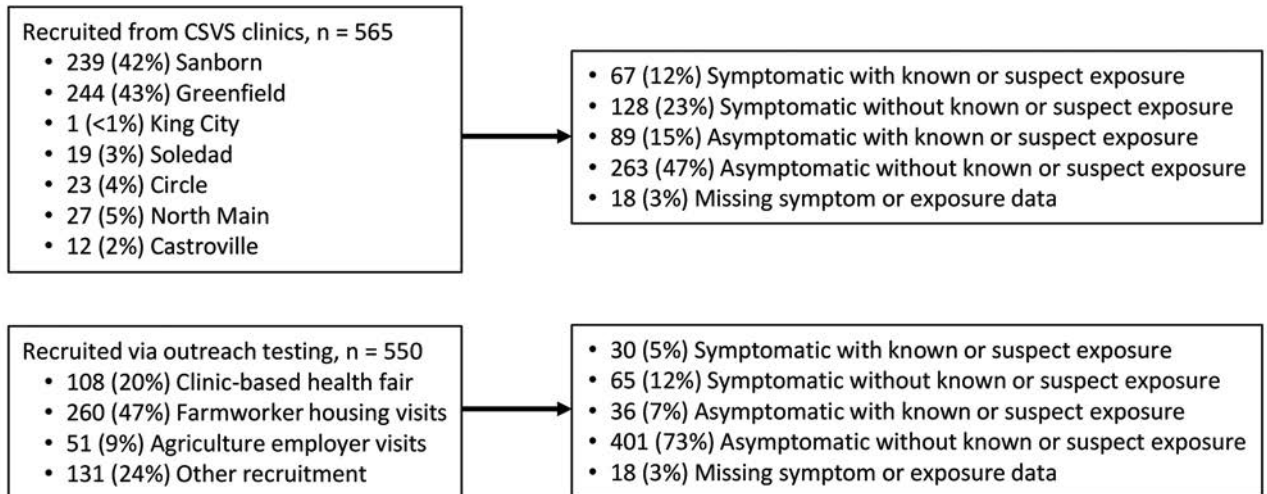


Figure 2. Participants recruited into the cross-sectional study of coronavirus disease (COVID-19) among farmworkers, Monterey County, California, USA, July 16–November 30, 2020. Number of farmworkers recruited at each participating CSVS clinic and outreach venues in the community. Number and proportion of participants reporting symptoms or exposure to known or suspected COVID-19 cases during the prior 2 weeks for both the clinic-based and outreach samples. CSVS, Clínica de Salud del Valle de Salinas.

farmworkers, coincided with the annual migration of many Salinas Valley farmworkers to Yuma, Arizona, and elsewhere (23).

Cross-Sectional Study

Our cross-sectional study recruited 1,115 farmworkers, including 565 who were tested at clinics and 550 tested through outreach efforts (Figure 2). SARS-CoV-2 TMA test results were obtained for 1,111 (99.6%) participants and ELISAs conducted for 1,058 (94.9%) participants (Table 2). Most of the farmworkers in this study were born in Mexico, spoke Spanish at home, had primary school-level education or less, earned <25,000 \$US per year (Table 2), and worked in the fields (Table 1); 36.3% lived in crowded housing (Table 1). Most (81.8%) were overweight or obese, but only 4.4% were current smokers (Table 1). Compared with farmworkers recruited via outreach, farmworkers recruited at clinics had lower levels of educational attainment and had been in the United States fewer years. More spoke indigenous languages at home (14.9% vs. 4.7%; Table 2) and reported contact with an individual experiencing respiratory symptoms in the 2 weeks prior to testing (17.9% vs. 3.3%; Table 1).

Overall, 27.2% of participants reported symptoms potentially related to COVID-19 in the previous 2 weeks and 41.2% reported symptoms since the start of the pandemic (Table 3). A higher proportion of farmworkers recruited at clinics compared with those recruited via outreach reported ≥ 1 symptom potentially attributable to COVID-19 in either the 2 weeks before testing (35.8% vs. 18.4%) or the period

since December 2019 (47.7% vs. 34.7%) (Table 2). Among all farmworkers, 12.7% tested TMA-positive for current SARS-CoV-2 infection, including 18.7% of farmworkers tested at clinics and 6.6% of those tested via outreach (Table 2). In contrast, 19.0% of farmworkers tested via ELISA were found to have antibody evidence of prior infection; similar prevalence was found among those tested in the clinics (18.4%) and via outreach (19.4%).

Of all farmworkers who had TMA-positive test results, 58.9% reported symptoms in the preceding 2 weeks, including 64.8% among those recruited from the clinic and 41.7% of those recruited via outreach (Table 3). Overall, 27.2% of those who had any potential COVID-19 symptoms in the 2 weeks before enrollment had current TMA-positive SARS-CoV-2 infection. Prevalence of current infection among farmworkers recruited in the clinic was 34.2% for those reporting any symptoms and prevalence was 10.1% for those reporting no symptoms. Among farmworkers recruited from outreach testing, current TMA-positive SARS-CoV-2 infection was detected in 14.9% of those reporting any symptoms and 4.7% among those reporting no symptoms (Table 3). After adjustment for age, sex, and recruitment setting, the aOR of a TMA-positive SARS-CoV-2 test result was 4.16 (95% CI 2.85–6.06) among farmworkers reporting any of the solicited symptoms in the previous 2 weeks compared with those reporting no symptoms (Figure 3).

Symptoms most strongly associated with current SARS-CoV-2 infection included shortness of

RESEARCH

breath (aOR 26.86, 95% CI 8.78–83.31), loss of smell (aOR 14.06, 95% CI 6.37–31.15), loss of taste (aOR 11.62, 95% CI 5.52–24.77), and self-reported fever (aOR 9.06, 95% CI 5.02–16.39). Each of these symptoms, however, was reported by <25% of persons with current SARS-CoV-2 infection. For the most

commonly reported symptoms among persons testing positive, headache (33.0%) was associated with 3.52-fold (95% CI 2.31–5.33) higher adjusted odds of SARS-CoV-2 RNA detection, and myalgia (31.6%) was associated with 6.13-fold (95% CI 3.83–9.77) higher adjusted odds.

Table 2. Demographic characteristics, socioeconomic status, and SARS-CoV-2 infection among persons recruited for cross-sectional study of farmworkers, Monterey County, California, USA, July 16–November 30, 2020*

Characteristics	Enrollees, no. (%)		
	All, n = 1,115	Clinic, n = 565	Outreach, n = 550
Age range, y			
18–29	277 (24.8)	140 (24.7)	137 (24.9)
30–39	274 (24.6)	136 (24.0)	138 (25.1)
40–49	298 (26.7)	163 (28.8)	135 (24.5)
50–59	200 (17.9)	90 (15.9)	110 (20.0)
≥60	66 (5.9)	36 (6.4)	30 (5.5)
Sex			
F	586 (52.6)	302 (53.5)	284 (51.6)
M	529 (47.4)	263 (46.5)	266 (48.4)
Country of birth			
Mexico	929 (83.3)	486 (86.0)	443 (80.5)
United States	142 (12.7)	49 (8.7)	93 (16.9)
Other	44 (3.9)	30 (5.3)	14 (2.5)
Language spoken at home			
Spanish	948 (85.0)	460 (81.4)	488 (88.7)
English	57 (5.1)	21 (3.7)	36 (6.5)
Indigenous language	110 (9.9)	84 (14.9)	26 (4.7)
Education	n = 1,114	n = 564	n = 550
Never attended school	62 (5.6)	48 (8.5)	14 (2.5)
Some primary school	430 (38.6)	229 (40.5)	201 (36.5)
Primary school complete	238 (21.3)	119 (21.1)	119 (21.6)
Some high school	142 (12.7)	68 (12.0)	74 (13.5)
High school complete	242 (21.7)	100 (17.7)	142 (25.8)
Family income, US \$	n = 1,059	n = 536	n = 523
<25,000	560 (52.8)	291 (54.3)	269 (51.4)
25,000–34,999	260 (24.6)	112 (20.9)	148 (28.3)
35,000–49,999	162 (15.3)	86 (16.0)	76 (14.5)
≥50,000	77 (7.3)	47 (8.8)	30 (5.7)
Years in United States	n = 1,114	n = 564	n = 550
<15	262 (26.9)	157 (30.4)	105 (23.0)
15–19	194 (19.9)	110 (21.3)	84 (18.4)
20–29	299 (30.7)	141 (27.3)	158 (34.6)
≥30	217 (22.3)	107 (20.7)	110 (24.1)
H2A visa holder	n = 960	n = 509	n = 451
Holds H2A visa	65 (6.8)	20 (4.0)	45 (10.0)
Body mass index	n = 1,087	n = 545	n = 542
<18.5, underweight	4 (0.4)	2 (0.4)	2 (0.4)
18.5–24.9, normal	194 (17.8)	106 (19.4)	88 (16.2)
25–29.9 overweight	423 (38.9)	212 (38.9)	211 (38.9)
≥30, obese	466 (42.9)	225 (41.3)	241 (44.5)
Smoking	n = 1,114	n = 564	n = 550
Never smoked	907 (81.4)	460 (81.6)	447 (81.3)
Former smoker	158 (14.2)	86 (15.2)	72 (13.1)
Current smoker	49 (4.4)	18 (3.2)	31 (5.6)
Recent COVID-19 symptoms	n = 1,108	n = 565	n = 543
Symptoms in preceding 2 weeks	301 (27.2)	200 (35.8)	101 (18.4)
History of COVID-19 symptoms	n = 1,108	n = 558	n = 550
Symptoms since pandemic started in December 2019	457 (41.2)	266 (47.7)	191 (34.7)
SARS-CoV-2 infection	n = 1,111	n = 563	n = 548
Positive TMA result	141 (12.7)	105 (18.7)	36 (6.6)
Prior SARS-CoV-2 infection	n = 1,058	n = 526	n = 532
Positive antibody result	201 (19.0)	97 (18.4)	104 (19.5)

*Clinic participants are those recruited on clinic premises, where they might have been seeking care for COVID-19 or any other illness. Outreach participants are those recruited at mobile testing operations in the community, who were not seeking medical care. COVID-19, coronavirus disease; SARS-CoV-2, severe acute respiratory syndrome coronavirus 2; TMA, transcription-mediated amplification nucleic acid assay.

Table 3. Prevalence of COVID-19 symptoms and severe acute respiratory syndrome coronavirus 2 infection among farm workers enrolled in a cross-sectional study, Monterey County, California, USA, July 16–November 30, 2020*

Symptoms	All participants, n = 1,108		Clinic participants, n = 558		Outreach participants, n = 550	
	Frequency	Infected	Frequency	Infected	Frequency	Infected
Any symptom	301 (27.2)	83 (27.7)	200 (35.8)	68 (34.2)	101 (18.4)	15 (14.9)
No symptoms	807 (72.8)	57 (7.1)	358 (64.2)	36 (10.1)	449 (81.6)	21 (4.7)
Nonproductive cough	68 (6.1)	31 (45.6)	47 (8.4)	26 (55.3)	21 (3.8)	5 (23.8)
Productive cough	68 (6.1)	25 (37.3)	51 (9.1)	21 (42.0)	17 (3.1)	4 (23.5)
Pain or pressure in the ears	24 (2.2)	10 (41.7)	19 (3.4)	10 (52.6)	5 (0.9)	0
Blocked nose	62 (5.6)	22 (36.1)	50 (9.0)	19 (38.8)	12 (2.2)	3 (25.0)
Runny nose	78 (7.0)	24 (31.2)	56 (10.0)	18 (32.7)	22 (4.0)	6 (27.3)
Sneezing	95 (8.6)	21 (22.3)	61 (10.9)	16 (26.7)	34 (6.2)	5 (14.7)
Watery eyes	57 (5.1)	14 (25.0)	48 (8.6)	14 (29.8)	9 (1.6)	0
Hoarseness	49 (4.4)	19 (38.8)	42 (7.5)	17 (40.5)	7 (1.3)	2 (28.6)
Self-reported fever†	56 (5.1)	33 (58.9)	47 (8.4)	29 (61.7)	9 (1.6)	4 (44.4)
Sweating	48 (4.3)	22 (45.8)	40 (7.2)	20 (50.0)	8 (1.5)	2 (25.0)
Chills	74 (6.7)	35 (47.3)	63 (11.3)	33 (52.4)	11 (2.0)	2 (18.2)
Headache	147 (13.3)	46 (31.5)	100 (17.9)	39 (39.4)	47 (8.5)	7 (14.9)
Tickle in throat	49 (4.4)	17 (34.7)	36 (6.5)	15 (41.7)	13 (2.4)	2 (15.4)
Sore throat	103 (9.3)	32 (31.1)	78 (14.0)	29 (37.2)	25 (4.5)	3 (12.0)
Myalgia	97 (8.8)	44 (45.8)	79 (14.2)	40 (51.3)	18 (3.3)	4 (22.2)
Chest pain	26 (2.3)	11 (42.3)	21 (3.8)	10 (47.6)	5 (0.9)	1 (20.0)
Sinus pain	17 (1.5)	7 (41.2)	14 (2.5)	7 (50.0)	3 (0.5)	0 (0.0)
Swollen glands	18 (1.6)	5 (27.8)	11 (2.0)	5 (45.5)	7 (1.3)	0 (0.0)
Loss of appetite	38 (3.4)	21 (55.3)	32 (5.7)	18 (56.2)	6 (1.1)	3 (50.0)
Difficulty breathing	34 (3.1)	18 (52.9)	27 (4.8)	16 (59.3)	7 (1.3)	2 (28.6)
Wheezing	15 (1.4)	6 (40.0)	12 (2.2)	6 (50.0)	3 (0.5)	0
Shortness of breath	22 (2.0)	18 (81.8)	19 (3.4)	16 (84.2)	3 (0.5)	2 (66.7)
Diarrhea	40 (3.6)	15 (37.5)	33 (5.9)	14 (42.4)	7 (1.3)	1 (14.3)
Nausea	39 (3.5)	13 (33.3)	32 (5.7)	13 (40.6)	7 (1.3)	0
Stomach pain	47 (4.2)	15 (31.9)	34 (6.1)	12 (35.3)	13 (2.4)	3 (23.1)
Trouble thinking	18 (1.6)	5 (27.8)	10 (1.8)	5 (50.0)	8 (1.5)	0 (0.0)
Fatigue	94 (8.5)	33 (35.5)	70 (12.5)	31 (44.9)	24 (4.4)	2 (8.3)
Loss of sense of taste	33 (3.0)	22 (66.7)	26 (4.7)	18 (69.2)	7 (1.3)	4 (57.1)
Loss of sense of smell	32 (2.9)	22 (68.8)	25 (4.5)	19 (76.0)	7 (1.3)	3 (42.9)
Pain or pressure in the eyes	25 (2.3)	6 (24.0)	16 (2.9)	6 (37.5)	9 (1.6)	0

*Testing was performed by using transcription-mediated amplification (TMA) assay. Percentages were calculated excluding persons for whom data were not available. Clinic participants are those recruited on clinic premises, where they might have been seeking care for COVID-19 or any other illnesses. Outreach participants are those recruited at mobile testing operations in the community, who were not seeking medical care. For frequency, proportions are computed among all tested. For infected, proportions indicate the prevalence of current, TMA-positive infection among those with the indicated symptom(s) in the previous 2 weeks. COVID-19, coronavirus disease.

†Participants were not asked to verify whether they recorded their body temperature.

Persons who recalled experiencing a blocked nose, sweating, chills, headache, a tickling sensation in the throat, a feeling of pain or pressure in the sinuses, loss of appetite, shortness of breath, fatigue, loss of taste, or loss of smell since December 2019 had higher antibody reactivity, on average, than persons who did not recall experiencing such symptoms (Figure 4, panel A). We also identified higher antibody reactivity among persons experiencing wheezing or loss of taste in the preceding 2 weeks, and suggestive associations of higher antibody measurements with persons reporting chest pain and loss of smell in the preceding 2 weeks (Figure 4, panel B). We found no statistically significant difference in quantitative antibody reactivity measures among persons who were currently infected with SARS-CoV-2 compared with persons who were not ($p = 0.3$), suggesting associations of antibody reactivity with recent symptoms were not attributable to current infection. Among 129 TMA-positive cases 30 (18%) met the threshold

for IgG seropositivity, as did 168/925 (23%) TMA-negative cases.

Reweighting the sample to adjust for differences among persons tested over time, we estimated the prevalence of current, TMA-positive SARS-CoV-2 infection within the population reached by outreach testing was 5.6% (95% CI 2.9%–10.6%) during July 16–August 31, 7.4% (95% CI 4.4%–12.4%) during September 1–30, 4.5% (95% CI 2.6%–7.5%) during October 1–31, and 8.0% (95% CI 5.5%–11.7%) during November 1–30 (Figure 5, panel A). These results closely tracked patterns in the proportion of tests yielding positive results among all farmworkers tested by CSVS (Figure 1, panel C). Over this period, we estimated 2.0% (95% CI 0.9%–4.4%) to 6.4% (95% CI 4.0%–10.2%) prevalence of current SARS-CoV-2 infection among asymptomatic persons and 7.7% (95% CI 3.7%–15.8%) to 17.4% (95% CI 10.4%–29.3%) prevalence of current SARS-CoV-2 infection among persons experiencing ≥ 1 symptom. Estimated seroprevalence increased from 10.5% (95%

CI 6.0%–18.4%) to 21.2% (95% CI 16.6%–27.4%) over the duration of the study, with similar results among symptomatic and asymptomatic persons during each period (Figure 5, panel B).

Discussion

Among all adults tested for SARS-CoV-2 infection by clinics serving the Monterey County farmworker

population, test positivity was 28% higher for farmworkers than for nonfarmworkers from the same communities. Test positivity was much higher (22.1%) among farmworkers tested by CSVS compared with the overall test-positive fraction (6.1%) observed in Monterey County over the same period (24). Within the cross-sectional study subpopulation, we identified sustained high prevalence of infection: TMA-positive

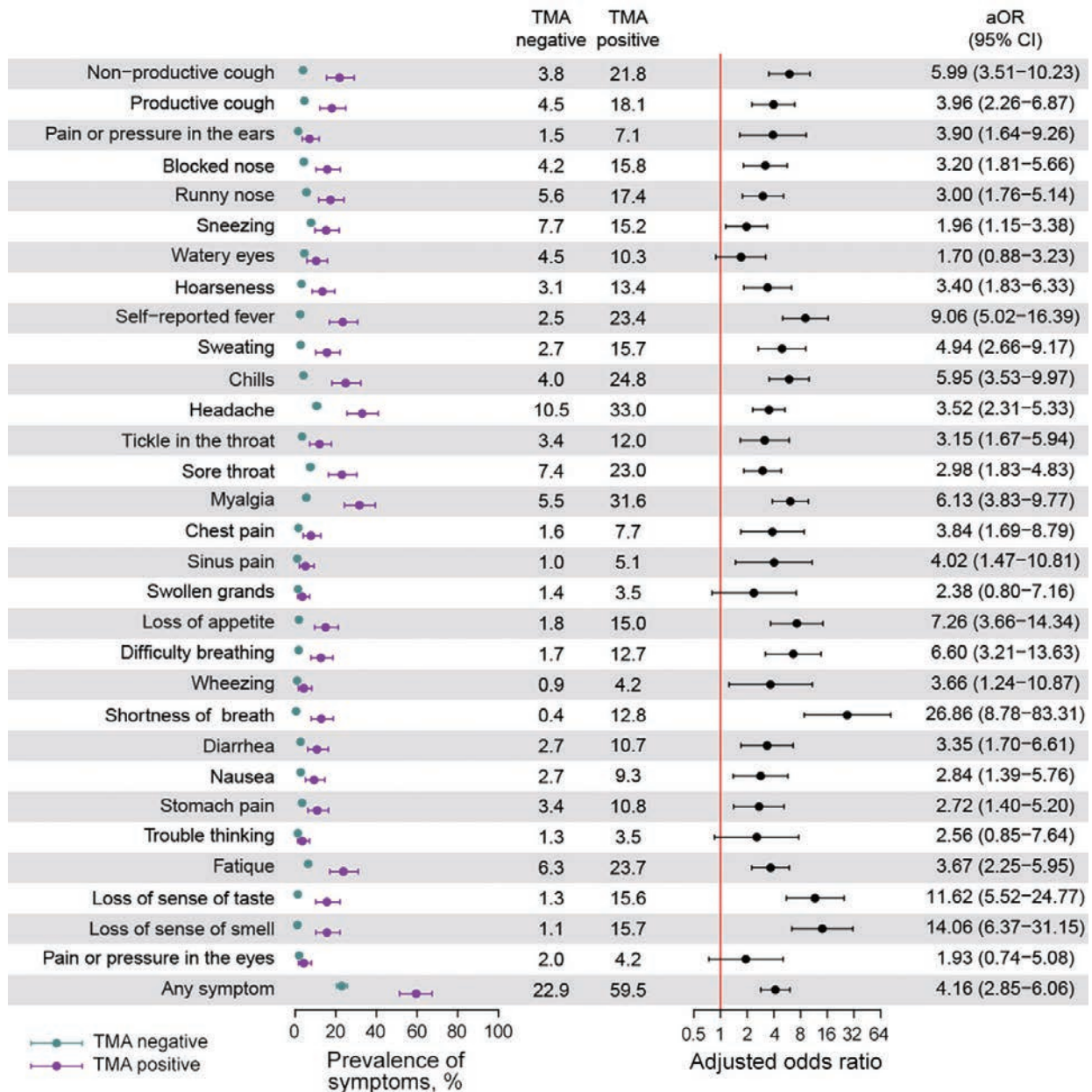


Figure 3. Association of symptoms and current TMA-positive severe acute respiratory syndrome coronavirus 2 (SARS-CoV-2) infection in cross-sectional study of farmworkers, Monterey County, California, USA, July 16–November 30, 2020. Illustration of the prevalence of each symptom during the 2 weeks preceding testing among persons who tested positive and negative for SARS-CoV-2 infection via TMA and the aOR conveying the association of each symptom with current infection. We used logistic regression to determine aORs, controlling for age group, sex, and recruitment venue (i.e., clinic-based or outreach sample). Bars denote 95% CIs around point estimates (circles). aOR, adjusted odds ratio; TMA, transcription-mediated amplification nucleic acid assay.

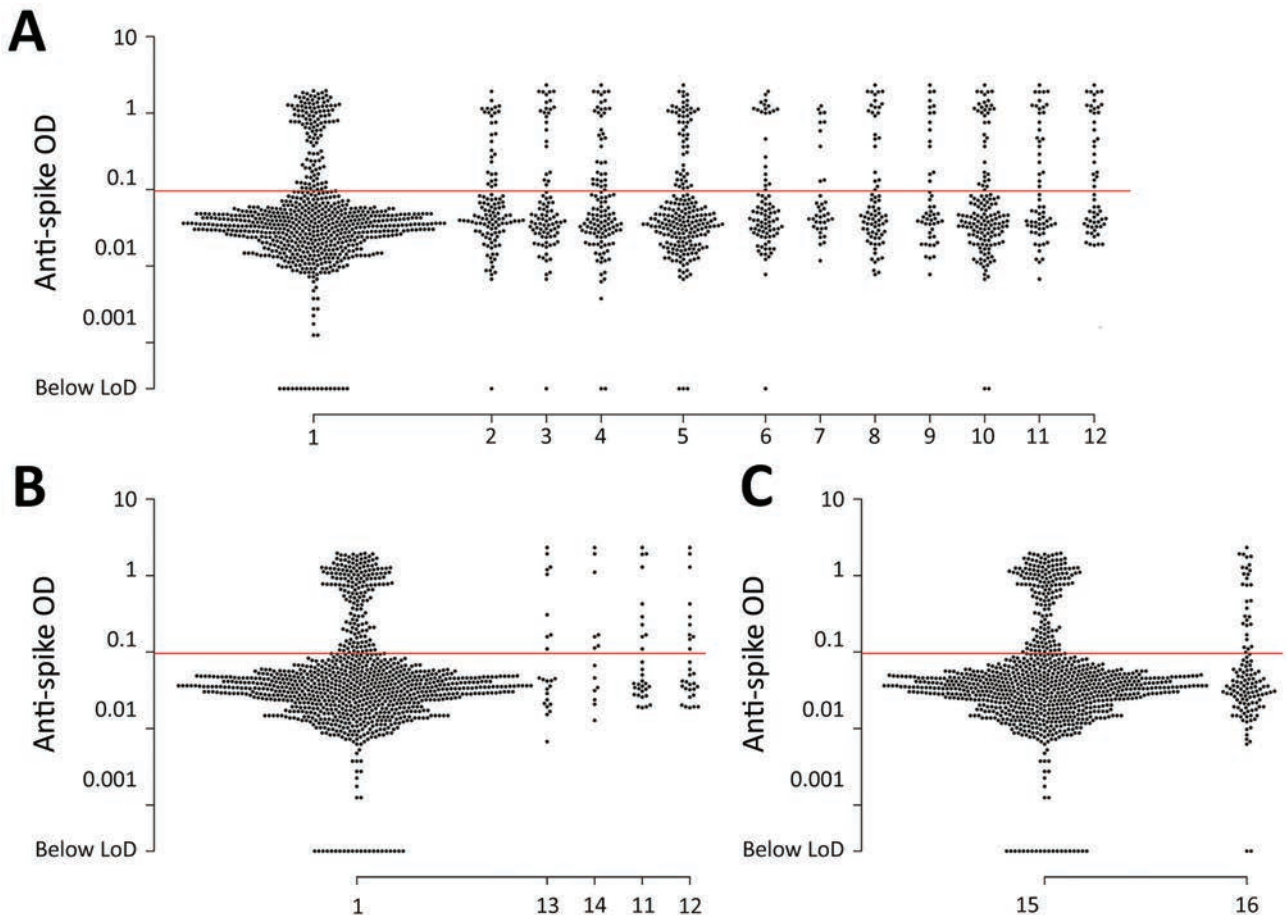


Figure 4. Scatter plot of anti-spike IgG reactivity and association with recalled coronavirus disease (COVID-19) symptoms in a cross-sectional study of farmworkers, Monterey County, California, USA, July 16–November 30, 2020. A) Reactivity among persons who reported experiencing or not experiencing various symptoms potentially associated with COVID-19 since December 2019: 1, none of the symptoms listed here; 2, blocked nose ($p = 0.027$); 3, sweating ($p = 0.010$); 4, chills ($p = 0.013$); 5, headache ($p = 0.034$); 6, tickling in throat ($p = 0.029$); 7, sinus pain or pressure ($p = 0.034$); 8, loss of appetite ($p < 0.001$); 9, shortness of breath ($p = 0.006$); 10, fatigue ($p = 0.032$); 11, loss of taste ($p < 0.001$); 12, loss of smell ($p < 0.001$). B) Reactivity among persons who reported experiencing or not experiencing various symptoms in the 2 weeks before enrollment (data not shown for symptoms with $p > 0.1$): 1, none of the symptoms listed here; 13, chest pain ($p = 0.061$); 14, wheezing ($p = 0.043$); 11, loss of taste ($p = 0.037$); 12, loss of smell ($p = 0.072$). C) Reactivity among persons who had a positive or negative severe acute respiratory syndrome coronavirus 2 transcription-mediated amplification (TMA) nucleic acid assay result at the enrollment visit: 15, TMA-positive ($p = 0.325$); 16, TMA-negative. Reported p values are measured in logistic regression models with the occurrence of each symptom as the outcome and antibody ELISA OD values (log-transformed) as predictors and adjusted for age group and sex. Red lines indicate assay LoD. LoD, limit of detection; OD, optical density.

results among 6.6% of persons tested in the community and 18.7% of those tested in clinics. We estimated $\approx 10\%$ of the farmworker population became infected over a 3-month period during the study, yielding $\approx 21\%$ seroprevalence by November 2020. This seroprevalence is well above the 5% seroprevalence noted among California adults in a large-scale assessment of blood specimens submitted for routine clinical screening or clinical management in September (25). A previous study in San Francisco likewise identified elevated infection risk in an urban low-income and predominantly Latino population, with 6.0% prevalence of current infection among frontline

workers and 7.7% seroprevalence by late April 2020 (26). Our findings demonstrate high infection risk among farmworkers during the ongoing pandemic.

We identified a diverse array of symptoms, including gastrointestinal and other nonrespiratory symptoms, associated with SARS-CoV-2 infection. Among persons found to be TMA-positive for current SARS-CoV-2 infection in our study, 41% did not report experiencing any symptoms in the 2 weeks preceding their test. Similar results have been reported in other studies (27). Of note, persons could have been presymptomatic at the time of their interview; in addition, asymptomatic persons who seek testing might

not represent the broader community (for instance, if testing is triggered by known SARS-CoV-2 exposure). The ≈2%–6% prevalence of infection among persons without symptoms in the community suggests substantial risk for exposure to clinically inapparent cases. Guidance issued for growers to screen farmworkers for fever or other COVID-19 symptoms likely is inadequate to prevent workplace infections (28). We also identified associations of higher antibody reactivity with current symptoms, including loss of taste and smell, chest pain, and wheezing. Participants in our study likely experienced these symptoms in a persisting manner beyond the acute infectious stage because seroconversion typically occurs 8–14 days after initial

symptoms (29). The clinical profile of long COVID has not been fully clarified, but the same symptoms we noted have been identified as prominent complaints in prior studies of prolonged COVID-19 illness, along with fatigue, joint pain, and headache (30,31; C.H. Sudra et al., unpub. data, <https://doi.org/10.1101/2020.10.19.20214494>).

Our study's limitations include that we cannot verify how well our sample represents the farmworker population, many of whom are hidden from population statistical measures (32); our findings should be taken to represent persons reached by testing. Because we excluded persons who did not speak Spanish or English well enough to participate in the cross-sectional

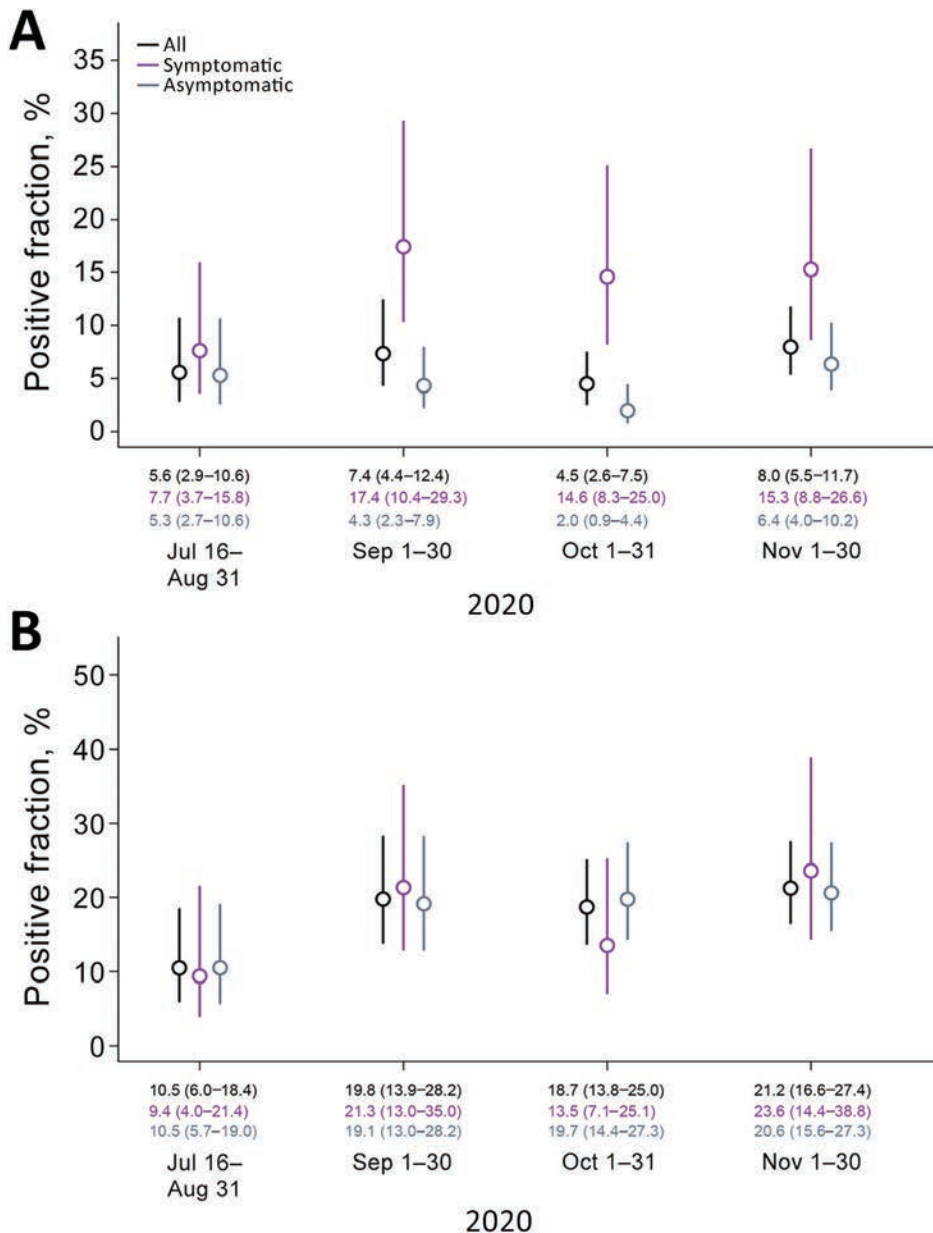


Figure 5. Prevalence of severe acute respiratory syndrome coronavirus 2 (SARS-CoV-2) positivity by transcription-mediated amplification (TMA) and seropositivity over time, Monterey County, California, USA, July 16–November 30, 2020. A) SARS-CoV-2 TMA; B) SARS-CoV-2 IgG ELISA. Estimated prevalence of SARS-CoV-2 infection and seropositivity in a sample population reached by outreach testing, reweighted to correct for differences in the population seeking testing over the course of the study. Lines delineate 95% CI around mean estimates (circles); medians and 95% CIs appear along the baseline.

study, our study likely underrepresents indigenous populations, which are estimated to be 13% of Salinas Valley farmworkers (11). Roughly half of our cross-sectional study participants were enrolled in clinic-based testing, among whom infection prevalence was higher. For this reason, our statistical framework accounted for differences between clinic-based and outreach samples. Last, waning antibody titers from infections acquired early in the pandemic might have contributed to underestimation of seroprevalence, particularly among persons who experienced mild or asymptomatic infection (33).

The recommendation of the Advisory Committee on Immunization Practices prioritized residents of long-term care facilities and healthcare workers for phase 1 vaccination programs (34), but prioritization of differing essential workforce groups among phase 2 recipients will be determined by states. Our study demonstrates high risk for SARS-CoV-2 infection, and both acute and persisting COVID-19 symptoms, among farmworkers in the Salinas Valley. These findings underscore the need to deliver vaccination and other preventive interventions to help reduce further illness among farmworkers and mitigate spread of COVID-19 in the United States.

This article was preprinted at <https://doi.org/10.1101/2020.12.27.20248894>.

Members of the CHAMACOS-Project-19 study team include Jose Camacho, Gardenia Casillas, Celeste Castro, Cynthia Chang, Lupe Flores, Lizari Garcia, Madison J. de Vere, Maria Reina Garcia, Terry Gomez, Carly Hyland, Daniel Lampert, Aaron McDowell-Sanchez, Dominic Pina Montes, Jacqueline Montoya, Lilibeth Nunez, Juanita “Liz” Orozco, Marbel Orozco, Nargis Rezai, Maria T. Rodriguez, Monica Romero, Hina Sheth, Jon Yoshiyama, and Litzi Zepeda.

This study received financial support from the Innovative Genomics Institute at the University of California Berkeley. J.A.L. discloses receipt of grants and fees from Pfizer unrelated to this study. All other authors declare no conflicts of interest.

About the Authors

Dr. Lewnard is an assistant professor of epidemiology at the School of Public Health, University of California, Berkeley, and his research interests include infectious disease transmission dynamics and control. Dr. Mora is an assistant researcher at the University of California, Berkeley, and an associate professor at Universidad Nacional, Heredia, Costa Rica. Her research interests include the health effects of exposures to environmental toxicants.

References

- Lewnard JA, Lo NC. Scientific and ethical basis for social-distancing interventions against COVID-19. *Lancet Infect Dis*. 2020;20:631-3. [https://doi.org/10.1016/S1473-3099\(20\)30190-0](https://doi.org/10.1016/S1473-3099(20)30190-0)
- The President's Coronavirus Guidelines for America. 30 days to slow the spread. 2020 Mar 16 [cited 2021 Jan 21]. https://trumpwhitehouse.archives.gov/wp-content/uploads/2020/03/16.20_coronavirus-guidance_8.5x11_315PM.pdf
- Dyal JW, Grant MP, Broadwater K, Bjork A, Waltenburg MA, Gibbins JD, et al. COVID-19 among workers in meat and poultry processing facilities – 19 states, April 2020. *MMWR Morb Mortal Wkly Rep*. 2020;69. <https://doi.org/10.15585/mmwr.mm6918e3>
- Steinberg J, Kennedy ED, Basler C, Grant MP, Jacobs JR, Ortbahn D, et al. COVID-19 outbreak among employees at a meat processing facility – South Dakota, March–April 2020. *MMWR Morb Mortal Wkly Rep*. 2020;69:1015-9. <https://doi.org/10.15585/mmwr.mm6931a2>
- Stephenson J. COVID-19 Outbreaks among food production workers may intensify pandemic's disproportionate effects on people of color. *JAMA Heal Forum*. 2020 Jun 19 [Epub ahead of print]. <https://doi.org/10.1001/jamahealthforum.2020.0783>
- Martin P. Immigration and farm labor: from unauthorized to H-2A for some? Migration Policy Institute. 2017 [cited 2021 Jan 21]. <https://www.migrationpolicy.org/research/immigration-and-farm-labor-unauthorized-h-2a-some>
- Barham BL, Melo A, Hertz T. Earnings, wages, and poverty outcomes of US farm and low-skill workers. *Appl Econ Perspect Policy*. 2020;42:307-34. <https://doi.org/10.1002/aep.13014>
- Kerwin D, Warren RUS. Foreign-born workers in the global pandemic: essential and marginalized. *J Migr Hum Secur*. 2020;8:282-300. <https://doi.org/10.1177/2331502420952752>
- Becot F, Inwood S, Bendixsen C, Henning-Smith C. Health care and health insurance access for farm families in the United States during COVID-19: essential workers without essential resources? *J Agromedicine*. 2020;25:374-7. <https://doi.org/10.1080/1059924X.2020.1814924>
- Carlisle-Cummins I. COVID-19 farmworker study (COFS): Historic pandemic worsens vulnerability of essential workers who feed us all. 2020 [cited 2021 Jan 21]. <http://covid19farmworkerstudy.org/preliminary-data>
- Villarejo D, Wadsworth G. Farmworker housing study and action plan for Salinas Valley and Pajaro Valley, April 2018. California Institute for Rural Studies. 2018 [cited 2021 Jan 21]. <https://www.co.monterey.ca.us/home/showdocument?id=63729>
- Eskenazi B, Bradman A, Gladstone EA, Jaramillo S, Birch K, Holland N. CHAMACOS, a longitudinal birth cohort study: lessons from the fields. *J Child Heal*. 2003;1:3-27. <https://doi.org/10.3109/713610244>
- Bradman A, Chevrier J, Tager I, Lipsett M, Sedgwick J, Macher J, et al. Association of housing disrepair indicators with cockroach and rodent infestations in a cohort of pregnant Latina women and their children. *Environ Health Perspect*. 2005;113:1795-801. <https://doi.org/10.1289/ehp.7588>
- Goldman L, Eskenazi B, Bradman A, Jewell NP. Risk behaviors for pesticide exposure among pregnant women living in farmworker households in Salinas, California. *Am J Ind Med*. 2004;45:491-9. <https://doi.org/10.1002/ajim.20012>
- Villarejo D. California's hired farm workers move to the cities: the outsourcing of responsibility for farm labor

- housing. Presented at California Rural Legal Assistance Priorities Conference; Asilomar, California; July 16, 2013 [cited 2021 Jan 21]. https://www.crla.org/sites/all/files/u6/2014/rju0214/VillarejoFrmLbrHsngHlth_CRLA_012414.pdf
16. Flocks J. The potential impact of COVID-19 on H-2A agricultural workers. *J Agromedicine*. 2020;25:367-9. <https://doi.org/10.1080/1059924X.2020.1814922>
 17. Smith E, Zhen W, Manji R, Schron D, Duong S, Berry GJ. Analytical and clinical comparison of three nucleic acid amplification tests for SARS-CoV-2 detection. *J Clin Microbiol*. 2020;58:e01134-20. <https://doi.org/10.1128/JCM.01134-20>
 18. Skittrall JP, Wilson M, Smielewska AA, Parmar S, Fortune MD, Sparkes D, et al. Specificity and positive predictive value of SARS-CoV-2 nucleic acid amplification testing in a low-prevalence setting. *Clin Microbiol Infect*. 2020 Oct 14 [Epub ahead of print]. <https://doi.org/10.1016/j.cmi.2020.10.003>
 19. Amanat F, Stadlbauer D, Strohmeier S, Nguyen THO, Chromikova V, McMahon M, et al. A serological assay to detect SARS-CoV-2 seroconversion in humans. *Nat Med*. 2020;26:1033-6. <https://doi.org/10.1038/s41591-020-0913-5>
 20. Cole SR, Hernán MA. Constructing inverse probability weights for marginal structural models. *Am J Epidemiol*. 2008;168:656-64. <https://doi.org/10.1093/aje/kwn164>
 21. Honaker J, King G, Blackwell M. Amelia II: a program for missing data. *J Stat Softw*. 2011;45: 1-47. <https://doi.org/10.18637/jss.v045.i07>
 22. Ripley B, Venables W, Ripley MP. Package ‘nnet.’ 2016 [cited 2021 Jan 21]. <https://cran.r-project.org/web/packages/nnet/nnet.pdf>
 23. Matthews J. Salinas and Yuma share a common (salad) bowl. *San Francisco Chronicle*. 2018 Oct 20 [cited 2021 Jan 21]. <https://www.sfchronicle.com/opinion/article/Salinas-and-Yuma-share-a-common-salad-bowl-13319515.php>
 24. Moreno E. COVID-19 data, metrics and updates. Monterey County Health Department, Public Health Bureau. 2020 [cited 2021 Jan 21]. <https://www.co.monterey.ca.us/home/showdocument?id=96259>
 25. Havers FP, Reed C, Lim T, Montgomery JM, Klens JD, Hall AJ, et al. Seroprevalence of antibodies to SARS-CoV-2 in 10 sites in the United States, March 23–May 12, 2020. *JAMA Intern Med*. 2020 Jul 21 [Epub ahead of print]. PubMed <https://doi.org/10.1001/jamainternmed.2020.4130>
 26. Chamie G, Marquez C, Crawford E, Peng J, Petersen M, Schwab D, et al. CLIAhub Consortium. SARS-CoV-2 community transmission disproportionately affects the Latinx population during shelter-in-place in San Francisco. *Clin Infect Dis*. 2020 Aug 21 [Epub ahead of print]. <https://doi.org/10.1093/cid/ciaa1234>
 27. Buitrago-Garcia D, Egli-Gany D, Counotte MJ, Hossmann S, Imeri H, Ipekci AM, et al. Occurrence and transmission potential of asymptomatic and presymptomatic SARS-CoV-2 infections: A living systematic review and meta-analysis. *PLoS Med*. 2020;17:e1003346. <https://doi.org/10.1371/journal.pmed.1003346>
 28. Advisory for agricultural worker protection during COVID-19 crisis on the Central Coast of California. Monterey County Health Department 2020 [cited 2021 Jan 21]. <https://www.co.monterey.ca.us/home/showdocument?id=88063>
 29. Long QX, Liu BZ, Deng HJ, Wu GC, Deng K, Chen YK, et al. Antibody responses to SARS-CoV-2 in patients with COVID-19. *Nat Med*. 2020;26:845-8. <https://doi.org/10.1038/s41591-020-0897-1>
 30. Mandal S, Barnett J, Brill SE, Brown JS, Denny EK, Hare SS, et al.; ARC Study Group. ‘Long-COVID’: a cross-sectional study of persisting symptoms, biomarker and imaging abnormalities following hospitalisation for COVID-19. *Thorax*. 2020 Nov 10 [Epub ahead of print]. <https://doi.org/10.1136/thoraxjnl-2020-215818>
 31. Carfi A, Bernabei R, Landi F; Gemelli Against COVID-19 Post-Acute Care Study Group. Persistent symptoms in patients after acute COVID-19. *JAMA*. 2020;324:603-5. <https://doi.org/10.1001/jama.2020.12603>
 32. Bail KM, Foster J, Dalmida SG, Kelly U, Howett M, Ferranti EP, et al. The impact of invisibility on the health of migrant farmworkers in the southeastern United States: a case study from Georgia. *Nurs Res Pract*. 2012;2012:760418. PubMed <https://doi.org/10.1155/2012/760418>
 33. Choe PG, Kang CK, Suh HJ, Jung J, Song KH, Bang JH, et al. Waning antibody responses in asymptomatic and symptomatic SARS-CoV-2 infection. *Emerg Infect Dis*. 2021;27:327-9. <https://doi.org/10.3201/eid2701.203515>
 34. Dooling K; ACIP COVID-19 Vaccines Work Group. Phased allocation of COVID-19 vaccines. Presented at the ACIP Meeting 2020 Dec 1 [cited 2021 Jan 21]. <https://www.cdc.gov/vaccines/acip/meetings/downloads/slides-2020-12/COVID-02-Dooling.pdf>

Address for correspondence: Joseph A. Lewnard, University of California, Berkeley, 2121 Berkeley Way, Rm 5410, Berkeley, CA 94720, USA; email: jlewnard@berkeley.edu

Herd Immunity against Severe Acute Respiratory Syndrome Coronavirus 2 Infection in 10 Communities, Qatar

Andrew Jeremijenko, Hiam Chemaitelly, Houssein H. Ayoub, Moza Alishaq, Abdul-Badi Abou-Samra, Jameela Ali A.A. Al Ajmi, Nasser Ali Asad Al Ansari, Zaina Al Kanaani, Abdullatif Al Khal, Einas Al Kuwari, Ahmed Al-Mohammed, Naema Hassan Abdulla Al Molawi, Huda Mohamad Al Naomi, Adeel A. Butt, Peter Coyle, Reham Awni El Kahlout, Imtiaz Gillani, Anvar Hassan Kaleeckal, Naseer Ahmad Masoodi, Anil George Thomas, Hanaa Nafady-Hego, Ali Nizar Latif, Riyazuddin Mohammad Shaik, Nourah B.M. Younes, Hanan F. Abdul Rahim, Hadi M. Yassine, Mohamed G. Al Kuwari, Hamad Eid Al Romaihi, Mohamed H. Al-Thani, Roberto Bertolini, Laith J. Abu-Raddad

We investigated what proportion of the population acquired severe acute respiratory syndrome coronavirus 2 (SARS-CoV-2) infection and whether the herd immunity threshold has been reached in 10 communities in Qatar. The study included 4,970 participants during June 21–September 9, 2020. Antibodies against SARS-CoV-2 were detected by using an electrochemiluminescence immunoassay. Seropositivity ranged from 54.9% (95% CI 50.2%–59.4%) to 83.8% (95% CI 79.1%–87.7%) across communities and showed a pooled mean of 66.1% (95% CI 61.5%–70.6%). A range of other epidemiologic measures indicated that active infection is rare, with limited if any sustainable infection transmission for clusters to occur. Only 5 infections were ever severe and 1 was critical in these young communities; infection severity rate of 0.2% (95% CI 0.1%–0.4%). Specific communities in Qatar have or nearly reached herd immunity for SARS-CoV-2 infection: 65%–70% of the population has been infected.

Since the start of the severe acute respiratory syndrome coronavirus 2 (SARS-CoV-2) pandemic, millions of infections have been confirmed through real-time reverse transcription PCR (RT-PCR) testing

(1), and millions probably have gone undocumented (2). Two key questions remain unanswered. Has any community reached herd immunity to render infection transmission chains unsustainable? What proportion of the population needs to be infected to reach herd immunity?

Qatar, a peninsula in the Arabian Gulf region that has a diverse population of 2.8 million (3), has experienced a large-scale SARS-CoV-2 epidemic (4,5). By January 14, 2021, the rate of real-time RT-PCR-confirmed infections exceeded 65 cases/1,000 persons (6). The epidemic, which is currently in an advanced stage (4), seems to have followed a classic susceptible-infected-recovered pattern, with an epidemic peak around May 20, followed by a steady decrease for the next 8 months (4).

The subpopulation most affected by this epidemic was expatriate craft and manual workers (CMWs) among whom community transmission was first identified (4). These workers constitute ~60% of the population in Qatar and are typically single men 20–49 years of age (7). CMWs at a given workplace

Author affiliations: Hamad Medical Corporation, Doha, Qatar (A. Jeremijenko, M. Alishaq, A.-B. Abou-Samra, J.A.A.A. Al Ajmi, N.A.A. Al Ansari, Z. Al Kanaani, A. Al Khal, E. Al Kuwari, A. Al-Mohammed, N.H.A. Al Molawi, H.M. Al Naomi, A.A. Butt, P. Coyle, R.A. El Kahlout, I. Gillani, A.H. Kaleeckal, N.A. Masoodi, A.G. Thomas, H. Nafady-Hego, A.N. Latif, R.H. Shaik, N.B.M. Younes); Weill Cornell Medicine–Qatar of Cornell University, Doha (H. Chemaitelly, L.J. Abu-Raddad); World Health Organization Collaborating Centre for Disease Epidemiology

Analytics on HIV/AIDS, Sexually Transmitted Infections, Doha (H. Chemaitelly, L.J. Abu-Raddad); Qatar University, Doha (H.H. Ayoub, H.F. Abdul Rahim, H.M. Yassine); Assiut University, Assiut, Egypt (H. Nafady-Hego); Primary Health Care Corporation, Doha (M.G. Al Kuwari); Ministry of Public Health, Doha (H.E. Al Romaihi, M.H. Al-Thani, R. Bertolini); Cornell University, New York, New York, USA (A.A. Butt, L.J. Abu-Raddad)

DOI: <https://doi.org/10.3201/eid2705.20.4365>

or company not only work together during the day but also live together as a community in large dormitories or housing complexes in which they share rooms, bathrooms, and cafeteria-style meals (4,8). These communities stay mostly in contact with their own community members and infrequently mingle with other communities, creating a geographic bubble that proved essential for the pattern of infection transmission (4). With reduced options for effective social and physical distancing, SARS-CoV-2 transmission in these CMW communities resembled that of influenza outbreaks in schools (4,9,10), and especially boarding schools (10). This finding is observed despite implementation of nonpharmaceutical control measures, such as a mask mandate after the World Health Organization (WHO) recommendation (11), promotion and facilitation of social and physical distancing, disinfection of surfaces, and awareness messaging in different languages. A similar transmission pattern has been documented among migrant workers in Singapore (12,13) and Spain (14).

Factors observed included the large number of diagnosed infections in CMWs (4), the large proportion of infections that were asymptomatic (4,15,16), the high real-time RT-PCR positivity rates in the random testing campaigns conducted around the epidemic peak in different CMW communities (4), the observed susceptible-infected-recovered epidemic curve with steady decreases in incidence for 8 months despite the gradual easing of the social and physical distancing restrictions (4,17), and evidence indicating an efficacy >90% for natural infection against reinfection that lasts for ≥ 7 months (18; L.J. Abu-Raddad et al., unpub. data). All of these factors raised questions of whether herd immunity might have been reached in at least some of these communities.

On the basis of these considerations, we hypothesized that at least some of the CMW communities have already reached the herd immunity threshold. To investigate this hypothesis, our specific objective was to assess the proportion of the population that has been infected by assessing the level of detectable antibodies. More than 90% of real-time RT-PCR-confirmed cases in Qatar show development of detectable antibodies (4); therefore, we operationally defined herd immunity as the proportion of the population that needs to have detectable antibodies before infection transmission/circulation becomes unsustainable in this population, with limited if any new infections occurring. The study was conducted to inform the national response and preparedness for potential future infection waves.

Methods

Data Sources

We conducted testing for detectable SARS-CoV-2-specific antibodies in blood specimens in 10 CMW communities during June 21–September 9, 2020. This testing was part of an a priori–designed study combined with a testing and surveillance program led by the Ministry of Public Health and Hamad Medical Corporation (HMC), the main public healthcare provider in Qatar and the nationally designated provider for all COVID-19 healthcare needs. The goal of this program was to assess the level of infection exposure in different subpopulations and economic sectors.

The study design was opportunistic using the Ministry of Public Health–HMC program and the need for rapid data collection to inform the national response. We specifically selected the 10 CMW communities for feasibility or given earlier random real-time RT-PCR testing campaigns or contact tracing that suggested substantial infection levels. For instance, CMW community 1 was part of a random real-time RT-PCR testing campaign that identified, by using nasopharyngeal swab specimens, a high positivity rate of 59% during late April 2020.

The population size of each of these communities ranged from a few hundred to a few thousand who live in shared accommodations provided by the employers. The companies that employ these workers belonged to the service or industrial sectors, but the bulk of the employees, even in the industrial companies, worked on providing services, such as catering, cleaning, and other janitorial services, warehousing, security, and port work.

Ten employers were contacted and were willing to participate and advertise the availability and location of testing sites to their employees. Participation was voluntary. Employees interested in being tested and in knowing their status were provided with transportation to HMC testing sites. Informed consent was able to be obtained in 9 languages (Arabic, Bengali, English, Hindi, Urdu, Nepali, Sinhala, Tagalog, and Tamil) to cater to the main language groups spoken in the CMW communities of Qatar.

We used self-administered questionnaires in these same languages only for CMW community 1; questionnaires were given by trained public health workers to collect data on sociodemographics and history of exposure and symptoms. We developed the questionnaire on the basis of suggestions from WHO (19). A blood specimen was obtained from all study participants, and in 6 communities, nasopharyngeal swab specimens were simultaneously collected for

real-time RT-PCR testing by licensed nurses. We applied national guidelines and standard of care to all identified real-time RT-PCR-positive case-patients, including requirement of isolation and other measures to prevent infection transmission. No action was mandated by the national guidelines to those persons found to be antibody positive but real-time RT-PCR negative, and thus no action was taken apart from notifying persons of their serostatus.

We subsequently linked results of the serologic testing to the HMC centralized and standardized database comprising all SARS-CoV-2 real-time RT-PCR testing conducted in Qatar since the start of the epidemic (4). The database also includes data on hospitalization and on the WHO severity classification (20) for each real-time RT-PCR-confirmed infection. Data were also linked to datasets of 2 recently completed national reinfection studies (18; L.J. Abu-Raddad et al., unpub. data) to identify reinfections. The study was approved by HMC and Weill Cornell Medicine-Qatar Institutional Review Boards.

Laboratory Methods

We performed testing for SARS-CoV-2-specific antibodies in serologic samples by using an electrochemiluminescence immunoassay (Roche Elecsys Anti-SARS-CoV-2, <https://www.roche.com>) (sensitivity 99.5%, specificity 99.8%) (21,22). We interpreted results according to the manufacturer's instructions: reactive for a cutoff index ≥ 1.0 and nonreactive for a cutoff index < 1.0 (22).

We performed real-time RT-PCR testing of aliquots of universal transport medium (Huachenyang Technology, <https://szhcy.en.alibaba.com>) used for collection of nasopharyngeal swab specimens. We extracted aliquots by using the QIASymphony Platform (QIAGEN, <https://www.qiagen.com>); tested them by using real-time PCR (TaqPath COVID-19 Combo Kit; Thermo Fisher Scientific, <https://www.thermo-fisher.com> (sensitivity 100%, specificity 100%) (23) in an ABI 7500 FAST System (ThermoFisher); extracted them by using a custom protocol (M.K. Kalikiri et al., Sidra Medicine, pers. comm., 2021 Feb 1) on a Hamilton Microlab STAR (<https://www.hamiltoncompany.com>); tested them by using the AccuPower SARS-CoV-2 Real-Time RT-PCR Kit (Bioneer, <https://www.bioneer.com>) (sensitivity 100%, specificity 100%) (24) on an ABI 7500 FAST System or loaded them directly into a Roche Cobas 6800 system; and assayed them by using the Cobas SARS-CoV-2 Test (sensitivity 95%, specificity 100%) (25). All laboratory testing was conducted at HMC Central Laboratory following standardized protocols.

Statistical Analysis

We used frequency distributions to describe characteristics of CMWs and to estimate different SARS-CoV-2 epidemiologic measures. We estimated the pooled mean for SARS-CoV-2 seropositivity across CMW communities by using meta-analysis. We applied a DerSimonian-Laird random-effects model (26) to pool seroprevalence measures that were weighted by using the inverse-variance method (27,28).

We used χ^2 tests and univariable logistic regressions to determine the association of each prespecified covariate (i.e., sex, age, nationality, and CMW community) with seropositivity. For CMW community 1, we also investigated associations of educational attainment, contact with an infected person, presence of symptoms in the previous 2 weeks, and whether symptoms required medical attention with seropositivity. Missing values were included as separate subcategories in the analyses. We generated summary statistics, as well as odds ratios (ORs), 95% CIs, and p values (Tables 1, 2; Appendix Tables 1, 2, <https://wwwnc.cdc.gov/EID/article/27/5/20-4365-App1.pdf>).

We performed multivariable logistic regressions to estimate the magnitude of the association of a specific covariate adjusting for other covariates in the model. Covariates with p values ≤ 0.2 in univariable regression analysis were included simultaneously in the multivariable logistic regression model. Covariates with p values ≤ 0.05 in the multivariable model were considered as showing evidence for an association with the outcome, and associated adjusted ORs (aORs), 95% CIs, and p values were generated and reported (Tables 1, 2; Appendix Tables 1, 2). No interactions were investigated. Statistical models' goodness of fit were reported. The distribution of real-time RT-PCR cycle threshold (C_t) values for persons who were real-time RT-PCR positive was further generated, and summary statistics were reported. Statistical analyses were performed by using STATA/SE version 16.1 (<https://www.stata.com>) (29).

We also conducted mathematical modeling simulations to highlight the effect of heterogeneity in the risk for exposure to the infection on the level of herd immunity. These simulations were generated by using a classic age-structured, susceptible-exposed-infectious-recovered mathematical model published elsewhere (17). Simulations were implemented by using MATLAB R2019a (<https://www.mathworks.com>) (30).

Results

A total of 4,970 CMWs from the 10 CMW communities participated in this study (Table 1). Participants

Table 1. Characteristics of 10 CMWs and associations with SARS-CoV-2 seropositivity, indicated by detectable antibodies in serologic samples, Qatar*

Characteristic	No. (%)†	SARS-CoV-2 seropositive			Univariable regression analysis		Multivariable regression analysis‡	
		No.	%§ (95% CI)	p value	OR (95% CI)	p value¶	OR (95% CI)	p value#
Sex								
M	4,721 (95.0)	3,153	66.8 (65.4–68.1)	<0.001	Referent		Referent	
F	249 (5.0)	46	18.5 (13.9–23.9)		0.11 (0.08–0.16)	<0.001	0.13 (0.09–0.19)	<0.001
Age, y								
<29	1,579 (31.8)	1,031	65.3 (62.9–67.6)	<0.001	Referent		Referent	
30–39	1,973 (39.7)	1,226	62.1 (60.0–64.3)		0.87 (0.76–1.00)	0.052	0.90 (0.78–1.05)	0.178
40–49	1,040 (20.9)	680	65.4 (62.4–68.3)		1.00 (0.85–1.18)	0.962	1.12 (0.93–1.35)	0.216
≥50	339 (6.8)	225	66.4 (61.1–71.4)		1.05 (0.82–1.34)	0.705	1.21 (0.92–1.59)	0.170
Missing	39 (0.8)	37	94.9 (82.7–99.4)		9.83 (2.36–40.95)	0.002	9.57 (2.22–41.32)	0.002
Nationality								
Other**	125 (2.5)	40	32.0 (23.9–40.9)	<0.001	Referent		Referent	
Filipino	186 (3.7)	68	36.6 (29.6–43.9)		1.22 (0.76–1.98)	0.408	2.23 (1.32–3.75)	0.003
Sri Lankan	147 (3.0)	77	52.4 (44.0–60.7)		2.34 (1.42–3.84)	0.001	2.81 (1.66–4.76)	<0.001
Kenyan	152 (3.1)	77	50.7 (42.4–58.9)		2.18 (1.33–3.57)	0.002	3.43 (1.99–5.90)	<0.001
Indian	1,647 (33.1)	1,035	62.8 (60.5–65.2)		3.59 (2.44–5.30)	<0.001	3.60 (2.40–5.41)	<0.001
Nepalese	2,136 (43.0)	1,468	68.7 (66.7–70.7)		4.67 (3.17–6.88)	<0.001	4.93 (3.27–7.42)	<0.001
Bangladeshi	577 (11.6)	434	75.2 (71.5–78.7)		6.45 (4.23–9.82)	<0.001	6.78 (4.31–10.66)	<0.001
CMW community								
5	443 (8.9)	243	54.9 (50.1–59.6)	<0.001	Referent		Referent	
4	534 (10.7)	330	61.8 (57.5–65.9)		1.33 (1.03–1.72)	0.028	1.12 (0.83–1.52)	0.449
10	957 (19.3)	620	64.8 (61.7–67.8)		1.51 (1.20–1.90)	<0.001	1.30 (1.02–1.65)	0.034
7	188 (3.8)	122	64.9 (57.6–71.7)		1.52 (1.07–2.17)	0.020	1.31 (0.91–1.89)	0.154
6	1,505 (30.3)	946	62.9 (60.4–65.3)		1.39 (1.12–1.73)	0.002	1.32 (1.06–1.66)	0.015
2	456 (9.2)	282	61.8 (57.2–66.3)		1.33 (1.02–1.74)	0.034	1.46 (1.08–1.96)	0.013
9	202 (4.1)	126	62.4 (55.3–69.1)		1.36 (0.97–1.92)	0.074	1.71 (1.18–2.48)	0.005
8	139 (2.8)	93	66.9 (58.4–74.6)		1.66 (1.12–2.48)	0.013	1.92 (1.25–2.95)	0.003
1	255 (5.1)	193	75.7 (69.9–80.8)		2.56 (1.82–3.61)	<0.001	2.52 (1.75–3.62)	<0.001
3	291 (5.9)	244	83.8 (79.1–87.9)		4.27 (2.97–6.15)	<0.001	3.49 (2.41–5.07)	<0.001

*CMW, craft and manual worker; OR, odds ratio; SARS-CoV-2, severe acute respiratory syndrome coronavirus 2.

†Percentage of total sample.

‡Pseudo-R² value in the multivariable logistic regression model is 7.1%.

§Percent seropositive of those tested.

¶Covariates with p ≤ 0.2 in univariable analysis (i.e., sex, age, nationality, and CMW community) were included in the multivariable analysis.

#Covariates with p ≤ 0.05 in multivariable analysis (i.e., sex, nationality, and CMW community) were considered predictors of SARS-CoV-2 seropositivity.

**Includes all other nationalities that contributed <10% of the sample in each community. These are: Canadian, Egyptian, Ethiopian, Georgian, Ghanaian, Indonesian, Iraqi, Jordanian, Lebanese, Nigerian, Pakistani, Palestinian, Somali, Tanzanian, Tunisian, Ugandan, and Yemeni.

were mostly men (95.0%); <40 years of age (71.5%); and of Nepalese (43.0%), Indian (33.1%), or Bangladeshi (11.6%) origin. Regression analyses identified each of sex, nationality, and CMW community to be independently associated with seropositivity.

Women had 87% lower odds of being seropositive than men (aOR 0.13, 95% CI 0.09–0.19) (Table 1). Compared with all other nationalities (Table 1), aOR was 6.78 (95% CI 4.31–10.66) for Bangladeshis, 4.93 (95% CI 3.27–7.42) for Nepalese, 3.60 (95% CI 2.40–5.41) for Indians, 3.43 (95% CI 1.99–5.90) for Kenyans, 2.81 (95% CI 1.66–4.76) for Sri Lankans, and 2.23 (95% CI 1.32–3.75) for Filipinos. Some differences in seropositivity by CMW community were noted (Table 1). No major differences in seropositivity by age group were found (Table 1).

We provide characteristics and associations with seropositivity (detectable antibodies in serologic samples) for only CMW community 1, in which a specific self-administered questionnaire was administered

and collected specific sociodemographic data and history of exposure and symptoms (Table 2). Nearly 40% of participants had intermediate or low educational attainment, and 31% had higher schooling levels or vocational training. University education was associated with a 75% (OR 0.25, 95% CI 0.09–0.67) lower odds of seropositivity compared with intermediate or lower educational attainment. No significant associations with seropositivity were found for contact with an infected person, presence of symptoms, or symptoms requiring medical attention. We provide characteristics and associations with SARS-CoV-2 seropositivity for CMW communities 2–10 (Appendix Table 1). For each of these communities, associations were found for sex and nationality, but no major associations were found for age group.

We provide key SARS-CoV-2 epidemiologic measures in the different CMW communities (Figure 1). Of 4,970 SARS-CoV-2 antibody test results for these CMWs, 3,199 (64.4%, 95% CI 63.0%–65.7%) were

seropositive. Seropositivity ranged from 54.9% (95% CI 50.2%–59.4%) for CMW community 5 to 83.8% (95% CI 79.1%–87.7%) for CMW community 3 (Figure 1, panel A). The pooled mean for SARS-CoV-2 seropositivity across the 10 CMW communities was 66.1% (95% CI 61.5%–70.6%).

Of 2,016 real-time RT-PCR tests using nasopharyngeal swab specimens collected during this study for these CMWs, 112 (5.6%, 95% CI 4.6%–6.6%) were positive. Real-time RT-PCR positivity ranged from 0.0% (95% CI 0.0%–3.9%) for CMW community 1 and 0.0% (95% CI 0.0%–9.0%) for CMW community 8 to 10.5% (95% CI 7.4%–14.8%) for CMW community 3 (Figure 1, panel B). Pooled mean real-time RT-PCR positivity across the 6 CMW communities in which real-time RT-PCR testing was conducted was 3.9% (95% CI 1.6%–6.9%). The C_t values ranged from 15.8 to

37.4 (median 34.0) (Figure 2). Most (79.5%) real-time RT-PCR-positive persons had C_t values >30, suggestive of no active infection (31,32). Major differences in real-time RT-PCR positivity were found by nationality and CMW community (Appendix Table 2).

Infection positivity (antibody or real-time RT-PCR positive) ranged from 62.5% (95% CI 58.3%–66.7%) for CMW community 4 to 83.8% (95% CI 79.1%–87.7%) for CMW community 3 (Figure 1, panel C). Pooled mean infection positivity across the 6 CMW communities with antibody and RT-PCR results was 69.5% (95% CI 62.8%–75.9%).

Data were linked to the national SARS-CoV-2 real-time RT-PCR testing and hospitalization database. Of the 3,199 antibody-positive CMWs, 1,012 (31.6%, 95% CI 30.0%–33.3%) were previously given a diagnosis of SARS-CoV-2 infection (had a record of a real-time

Table 2. Characteristics of CMW community 1 and associations with SARS-CoV-2 seropositivity (detectable antibodies in serologic samples) including sociodemographics, history of exposure, and symptoms, Qatar*

Characteristic	No. (%)† tested	SARS-CoV-2 seropositive			Univariable regression analysis‡	
		No.	%§ (95% CI)	p value	OR (95% CI)	p value¶
Sex						
M	240 (94.1)	189	78.8 (73.0–83.7)	<0.001	Referent	
F	15 (5.9)	4	26.7 (7.8–55.1)		0.10 (0.03–0.32)	<0.001
Age, y						
<29	105 (41.2)	84	80.0 (71.1–87.2)	0.322	Referent	
30–39	111 (43.5)	83	74.8 (65.6–82.5)		0.74 (0.39–1.41)	0.360
40–49	27 (10.6)	19	70.4 (49.8–86.2)		0.59 (0.23–1.54)	0.284
≥50	12 (4.7)	7	58.3 (27.7–84.8)		0.35 (0.10–1.21)	0.098
Nationality						
Other#	48 (18.8)	23	47.9 (33.3–62.8)	<0.001	Referent	
Indian	32 (12.5)	20	62.5 (43.7–78.9)		1.81 (0.73–4.51)	0.202
Nepalese	157 (61.6)	132	84.1 (77.4–89.4)		5.74 (2.82–11.67)	<0.001
Bangladeshi	18 (7.1)	18	100.0 (81.5–100.0)		Omitted by model	NA
Education level						
Intermediate or lower	101 (39.6)	88	87.1 (79.0–93.0)	<0.001	Referent	
Secondary/high school/vocational	80 (31.4)	69	86.3 (76.7–92.9)		0.93 (0.39–2.20)	0.863
University	27 (10.6)	17	63.0 (42.4–80.6)		0.25 (0.09–0.67)	0.005
Missing	47 (18.4)	19	40.4 (26.4–55.7)		0.10 (0.04–0.23)	<0.001
Contact with an infected person						
No	124 (48.6)	93	75.0 (66.4–82.3)	0.303	Referent	
Yes	14 (5.5)	13	92.9 (66.1–99.8)		4.33 (0.54–34.48)	0.166
Unknown/missing	117 (45.9)	87	74.4 (65.5–82.0)		0.97 (0.54–1.73)	0.909
Symptoms in the past 2 weeks**						
Asymptomatic	184 (72.2)	148	80.4 (74.0–85.9)	<0.001	Referent	
1	16 (6.3)	16	100.0 (79.4–100.0)		Omitted by model	NA
≥2	12 (4.7)	12	100.0 (73.5–100.0)		Omitted by model	NA
Missing	43 (16.9)	17	39.5 (25.0–55.6)		0.16 (0.08–0.32)	<0.001
Symptoms required medical attention						
No	210 (82.4)	174	82.9 (77.1–87.7)	<0.001	Referent	
Yes	3 (1.2)	3	100.0 (29.2–100.0)		Omitted by model	NA
Unknown/missing	42 (16.5)	16	38.1 (23.6–54.4)		0.13 (0.06–0.26)	<0.001

*CMW, craft and manual worker; NA, not applicable; OR, odds ratio; SARS-CoV-2, severe acute respiratory syndrome coronavirus 2.

†Percentage of total sample.

‡Overall sample size and numbers per stratum were too small to warrant conduct of meaningful multivariable regression analysis.

§Percent seropositive of those tested.

¶Covariates with $p \leq 0.05$ in univariable analysis (i.e., sex, nationality, and education level were considered as showing evidence for an association with SARS-CoV-2 seropositivity).

#Includes all other nationalities that contributed <10% of the sample. These are Filipino, Georgian, Kenyan, Sri Lankan, and Tunisian.

**Symptoms were based on self-report and included fever, chills, muscle ache/myalgia, sore throat, cough, runny nose/rhinorrhea, shortness of breath, wheezing, chest pain, other respiratory symptoms, headache, nausea and vomiting, abdominal pain, diarrhea, loss of sense of smell, and loss of sense of taste.

RT-PCR-confirmed positive result before this study). No records of previous real-time RT-PCR positive test results were found for the remaining 2,187 antibody-positive CMWs. For the CMW communities that were previously part of broad real-time RT-PCR testing because of a case identification or a random testing campaign, the diagnosis rate ranged from 28.0% (95% CI 19.1%–38.2%) for CMW community 8 to 82.9% (95% CI 76.8%–87.9%) for CMW community 1. In instances in which no such broad real-time RT-PCR testing was conducted, the diagnosis rate was only 13.2% (95% CI 10.7%–16.1%) for CMW community 10, 7.4% (95% CI 4.7%–11.2%) for CMW community 2, and 0.4% (95% CI 0.0%–2.3%) for CMW community 3. Only a small fraction of antibody-negative persons, 14 of 1,771 (0.8%, 95% CI 0.4%–1.3%), had been previously given a diagnosis of being real-time RT-PCR positive (Appendix Table 3).

Of the total sample, 21 persons had a hospitalization record associated with a SARS-CoV-2 infection diagnosis, of whom, infection severity per WHO classification was mild for 5, moderate for 10, severe for 5, and critical for 1. All 21 persons eventually cleared their infection and were discharged from the hospital. All of these persons were also antibody positive. Accordingly, the proportion of those persons who had a confirmed severe or critical infection of the 3,233 persons who had a laboratory-confirmed infection (antibody or real-time RT-PCR positive result) was 0.2% (95% CI 0.1%–0.4%).

We linked our data to records of 2 recently completed studies. These studies, which assessed reinfection in Qatar in a cohort of >130,000 real-time RT-PCR-confirmed infected persons (18) and a cohort of >43,000 antibody-positive persons (L.J. Abu-Raddad et al., unpub. data), identified no reinfections in these

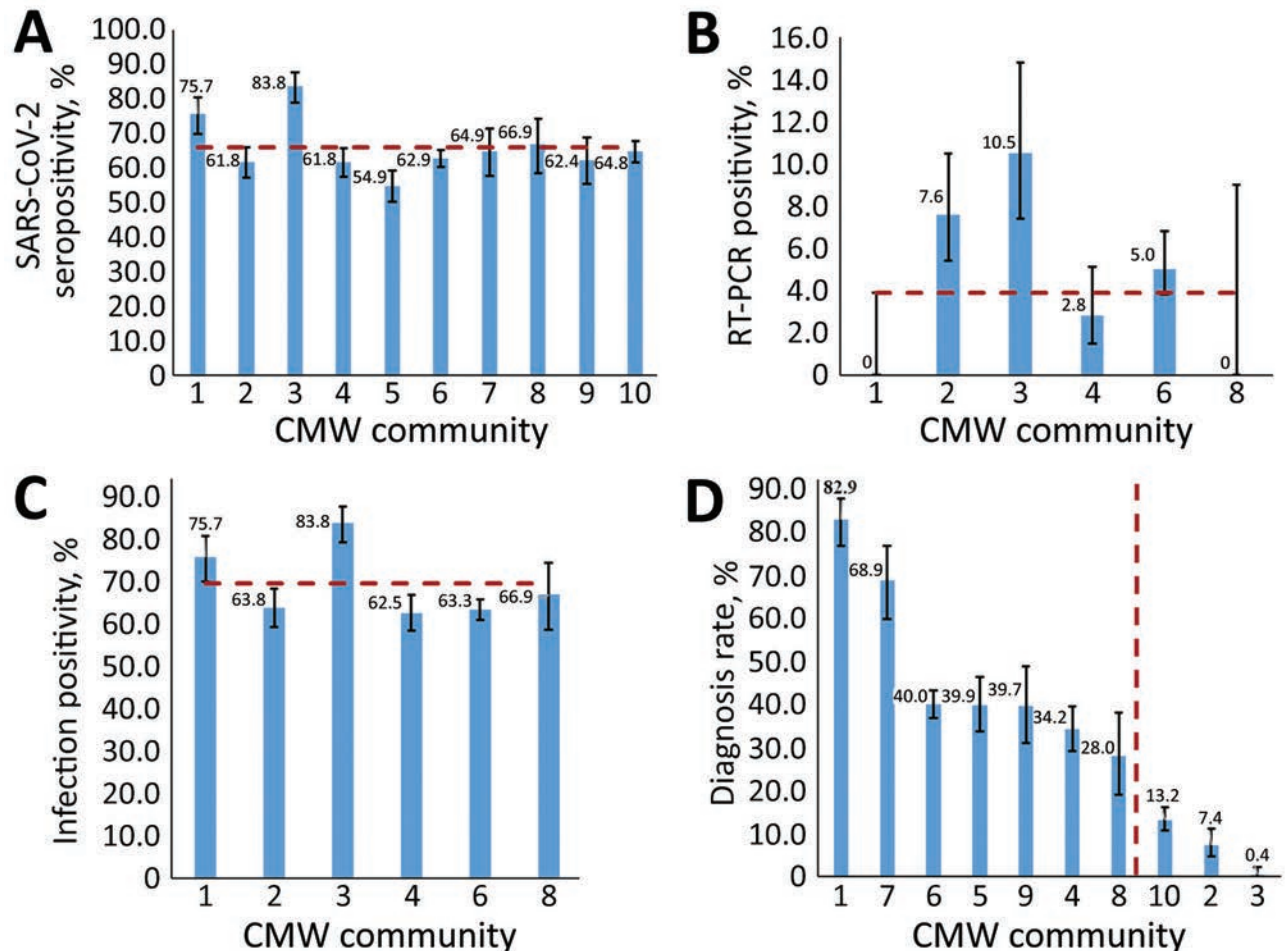


Figure 1. Measures of SARS-CoV-2 infection across 10 craft and manual worker communities, Qatar. A) Seropositivity (antibody positivity), B) real-time RT-PCR positivity, C) infection positivity (antibody or real-time RT-PCR positive), and D) diagnosis rate. Panels B and D show results for only the 6 communities for whom real-time RT-PCR testing was performed. Percentages are shown above bars. Numbers along the x-axes of each panel indicate the community number. Error bars indicate 95% CIs. CMW, craft and manual workers; RT-PCR, real-time reverse transcription PCR; SARS-CoV-2, severe acute respiratory syndrome coronavirus 2.

study participants whose results were confirmed by using viral genome sequencing.

Discussion

Our results support that herd immunity has been reached (or at least nearly reached) in these CMW communities, and that the level of herd immunity needed for SARS-CoV-2 infection is a proportion of the population infected of $\approx 65\%$ – 70% . This conclusion has been reached considering the following lines of evidence. First, these CMW communities had comparable seroprevalences of $\approx 65\%$ – 70% . Second, real-time RT-PCR positivity was low and most of those who were real-time RT-PCR positive had a high C_t suggestive of an earlier rather than recent infection (31,32). Third, only a few persons had active infection ($C_t < 25$) and no major infection cluster was identified in any of these CMW communities during this study or thereafter (suggestive of isolated infections and unsustainable infection transmission for clusters to occur). Fourth, 2 recent studies from Qatar reported an efficacy $>90\%$ for natural infection against reinfection for ≥ 7 months after primary infection (18; L.J. Abu-Raddad et al., unpub. data), in addition to other evidence on the durability of immunity (33–35). Fifth, the level of 65% – 70% infection exposure is in concordance with that predicted by using the classical formula for herd immunity of $1 - 1/R_0$ (36,37); R_0 , the basic reproduction number, as 2.5–4.0 (38,39).

Although large clusters of infection were common in such CMW communities before and around the epidemic peak toward end of May, that time is several weeks before the launch of this study. Thus, no such major cluster has been subsequently identified in such CMW communities in Qatar, despite the progressive easing of the social and physical distancing restrictions since June 15, 2020.

These findings indicate that reaching herd immunity in such largely homogenous communities requires high exposure levels of $\approx 65\%$ – 70% . However, true herd immunity might have been reached even at a lower proportion of the population infected. Mathematical modeling indicates that infection exposure for a novel infection (especially in the first cycle) can considerably overshoot the classical herd immunity level of $1 - 1/R_0$ more so if the social contact rate within this community is homogeneous (Appendix Figure 1). Heterogeneity in the social contact rate can reduce the final proportion of the population that needs to be infected to reach herd immunity (Appendix Figure 1) (37; R. Aguas et al., Oxford University, pers. comm., 2021 Feb 1).

The severity rate for SARS-CoV-2 infection was low (0.2%), possibly because of the young age of the

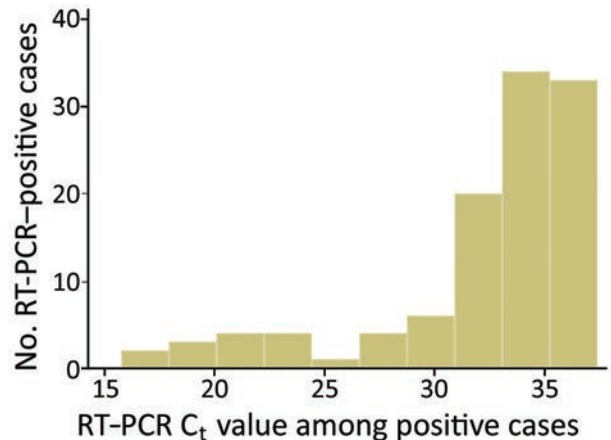


Figure 2. Distribution of real-time RT-PCR C_t values among craft and manual workers identified as real-time RT-PCR positive for severe acute respiratory syndrome coronavirus 2, Qatar. C_t , cycle threshold; RT-PCR, real-time reverse transcription PCR.

CMWs. No COVID-19 deaths were reported in these CMW communities. In communities in which no previous, broad real-time RT-PCR testing was conducted, $<15\%$ of the antibody-positive persons had ever been given a diagnosis as being real-time RT-PCR positive before this study. There was a large difference in infection exposure between women and men (Table 1). This difference, with the variable proportion of women across these communities, also explains part of the variation seen in the overall seroprevalence across these communities (Figure 1; Appendix Figure 2). This finding might be attributed to women and men living in different housing accommodations and having different work roles. Women, a small minority in these CMW communities, live in small shared accommodations as opposed to the large ones hosting men.

Differences in results by nationality (Table 1), are explained by nearly all Bangladeshis and Nepalese and most Indians being the workers in these communities, because a proportion of Indians and much of the other nationalities held administrative or managerial positions that had lower social contact rates and possibly lived in different accommodations than most of the workers. No major differences in infection exposure by age were found, although there was a tendency for persons >40 years of age to have lower infection exposure (Appendix Table 1), possibly caused by different occupations within these communities.

Our study's limitations included that, by design, the study was specifically conducted in select CMW communities, and therefore findings might not be representative nor generalizable to the wider CMW population in Qatar. The small and variable proportion of women in these communities suggests that

findings might not also be generalizable to women in these communities. Response rate could not be precisely ascertained given uncertainty around the number of CMWs who were aware of the invitation to participate, but on the basis of employer-reported counts of the size of each community, the response rate was >50%, and participants expressed high interest in knowing their antibody status. The validity of study outcomes is contingent on the sensitivity and specificity of the used assays. However, laboratory methods were based on high-quality commercial platforms, and each diagnostic method was validated in the laboratory before its use. The antibody assay is one of the best available and extensively used and investigated commercial platforms; it has a specificity $\geq 99.8\%$ (22,40,41), indicating that false-positive results, or positive results due to cross-reactivity with other common cold coronaviruses, are not likely.

In conclusion, some of the CMW communities in Qatar, who constituted $\approx 60\%$ of the total population (7), have reached or nearly reached herd immunity for SARS-CoV-2 infection. Although achieving herd immunity at a national level is difficult within a few months (42), herd immunity could be achieved in specific communities within a few months. In such relatively homogenous communities, reaching herd immunity required infection of 65%–70% of the members of the community. These findings suggest that the SARS-CoV-2 epidemic in a homogenous population is likely to be sustainable until at least two thirds of the population become infected. This finding also suggests that a SARS-CoV-2 vaccine needs at least 65%–70% efficacy at universal coverage for herd immunity to be achieved in a population not exposed to SARS-CoV-2 infection (43,44; H.H. Ayoub et al., unpub. data). Alternatively, herd immunity might be reached at a vaccination coverage of $\approx 75\%$ if vaccine efficacy is 95%, similar to that of the recently licensed SARS-CoV-2 vaccines (45,46).

Acknowledgments

We thank Hanan Al Kuwari for providing vision, guidance, leadership, and support; Saad Al Kaabi for providing leadership, analytical insights, and an instrumental role in enacting data information systems that made these studies possible; the SWICC Committee and the Scientific Reference and Research Taskforce (SRRT) members for providing informative input, scientific technical advice, and enriching discussions; Mariam Abdulmalik and members of the Tactical Community Command Group on COVID-19 for providing support to the teams that worked on field surveillance;

Nahla Afifi, Tasneem Al-Hamad, Eiman Al-Khayat, and the rest of the Qatar Biobank for Medical Research team for providing unwavering support in retrieving and analyzing samples and in compiling and generating databases for COVID-19 infection; Asmaa Al-Thani for providing leadership; the Clinical Coding Team and the COVID-19 Mortality Review Team (both at Hamad Medical Corporation) and Surveillance Team at the Ministry of Public Health for providing dedicated efforts; Ziad Yehya at Qatargas for providing dedicated logistical and resource support; and all companies that facilitated the participation of their employees in this study.

This study was supported by the Hamad Medical Corporation, Ministry of Public Health, and the Biomedical Research Program and the Biostatistics, Epidemiology, and Biomathematics Research Core, both at Weill Cornell Medicine-Qatar.

A.J. and L.J.A. conceived and designed the study; A.J. collected data; H.C. performed data analyses and wrote the first draft of the manuscript; and H.H.A. contributed to analysis of data. All authors contributed to data acquisition, database development, testing, program development, discussion and interpretation of the results, and writing the manuscript. All authors have read and approved the final manuscript. All data are available in an aggregate form in the main text and Appendix.

About the Author

Dr. Jeremijenko is a senior consultant in occupational and environmental medicine at Hamad Medical Corporation, Doha, Qatar. His research interests are multidisciplinary, with an emphasis on occupational medicine, toxicology, and infectious diseases.

References

1. Worldometer. COVID-19 outbreak live update [cited 2020 Sep 6]. <https://www.worldometers.info/coronavirus>
2. Ioannidis J. Infection fatality rate of COVID-19 inferred from seroprevalence data. *Bull World Health Organ*. 2020 [cited 2021 Jan 21]. https://www.who.int/bulletin/online_first/BLT.20.265892.pdf
3. Planning and Statistics Authority. State of Qatar. Qatar monthly statistics [cited 2020 May 26]. <https://www.psa.gov.qa/en/pages/default.aspx>
4. Abu-Raddad LJ, Chemaitelly H, Ayoub HH, Al Kanaani Z, Al Khal A, Al Kuwari E, et al. Characterizing the Qatar advanced-phase SARS-CoV-2 epidemic. *Sci Rep*. 2021;11:6233–48. <https://doi.org/10.1038/s41598-021-85428-7>
5. Al Kuwari HM, Abdul Rahim HF, Abu-Raddad LJ, Abou-Samra A-B, Al Kanaani Z, Al Khal A, et al. Epidemiological investigation of the first 5685 cases of SARS-CoV-2 infection in Qatar, 28 February–18 April 2020. *BMJ Open*. 2020;10:e040428. <https://doi.org/10.1136/bmjopen-2020-040428>

6. Ministry of Public Health. State of Qatar. Coronavirus disease 2019 (COVID-19) [cited 2020 May 25]. <https://covid19.moph.gov.qa/EN/Pages/default.aspx>
7. Planning and Statistics Authority. State of Qatar. Labor force sample survey [cited 2020 May 1]. https://www.psa.gov.qa/en/statistics/Statistical%20Releases/Social/LaborForce/2017/statistical_analysis_labor_force_2017_En.pdf
8. De Bel-Air F. Demography, migration, and labour market in Qatar [cited 2020 May 1]. https://www.researchgate.net/publication/323129801_Demography_Migration_and_Labour_Market_in_Qatar_UPDATED_June_2017
9. Jackson C, Vynnycky E, Hawker J, Olowokure B, Mangtani P. School closures and influenza: systematic review of epidemiological studies. *BMJ Open*. 2013;3:e002149. <https://doi.org/10.1136/bmjopen-2012-002149>
10. Glatman-Freedman A, Portelli I, Jacobs SK, Mathew JJ, Slutzman JE, Goldfrank LR, et al. Attack rates assessment of the 2009 pandemic H1N1 influenza A in children and their contacts: a systematic review and meta-analysis. *PLoS One*. 2012;7:e50228. <https://doi.org/10.1371/journal.pone.0050228>
11. Cheng KK, Lam TH, Leung CC. Wearing face masks in the community during the COVID-19 pandemic: altruism and solidarity. *Lancet*. 2020;Apr 16:[Epub ahead of print]. [https://doi.org/10.1016/S0140-6736\(20\)30918-1](https://doi.org/10.1016/S0140-6736(20)30918-1)
12. Koh D. Migrant workers and COVID-19. *Occup Environ Med*. 2020;77:634-6. <https://doi.org/10.1136/oemed-2020-106626>
13. Bagdasarian N, Fisher D. Heterogenous COVID-19 transmission dynamics within Singapore: a clearer picture of future national responses. *BMC Med*. 2020;18:164. <https://doi.org/10.1186/s12916-020-01625-7>
14. Guijarro C, Pérez-Fernández E, González-Piñero B, Meléndez V, José Goyanes M, Renilla ME, et al. Differential risk for COVID-19 in the first wave of the disease among migrants from several areas of the world living in Spain [in Spanish]. *Rev Clin Esp*. 2020;Nov 20 [Epub ahead of print]. <https://doi.org/10.1016/j.rce.2020.10.10.006>
15. Nikolai LA, Meyer CG, Kremsner PG, Velavan TP. Asymptomatic SARS coronavirus 2 infection: invisible yet invincible. *Int J Infect Dis*. 2020;100:112-6. <https://doi.org/10.1016/j.ijid.2020.08.076>
16. Oran DP, Topol EJ. Prevalence of asymptomatic SARS-CoV-2 infection: a narrative review. *Ann Intern Med*. 2020;173:362-7. <https://doi.org/10.7326/M20-3012>
17. Ayoub HH, Chemaitelly H, Seedat S, Makhoul M, Al Kanaani Z, Al Khal A, et al. Mathematical modeling of the SARS-CoV-2 epidemic in Qatar and its impact on the national response to COVID-19. *J Glob Health*. 2021;11:05005. <https://doi.org/10.7189/jogh.11.05005>
18. Abu-Raddad LJ, Chemaitelly H, Malek JA, Ahmed AA, Mohamoud YA, Younuskuunju S, et al. Assessment of the risk of SARS-CoV-2 reinfection in an intense re-exposure setting. *Clin Infect Dis*. 2020 Dec 14:[Epub ahead of print]. <https://doi.org/10.1093/cid/ciaa1846>
19. World Health Organization. Population-based age-stratified seroepidemiological investigation protocol for COVID-19 virus infection [cited 2020 Apr 15]. <https://apps.who.int/iris/handle/10665/331656>
20. World Health Organization. Clinical management of COVID-19 [cited 2020 May 31]. <https://www.who.int/publications-detail/clinical-management-of-covid-19>
21. Muench P, Jochum S, Wenderoth V, Ofenloch-Haehnle B, Hombach M, Strobl M, et al. Development and validation of the Elecsys Anti-SARS-CoV-2 immunoassay as a highly specific tool for determining past exposure to SARS-CoV-2. *J Clin Microbiol*. 2020;58:e01694-20. <https://doi.org/10.1128/JCM.01694-20>
22. The Roche Group. Roche's COVID-19 antibody test receives FDA emergency use authorization and is available in markets accepting the CE mark [cited 2020 Jun 5]. <https://www.roche.com/media/releases/med-cor-2020-05-03.htm>
23. Thermo Fisher Scientific. TaqPath™ COVID-19 CE-IVD RT-PCR Kit instructions for use [cited 2020 Dec 2]. https://assets.thermofisher.com/TFS-Assets/LSG/manuals/MAN0019215_TaqPathCOVID-19_CE-IVD_RT-PCR%20Kit_IFU.pdf
24. Kubina R, Dziedzic A. Molecular and serological tests for COVID-19 a comparative review of SARS-CoV-2 coronavirus laboratory and point-of-care diagnostics. *Diagnostics (Basel)*. 2020;10:E434. <https://doi.org/10.3390/diagnostics10060434>
25. US Food and Drug Administration. Cobas® SARS-CoV-2: Qualitative assay for use on the cobas® 6800/8800 systems [cited 2020 Dec 2]. <https://www.fda.gov/media/136049/download>
26. DerSimonian R, Laird N. Meta-analysis in clinical trials. *Control Clin Trials*. 1986;7:177-88. [https://doi.org/10.1016/0197-2456\(86\)90046-2](https://doi.org/10.1016/0197-2456(86)90046-2)
27. Miller JJ. The inverse of the Freeman-Tukey double arcsine transformation. *Am Stat*. 1978;32:138 [cited 2020 Dec 2]. <https://www.tandfonline.com/doi/abs/10.1080/00031305.1978.10479283>
28. Barendregt JJ, Doi SA, Lee YY, Norman RE, Vos T. Meta-analysis of prevalence. *J Epidemiol Community Health*. 2013;67:974-8. <https://doi.org/10.1136/jech-2013-203104>
29. StataCorp. Statistical Software: Release 16.1. College Station (TX): Stata Corporation; 2019.
30. MATLAB®. The language of technical computing. Natick (MA): The MathWorks, Inc.; 2019.
31. Sethuraman N, Jeremiah SS, Ryo A. Interpreting diagnostic tests for SARS-CoV-2. *JAMA*. 2020;323:2249-51. <https://doi.org/10.1001/jama.2020.8259>
32. Wajnberg A, Mansour M, Leven E, Bouvier NM, Patel G, Firpo-Betancourt A, et al. Humoral response and PCR positivity in patients with COVID-19 in the New York City region, USA: an observational study. *Lancet Microbe*. 2020;1:e283-9. [https://doi.org/10.1016/S2666-5247\(20\)30120-8](https://doi.org/10.1016/S2666-5247(20)30120-8)
33. Dan JM, Mateus J, Kato Y, Hastie KM, Yu ED, Faliti CE, et al. Immunological memory to SARS-CoV-2 assessed for up to 8 months after infection. *Science*. 2021;371:eabf4063. <https://doi.org/10.1126/science.abf4063>
34. Wajnberg A, Amanat F, Firpo A, Altman DR, Bailey MJ, Mansour M, et al. Robust neutralizing antibodies to SARS-CoV-2 infection persist for months. *Science*. 2020;370:1227-30. <https://doi.org/10.1126/science.abd7728>
35. Lumley SF, O'Donnell D, Stoesser NE, Matthews PC, Howarth A, Hatch SB, et al.; Oxford University Hospitals Staff Testing Group. Antibody status and incidence of SARS-CoV-2 infection in health care workers. *N Engl J Med*. 2021;384:533-40. <https://doi.org/10.1056/NEJMoa2034545>
36. Anderson RM, Heesterbeek H, Klinkenberg D, Hollingsworth TD. How will country-based mitigation measures influence the course of the COVID-19 epidemic? *Lancet*. 2020;395:931-4. [https://doi.org/10.1016/S0140-6736\(20\)30567-5](https://doi.org/10.1016/S0140-6736(20)30567-5)
37. Britton T, Ball F, Trapman P. A mathematical model reveals the influence of population heterogeneity on herd immunity to SARS-CoV-2. *Science*. 2020;369:846-9. <https://doi.org/10.1126/science.abc6810>

38. He W, Yi GY, Zhu Y. Estimation of the basic reproduction number, average incubation time, asymptomatic infection rate, and case fatality rate for COVID-19: Meta-analysis and sensitivity analysis. *J Med Virol*. 2020;92:2543–50. <https://doi.org/10.1002/jmv.26041>
39. Online MIDAS. COVID-19 portal. COVID-19 parameter estimates: basic reproduction number [cited 2020 May 19]. https://github.com/midas-network/COVID-19/tree/master/parameter_estimates/2019_novel_coronavirus
40. Public Health England. Evaluation of Roche Elecsys AntiSARS-CoV-2 serology assay for the detection of anti-SARS-CoV-2 antibodies [cited 2020 Jun 5]. https://assets.publishing.service.gov.uk/government/uploads/system/uploads/attachment_data/file/891598/Evaluation_of_Roche_Elecsys_anti_SARS_CoV_2_PHE_200610_v8.1_FINAL.pdf
41. Oved K, Olmer L, Shemer-Avni Y, Wolf T, Supino-Rosin L, Prajrod G, et al. Multi-center nationwide comparison of seven serology assays reveals a SARS-CoV-2 non-responding seronegative subpopulation. *EClinicalMedicine*. 2020; 29:100651. <https://doi.org/10.1016/j.eclinm.2020.100651>
42. Pollán M, Pérez-Gómez B, Pastor-Barriuso R, Oteo J, Hernán MA, Pérez-Olmeda M, et al.; ENE-COVID Study Group. Prevalence of SARS-CoV-2 in Spain (ENE-COVID): a nationwide, population-based seroepidemiological study. *Lancet*. 2020;396:535–44. [https://doi.org/10.1016/S0140-6736\(20\)31483-5](https://doi.org/10.1016/S0140-6736(20)31483-5)
43. Makhoul M, Ayoub HH, Chemaitelly H, Seedat S, Mumtaz GR, Al-Omari S, et al. Epidemiological impact of SARS-CoV-2 vaccination: mathematical modeling analyses. *Vaccines (Basel)*. 2020;8:E668. <https://doi.org/10.3390/vaccines8040668>
44. Makhoul M, Chemaitelly H, Ayoub HH, Seedat S, Abu-Raddad LJ. Epidemiological differences in the impact of COVID-19 vaccination in the United States and China. *Vaccines (Basel)*. 2021;9:223–36. <https://doi.org/10.3390/vaccines9030223>
45. Jackson LA, Anderson EJ, Roupheal NG, Roberts PC, Makhene M, Coler RN, et al.; mRNA-1273 Study Group. An mRNA vaccine against SARS-CoV-2: preliminary report. *N Engl J Med*. 2020;383:1920–31. <https://doi.org/10.1056/NEJMoa2022483>
46. Polack FP, Thomas SJ, Kitchin N, Absalon J, Gurtman A, Lockhart S, et al.; C4591001 Clinical Trial Group. Safety and efficacy of the BNT162b2 mRNA COVID-19 vaccine. *N Engl J Med*. 2020;383:2603–15. <https://doi.org/10.1056/NEJMoa2034577>

Address for correspondence: Andrew Jeremijenko, Hamad Medical Corporation, PO Box 3050, Doha, Qatar; email: ajeremijenko@hamad.qa or Laith J. Abu-Raddad, Infectious Disease Epidemiology Group, World Health Organization Collaborating Centre for Disease Epidemiology Analytics on HIV/AIDS, Sexually Transmitted Infections, and Viral Hepatitis, Weill Cornell Medicine, Qatar, Qatar Foundation, Education City, PO Box 24144, Doha, Qatar; email: lja2002@qatar-med.cornell.edu

EID Podcast: Endotheliopathy and Platelet Dysfunction as Hallmarks of Fatal Lassa Fever

Lassa fever, a virus spread through the inhalation of rodent excreta, often causes mild, influenza-like symptoms. But in severe cases, patients can face bleeding, neurological symptoms, and a death rate up to 70 percent.

Lassa fever alters platelet function and blood clotting, but the exact mechanisms involved remain a mystery.

Now, researchers are searching for answers.

In this EID podcast, Dr. Brian Sullivan, a researcher and instructor at La Jolla Institute for Immunology, discusses how Lassa fever affects the vascular system.

Visit our website to listen: <https://go.usa.gov/xsTNp>

**EMERGING
INFECTIOUS DISEASES**

Symptom Diary–Based Analysis of Disease Course among Patients with Mild Coronavirus Disease, Germany, 2020

Patricia Nicole Wiegele,¹ Iyad Kabar,¹ Laura Kerschke, Christopher Froemmel, Anna Hüsing-Kabar, Hartmut Schmidt, Elena Vorona, Richard Vollenberg, Phil-Robin Tepassee

Limited information is available on the clinical course of outpatients with mild coronavirus disease (COVID-19). This information is critically important to inform public health prevention strategies and to provide anticipatory guidance to patients, primary care providers, and employers. We retrospectively assessed the daily prevalence of symptoms in 313 COVID-19 outpatients for the first 20 days of illness. Generalized estimating equations were used to assess the probability of symptom occurrence over time. Fatigue (91%), cough (85%), and headache (78%) were the most common symptoms and occurred a median of 1 day from symptom onset. Neurologic symptoms, such as loss of taste (66%) and anosmia (62%), and dyspnea (51%) occurred considerably later (median 3–4 days after symptom onset). Symptoms of COVID-19 are similar to those of other respiratory pathogens, so symptomatic patients should be tested more frequently for severe acute respiratory syndrome coronavirus 2 during influenza season to prevent further spread of COVID-19.

Coronavirus disease (COVID-19) is a highly contagious disease caused by severe acute respiratory syndrome coronavirus 2 (SARS-CoV-2) (1). SARS-CoV-2 was first identified in December 2019 in Wuhan, China, and quickly spread across the world (2). At the beginning of the COVID-19 pandemic, studies mainly focused on the epidemiologic and clinical characteristics of hospitalized and critically ill patients (3–6). Fever, cough, and dyspnea were identified as the most common symptoms in critically

ill patients (7,8). Chemosensory symptoms, including loss of taste and smell, were highly prevalent in mildly ill patients and thus more common in COVID-19 than in other respiratory viral diseases (9,10). Male sex, older age, obesity, and underlying conditions such as diabetes and cardiovascular disease are risk factors for severe or fatal disease (11–13). As the pandemic has spread worldwide, the numbers of COVID-19 outpatients with mild clinical manifestations have increased steadily, and such patients currently represent ≈80% of all confirmed cases (14). To prevent further spread of SARS-CoV-2, detecting such cases early is essential because both asymptomatic and oligosymptomatic patients can transmit the virus (15). To help in early identification of mild SARS-CoV-2 infections, we investigated symptom prevalence and severity on a daily basis in COVID-19 patients with a mild disease course.

Methods

Study Population

In March 2020, the University Hospital of Muenster (Muenster, Germany) started outreach to the public to identify persons who recovered from SARS-CoV-2 infection through press briefings and social media. The outreach did not imply any conditions for participation. A total of 2,136 persons who had recovered from SARS-CoV-2 infection reported back (by email, telephone, and mail), stated that the infection was confirmed by PCR testing of nasopharyngeal swab specimens, and reported their willingness to participate in further studies. They were asked for the availability of an individual symptom diary by email. Among the 2,136 case-patients, 736 stated that they kept a detailed symptom diary during the disease

Author affiliations: University Hospital Muenster Department of Medicine B for Gastroenterology, Hepatology, Endocrinology, and Clinical Infectiology, Muenster, Germany (P.N. Wiegele, I. Kabar, C. Froemmel, A. Hüsing-Kabar, H. Schmidt, E. Vorona, R. Vollenberg, P.-R. Tepassee); University of Muenster Institute of Biostatistics and Clinical Research, Muenster (L. Kerschke)

DOI: <https://doi.org/10.3201/eid2705.204507>

¹These authors contributed equally to this article.

course. These 736 participants received a detailed online questionnaire inquiring retrospectively on a daily basis about COVID-19 symptom prevalence, severity, duration, and timing. By filling out the online questionnaire, participants transferred their own symptom diary to the online questionnaire and provided structured data for further analyses. The time interval from positive pharyngeal swab specimen test result to filling out the online questionnaire was 8–12 weeks. The study was approved by the Ethics Committee of Muenster University. All patients provided written informed consent.

Epidemiologic and Clinical Data

In the online questionnaire, 736 participants were asked for the date when their first COVID-19 symptoms occurred. This date was defined as baseline (day 1). Within 20 days of symptom onset, participants had to indicate on a daily basis the presence or absence of various predefined symptoms of COVID-19 according to current literature (16,17). For every single day and every single symptom (Table 1), patients had to choose from a dropdown menu between absence versus presence. In case of presence of abdominal pain, nausea, loss of taste, vision disorders, hearing loss, loss of smell, cough, rhinitis, sore throat, myalgia, headache, and fatigue, participants further had to rate the intensity on a numeric rating scale (NRS) from 0 to

10 by using a dropdown menu. NRS data were classified into 5 different symptom severity grades: grade 0 (NRS 0), grade 1 (NRS 1–2), grade 2 (NRS 3–5), grade 3 (NRS 6–8), and grade 4 (NRS 9–10). Severity of dyspnea was measured using the 5-point modified Medical Research Council dyspnea scale from 0 to 4 (18). The indication of fever was based on a subjective assessment. Skin lesions (alterations of any kind in the area of the skin), mucosal lesions (alterations of any kind in the area of the mucous membrane), and vision disorders were not further specified in the questionnaire. Symptom prevalence indicates the number of participants who experienced a particular symptom at least once during the entire illness. If a symptom persisted for longer than 20 days, participants had to indicate the date when they experienced the symptom for the last time. When calculating the median symptom onset, we included in the analysis only persons who experienced the symptom ≥ 1 day during the illness. In addition, participant demographic characteristics, including age, sex, and body mass index (BMI) were collected. Among the 736 case-patients who received the questionnaire, 332 completed the questionnaire in its entirety. Nineteen persons reported hospitalization during the disease course and were excluded. Data from 313 persons were included in further analyses.

Statistical Analysis

We performed statistical analyses by using SPSS Statistics 26 for Macintosh (IBM, <https://www.ibm.com>) and R version 3.6.0 (R Project for Statistical Computing, <https://www.r-project.org>). Inferential statistics were intended to be exploratory (i.e., hypothesis generating). We interpreted p values as a metric weight of evidence against the respective null hypothesis of no effect, and no adjustment for multiple testing was made; p values ≤ 0.05 were considered statistically significant. We analyzed patient and symptom characteristics using standard descriptive statistics. We presented normally distributed continuous variables as means \pm SDs, minima, and maxima, categorical variables as counts and relative frequencies, and non-normally distributed continuous variables as medians, minima, and maxima. For each COVID-19 symptom, generalized estimating equations were used to assess the effect of time since symptom onset, age, sex, and BMI on the odds of being affected by the symptom. To account for the nonlinear relationship between time since symptom onset and symptom presence, the models also included a quadratic effect of time. Dependencies between longitudinal measurements in the same

Table 1. COVID-19 symptom characteristics in 313 patients participating in a symptom diary–based analysis of COVID-19 disease course, Germany, 2020*

Symptom	Prevalence, no. (%)†	Median day of onset (minimum–maximum)‡
Fatigue	285 (91.1)	1.0 (1–18)
Cough	266 (85.0)	1.0 (1–15)
Headache	244 (78.0)	1.0 (1–13)
Myalgia	229 (73.2)	1.0 (1–18)
Rhinitis	220 (70.3)	1.0 (1–20)
Loss of taste	208 (66.5)	4.0 (1–19)
Sore throat	204 (65.2)	1.0 (1–10)
Loss of smell	195 (62.3)	3.0 (1–19)
Fever	191 (61.0)	2.0 (1–20)
Dysgeusia	162 (51.8)	4.0 (1–2)
Dyspnea	160 (51.1)	3.0 (1–15)
Loss of appetite	140 (44.7)	3.0 (1–13)
Dizziness	126 (40.3)	2.0 (1–20)
Diarrhea	102 (32.6)	4.0 (1–20)
Nausea	100 (31.9)	3.0 (1–20)
Abdominal pain	88 (28.1)	2.5 (1–20)
Hearing loss	62 (19.8)	3.0 (1–16)
Vision disorders	58 (18.5)	3.0 (1–20)
Mucosal lesions	43 (13.7)	2.0 (1–12)
Skin lesions	31 (9.9)	6.0 (1–13)
Vomiting	10 (3.2)	5.0 (1–11)

*COVID-19, coronavirus disease.

†Symptom occurrence within the observation period was based on the overall cohort. Results shown as absolute and relative frequencies.

‡Day of symptom onset. Calculations of median days to symptom onset were restricted to patients who reported experiencing that symptom.

patient were modeled by a first-order autoregressive correlation structure. Results were reported as odds ratios (ORs), corresponding 95% CIs, and p values. An ordinal regression analysis based on proportional odds cumulative logit models was performed to evaluate the association between the maximum intensity of the symptoms loss of taste and loss of smell (because these manifestations are more common in COVID-19 than in other respiratory viral diseases) that was observed within the 20-day period of symptom onset and the independent parameters age, sex, and BMI. The symptom intensity was modeled on the basis of all patients who were affected by the respective symptom. Results are reported as ORs, 95% CIs, and p values.

Results

Characteristics of Study Participants

A total of 313 participants completely filled out the online questionnaire and were included in the analyses. We summarized the characteristics of the study population (Table 2).

First Appearance of COVID-19 Symptoms

Fatigue (91.1%), cough (85.0%), and headache (78.0%) were the most common symptoms and occurred within a median of 1 day after symptom onset. Further common general symptoms were myalgia (73.2%), rhinitis (70.3%), and sore throat (65.2%), occurring within a median of 1 day. Fever was reported by 61% of study participants within a median of 2 days after symptom onset. Symptoms of the lower respiratory tract (dyspnea) were reported by 51.1% of all participants and occurred within a median of 3 days after symptom onset, notably later than most other symptoms. The first appearance of neurologic symptoms including loss of taste (66.5%), dysgeusia (51.8%), and loss of smell (62.3%) was reported within a median of 3–4 days after symptom onset, also notably later than most other symptoms. Gastrointestinal symptoms including nausea (31.9%), vomiting (3.2%), and diarrhea (32.6%) also occurred notably later, within a median of 3–5 days.

Prevalence of COVID-19 Symptoms over Time

We compiled the daily prevalence of neurologic, general, gastrointestinal, lower respiratory, upper respiratory, and dermatologic symptoms within 20 days of symptom onset (Figure 1). Neurologic symptoms (Figure 1, panel A), such as dysgeusia, loss of taste, and loss of smell, had almost identical and quadratically shaped prevalence time courses. Within the first week

Table 2. Characteristics of 313 COVID-19 patients participating in a symptom diary–based analysis of COVID-19 disease course, Germany, 2020*

Characteristic	No. (%)
Age, y, mean ± SD (range)	45.5 ± 13.1 (17–92)
Sex	
M	142 (45.4)
F	171 (54.6)
BMI, mean ± SD (range)	24.7 ± 4.2 (17.7–46.3)
Underlying condition	
Diabetes mellitus	5 (1.6)
Cardiovascular disease	36 (11.5)
Liver disease	3 (1.0)
Thyroid disease	18 (5.8)
Pulmonary disease	20 (6.4)
Hospitalization	0
Invasive ventilation	0
Oxygen supply	0
Intensive-care unit	0

*Values are no. (%) except as indicated. BMI, body mass index; COVID-19, coronavirus disease.

of symptom onset, the number of participants affected by these symptoms increased rapidly. Dysgeusia reached the maximum on days 8 and 9 (34.5%), loss of taste on days 9 and 10 (47.3%), and loss of smell on day 9 (44.4%). General symptoms such as fever, myalgia, and fatigue (Figure 1, panel B) were frequently present from the beginning of COVID-19 symptom onset. The prevalence of these symptoms increased only slightly within the first days. Fatigue peaked on day 3 (74.1%), fever on day 2 (36.4%), and myalgia on day 3 (53.4%). Gastrointestinal symptoms showed a flat curve in symptom occurrence over time (Figure 1, panel C). The prevalence of upper respiratory symptoms, such as rhinitis, cough, stand sore throat, peaked during days 1–4, whereas the prevalence of a lower respiratory symptom (dyspnea) reached its maximum on day 8 (33.3%) (Figure 1, panel D).

Results from the generalized estimating equation analysis assessed the effect of time, age, sex, and BMI on symptom presence (Appendix Table, <https://wwwnc.cdc.gov/EID/article/27/5/20-4507-App1.pdf>). Age was positively associated with the odds of hearing loss, general symptoms (fatigue, fever, and myalgia), gastrointestinal symptoms (nausea, abdominal pain, and loss of appetite), and respiratory symptoms (dyspnea and cough) (ORs 1.02–1.05; $p < 0.05$). Women were more likely than men to be affected by neurologic symptoms (dysgeusia, loss of taste, loss of smell, headache, dizziness, and vision disorders), fatigue, myalgia, skin lesions, diarrhea, loss of appetite, rhinitis, and dyspnea (ORs 1.41–2.95; $p < 0.05$). The odds of all symptoms except for fever, mucosal lesions, skin lesions, sore throat, diarrhea, and loss of appetite increased with increasing BMI (ORs 1.05–1.11; $p < 0.05$).

In line with the descriptive analysis of daily symptom prevalence we have outlined, the odds of

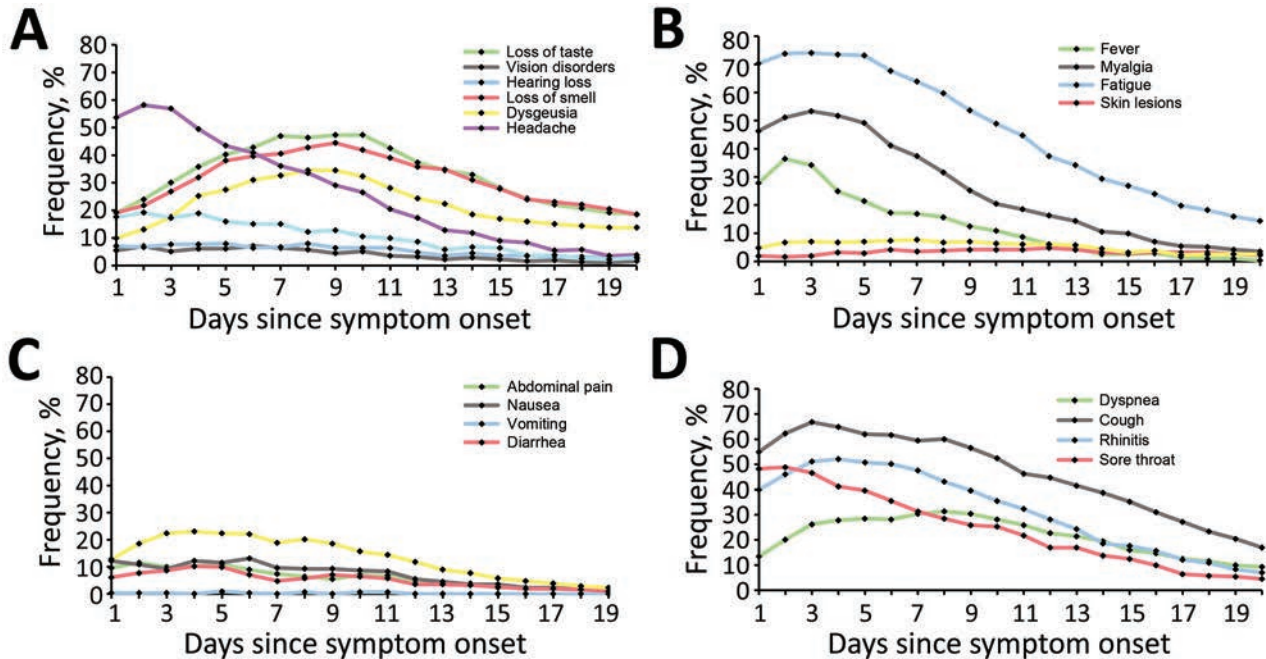


Figure 1. Prevalence of coronavirus disease symptoms over time among 313 patients participating in a symptom diary–based analysis of disease course, Germany, 2020. Line graphs show the occurrence of neurologic symptoms (A), general symptoms (B), gastrointestinal symptoms (C), and respiratory symptoms (D) within 20 days of symptom onset.

the presence of most symptoms showed a quadratic trend over time since symptom onset (ORs of the quadratic effect of day 0.98–0.996; $p < 0.05$). The quadratic trends were characterized by an initial increase and a

subsequent decrease in the odds of dysgeusia, loss of taste, loss of smell, hearing loss, mucosal lesions, loss of appetite, diarrhea, nausea, cough, rhinitis, and dyspnea. For all other symptoms, we observed an almost

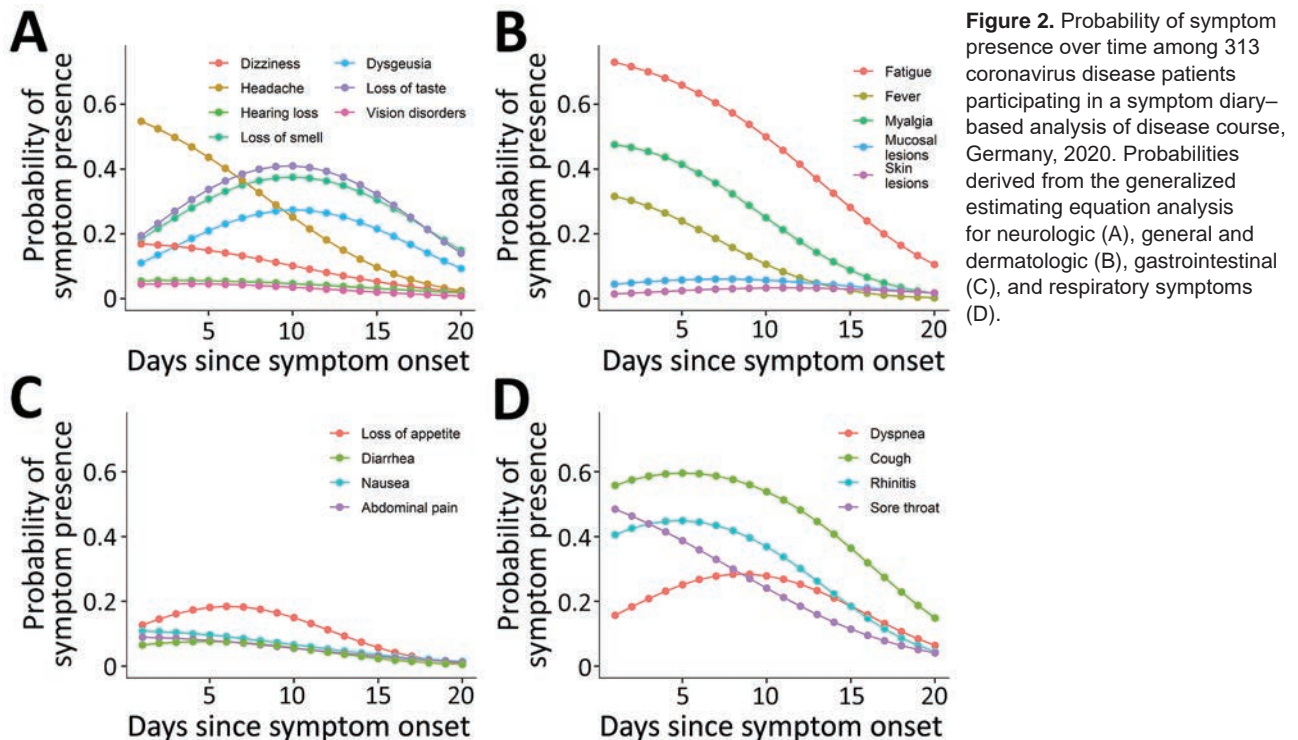


Figure 2. Probability of symptom presence over time among 313 coronavirus disease patients participating in a symptom diary–based analysis of disease course, Germany, 2020. Probabilities derived from the generalized estimating equation analysis for neurologic (A), general and dermatologic (B), gastrointestinal (C), and respiratory symptoms (D).

linear monotonic decrease in the odds of symptom presence over time (Figure 2).

Maximum Intensity of COVID-19 Symptoms

For the overall cohort, Figure 3 shows the distribution of maximal symptom intensity by severity grades 0–4 occurring within 20 days of COVID-19 symptom onset. Fatigue (57.2%), headache (54.0%), loss of taste (45.3%), loss of smell (41.9%), and myalgia (41.9%) were most frequently reported with severity grades 3 and 4.

For the overall cohort, Figure 3 shows the distribution of maximal symptom intensity by severity grades 0–4 occurring within 20 days of COVID-19 symptom onset. Fatigue (57.2%), headache (54.0%), loss of taste (45.3%), loss of smell (41.9%), and myalgia (41.9%) were most frequently reported with severity grades 3 and 4.

We determined that multiple factors were associated with severe symptom intensity within 20 days after symptom onset among all study participants (Table 3). Women were found to be at increased risk for having a severe course of loss of taste (OR 2.796 [95% CI 1.35–5.88]; $p = 0.006$) and loss of smell (OR 2.694 [95% CI 1.53–4.78]; $p = 0.001$). Age was negatively associated with the maximum symptom severity of smell loss (OR 0.968 [95% CI 0.95–0.99]; $p = 0.004$).

Time Course of COVID-19 Symptom Intensity

We assessed the distributions of symptom intensity grades reported within 20 days of COVID-19

symptom onset (Figure 4). Loss of taste and loss of smell were characterized by relatively high rates of grade 3 and 4 symptom severities. These symptoms showed a steady increase within the first week of symptom onset and reached maximums on day 8 (30.4% for loss of taste, 30.0% for loss of smell). In comparison, cough and headache showed less severity, with a steady decrease in intensity during the first week, except for day 4, when a notable increase in grade 3 headaches occurred compared with day 3 (14.7% vs. 38.0%).

Discussion

Our study examined the daily prevalence and severity of COVID-19 symptoms occurring within 20 days of symptom onset in mildly ill outpatients and revealed new insights in symptom development during the disease course. Fatigue, cough, chemosensory disorder, and dyspnea were highly prevalent in mild COVID-19. We were able to show that lower respiratory and chemosensory symptoms, which are considered more characteristic of COVID-19, appear significantly later than general and nonspecific symptoms such as fatigue and upper respiratory symptoms. Results of our study highlight the positive associations of BMI, age, and especially female sex with the frequency of characteristic disease symptoms.

In line with previous studies, we showed that chemosensory symptoms such as smell and taste disorders were highly prevalent among mildly ill COVID-19 patients, usually occurring 3–4 days

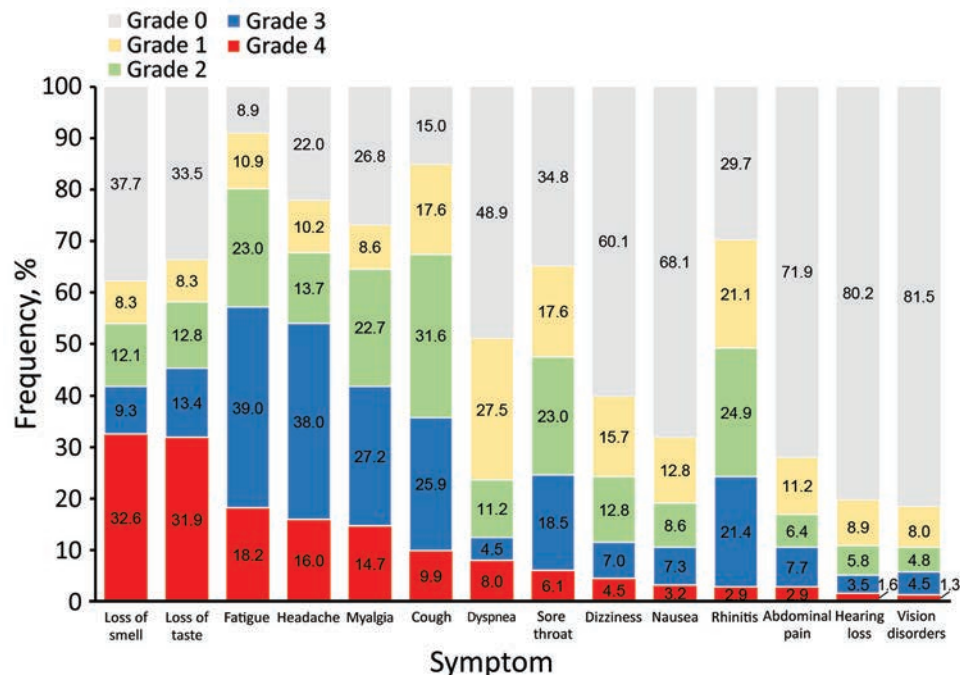


Figure 3. Maximum severity of coronavirus disease symptoms within 20 days of symptom onset among 313 patients participating in a symptom diary–based analysis of disease course, Germany, 2020. Bar plots show the frequencies of all participants experiencing symptoms of intensity grade 0 (none), grade 1 (mild), grade 2 (moderate), grade 3 (severe), or grade 4 (maximum imaginable) within 20 days of symptom onset. For each patient, the highest reported intensity in the 20-day period was chosen.

Table 3. Factors associated with severe COVID-19 symptom intensity within 20 days of symptom onset among 313 COVID-19 patients participating in a symptom diary–based analysis of COVID-19 disease course, Germany, 2020*

Symptom	Age		Female		BMI	
	OR (95% CI)	p value	OR (95% CI)	p value	OR (95% CI)	p value
Loss of taste	0.977 (0.95–1.01)	0.117	2.796 (1.35–5.88)	0.006	0.965 (0.89–1.05)	0.385
Loss of smell	0.968 (0.95–0.99)	0.004	2.694 (1.53–4.78)	0.001	1.000 (0.93–1.08)	0.989

*BMI, body mass index; COVID-19, coronavirus disease; OR, odds ratio..

after symptom onset (19–23). Both the number of patients affected by these symptoms and the proportion of patients experiencing these symptoms with severe intensity increased steadily during the first week, suggesting progressive central nervous system involvement. In our study, the appearance of neurologic symptoms (except for headache) was delayed compared with general and respiratory manifestations.

Gastrointestinal symptoms (nausea, vomiting, and diarrhea) also occurred notably later, within a median of 3–5 days, compared with general and upper airway symptoms, which is consistent with previous studies (24,25). Nobel et al. (26) showed an increased probability of SARS-CoV-2 infection in patients who had gastrointestinal symptoms in addition to further symptoms characteristic of COVID-19, compared with patients without gastrointestinal symptoms; these findings and our data suggest that physicians must be aware of SARS-CoV-2 infection in case of coexisting general and

gastrointestinal symptoms. Nevertheless, because gastrointestinal symptom onset appears later in disease, the risk for misdiagnosis at the very beginning of disease might be increased.

In our cohort, general and upper airway symptoms were prominent early indications of COVID-19, occurring within a median of 1 day after symptom onset. At symptom onset, fatigue (70.3%) and cough (55.0%) were the most frequently observed symptoms. In contrast, chemosensory and lower pulmonary symptoms (e.g., dyspnea), which are considered characteristic of COVID-19 (27,28), occurred within a median of 3–4 days after symptom onset and peaked during the second week. Our results show that multiple characteristic symptoms, including loss of smell (19.2% vs. 44.4%), dyspnea (13.4% vs. 31.3%), loss of taste (19.2% vs. 47.3%), and dysgeusia (9.9% vs. 34.5%), rarely occurred on the first day of COVID-19 symptom onset compared with the day of maximal frequency. In agreement with other studies, we found a delay of up to 1 week between the emergence of

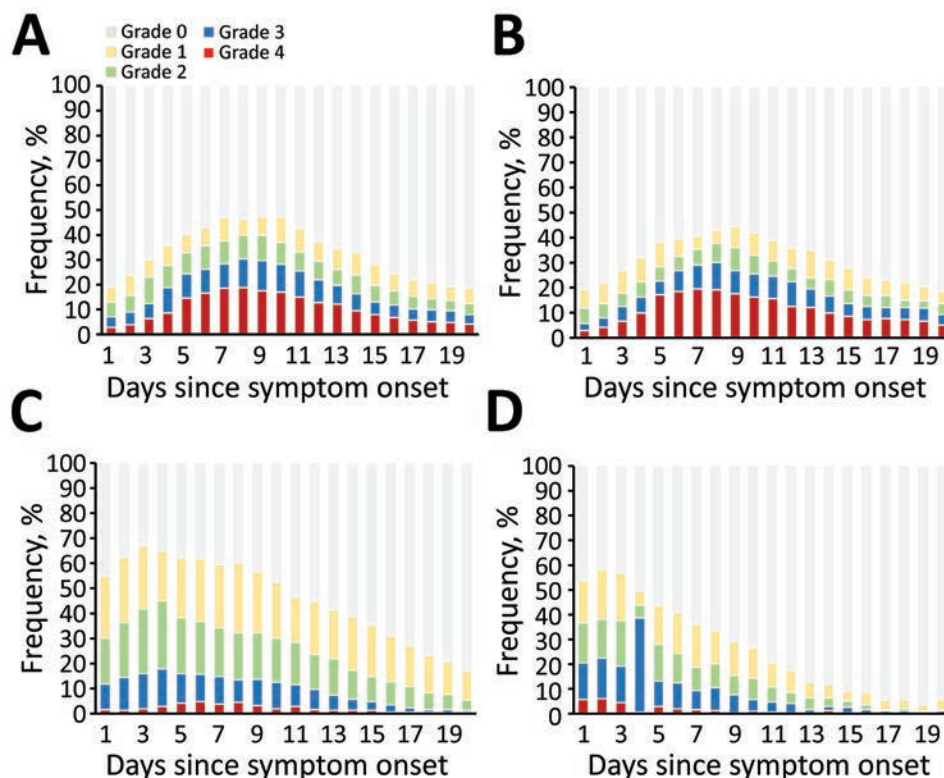


Figure 4. Time course of coronavirus disease symptom severity among 313 patients participating in a symptom diary–based analysis of disease course, Germany, 2020. Bar charts show the distributions of symptom severities: grade 0 (none), grade 1 (mild), grade 2 (moderate), grade 3 (severe), or grade 4 (maximum imaginable). Severity of loss of taste (A), loss of smell (B), cough (C), and headache (D) were evaluated over 20 days from symptom onset.

upper respiratory symptoms and pulmonary manifestations, including dyspnea (16,17). This finding might indicate that viral movement from the upper airway to deeper levels occurs within a week. The late development of more specific symptoms, such as dyspnea, loss of taste, dysgeusia, and loss of smell, might lead to delays in diagnosis, especially during the season of seasonal colds and influenza, because of increased occurrence of seasonal pathogens producing nonspecific symptoms (29–32). Our data highlight a critical period of up to 4 days after symptom onset with the potential for delayed diagnosis and further disease spread; infected persons can be highly contagious within 2 days before symptom onset and up to 10 days thereafter (33–35). Our data are in line with data from Yousaf et al. (21), who prospectively analyzed symptom profiles of 47 nonhospitalized household contacts with SARS-CoV-2 infection. However, there are differences in methodology and results between that report and this one.

According to our data, female sex was strongly associated with the occurrence of neurologic symptoms. Furthermore, women were more frequently affected by fatigue, myalgia, skin lesions, diarrhea, loss of appetite, rhinitis, and dyspnea. In line with our findings, Lechien et al. (36) reported that loss of smell, headache, and fatigue were significantly more prevalent in women. We extend these findings by showing that women suffer loss of taste and loss of smell with higher intensity during the first 20 days after symptom onset compared with men (Table 3).

In our study, higher BMI was significantly associated with the occurrence of general symptoms, respiratory symptoms, and neurologic symptoms. In addition, we were able to show that in mildly affected patients the likelihood of having onset of hearing loss, gastrointestinal symptoms, general symptoms, and respiratory symptoms increases with age. In contrast to Lee et al. (37), we could not prove that young participants were more often affected by loss of smell, but we found that they suffer this symptom with a higher intensity during the first 20 days after symptom onset. These findings suggest that older patients infected with SARS-CoV-2 are more likely to have general COVID-19 symptoms than specific symptoms such as loss of smell, potentially increasing the risk for misdiagnosis.

Our study's first limitation is that using social media and press briefings could have biased our results toward young persons who use social media and would be exposed to the press briefings. Using online symptom diaries might have limited participation by less technologically literate persons,

persons without internet at home, and persons who did not record symptom diaries or have time to complete the online form. Second, recall bias might have affected results. Participants kept an individual symptom diary during disease and retrospectively transferred these data into the online questionnaire 8–12 weeks after onset of the first symptom. Patients might have added information that was not in their original diaries. In addition, they had to choose the absence or presence of predefined symptoms, and the predefinition might have influenced symptoms reported by participants. Third, the data evaluated in this study were based on subjective patient statements. Unlike some other studies, no validated chemosensory tests were performed (38,39). Fourth, only ≈50% of persons who were eligible participated, potentially affecting the representativeness of the findings.

We describe the probability of the occurrence of different symptoms in mild COVID-19 on a daily basis by analysis of information directly obtained from the patient in a large cohort with mild disease symptoms. Despite the retrospective design, data were well preserved by patient's diaries, which might limit the potential recall bias we have described. To identify infected persons early in the disease course, exact knowledge of symptom prevalence in this period is very important, and our study provides useful data that could substantially improve early diagnosis of COVID-19.

In conclusion, our study found that general and upper airway symptoms appear soon after COVID-19 symptom onset in mild cases but lower respiratory tract and neurologic symptoms, both considered characteristic of COVID-19, occur significantly later. Older men might experience less frequent and less severe neurologic symptoms. Particularly in the season for seasonal colds and influenza, extreme caution is required in early identification of patients infected with SARS-CoV-2 because other seasonal viral diseases can initially produce very similar symptoms and because symptoms most characteristic of COVID-19 rarely occur on the first day of disease.

About the Author

Dr. Kabar is a professor in the Department of Gastroenterology, Hepatology, Endocrinology, and Clinical Infectiology and Deputy Director of the Department of Medicine B of the University Hospital Münster. Ms. Wiegele is a research assistant at the Department of Medicine B of the University Hospital Münster. In September 2020, she started her professional career as a dentist.

References

1. Coronaviridae Study Group of the International Committee on Taxonomy of Viruses. The species severe acute respiratory syndrome-related coronavirus: classifying 2019-nCoV and naming it SARS-CoV-2. *Nat Microbiol.* 2020; 5:536–44. <https://doi.org/10.1038/s41564-020-0695-z>
2. World Health Organization. Novel coronavirus [cited 2020 Jul 19]. <https://www.who.int/csr/don/12-january-2020-novel-coronavirus-china/en>
3. Chen N, Zhou M, Dong X, Qu J, Gong F, Han Y, et al. Epidemiological and clinical characteristics of 99 cases of 2019 novel coronavirus pneumonia in Wuhan, China: a descriptive study. *Lancet.* 2020;395:507–13. [https://doi.org/10.1016/S0140-6736\(20\)30211-7](https://doi.org/10.1016/S0140-6736(20)30211-7)
4. Zhou F, Yu T, Du R, Fan G, Liu Y, Liu Z, et al. Clinical course and risk factors for mortality of adult inpatients with COVID-19 in Wuhan, China: a retrospective cohort study. *Lancet.* 2020;395:1054–62. [https://doi.org/10.1016/S0140-6736\(20\)30566-3](https://doi.org/10.1016/S0140-6736(20)30566-3)
5. Yang X, Yu Y, Xu J, Shu H, Xia J, Liu H, et al. Clinical course and outcomes of critically ill patients with SARS-CoV-2 pneumonia in Wuhan, China: a single-centered, retrospective, observational study. *Lancet Respir Med.* 2020;8:475–81. [https://doi.org/10.1016/S2213-2600\(20\)30079-5](https://doi.org/10.1016/S2213-2600(20)30079-5)
6. Xie J, Tong Z, Guan X, Du B, Qiu H. Clinical characteristics of patients who died of coronavirus disease 2019 in China. *JAMA Netw Open.* 2020;3:e205619. <https://doi.org/10.1001/jamanetworkopen.2020.5619>
7. Cholankeril G, Podboy A, Aivaliotis VI, Tarlow B, Pham EA, Spencer SP, et al. High prevalence of concurrent gastrointestinal manifestations in patients with severe acute respiratory syndrome coronavirus 2: early experience from California. *Gastroenterology.* 2020;159:775–7. <https://doi.org/10.1053/j.gastro.2020.04.008>
8. Guan W-J, Ni Z-Y, Hu Y, Liang W-H, Ou C-Q, He J-X, et al.; China Medical Treatment Expert Group for Covid-19. Clinical characteristics of coronavirus disease 2019 in China. *N Engl J Med.* 2020;382:1708–20. <https://doi.org/10.1056/NEJMoa2002032>
9. Roland LT, Gurrola JG II, Loftus PA, Cheung SW, Chang JL. Smell and taste symptom-based predictive model for COVID-19 diagnosis. *Int Forum Allergy Rhinol.* 2020; 10:832–8. <https://doi.org/10.1002/alf.22602>
10. D'Ascanio L, Pandolfini M, Cingolani C, Latini G, Gradoni P, Capalbo M, et al. Olfactory dysfunction in COVID-19 patients: prevalence and prognosis for recovering sense of smell. *Otolaryngol Head Neck Surg.* 2021;164:82–6. <https://doi.org/10.1177/0194599820943530>
11. Wang D, Yin Y, Hu C, Liu X, Zhang X, Zhou S, et al. Clinical course and outcome of 107 patients infected with the novel coronavirus, SARS-CoV-2, discharged from two hospitals in Wuhan, China. *Crit Care.* 2020;24:188. <https://doi.org/10.1186/s13054-020-02895-6>
12. Du R-H, Liang L-R, Yang C-Q, Wang W, Cao T-Z, Li M, et al. Predictors of mortality for patients with COVID-19 pneumonia caused by SARS-CoV-2: a prospective cohort study. *Eur Respir J.* 2020;55:2000524. <https://doi.org/10.1183/13993003.00524-2020>
13. Cai Q, Chen F, Wang T, Luo F, Liu X, Wu Q, et al. Obesity and COVID-19 severity in a designated hospital in Shenzhen, China. *Diabetes Care.* 2020;43:1392–8. <https://doi.org/10.2337/dc20-0576>
14. World Health Organization. 2019 (COVID-19) situation report 41 [cited 2020 Mar 28]. <https://www.who.int/docs/default-source/coronaviruse/situation-reports/20200301-sitrep-41-covid-19.pdf>
15. Zou L, Ruan F, Huang M, Liang L, Huang H, Hong Z, et al. SARS-CoV-2 viral load in upper respiratory specimens of infected patients. *N Engl J Med.* 2020;382:1177–9. <https://doi.org/10.1056/NEJMc2001737>
16. Huang C, Wang Y, Li X, Ren L, Zhao J, Hu Y, et al. Clinical features of patients infected with 2019 novel coronavirus in Wuhan, China. *Lancet.* 2020;395:497–506. [https://doi.org/10.1016/S0140-6736\(20\)30183-5](https://doi.org/10.1016/S0140-6736(20)30183-5)
17. Cohen PA, Hall LE, John JN, Rapoport AB. The early natural history of SARS-CoV-2 infection: clinical observations from an urban, ambulatory COVID-19 clinic. *Mayo Clin Proc.* 2020;95:1124–6. <https://doi.org/10.1016/j.mayocp.2020.04.010>
18. Mahler DA, Wells CK. Evaluation of clinical methods for rating dyspnea. *Chest.* 1988;93:580–6. <https://doi.org/10.1378/chest.93.3.580>
19. Spinato G, Fabbris C, Polese J, Cazzador D, Borsetto D, Hopkins C, et al. Alterations in smell or taste in mildly symptomatic outpatients with SARS-CoV-2 infection. *JAMA.* 2020;323:2089–90. <https://doi.org/10.1001/jama.2020.6771>
20. Lechien JR, Chiesa-Estomba CM, De Siati DR, Horoi M, Le Bon SD, Rodriguez A, et al. Olfactory and gustatory dysfunctions as a clinical presentation of mild-to-moderate forms of the coronavirus disease (COVID-19): a multicenter European study. *Eur Arch Otorhinolaryngol.* 2020; 277:2251–61. <https://doi.org/10.1007/s00405-020-05965-1>
21. Yousaf AR, Duca LM, Chu V, Reses HE, Fajans M, Rabold EM, et al. A prospective cohort study in non-hospitalized household contacts with SARS-CoV-2 infection: symptom profiles and symptom change over time. *Clin Infect Dis.* 2020 Jul 28 [Epub ahead of print]. <https://doi.org/10.1093/cid/ciaa1072>
22. Lapostolle F, Schneider E, Vianu I, Dollet G, Roche B, Berdahl J, et al. Clinical features of 1487 COVID-19 patients with outpatient management in the greater Paris: the COVID-call study. *Intern Emerg Med.* 2020;15:813–7. <https://doi.org/10.1007/s11739-020-02379-z>
23. Karimi-Galougahi M, Safavi Naini A, Ghorbani J, Raad N, Raygani N. Emergence and evolution of olfactory and gustatory symptoms in patients with COVID-19 in the outpatient setting. *Indian J Otolaryngol Head Neck Surg.* 2020 Sep 28 [Epub ahead of print]. <https://doi.org/10.1007/s12070-020-02166-4>
24. Lin L, Jiang X, Zhang Z, Huang S, Zhang Z, Fang Z, et al. Gastrointestinal symptoms of 95 cases with SARS-CoV-2 infection. *Gut.* 2020;69:997–1001. <https://doi.org/10.1136/gutjnl-2020-321013>
25. Klopfenstein T, Kadiane-Oussou NJ, Royer P-Y, Toko L, Gendrin V, Zayet S. Diarrhea: an underestimated symptom in coronavirus disease 2019. *Clin Res Hepatol Gastroenterol.* 2020;44:282–3. <https://doi.org/10.1016/j.clinre.2020.04.002>
26. Nobel YR, Phipps M, Zucker J, Leibold B, Wang TC, So-bieszczyk ME, et al. Gastrointestinal symptoms and coronavirus disease 2019: a case-control study from the United States. *Gastroenterology.* 2020;159:373–375.e2. <https://doi.org/10.1053/j.gastro.2020.04.017>
27. Sedaghat AR, Gengler I, Speth MM. Olfactory dysfunction: a highly prevalent symptom of COVID-19 with public health significance. *Otolaryngol Head Neck Surg.* 2020;163:12–5. <https://doi.org/10.1177/0194599820926464>
28. Bhatraju PK, Ghassemieh BJ, Nichols M, Kim R, Jerome KR, Nalla AK, et al. Covid-19 in critically ill patients in the Seattle region – case series. *N Engl J Med.* 2020;382:2012–22. <https://doi.org/10.1056/NEJMoa2004500>
29. Tabatabai J, Prifert C, Pfeil J, Grulich-Henn J, Schnitzler P. Novel respiratory syncytial virus (RSV) genotype ON1

- predominates in Germany during winter season 2012–13. *PLoS One*. 2014;9:e109191. <https://doi.org/10.1371/journal.pone.0109191>
30. Neuzil KM, Maynard C, Griffin MR, Heagerty P. Winter respiratory viruses and health care use: a population-based study in the northwest United States. *Clin Infect Dis*. 2003;37:201–7. <https://doi.org/10.1086/375604>
 31. Viegas M, Barrero PR, Maffey AF, Mistchenko AS. Respiratory viruses seasonality in children under five years of age in Buenos Aires, Argentina: a five-year analysis. *J Infect*. 2004;49:222–8. <https://doi.org/10.1016/j.jinf.2003.10.006>
 32. Taubenberger JK, Morens DM. The pathology of influenza virus infections. *Annu Rev Pathol*. 2008;3:499–522. <https://doi.org/10.1146/annurev.pathmechdis.3.121806.154316>
 33. Ganyani T, Kremer C, Chen D, Torneri A, Faes C, Wallinga J, et al. Estimating the generation interval for COVID-19 based on symptom onset data, March 2020. *Euro Surveill*. 2020;25:2000257. <https://doi.org/10.2807/1560-7917.ES.2020.25.17.2000257>
 34. He X, Lau EHY, Wu P, Deng X, Wang J, Hao X, et al. Temporal dynamics in viral shedding and transmissibility of COVID-19. *Nat Med*. 2020;26:672–5. <https://doi.org/10.1038/s41591-020-0869-5>
 35. Cheng H-Y, Jian S-W, Liu D-P, Ng T-C, Huang W-T, Lin H-H; Taiwan COVID-19 Outbreak Investigation Team. Contact tracing assessment of COVID-19 transmission dynamics in Taiwan and risk at different exposure periods before and after symptom onset. *JAMA Intern Med*. 2020;180:1156–63. <https://doi.org/10.1001/jamainternmed.2020.2020>
 36. Lechien JR, Chiesa-Estomba CM, Place S, Van Laethem Y, Cabaraux P, Mat Q, et al.; COVID-19 Task Force of YO-IFOS. Clinical and epidemiological characteristics of 1420 European patients with mild-to-moderate coronavirus disease 2019. *J Intern Med*. 2020;288:335–44. <https://doi.org/10.1111/joim.13089>
 37. Lee Y, Min P, Lee S, Kim S-W. Prevalence and Duration of Acute Loss of Smell or Taste in COVID-19 Patients. *J Korean Med Sci*. 2020;35:e174. <https://doi.org/10.3346/jkms.2020.35.e174>
 38. Moein ST, Hashemian SMR, Mansourafshar B, Khorram-Tousi A, Tabarsi P, Doty RL. Smell dysfunction: a biomarker for COVID-19. *Int Forum Allergy Rhinol*. 2020;10:944–50. <https://doi.org/10.1002/alr.22587>
 39. Hornuss D, Lange B, Schröter N, Rieg S, Kern WV, Wagner D. Anosmia in COVID-19 patients. *Clin Microbiol Infect*. 2020;26:1426–7. <https://doi.org/10.1016/j.cmi.2020.05.017>

Address for correspondence: Phil-Robin Tepaspe, Department of Gastroenterology, Hepatology, Endocrinology, and Clinical Infectiology, University Hospital Muenster, Albert-Schweitzer-Campus 1, 48149 Muenster, Germany; email: phil-robin.tepaspe@ukmuenster.de

EID Podcast: Role of Oral Rabies Vaccines in Eliminating Death in People from Dog Bites

Rabies vaccines are highly effective, but delivering them can be challenging. The challenge is even greater for stray animals, which might not trust a stranger trying to deliver a life-saving vaccination.

How can public health officials ensure that stray dogs (and the people around them) are protected against rabies? Some researchers may have an answer: oral vaccines in dog treats.

In this EID podcast, Dr. Ryan Wallace, a CDC veterinary epidemiologist, explains an innovative strategy for delivering safe and effective oral vaccines.

Visit our website to listen: <https://go.usa.gov/xs5f6>

**EMERGING
INFECTIOUS DISEASES**

Serologic Screening of Severe Acute Respiratory Syndrome Coronavirus 2 Infection in Cats and Dogs during First Coronavirus Disease Wave, the Netherlands

Shan Zhao, Nancy Schuurman, Wentao Li, Chunyan Wang, Lidwien A.M. Smit, Els M. Broens, Jaap A. Wagenaar, Frank J.M. van Kuppeveld, Berend-Jan Bosch, Herman Egberink

Severe acute respiratory syndrome coronavirus 2 (SARS-CoV-2) can infect many animal species, including minks, cats, and dogs. To gain insights into SARS-CoV-2 infections in cats and dogs, we developed and validated a set of serologic assays, including ELISA and virus neutralization. Evaluation of samples from animals before they acquired coronavirus disease and samples from cats roaming SARS-CoV-2–positive mink farms confirmed the suitability of these assays for specific antibody detection. Furthermore, our findings exclude SARS-CoV-2 nucleocapsid protein as an antigen for serologic screening of cat and dog samples. We analyzed 500 serum samples from domestic cats and dogs in the Netherlands during April–May 2020. We showed 0.4% of cats and 0.2% of dogs were seropositive. Although seroprevalence in cats and dogs that had unknown SARS-CoV-2 exposure was low during the first coronavirus disease wave, our data stress the need for development of continuous serosurveillance for SARS-CoV-2 in these 2 animal species.

A novel human coronavirus (HCoV), severe acute respiratory syndrome coronavirus 2 (SARS-CoV-2), emerged in Wuhan, China, during December 2019 and caused a severe pandemic of coronavirus disease (COVID-19) (1,2). As of January 2021, SARS-CoV-2 had spread to 223 countries and caused >88 million infections, which occurred by human-to-human transmission and mostly affected elderly and immunocompromised persons (3).

SARS-CoV-2 is a zoonotic virus and was shown able to infect many animal species, such as cats, dogs,

ferrets, fruit bats, hamsters, and several nonhuman primates under experimental condition (4–6). Recently, transmission of SARS-CoV-2 from humans to cats and dogs shown by viral RNA or antibody detection has been reported, resulting in asymptomatic infections in dogs, and symptomatic and asymptomatic infections in cats (7–15). There is currently no evidence that pets play a role in spread of the virus. Nevertheless, close contacts between owners and pets and interactions between dogs and cats from different households raise the question about the role of these animals in SARS-CoV-2 transmission.

Diagnosis of SARS-CoV-2 is currently made by using molecular assays, such as real-time PCR. However, viral nucleic acid is only detectable within a limited timeframe after infection, and serologic screening of SARS-CoV-2–specific antibodies in cats and dogs is needed for insights into the prevalence of this infection and possible modes of transmission (human-to-animal, animal-to-animal, and animal-to-human).

We developed and validated SARS-CoV-2–specific serologic assays. Serum samples were first tested with ELISAs by using different antigens, including spike protein subunit (S1) of endemic feline and canine coronaviruses and SARS-CoV-2 antigens (S1, receptor binding domain [RBD], and nucleocapsid [N] protein), and subsequently analyzed by using virus neutralization titer (VN) assays with SARS-CoV-2 spike pseudotyped virus. Using these assay platforms, we conducted serosurveillance study of SARS-CoV-2 in cats and dogs of unknown SARS-CoV-2 exposure during the first wave of COVID-19 pandemic (April–May 2020) in the Netherlands.

Author affiliation: Utrecht University, Utrecht, the Netherlands

DOI: <https://doi.org/10.3201/eid2705.204055>

Materials and Methods

Serum Samples

Cat and dog serum samples collected during 2019 (pre-COVID-19 cohort, $n = 45$ each) were obtained from the serum bank of Utrecht University (Utrecht, the Netherlands). Paired and postinfection serum samples of feline coronavirus (FCoV) type I-infected specific pathogen-free (SPF) cats ($n = 9$) were obtained from SPF cats infected with FCoV strain UU2 or RM in a previous study (16). The SARS-CoV-2-exposed cohort consisted of 44 serum samples from stray cats roaming on SARS-CoV-2-positive mink farms (17) and 1 serum sample of a dog from a COVID-19-confirmed household. The 2020 cohort is composed of domestic cat and dog serum or plasma samples ($n = 500$ each) that were sent to the University Veterinary Diagnostic Laboratory or the Veterinary Microbiological Diagnostic Center at Utrecht University for routine diagnostics during April–May 2020. Data on SARS-CoV-2 exposure of these animals was not available. All samples were stored at -20°C until use and heat-inactivated at 56°C for 30 min before use.

Antigen Preparation

We produced streptavidin-tagged SARS-CoV-2 S1 and RBD proteins in eukaryotic cells as described (18,19), and cloned and similarly produced streptavidin-tagged bovine coronavirus (BCoV) S1 and HCoV-229E S1. SARS-CoV-2 N protein was obtained from Sino Biological (<https://www.sinobiological.com>). We produced mouse Fc-tagged FCoV type I S1, FCoV type II S1, or BCoV S1 proteins as described (20). Vesicular stomatitis virus (VSV) pseudotyped with SARS-CoV-2 S protein (SARS2-VSV) was prepared as described (18) and titrated on Vero E6 cells.

ELISA

We first screened samples from the 3 cohorts with indirect ELISAs for the different proteins as described (20). In brief, high-binding microtiter plates were coated with equal molar amounts of protein (1 pmol/L well after optimizing by using checkerboard titration), diluted in phosphate-buffered saline, and blocked with blocking buffer (phosphate-buffered saline containing 0.05% Tween-20 and 5% milk powder). A standard 1:50 dilution of serum samples or serial 2-fold dilutions of serum samples starting at a 1:50 dilution were added to the wells. After incubation for 1 h at 37°C , plates were washed and subsequently incubated with horseradish peroxidase (HRP)-conjugated secondary antibody (1:4,000 for goat anti-cat IgG/HRP; Rockland Immunochemicals, Inc., <https://rockland-inc.com>)

and 1:6,000 for goat anti-dog IgG/HRP; Cappel, <http://ziobio.com>) diluted in blocking buffer for 1 h at 37°C . Peroxidase reactions were visualized by incubation with 3,3',5,5'-tetramethylbenzidine (10 min at room temperature) and quenching with sulfuric acid. Optical densities (ODs) were measured at 450 nm. Cutoff values were determined at 6-fold SDs above the mean value of reactivity of all negative serum samples from the pre-COVID-19 cohort (19).

S1 Adsorption Assay

To verify that the 2 betacoronavirus infections in dogs (SARS-CoV-2 and canine respiratory coronavirus [CRCoV]) can be distinguished serologically, we designed an antigen S1 adsorption assay. We incubated serum samples with Strep-Tactin Sepharose Beads (IBA Lifesciences, <https://www.iba-lifesciences.com>) conjugated with S1 protein of SARS-CoV-2, BCoV, or HCoV-229E and titrated mock-absorbed and protein-absorbed serum samples in the ELISA. We expressed IgG titers as the reciprocal of highest serum dilution resulting in OD values above the cutoff value.

Virus Neutralization Assay

We conducted a VN assay by using luciferase-encoding VSV particles pseudotyped with S protein of SARS-CoV-2 (SARS2-VSV), which was conducted on Vero E6 cells in a 96-well plate (18). Antigenicity of SARS2-VSV was validated previously, and VN titers (VNTs) for SARS2-VSV correlated well with those for live SARS-CoV-2 (18). Samples (starting at a 1:8 dilution) were serially diluted 2-fold and mixed 1:1 with SARS-2-VSV. Mixtures were preincubated at 37°C for 1 h and used for inoculation on cells. Twenty-four hours postinfection, cells were lysed and relative luminescence units (RLU) of luciferase activity was determined as described (18). RLU reduction rates of samples were calculated by using the formula

$$\text{Reduction rate (\%)} = \frac{\text{RLU}_{\text{SARS2-VSV}} - \text{RLU}_{\text{mixture}}}{\text{RLU}_{\text{SARS2-VSV}} - \text{RLU}_{\text{blank}}} \times 100\%$$

Sample neutralization titers were determined by using the reciprocal of the highest dilution that resulted in >50% reduction of luciferase activity. A VNT ≥ 16 was considered positive (21).

Statistical Analyses

All statistical analyses were performed by using Prism version 7.04 for Windows (GraphPad, <https://www.graphpad.com>). The Pearson correlation coefficient was calculated to determine

the correlation between different ELISA ODs and VNTs. The 95% CIs were determined by using the modified Wald method.

Results

Pre-COVID-19 Cohort

Serum samples from the pre-COVID-19 cohort were tested against SARS-CoV-2 antigens to screen for potential cross-reactive antibodies elicited by endemic coronaviruses in cats and dogs because they are natural reservoirs of several coronaviruses (i.e., FCoV [genus *Alphacoronavirus*] in cats, canine coronavirus [CCoV; genus *Alphacoronavirus*] and CRCoV [genus *Betacoronavirus*] in dogs) (20,22,23). We summarized sequence identities of SARS-CoV-2 antigens used and matching endemic coronavirus antigens (Table 1). FCoV type I S1 was used as an additional antigen to assess the reactivity of cat serum samples. For dog serologic analysis, FCoV type II S1 (92.1% similar to S1 of CCoV) was used as a proxy antigen for CCoV, and BCoV S1 (95.7% similar to S1 of CRCoV) was used as a proxy antigen for CRCoV. Many serum samples were positive for FCoV and BCoV S1, but all samples were negative for antibodies against SARS-CoV-2 S1 and RBD (Figure 1). Because of limited sample volumes, a selection of serum samples ($n = 34$ for cats and $n = 24$ for dogs) was tested for SARS-CoV-2 S-bearing VSV pseudovirus (SARS2-VSV) neutralization, and all showed negative results (VNT <16).

A total of 8 (17.8%) of 45 pre-COVID-19 cat serum samples and 1 (2.2%) of 45 dog serum samples showed positive results in the SARS-CoV-2 N protein ELISA (Figure 1, panels A, B). To explore this finding, we analyzed paired serum samples of SPF cats infected with FCoV (Figure 1, panel C). Serum samples from uninfected SPF cats were negative. After FCoV infection, 8 (88.9%) of 9 cats had antibodies reacting with SARS-CoV-2 N protein. When compared with S1 and RBD proteins, we found that the N protein was more conserved among CoVs (Table 1), which

might explain the cross-reactivity between FCoV and SARS-CoV-2 detected in our ELISAs.

SARS-CoV-2-Exposed Cohort

We tested the serum of a dog from a COVID-19-confirmed household, as well as serum samples from SARS-CoV-2-exposed stray cats found in the surroundings of SARS-CoV-2-positive mink farms (17). These cats had access to the stables and cages in which the minks were housed. This cohort was expected to contain a higher number of SARS-CoV-2-positive samples because of close contact between the cats and minks and the dog and its owner and was a source of suitable samples for validation of our ELISA and VNT. A total of 11 (24.4%, 95% CI 14.1%–38.8%) of 45 serum samples from 10 cats and 1 dog were positive by ELISA for SARS-CoV-2 S1 and RBD, and 10 (22.2%, 95% CI 12.4%–36.5%) of 45 samples (were reactive against SARS-CoV-2 N protein (Figure 2, panel A). All S1- and RBD-positive samples could neutralize SARS2-VSV infections, but N protein positivity and VN ability were not well associated (Figure 2, panel B).

OD values obtained for the SARS-CoV-2 S1 and RBD ELISAs showed a strong correlation with each other ($R = 0.95$), and both correlated well with VNT ($R = 0.87$) (Figure 3, panels A–C). Conversely, only a poor correlation was observed between OD values obtained for N protein ELISA and VNT ($R = 0.57$) (Figure 3, panel D). These data validate SARS-CoV-2 S1 and RBD and exclude N protein as antigen for serologic screening of cat and dog serum samples.

SARS-CoV-2 Seroprevalence in Domestic Cats

A total of 500 cat samples from the 2020 cohort were tested by using SARS-CoV-2 S1 and RBD ELISAs (Figure 4, panels A, C). FCoV type I S1 was included as an additional antigen in the ELISA, and 71% of cat samples were FCoV type I antibody positive. Six cat samples were positive for SARS-CoV-2 S1 and RBD, and an additional 6

Table 1. Percentage amino acid identity of canine and feline coronavirus spike and nucleocapsid proteins with SARS-CoV-2 proteins, the Netherlands*

Genus	Virus	SARS-CoV-2			
		N	S	S1	RBD
Betacoronavirus	CRCoV	32.4	28.5	20.0	15.6
Alphacoronavirus	FCoV type I	29.0	24.0	16.8	7.7
Alphacoronavirus	FcoV type II	27.8	25.3	17.7	8.9
Alphacoronavirus	CCoV	28.0	25.1	16.9	8.9

*SARS-CoV-2, CRCoV, FCoV type I, FCoV type II, CCoV (GB: NC_045512.2, JX860640.1, FJ938060.1, AY994055.1, KC175341.1). Amino acid sequences were aligned by using Clustal W (<https://www.ebi.ac.uk/Tools/msa/clustalo>), and pairwise identities were calculated by using the needle method in the EMBOSS pairwise alignment algorithms program (http://www.ebi.ac.uk/Tools/psa/emboss_needle). CCoV, canine coronavirus; CRCoV, canine respiratory coronavirus; FCoV, feline coronavirus; N, nucleocapsid protein; RBD, receptor-binding domain; S, spike protein; SARS-CoV-2, severe acute respiratory syndrome coronavirus 2; S1, spike protein subunit 1.

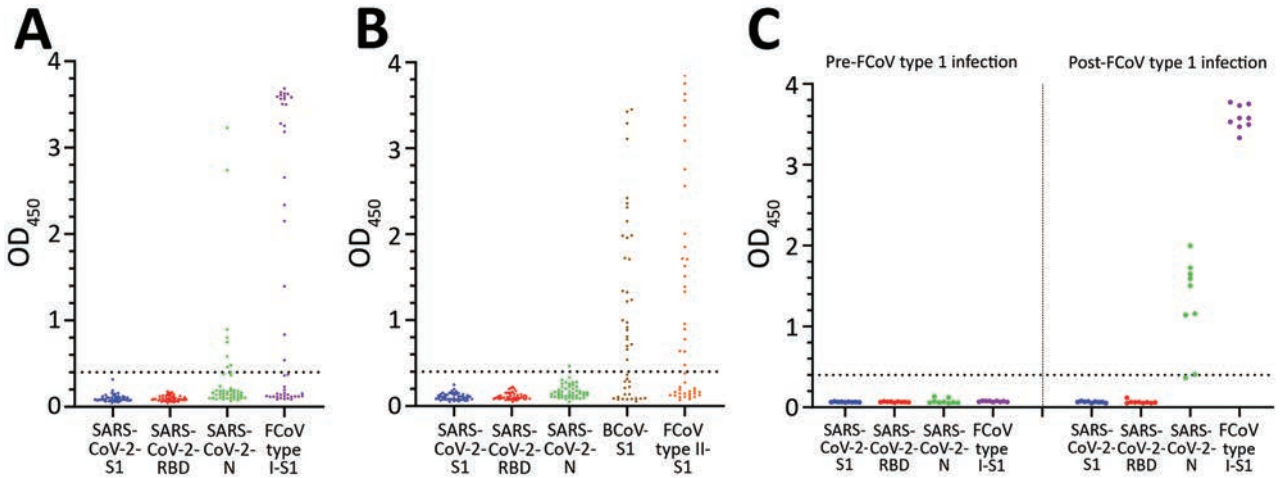


Figure 1. ELISA reactivities against different antigens of pre-coronavirus disease (COVID-19) cat and dog serum samples and paired samples of FCoV type I infection, the Netherlands. A) Reactivities of pre-COVID-19 cat serum samples against SARS-CoV-2 S1, RBD, N, and FCoV type I S1. B) Reactivities of pre-COVID-19 dog serum samples against SARS-CoV-2 S1, RBD, N, BCoV S1, and FCoV type II S1. C) Reactivities of paired SPF cat serum samples (left panel) and FCoV type I-specific serum samples (right panel) to SARS-CoV-2 S1, subunit; RBD, N, and FCoV S1 protein levels were determined by ELISA. Dotted lines indicate positive cutoff levels. BCoV, bovine coronavirus; FCoV, feline coronavirus; N, nucleocapsid; OD, optical density; RBD, receptor-binding domain; S1, spike protein subunit 1; SARS-CoV-2, severe acute respiratory syndrome coronavirus 2; SPF, specific pathogen free.

samples were positive only for RBD (Figure 4, panel C). We have summarized results of different tests (Table 2). We tested by VN assay all samples positive for SARS-CoV-2 S1 or RBD by ELISA, together with 50 randomly chosen samples that showed negative results in the S1 and RBD ELISAs. Two samples that reacted with SARS-CoV-2 S1 and RBD were able to neutralize SARS2-VSV infection, and all ELISA-negative samples were also negative in the VN assay (Table 2; Figure 4,

panel C). On the basis of results obtained for SARS-CoV-2-exposed animals, we defined a seropositive sample as any sample being ELISA positive for SARS-CoV-2 S1 and RBD, and with a VNT ≥ 16 . Samples that did not consistently show diagnostic thresholds (ELISA positive for S1 and RBD, but VNT < 16) were considered as being suspected (Table 2). Accordingly, 2 (0.4%, 95% CI 0.01%–1.55%) of 500 domestic cat samples with unknown SARS-CoV-2 exposure had reached the diagnostic thresholds,

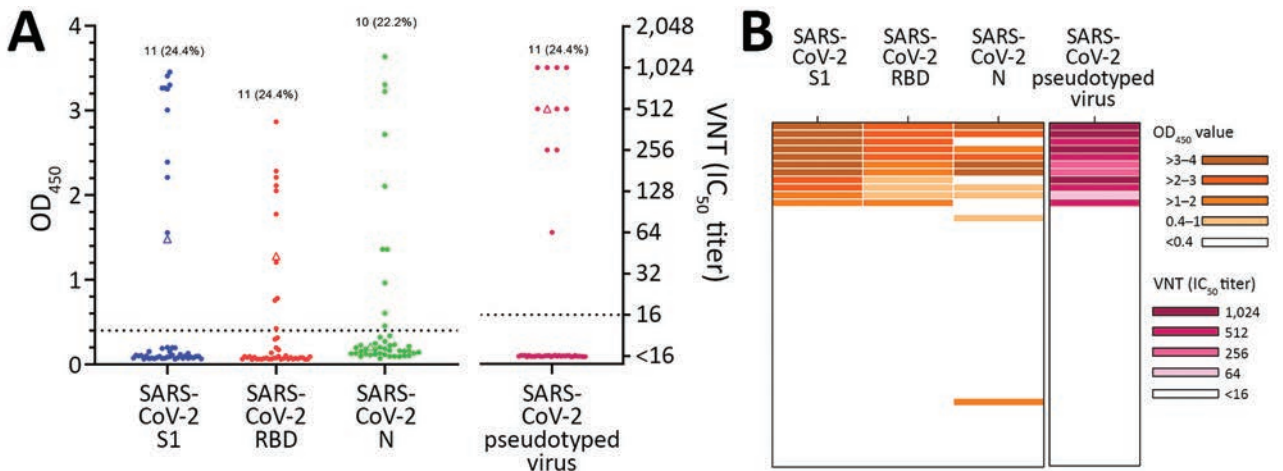


Figure 2. Serologic analyses of cat and dog serum samples from SARS-CoV-2-exposed cohort, the Netherlands. A) ELISA against SARS-CoV-2 S1, RBD, and N proteins, and VN analysis with SARS-CoV-2 pseudotyped virus. Dots indicate cat serum samples (n = 44) and triangle indicates dog sample (n = 1). B) Combination of results tested by different assays expressed as a heatmap. Dotted lines indicate positive cutoff levels. IC₅₀, 50% inhibitory concentration; N, nucleocapsid; OD, optical density; RBD, receptor-binding domain; S1, spike protein subunit 1; SARS-CoV-2, severe acute respiratory syndrome coronavirus 2; VN, virus neutralization.

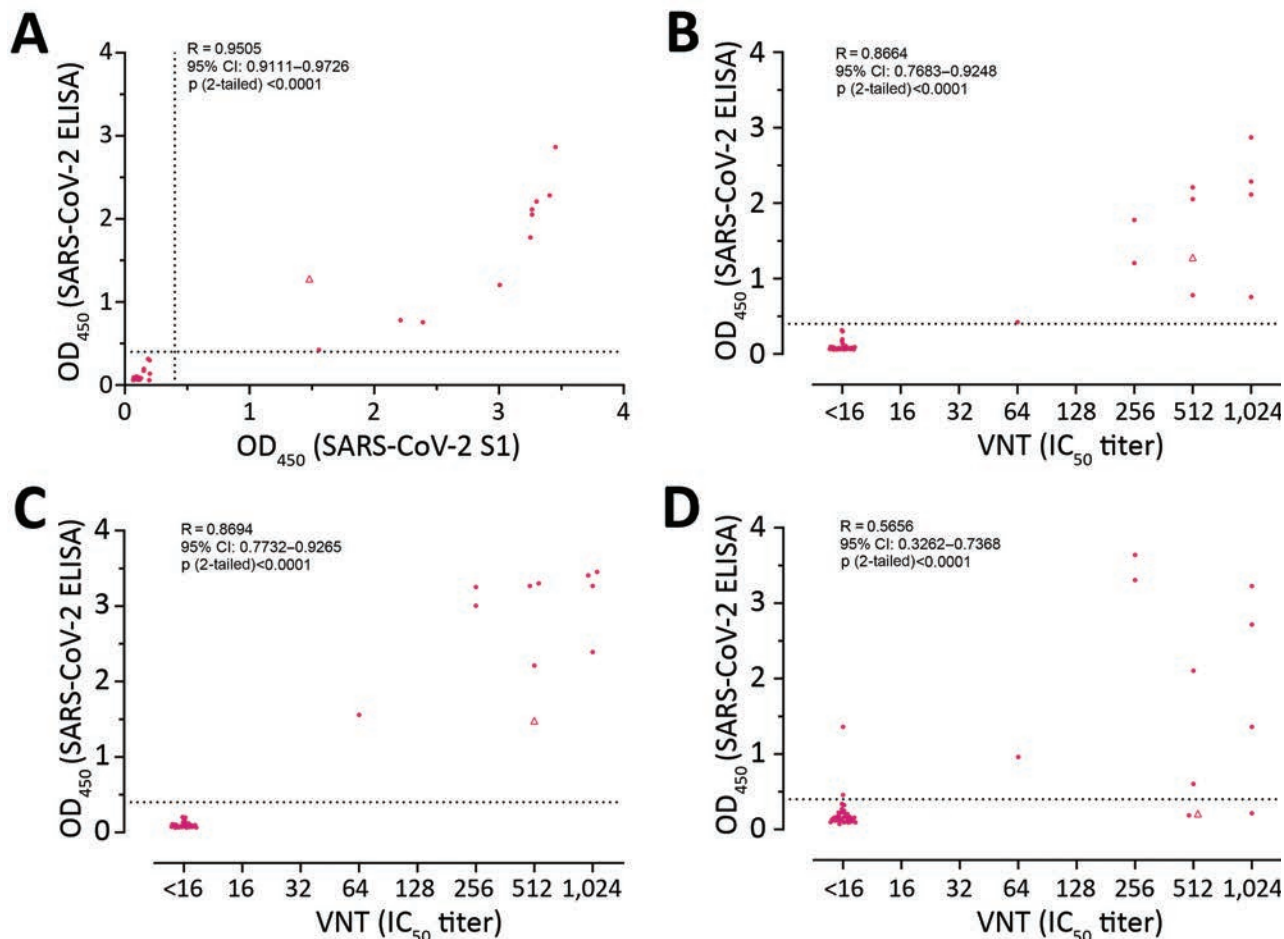


Figure 3. Pairwise correlation analyses of reactivities acquired for serologic analyses of SARS-CoV-2-exposed cohort, the Netherlands. Pearson correlation coefficient was calculated to determine the correlation between the reactivities of RBD ELISA vs. S1 ELISA (A), RBD ELISA vs. VNT (B), S1 ELISA vs. VNT (C), and N ELISA vs. VNT (D). Cat serum samples ($n = 44$) were indicated in dots and the dog sample ($n = 1$) in triangle. Dotted lines show the positive cutoff levels. IC₅₀, 50% inhibitory concentration; N, nucleocapsid; OD, optical density; RBD, receptor-binding domain; S1, spike protein subunit 1; SARS-CoV-2, severe acute respiratory syndrome coronavirus 2; VNT, virus neutralization titer.

and henceforth were confirmed as seropositive. Four serum samples were defined as suspected.

SARS-CoV-2 Seroprevalence in Domestic Dogs

We tested 500 dog samples by using the SARS-CoV-2 S1 and RBD ELISAs (Figure 4, panels B, D). FCoV type II S1 was included as an additional antigen, and results showed that 40.4% were positive for FCoV type II S1 antibody (indicator of CCoV exposure). Nine samples were positive for SARS-CoV-2 S1, of which only 1 was positive for RBD (Table 2; Figure 4, panel D). Only the sample that reacted with SARS-CoV-2 S1 and RBD was able to neutralize SARS2-VSV. Randomly chosen ELISA negative samples ($n = 50$) were negative in the VN assay (Table 2; Figure 4, panel D). Thus, 1 (0.2%, 95% CI, <0.01%–1.24%) of 500 of domestic dog

samples with unknown SARS-CoV-2 exposure was considered seropositive.

Confirmation of SARS-CoV-2-Specific Antibodies in Dog Samples by using Adsorption Assays

The 2 seropositive dog samples also contained antibodies against CRCoV, which belongs to genus *Betacoronavirus*, as does SARS-CoV-2 (Figure 5). To corroborate SARS-CoV-2 seropositivity, we performed an antigen S1 adsorption assay with S1 proteins of SARS-CoV-2 or BCoV (proxy for CRCoV). HCoV-229E (genus *Alphacoronavirus*) S1 was used as a control. Although adsorption of 229E S1 did not change ELISA reactivity for serum samples against SARS-CoV-2 and BCoV antigens, adsorption of SARS-CoV-2 and BCoV S1 specifically removed ELISA reactivity against the corresponding protein

(Figure 5). These data confirmed that ELISA reactivity against SARS-CoV-2 for these 2 dog samples is specific, in accordance with the screening of CRCoV-positive pre-COVID-19 dog samples described earlier, which did not show cross-reactivity with SARS-CoV-2 S1 in our ELISAs.

Discussion

Because SARS-CoV-2 can infect cats and dogs, the virus might spread in this population and animals might act as a reservoir with the possibility of animal-to-human transmission. Although so far the pandemic has been driven by human-to-human transmission, it is useful to know whether domestic animals can play a role in maintenance and spread of SARS-CoV-2 infections, as underscored by the recent reports that workers from mink farms had acquired SARS-CoV-2 from minks (24,25). For these studies, verified serologic assays that detect virus-specific antibody responses in cats and dogs are needed. In our study, we modified assays used in human epidemiologic studies and validated ELISAs to detect SARS-CoV-2 S1 and RBD antibodies and VN by using pseudotyped

SARS2-VSV for screening cat and dog samples. We defined seropositivity on the basis of results for positive samples from the SARS-CoV-2-exposed cohort.

We also showed that N protein, which is used in serologic studies with human samples (19,26), lacks discriminating power. We found a poor correlation between the results of the N protein ELISA and the VNT and the S1 and RBD ELISAs. Several of the pre-COVID-19 samples were positive in the N protein ELISA, probably because of antigenic cross-reactivity between SARS-CoV-2 and FCoV type I N proteins. These data validate SARS-CoV-2 S1 and RBD and exclude N protein as antigens for serologic screening of cat and dog serum samples. A similar phenomenon was also reported between porcine epidemic diarrhea virus and porcine transmissible gastroenteritis virus (27). Therefore, N protein cannot be used for serologic screening of samples from cats and dogs.

To date, most studies focused on molecular detection of SARS-CoV-2 in exposed animals, and virus detection is also used as the case definition by the World Organisation for Animal Health (28). However, serologic studies are needed to gain insights into

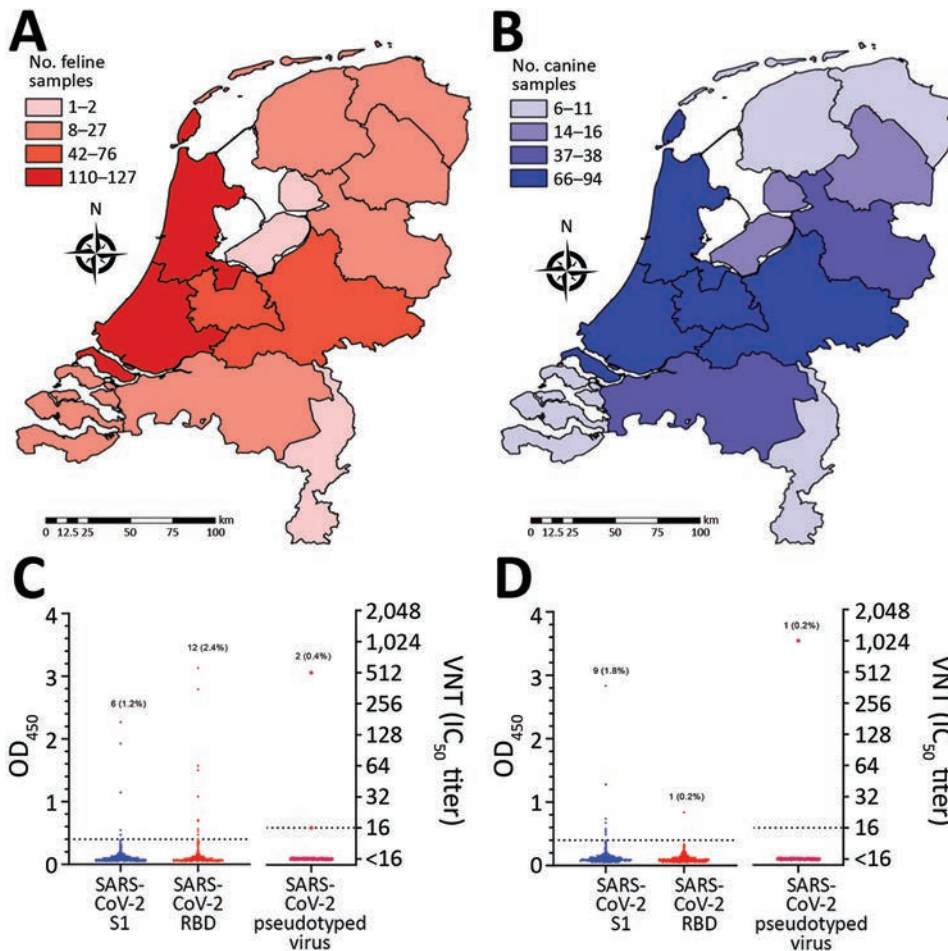


Figure 4. Geographic coverage and serologic analysis of cat (A, C) and dog (B, D) samples of 2020 cohorts for SARS-CoV-2, the Netherlands. A, B) Geographic distribution. Choropleth maps were produced by using ArcGIS version 9.3.1 (Esri, <https://www.esri.com>). C, D) ELISA and VNT analysis. Number and percentages of positive samples are indicated. Dotted lines indicate positive cutoff levels. Samples that had a VNT ≥ 16 were considered positive. IC₅₀, 50% inhibitory concentration; OD, optical density; RBD, receptor-binding domain; S1, spike protein subunit 1; SARS-CoV-2, severe acute respiratory syndrome coronavirus 2; VNT, virus neutralization titer.

Table 2. Serologic results for animal samples tested in different serologic assays, the Netherlands*

Animal	Cohort	SARS-CoV-2 S1	SARS-CoV-2		No. samples	Result
		ELISA†	RBD	ELISA†		
Cat	SARS-CoV-2 exposed, n = 44	+	+	+	10	Seropositive
		-	-	-	34	Seronegative
	2020, n = 500	+	+	+	2	Seropositive
		+	+	-	4	Suspected
		-	+	-	6	Seronegative
		-	-	-/NA	488	Seronegative
Dog	SARS-CoV-2 exposed, n = 1	+	+	+	1	Seropositive
		+	+	+	1	Seropositive
	2020, n = 500	+	-	-	8	Seronegative
		-	-	-/NA	491	Seronegative

*NA, not applicable; RBD, receptor-binding domain; SARS-CoV-2, severe acute respiratory syndrome coronavirus 2; S1, spike protein subunit 1; VNT, virus neutralization titer; -, negative; +, positive.
 †An ELISA optical density value greater than or equal to the cutoff value of 0.4 is a positive result, and an ELISA OD value less than the cutoff value is a negative result.
 ‡Neutralization titers of samples were determined by using the reciprocal of the highest dilution that resulted in >50% reduction of luciferase activity in pseudovirus virus neutralization. A VNT greater than or equal to the cutoff value of 16 is a positive result, and a VNT less than the cutoff value is a negative result.

the role of domestic animals in the epidemiology of the disease because they serve as a strong functional complement of molecular detection. In a recent molecular survey, no positive samples were detected for 4,000 samples from companion animals (cats, dogs, and horses) (29). However, serologic screening was not performed. In our study of samples from domestic animals with unknown SARS-CoV-2 exposure, we determined seroprevalences for SARS-CoV-2 of 0.4% for cats and 0.2% for dogs, which is lower than the prevalence rate of endemic coronaviruses, such as FCoV and CCoV, and also lower than the seroprevalence estimate in human populations in the Netherlands (2.7%–9.5%) at the period of sample collection (30,31). In our study, we also found a much lower seroprevalence than for domestic cats and dogs in

northern Italy, where >3% of samples were seropositive (32). However, all of these animals lived in SARS-CoV-2–positive households or in severely affected geographic areas. Such observations demonstrate that cats and dogs can acquire SARS-CoV-2 infection, but that the virus was not widely circulating in the cat and dog populations of the Netherlands at the time of sampling (April–May 2020).

VN assays are considered to be the reference standard for assessing immunity to many coronavirus infections based on their exceptional specificity (33). Therefore, we defined a sample positive when the S1 and RBD ELISA results were positive and confirmed by VN. In our screening, 4 cat samples were positive for S1 and RBD by ELISAs, but failed to neutralize SARS2-VSV infection and were defined as suspected.

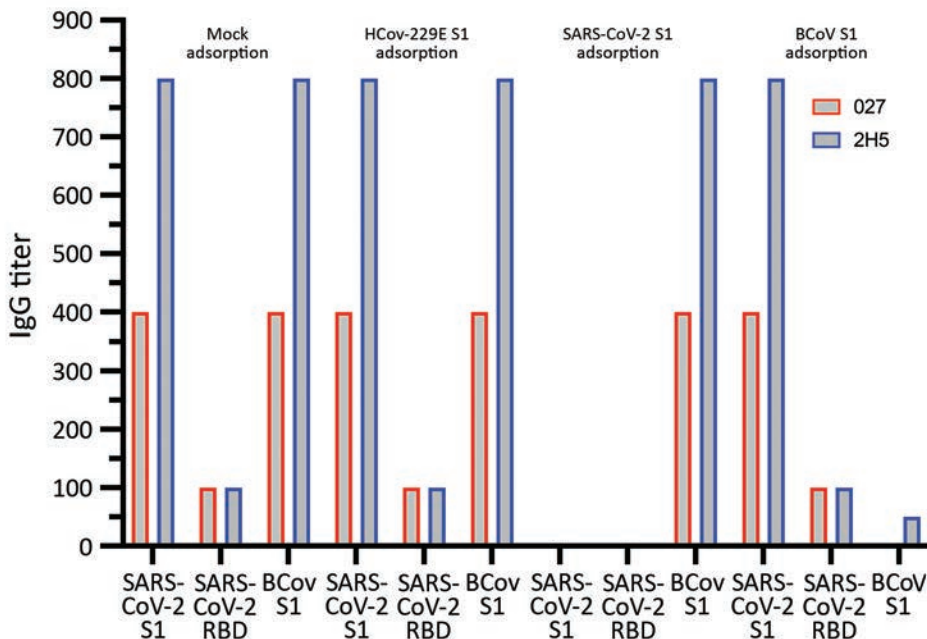


Figure 5. Corroboration of SARS-CoV-2 seropositivity in dog samples with adsorption assays, the Netherlands. ELISA reactivities of the 2 positive dog samples were determined against SARS-CoV-2 S1, RBD, and BCoV S1 after mock adsorption or adsorption with HCoV-229E S1, SARS-CoV-2 S1, or BCoV S1 proteins. The 2 seropositive dog samples (027 and 2H5) are from the SARS-CoV-2–exposed cohort and 2020 cohort, respectively. BCoV, bovine coronavirus; HCoV, human coronavirus; RBD, receptor-binding domain; S1, spike protein subunit 1; SARS-CoV-2, severe acute respiratory syndrome coronavirus 2.

This finding might be related to individual differences in development of neutralizing antibodies, such as different levels of SARS-CoV-2 exposure and time of sampling postinfection. In humans with asymptomatic or mild infection of Middle East respiratory syndrome coronavirus and SARS-CoV-2, samples were seropositive but failed to neutralize virus infection (33,34). Moreover, 14 samples reacted only with S1 or RBD in ELISAs and were defined as seronegative because they did not reach our diagnostic threshold (Table 2).

One limitation of our study is that lack of knowledge on the kinetics of SARS-CoV-2 antibodies in cats and dogs limits the setup of validated serologic assays. VN assays are considered to be a standard, but little is known regarding sensitivity compared with S1 or RBD ELISAs for identifying SARS-CoV-2 infections. Future studies require systematic analyses of development of antibody responses against different antigens in cats and dogs experimentally infected with SARS-CoV-2. In addition, regarding sampling methods used for the 2020 cohort, it is not possible to trace the health status and the level of SARS-CoV-2 exposure for those animals. Therefore, we cannot make any associations between antibody levels and clinical status. Also, our data report mainly SARS-CoV-2 seroprevalence during the first wave of the COVID-19 pandemic (April–May 2020). Whether seroprevalence is different during the second wave of the pandemic remains unknown. Moreover, possible implication of the emergence of new SARS-CoV-2 variant strains on the infection of animals remains to be established.

Overall, we developed and validated a set of serologic assays, and conducted seroprevalence study of SARS-CoV-2 infection in domestic cats and dogs in the Netherlands. The general prevalence rate was low at the time of sampling, indicating that cats and dogs are probably incidental hosts because of occasional SARS-CoV-2 spillover from humans. However, continued serosurveillance is needed to monitor possible, sustained transmission of SARS-CoV-2 infection in companion animals and a wider range of other animal species. This need is especially required because the incidence of COVID-19 in humans is still increasing in several parts of the world.

Acknowledgments

We thank Carien Radstake and the team at the Veterinary Microbiological Diagnostic Center (Utrecht, the Netherlands) for their contributions and Jie Chen for creating the choropleth map.

This study was supported by the Dutch Ministry of Agriculture, Nature and Food Quality. S.Z. was supported

by a grant from the China Scholarship Council (File no. 201606910061).

About the Author

Ms. Zhao is a doctoral candidate in the Virology Division, Faculty of Veterinary Medicine, Utrecht University, Utrecht. The Netherlands. Her primary research interest is seroepidemiologic studies of coronavirus and influenza A virus infections in companion animals.

References

- Zhou P, Yang XL, Wang XG, Hu B, Zhang L, Zhang W, et al. A pneumonia outbreak associated with a new coronavirus of probable bat origin. *Nature*. 2020;579:270–3. <https://doi.org/10.1038/s41586-020-2012-7>
- Wang C, Horby PW, Hayden FG, Gao GF. A novel coronavirus outbreak of global health concern. *Lancet*. 2020;395:470–3. [https://doi.org/10.1016/S0140-6736\(20\)30185-9](https://doi.org/10.1016/S0140-6736(20)30185-9)
- World Health Organization. Coronavirus disease (COVID-19) situation reports [cited 2021 Jan 15]. <https://www.who.int/publications/m/item/weekly-epidemiological-update-12-january-2021>
- Shi J, Wen Z, Zhong G, Yang H, Wang C, Huang B, et al. Susceptibility of ferrets, cats, dogs, and other domesticated animals to SARS-coronavirus 2. *Science*. 2020;368:1016–20. <https://doi.org/10.1126/science.abb7015>
- Lu S, Zhao Y, Yu W, Yang Y, Gao J, Wang J, et al. Comparison of nonhuman primates identified the suitable model for COVID-19. *Signal Transduct Target Ther*. 2020;5:157. <https://doi.org/10.1038/s41392-020-00269-6>
- Schlottau K, Rissmann M, Graaf A, Schön J, Sehl J, Wylezich C, et al. SARS-CoV-2 in fruit bats, ferrets, pigs, and chickens: an experimental transmission study. *Lancet Microbe*. 2020;1:e218–25. [https://doi.org/10.1016/S2666-5247\(20\)30089-6](https://doi.org/10.1016/S2666-5247(20)30089-6)
- Newman A, Smith D, Ghai RR, Wallace RM, Torchetti MK, Loiacono C, et al. First reported cases of SARS-CoV-2 infection in companion animals – New York, March–April 2020. *MMWR Morb Mortal Wkly Rep*. 2020;69:710–3. <https://doi.org/10.15585/mmwr.mm6923e3>
- Sit TH, Brackman CJ, Ip SM, Tam KW, Law PY, To EM, et al. Infection of dogs with SARS-CoV-2. *Nature*. 2020;586:776–8. <https://doi.org/10.1038/s41586-020-2334-5>
- Sailleau C, Dumarest M, Vanhomwegen J, Delaplace M, Caro V, Kwasiborski A, et al. First detection and genome sequencing of SARS-CoV-2 in an infected cat in France. *Transbound Emerg Dis*. 2020;67:2324–8. <https://doi.org/10.1111/tbed.13659>
- Ruiz-Arrondo I, Portillo A, Palomar AM, Santibáñez S, Santibáñez P, Cervera C, et al. Detection of SARS-CoV-2 in pets living with COVID-19 owners diagnosed during the COVID-19 lockdown in Spain: A case of an asymptomatic cat with SARS-CoV-2 in Europe. *Transbound Emerg Dis*. 2020 Aug 18 [Epub ahead of print]. <https://doi.org/10.1111/tbed.13803>
- Barrs VR, Peiris M, Tam KW, Law PY, Brackman CJ, To EM, et al. SARS-CoV-2 in quarantined domestic cats from COVID-19 households or close contacts, Hong Kong, China. *Emerg Infect Dis*. 2020;26:3071–4. <https://doi.org/10.3201/eid2612.202786>
- Garigliany M, Van Laere AS, Clercx C, Giet D, Escriou N, Huon C, et al. SARS-CoV-2 natural transmission from human

- to cat, Belgium, March 2020. *Emerg Infect Dis.* 2020;26:3069–71. <https://doi.org/10.3201/eid2612.202223>
13. Fritz M, Rosolen B, Krafft E, Becquart P, Elguero E, Vratskikh O, et al. High prevalence of SARS-CoV-2 antibodies in pets from COVID-19+ households. *One Health.* 2021;11:100192. <https://doi.org/10.1016/j.onehlt.2020.100192>
 14. Neira V, Brito B, Agüero B, Berríos F, Valdés V, Gutierrez A, et al. A household case evidences shorter shedding of SARS-CoV-2 in naturally infected cats compared to their human owners. *Emerg Microbes Infect.* 2020;Dec 15:1–22. <https://doi.org/10.1080/22221751.2020.1863132>
 15. Michelitsch A, Hoffmann D, Wernike K, Beer M. Occurrence of antibodies against SARS-CoV-2 in the domestic cat population of Germany. *Vaccines (Basel).* 2020;8:1–10. <https://doi.org/10.3390/vaccines8040772>
 16. Vogel L, Van der Lubben M, te Lintelo EG, Bekker CP, Geerts T, Schuijff LS, et al. Pathogenic characteristics of persistent feline enteric coronavirus infection in cats. *Vet Res.* 2010;41:71. <https://doi.org/10.1051/vetres/2010043>
 17. Oreshkova N, Molenaar RJ, Vreman S, Harders F, Oude Munnink BB, Hakze-van der Honing RW, et al. SARS-CoV-2 infection in farmed minks, the Netherlands, April and May 2020. *Euro Surveill.* 2020;25:2001005. <https://doi.org/10.2807/1560-7917.ES.2020.25.23.2001005>
 18. Wang C, Li W, Drabek D, Okba NM, van Haperen R, Osterhaus AD, et al. A human monoclonal antibody blocking SARS-CoV-2 infection. *Nat Commun.* 2020;11:2251. <https://doi.org/10.1038/s41467-020-16256-y>
 19. Okba NM, Müller MA, Li W, Wang C, GeurtsvanKessel CH, Corman VM, et al. Severe acute respiratory syndrome coronavirus 2-specific antibody responses in coronavirus disease patients. *Emerg Infect Dis.* 2020;26:1478–88. <https://doi.org/10.3201/eid2607.200841>
 20. Zhao S, Li W, Schuurman N, van Kuppeveld F, Bosch B-J, Egberink H. Serological screening for coronavirus infections in cats. *Viruses.* 2019;11:743. <https://doi.org/10.3390/v11080743>
 21. Qiu C, Huang Y, Zhang A, Tian D, Wan Y, Zhang X, et al. Safe pseudovirus-based assay for neutralization antibodies against influenza A(H7N9) virus. *Emerg Infect Dis.* 2013;19:1685–7. <https://doi.org/10.3201/eid1910.130728>
 22. Haake C, Cook S, Pusterla N, Murphy B. Coronavirus infections in companion animals: virology, epidemiology, clinical and pathologic features. *Viruses.* 2020;12:E1023. <https://doi.org/10.3390/v12091023>
 23. Hohdatsu T, Okada S, Ishizuka Y, Yamada H, Koyama H. The prevalence of types I and II feline coronavirus infections in cats. *J Vet Med Sci.* 1992;54:557–62. <https://doi.org/10.1292/jvms.54.557>
 24. Hammer AS, Quaade ML, Rasmussen TB, Fonager J, Rasmussen M, Mundbjerg K, et al. SARS-CoV-2 transmission between mink (*Neovison vison*) and humans, Denmark. *Emerg Infect Dis.* 2021;27:547–51. <https://doi.org/10.3201/eid2702.203794>
 25. Oude Munnink BB, Sikkema RS, Nieuwenhuijse DF, Molenaar RJ, Munger E, Molenkamp R, et al. Transmission of SARS-CoV-2 on mink farms between humans and mink and back to humans. *Science.* 2021;371:172–7. <https://doi.org/10.1126/science.abe5901>
 26. Long QX, Tang XJ, Shi QL, Li Q, Deng HJ, Yuan J, et al. Clinical and immunological assessment of asymptomatic SARS-CoV-2 infections. *Nat Med.* 2020;26:1200–4. <https://doi.org/10.1038/s41591-020-0965-6>
 27. Xie W, Ao C, Yang Y, Liu Y, Liang R, Zeng Z, et al. Two critical N-terminal epitopes of the nucleocapsid protein contribute to the cross-reactivity between porcine epidemic diarrhea virus and porcine transmissible gastroenteritis virus. *J Gen Virol.* 2019;100:206–16. <https://doi.org/10.1099/jgv.0.001216>
 28. World Organisation for Animal Health. Considerations for sampling, testing, and reporting of SARS-CoV-2 in animals. 2020;33(May):1–6 [cited 2021 Feb 21]. https://www.oie.int/fileadmin/Home/eng/Our_scientific_expertise/docs/pdf/COV-19/Sampling_Testing_and_Reporting_of_SARS-CoV-2_in_animals_final_7May_2020.pdf
 29. IDEXX. Overview of IDEXX SARS-CoV-2 (COVID-19) RealPCR test-IDEXX US [cited 2020 Jun 28]. <https://www.idexx.com/en/veterinary/reference-laboratories/overview-idexx-sars-cov-2-covid-19-realpcr-test>
 30. Slot E, Hogema BM, Reusken CB, Reimerink JH, Molier M, Karregat JH, et al. Low SARS-CoV-2 seroprevalence in blood donors in the early COVID-19 epidemic in the Netherlands. *Nat Commun.* 2020;11:5744. <https://doi.org/10.1038/s41467-020-19481-7>
 31. Vos ER, den Hartog G, Schepp RM, Kaaijk P, van Vliet J, Helm K, et al. Nationwide seroprevalence of SARS-CoV-2 and identification of risk factors in the general population of the Netherlands during the first epidemic wave. *J Epidemiol Community Health.* 2020;jech-2020-215678. <https://doi.org/10.1136/jech-2020-215678>
 32. Patterson EI, Elia G, Grassi A, Giordano A, Desario C, Medardo M, et al. Evidence of exposure to SARS-CoV-2 in cats and dogs from households in Italy. *Nat Commun.* 2020;11:6231. <https://doi.org/10.1038/s41467-020-20097-0>
 33. GeurtsvanKessel CH, Okba NM, Igloi Z, Bogers S, Embregts CW, Laksono BM, et al. An evaluation of COVID-19 serological assays informs future diagnostics and exposure assessment. *Nat Commun.* 2020;11:3436. <https://doi.org/10.1038/s41467-020-17317-y>
 34. Okba NM, Raj VS, Widjaja I, GeurtsvanKessel CH, de Bruin E, Chandler FD, et al. Sensitive and specific detection of low-level antibody responses in mild Middle East respiratory syndrome coronavirus infections. *Emerg Infect Dis.* 2019;25:1868–77. <https://doi.org/10.3201/eid2510.190051>

Address for correspondence: Herman Egberink, Department of Biomolecular Health Sciences, Infectious Diseases and Immunology, Virology Division, Faculty of Veterinary Medicine, Utrecht University, Utrecht, the Netherlands; email: h.f.egberink@uu.nl

Active Case Finding of Current Bornavirus Infections in Human Encephalitis Cases of Unknown Etiology, Germany, 2018–2020

Philip Eisermann,¹ Dennis Rubbenstroth,¹ Daniel Cadar, Corinna Thomé-Bolduan, Petra Eggert, Alexander Schlaphof, Frank Leypoldt, Martin Stangel, Thorsten Fortwängler, Florian Hoffmann, Andreas Osterman, Sabine Zange, Hans-Helmut Niller, Klemens Angstwurm, Kirsten Pörtner, Christina Frank, Hendrik Wilking, Martin Beer, Jonas Schmidt-Chanasit, Dennis Tappe

Human bornavirus encephalitis is a severe and often fatal infection caused by variegated squirrel bornavirus 1 (VSBV-1) and Borna disease virus 1 (BoDV-1). We conducted a prospective study of bornavirus etiology of encephalitis cases in Germany during 2018–2020 by using a serologic testing scheme applied along proposed graded case definitions for VSBV-1, BoDV-1, and unspecified bornavirus encephalitis. Of 103 encephalitis cases of unknown etiology, 4 bornavirus infections were detected serologically. One chronic case was caused by VSBV-1 after occupational-related contact of a person with exotic squirrels, and 3 acute cases were caused by BoDV-1 in virus-endemic areas. All 4 case-patients died. Bornavirus etiology could be confirmed by molecular methods. Serologic testing for these cases was virus specific, discriminatory, and a practical diagnostic option for living patients if no brain tissue samples are available. This testing should be guided by clinical and epidemiologic suspicions, such as residence in virus-endemic areas and animal exposure.

Human bornavirus encephalitis is a severe and often fatal disease caused by 2 related zoonotic members of the family Bornaviridae, variegated squirrel bornavirus 1 (VSBV-1, species *Mammalian 2 orthobornavirus*) and Borna disease virus 1 (BoDV-1,

species *Mammalian 1 orthobornavirus*). In 2015, VSBV-1 was detected as causative agent of fatal human encephalitis in a cluster of private breeders of exotic squirrels in Germany (1). In 2018, BoDV-1 was shown to be responsible for a cluster of transplant-related encephalitis cases (2) and individual encephalitis (3) in Germany. VSBV-1 has been detected in several holdings in Europe (private husbandries and zoologic gardens) of exotic squirrel species from the family Sciuridae of non-European descent (4–6). The geographic origin of the virus and potential additional wild animal reservoirs are unknown. In contrast, BoDV-1 is harbored by bicolored white-toothed shrews (*Crocidura leucodon*) native to Europe and is known to cause animal Borna disease (BD) after spillover infection in domestic animals in Europe. BD is a meningo-myeloencephalitis found predominantly in horses and sheep and is endemic to parts of Germany, as well as Austria, Liechtenstein, and Switzerland (7,8).

Although clinical disease and the underlying (immuno)pathology (9,10) have been described for human VSBV-1 encephalitis (1,11) and BoDV-1 encephalitis (3,12,13), many questions regarding the epidemiology

Author affiliations: Bernhard-Nocht-Institut für Tropenmedizin, Hamburg, Germany (P. Eisermann, D. Cadar, C. Thomé-Bolduan, P. Eggert, A. Schlaphof, J. Schmidt-Chanasit, D. Tappe); Federal Research Institute for Animal Health, Greifswald-Insel Riems, Germany (D. Rubbenstroth, M. Beer); University Medical Center Schleswig-Holstein, Kiel, Germany (F. Leypoldt); Medizinische Hochschule Hannover, Hannover, Germany (M. Stangel); Donau-Isar-Klinikum Deggendorf, Deggendorf, Germany (T. Fortwängler); Ludwig-Maximilians-University, Munich, Germany (F. Hoffmann); Max von Pettenkofer Institute, Munich (A. Osterman);

German Center for Infection Research, Munich (A. Osterman); Bundeswehr Institute of Microbiology, Munich (S. Zange); Regensburg University Hospital, Regensburg, Germany (H.-H. Niller, K. Angstwurm); Postgraduate Training for Applied Epidemiology, Berlin, Germany (K. Pörtner); European Centre for Disease Prevention and Control, Stockholm, Sweden (K. Pörtner); Robert Koch Institute, Berlin (K. Pörtner, C. Frank, H. Wilking)

DOI: <https://doi.org/10.3201/eid2705.204490>

¹These authors contributed equally to this article.

of human VSBV-1 (6) and BoDV-1 (12) infections are still unanswered. Therefore, in March 2020, the direct detection of bornavirus infections became notifiable in Germany for humans (German Infection Protection Act [Infektionsschutzgesetz, IfSG]) and mammals (Verordnung über meldepflichtige Tierkrankheiten, TKrMeldpflV). Moreover, diagnostic external quality assurance tests are being prepared for serologic and molecular testing to equip participating laboratories with the skills and techniques to diagnose such infections and to provide reference materials in the future.

We report the results of a prospective screening study for bornavirus infections in human cases of encephalitis of unknown etiology in Germany during 2018–2020. Screening was based on a newly developed serologic testing scheme and using graded case definitions for VSBV-1 encephalitis, BoDV-1 encephalitis, and unspecified bornavirus encephalitis (i.e., bornavirus encephalitis in which the exact bornavirus species could not be determined).

Patients, Materials, and Methods

Patient Groups

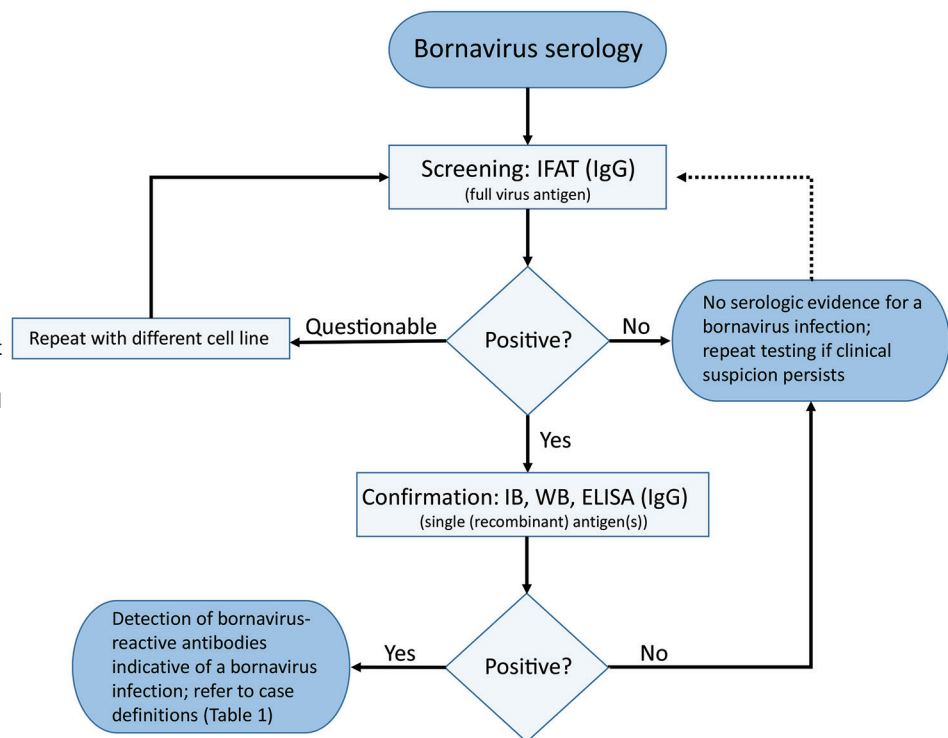
We tested 2 patient groups. For the first group, neurologic hospital departments in Germany and researchers

specializing in autoimmune encephalitis within the German Network for Research on Autoimmune Encephalitis (GENERATE, <https://www.generate-net.de>) were alerted about bornavirus encephalitis cases by email. In response, serum and cerebrospinal fluid (CSF) samples of patients with encephalitis of unknown etiology were sent to the Bernhard Nocht Institute for Tropical Medicine (Hamburg, Germany) during January 2018–August 2020 for analysis of possible bornavirus infections. Samples were analyzed for antibodies against VSBV-1 and BoDV-1. For the second group, serum samples from patients without a clinical history of encephalitis but for whom a bornavirus serologic analysis was nonetheless requested by the treating physicians during the same period were also analyzed.

Serologic Testing Scheme and Case Definition

We developed and used a serologic testing scheme (Figure 1) in conjunction with graded case definitions (confirmed, probable, and possible cases) for human VSBV-1 encephalitis, BoDV-1 encephalitis, and unspecified bornavirus encephalitis (Table 1). We defined encephalitis or encephalopathy according to Venkatesan et al. (14). We performed screening of serum and CSF samples for bornavirus-reactive IgG by using an indirect immunofluorescence antibody test

Figure 1. Serologic testing scheme for human bornavirus encephalitis, Germany, 2018–2020. Scheme was based on serologic screening and confirmatory assays and in conjunction with a case definition for variegated squirrel bornavirus 1 (VSBV-1) and Borna disease virus 1 (BoDV-1) encephalitis (Table 1) was diagnosed. Screening of serum samples and cerebrospinal fluid for bornavirus-reactive IgG was conducted by using an indirect immunofluorescence antibody test. A persistently BoDV-1-infected cell line was used with uninfected cells of the same cell line as controls (Vero cells or Crandell-Rees feline kidney cells). For confirmation of a positive IFAT screening result, a line blot with recombinant VSBV-1 and BoDV-1 phosphoprotein proteins was used in our study, but alternative assays, such as WB or ELISA with recombinant antigen(s) or antigen(s) derived from infected cells, might also be appropriate after sufficient validation. Adequate control serum samples from confirmed human VSBV-1 and BoDV-1 encephalitis cases and a pooled serum of 20 healthy blood donors were used for the IFAT and the line blot. IFAT, indirect immunofluorescence antibody test; IB, immunoblot; WB, Western blotting.



(IFAT) and Crandell-Rees Feline Kidney (CRFK) cells persistently infected with BoDV-1 strain V and uninfected cells of the same cell line as controls (11,15).

Because of high antigenic cross-reactivity within the genus *Orthobornavirus*, the BoDV-1 IFAT also detects antibodies against VSBV-1 (1,11,16). All serum or CSF samples with intranuclear IFAT patterns indicative for bornavirus infections (11,15) at dilutions $\geq 1:10$ were considered positive. End-point titers are indicated as the reciprocal value of the highest positive dilution factor. We used a line blot (immunoblot) with recombinant phosphoprotein (P) from VSBV-1 and BoDV-1 as a confirmatory assay (11,15). The P protein was chosen because it was shown to be more specific than the nucleoprotein for serologic analysis (11). The cutoff value of the line blot was 16 arbitrary units per antigen, as validated by the manufacturer (Euroimmun, <https://www.euroimmun.com>) by using bornavirus-positive serum and CSF samples in comparison to >200 controls without evidence of bornavirus encephalitis. In our study, we used serum samples from laboratory-confirmed human VSBV-1 and BoDV-1 encephalitis cases as positive controls and pooled serum samples from 20 healthy blood donors as negative control for both the IFAT and the line blot.

Molecular Assays and Cell Culture

We performed VSBV-1-specific (1) and BoDV-1-specific (2) quantitative reverse transcription PCRs (qRT-PCRs) for CSF and brain tissue of seropositive patients, if available. In positive cases, we used next-generation sequencing (NGS) to generate full-length virus genomes (1,11,12). We performed virus isolation in Vero or CRFK cells (12) and confirmed by direct immunofluorescence test using polyclonal antibodies (11,12) against VSBV-1 and BoDV-1.

Ethics

The planning, conduct, and reporting of this study was in accordance with the Declaration of Helsinki, as revised in 2013. Ethical clearance was obtained from the Medical Board of Hamburg (no. PV5616).

Results

For group 1, serum and CSF samples from 103 patients with encephalitis (at that time of unknown etiology) were received and tested during the study. Samples were from 60 male and 43 female patients; age range was 1–89 years (median age 48 years). For group 2, bornavirus serologic analysis was conducted for serum samples from 121 patients who had no clinical history of encephalitis but for whom bornavirus serologic analysis was requested. Samples were from 55

male and 66 female patients; age range was 4–84 years (median age 45 years).

For group 1, a total of 4 (3.9%) confirmed bornavirus encephalitis case-patients were detected: 1 VSBV-1 case-patient in northern Germany (Schleswig-Holstein) (case-patient 1) and 3 BoDV-1 case-patients in Bavaria in southern Germany (case-patients 2–4; Figure 2). None of these case-patients had a travel history outside Germany in the 5 months before symptom onset. Initial testing by IFAT resulted in detection of bornavirus-reactive anti-

Table 1. Case definitions for BoDV-1 or VSBV-1 encephalitis/encephalopathy, Germany, 2018–2020*
Case definition

Confirmed case of BoDV-1 or VSBV encephalitis/encephalopathy
Encephalitis or encephalopathy AND detection of BoDV-1 or VSBV-1 RNA in CSF or CNS tissue OR detection of BoDV-1 or VSBV-1 antigen by IHC with virus-specific monoclonal antibodies in CNS tissue
Confirmed case of unspecified bornavirus encephalitis/encephalopathy
Encephalitis or encephalopathy AND detection of bornavirus antigen by IHC with cross-reactive monoclonal antibodies or polyclonal serum in CNS tissue
Probable case of BoDV-1 or VSBV-1 encephalitis/encephalopathy
Encephalitis or encephalopathy AND detection of bornavirus-reactive IgG in a serum or CSF sample by screening test (with full virus antigen, e.g., IFAT) and suitable confirmation assay detecting antibodies against individual bornavirus antigens (derived from infected cells or recombinant antigens, e.g., Western blot, immunoblot, or ELISA) AND suitable comparative antibody quantification assay able to distinguish antibodies specific for BoDV-1, VSBV-1 or other orthobornaviruses (e.g., IFAT, immunoblot, ELISA) OR exposure to VSBV-1-positive squirrels or epidemiologic link to BoDV-1-endemic regions AND no evidence of other reasons for the clinical picture
Probable case of unspecified bornavirus encephalitis/encephalopathy
Encephalitis or encephalopathy AND detection of bornavirus-reactive IgG in a serum or CSF sample by screening test (with full virus antigen, e.g., IFAT) and suitable confirmation assay detecting antibodies against individual bornavirus antigens (derived from infected cells or recombinant antigens, e.g., Western blot, immunoblot, or ELISA) AND detection of bornavirus-reactive IgG in a serum or CSF sample by screening test (with full virus antigen, e.g., IFAT) and suitable confirmation assay detecting antibodies against individual bornavirus antigens (derived from infected cells or recombinant antigens, e.g., Western blot, immunoblot, or ELISA)
Possible case of BoDV-1 or VSBV-1 encephalitis/encephalopathy
Encephalitis or encephalopathy AND residence in BoDV-1-endemic area or exposure to VSBV-1-positive squirrels AND no evidence of other reasons for the clinical picture

*Case definitions replace those of Tappe et al. (6). Encephalitis or encephalopathy was defined according to Venkatesan et al. (14). BoDV-1, Borna disease virus 1; CNS, central nervous system; CSF, cerebrospinal fluid; IFAT, immunofluorescence antibody test; IHC, immunohistochemical analysis; VSBV-1, variegated squirrel bornavirus 1.

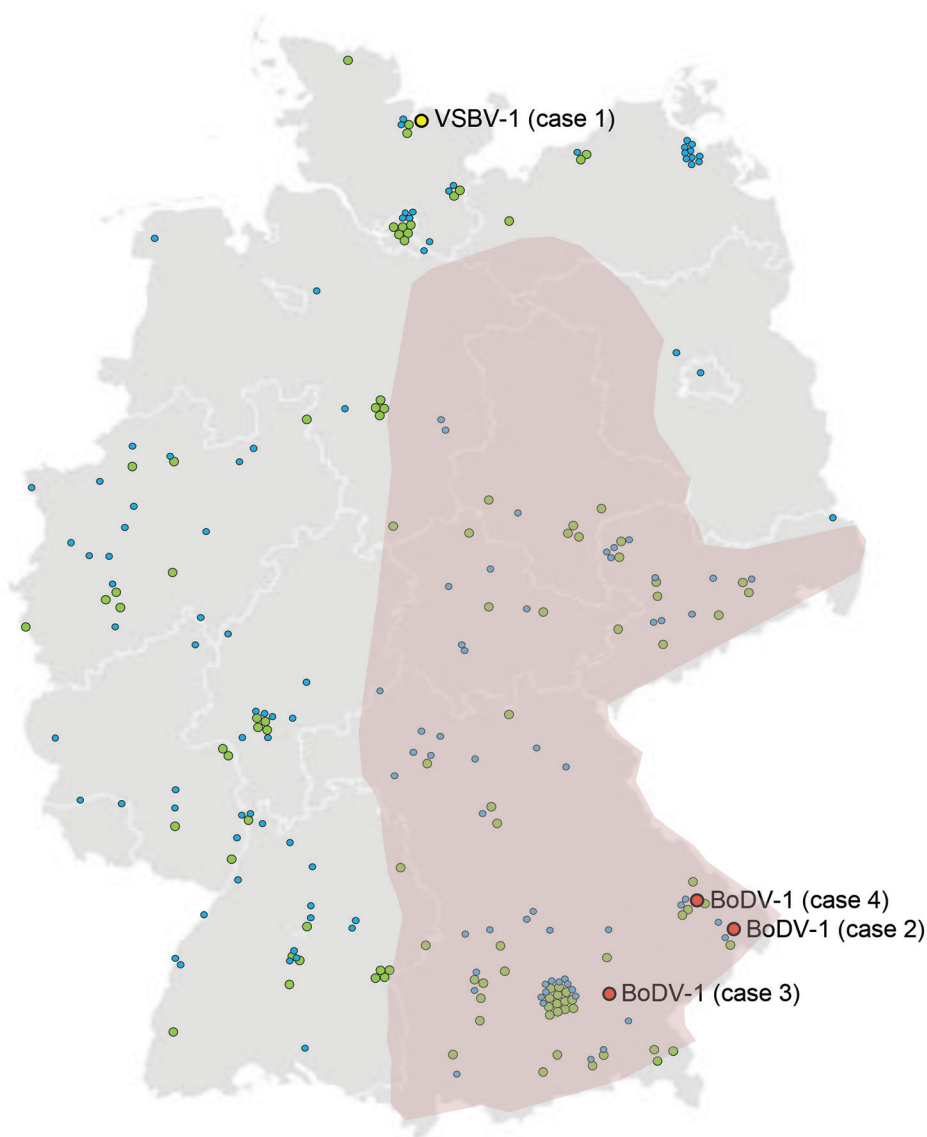


Figure 2. Germany showing locations of residences of human case-patients who had encephalitis and other conditions and were tested for bornavirus etiology, 2018–2020. Among 103 encephalitis cases with unknown etiology, 4 bornavirus cases were found: 1 chronic VSBV-1 infection in northern Germany (case 1) and 3 BoDV-1 infections in southern Germany (cases 2, 3, and 4). Encephalitis cases without a bornavirus etiology are indicated as green circles. Among 121 cases without a clinical history of encephalitis but for whom a bornavirus serologic analysis was requested, no bornavirus infections were detected (blue circles). Purple indicates regions known to be endemic for BoDV-1. BoDV-1, Borna disease virus 1; VSBV-1, variegated squirrel bornavirus 1.

bodies in serum and CSF samples for all 4 case-patients (Table 2). Samples of case-patients 1–3 also showed positive results for a bornavirus P line blot assay. Serum and CSF samples from case-patient 1 showed higher signals for VSBV-1 P than BoDV-1 P, and serum samples from case-patients 2 and 3 showed higher signals for BoDV-1 P (Table 2). The discriminatory potential of this test was confirmed by analysis of reference serum samples from several laboratory-confirmed BoDV-1 and VSBV-1 encephalitis cases (Figure 3). qRT-PCR and full-genome sequencing confirmed the bornavirus infection for all 4 case-patients.

Case-Patient 1: Chronic VSBV-1 Encephalitis/Encephalopathy

Case-patient 1 was a 41-year-old man, a former zoo animal caretaker, from northern Germany who was

given a diagnosis of VSBV-1 infection at the Bernhard Nocht Institute for Tropical Medicine during February 2019. Acute encephalitis had developed in the patient in 2007; by 2019, he was living in a nursing home and showed severe neurologic deficits and disabilities. The patient had cared for exotic squirrel species in the same zoo (zoo D [6]) in which a woman (another zoo animal caretaker) showed development of VSBV-1 encephalitis during 2013 after contact with exotic squirrels; her case had been retrospectively detected in 2018 (11).

IFAT titers for case-patient 1 in February 2019 were extremely high (655,360 for serum and 20,480 for CSF). Line blot results for antibodies against VSBV-1 P were 62 units for serum and 49 units for CSF (Table 2). qRT-PCR results were negative for VSBV-1 in stored CSF obtained during 2007 but positive in

an archived formalin-fixed brain biopsy specimen obtained the same year (cycle quantitation [Cq] value 30.9). Five months after the diagnosis of VSBV-1 encephalitis, the patient died of urosepsis, 12 years after onset of neurologic illness.

Case-Patient 2: Acute BoDV-1 Encephalitis

Case-patient 2 was a 55-year-old woman, a part-time cleaner from Bavaria who was given a diagnosis of BoDV-1 infection in February 2019. The patient had encephalitis, fever, headache, and coma develop in mid-January 2019. IFAT titer was 640 for serum and 80 for CSF. Line blot results for antibodies against BoDV-1 P were 30 units for serum and 4 units for CSF (Table 2). A qRT-PCR result for BoDV-1 in CSF was weakly positive (Cq 35.3). Case-patient 2 died 1 day after diagnosis and 3 weeks after onset of disease. Postmortem virus isolation and sequencing from brain tissue were successful (GenBank accession no. LR722643; Figure 4) (12). This case-patient was included in a recent case series from Bavaria as case-patient P8 by Niller et al. (12), and histopathologic results were described in detail as case-patient 6 by Liesche et al. (10).

Case-Patient 3: Acute BoDV-1 Encephalitis

Case-patient 3 was an 11-year-old girl from a rural region of Bavaria who was given a diagnosis of BoDV-1 infection in November 2019. The patient had encephalitis, fever, headache, and epileptic seizures develop during mid-October 2019. IFAT titer was 2,560 for serum and 160 for CSF. Line blot results for antibodies against BoDV-1 P were 17 units for serum and 2 units for CSF (Table 2). A qRT-PCR result for BoDV-1 in CSF was positive (Cq 33.0). A full-length virus genome was obtained by NGS from brain tissue attached to a CSF pressure probe removed after death (GenBank accession no. MT364324; Figure 4). Virus isolation from brain material was successful in CRFK cells after 2 passages of the inoculated cells. Case-patient 3 died 2 days after diagnosis and 4 weeks after onset of illness. No autopsy was performed.

Case-Patient 4: Acute BoDV-1 Encephalitis

Case-patient 4 was a 79-year-old man, a farmer from a rural region of Bavaria who was given a diagnosis

of BoDV-1 infection in June 2020. The patient had encephalitis, fever, and confusion develop at the end of May 2020. IFAT titer was 2,560 for serum and 160 for CSF. Line blot results for antibodies against BoDV-1 P were 1 unit for serum and 0 units for CSF (Table 2). A qRT-PCR result for BoDV-1 in CSF was positive (Cq 34.0). Virus isolation from CSF was not successful, but a full-length virus genome was obtained by NGS (GenBank accession no. MW053459; Figure 4). Case-patient 4 patient died 1 day after diagnosis and 4 weeks after onset of illness. No autopsy was performed.

All 4 case-patients fulfilled the case definition for confirmed VSBV-1 or BoDV-1 encephalitis. No unspecified bornavirus encephalitis cases and no probable or possible cases were identified in this study. Consistent with their geographic origin, we found that BoDV-1 sequences from case-patients 2–4 (GenBank accession nos. LR722643, MT364324, and MW053459) were closely related to human- and animal-derived sequences in BoDV-1 cluster 1A from home regions of the patients in southeastern Bavaria (Figure 4). Case-patients 2 and 4 lived <50 km from each other (Figure 2). Their BoDV-1 genome sequences showed higher nucleotide identity to each other (99.6%; Figure 4) than to the viral sequence obtained from patient 3 (98.6%), who lived ≈80 km southwest of case-patients 2 and 4. In congruence with previous confirmed human BoDV-1 infections, phylogenetic analysis suggested that zoonotic transmission occurred from the natural reservoir of the viruses near the most recent residences of the patients (2,12). For the nonencephalitis patients in group 2, we found no persons who had bornavirus-reactive antibodies in the IFAT or the IFAT plus line blot (Figure 2).

Discussion

The epidemiology of human bornavirus encephalitis is still largely unknown. In our prospective study, we identified 4 bornavirus case-patients (3.9%) in a group of 103 case-patients who had cryptic encephalitis. The VSBV-1 case-patient had a disease course during 2007–2019, whereas the BoDV-1 case-patients died from acute infection during 2019 and 2020. Regarding incidence of infection, bornavirus encephalitis cases caused by VSBV-1 and BoDV-1 appear to

Table 2. Line blot results for 4 case-patients who had bornavirus encephalitis, Germany, 2018–2020*

Case no.	Virus	Serum			Cerebrospinal fluid		
		IFAT	VSBV-1 P	BoDV-1 P	IFAT	VSBV-1 P	BoDV-1 P
1	VSBV-1	655,360	62	54	20,480	49	32
2	BoDV-1	640	9	30	80	2	4
3	BoDV-1	2,560	4	17	160	2	2
4	BoDV-1	2,560	2	1	160	1	0

*Cutoff value is 16 arbitrary units per antigen; positive results are indicated in bold. Results of antibody testing against heterologous antigens are indicated in italics. BoDV-1, Borna disease virus 1; IFAT, immunofluorescence antibody test; P, phosphoprotein; VSBV-1, variegated squirrel bornavirus 1.

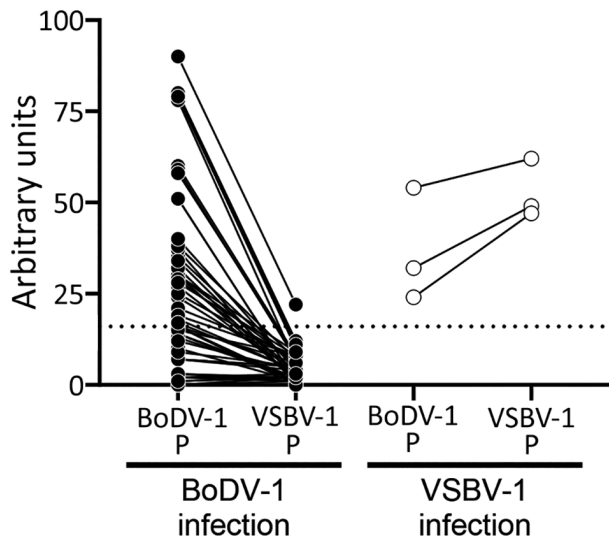


Figure 3. Reactivity of samples from BoDV-1- and VSBV-1-infected patients with homologous and heterologous bornavirus P antigens, Germany. Bornavirus indirect immunofluorescence antibody test–positive serum and cerebrospinal fluid samples were tested by using the Euroimmun (<https://www.euroimmun.com>) line blot with BoDV-1 P and VSBV-1 P antigens (BoDV-1: 52 samples from 14 patients; VSBV-1: 3 samples from 2 patients). Samples originated from patients with laboratory-confirmed BoDV-1 or VSBV-1 infection (2,10–12; this study). Results are indicated as arbitrary units. Dotted line indicates cutoff value of 16 as defined by the manufacturer. BoDV-1, Borna disease virus 1; P, phosphoprotein; VSBV-1, variegated squirrel bornavirus 1.

be rare. Cases were only found among the group of encephalitis patients and not among patients with unspecified symptoms for whom a bornavirus serologic analysis was nonetheless requested. This finding supports previous studies that scientific evidence for a possible bornavirus etiology for other clinical entities apart from encephalitis continues to be lacking (15,17,18).

The cases detected in our study confirm previously identified risk factors: acquiring VSBV-1 encephalitis through contact with exotic squirrel species and association of BoDV-1 encephalitis with residence in mainly rural environments in areas endemic for animal BD and thus BoDV-1. The incidence of human VSBV-1 continues to be restricted to the small group of zoo animal caretakers and squirrel owners exposed to infected exotic squirrels. The denominator of this group is unknown, but small. Known confirmed human case-patients include 3 private breeders (1) and 2 zoo animal caretakers (case-patient 1 reported here; case reported in 11). All of these patients died, although the patient identified in this study survived for 12 years after the acute phase. In another study (6), a squirrel breeder had a serologically positive result

after recovery from a transient neurologic disease. This case was classified as a probable case because diagnostic material suitable for confirmation of the infection by direct virus detection (Table 1) was not available. Two additional breeders identified in the same study had died of unclear encephalitis, but no archived diagnostic materials were available. These cases were categorized as possible cases (Table 1).

The incidence of diagnosed BoDV-1 encephalitis cases is currently ≈ 2 cases/year in Germany; there is a strong restriction to known areas to which BoDV-1 is endemic (12). In these regions, BoDV-1 might be a major cause of previously cryptic encephalitis: In a recent study of archived brain tissue material from patients who had fatal encephalitis without a known cause from 1 center in Bavaria in an area to which animal BD is endemic, 7 (78%) of 9 had a BoDV-1 infection (12). At the same time, a seroprevalence study performed in BoDV-1–endemic areas found only 1 seropositive person among a presumed risk group of 736 veterinarians (0.14%; clinical and diagnostic follow-up was not possible) and none among 373 healthy blood donors (0%; 15). Thus, these data suggest that BoDV-1 infection and BoDV-1–induced encephalitis are rare, even in virus-endemic areas, but have a high case-fatality rate.

Bornavirus encephalitis cases caused by VSBV-1 and BoDV-1 are clinically similar, severe, and in nearly all reported cases fatal. The course of BoDV-1 encephalitis appears to be more rapid (1–3,10–13). All but 1 case-patient who had confirmed bornavirus encephalitis died; only in a transplant-associated BoDV-1 encephalitis cluster did 1 patient survive but had neurologic sequelae (2). In our study, all 4 patients died of the disease; however, a patient who had severe VSBV-1 encephalitis/encephalopathy had a 12-year chronic course of disease. More thus far undetected chronic bornavirus infections in persons who have neurologic deficits after encephalitis or chronic encephalopathy might be present and should undergo diagnostic testing for a bornavirus etiology. Clinical awareness, particularly for severe encephalitis cases in areas to which BoDV-1 is endemic or after contact with exotic squirrel species, should lead to early testing for a possible bornavirus etiology while the person is still alive. Bornavirus infection needs to become a routine target for differential diagnostics. An early diagnosis would be a prerequisite for antiviral chemotherapy.

Following graded case definitions for VSBV-1, BoDV-1, and unspecified bornavirus encephalitis/encephalopathy (Table 1), we used a serologic testing scheme (Figure 1) for rapid initial *intra vitam* diagnosis of bornavirus encephalitis. Positive serologic

results were subsequently confirmed by direct pathogen detection for all 4 bornavirus encephalitis cases. In this study, as well as in previous studies, higher and earlier detectable antibody titers were usually observed in serum samples than in CSF samples (2,12,13). The time of seroconversion during human bornavirus encephalitis is variable; some patients are already seropositive at the time

of hospitalization, and others show development of detectable antibodies only shortly before death (2,12). Thus, serologic follow-up testing (likely within days) should be performed in encephalitis case-patients who have epidemiologic risk factors but initially negative results because such patients might be infected with zoonotic bornaviruses but might not yet have seroconverted.

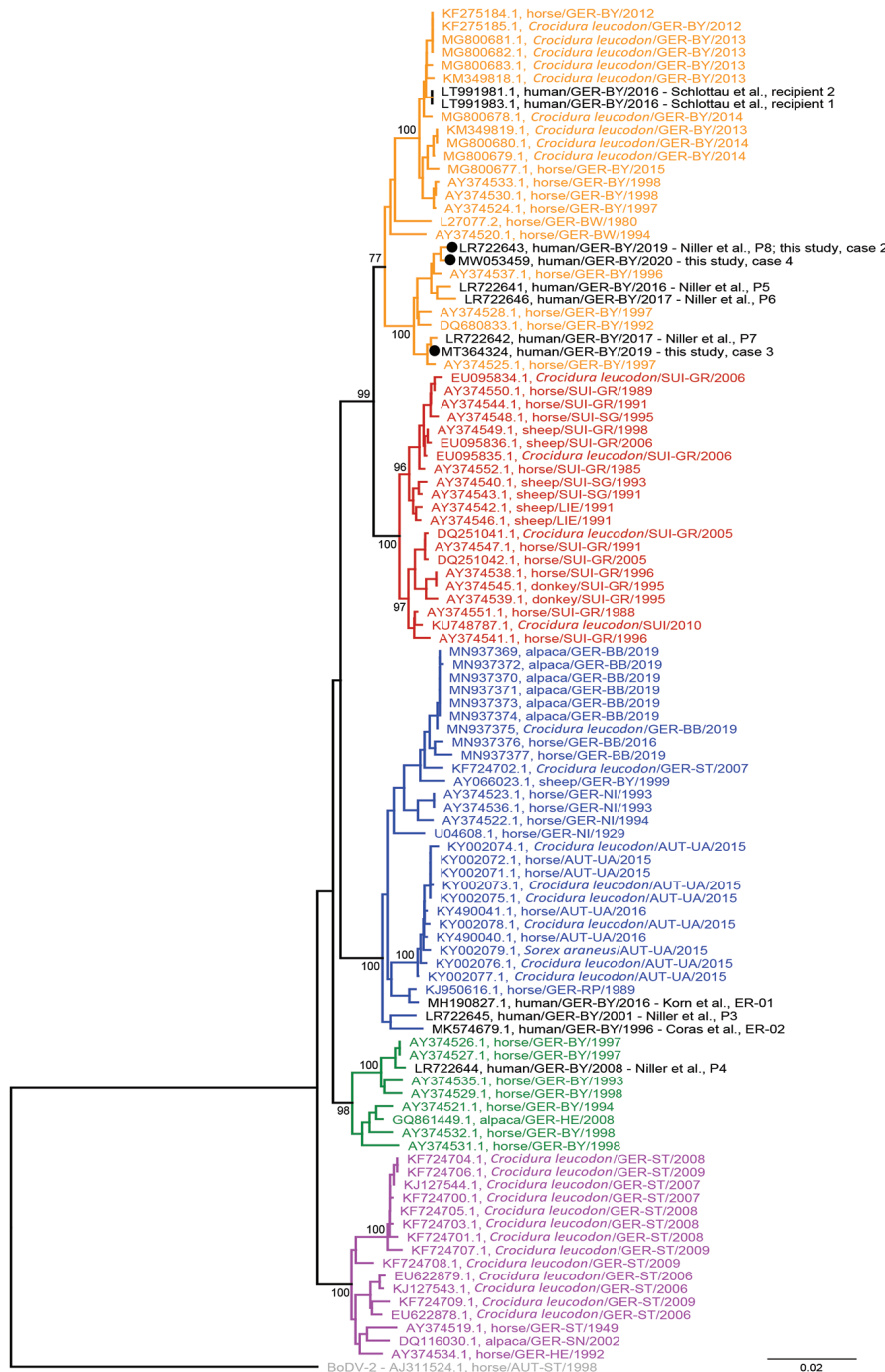


Figure 4. Phylogenetic analysis of BoDV-1 nucleotide sequences from virus-endemic areas, Germany. Shown are partial bornavirus sequences (nucleoprotein gene to phosphoprotein gene, 1,824 nt, representing genome positions 54–1877 of BoDV-1 reference genome U04608), including BoDV-1 sequences from animals and humans in virus-endemic regions in Germany, Austria, Switzerland, and Liechtenstein. BoDV-2 was used as an outgroup. Analysis was performed by using the neighbor-joining algorithm and the Jukes–Cantor distance model in Geneious Prime (<https://www.geneious.com>) and the tree was rooted for the VSBV-1 clade. Human sequences are indicated in black. Sequences of cases 1–4 included in this study are indicated in bold. Values at branches represent support in 1,000 bootstrap replicates. Only bootstrap values ≥ 70 at major branches are shown. Cluster designations, host, and geographic origin are indicated according to previously published studies (2,7,8,12,17–23). Colors and numbers at right indicate clusters. Scale bar indicates nucleotide substitutions per site. AUT, Austria; UA, Upper Austria; ST, Styria. GER, Germany: BB, Brandenburg; BW, Baden-Wuerttemberg; BY, Bavaria; HE, Hesse; NI, Lower Saxony; RP, Rhineland-Palatinate; SN, Saxony; ST Saxony-Anhalt. LIE, Liechtenstein. SUI, Switzerland: GR, Grisons; SG, St. Gall.

IFAT appears to be more sensitive than the line blot assay used in this study and previous studies (12). In this study, line blot results were below the cutoff value for case-patient 4 in serum and CSF samples. This finding emphasizes the need for serologic follow-up testing for some case-patients, with the expectation that the screening test result will be confirmed by positive single-antigen assay results in follow-up samples that have increased antibody titers. Without the molecular confirmation, case-patient 4 would have been classified as having a possible case, stressing the need for molecular testing. In addition to sensitivity, specificity is a crucial issue of serologic testing for bornavirus infections, emphasizing the need for careful evaluation of IFAT results with a specific granular intranuclear pattern observed only in the bornavirus-infected cells (2,11,15,16).

Orthobornaviruses show considerable cross-reactivity among each other (16). Furthermore, antibodies against individual antigenic epitopes might be detected despite lack of any known previous bornavirus contact, leading to false-positive results (19). Establishing and optimizing assays such as Western blot, line blot, or ELISA, for detection of antibodies against individual bornavirus antigens are needed to enable subsequent confirmation of positive IFAT results and help to partly overcome the shortcomings of bornavirus serologic analysis. Furthermore, comparative testing by using antigens from different orthobornaviruses by IFAT (16) or line blot (as shown in this study) can enable discriminatory prediction of VSBV-1, BoDV-1, or other orthobornavirus infections. In the line blot used in this study, serum samples from VSBV-1-infected and BoDV-1-infected patients reliably showed higher arbitrary antibody units for the respective homologous P antigen than for heterologous antigen (Table 2). This provisional discrimination might be useful for prognosis because BoDV-1 infections appear to be more rapidly fatal than VSBV-1 infections. Despite these measures, incidental, singular, bornavirus-reactive antibodies might remain indistinguishable from truly positive results.

Because of these limitations of serologic testing, direct pathogen detection is mandatory to confirm the initial serologic diagnosis and discrimination of VSBV-1 and BoDV-1 infections, as indicated in the graded case definitions (Table 1). However, *intra vitam* direct detection of the virus is severely hampered by the strong cell-associated and neurotropic nature of the virus and its almost exclusive restriction to the central nervous system in dead-end hosts, such as humans (2,11,12). The virus is not detectable in blood, and viral RNA

detection by qRT-PCR in CSF samples often shows negative or only weakly positive results; the negative predictive value appears to be low (12). Bornavirus RNA detection in biopsy specimens from affected brain areas seems to be the most sensitive diagnostic method, but the difficulties with these procedures are high and unlikely to be met early in the disease course. Postmortem, unequivocal confirmation of infection can be made by using qRT-PCR, *in situ* hybridization, and immunohistochemical analysis of brain tissue (2,3,9–13). Sequencing the viral genome and subsequent phylogeographic analysis might provide information on the regional source of infection (2,12).

The first limitation of this study is that, although it was a large screening program of encephalitis cases for bornavirus infections, a complete or representative sampling was not performed. Thus, the prevalence of human bornavirus encephalitis remains to be investigated. Second, only a few bornavirus cases were found, which was partly caused by the overall low incidence of bornavirus encephalitis in humans. This limitation also emphasizes the need for increased awareness for this disease. Detection of future cases will provide further opportunity to approve the herein proposed case definition criteria. Third, only encephalitis cases from Germany were investigated in this study. However, the virus-endemic region for BoDV-1 also includes neighboring Austria, Liechtenstein, and Switzerland. Undetected human BoDV-1 cases are also expected in these countries.

In conclusion, human bornavirus encephalitis cases remain rare in the general population in Germany, even for BoDV-1 infections in areas to which animal BD is endemic. Human bornavirus encephalitis is often fatal. Chronic cases occur at least for VSBV-1 infections, but might be exceptional. There is no evidence that zoonotic bornaviruses might cause diseases other than encephalitis (e.g., encephalomyelitis, encephalomyelorradiculitis) in humans. Antibody testing in serum samples is sensitive but requires confirmation by direct detection of virus. The proposed testing scheme and case definitions proved useful. All patients who have encephalitis (especially a severe course) from virus-endemic areas or after contact with exotic squirrels should be tested for a bornavirus infection, ideally early in the disease course by antibody testing in serum samples.

The study was supported by the Federal Ministry of Education and Research within the Zoonotic Bornavirus Consortium, a project of the National Network of Zoonotic Infectious Diseases in Germany (grant no. 01KI2005C).

About the Author

Dr. Eisermann is a clinical microbiologist at the Bernhard Nocht Institute, Hamburg, Germany. His research interests focus on emerging viral diseases.

References

- Hoffmann B, Tappe D, Höper D, Herden C, Boldt A, Mawrin C, et al. A variegated squirrel bornavirus associated with fatal human encephalitis. *N Engl J Med*. 2015;373:154–62. <https://doi.org/10.1056/NEJMoa1415627>
- Schlottau K, Forth L, Angstwurm K, Höper D, Zecher D, Liesche F, et al. Fatal encephalitic borna disease virus 1 in solid-organ transplant recipients. *N Engl J Med*. 2018;379:1377–9. <https://doi.org/10.1056/NEJMc1803115>
- Korn K, Coras R, Bobinger T, Herzog SM, Lücking H, Stöhr R, et al. Fatal encephalitis associated with borna disease virus 1. *N Engl J Med*. 2018;379:1375–7. <https://doi.org/10.1056/NEJMc1800724>
- Schlottau K, Jenckel M, van den Brand J, Fast C, Herden C, Höper D, et al. Variegated squirrel bornavirus 1 in squirrels, Germany and the Netherlands. *Emerg Infect Dis*. 2017;23:477–81. <https://doi.org/10.3201/eid2303.161061>
- Schlottau K, Hoffmann B, Homeier-Bachmann T, Fast C, Ulrich RG, Beer M, et al. Multiple detection of zoonotic variegated squirrel bornavirus 1 RNA in different squirrel species suggests a possible unknown origin for the virus. *Arch Virol*. 2017;162:2747–54. <https://doi.org/10.1007/s00705-017-3432-z>
- Tappe D, Frank C, Homeier-Bachmann T, Wilking H, Allendorf V, Schlottau K, et al. Analysis of exotic squirrel trade and detection of human infections with variegated squirrel bornavirus 1, Germany, 2005 to 2018. *Euro Surveill*. 2019;24:1800483 <https://doi.org/10.2807/1560-7917.ES.2019.24.8.1800483>
- Dürwald R, Kolodziejek J, Weissenböck H, Nowotny N. The bicolored white-toothed shrew *Crocidura leucodon* (HERMANN 1780) is an indigenous host of mammalian borna disease virus. *PLoS One*. 2014;9:e93659. <https://doi.org/10.1371/journal.pone.0093659>
- Weissenböck H, Bagó Z, Kolodziejek J, Hager B, Palmethofer G, Dürwald R, et al. Infections of horses and shrews with bornaviruses in upper Austria: a novel endemic area of borna disease. *Emerg Microbes Infect*. 2017;6:e52. <https://doi.org/10.1038/emi.2017.36>
- Tappe D, Schmidt-Chanasit J, Rauch J, Allartz P, Herden C. Immunopathology of fatal human variegated squirrel bornavirus 1 encephalitis, Germany, 2011–2013. *Emerg Infect Dis*. 2019;25:1058–65. <https://doi.org/10.3201/eid2506.181082>
- Liesche F, Ruf V, Zoubaa S, Kaletka G, Rosati M, Rubbenstroth D, et al. The neuropathology of fatal encephalomyelitis in human borna virus infection. *Acta Neuropathol*. 2019;138:653–65. <https://doi.org/10.1007/s00401-019-02047-3>
- Tappe D, Schlottau K, Cadar D, Hoffmann B, Balke L, Bewig B, et al. Occupation-associated fatal limbic encephalitis caused by variegated squirrel bornavirus 1, Germany, 2013. *Emerg Infect Dis*. 2018;24:978–87. <https://doi.org/10.3201/eid2406.172027>
- Niller HH, Angstwurm K, Rubbenstroth D, Schlottau K, Ebinger A, Giese S, et al. Zoonotic spillover infections with borna disease virus 1 leading to fatal human encephalitis, 1999–2019: an epidemiological investigation. *Lancet Infect Dis*. 2020;20:467–77. [https://doi.org/10.1016/S1473-3099\(19\)30546-8](https://doi.org/10.1016/S1473-3099(19)30546-8)
- Coras R, Korn K, Kuerten S, Huttner HB, Ensser A. Severe bornavirus-encephalitis presenting as Guillain-Barré-syndrome. *Acta Neuropathol*. 2019;137:1017–9. <https://doi.org/10.1007/s00401-019-02005-z>
- Venkatesan A, Tunkel AR, Bloch KC, Luring AS, Sejvar J, Bitnun A, et al.; International Encephalitis Consortium. Case definitions, diagnostic algorithms, and priorities in encephalitis: consensus statement of the international encephalitis consortium. *Clin Infect Dis*. 2013;57:1114–28. <https://doi.org/10.1093/cid/cit458>
- Tappe D, Frank C, Offergeld R, Wagner-Wiening C, Stark K, Rubbenstroth D, et al. Low prevalence of borna disease virus 1 (BoDV-1) IgG antibodies in humans from areas endemic for animal borna disease of southern Germany. *Sci Rep*. 2019;9:20154. <https://doi.org/10.1038/s41598-019-56839-4>
- Zimmermann V, Rinder M, Kaspers B, Staeheli P, Rubbenstroth D. Impact of antigenic diversity on laboratory diagnosis of Avian bornavirus infections in birds. *J Vet Diagn Invest*. 2014;26:769–77. <https://doi.org/10.1177/1040638714547258>
- Kolodziejek J, Dürwald R, Herzog S, Ehrensperger F, Lussy H, Nowotny N. Genetic clustering of borna disease virus natural animal isolates, laboratory and vaccine strains strongly reflects their regional geographical origin. *J Gen Virol*. 2005;86:385–98. <https://doi.org/10.1099/vir.0.80587-0>
- Dürwald R, Kolodziejek J, Herzog S, Nowotny N. Meta-analysis of putative human bornavirus sequences fails to provide evidence implicating Borna disease virus in mental illness. *Rev Med Virol*. 2007;17:181–203. <https://doi.org/10.1002/rmv.530>
- Nobach D, Bourg M, Herzog S, Lange-Herbst H, Encarnação JA, Eickmann M, et al. Shedding of infectious borna disease virus-1 in living bicolored white-toothed shrews. *PLoS One*. 2015;10:e0137018. <https://doi.org/10.1371/journal.pone.0137018>
- Schulze V, Große R, Fürstenau J, Forth LF, Ebinger A, Richter MT, et al. Borna disease outbreak with high mortality in an alpaca herd in a previously unreported endemic area in Germany. *Transbound Emerg Dis*. 2020;67:2093–107. <https://doi.org/10.1111/tbed.13556>
- Hornig M, Briesche T, Licinio J, Khabbaz RF, Altshuler LL, Potkin SG, et al. Absence of evidence for bornavirus infection in schizophrenia, bipolar disorder and major depressive disorder. *Mol Psychiatry*. 2012;17:486–93. <https://doi.org/10.1038/mp.2011.179>
- Rubbenstroth D, Schlottau K, Schwemmler M, Rissland J, Beer M. Human bornavirus research: back on track! *PLoS Pathog*. 2019;15:e1007873. <https://doi.org/10.1371/journal.ppat.1007873>
- Billich C, Sauder C, Frank R, Herzog S, Bechter K, Takahashi K, et al. High-avidity human serum antibodies recognizing linear epitopes of borna disease virus proteins. *Biol Psychiatry*. 2002;51:979–87. [https://doi.org/10.1016/S0006-3223\(02\)01387-2](https://doi.org/10.1016/S0006-3223(02)01387-2)

Address for correspondence: Dennis Tappe, Bernhard-Nocht-Institut für Tropenmedizin, Bernhard-Nocht-Strasse 74, Hamburg 20359, Germany; email: tappe@bnitm.de

Susceptibility to SARS-CoV-2 of Cell Lines and Substrates Commonly Used to Diagnose and Isolate Influenza and Other Viruses

Li Wang, Xiaoyu Fan, Gaston Bonenfant, Dan Cui, Jaber Hossain, Nannan Jiang, Gloria Larson, Michael Currier, Jimma Liddell, Malania Wilson, Azaibi Tamin, Jennifer Harcourt, Jessica Ciomperlik-Patton, Hong Pang, Naomi Dybdahl-Sissoko, Ray Campagnoli, Pei-Yong Shi, John Barnes, Natalie J. Thornburg, David E. Wentworth, Bin Zhou

Co-infection with severe acute respiratory syndrome coronavirus 2 (SARS-CoV-2) and other viruses has been reported. We evaluated cell lines commonly used to isolate viruses and diagnose related diseases for their susceptibility to SARS-CoV-2. Although multiple kidney cell lines from monkeys were susceptible to SARS-CoV-2, we found many cell types derived from humans, dogs, minks, cats, mice, and chicken were not. We analyzed MDCK cells, which are most commonly used for surveillance and study of influenza viruses, and found that they were not susceptible to SARS-CoV-2. The low expression level of the angiotensin converting enzyme 2 receptor and lower receptor affinity to SARS-CoV-2 spike, which could be overcome by overexpression of canine angiotensin converting enzyme 2 in trans, strengthened the cellular barrier to productive infection. Moreover, a D614G mutation in the spike protein did not appear to affect SARS-CoV-2 cell tropism. Our findings should help avert inadvertent propagation of SARS-CoV-2 from diagnostic cell lines.

Coronavirus disease (COVID-19) has resulted in >70 million laboratory-confirmed cases and >1.6 million deaths in <1 year since the first case was confirmed. Co-infection with severe acute respiratory

syndrome coronavirus 2 (SARS-CoV-2) and other viruses, such as influenza virus, has been reported (1–4). Because cases of COVID-19 continue to climb sharply, more coinfections are expected, especially in the current and future influenza seasons.

Isolating and propagating viruses from clinical specimens in cell cultures or embryonated chicken eggs is widely used to identify multiple viruses and produce vaccines, mostly under Biosafety Level 2 containment. Currently, SARS-CoV-2 must be isolated and propagated under Biosafety Level 3 containment because of its risk to laboratorians and the general public. Therefore, if any of these cell lines or eggs support productive replication of SARS-CoV-2, then a validated procedure should be implemented to rule out the presence of SARS-CoV-2 in the specimens before their inoculation. However, adding a diagnostic step specific to SARS-CoV-2 in many circumstances is impractical or substantially increases the cost and labor required.

We conducted this study to determine whether cell lines and eggs commonly used to isolate and propagate influenza viruses, poliovirus, and other human viruses can support productive replication of SARS-CoV-2. If a substrate is confirmed to be insensitive to SARS-CoV-2, modifying procedures to diagnose and isolate susceptible viruses in that substrate may be unnecessary. Although we repeated all results under the same or slightly different conditions, some of our results were further confirmed using multiple assay methods on divergent SARS-CoV-2 strains and in cell lines from different sources. Our study provides additional information on the risk of inadvertently propagating SARS-CoV-2 in cell lines and substrates when isolating, identifying, propagating, or producing vaccines for other viruses.

Author affiliations: Centers for Disease Control and Prevention, Atlanta, Georgia, USA (L. Wang, X. Fan, J. Hossain, M. Currier, M. Wilson, A. Tamin, J. Harcourt, J. Ciomperlik-Patton, H. Pang, N. Dybdahl-Sissoko, R. Campagnoli, J. Barnes, N.J. Thornburg, D.E. Wentworth, B. Zhou); Oak Ridge Institute for Science and Education, Oak Ridge, Tennessee, USA (G. Bonenfant, N. Jiang, G. Larson); Battelle Memorial Institute, Atlanta, Georgia, USA (D. Cui, J. Liddell); University of Texas Medical Branch, Galveston, Texas, USA (P.-Y. Shi)

DOI: <https://doi.org/10.3201/eid2705.210023>

Materials and Methods

Viruses

We used 3 virus stocks for our investigation. The SARS-CoV-2/USA-WA1/2020 (USA-WA1) viral strain was isolated from the specimen of the first confirmed case in the United States (5). SARS-CoV-2/Massachusetts/VPT1/2020 (MA/VPT1) was

isolated in Vero E6 cells from a nasopharyngeal specimen collected in April 2020. The recombinant fluorescent reporter virus icSARS-CoV-2-mNG was generated as described elsewhere (6). We sequenced the spike genes of all working stocks. Although USA-WA1 and MA/VPT1 did not have mutations or variations (at the 20% cutoff level), icSARS-CoV-2-mNG acquired a 5-residue insertion at the furin

Table 1. Overview of commercial cell lines used in study of susceptibility to SARS-CoV-2 of cell lines and substrates used to diagnose and isolate influenza and other viruses*

Cell line	Organism	Tissue	Type/ morphology	Virus susceptibility profile†	SARS-CoV-1 susceptible (references)	SARS-CoV-2 susceptible
Vero	African green monkey	Kidney	Epithelial	AdV, coxsackie B, measles, mumps, rotavirus, rubella, influenza	Yes (32,38)	Yes
Vero 76	African green monkey	Kidney	Epithelial	AdV, coxsackie B, measles, mumps, poliovirus, rotavirus, rubella, West Nile Virus	Yes (39)	Yes
BGMK	African green monkey	Kidney	Epithelial	coxsackie B, poliovirus	Yes (32)	Yes
CV-1	African green monkey	Kidney	Fibroblast	measles, mumps, rotavirus	Yes (32)	No
LLC-MK2	Rhesus macaque	Kidney	Epithelial	enterovirus, myxovirus and poxvirus groups, poliovirus type 1, rhinovirus	Yes (32)	Yes
RhMK	Rhesus macaque	Kidney	Epithelial	enteroviruses, influenza, parainfluenza	Yes (35)	Yes
A549	Human	Lung	Epithelial	AdV, influenza, measles, mumps, parainfluenza, poliovirus, RSV, rotavirus	No (32,34,35); Yes (40)	No
HEL	Human	Lung	Fibroblast	AdV, CMV, echovirus, HSV, poliovirus, rhinovirus	No (32,35)	No
HeLa	Human	Cervix	Epithelial	AdV, CMV, echovirus, HSV, poliovirus, rhinovirus	No (32)	No
HeLa 229	Human	Cervix	Epithelial	AdV, CMV, echovirus, HSV, poliovirus, rhinovirus	Unknown	No
HEp2	Human	Cervix	Epithelial	AdV, coxsackie B, HSV, measles, parainfluenza, poliovirus, RSV	No (32)	No
MRC-5	Human	Lung	Fibroblast	AdV, CMV, echovirus, HSV, influenza, mumps, poliovirus, rhinovirus	No (35)	No
MRHF	Human	Foreskin	Fibroblast	AdV, CMV, echovirus, HSV, mumps, poliovirus, rhinovirus	Unknown	No
NCI-H292	Human	Lung	Epithelial	AdV, HSV, influenza A, measles virus, RSV, rhinoviruses, vaccinia virus	No (34,37,40)	No
RD	Human	Muscle	Spindle; multinucleated	AdV, echovirus, HSV, poliovirus	No (32,36)	No
WI-38	Human	Lung	Fibroblast	AdV, CMV, echovirus, HSV, influenza, mumps, poliovirus, rhinovirus, RSV	Unknown	No
McCoy	Mouse	Unknown	Fibroblast	HSV	Unknown	No
MNA	Mouse	Nerve	Neuroblastoma	Rabies	Unknown	No
MDCK	Dog	Kidney	Epithelial	AdV, coxsackie virus, influenza, reoviruses	No (29,32,33,35,37)	No
CRFK	Cat	Kidney	Epithelial	canine parvovirus, feline calicivirus, feline panleukopenia virus, rabies virus	Yes (29)	Yes (limited)
Mv1Lu	American mink	Lung	Epithelial	CMV, influenza	Yes (35,38)	No
H&V-Mix	CV-1 and MRC-5	Mixture	Mixture	AdV, CMV, echovirus, HSV, influenza, poliovirus type 1, SV40 virus, VZV	Unknown	No
R-Mix	Mv1Lu and A549	Mixture	Mixture	AdV, CMV, HSV, influenza, measles, mumps, poliovirus, RSV, rotavirus	Yes (35)	No
R-Mix Too	MDCK and A549	Mixture	Mixture	AdV, HSV, influenza, MPV, measles, mumps, poliovirus, RSV, rotavirus, VZV	Unknown	No
Super E-Mix	BGMK and A549	Mixture	Mixture	AdV, HSV, influenza, measles, mumps, poliovirus, RSV, rotavirus, VZV	Unknown	Yes

*AdV, adenovirus; CMV, cytomegalovirus; HSV, herpes simplex virus; RhMK, rhesus monkey kidney; RSV, respiratory syncytial virus; VZV, varicella zoster virus.

†Virus susceptibility profiles listed are as reported by Quidel (<https://www.quidel.com>) and not verified in this study.

Table 2. Primers and probes used for the quantification of ACE2 mRNA in various cell lines in study of susceptibility to SARS-CoV-2 of cell lines and substrates used to diagnose and isolate influenza and other viruses

Assay identification	Applicable cell lines	Primers/probes*	Sequence, 5' → 3'
ACE2.FAM.10	Vero E6, A549, CRFK, CV-1	Forward Probe Reverse	CCCAGAATCCTTGAGTCAT TACTGATGCAATGGTGAACC TTGGACAGAAACCAACATAG
ACE2.FAM.11	Vero E6, CRFK	Forward Probe Reverse	GGGTCACAGTATGTTTCATC TATCTCTCGTTCATCTCCC GGAGGTGGATGGTCTTTA
ACE2.FAM.12	Vero E6, MDCK-NBL-2, MDCK-SIAT1	Forward Probe Reverse	TGGTCTTTGGGAATTTCA TAAAGACCATCCACCTCCAC GAAATCATGTCACTTTCTGC
ACE2.FAM.13	Vero E6, MDCK-NBL-2, MDCK-SIAT1	Forward Probe Reverse	AACATGGAACAGAGATGC CCAAAGACCAGTGGATGAAA GGAGGTGGATGGTCTTTA
ACE2.FAM.14	Vero E6, Mv1Lu	Forward Probe Reverse	CTTCATAGTCTCCTCTCCAATAA CTCTTCATATAATGGCCTCAGC CTACAATGAGAGGCTCTGG
ACE2.FAM.15	Vero E6, Mv1Lu	Forward Probe Reverse	CTCTTCATATAATGGCCTCAG AGACTACAATGAGAGGCTCT ATGAGCACCATCTACAGT
ACE2.FAM.16	Vero E6, A549, CV-1	Forward Probe Reverse	GGGTCACAGTATGTTTCATC TATCTCTCGTTCATCTCCC GGAGGTGGATGGTCTTTA

*Probes labeled at the 5'-end with the reporter molecule 6-carboxyfluorescein (FAM), internally with the quencher ZEN, and at the 3'-end with Iowa Black FQ (Integrated DNA Technologies, <https://www.idtdna.com>).

cleavage site resulting in a sequence change from “PRRARS” to “PRRNIGERARS” in most ($\approx 70\%$) of the viral population. Although furin cleavage site mutations were reported to decrease entry and infection efficiency to various degrees in lung epithelial cells (7–9), because $\approx 30\%$ of the population in our working stock contains the intact furin cleavage site, we still used it in the qualitative assessment of SARS-CoV-2 entry of various cell lines.

Cells

We obtained MDCK-Atlanta, MDCK-London, and MDCK-SIAT1 cells from International Reagent Resources (<https://www.internationalreagentresource.org>) and MDCK-hCK cells from the University of Wisconsin–Madison (<https://www.wisc.edu>). We obtained MDCK-NBL2, Vero E6, CV-1, A549, Crandell-Rees Feline Kidney (CRFK) cells, Mv1Lu, RD, Hep-2c, HeLa, and L20B cells from American Type Culture Collection (<https://www.atcc.org>); these cells were maintained at Division of Scientific Resources, National Center for Emerging and Zoonotic Infectious Diseases, Centers for Disease Control and Prevention (Atlanta, GA, USA). We obtained chicken embryo fibroblasts from Charles River Laboratories (<https://www.criver.com>). We obtained an additional 25 cell lines (Table 1) from Quidel Corporation (<https://www.quidel.com>); these lines were preseeded in 24-well plates, except for CRFK and rhesus monkey kidney cells, which were obtained in T-75 flasks and seeded into 24-well plates in the laboratory 1 day before infection.

Virus Infection of Cell Lines

We seeded cells in 6-, 12-, or 24-well plates 1 day before infection or used them directly upon receipt from Quidel. Infection dose for each experiment is specified in the results section or figure legends. In general, inoculum was saved for back titration and the result is shown as 0 hours postinoculation (hpi) in some figures. We then washed cells at 1–2 hpi and collected supernatants or cell lysates daily for up to 3 days for infectious virus titration and up to 5 days hpi for viral RNA quantification. We observed cytopathic effect and fluorescence signals for icSARS-CoV-2-mNG daily.

Virus Infection of Embryonated Chicken Eggs

We obtained specific pathogen-free embryonated chicken eggs from Charles River Laboratories. We inoculated USA-WA1 into the allantoic cavity of twenty-four 8- to 12-day-old eggs at 10^5 median tissue culture infectious dose ($TCID_{50}$)/egg and incubated them at 37°C for 3 days. Allantoic fluid was collected from individual eggs separately as E1 samples. We passaged 100 μL of each E1 sample into a corresponding egg and collected 24 E2 samples after 3 days of incubation. We also generated 24 E3 samples from passage of E2 samples in 24 eggs. We titrated all E1, E2, and E3 samples, as well as samples from cell lines, with $TCID_{50}$ assay using VeroE6 cells; viral RNAs were quantified by real-time reverse transcription PCR (rRT-PCR) (10). We used synthetic RNA in the rRT-PCR assay to generate the standard curve for absolute quantification.

Immunoblot Detection and PCR Quantification of Angiotensin-Converting Enzyme 2

Cells were lysed in NP-40 lysis buffer and we determined protein concentrations using a Pierce BCA protein assay kit (<https://www.thermofisher.com>). We immunoblotted cell lysates and recombinant

angiotensin-converting enzyme (ACE) 2 protein control (Sino Biological; <https://www.sinobiological.com>) for ACE2 and β -actin using 1:500 polyclonal goat anti-human ACE2 AF933 (R&D Systems; <https://www.rndsystems.com>) and 1:1,000 monoclonal mouse anti- β -Actin AB8226 (Abcam;

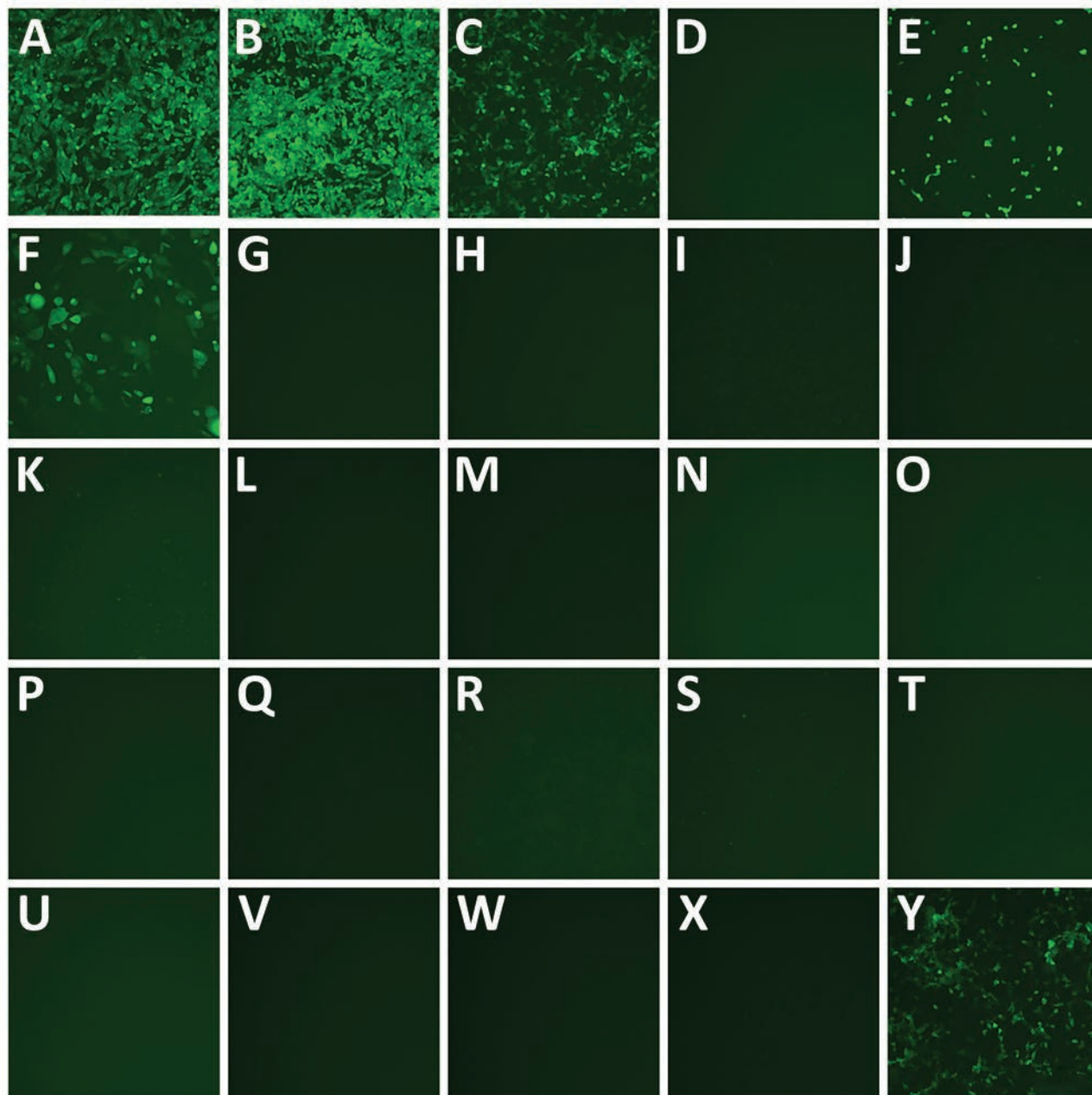


Figure 1. Select commercially sourced cell lines infected by severe acute respiratory syndrome coronavirus 2 (SARS-CoV-2) in study of susceptibility to SARS-CoV-2 of cell lines and substrates used to diagnose and isolate influenza and other viruses. A) Vero; B) Vero 76; C) BGMK; D) CV-1; E) LLC-MK2; F) RhMK; G) A549; H) HEL; I) HeLa; J) Hela 229; K) Hep-2; L) MRC-5; M) MRHF; N) NCI-H292; O) RD; P) WI-38; Q) McCoy; R) MNA; S) MDCK; T) CRFK; U) Mv1Lu; V) H&V-Mix; W) R-Mix; X) R-Mix Too; Y) Super E-Mix. Cell lines were inoculated with the SARS-CoV-2 reporter virus encoding mNeonGreen (icSARS-CoV-2-mNG) and infected cells (green fluorescence). Microscopy images (original magnification $\times 10$) captured 1 day postinfection, but similar results were observed through 5 days postinfection; all mNeonGreen-negative cell lines remained negative.

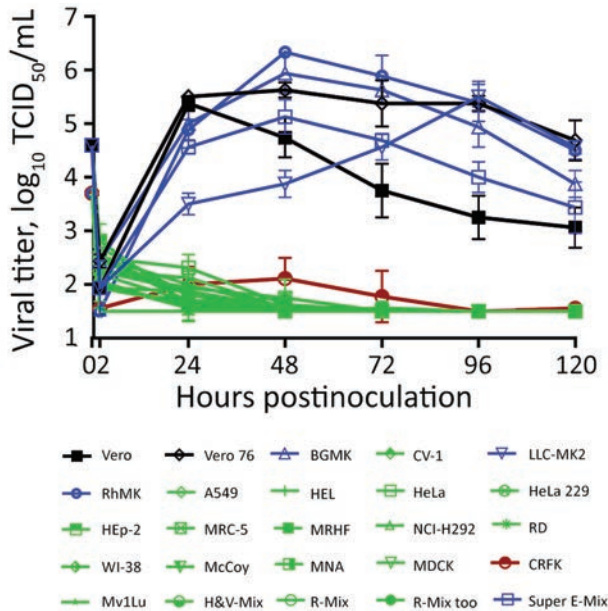


Figure 2. Varied severe acute respiratory syndrome coronavirus 2 (SARS-CoV-2) viral replication kinetics in commercially sourced cell lines in study of susceptibility to SARS-CoV-2 of cell lines and substrates used to diagnose and isolate influenza and other viruses. Data are mean of $n = 4 \pm$ SD. TCID₅₀, median tissue culture infectious dose.

<https://www.abcam.com>) primary antibodies followed by Abcam 1:4,000 donkey anti-goat and 1:4,000 goat anti-mouse secondary antibodies (Bio-rad; <https://www.bio-rad-antibodies.com> or KPL; <https://www.seracare.com>). We developed immunoblots using ThermoFisher SuperSignal West Pico PLUS chemiluminescent substrate. Qualitative RT-PCR (qRT-PCR) was used to determine the relative mRNA ACE2 levels in different cell lines. Two sets of primers and probes (Table 2) were used for each cell type targeting identical regions of ACE2 mRNA multiplexed with Applied Biosystems 4310893E eukaryotic 18S rRNA (<https://www.thermofisher.com>). We used the comparative cycle threshold ($\Delta\Delta$ Ct) method to quantify relative ACE2 gene expression. For each cell type and primer/probe set, we normalized ACE2 cycle threshold against 18S rRNA and then standardized to Vero E6.

Expression of Recombinant ACE2 Proteins and Biolayer Interferometry Assay

We used the ThermoFisher Expi293 Expression system to produce histidine-tagged ACE2 (ectodomain) proteins and purified them using HisTrap FF column (GE Life Sciences, <https://www.cytivalife-sciences.com>) as described elsewhere (11). We evaluated affinity between Sino Biologic 40591-V02H

SARS-CoV-2 S1 and human ACE2 or canine ACE2 using ForteBio anti-penta-His (HIS1K) biosensors (<https://www.sartorius.com>) on Octet RED96 at 30°C with a shaking speed at 1,000 RPM. We corrected the data by subtracting reference sample and used 1:2 bivalent binding model with global fit to determine affinity constants.

Exogenous Expression of ACE2 in MDCK Cells and ACE2 Sequence Alignment

We generated constructs coexpressing full-length human ACE2 (hACE2) or canine ACE2 (cACE2) with mCherry2 protein (CMV promoter-ACE2-IRES-mCherry2) and transfected them into MDCK-SIAT1 cells through electroporation with the Lonza Nucleofector system (<https://bioscience.lonza.com>) using the manufacturer's protocol with program A024. We transfected 1.5×10^6 MDCK-SIAT1 cells with 10 μ g DNA (pCMV-hACE2-IRES-mCherry2, pCMV-cACE2-IRES-mCherry2, or pCMV-IRES-mCherry2 empty control). One day posttransfection, we inoculated the cells with USA-WA1 or icSARS-CoV-2-mNG. We aligned ACE2 protein sequences for human (GenBank accession no. NP_001358344.1), African green monkey (accession no. AAY57872.1), rhesus macaque (accession no. ACI04564.1), mouse (accession no. NP_001123985.1), dog (accession no. XP_005641049.1), cat (accession no. NP_001034545.1), American mink (accession no. QPL12211), and chicken (accession no. XP_416822.2) using MUSCLE alignment in Geneious Prime software version 2019.2.3 (<https://www.geneious.com>).

Results

Replication of SARS-CoV-2 in a Large Set of Cell Substrates

We seeded the 25 cell lines from Quidel in 24-well plates and inoculated with 5×10^4 TCID₅₀/well of a fluorescent reporter virus in which the open reading frame 7a gene was replaced by the mNeonGreen gene (icSARS-CoV-2-mNG), allowing successful infection to be visualized by a green fluorescence signal (6). Almost all nonhuman primate cell lines were susceptible to icSARS-CoV-2-mNG infection except for CV-1 cells (Figure 1). In contrast, none of the tested human, mouse, mink, dog, or cat cell lines yielded fluorescent cells after infection. The Super-E Mix cells were likely susceptible because this cell culture is a mixture containing BGMK cells, which were found to be susceptible to SARS-CoV-2 (Figure 1). We then inoculated all these cell lines with 5×10^4 TCID₅₀/well

of the wild type SARS-CoV-2/USA-WA1/2020 (USA-WA1) strain and titrated supernatants collected over 5 days. Consistent with the results from icSARS-CoV-2-mNG infection, all nonhuman primate cell lines except CV-1 cells supported productive virus replication, whereas all other cell lines failed to generate infectious virus (Figure 2). It should be noted that viral titers in CRFK cells increased slightly at 2 days postinfection (dpi) (Figure 2), suggesting that this cell line may support a low level of replication.

Replication of SARS-CoV-2 in Influenza Virus Substrates

Laboratories use multiple lineages or derivatives of MDCK cells and embryonated chicken eggs to isolate and propagate different types or subtypes of influenza viruses. Some lineages, such as MDCK-SIAT1 and hCK cells, were genetically modified and cloned from

single cells, resulting in altered cell morphology and enhanced susceptibility to some subtypes of influenza viruses compared with susceptibility in their parental MDCK cell lines (12,13). The different lineages of MDCK cells have altered gene expression profiles and surface glycans and it is unclear whether that would affect their susceptibility to SARS-CoV-2. Therefore, we examined the susceptibility to SARS-CoV-2 in representative lineages of MDCK cells that are widely used in different laboratories, including MDCK-NBL-2, MDCK-Atlanta, MDCK-London, MDCK-SIAT1, and MDCK-hCK.

We inoculated Vero E6 cells as a positive control and various MDCK cell lines with 5×10^4 TCID₅₀/well of USA-WA1 and incubated for 1–2 hours at 37°C. We then washed cells to remove the inoculum and influenza virus infection media containing TPCK-trypsin and added bovine serum albumin to mimic the conditions used to isolate influenza

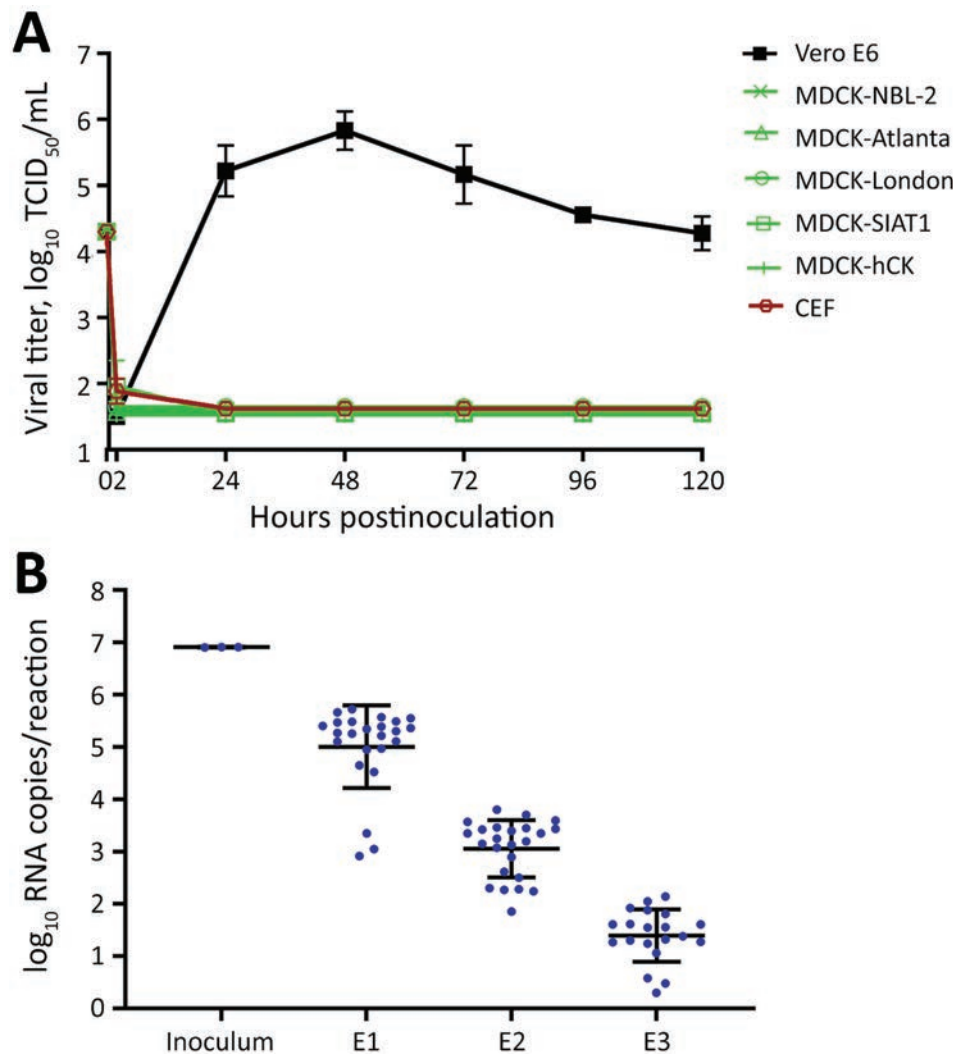


Figure 3. Influenza virus substrates not infected by severe acute respiratory syndrome coronavirus 2 (SARS-CoV-2) in study of susceptibility to SARS-CoV-2 of cell lines and substrates used to diagnose and isolate influenza and other viruses. A) Vero E6, MDCK-NBL-2, MDCK-Atlanta, MDCK-London, MDCK-SIAT1, MDCK-hCK, and chicken embryo fibroblast cells inoculated with USA-WA1 at 5×10^4 TCID₅₀/well in 12-well plates (MOI 0.1 to ≈ 0.3 , depending on cell line). B) USA-WA1 total viral RNA levels in allantoic fluid from infected eggs quantified by real-time reverse transcription PCR using a standard curve generated by synthetic RNA. Four eggs with undetectable RNA not plotted for E3. Data are mean of $n = 3 \pm SD$ (cells) or $n = 24 \pm SD$ (eggs). TCID₅₀, median tissue culture infectious dose.

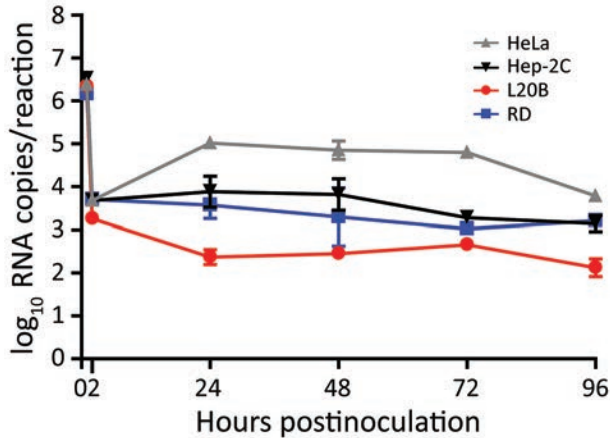


Figure 4. Poliovirus and enterovirus substrates not infected by severe acute respiratory syndrome coronavirus 2 (SARS-CoV-2) in study of susceptibility to SARS-CoV-2 of cell lines and substrates used to diagnose and isolate influenza and other viruses. Total viral RNA levels determined by real-time reverse transcription PCR (standard curve generated by synthetic RNA) from RNA extracted from cell lines inoculated with USA-WA1 at MOI 0.1 in 6-well plates. Data points at 1 h represented by RNA from the inoculum; ≥ 2 h time points from RNA extracted from cell lysates. Data are mean of $n = 3 \pm \text{SD}$.

viruses. We collected supernatants at the indicated times postinfection and measured viral titers. Vero E6 cells supported robust viral replication and reached peak titer in ≤ 2 days (Figure 3, panel A), and infection killed most cells (data not shown). In contrast, none of the 5 MDCK cell lines tested supported SARS-CoV-2 replication. Although residual infectious virus was present in some MDCK supernatant samples at 2 hpi, it was below the limit of detection at 1 dpi and did not cause any cytopathic effect through 5 dpi. We conducted similar

experiments with the MDCK cell lines in which the infection media contained fetal bovine serum rather than bovine serum albumin and again SARS-CoV-2 failed to replicate in any of the 5 MDCK cell lines (data not shown but almost identical to Figure 3, panel A).

Embryonated chicken eggs are another common substrate for isolating, propagating, and producing vaccines for influenza viruses. We inoculated 24 eggs each with 10^5 TCID₅₀ of USA-WA1 and blindly passaged the virus in eggs for 3 passages (E1, E2, and E3). Viral titers in the allantoic fluid of E1, E2, and E3 eggs were below the limit of detection ($10^{1.5}$ TCID₅₀/mL) even in E1 eggs (data not shown). We then used an rRT-PCR assay to quantify the viral RNA levels in the inoculum and allantoic fluid samples (10). Viral RNA decreased steadily over the 3 passages in eggs (Figure 3, panel B). We also inoculated chicken embryo fibroblasts with USA-WA1; no infectious virus was produced from the cells (Figure 3, panel A). These results clearly demonstrate that embryonated chicken eggs are not a susceptible substrate for SARS-CoV-2 replication. Collectively, the data show that substrates commonly used to culture influenza A and B viruses are not susceptible to SARS-CoV-2 infection.

Replication of SARS-CoV-2 in Polio and Enterovirus Substrates

Stool specimens from patients potentially infected with polio or enteroviruses are used to inoculate appropriate cell lines for surveillance. Because SARS-CoV-2 virus can infect multiple organs and tissues and its presence in stool specimens has been reported (14–20), it is important to determine if

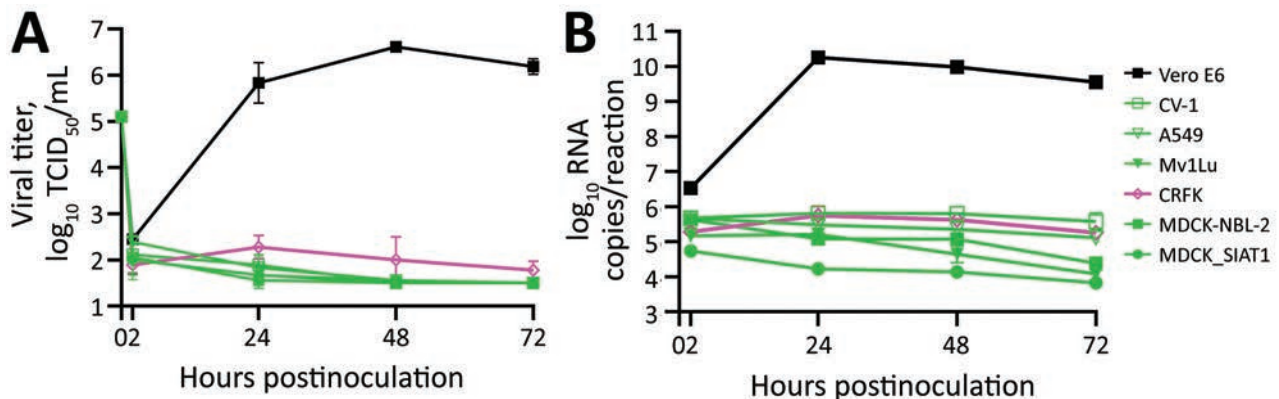


Figure 5. Infection of severe acute respiratory syndrome coronavirus 2 (SARS-CoV-2) with spike G614 in study of susceptibility to SARS-CoV-2 of cell lines and substrates used to diagnose and isolate influenza and other viruses. Vero E6, CV-1, A549, Mv1Lu, CRFK, MDCK-NBL-2, and MDCK-SIAT1 cell lines inoculated with MA/VPT1 at 5×10^5 TCID₅₀/well in 12-well plates (MOI 1 to ≈ 5 depending on cell line). A) Supernatants collected at indicated times and used to determine viral replication kinetics by TCID₅₀. B) Total viral RNA levels extracted from cells inoculated for the indicated times as determined by real-time reverse transcription PCR. Data are mean of $n = 3 \pm \text{SD}$. TCID₅₀, median tissue culture infectious dose.

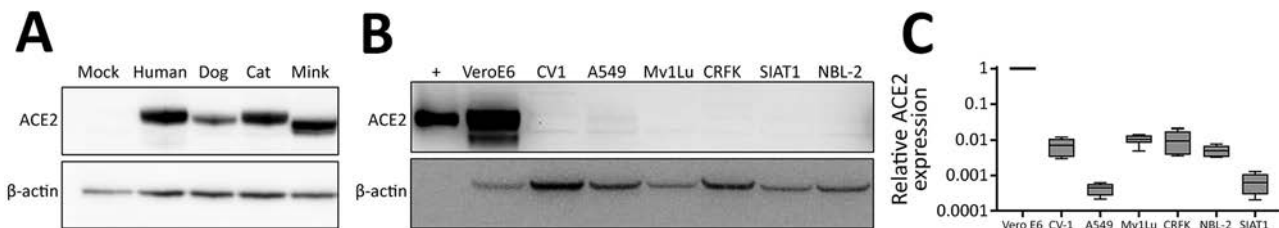


Figure 6. ACE2 differentially expressed across cell lines in study of susceptibility to severe acute respiratory syndrome coronavirus 2 of cell lines and substrates used to diagnose and isolate influenza and other viruses. A) Mock transfected 293T cells or 293T cells transfected with plasmids expressing human, dog, cat, or mink ACE2 immunoblotted for ACE2 protein expression. B) Whole-cell lysate from uninoculated Vero E6, CV-1, A549, Mv1Lu, CRFK, MDCK-NBL-2, and MDCK-SIAT1 cell lines immunoblotted for endogenous ACE2 expression. Recombinant human ACE2 used as a positive control for detecting human ACE2. C) Relative ACE2 expression determined by real-time quantitative PCR. Data are mean of $n = 6 \pm SD$. Boxes are 1 SD away from the mean, and whiskers indicate the minimum and maximum. ACE, angiotensin-converting enzyme 2.

cell lines commonly used for polio and enterovirus culture could inadvertently propagate SARS-CoV-2. Therefore, we inoculated RD, HeLa, Hep-2C, and L20B cells with USA-WA1 at a multiplicity of infection (MOI) of 0.1 and incubated for 2 hours after which we removed the inoculum and washed the cells 3 times to remove residual virus. We observed no cytopathic effect over a 4-day period and SARS-CoV-2 was not detectable in supernatant collected at 1–4 dpi (data not shown). This result was confirmed by rRT-PCR of cell lysate, which revealed that the total viral RNA levels decreased relative to the inoculum, indicating that virus did not efficiently initiate RNA transcription or replication (Figure 4). These results indicate that cell substrates

regularly used for polio and enterovirus cultures are not susceptible to SARS-CoV-2 infection when cultured under standard conditions.

Replication of SARS-CoV-2 with Spike D614G Substitution

During this study, we noticed that the proportion of naturally circulating virus containing a D614G substitution in the spike protein was rapidly increasing. The USA-WA1 strain is an early isolate that expresses spike with D614. To confirm that the cell susceptibility data obtained using this virus were valid with recent strains, a subset of representative cell lines were inoculated with a high titer (5×10^5 TCID₅₀/well) of SARS-CoV-2/Massachusetts/

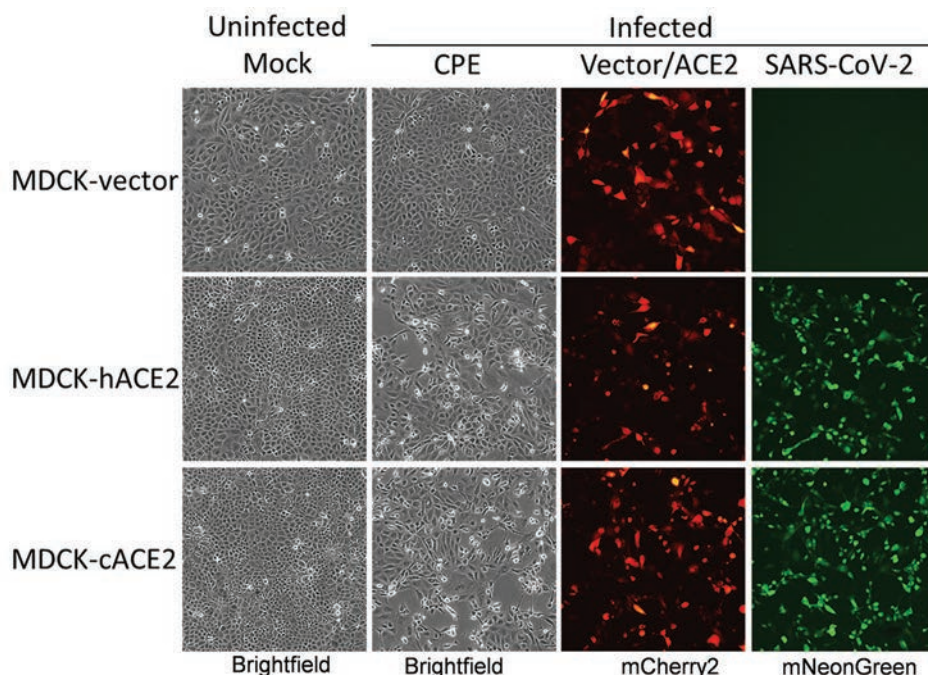


Figure 7. Overexpression of canine ACE2 in MDCK cells in study of susceptibility to severe acute respiratory syndrome coronavirus 2 of cell lines and substrates used to diagnose and isolate influenza and other viruses. Cells inoculated with icSARS-CoV-2-mNG reporter virus. Representative images at 1 dpi are shown (original magnification $\times 10$). ACE, angiotensin-converting enzyme 2.

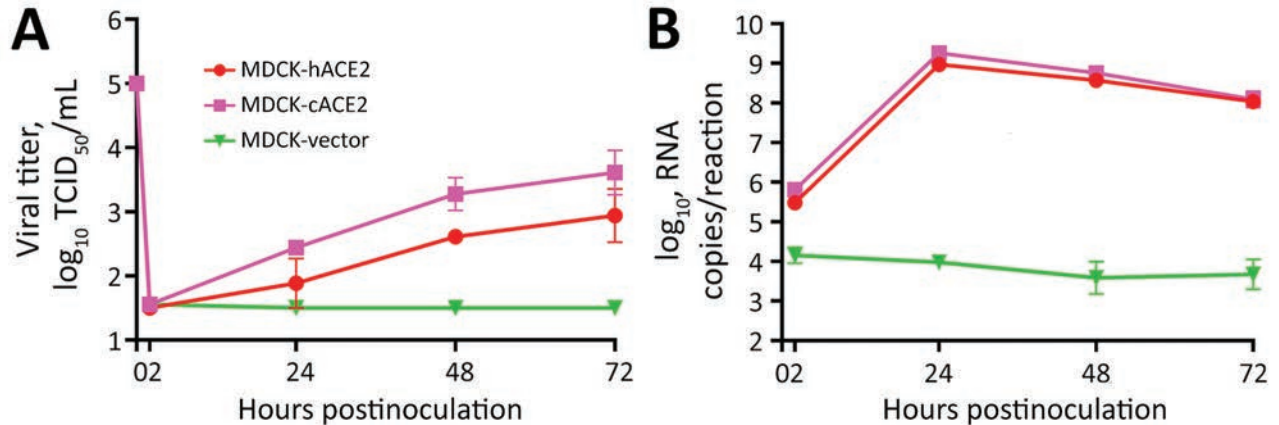


Figure 8. MDCK-vector, MDCK-hACE2, and MDCK-cACE2 cells inoculated with USA-WA1 at 5×10^5 TCID₅₀/well in 12-well plates in study of susceptibility to severe acute respiratory syndrome coronavirus 2 of cell lines and substrates used to diagnose and isolate influenza and other viruses. Supernatants collected at the indicated times. A) Viral titers determined by TCID₅₀ assay; B) total viral RNA determined using real-time reverse transcription PCR (standard curve generated by synthetic RNA). Data for both panels are mean of $n = 3 \pm$ SD. ACE, angiotensin-converting enzyme 2; cACE2, canine ACE2; hACE2, human ACE2; TCID₅₀, median tissue culture infectious dose.

VPT1/2020 (MA/VPT1), which encodes a spike with G614. In selecting cell lines for the subset, we included Vero E6 cells as a cell line that should support replication of MA/VPT1 given our previous findings with USA-WA1 (Figure 3, panel A). Indeed, Vero E6 cells supported similar replication kinetics for MA/VPT1 and USA-WA1 (Figure 5, panel A). Even with a 10-fold higher inoculum of MA/VPT1 than previously used for USA-WA1 tests (5×10^4 TCID₅₀/well), CV-1, A549, Mv1Lu, MDCK-NBL-2, and MDCK-SIAT1, cell lines were not susceptible to this SARS-CoV-2 strain encoding spike G614. CRFK cells inoculated with MA/VPT1 generated virus titers slightly above the limit of detection at 1 dpi, after which titers decreased

(Figure 5, panel A). We further confirmed viral titers by rRT-PCR. Consistent with the virus titer data, inoculated CRFK cells had a 5-fold increase of viral RNA at 1 dpi compared to 2 hpi, but the RNA levels decreased over the next 2 days. In contrast, CV-1, A549, Mv1Lu, MDCK-NBL-2, and MDCK-SIAT1 cells did not show any noticeable increase of viral RNA levels during the time course of this study (Figure 5, panel B). All 7 cell lines in this subset demonstrated very similar viral replication kinetics for both MA/VPT1 and USA-WA1 virus strains (Figures 2–5), indicating that the currently dominant virus strains with spike G614 likely have the same cell susceptibility profile as earlier strains encoding spike D614.

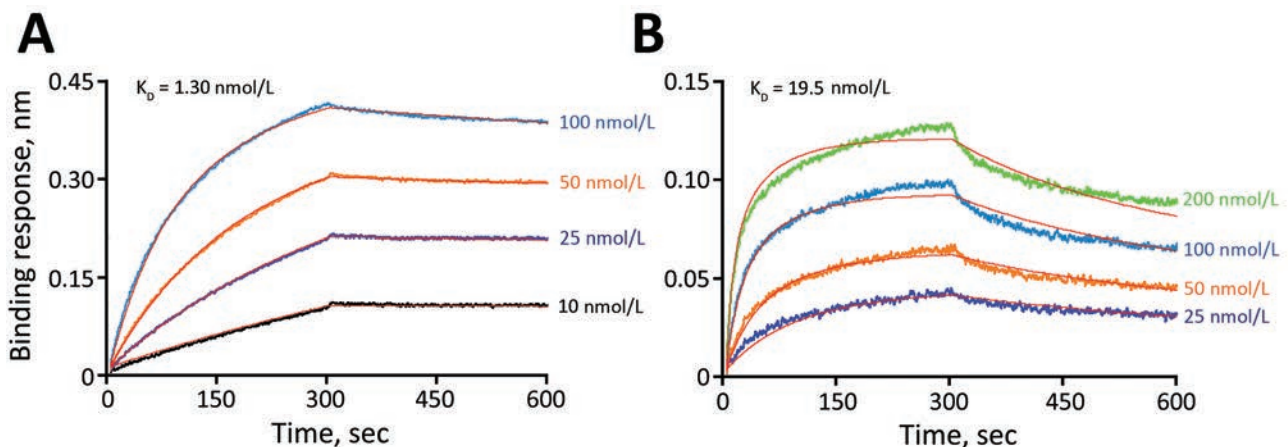


Figure 9. Canine ACE2 affinity to severe acute respiratory syndrome coronavirus 2 (SARS-CoV-2) spike protein compared with that for human ACE2 in study of susceptibility to SARS-CoV-2 of cell lines and substrates used to diagnose and isolate influenza and other viruses. Bioluminescence resonance energy transfer assay used to determine K_d, the equilibrium dissociation constant of human (A) or canine (B) ACE2 protein with SARS-CoV-2 spike protein.

Amino acid residue	24	27	28	30	31	34	35	37	38	41	42	79	82	83	350	353	354	355	357	393	Protein length, aa	% Identity to hACE2
Human	Q	T	F	D	K	H	E	E	D	Y	Q	L	M	Y	N	K	G	D	R	R	805	–
Rhesus macaque	Q	T	F	D	K	H	E	E	D	Y	Q	L	M	Y	N	K	G	D	R	R	805	95.2
African green monkey	Q	T	F	D	K	H	E	E	D	Y	Q	L	M	Y	N	K	G	D	R	R	805	94.5
Cat	L	T	F	E	K	H	E	E	E	Y	Q	L	T	Y	N	K	G	D	R	R	805	85.2
Dog	L	T	F	E	K	Y	E	E	E	Y	Q	L	T	Y	N	K	G	D	R	R	804	84.1
American mink	L	T	F	E	K	Y	E	E	E	Y	Q	H	T	Y	N	K	H	D	R	R	805	83.0
Mouse	N	T	F	N	N	Q	E	E	D	Y	Q	T	S	F	N	H	G	D	R	R	805	82.1
Chicken	–	T	F	A	E	V	R	E	D	Y	E	N	R	F	N	K	N	D	R	R	808	65.6

Figure 10. Aligned ACE2 protein sequences from human, rhesus macaque, African green monkey, cat, dog, American mink, mouse, and chicken cells in study of susceptibility to severe acute respiratory syndrome coronavirus 2 (SARS-CoV-2) of cell lines and substrates used to diagnose and isolate influenza and other viruses. Residues involved in interaction with SARS-CoV-2 spike protein (41–44) shown using hACE2 numbering; yellow indicates residues varying from hACE2. Dash indicates gap in alignment. Percentage identity to hACE2 across the entire protein is shown. ACE, angiotensin-converting enzyme 2; cACE2, canine ACE2; hACE2, human ACE2.

ACE2 as a Critical Determinant in Susceptibility and Species Specificity

Coronavirus spike-host receptor interactions play the major role in species specificity (21). SARS-CoV-2 uses hACE2 as the host cell receptor (22). Multiple species, including humans, monkeys, cats, minks, ferrets, hamsters, and dogs, have been infected by SARS-CoV-2 in experimental and natural settings (23–28). To further investigate the mechanism of susceptibility or resistance and gain insight into SARS-CoV-2 species specificity, we analyzed the ACE2 expression levels in various cell lines. Multiple ACE2 antibodies were screened to identify a polyclonal antibody that reacts with transiently overexpressed ACE2 in humans, dogs, cats, and minks (Figure 6, panel A). Using this antibody, we determined by immunoblot that endogenous ACE2 levels were very high in Vero E6 cells derived from African green monkey kidneys but extremely low in the other African green monkey kidney cell line, CV-1, which could explain the drastic difference in infectivity between these 2 cell lines (Figure 6, panel B). Canine ACE2 protein was not detectable in MDCK cells, which surely plays a role in their resistance to SARS-CoV-2 infection. Similarly, feline CRFK, mink Mv1Lu, and human A549 cells had very low or undetectable endogenous ACE2 expression (Figure 6, panel B). The low protein levels of ACE2 in those cells coincided with low mRNA levels determined by rRT-PCR (Figure 6, panel C).

Since MDCK cells are the most important cell line for isolating and propagating influenza viruses and dogs have been infected with SARS-CoV-2, we selected cACE2 for additional analysis. To better

understand resistance of MDCK cells to SARS-CoV-2, we transfected constructs coexpressing hACE2 or cACE2 proteins under a cytomegalovirus promoter and mCherry2 protein through an IRES element into MDCK-SIAT1 cells. MDCK cells expressing hACE2 (MDCK-hACE2) or cACE2 (MDCK-cACE2) as determined by mCherry2 expression were efficiently infected by icSARS-CoV-2-mNG (Figure 7). We also transfected MDCK cells with an empty vector plasmid that expresses mCherry2 via the IRES element but does not encode an ACE2 protein (MDCK-vector) as a control. Like wild-type MDCK cells, the MDCK-vector control cells were not susceptible to SARS-CoV-2 (Figure 7). We further confirmed these results by infecting MDCK-hACE2 and MDCK-cACE2 cells with the wild-type virus USA-WA1 and assaying viral replication kinetics. Viral infectious titers and viral RNA levels were elevated in MDCK cells overexpressing either hACE2 or cACE2 relative to MDCK-vector cells (Figure 8, panels A, B).

These results indicate that MDCK cell resistance to SARS-CoV-2 occurs at the virus entry step. Once bound, the genome is released, transcribed, translated, replicated, and packaged into particles that efficiently bud from infected cells. However, overexpression of ACE2 in MDCK cells could result in greater ACE2 expression than in most natural cell lines. Therefore, even if cACE2 does not bind the spike protein as efficiently as hACE2, overexpression could facilitate entry of SARS-CoV-2 into MDCK-cACE2 cells. To determine if cACE2-binding affinity to SARS-CoV-2 spike was an additional factor preventing infection of MDCK cells, we conducted biolayer interferometry assays to compare the binding affinity

of spike with cACE2 and hACE2. We identified that the SARS-CoV-2 spike bound to cACE2 (equilibrium dissociation constant $[K_D] = 19.5 \text{ nmol/L}$) 15-fold less efficiently than to hACE2 ($K_D = 1.30 \text{ nmol/L}$) (Figure 9). The reduced binding affinity to cACE2 is likely a result of the sequence differences between the hACE and cACE2 in regions directly involved in spike binding (Figure 10). Therefore, both low expression of cACE2 by MDCK cells and low binding affinity of cACE2 to SARS-CoV-2 spike contribute to the resistance of MDCK cells to SARS-CoV-2.

Discussion

In this study, we determined the SARS-CoV-2 susceptibility of >30 cell lines and derivatives and embryonated chicken eggs. Findings from our study corroborate and complement those from other susceptibility studies published in recent months (29,30), including that MDCK cells and embryonated eggs do not support productive SARS-CoV-2 infection (30). In addition, our infectious virus titration assay data further showed that SARS-CoV-2 loses infectivity rapidly in cells and eggs, whereas the viral RNA levels decreased slowly. In addition, most circulating strains contain the D614G substitution in the spike protein, which could affect binding, entry, and species specificity; viruses with this change were not tested in previous studies. Herein, we showed that the spike D614G substitution does not alter susceptibility of the cell lines tested including those with low levels of human (A549), nonhuman primate (CV-1), mink (Mv1Lu), cat (CRFK), or dog (MDCK) ACE2. In the future, even in the unlikely event that other spike substitutions render the binding of spike to cACE2 stronger (Figure 9), the low expression level of cACE2 in MDCK cells (Figure 6) still poses a high barrier for SARS-CoV-2 to overcome. Therefore, 2 independent studies together illustrate that MDCK cells and commonly used derivatives are not susceptible to SARS-CoV-2 and can be safely used for isolating and propagating influenza viruses and producing vaccines. In addition, chicken eggs, which are used to manufacture most influenza virus vaccines, do not support replication of SARS-CoV-2.

We expanded our examination to other clinically relevant cell lines used in diagnosis and isolation of a wide array of human viruses, particularly respiratory viruses (Table 1). Although many of those cells were tested with SARS-CoV-1 virus previously (29,31–40), it is worth noting that cell susceptibility conclusions derived from SARS-CoV-1 studies do not always apply to SARS-CoV-2. For example, we and others previously showed that Mv1Lu cells supported a moderate

level of SARS-CoV-1 virus replication (35,38), but they are not susceptible to SARS-CoV-2 replication, as demonstrated in this study. This finding could be justified by the difference in ACE2 binding positions between SARS-CoV-1 and SARS-CoV-2 (41–44). Considering that mink ACE2 is only 83% identical to human ACE2 (Figure 10), some of the different ACE2 residues may have more adverse effect on SARS-CoV-2 entry than on SARS-CoV-1 entry. This idea does not necessarily contradict recent reports of SARS-CoV-2 infections among minks on farms (24,45–48); ACE2 expression is relatively low in Mv1Lu cells (Figure 6) but likely higher in various epithelial cells in vivo, enabling productive infection in minks in spite of a weaker spike-receptor interaction.

Overall, our study provides useful information on multiple cell lines and chicken eggs regarding their susceptibility to SARS-CoV-2. Of note, from a biosafety standpoint, humans can be co-infected with multiple pathogens. Specimens collected for testing and culture of other viruses may contain SARS-CoV-2; these data should help laboratories avoid inadvertent propagation. The data on canine ACE2 shed light on the relationship between SARS-CoV-2 susceptibility and ACE2 receptor affinity (species specificity) and expression level, suggesting that even ACE2 proteins with several substitutions at key residues that contact SARS-CoV-2 spike protein can still serve as functional receptors when expressed at high levels.

Acknowledgements

We thank the US Centers for Disease Control and Prevention COVID-19 Response Laboratory and Testing Task Force for their support and guidance and the Division of Scientific Resources for providing some cell lines and other materials. We also thank Yoshihiro Kawaoka of University of Wisconsin-Madison for providing MDCK-hCK cells.

About the Author

Dr. Wang is a biologist in the Influenza Division, National Center for Immunization and Respiratory Diseases, Centers for Disease Control and Prevention, whose main responsibility is to develop candidate vaccine viruses for influenza viruses with pandemic potential. She has been deployed to the CDC COVID-19 response and leads the efforts on assessment of cell lines and substrates for their susceptibility to SARS-CoV-2.

References

1. Kim D, Quinn J, Pinsky B, Shah NH, Brown I. Rates of co-infection between SARS-CoV-2 and other respiratory pathogens. *JAMA*. 2020;323:2085–6. <https://doi.org/10.1001/jama.2020.6266>

2. Li Z, Chen ZM, Chen LD, Zhan YQ, Li SQ, Cheng J, et al. Coinfection with SARS-CoV-2 and other respiratory pathogens in patients with COVID-19 in Guangzhou, China. *J Med Virol*. 2020;92:2381–3. <https://doi.org/10.1002/jmv.26073>
3. Konala VM, Adapa S, Naramala S, Chenna A, Lamichhane S, Garlapati PR, et al. A case series of patients coinfecting with influenza and COVID-19. *J Investig Med High Impact Case Rep*. 2020;8:2324709620934674. <https://doi.org/10.1177/2324709620934674>
4. Yue H, Zhang M, Xing L, Wang K, Rao X, Liu H, et al. The epidemiology and clinical characteristics of co-infection of SARS-CoV-2 and influenza viruses in patients during COVID-19 outbreak. *J Med Virol*. 2020;92:2870–3. <https://doi.org/10.1002/jmv.26163>
5. Harcourt J, Tamin A, Lu X, Kamili S, Sakthivel SK, Murray J, et al. severe acute respiratory syndrome coronavirus 2 from patient with coronavirus disease, United States. *Emerg Infect Dis*. 2020;26:1266–73. <https://doi.org/10.3201/eid2606.200516>
6. Xie X, Muruato A, Lokugamage KG, Narayanan K, Zhang X, Zou J, et al. An infectious cDNA clone of SARS-CoV-2. *Cell Host Microbe*. 2020;27:841–848.e3. <https://doi.org/10.1016/j.chom.2020.04.004>
7. Hoffmann M, Kleine-Weber H, Pöhlmann S. A multibasic cleavage site in the spike protein of SARS-CoV-2 is essential for infection of human lung cells. *Mol Cell*. 2020;78:779–784.e5. <https://doi.org/10.1016/j.molcel.2020.04.022>
8. Chu H, Hu B, Huang X, Chai Y, Zhou D, Wang Y, et al. Host and viral determinants for efficient SARS-CoV-2 infection of the human lung. *Nat Commun*. 2021;12:134. <https://doi.org/10.1038/s41467-020-20457-w>
9. Johnson BA, Xie X, Bailey AL, Kalveram B, Lokugamage KG, Muruato A, et al. Loss of furin cleavage site attenuates SARS-CoV-2 pathogenesis. *Nature*. 2021;591:293–9. <https://doi.org/10.1038/s41586-021-03237-4>
10. Lu X, Wang L, Sakthivel SK, Whitaker B, Murray J, Kamili S, et al. US CDC Real-time reverse transcription PCR panel for detection of severe acute respiratory syndrome coronavirus 2. *Emerg Infect Dis*. 2020;26:1654–65. <https://doi.org/10.3201/eid2608.201246>
11. Zhou B, Thao TTN, Hoffmann D, Taddeo A, Ebert N, Labrousseau F, et al. SARS-CoV-2 spike D614G variant confers enhanced replication and transmissibility. *Nature*. 2021 Feb 26 [Epub ahead of print]. <https://doi.org/10.1038/s41586-021-03361-1>
12. Matrosovich M, Matrosovich T, Carr J, Roberts NA, Klenk HD. Overexpression of the alpha-2,6-sialyltransferase in MDCK cells increases influenza virus sensitivity to neuraminidase inhibitors. *J Virol*. 2003;77:8418–25. <https://doi.org/10.1128/JVI.77.15.8418-8425.2003>
13. Takada K, Kawakami C, Fan S, Chiba S, Zhong G, Gu C, et al. A humanized MDCK cell line for the efficient isolation and propagation of human influenza viruses. *Nat Microbiol*. 2019;4:1268–73. <https://doi.org/10.1038/s41564-019-0433-6>
14. Wang W, Xu Y, Gao R, Lu R, Han K, Wu G, et al. Detection of SARS-CoV-2 in different types of clinical specimens. *JAMA*. 2020;323:1843–4. <https://doi.org/10.1001/jama.2020.3786>
15. Cheung KS, Hung IFN, Chan PPY, Lung KC, Tso E, Liu R, et al. Gastrointestinal manifestations of SARS-CoV-2 infection and virus load in fecal samples from a Hong Kong cohort: systematic review and meta-analysis. *Gastroenterology*. 2020;159:81–95. <https://doi.org/10.1053/j.gastro.2020.03.065>
16. Young BE, Ong SWX, Kalimuddin S, Low JG, Tan SY, Loh J, et al.; Singapore 2019 Novel Coronavirus Outbreak Research Team. Singapore 2019 novel coronavirus outbreak research team. epidemiologic features and clinical course of patients infected with SARS-CoV-2 in Singapore. *JAMA*. 2020;323:1488–94. <https://doi.org/10.1001/jama.2020.3204>
17. Xu Y, Li X, Zhu B, Liang H, Fang C, Gong Y, et al. Characteristics of pediatric SARS-CoV-2 infection and potential evidence for persistent fecal viral shedding. *Nat Med*. 2020;26:502–5. <https://doi.org/10.1038/s41591-020-0817-4>
18. Zheng S, Fan J, Yu F, Feng B, Lou B, Zou Q, et al. Viral load dynamics and disease severity in patients infected with SARS-CoV-2 in Zhejiang province, China, January–March 2020: retrospective cohort study. *BMJ*. 2020;369:m1443. <https://doi.org/10.1136/bmj.m1443>
19. Tang A, Tong ZD, Wang HL, Dai YX, Li KF, Liu JN, et al. Detection of novel coronavirus by RT-PCR in stool specimen from asymptomatic child, China. *Emerg Infect Dis*. 2020;26:1337–9. <https://doi.org/10.3201/eid2606.200301>
20. COVID-19 Investigation Team. Clinical and virologic characteristics of the first 12 patients with coronavirus disease 2019 (COVID-19) in the United States. *Nat Med*. 2020;26:861–8. <https://doi.org/10.1038/s41591-020-0877-5>
21. Wentworth DE, Holmes KV. Coronavirus binding and entry. Thiel V, editor. *Coronaviruses: molecular and cellular biology*. Norfolk (UK): Caister Academic Press; 2007. p. 3–31
22. Zhang H, Penninger JM, Li Y, Zhong N, Slutsky AS. Angiotensin-converting enzyme 2 (ACE2) as a SARS-CoV-2 receptor: molecular mechanisms and potential therapeutic target. *Intensive Care Med*. 2020;46:586–90. <https://doi.org/10.1007/s00134-020-05985-9>
23. Abdel-Moneim AS, Abdelwhab EM. Evidence for SARS-CoV-2 infection of animal hosts. *Pathogens*. 2020; 9:E529. <https://doi.org/10.3390/pathogens9070529>
24. Oreshkova N, Molenaar RJ, Vreman S, Harders F, Oude Munnink BB, Hakze-van der Honing RW, et al. SARS-CoV-2 infection in farmed minks, the Netherlands, April and May 2020. *Euro Surveill*. 2020;25:2001005.
25. Munster VJ, Feldmann F, Williamson BN, van Doremalen N, Pérez-Pérez L, Schulz J, et al. Respiratory disease in rhesus macaques inoculated with SARS-CoV-2. *Nature*. 2020;585:268–72. <https://doi.org/10.1038/s41586-020-2324-7>
26. Bosco-Lauth AM, Hartwig AE, Porter SM, Gordy PW, Nehring M, Byas AD, et al. Experimental infection of domestic dogs and cats with SARS-CoV-2: Pathogenesis, transmission, and response to reexposure in cats. *Proc Natl Acad Sci U S A*. 2020;117:26382–8. <https://doi.org/10.1073/pnas.2013102117>
27. Halfmann PJ, Hatta M, Chiba S, Maemura T, Fan S, Takeda M, et al. Transmission of SARS-CoV-2 in domestic cats. *N Engl J Med*. 2020;383:592–4. <https://doi.org/10.1056/NEJMc2013400>
28. Singla R, Mishra A, Joshi R, Jha S, Sharma AR, Upadhyay S, et al. Human animal interface of SARS-CoV-2 (COVID-19) transmission: a critical appraisal of scientific evidence. *Vet Res Commun*. 2020;44:119–30. <https://doi.org/10.1007/s11259-020-09781-0>
29. Chu H, Chan JF, Yuen TT, Shuai H, Yuan S, Wang Y, et al. Comparative tropism, replication kinetics, and cell damage profiling of SARS-CoV-2 and SARS-CoV with implications for clinical manifestations, transmissibility, and laboratory studies of COVID-19: an observational study. *Lancet Microbe*. 2020;1:e14–23. [https://doi.org/10.1016/S2666-5247\(20\)30004-5](https://doi.org/10.1016/S2666-5247(20)30004-5)
30. Barr IG, Rynehart C, Whitney P, Druce J. SARS-CoV-2 does not replicate in embryonated hen's eggs or in

- MDCK cell lines. *Euro Surveill.* 2020;25:2001122. 10.2807/1560-https://doi.org/10.2807/1560-7917.ES.2020.25.25.2001122
31. Hattermann K, Müller MA, Nitsche A, Wendt S, Donoso Mantke O, Niedrig M. Susceptibility of different eukaryotic cell lines to SARS-coronavirus. *Arch Virol.* 2005;150:1023–31. https://doi.org/10.1007/s00705-004-0461-1
 32. Kaye M, Druce J, Tran T, KostECKi R, Chibo D, Morris J, et al. SARS-associated coronavirus replication in cell lines. *Emerg Infect Dis.* 2006;12:128–33. https://doi.org/10.3201/eid1201.050496
 33. Yamashita M, Yamate M, Li GM, Ikuta K. Susceptibility of human and rat neural cell lines to infection by SARS-coronavirus. *Biochem Biophys Res Commun.* 2005;334:79–85. https://doi.org/10.1016/j.bbrc.2005.06.061
 34. Drosten C, Günther S, Preiser W, van der Werf S, Brodt HR, Becker S, et al. Identification of a novel coronavirus in patients with severe acute respiratory syndrome. *N Engl J Med.* 2003;348:1967–76. https://doi.org/10.1056/NEJMoa030747
 35. Gillim-Ross L, Taylor J, Scholl DR, Ridenour J, Masters PS, Wentworth DE. Discovery of novel human and animal cells infected by the severe acute respiratory syndrome coronavirus by replication-specific multiplex reverse transcription-PCR. *J Clin Microbiol.* 2004;42:3196–206. https://doi.org/10.1128/JCM.42.7.3196-3206.2004
 36. Hattermann K, Müller MA, Nitsche A, Wendt S, Donoso Mantke O, Niedrig M. Susceptibility of different eukaryotic cell lines to SARS-coronavirus. *Arch Virol.* 2005;150:1023–31. https://doi.org/10.1007/s00705-004-0461-1
 37. Ksiazek TG, Erdman D, Goldsmith CS, Zaki SR, Peret T, Emery S, et al.; SARS Working Group. A novel coronavirus associated with severe acute respiratory syndrome. *N Engl J Med.* 2003;348:1953–66. https://doi.org/10.1056/NEJMoa030781
 38. Mossel EC, Huang C, Narayanan K, Makino S, Tesh RB, Peters CJ. Exogenous ACE2 expression allows refractory cell lines to support severe acute respiratory syndrome coronavirus replication. *J Virol.* 2005;79:3846–50. https://doi.org/10.1128/JVI.79.6.3846-3850.2005
 39. Severson WE, Shindo N, Sosa M, Fletcher T III, White EL, Ananthan S, et al. Development and validation of a high-throughput screen for inhibitors of SARS CoV and its application in screening of a 100,000-compound library. *J Biomol Screen.* 2007;12:33–40. https://doi.org/10.1177/1087057106296688
 40. Yen YT, Liao F, Hsiao CH, Kao CL, Chen YC, Wu-Hsieh BA. Modeling the early events of severe acute respiratory syndrome coronavirus infection in vitro. *J Virol.* 2006;80:2684–93. https://doi.org/10.1128/JVI.80.6.2684-2693.2006
 41. Yan R, Zhang Y, Li Y, Xia L, Guo Y, Zhou Q. Structural basis for the recognition of SARS-CoV-2 by full-length human ACE2. *Science.* 2020;367:1444–8. https://doi.org/10.1126/science.abb2762
 42. Wang Q, Zhang Y, Wu L, Niu S, Song C, Zhang Z, et al. Structural and functional basis of SARS-CoV-2 entry by using human ACE2. *Cell.* 2020;181:894–904.e9. https://doi.org/10.1016/j.cell.2020.03.045
 43. Lan J, Ge J, Yu J, Shan S, Zhou H, Fan S, et al. Structure of the SARS-CoV-2 spike receptor-binding domain bound to the ACE2 receptor. *Nature.* 2020;581:215–20. https://doi.org/10.1038/s41586-020-2180-5
 44. Shang J, Ye G, Shi K, Wan Y, Luo C, Aihara H, et al. Structural basis of receptor recognition by SARS-CoV-2. *Nature.* 2020;581:221–4. 10.1038/s41586-020-2179-y https://doi.org/10.1038/s41586-020-2179-y
 45. Enserink M. Coronavirus rips through Dutch mink farms, triggering culls. *Science.* 2020;368:1169. https://doi.org/10.1126/science.368.6496.1169
 46. Molenaar RJ, Vreman S, Hakze-van der Honing RW, Zwart R, de Rond J, Weesendorp E, et al. Clinical and pathological findings in SARS-CoV-2 disease outbreaks in farmed mink (*Neovison vison*). *Vet Pathol.* 2020;57:653–7. https://doi.org/10.1177/0300985820943535
 47. Hammer AS, Quaade ML, Rasmussen TB, Fonager J, Rasmussen M, Mundbjerg K, et al. SARS-CoV-2 Transmission between mink (*Neovison vison*) and humans, Denmark. *Emerg Infect Dis.* 2021;27:547–51. https://doi.org/10.3201/eid2702.203794
 48. Oude Munnink BB, Sikkema RS, Nieuwenhuijse DF, Molenaar RJ, Munger E, Molenkamp R, et al. Transmission of SARS-CoV-2 on mink farms between humans and mink and back to humans. *Science.* 2021;371:172–7. https://doi.org/10.1126/science.abe5901

Address for correspondence: Bin Zhou, Centers for Disease Control and Prevention, 1600 Clifton Rd NE, Mailstop H17-5, Atlanta, GA 30329-4027, USA; email: bzhou@cdc.gov

Epidemiologic History and Genetic Diversity Origins of Chikungunya and Dengue Viruses, Paraguay

Tiago Gräf,¹ Cynthia Vazquez,¹ Marta Giovanetti,¹ Fernanda de Bruycker-Nogueira,¹ Vagner Fonseca,¹ Ingra Morales Claro, Jaqueline Goes de Jesus, Andrea Gómez, Joilson Xavier, Marcos Cesar Lima de Mendonça, Shirley Villalba, Juan Torales, Maria Liz Gamarra, Julien Thézé, Ana Maria Bispo de Filippis, Vasco Azevedo, Tulio de Oliveira, Leticia Franco, Carlos F. Campelo de Albuquerque, Sandra Irala, Edward Charles Holmes, Jairo Andrés Méndez Rico, Luiz Carlos Junior Alcantara

Paraguay has been severely affected by emergent Zika and chikungunya viruses, and dengue virus is endemic. To learn more about the origins of genetic diversity and epidemiologic history of these viruses in Paraguay, we deployed portable sequencing technologies to strengthen genomic surveillance and determine the evolutionary and epidemic history of arthropod-borne viruses (arboviruses). Samples stored at the Paraguay National Central Laboratory were sequenced and subjected to phylogenetic analysis. Among 33 virus genomes generated, we identified 2 genotypes of chikungunya and 2 serotypes of dengue virus that circulated in Paraguay during 2014–2018; the main source of these virus lineages was estimated to be Brazil. The evolutionary history inferred by our analyses precisely matched the available travel history of the patients. The genomic surveillance approach used was valuable for describing the epidemiologic history of arboviruses and can be used to determine the origins and evolution of future arbovirus outbreaks.

Chikungunya virus (CHIKV), dengue virus (DENV), and Zika virus (ZIKV) are 3 of the most common arthropod-borne viruses (arboviruses)

that infect humans. All are transmitted by the anthropophilic and urban-adapted *Aedes aegypti* and *Ae. albopictus* mosquito vectors (1). Driven by human movement and climate trends, the distribution of these mosquitoes is expanding along with the arboviruses they transmit (2). In Latin America, CHIKV and ZIKV have emerged since the mid-2000s, joining DENV, which is already endemic there (3). In this region, only Uruguay and Chile did not report autochthonous transmissions of one of these arboviruses during 2014–2019, highlighting the current state of endemicity (4).

Paraguay is a landlocked country in the center of South America; it borders Bolivia, Brazil, and Argentina. DENV is endemic to Paraguay, and all 4 serotypes (DENV-1–4) have been detected there; in some seasons, multiple serotypes co-circulate (5,6). Phylogenetic analysis has shown that DENV genetic diversity in Paraguay is closely related to that in neighboring countries, particularly Brazil (7,8). However, more genomic surveillance studies in Paraguay are needed to learn more about this epidemiologic pattern. Cases

Author affiliations: Fundação Oswaldo Cruz, Salvador, Brazil (T. Gräf, J.G. de Jesus); Fundação Oswaldo Cruz, Rio de Janeiro, Brazil (C. Vazquez, M. Giovanetti, F. de Bruycker-Nogueira, V. Fonseca, J. Xavier, M.C.L. de Mendonça, A.M. Bispo de Filippis, L.C.J. Alcantara); Laboratorio Central de Salud Pública, Asunción, Paraguay (C. Vazquez, A. Gómez, S. Villalba, J. Torales, M.L. Gamarra); Instituto de Ciências Biológicas, Universidade Federal de Minas Gerais, Belo Horizonte, Brazil (M. Giovanetti, V. Fonseca, J. Xavier, V. Azevedo, L.C.J. Alcantara); University of KwaZulu-Natal, Durban, South Africa (V. Fonseca, T. de Oliveira); Universidade de São Paulo, São Paulo, Brazil (I.M. Claro); University of Oxford, Oxford, UK (J. Thézé); University

of Washington, Seattle, Washington, USA (T. de Oliveira); Organización Panamericana de la Salud / Organización Mundial de la Salud, Panama City, Panama (L. Franco); Organização Pan-Americana da Saúde/Organização Mundial da Saúde, Brasília, Brazil (C.F. Campelo de Albuquerque); Dirección General de Vigilancia de la Salud Paraguay, Asunción (S. Irala); The University of Sydney, Sydney, New South Wales, Australia (E.C. Holmes); Pan American Health Organization/World Health Organization, Washington, DC, USA (J.A.M. Rico)

DOI: <https://doi.org/10.3201/eid2705.204244>

¹These first authors contributed equally to this article.

of chikungunya fever in Paraguay were first reported in June 2014; autochthonous cases were first detected in 2015, and CHIKV caused seasonal outbreaks every year until 2018. Zika was first detected in November 2015, and autochthonous infections were confirmed soon after (9). To date, however, little is known about the genetic diversity of CHIKV and ZIKV that circulate in Paraguay.

The potential triple epidemic scenario (i.e., CHIKV, DENV, ZIKV) in Paraguay could pose serious public health and economic burdens. Arbovirus surveillance is critical for assisting health services with preparedness, providing key information about the seasonality of infections and diversity of circulating viral lineages. When resources allow, such surveillance can now involve genomic surveillance via portable sequencing technologies. For example, this approach was successfully used to study the ZIKV epidemic in the Americas (10,11), the reemergence of yellow fever virus in Brazil (12,13), and recurrent outbreaks of CHIKV in several regions of Brazil (14–16).

To help reinforce arbovirus surveillance in Paraguay, we performed portable genome sequencing under the scope of the ZIBRA project (<http://zibra-project.org>) at the Laboratorio Central de Salud Pública in Asunción, Paraguay. During July 16–20, 2018, a team of molecular biologists from Brazil and Paraguay worked on a group of samples selected to determine the recent history of arboviruses in the country, generating 33 viral genomes and building capacity skills among the local laboratory staff. We report the analysis of the origins and spread of CHIKV in Paraguay as well as the current dynamics of DENV. The project was reviewed and approved by the Comissão Nacional de Ética em Pesquisa (CONEP) from the Brazilian Ministry of Health as part of the arbovirus genomic surveillance efforts within the terms of CONEP Resolution 510/2016 by the Pan American Health Organization Ethics Review Committee (PAHO-2016-08-0029) and by the Paraguayan Ministry of Public Health and Social Welfare (MSPyBS/S.G. no. 0944/18).

Methods

Sample and Data Collection

This study was necessarily based on convenience sampling; de-identified samples were obtained from material exceeding the routine number of arbovirus diagnoses and stored at the Laboratorio Central de Salud Pública de Asunción, Paraguay, which concentrates biological samples collected throughout the country. On the basis of resources and time

availability, we selected 50 acute-phase serum samples that were positive for DENV or CHIKV with PCR cycle threshold (C_t) values <28 at the time of diagnosis. Using epidemiologic data, we chose samples to represent geographic departments in Paraguay with the highest number of cases. ZIKV-positive samples with low C_t and historical samples for DENV were unavailable; hence, for DENV, we studied only the 2018 epidemic. The Dirección General de Vigilancia de la Salud of Paraguay provided temporal data on the incidence of chikungunya and dengue cases by department within Paraguay.

Virus Amplification and Whole-Genome Sequencing

We extracted viral RNA from the selected samples by using the QIAamp Viral RNA Mini Kit (QIAGEN, <https://www.qiagen.com>) and subjected the RNA to real-time reverse transcription quantitative PCR to detect CHIKV and DENV serotypes 1–4 as described previously (17–19). To increase the genome coverage, we selected only samples with $C_t \leq 35$ for sequencing. Extracted RNA was converted to cDNA by using the Protoscript II First Strand cDNA Synthesis Kit (New England Biolabs, Inc., <https://www.neb.uk.com>) and random hexamer priming. We attempted whole-genome amplification by multiplex PCR as previously described (20).

We purified amplicons by using 1x AMPure XP Beads (Beckman Coulter, <https://www.beckman.com>) and quantified them on a Qubit 3.0 fluorimeter by using a Qubit dsDNA HS Assay Kit (ThermoFisher Scientific, <https://www.thermofisher.com>). We performed DNA library preparation by using a Ligation Sequencing Kit and Native Barcoding Kit (NBD103; Oxford Nanopore Technologies, <https://nanoporetech.com>). We generated sequencing libraries from the barcoded products by using the Genomic DNA Sequencing Kit SQK-MAP007/SQK-LSK208 and loaded them into an R9.4 flow cell (Oxford Nanopore Technologies).

Generation of Consensus Sequences

We base-called raw files by using Albacore software, demultiplexed and trimmed by using Porechop software (<https://github.com>) and then mapped with Burrows-Wheeler Aligner software to a reference genome. On the basis of PCR analyses, we used GenBank accession nos. KP164568 for CHIKV, KF672760 for DENV-1, and JN559741 for DENV-4 as reference sequences. To detect single-nucleotide variants to the reference genome, we applied Nanopolish software variant calling (<https://nanoporetech.com>) to the assembly. Nonoverlapped primer binding sites and

sites for which coverage was $<20\times$ were replaced with ambiguity code N.

Phylogenetic Analyses

We first investigated sequence genotypes by using the arbovirus genotyping tool (21). To investigate the origins and spatial dynamics of arboviruses in Paraguay, we downloaded all sequences assigned as CHIKV, DENV-1, and DENV-4 from GenBank. We excluded sequences without sampling date and location and sequences covering $<50\%$ of the virus genome. Sequence alignment was performed by using MAFFT (22) (FFT-NS-2 algorithm) and visually inspected in Aliview (23). We estimated maximum-likelihood phylogenies in IQ-TREE (24) by using the best-fit model of nucleotide substitution as indicated by the ModelFinder application (implemented in IQ-TREE). Branch support was assessed by the SH-like approximate-likelihood ratio test, and we submitted highly supported (>0.9) clades containing the DENV genomes from Paraguay (Appendix 1 Figure 1, <https://wwwnc.cdc.gov/EID/article/27/5/20-4224-App1.pdf>) and the clades of CHIKV from the Americas to TempEst (25) to assess the strength of temporal signal in these data.

Time-scaled phylogenetic trees were inferred by using the BEAST package (26). We chose the uncorrelated relaxed molecular clock model as indicated by the marginal likelihood estimation model test procedure. We also used the codon-based SRD06 model of nucleotide substitution and the nonparametric Bayesian Skygrid coalescent model. A discrete phylogeographical model (27) was used to reconstruct the spatial diffusion of the virus across the compiled dataset sampling locations (Appendix 2, <https://wwwnc.cdc.gov/EID/article/27/5/20-4224-App2.xlsx>). Phylogeographic analyses were performed by applying an asymmetric model of location transitioning coupled with the Bayesian stochastic search variable selection procedure. We complemented this analysis with Markov jump estimation that counts location transitions per unit time along the tree. We ran Monte Carlo Markov chains long enough to ensure stationarity and an adequate effective sample size of >200 .

Results

Of the 50 samples tested, 25 were positive for CHIKV, 14 for DENV-1, and 11 for DENV-4. For positive samples, the average PCR C_t value was 26.36 (range 16–37). From the 50 samples, we were able to generate 33 complete or near-complete genome sequences (17 CHIKV and 16 DENV genomes) (Table). The GenBank accession numbers of newly generated sequences

are MT038393–409 (CHIKV) and MT040672–87 (DENV). The collection dates of the samples sequenced were November 3, 2014, through July 10, 2018, and locations covered 15 municipalities and 8 departments (the first-level administrative subdivisions) of Paraguay (Figure 1). Women accounted for 58% of the samples, and the median patient age was 34 years. A TempEst analysis of all arbovirus lineages found here revealed a strong correlation between the sampling time and the root-to-tip divergence (Appendix 1 Figure 2).

The CHIKV Epidemic in Paraguay during 2014–2018

Of the 17 CHIKV genomes, 12 were classified as Asian genotype (sampled during 2014–2016) and 5 as East/Central/South African (ECSA) genotype (sampled during 2018). The oldest CHIKV sample analyzed (patient PY45) was obtained in November 2014 from the department of Amambay and was identified as an Asian genotype (Figure 1). However, autochthonous transmission of CHIKV was not confirmed until February 2015, followed by an increased number of reported infections (9) (Figure 2, panel A). Phylogeographic analysis revealed that the most likely origin of PY45 was Central or South America (Figure 3, panel A). The travel history for PY45 is in agreement with these results because the patient reported having visited Panama and San Andrés, a Colombian cluster of islands in the Caribbean region. In November 2014, another introduction of CHIKV in Paraguay was detected in the Central Department. That sequence (patient PY44) clustered with high support (posterior probability [PP] = 1) among sequences from Colombia and 1 sequence from Nicaragua, and the ancestral state of the most recent common ancestor (MRCA) of this clade was South America (PP = 0.8). Patient PY44 reported traveling to Cartagena, Colombia, supporting the origin estimated by the phylogeographic analysis.

In 2015, a large CHIKV epidemic occurred in Paraguay, resulting in $\approx 10,000$ cases (suspected and confirmed); the main affected departments were Central, Asunción, and Paraguarí (Figure 2, panel A). All genomes generated from the 4 samples from 2015 were classified as members of the Asian genotype and grouped together with high support (PP = 1) (Figure 3, panel A) in a clade for which time to MRCA (tMRCA) was October 2014 (95% highest posterior density [HPD] May 2014 to November 2014) (Figure 2, panel B). From our analysis, we estimated that the geographic origin of the variant circulating in Paraguay in 2015 was Puerto Rico (PP = 0.98) (Figure 3, panel A). The first patient with autochthonous

CHIKV infection in Paraguay is believed to be the housemaid of a family returning from Puerto Rico in October 2014, who sought healthcare services for symptoms of chikungunya fever. CHIKV infections were confirmed for the housemaid and the family, and our phylogenetic analysis confirmed this epidemiologic history.

The time distributions of CHIKV infection cases from 2016 were very similar to those in 2015 (Figure 2, panel A), although they did reveal that at least 2 lineages were circulating in the country (Figure 3,

panel A). A new introduction is likely to have occurred in the Paraguari Department at the mean time point of November 2015 (95% HPD June 2015 to January 2016); the most likely place of origin was Central America (PP = 0.76) (Figure 3, panel A). However, the sequence from Amambay Department, isolated in 2014, is positioned basally to the Paraguari cluster, suggesting that the same variant persisted in the country up to 2016. Year-round persistence of a CHIKV strain is clearly observed in the Central/Asunción Department cluster in which the genome

Table. Patient demographic and virus sequencing data for samples from the Laboratorio Central de Salud Publica de Asunción, Paraguay, 2014–2018*

Sample	Virus	Department, municipality	Collection date	Patient age, y/sex	C _t	Reads	Genome coverage, %
PY02	CHIKV-Asian genotype	Paraguari, Yaguaron	2016 Jan 20	40/M	23.6	204,763	88.1
PY03	CHIKV-Asian genotype	Paraguari, Yaguaron	2016 Jan 21	67/M	16.9	215,137	87.0
PY06	CHIKV-Asian genotype	Paraguari, Yaguaron	2016 Feb 16	9/M	26.9	282,182	88.3
PY07	CHIKV-Asian genotype	Paraguari, Yaguaron	2016 Feb 19	34/F	29.7	267,784	87.2
PY08	CHIKV-Asian genotype	Paraguari, Yaguaron	2016 Feb 22	39/F	30.2	142,555	87.1
PY09	CHIKV-Asian genotype	Asunción, Asunción	2016 Mar 21	27/F	28	265,596	87.9
PY12	CHIKV-ECSA/BR	Amambay, Pedro Juan Caballero	2018	21/M	29	236,285	84.8
PY13	CHIKV-ECSA/BR	Amambay, Pedro Juan Caballero	2018 Jun 25	35/F	28	175,112	85.3
PY15	CHIKV-ECSA/BR	Amambay, Bella Vista Norte	2018 Jun 29	40/F	34	17,030	70.9
PY17	CHIKV-ECSA/BR	Amambay, Bella Vista Norte	2018 Jul 3	22/M	34	320,142	86.8
PY18	CHIKV-ECSA/BR	Amambay, Bella Vista Norte	2018 Jul 10	57/M	29	315,588	86.0
PY19	DENV-4	Guairá, Villarrica	2018 Apr 23	38/F	23	22,041	82.3
PY21	DENV-4	Guairá, Villarrica	2018 Apr 26	68/F	22	21,042	96.0
PY22	DENV-4	Guairá, Villarrica	2018 Apr 27	52/M	22	13,213	96.0
PY23	DENV-4	Central, San Lorenzo	2018 May 6	19/M	27	11,548	74.6
PY24	DENV-1	San Pedro, San Pedro De Ycuamandju	2018 May 4	29/F	20	7,265	89.1
PY25	DENV-4	Central, San Lorenzo	2018 May 5	38/F	21	17,299	96.0
PY27	DENV-4	Alto Paraná, Domingo Martinez De Irala	2018 May 9	27/F	19	21,188	96.0
PY28	DENV-4	Alto Paraná, Hernandarias	2018 May	30/M	21	22,800	86.6
PY31	DENV-4	Alto Paraná, Hernandarias	2018 May 22	14/M	32	8,770	95.9
PY32	DENV-4	Central, San Lorenzo	2018 May 31	28/M	28	6,907	96.0
PY33	DENV-1	Asunción, Asunción	2018 May 31	3/F	22	9,846	76.8
PY34	DENV-4	Alto Paraná, Juan Leon Mallorquin	2018 May 28	47/F	26	7,945	96.0
PY35	DENV-1	Itapúa, Encarnacion	2018 Jun 7	62/F	23	119,293	89.1
PY36	DENV-1	Itapúa, Encarnacion	2018 Jun 8	61/M	23	6,448	76.8
PY38	DENV-1	Itapúa, Cambyreta	2018 Jun 8	6/F	25	111,057	89.1
PY43	DENV-1	Guairá, Villarrica	2018 Jun 4	53/F	25	8,779	89.1
PY44	CHIKV-Asian genotype	Central, Luque	2014 Nov 30	33/F	24	13,687	85.1
PY45	CHIKV-Asian genotype	Amambay, Pedro Juan Caballero	2014 Nov 3	54/M	24	12,214	86.6
PY47	CHIKV-Asian genotype	Central, Guarambare	2015 Apr 26	25/M	17	9,536	85.2
PY48	CHIKV-Asian genotype	Central, Fernando De La Mora	2015 Apr 28	50/F	18	6,002	86.6
PY49	CHIKV-Asian genotype	Central, Fernando De La Mora	2015 May 3	12/F	27	53,928	86.4
PY50	CHIKV-Asian genotype	Central, Fernando De La Mora	2015 May 6	25/F	16	49,813	86.8

*CHIKV, chikungunya virus; C_t, cycle threshold; DENV, dengue virus; ECSA/BR, East/Central/South African genotype from Brazil.

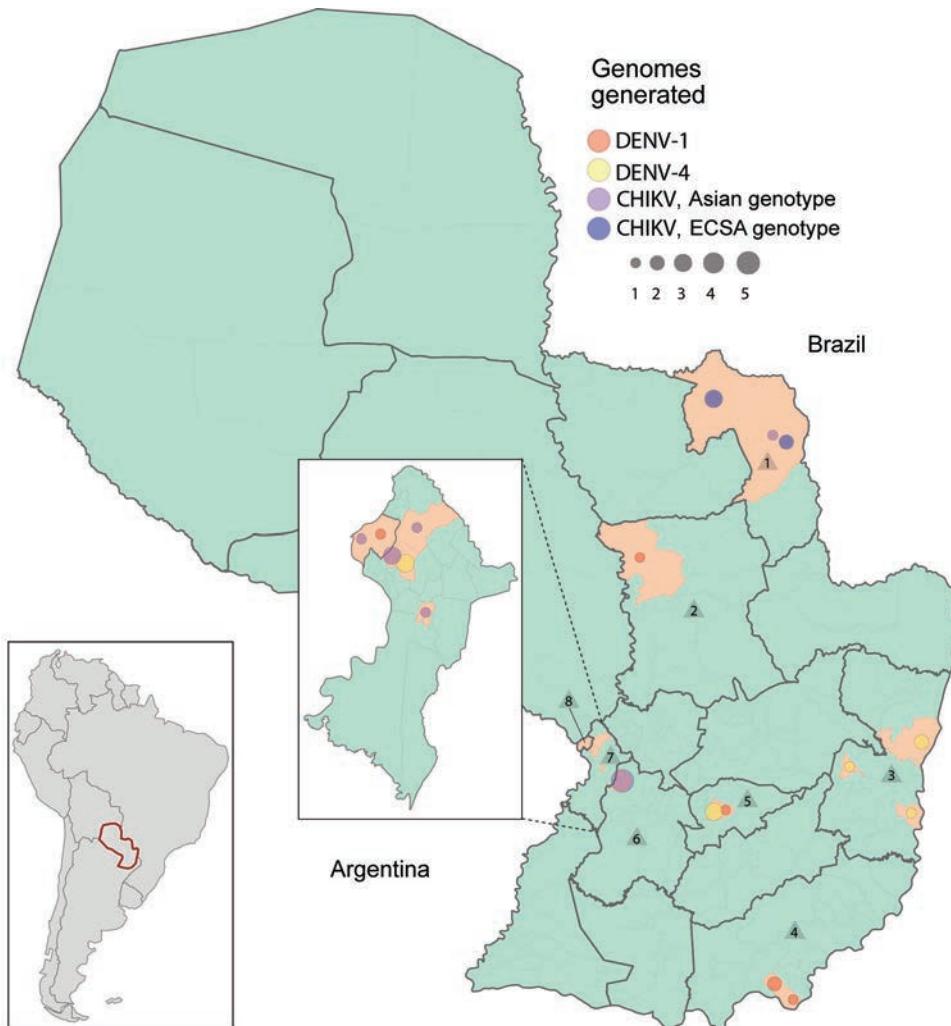


Figure 1. Geopolitical map of Paraguay showing locations of sampling for dengue virus (DENV) and chikungunya virus (CHIKV). Circle sizes are scaled to represent the number of genomes isolated in each municipality. Numbers inside triangles indicate sampled departments: 1, Amambay; 2, San Pedro; 3, Alto Paraná; 4, Itapúa; 5, Guairá; 6, Paraguari; 7, Central; 8, Asunción. Callout map shows the Central and Asunción Departments of Paraguay; inset map shows the location of Paraguay in South America.

isolated in 2016 clustered with the genomes isolated in 2015 (Figure 3, panel A).

Besides the Asian genotype of CHIKV, an outbreak of the ECSA genotype occurred in Paraguay in 2018. After a year of very few CHIKV infections in 2017 (Figure 2, panel A), a new outbreak was observed in 2018 (although milder than that of 2015 and 2016), and the main affected department was Amambay. Five genomes from this department revealed circulation of the CHIKV ECSA genotype in 2018, and the mean tMRCA of this cluster was December 2017 (95% HPD July 2017 to April 2018) (Figure 2, panel B). The source of introduction of this new CHIKV lineage in Paraguay was estimated to be Brazil, most likely the Northeast Region (PP = 0.64), or perhaps the North Region (PP = 0.32) (Figure 3, panel B).

We also summarized all geographic locations that had significantly (Bayes factor >3) seeded new CHIKV lineages to Paraguay and superimposed it onto the

tMRCA of the 3 main CHIKV clusters detected there (Figure 2, panel B). Most transitions in the Asian genotype occurred in 2014, when CHIKV was spreading rapidly through the Americas. Far fewer transitions were estimated to have occurred in 2015, which accords with the hypothesis that the 2016 outbreak in Paraguari was caused by a lineage already circulating in the country. For the ECSA genotype of CHIKV, the importations from Brazil were widespread between the middle of 2015 and the beginning of 2019. These widespread importations result from the long branch connecting the Paraguay ECSA cluster to the Brazilian sequences (Figure 3, panel B), increasing uncertainty in the relevant parameter estimates.

Genetic Diversity of DENV in 2018

The number of DENV cases in Paraguay during 2015–2018 shows a very similar pattern to that for CHIKV (Figure 2, panel A; Figure 4, panel A). Case numbers

were higher at the beginning of each year, except for 2017 when the DENV season was atypically mild. Our sampling from 2018 captured the 2 DENV serotypes (DENV-1 and DENV-4) circulating in the country (9), and molecular clock analyses estimated that DENV-4 was introduced in Paraguay just before the beginning of the 2018 outbreak, whereas DENV-1 was already circulating in 2017 (Figure 4, panel B).

DENV-1 and DENV-4 sequences from Paraguay clustered together with high support ($PP > 0.9$) and belonged to genotypes V and II, respectively, which predominate in Latin America (Figure 5). The most likely origin of the DENV-1 strain circulating in Paraguay in 2018 was estimated to be Brazil ($PP = 0.75$) (Figure 5, panel A), and the mean tMRCA was estimated to be October 2016 (95% HPD February 2016 to May 2017) (Figure 4, panel B). DENV-4 was also estimated to have an origin in Brazil; the best-supported regions of origin were Central-West ($PP = 0.64$) and North ($PP = 0.34$) (Figure 5, panel B). The mean tMRCA of DENV-4 was September 2017 (95% HPD April 2017 to February 2018), ≈ 1 year later than DENV-1. Examining the DENV-4 cluster in Paraguay in more detail revealed that sequences from the Alto Paraná Department are basal and that sequences from the Central and Guairá Departments group together in a highly supported ($PP > 0.9$) and distal cluster (Figure 5, panel B). Alto Paraná borders Brazil, and although not formally tested because of the small

number of sequences, Alto Paraná could be the point of introduction of the current DENV-4 lineage into Paraguay.

Discussion

The first CHIKV outbreaks in the Americas (the Asian genotype) were reported for the French Caribbean islands of Saint Martin and Martinique in December 2013 (28). The virus rapidly spread throughout the Caribbean and Central America in 2014, and autochthonous transmissions were reported in almost all countries/territories of these regions. In 2014, Paraguay reported imported cases only, mostly in persons with a history of travel to Central America or the Caribbean. Our analysis of virus sequences from 2 of these persons with imported cases, and the virus phylogenetic relatedness to foreign viruses, matched the travel history with precision. In addition, the estimated origin of the first outbreak of CHIKV in Paraguay in 2015 agreed both in time (October 2015) and location (Puerto Rico) with the travel data collected by the Paraguay surveillance system.

The CHIKV epidemic in Paraguay in 2016 was very similar to that in 2015, when the most affected departments were Central, Asunción, and Paraguari. These neighboring departments are located in the most densely populated region of Paraguay, which might lead to consecutive outbreaks. In our sampling, most sequences from 2016 were from the Paraguari Department and formed a separate clade

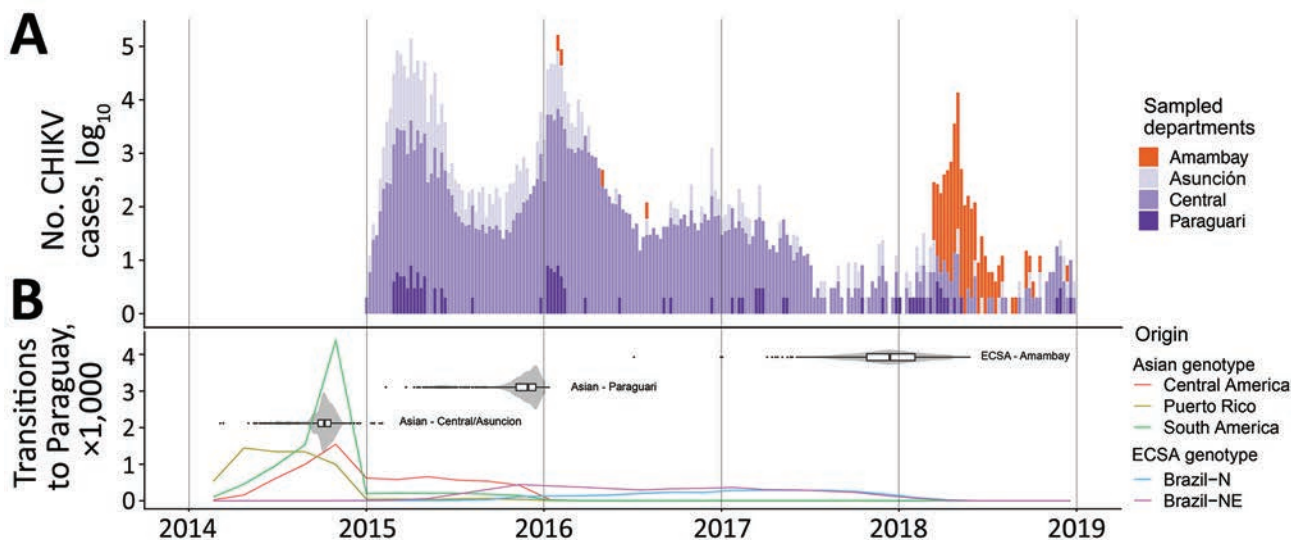


Figure 2. Chikungunya virus (CHIKV) outbreaks in Paraguay during 2014–2018 and the spatial–temporal history of virus diffusion. A) Total number of cases of CHIKV infection reported by epidemiologic week in the departments from which genome sequences were available. B) Location transitions to Paraguay inferred from the posterior distribution of phylogenetic trees by the Markov jump approach, and the time to most recent common ancestor for the CHIKV clusters detected in the country. Lines are colored according to the origin of the estimated transition toward Paraguay. Violin plots show 95% CIs with internal boxplots showing median and interquartile ranges. Brazil-N, Brazil North Region; Brazil-NE, Brazil Northeast Region; ECSA, East/Central/South African genotype.

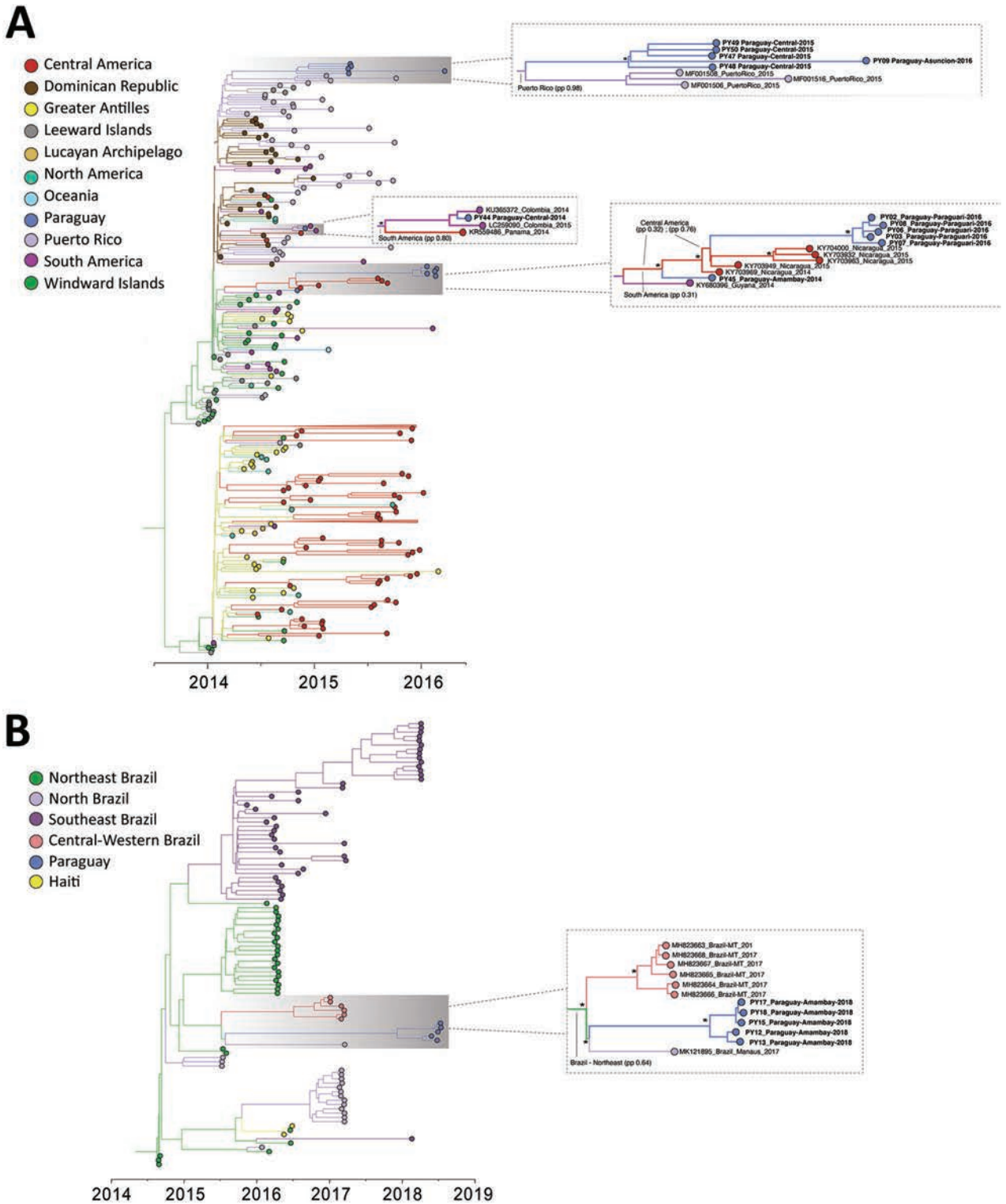


Figure 3. Time-scaled phylogenetic trees of chikungunya virus (CHIKV) genomes isolated in the Americas. A) CHIKV Asian genotype; B) CHIKV East/Central/South African genotype from Brazil. Tips and internal branches are colored according to the most likely geographic location, and ancestral states were estimated by phylogeographic methods. Clusters relevant to the epidemic in Paraguay are shown in detail where the most likely ancestral state estimation is annotated. Asterisks indicate highly supported clusters (posterior probability >0.9).

from the 2015 epidemic, suggesting a new introduction event. However, because of the co-clustering of sequences from the Asunción and Central Departments isolated in 2015 and 2016, we cannot exclude year-round persistence of the virus. Models of *Aedes* spp. mosquito competence for DENV transmission have shown that the Paraguay climate is conducive to year-round persistence (29).

In Brazil, 2 distinct lineages of CHIKV were detected at the end of 2014, the ECSA genotype in the Northeast Region and the Asian genotype in the North Region (30). Whereas the CHIKV outbreak of the Asian genotype remained restricted to a small number of cases, the ECSA lineage spread throughout Brazil. In this study, we determined that the ECSA genotype was the causative agent of a CHIKV outbreak in Amambay (a Paraguay department on the Brazil border) in 2018. To our knowledge, these are the only 2 countries in the Americas to report outbreaks of both the Asian and ECSA genotypes to date. Our analysis revealed a mean time of entry into Paraguay of around December 2017, most likely from the Northeast Region in Brazil. However, because of the small number of samples from states in Brazil that border Paraguay, all such inferences of geographic origins should be interpreted with caution. It is possible that previous exposure to the CHIKV Asian genotype may have created some population immunity that restricted ECSA circulation in other parts of Paraguay (e.g., Central and Asunción Departments) in 2018. Unfortunately, no data on CHIKV seroprevalence in Paraguay are available to test this hypothesis. Amambay, on the other hand, reported few CHIKV cases during the epidemics of 2015 and 2016 (Figure 2, panel A), potentially enabling the emergence of the ECSA genotype in 2018.

The 2018 dengue season in Paraguay was dominated by DENV-1, reported in all departments (9). Three departments (Central, Alto Paraná, and Guairá) also reported the circulation of DENV-4. Our analysis suggests that the origin of both serotypes in Paraguay is Brazil, supporting findings of previous studies (31). Although our sampling was restricted to 2018, we observed that the tMRCA of DENV-1 was much earlier (October 2016), suggesting that this lineage may have persisted during the 2017 and 2018 seasons, when it may have been responsible for most cases (9). DENV-4, on the other hand, was introduced in September 2017, just before the start of the dengue season, and was responsible for few infections until the 2019–20 season, when it dominated the epidemic (32, 33).

Despite screening all publicly available (GenBank) sequences of DENV from the Americas, we found that the DENV datasets were sparsely distributed in time (DENV-4) or contained large temporal gaps (DENV-1) (Appendix 1 Figure 2), potentially biasing our results. The paucity of available DENV complete genomes in South America constrains the applicability of phylogenetic tools for studying virus population dynamics. It also highlights the value of intensifying sequencing efforts in line with the genomic surveillance approach and for real-time generating and sharing of data. The CHIKV datasets were much more comprehensive; for instance, the Asian lineage dataset analyzed included 291 genomes sampled during 2014–2018, representing 38 countries/territories (Appendix 2). The more comprehensive CHIKV datasets reflect the fact that CHIKV emerged in the Americas in the era of next-generation sequencing, when the development of numerous platforms reduced the cost and shortened the time from sample preparation to

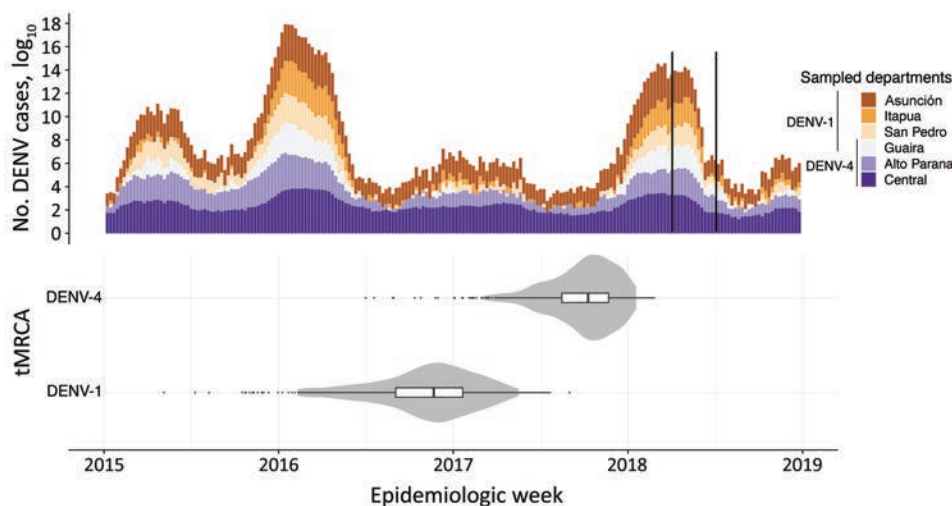


Figure 4. Dengue virus (DENV) outbreaks in Paraguay during 2015–2018 and tMRCA of serotypes 1 and 4. A) Total cases of DENV infections reported by epidemiologic week in the departments from which genome sequences were available. The black bars in 2018 delimit the sampling time range for the DENV genomes. B) tMRCA for DENV-1 and DENV-4 in the same timescale as the number of cases reported. Violin plots show 95% CIs; internal boxplots show medians and interquartile ranges. tMRCA, time to most recent common ancestor.

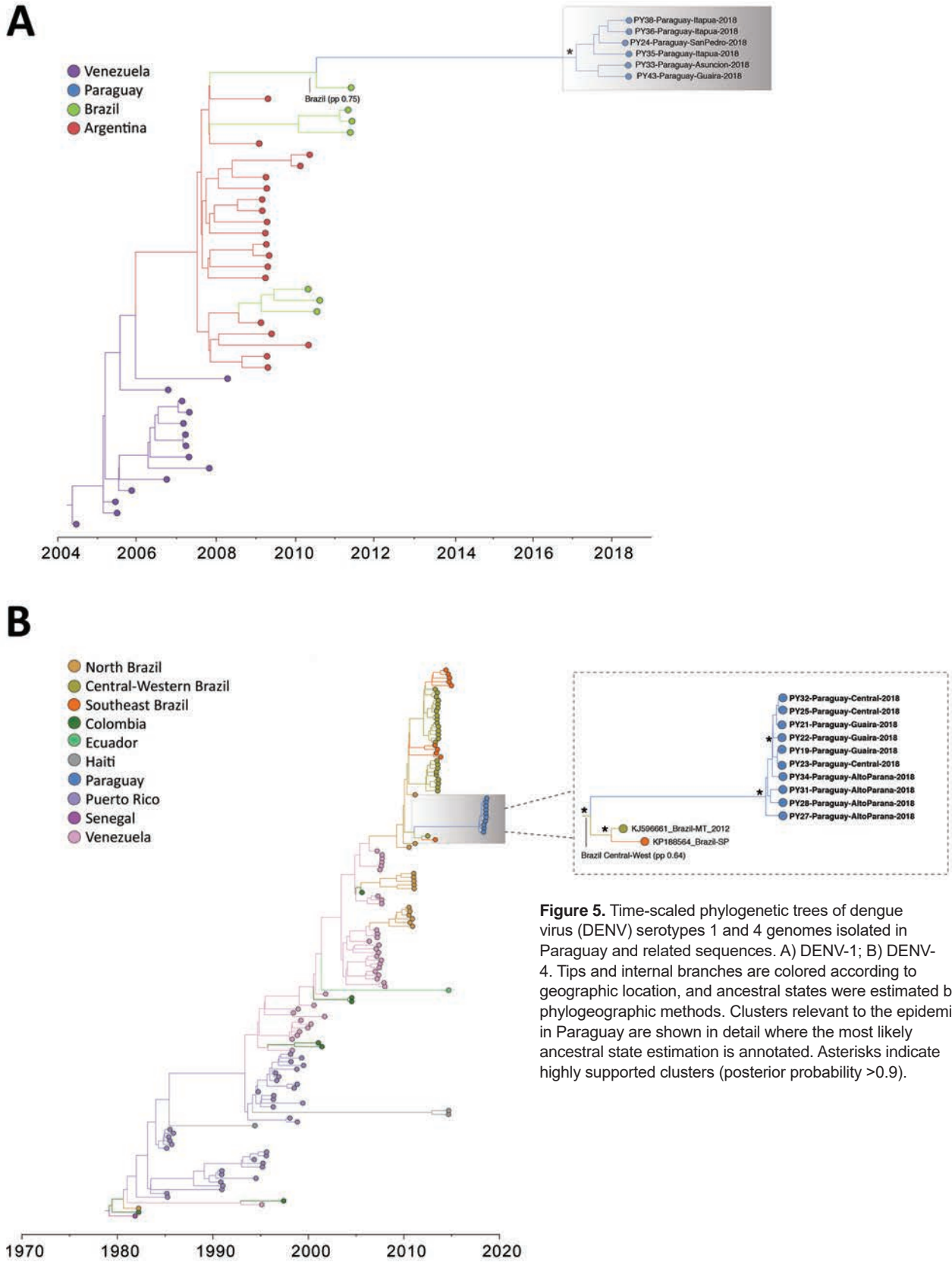


Figure 5. Time-scaled phylogenetic trees of dengue virus (DENV) serotypes 1 and 4 genomes isolated in Paraguay and related sequences. A) DENV-1; B) DENV-4. Tips and internal branches are colored according to geographic location, and ancestral states were estimated by phylogeographic methods. Clusters relevant to the epidemic in Paraguay are shown in detail where the most likely ancestral state estimation is annotated. Asterisks indicate highly supported clusters (posterior probability >0.9).

data generation. Hence, this increased availability of CHIKV virus genomes allowed a more detailed analysis of the virus's spatiotemporal history in Paraguay. However, another study limitation is the convenience sampling used, with a narrow breadth, potentially biasing molecular clock dating and location ancestral reconstruction. The limited availability of stored samples from years before 2018, and their possibly limited RNA integrity, impaired genome sequencing from previous outbreaks. Nevertheless, we suggest that the 33 genomes generated here are representative of the current DENV diversity and the recent CHIKV evolutionary history in Paraguay.

Of note, the mean tMRCAs for the 3 clusters of CHIKV and the 2 clusters of DENV were estimated in the last trimester of the year (September–December), the start of arbovirus season in many tropical and subtropical regions in the Southern Hemisphere (e.g., Paraguay). A previous study (34) has modeled the timing and scale of arbovirus transmission potential and found that in many cities in Brazil with climates similar to that of Paraguay, transmission starts to increase around September. Thus, the tMRCAs estimated here probably reflect the onset of the arbovirus season, which peaks during January–March. Oddly, the 2017 season was marked by a noticeable reduction in cases of both DENV and CHIKV in Paraguay (Figure 2, panel A; Figure 5, panel A). This pattern was observed for dengue throughout the Americas, where cases decreased by 73% in 2017 compared with 2016 (35). It is possible that the mild season in 2017 might be explained by a transient strengthening of vector control interventions, implemented after the arrival of CHIKV and ZIKV in the Americas and the consequent public health emergency triggered by these pathogens. In addition, cross-immunity between ZIKV and DENV has been observed in the laboratory (36). Hence, population immunity to ZIKV after the 2015–2016 epidemic may have provided some transitory protection against DENV, resulting in lower incidence in 2017 (37,38), although this protection alone would not explain the decreased CHIKV cases in 2017 in Paraguay.

In conclusion, our study reveals a complex pattern of arbovirus circulation in Paraguay. We identify Brazil as a source of CHIKV and DENV lineages and show that other countries from South America and the Caribbean, mainly tourist destinations, were also hubs of virus spread toward Paraguay. Our sequencing and phylogenetic analyses proved to be

powerful tools for revealing the transmission dynamics between the sampled locations and matched, with striking precision, available patient travel history. With support from the Pan American Health Organization, this project developed capacity-building skills in Paraguay, which can be applied in future arbovirus outbreaks.

This work was supported by Decit/SCTIE/MoH and CNPq (440685/2016-8 and 440856/2016-7); by CAPES (88887.130716/2016-00, 88881.130825/2016-00, and 88887.130823/2016-00), and by the EU Horizon 2020 Programme through ZIKAlliance (PRES-005-FEX-17-4-2-33). M.G. is supported by the Fundação de Amparo à Pesquisa do Estado do Rio de Janeiro–FAPERJ. E.C.H. is supported by an Australian Research Council Australian Laureate Fellowship (FL170100022). A.M.B.F. was supported by International Development Research Centre, Canada (grant 108411-001) and by Horizon 2020 through ZikaPlan and ZikAction (grant agreement nos. 734584 and 734857).

About the Author

Dr. Gräf is a public health researcher at the Gonçalo Moniz Institute of the Oswaldo Cruz Foundation, Salvador, Brazil. His research interests focus on molecular epidemiology and the application of phylogenetics to study viral evolution and epidemic spread.

References

1. Paixão ES, Teixeira MG, Rodrigues LC. Zika, chikungunya and dengue: the causes and threats of new and reemerging arboviral diseases. *BMJ Glob Health* 2018;3:e000530.
2. Kraemer MUG, Reiner RC Jr, Brady OJ, Messina JP, Gilbert M, Pigott DM, et al. Past and future spread of the arbovirus vectors *Aedes aegypti* and *Aedes albopictus*. *Nat Microbiol.* 2019;4:854–63. <https://doi.org/10.1038/s41564-019-0376-y>
3. Mayer SV, Tesh RB, Vasilakis N. The emergence of arthropod-borne viral diseases: a global prospective on dengue, chikungunya and zika fevers. *Acta Trop.* 2017;166:155–63. <https://doi.org/10.1016/j.actatropica.2016.11.020>
4. Pan American Health Organization. Health information platform for the Americas (PLISA) [cited 2019 Jan 29]. <http://www.paho.org/data/index.php/en>
5. Vazquez C, Villalba S, Oviedo E, Gamarrá ML, Oviedo E, Oviedo A, et al. Características virológicas y serológicas de pacientes con dengue grave y fallecidos por dengue durante la epidemia del año 2011 en Paraguay. *Rev Inst Med Trop.* 2012;77:8–18.
6. Flores Rodríguez LE, Díaz Duba S, Torales J, Agüero R, Román L, Adorno J, et al. Características clínicas de la epidemia de dengue en el Servicio de Urgencias del Hospital de Clínicas. *Rev Salud Pública Paraguay.* 2016;6:2–7.
7. Aquino VH, Anatriello E, Gonçalves PF, DA Silva EV, Vasconcelos PF, Vieira DS, et al. Molecular epidemiology of dengue type 3 virus in Brazil and Paraguay, 2002–2004. *Am*

- J Trop Med Hyg. 2006;75:710–5. <https://doi.org/10.4269/ajtmh.2006.75.710>
8. Avilés G, Rowe J, Meissner J, Manzur Caffarena JC, Enria D, St Jeor S. Phylogenetic relationships of dengue-1 viruses from Argentina and Paraguay. *Arch Virol*. 2002;147:2075–87. <https://doi.org/10.1007/s00705-002-0886-3>
 9. Direccion General de Vigilancia de la Salud. Paraguay. Boletín epidemiológico Semanal. 2018 [cited 2021 Mar 16]. http://dgvs.mspbs.gov.py/webdgvs/files/boletines/SE52_2018_Boletin.pdf
 10. Faria NR, Quick J, Claro IM, Thézé J, de Jesus JG, Giovanetti M, et al. Establishment and cryptic transmission of Zika virus in Brazil and the Americas. *Nature*. 2017;546:406–10. <https://doi.org/10.1038/nature22401>
 11. Giovanetti M, Faria NR, Lourenço J, Goes de Jesus J, Xavier J, Claro IM, et al. Genomic and epidemiological surveillance of Zika virus in the Amazon Region. *Cell Rep*. 2020;30:2275–2283.e7. <https://doi.org/10.1016/j.celrep.2020.01.085>
 12. Faria NR, Kraemer MUG, Hill SC, Goes de Jesus J, Aguiar RS, Iani FCM, et al. Genomic and epidemiological monitoring of yellow fever virus transmission potential. *Science*. 2018;361:894–9. <https://doi.org/10.1126/science.aat7115>
 13. Giovanetti M, de Mendonça MCL, Fonseca V, Mares-Guia MA, Fabri A, Xavier J, et al. Yellow fever virus re-emergence and spread in Southeast Brazil, 2016–2019. *J Virol*. 2019;94:e01623–19. <https://doi.org/10.1128/JVI.01623-19>
 14. Naveca FG, Claro I, Giovanetti M, de Jesus JG, Xavier J, Iani FCM, et al. Genomic, epidemiological and digital surveillance of chikungunya virus in the Brazilian Amazon. *PLoS Negl Trop Dis*. 2019;13:e0007065. <https://doi.org/10.1371/journal.pntd.0007065>
 15. Pereira Gusmão Maia Z, Mota Pereira F, do Carmo Said RF, Fonseca V, Gräf T, de Bruycker Nogueira F, et al. Return of the founder chikungunya virus to its place of introduction into Brazil is revealed by genomic characterization of exanthematic disease cases. *Emerg Microbes Infect*. 2019;9:53–7. <https://doi.org/10.1080/22221751.2019.1701954>
 16. Xavier J, Giovanetti M, Fonseca V, Thézé J, Gräf T, Fabri A, et al. Circulation of chikungunya virus East/Central/South African lineage in Rio de Janeiro, Brazil. *PLoS One*. 2019;14:e0217871. <https://doi.org/10.1371/journal.pone.0217871>
 17. Lanciotti RS, Kosoy OL, Laven JJ, Velez JO, Lambert AJ, Johnson AJ, et al. Genetic and serologic properties of Zika virus associated with an epidemic, Yap State, Micronesia, 2007. *Emerg Infect Dis*. 2008;14:1232–9. <https://doi.org/10.3201/eid1408.080287>
 18. Lanciotti RS, Calisher CH, Gubler DJ, Chang GJ, Vorndam AV. Rapid detection and typing of dengue viruses from clinical samples by using reverse transcriptase-polymerase chain reaction. *J Clin Microbiol*. 1992;30:545–51. <https://doi.org/10.1128/JCM.30.3.545-551.1992>
 19. Lanciotti RS, Kosoy OL, Laven JJ, Panella AJ, Velez JO, Lambert AJ, et al. Chikungunya virus in US travelers returning from India, 2006. *Emerg Infect Dis*. 2007;13:764–7. <https://doi.org/10.3201/eid1305.070015>
 20. Quick J, Grubaugh ND, Pullan ST, Claro IM, Smith AD, Gangavarapu K, et al. Multiplex PCR method for MinION and Illumina sequencing of Zika and other virus genomes directly from clinical samples. *Nat Protoc*. 2017;12:1261–76. <https://doi.org/10.1038/nprot.2017.066>
 21. Fonseca V, Libin PJK, Theys K, Faria NR, Nunes MRT, Restovic MI, et al. A computational method for the identification of dengue, Zika and chikungunya virus species and genotypes. *PLoS Negl Trop Dis*. 2019;13:e0007231. <https://doi.org/10.1371/journal.pntd.0007231>
 22. Katoh K, Kuma K, Toh H, Miyata T. MAFFT version 5: improvement in accuracy of multiple sequence alignment. *Nucleic Acids Res*. 2005;33:511–8. <https://doi.org/10.1093/nar/gki198>
 23. Larsson A. AliView: a fast and lightweight alignment viewer and editor for large datasets. *Bioinformatics*. 2014;30:3276–8. <https://doi.org/10.1093/bioinformatics/btu531>
 24. Nguyen LT, Schmidt HA, von Haeseler A, Minh BQ. IQ-TREE: a fast and effective stochastic algorithm for estimating maximum-likelihood phylogenies. *Mol Biol Evol*. 2015;32:268–74. <https://doi.org/10.1093/molbev/msu300>
 25. Rambaut A, Lam TT, Max Carvalho L, Pybus OG. Exploring the temporal structure of heterochronous sequences using TempEst (formerly Path-O-Gen). *Virus Evol*. 2016;2:vew007. <https://doi.org/10.1093/ve/vew007>
 26. Suchard MA, Lemey P, Baele G, Ayres DL, Drummond AJ, Rambaut A. Bayesian phylogenetic and phylodynamic data integration using BEAST 1.10. *Virus Evol*. 2018;4:vey016. <https://doi.org/10.1093/ve/vey016>
 27. Lemey P, Rambaut A, Drummond AJ, Suchard MA. Bayesian phylogeography finds its roots. *PLOS Comput Biol*. 2009;5:e1000520. <https://doi.org/10.1371/journal.pcbi.1000520>
 28. Leparc-Goffart I, Nougairède A, Cassadou S, Prat C, de Lamballerie X. Chikungunya in the Americas. *Lancet*. 2014;383:514. [https://doi.org/10.1016/S0140-6736\(14\)60185-9](https://doi.org/10.1016/S0140-6736(14)60185-9)
 29. Brady OJ, Golding N, Pigott DM, Kraemer MU, Messina JP, Reiner RC Jr, et al. Global temperature constraints on *Aedes aegypti* and *Ae. albopictus* persistence and competence for dengue virus transmission. *Parasit Vectors*. 2014;7:338. <https://doi.org/10.1186/1756-3305-7-338>
 30. Nunes MRT, Faria NR, de Vasconcelos JM, Golding N, Kraemer MU, de Oliveira LF, et al. Emergence and potential for spread of chikungunya virus in Brazil. *BMC Med*. 2015;13:102. <https://doi.org/10.1186/s12916-015-0348-x>
 31. de Bruycker-Nogueira F, Souza TMA, Chouin-Carneiro T, da Costa Faria NR, Santos JB, Torres MC, et al. DENV-1 genotype V in Brazil: spatiotemporal dispersion pattern reveals continuous co-circulation of distinct lineages until 2016. *Sci Rep*. 2018;8:17160. <https://doi.org/10.1038/s41598-018-35622-x>
 32. Direccion General de Vigilancia de la Salud. Paraguay. Boletín epidemiológico Semanal. 2019 [cited 2021 Mar 16]. http://dgvs.mspbs.gov.py/files/boletines/SE40_2019_Boletin.pdf
 33. Direccion General de Vigilancia de la Salud. Paraguay. Boletín epidemiológico Semanal, 2020 [cited 2021 Mar 16]. http://dgvs.mspbs.gov.py/files/boletines/SE40_2020_Boletin.pdf
 34. Obolski U, Perez PN, Villabona-Arenas CJ, Thézé J, Faria NR, Lourenço J. MVSE: an R-package that estimates a climate-driven mosquito-borne viral suitability index. *Methods Ecol Evol*. 2019;10:1357–70. <https://doi.org/10.1111/2041-210X.13205>
 35. Perez F, Llau A, Gutierrez G, Bezerra H, Coelho G, Ault S, et al. The decline of dengue in the Americas in 2017: discussion of multiple hypotheses. *Trop Med Int Health*. 2019;24:442–53. <https://doi.org/10.1111/tmi.13200>
 36. Priyamvada L, Quicke KM, Hudson WH, Onlamoon N, Sewatanon J, Edupuganti S, et al. Human antibody responses after dengue virus infection are highly cross-reactive to Zika virus. *Proc Natl Acad Sci U S A*. 2016;113:7852–7. <https://doi.org/10.1073/pnas.1607931113>
 37. Pérez-Guzmán EX, Pantoja P, Serrano-Collazo C, Hassert MA, Ortiz-Rosa A, Rodríguez IV, et al. Time elapsed between Zika

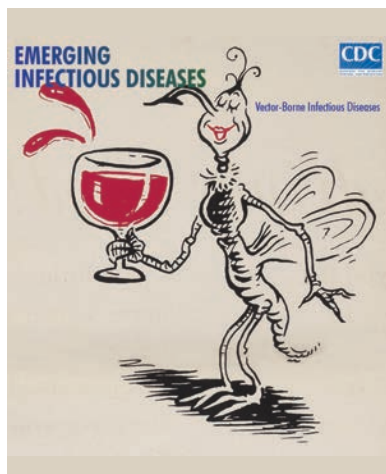
- and dengue virus infections affects antibody and T cell responses. *Nat Commun.* 2019;10:4316. <https://doi.org/10.1038/s41467-019-12295-2>
38. Mugabe VA, Borja LS, Cardoso CW, Weaver SC, Reis MG, Kitron U, et al. Changes in the dynamics of dengue incidence in South and Central America are possibly due to cross-population immunity after Zika virus epidemics. *Trop Med Int Health.* 2021;26:272–80.

Address for correspondence: Luiz Carlos Junior Alcantara, Laboratório de Flavivirus, Instituto Oswaldo Cruz, Fundação Oswaldo Cruz, Rio de Janeiro, RJ, Brazil; email: luiz.alcantara@ioc.fiocruz.br; Jairo Andrés Méndez Rico, Pan American Health Organization/World Health Organization, 525 23rd St NW, Washington, DC 20037, USA; email: ricoj@paho.org

February 2021

Vectorborne Infectious Diseases

- Childcare Exposure to Severe Acute Respiratory Syndrome Coronavirus 2 for 4-Year-Old Presymptomatic Child, South Korea
- Characteristics of Patients Co-infected with Severe Acute Respiratory Syndrome Coronavirus 2 and Dengue Virus, Buenos Aires, Argentina, March–June 2020
- Characteristics and Timing of Initial Virus Shedding in Severe Acute Respiratory Syndrome Coronavirus 2, Utah, USA
- Zika Virus–Associated Birth Defects, Costa Rica, 2016–2018
- *Plasmodium ovale wallikeri* and *P. ovale curtisi* Infections and Diagnostic Approaches to Imported Malaria, France, 2013–2018
- Symptom Profiles and Progression in Hospitalized and Nonhospitalized Patients with Coronavirus Disease, Colorado, USA, 2020
- Addressing COVID-19 Misinformation on Social Media Preemptively and Responsively
- Universal Admission Screening for SARS-CoV-2 Infections among Hospitalized Patients, Switzerland, 2020
- Excess Deaths during Influenza and Coronavirus Disease and Infection–Fatality Rate for Severe Acute Respiratory Syndrome Coronavirus 2, the Netherlands
- Murine Typhus in Canary Islands, Spain, 1999–2015



- Rapid Transmission of Severe Acute Respiratory Syndrome Coronavirus 2 in Detention Facility, Louisiana, USA, May–June, 2020
- Plasma MicroRNA Profiling of *Plasmodium falciparum* Biomass and Association with Severity of Malaria Disease
- Increasing Incidence of Invasive Group A *Streptococcus* Disease in First Nations Population, Alberta, Canada, 2003–2017
- Outbreak of Severe Vomiting in Dogs Associated with a Canine Enteric Coronavirus, United Kingdom
- Spread of Multidrug-Resistant *Rhodococcus equi*, United States
- SARS-CoV-2 Infections among Recent Organ Recipients, March–May 2020, United States
- *Plasmodium falciparum* Histidine-Rich Protein 2 and 3 Gene Deletions in Strains from Nigeria, Sudan, and South Sudan
- Hepatitis C Virus Transmission Clusters in Public Health and Correctional Settings, Wisconsin, USA, 2016–2017
- Prolonged Maternal Zika Viremia as a Marker of Adverse Perinatal Outcomes
- Use of Commercial Claims Data for Evaluating Trends in Lyme Disease Diagnoses, United States, 2010–2018
- Highly Pathogenic Avian Influenza A(H5N8) Virus Spread by Short- and Long-Range Transmission, France, 2016–17
- Emergence of Lyme Disease on Treeless Islands, Scotland, United Kingdom
- SARS-CoV-2 Transmission between Mink (*Neovison vison*) and Humans, Denmark
- Shuni Virus in Cases of Neurological Disease in Humans, South Africa
- SARS-CoV-2 Transmission between Mink (*Neovison vison*) and Humans, Denmark
- Effects of Social Distancing Measures during the First Epidemic Wave of Severe Acute Respiratory Syndrome Coronavirus 2, Greece

**EMERGING
INFECTIOUS DISEASES**

To revisit the February 2021 issue, go to:
<https://wwwnc.cdc.gov/eid/articles/issue/27/2/table-of-contents>

Monitoring SARS-CoV-2 Circulation and Diversity through Community Wastewater Sequencing, the Netherlands and Belgium

Ray Izquierdo-Lara, Goffe Elsinga, Leo Heijnen, Bas B. Oude Munnink, Claudia M.E. Schapendonk, David Nieuwenhuijse, Matthijs Kon, Lu Lu, Frank M. Aarestrup, Samantha Lycett, Gertjan Medema,¹ Marion P.G. Koopmans,¹ Miranda de Graaf¹

Severe acute respiratory syndrome coronavirus 2 (SARS-CoV-2) has rapidly become a major global health problem, and public health surveillance is crucial to monitor and prevent virus spread. Wastewater-based epidemiology has been proposed as an addition to disease-based surveillance because virus is shed in the feces of ~40% of infected persons. We used next-generation sequencing of sewage samples to evaluate the diversity of SARS-CoV-2 at the community level in the Netherlands and Belgium. Phylogenetic analysis revealed the presence of the most prevalent clades (19A, 20A, and 20B) and clustering of sewage samples with clinical samples from the same region. We distinguished multiple clades within a single sewage sample by using low-frequency variant analysis. In addition, several novel mutations in the SARS-CoV-2 genome were detected. Our results illustrate how wastewater can be used to investigate the diversity of SARS-CoV-2 viruses circulating in a community and identify new outbreaks.

Since its discovery, severe acute respiratory syndrome coronavirus 2 (SARS-CoV-2) has caused >100 million confirmed cases of coronavirus disease (COVID-19). The global effects of SARS-CoV-2 and the need to learn more about its origin and epidemiology have resulted in the sequencing of >416,000 genomes as of January 2021 (1). This work has enabled the identification of groups of viruses that, on

the basis of their genetic diversity, can be associated with geographic and temporal patterns of virus spread (2). Nextstrain (<https://nextstrain.org>) currently divides SARS-CoV-2 diversity into 12 major global clades (19A, 19B, and 20A–20J), on the basis of high prevalence, signature mutations, and geographic spread (3).

Although SARS-CoV-2 primarily affects respiratory tract tissues, it can also replicate in the gastrointestinal tract, as evidenced by *in vitro* infection of enteroids (4), presence of viral proteins in gastrointestinal epithelium biopsy specimens (5), and detection of infectious virus in stool samples (6). Viral RNA is shed in the feces of ~40% of infected persons, often for longer periods than the virus can be detected in nasal swab specimens. SARS-CoV-2 RNA has been detected in urine occasionally (<5% of infected patients) (7–9).

Because of the rapid spread of SARS-CoV-2, individual screening of clinical cases and study of viral diversity on a population level are challenging. Various reports have demonstrated that enteric and respiratory viruses can be detected in wastewater (10–18). This finding has led to the recognition of wastewater-based epidemiology as a potentially valuable tool to assess the spread of the disease at a community level. Recently, the Water Research Institute in the Netherlands and other groups have demonstrated temporal correlations between SARS-CoV-2 RNA titers in sewage and the number of reported cases in a city or county when ≥ 26 gene copies per liter could be detected (14,19–21). Therefore, sewage testing is currently considered globally to be an adjunct to patient-based surveillance and demonstrates promise as an early warning indicator of increasing virus circulation.

Author affiliations: Erasmus University Medical Center, Rotterdam, the Netherlands (R. Izquierdo-Lara, B.B. Oude Munnink, C.M.E. Schapendonk, D. Nieuwenhuijse, M. Kon, M.P.G. Koopmans, M. de Graaf); KWR Water Research Institute, Nieuwegein, the Netherlands (G. Elsinga, L. Heijnen, G. Medema); University of Edinburgh, Edinburgh, Scotland, UK (L. Lu, S. Lycett); Technical University of Denmark, Kongens Lyngby, Denmark (F.M. Aarestrup)

¹These senior authors contributed equally to this article.

DOI: <https://doi.org/10.3201/eid2705.204410>

Enhanced surveillance is a key pillar of the current strategy to control the spread of SARS-CoV-2 and includes frequently testing mildly symptomatic persons, investigating infection clusters to identify possible common exposures, and monitoring hospital admission rates. Whole-genome sequencing of SARS-CoV-2 from clinical samples has been adopted as an additional tool to identify clusters. Particularly in geographic areas with minimal virus circulation, sequencing can help identify possible sources, provided that sufficient background sequencing has been performed. So far, little work has been done to correlate SARS-CoV-2 diversity in sewage samples with diversity in patients (22,23). We used next-generation sequencing (NGS) of SARS-CoV-2 from wastewater samples to assess whether these samples reflect the diversity of SARS-CoV-2 circulating within the population of the Netherlands and Belgium.

Methods

Sample Preparation

Wastewater specimens were collected as 24-h flow-dependent composite samples and processed as previously described (14). Debris of 100–200 mL of sewage samples was pelleted and the supernatant was concentrated by using 100 kDa Centricon ultrafilters (Millipore Sigma, <https://www.emdmillipore.com>); *in vitro*-transcribed dengue virus type-2 RNA was added as an internal extraction control. RNA was extracted by using the Nuclisens kit (bio-Mérieux, <https://www.biomerieux.com>) and King-Fisher purification system (Thermo Fisher Scientific, <https://www.thermofisher.com>) (14). RNA was screened by quantitative reverse transcription PCR (qRT-PCR) with 5 primer–probe sets targeting the SARS-CoV-2 nucleocapsid (N) gene (N1–N3) (24), envelope (E) gene for all sarbecoviruses (25), and the internal control.

NGS

We performed SARS-CoV-2-specific multiplex PCR for nanopore sequencing as described previously (26). Primers for 89 overlapping amplicons spanning the genome were used in 2 PCR pools. Libraries were generated by using the Oxford Nanopore native barcode kits (Oxford Nanopore Technologies, <https://nanoporetech.com>) and sequenced on a R9.4 flow cell.

Illumina sequencing was performed as described previously (27). Amplicons were generated by the multiplex PCR described previously. Amplicons were purified with 0.8X AMPure XP beads (Beckman Coulter, <https://www.beckmancoulter.com>)

and 100 ng of DNA was converted into paired-end Illumina sequencing libraries by using the KAPA HyperPlus library preparation kit (Roche, <https://www.roche.com>). We used the KAPA Unique Dual-Indexed Adapters Kit (Roche) to enable subsequent sequencing of multiple libraries in a single Illumina MiSeq version 3 flowcell (2 × 300 cycles) (Illumina, <https://www.illumina.com>).

Nanopore Sequence Analysis

Raw sequence data were processed as previously described (26). We used a snakemake script to demultiplex fastq raw reads by using Porechop (<https://github.com/rrwick/Porechop>), to trim primers by using Cutadapt (28), and to perform a reference-based alignment by using minimap2 to GISAID sequence EPI_ISL_412973 (<https://www.gisaid.org>). The run was monitored by using RAMPART (<https://artic-network.github.io/rampart>). The consensus genome was extracted by using 2 analyses for which positions with a coverage <10X or <30X were replaced with an N. We confirmed mutations in the genome by manually checking the alignment in Ugene (29) and resolved homopolymeric regions by consulting reference genomes. On the basis of previous studies (30), we considered mutations with >30X coverage high quality, whereas mutations $\geq 10X$ and $\leq 30X$ coverage were considered low quality.

Illumina Sequence Analysis

We used a customized Galaxy workflow (31) for all processing, reference-based alignment, and variant analysis. Raw sequencing reads were filtered by using Fastp (32) to remove adaptor contamination, ambiguous bases, low quality reads (Phred score <30), and fragments <50 nt. Reads were mapped against GISAID sequence EPI_ISL_412973 by using the default settings of BWA-MEM (H. Li, unpub. data, <https://arxiv.org/abs/1303.3997>). Reads were realigned by using the leftalign utility from FreeBayes (E. Garrison, unpub. data, <https://arxiv.org/abs/1207.3907>). All reads with mapping scores of <30 were discarded. Consensus sequences and variants were generated by using iVar (33). Final consensus sequences (frequency >50%) were constructed by using all mapped reads with a coverage of >5X and Phred score of >30. For detection of low-frequency variants (LFVs), we used parameters as follows: minimum coverage of 50X, Phred score >30, and a minimum frequency threshold of 10%. Variant calling was confirmed by manual inspection of the aligned reads in Ugene (29). Variant positions are given with respect to the Wuhan-Hu-1 strain (MN908947) (34). We uploaded all consensus

sequences with coverage >50% to GISAID (accession nos. EPI_ISL_539300–25).

Phylogenetic Analysis

The first dataset included all full-length SARS-CoV-2 genomes from the Netherlands (1,544 genomes) and Belgium (888 genomes) from GISAID as of July 8, 2020. The second dataset was a subsample representative of the global diversity of all SARS-CoV-2 sequences in GISAID as of June 1, 2020. This global dataset contained 2,552 subsampled sequences (full length with Ns <5%) to include 1 unique genome per country or state per week. We aligned sequences with >75% genome coverage by using MAFFT (<https://mafft.cbrc.jp/alignment/server>) and inferred maximum-likelihood trees by using the best predicted models general time-reversible plus F plus R3 (global subsample) and general time-reversible plus F plus R2 (Netherlands-Belgium dataset) and bootstrap with 1,000 replicates. Trees were visualized by using Figtree version 1.4.4 (<http://tree.bio.ed.ac.uk/software/figtree>). Clades were assigned by using the Nextclade tool.

Results

Correlation between qRT-PCR and Percentage of Genome Recovered

Previously, sewage samples collected from 6 locations in the Netherlands (and Schiphol Airport) were tested by qRT-PCR to investigate the levels of SARS-CoV-2 RNA (14). To further investigate the genetic diversity of SARS-CoV-2, we subjected 55 wastewater samples obtained from 13 locations in the Netherlands (48 samples) and 7 locations in Belgium (7 samples) with cycle threshold (C_t) values of <36 to whole-genome sequencing by using nanopore technology. The wastewater treatment plants in the Netherlands served \approx 200,000–980,000 inhabitants; Schiphol was estimated to serve 54,000 persons (14). The samples covered a period of 70 days (March 25–June 3, 2020); of all 55 samples, 2 (Franeker-92719 and AmsterdamWest-92852) were sequenced by nanopore twice. Of the 55 samples, 24 were also sequenced by Illumina (Table 1).

We used 4 primer–probe sets targeting the N (N1–N3) genes and E gene to evaluate the concentration of SARS-CoV-2 in sewage samples (Table 1) (14). The percentage of the genome covered by the assembly of nanopore reads (>10X coverage) ranged from 0% to 99.2%. We found an inverse sigmoidal correlation between the percentage of the genome assembled from nanopore sequencing reads and the N and E gene C_t values (Figure 1). The C_t values at

which half of the genome could be obtained were 34.6 for N1, 33.8 for N2, 33.2 for N3, and 32.5 for E. No correlation was observed between C_t values and the percentage of the genome assembled from Illumina reads (Appendix Figure 1, <https://wwwnc.cdc.gov/EID/article/27/5/20-4410-App1.pdf>).

Consensus Sequences

We performed phylogenetic analysis to assess whether consensus sequences from sewage could be associated with clinical samples from the same region. A total of 22 genomes (20 from nanopore and 2 from Illumina runs) with a coverage >75% of the genome were obtained from 20 samples. We used these sequences to infer a maximum-likelihood tree using all sequences from the Netherlands and Belgium available in GISAID and a maximum-likelihood tree using a subset representative of the global diversity of SARS-CoV-2 in GISAID. In general, the sequences from the Netherlands and Belgium grouped into 5 clades (Figure 2, panel A), and most of the sequences belonged to clade 20A (52.0% for the Netherlands and 47.7% for Belgium). The clades 19B and 20C were less prevalent; 8.9% of sequences from the Netherlands belonged to 19B and 1.2% to 20C, whereas 10.4% of Belgium sequences belonged to 19B and 0.3% to 20C. Both trees showed that sewage samples grouped within clades 19A, 20A, and 20B (Figure 2). Samples Franeker-92719 and HeeswijkDinther-92499 clustered with sequences isolated from patients from the same region (Figure 2, panel A), indicating that sewage samples can be linked to specific outbreaks. Included in the phylogenetic trees were 2 samples with 2 consensus sequences (AmsterdamWest-92852 and Franeker-92719), which demonstrated 2-mutation differences between consensus sequences of the same sample (Appendix Table 1). Despite this discrepancy, consensus sequences from the same sample clustered within the same clade (Appendix Figures 2, 3). Some sequences clustered close to the root of the tree, probably because of the presence of multiple strains within 1 sample, which resulted in a combination of mutations in their consensus sequences.

To associate samples with a particular clade or cluster, we compared all consensus sequences, including partial sequences, with the Wuhan-Hu-1 reference isolate. A total of 145 single-nucleotide polymorphisms (SNPs) were detected in our dataset (Appendix Table 1). Of these, 24 SNPs were detected in >1 sequence. We also detected SNPs in the Netherlands sewage sequences with a geographic regional signal, which were present in the Netherlands clinical samples at much higher frequencies than in global or

Belgium clinical samples, such as T514C and C1594T (Appendix Table 2).

Finding clade-defining mutations in the consensus sequence suggests the dominance of a certain

Table 1. Overview of SARS-CoV-2 wastewater samples sequenced during study of circulation and diversity through community wastewater sequencing, the Netherlands and Belgium*

Sample no.	Sample ID	Date	Country	Sampling location	Target Ct†				Coverage, %	
					N1	N2	N3	E	Nanopore	Illumina
1	92499	2020 Mar 25	Netherlands	Heeswijk-Dinther	32.9	32.1	30.7	30.8	94.4	ND
2	92502	2020 Mar 25	Netherlands	Apeldoorn	36.6	34.9	33.2	33.3	74.9	19.4
3	92503	2020 Mar 25	Netherlands	Amersfoort	34.9	33.1	31.8	32.1	87.8	ND
4	92504	2020 Mar 25	Netherlands	Utrecht	31.8	30.9	29.8	29.9	95.2	ND
5	92505	2020 Mar 25	Netherlands	Utrecht Overvecht	32.3	31.1	30.1	30.1	92.4	ND
6	92506	2020 Mar 25	Netherlands	Schiphol	32.7	32.0	30.8	30.7	92.2	65.6
7	92508	2020 Mar 25	Netherlands	Amsterdam West	31.8	30.7	29.7	29.9	97.0	ND
8	92509	2020 Mar 25	Netherlands	Tilburg	33.0	32.2	31.2	31.0	78.8	65.5
9	92719	2020 Mar 30	Netherlands	Franeker	31.8	30.8	31.2	30.7	97.7/50.9‡	78.2
10	92721	2020 Mar 30	Netherlands	Beverwijk	32.6	31.4	31.8	30.8	93.7	47.7
11	92722	2020 Mar 30	Netherlands	Katwoude	32.9	32.6	32.7	31.4	84.6	53.9
12	92723	2020 Mar 30	Netherlands	Wervershoof	33.1	32.3	32.5	31.1	96.6	43.2
13	92848	2020 Apr 1	Netherlands	Amersfoort	33.6	32.1	32.3	31.6	96.6	39.4
14	92849	2020 Apr 1	Netherlands	Utrecht	32.4	31.4	31.8	30.6	57.8	48.5
15	92851	2020 Apr 1	Netherlands	Schiphol	33.7	33.1	33.4	32.3	89.4	53.5
16	92852	2020 Apr 1	Netherlands	Amsterdam West	31.8	30.6	30.9	29.9	99.2/97.1‡	59.1
17	92853	2020 Apr 1	Netherlands	Tilburg	33.5	32.6	32.6	32.0	91.2	ND
18	92943	2020 Apr 2	Belgium	Langemark	33.2	33.3	33.1	32.2	60.3	ND
19	92947	2020 Apr 2	Belgium	Lo-Reninge	34.6	34.2	34.5	33.4	71.3	ND
20	92949	2020 Apr 2	Belgium	Properinge	34.5	33.4	33.4	32.4	65.6	65.6
21	92965	2020 Apr 2	Netherlands	Delft	32.9	32.9	32.9	31.5	91.7	52.4
22	93030	2020 Apr 5	Belgium	Aartselaar	33.2	32.4	31.6	31.4	89.9	61.2
23	93032	2020 Apr 5	Belgium	Gent	34.2	33.7	32.6	32.1	63.2	46.9
24	93034	2020 Apr 5	Belgium	Leuven	33.6	33.4	32.1	31.4	70.2	37.6
25	93036	2020 Apr 5	Belgium	Tienen	33.3	32.6	31.2	30.8	88.1	41.5
26	93818	2020 Apr 8	Netherlands	Amersfoort	34.9	34.3	33.4	32.4	37.5	ND
27	93820	2020 Apr 9	Netherlands	Utrecht	32.8	32.2	31.2	30.8	55.2	ND
28	93822	2020 Apr 9	Netherlands	Amsterdam West	32.6	25.1	31.6	30.9	87.3	ND
29	93823	2020 Apr 9	Netherlands	Schiphol	33.0	33.2	32.2	31.3	67.3	43.5
30	93825	2020 Apr 8	Netherlands	Delft	33.9	33.7	32.7	32.0	63.9	64.3
31	93828	2020 Apr 9	Netherlands	Tilburg	35.2	34.6	33.1	32.7	31.2	ND
32	93948	2020 Apr 14	Netherlands	Heeswijk-Dinther	35.8	34.6	33.6	32.7	18.8	ND
33	93950	2020 Apr 15	Netherlands	Wervershoof	34.9	34.3	33.1	32.5	60.7	ND
34	94330	2020 Apr 21	Netherlands	Utrecht1	35.1	34.4	33.2	33.5	41.7	ND
35	94331	2020 Apr 21	Netherlands	Utrecht2	35.7	34.1	34.2	33.7	38.6	ND
36	94334	2020 Apr 21	Netherlands	Amsterdam West	34.0	33.3	32.4	32.0	66.7	ND
37	94335	2020 Apr 21	Netherlands	Schiphol	33.8	34.1	32.9	33.7	40.1	43.0
38	94337	2020 Apr 21	Netherlands	Delft	35.7	34.1	34.1	33.8	34.2	ND
39	94339	2020 Apr 21	Netherlands	Tilburg	34.8	35.4	34.7	36.0	11.2	80.3
40	94602	2020 Apr 29	Netherlands	Utrecht	35.6	34.3	33.0	34.2	29.6	ND
41	94604	2020 Apr 29	Netherlands	Amsterdam West	34.9	34.6	32.8	33.6	15.0	ND
42	94605	2020 Apr 29	Netherlands	Schiphol	34.6	35.1	33.6	33.2	21.3	35.2
43	94607	2020 Apr 25	Netherlands	Delft	35.8	36.2	34.4	34.0	15.3	ND
44	94976	2020 May 7	Netherlands	Utrecht	35.5	36.0	35.1	33.5	6.3	ND
45	94978	2020 May 7	Netherlands	Amsterdam West	35.0	34.8	34.5	33.7	19.8	ND
46	94982	2020 May 6	Netherlands	Delft	35.1	35.9	34.7	33.7	18.7	ND
47	95550	2020 May 13	Netherlands	Utrecht	ND	34.4	ND	32.0	3.0	ND
48	95552	2020 May 13	Netherlands	Amsterdam West	ND	34.2	ND	32.8	20.4	ND
49	95556	2020 May 12	Netherlands	Delft	ND	34.4	ND	34.1	0	ND
50	95558	2020 May 13	Netherlands	Tilburg	ND	34.3	ND	36.1	0	ND
51	95793	2020 May 19	Netherlands	Utrecht	ND	35.1	ND	34.9	0	ND
52	95794	2020 May 19	Netherlands	Amsterdam West	ND	35.1	ND	34.2	7.7	ND
53	96925	2020 Jun 2	Netherlands	Utrecht	ND	35.2	ND	37.1	0	ND
54	96927	2020 Jun 2	Netherlands	Schiphol	ND	32.5	ND	31.1	30.8	34.0
55	97044	2020 Jun 3	Netherlands	Delft	ND	35.7	ND	33.5	8.2	ND

*Ct, cycle threshold; E, envelope; N, nucleocapsid; ND, not determined; SARS-CoV-2, severe acute respiratory syndrome coronavirus 2.

†Three primer-probe sets targeting the N1–N3 genes and 1 targeting the E gene.

‡These samples were sequenced twice.

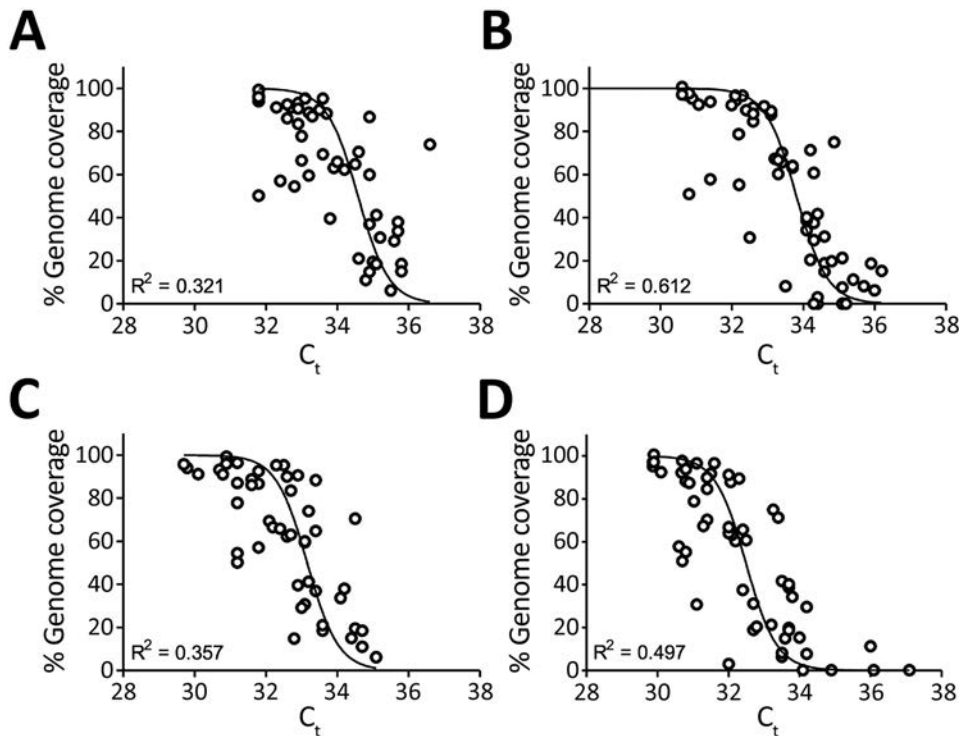


Figure 1. Quantitative reverse transcription PCR C_t of severe acute respiratory syndrome coronavirus 2 RNA in sewage samples as determined by N gene (N1–N3) and E gene assays against the percentage of genome covered (>10×) by nanopore reads, the Netherlands and Belgium. A) N1 gene; B) N2 gene; C) N3 gene; D) E gene. C_t, cycle threshold.

clade within a sample; the presence of these mutations can also aid in the detection of virus mixtures in a sample. During the period of wastewater-sample collection, Nextstrain defined 5 major clades (19A, 19B, 20A, 20B, and 20C). Each clade is defined by the presence of ≥ 2 linked mutations. Clade 19A is the root clade and contains the Wuhan-Hu-1 reference sequence. Both 19B and 20A emerged from 19A, where 2 and 3 linked mutations define these major clades: T28144C and C8782T define 19B; and C3037T, C14408T, and A23403G define 20A. Clades 20B and 20C emerged from 20A, where the trinucleotide substitution GGG28881–28883AAC defines 20B and the linked mutations C1059T and G25563T define 20C. Nucleotide substitution A23403G, a signature mutation of clades 20A, 20B, and 20C that generates the D614G amino-acid substitution in the S glycoprotein, was detected in 83.6% (51/61) of the samples that were sequenced at this region (Appendix Table 1). The GGG28881–28883AAC substitution was detected in 41.9% (18/43) of the sequences. One of the 2 mutations defining the low-prevalence clades 20C and 19B (C1059T and T28144C) was found in 2 and 3 consensus sequences. However, these sequences could not be assigned to these clades because regions containing the additional clade-defining mutations were not sequenced with sufficient coverage. The hCoV-19/Netherlands/Amersfoort-92503-N/2020 sequence contained a mix of clade-defining mutations: C1059T,

which defines 20C; T28144C, which defines 19B; and GGG28881–28883AAC, which defines 20B. This finding indicates that the obtained consensus sequence does not represent a single strain.

In addition to the clade-defining mutations, we detected 49 and 63 SNPs that were not present in either the Netherlands (1,544 sequences) or Belgium (888 sequences) datasets but were seen in the global dataset (55,074 sequences), although with <1% prevalence (Appendix Table 2). Moreover, we detected 51 novel mutations in sewage consensus sequences that were not previously reported, of which 48 were supported by coverage above the thresholds set for high quality (coverage >30× for Nanopore and coverage >5× and Phred score >30 for Illumina). Discrepancies between consensus sequences of the same sewage sample can occur. AmsterdamWest-92852 was sequenced 3 times and 4 positions varied (Appendix Table 1). These differences are explained by the presence of variant sites in a single sample in similar percentages, which resulted in differences in consensus sequences between sequencing runs.

LFV Analysis

Given that sewage samples are likely to contain a mixture of SARS-CoV-2 strains, we performed a variant analysis with Illumina data to distinguish multiple strains within single samples. By using a coverage >50×, Phred score >30, and a frequency threshold of

>10% as settings, we found 21 positions with at least 1 sample containing major and minor variants (Table 2). Of these, 14 mutations resulted in changes at the amino acid level (12 nonsynonymous mutations and 2 deletions). Of note, 8 of these (4497C, 10514C, 11484T, 13046A, 16538_16540delATA, 16777T, 16823T, and 28736A) are novel mutations that did not

appear in the Netherlands–Belgium or global datasets. The other 7 variants appeared but demonstrated low prevalence in both datasets (0.002%–0.130%). The most prominent of these was the 28139A mutation in a wastewater sample from March, which was detected in only 4 sequences worldwide and demonstrated both a strong temporal (all detected in March 2020)

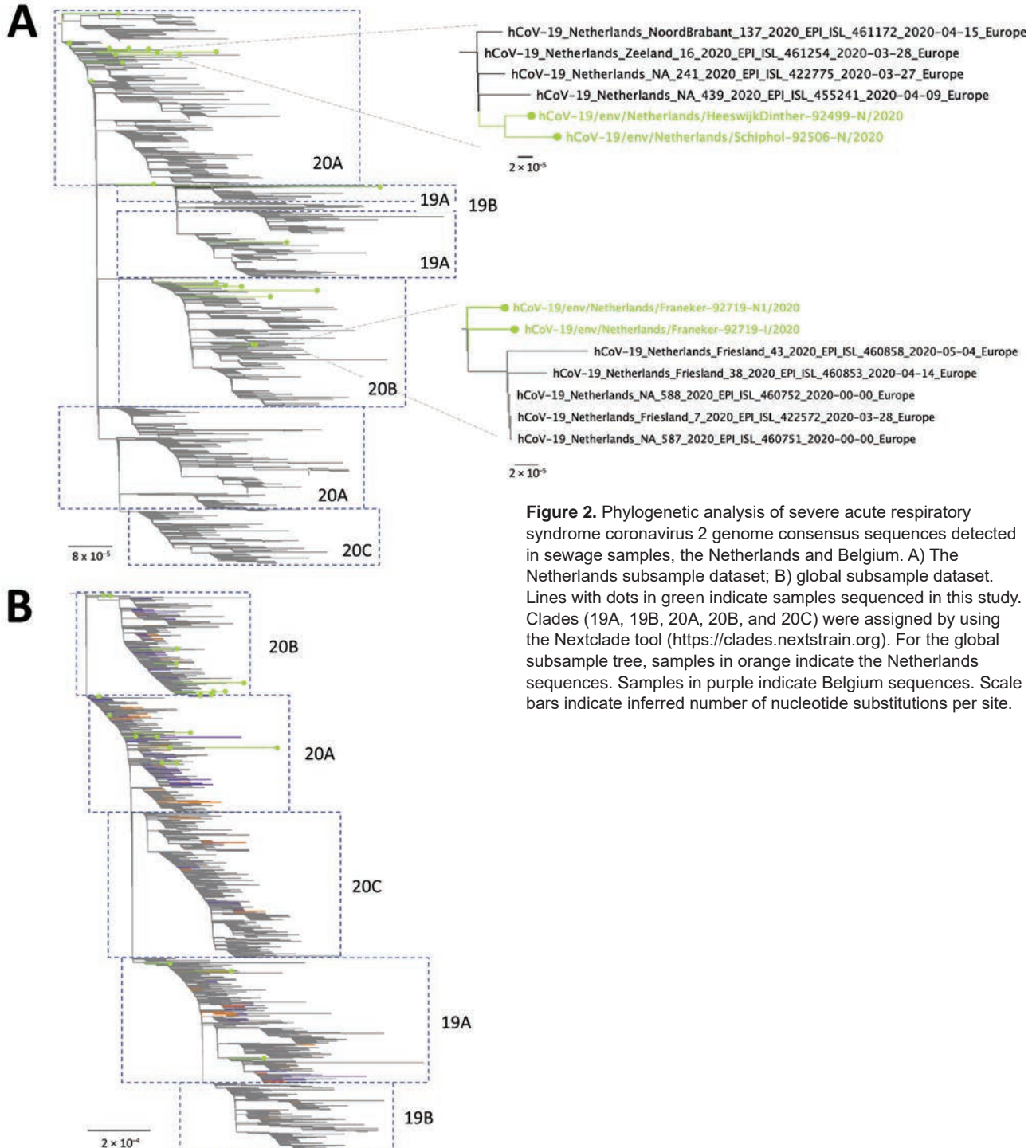


Figure 2. Phylogenetic analysis of severe acute respiratory syndrome coronavirus 2 genome consensus sequences detected in sewage samples, the Netherlands and Belgium. A) The Netherlands subsample dataset; B) global subsample dataset. Lines with dots in green indicate samples sequenced in this study. Clades (19A, 19B, 20A, 20B, and 20C) were assigned by using the Nextclade tool (<https://clades.nextstrain.org>). For the global subsample tree, samples in orange indicate the Netherlands sequences. Samples in purple indicate Belgium sequences. Scale bars indicate inferred number of nucleotide substitutions per site.

Table 2. Summary of LFVs detected in wastewater samples determined by Illumina sequencing in study of SARS-CoV-2 circulation and diversity through community wastewater sequencing, the Netherlands and Belgium*

Position†	Sample	MV	LFV	LFV, %	Total depth	Feature	AA	MV	LFV	Frequency, %‡		
										NL	BE	Global
1440	NL/Schiphol-92506-I	G	A	13.2	53	ORF1a	G	N	N	1.619	4.167	1.903
3549	NL/Franeker-92719-I	GACCACTTA	-\$	46.8	201	ORF1a	GPLK	E	E	0	0	0
4497	NL/Beverwijk-92721-I	T	C	42.6	479	ORF1a	I	T	T	0	0	0.000
10514	NL/AmsterdamWest-92852-I	T	C	12.5	1,656	ORF1a	Y	H	H	0	0	0
10933	BE/Aartselaar-93030-I	C	T	18.0	50	ORF1a	P	P	P	100.000	100.000	99.996
	NL/Tilburg-94339-I	T	C	11.1	63	ORF1a	P	P	P	0	0	0.004
11083	BE/Properinge-92949-I	G	T	12.1	58	ORF1a	L	F	F	5.635	7.320	11.007
	BE/Aartselaar-93030-I	T	G	26.4	129	ORF1a	F	L	L	94.430	92.680	88.069
	NL/Tilburg-94339-I	G	T	12.7	150	ORF1a	L	F	F	5.635	7.320	11.007
11109	NL/AmsterdamWest-92852-I	C	T	48.3	230	ORF1a	A	V	V	15.220	0.338	0.534
	NL/Tilburg-94339-I	C	T	21.2	66	ORF1a	A	V	V	15.220	0.338	0.534
11484	NL/Beverwijk-92721-I	C	T	44.0	84	ORF1a	A	V	V	0	0	0
11494	NL/Franeker-92719-I	C	T	13.5	104	ORF1a	N	N	N	0	0	0.002
	BEAartselaar-93030-I	C	T	43.5	370	ORF1a	N	N	N	0	0	0.002
	NL/Tilburg-94339-I	C	T	13.8	247	ORF1a	N	N	N	0	0	0.002
13046	BE/Aartselaar-93030-I	C	A	36.7	98	ORF1a	P	T	T	0	0	0
13426	BE/Gent-93032-I	C	T	22.6	115	ORF1a	R	R	R	0	0	0.038
16538	BE/Gent-93032-I	-	ATA	27.6	348	ORF1b	-	N	N	100.000	100.000	100.000
16777	NL/Schiphol-92851-I	G	T	30.2	404	ORF1b	V	F	F	0	0	0
16806	NL/Tilburg-94339-I	C	A	22.1	77	ORF1b	N	K	K	0	0	0.016
16823	BE/Aartselaar-93030-I	G	T	12.0	192	ORF1b	G	V	V	0	0	0
24862	NL/Katwoude-92722-I	A	G	34.0	53	S	T	T	T	8.614	0.338	0.463
28115	NL/Delft-92965-I	T	C	47.8	67	ORF8	I	I	I	100.000	100.000	99.993
28139	NL/Tilburg-94339-I	C	A	36.0	136	ORF8	S	S	S	0.130	0.113	0.007
28375	NL/Tilburg-94339-I	G	A	30.8	146	N	G	G	G	0	0	0.002
28394	NL/AmsterdamWest-92852-I	C	T	31.5	54	N	R	W	W	0	0	0.004
	BE/Properinge-92949-I	C	T	16.7	60	N	R	W	W	0	0	0.004
	NL/Tilburg-94339-I	C	T	13.6	191	N	R	W	W	0	0	0.004
28736	BE/Leuven-93034-I	A	G	22.0	363	N	A	T	T	100.000	100.000	100.000

*BE, Belgium; LFV, low-frequency variant; MV, major variant; NL, Netherlands; SARS-CoV-2, severe acute respiratory syndrome coronavirus 2.

†Positions are given with respect to Wuhan-Hu-1 (GenBank accession no. MN908947).

‡Frequency of the LFV of sample against GISAID database (as of July 8, 2020) of the Netherlands, Belgium, and global samples.

§Dashes represent a gap at the given region, either as a MV or LFV.

and regional signal (2 sequences from the Netherlands [EPI_ISL_422640 and EPI_ISL_422880], 1 from Denmark [EPI_ISL_444879], and 1 from Belgium [EPI_ISL_458209]).

Finally, 4 variants (1440A, 11083T, 11109T, and 24862G) appeared at higher levels in both datasets (>0.5%); 11109T and 24862G were 28.5 and 14.3 times more prevalent in the Netherlands dataset than in the global dataset (Table 2). The other variants appeared at similar frequencies in all datasets.

In addition to consensus sequences, LFV analysis is of value for identifying potential local outbreaks. This identification could be achieved by detecting cluster-defining mutations that are associated with sequences from a particular geographic area. To associate the presence of a minor variant to sequences belonging to unique clusters, we mapped the 4 most prevalent LFVs onto the Netherlands-Belgium subsample and global subsample phylogenetic trees (Figure 3). For 3 variants (1440A, 11109T, and 24862G),

the presence of the mutation and their clustering on the phylogenies were clearly associated. However, when 1 of these 3 variants was detected as an LFV in a sewage sample, the consensus sequence of this sample did not group with the cluster of clinical samples that contains the variant. For example, the 24862G variant in sample Tilburg-94339 was detected in 2 unique clusters within clade 20A, whereas its consensus sequence (hCoV-19/env/Netherlands/Tilburg-94339-I/2020) clustered within clade 20B, suggesting the presence of both clades in this sample. Although mutation 11083T was most prevalent in clade 19A, it was also scattered along the trees, indicating poor association with a particular clade.

Discussion

The use of wastewater sampling as a tool to learn more about the epidemiology and diversity of SARS-CoV-2 at a community level offers many advantages over human sampling. Sewage samples are relatively easy to

collect, sampling bias toward severe cases does not occur, ethical issues are limited, and potentially fewer samples are required to determine temporal changes of viral infections in the community (35,36). Nevertheless, comprehensive comparisons with clinical surveillance are required to determine the extent and limits of using sewage as a surveillance or early-warning tool.

We used nanopore and Illumina NGS analysis to study the diversity of SARS-CoV-2 in sewage and compared these results to the viral diversity found in clinical samples. To evaluate this diversity in a comprehensive fashion, we used the Nextstrain clade classification system because it is based on the use of signature mutations to assign sequences to a clade (3), enabling the association of SNPs or LFV to a particular clade, especially for genome sequences with <75% coverage.

Our method enabled us to obtain complete or near-complete genomes from wastewater samples with C_t values of ≥ 5 C_t s below the limit of detection and partial genomes for samples with higher C_t values. To increase the percentage of genome covered, a threshold of 10 \times coverage per position was used to generate consensus sequences from nanopore reads. The error rate with this threshold is <0.03%, and most of the mutations (132/145) listed have a coverage of >30 \times , which produces an error rate of 1/585,000 nt (30).

Of note, we found sewage samples that clustered with sequences isolated from patients of the same region and LFV with a strong regional signal. In a recent

study from the United States, wastewater contained SARS-CoV-2 genomes identical to those in clinical samples from the same region (37). Sewage samples can contain a mixture of SARS-CoV-2 viruses, which can be an indication of multiple viruses circulating within a community and perhaps in domestic and livestock animals (38–42). We applied a targeted amplification method and thus did not assess the presence of other viruses. Consensus sequence genomes from a wastewater sample can identify the predominant virus strain in a population, which is suitable for locations with few introductions of the virus (22,23). However, this approach is not appropriate for a population in which multiple virus strains are circulating in parallel. Moreover, it might lead to artificial consensus genomes that do not represent an existing virus.

NGS analysis can unravel the diversity of viruses within a complex sample such as wastewater, particularly by using unbiased sequencing of the sewage virome (43). Nevertheless, the detection of variants of a virus in a single sample can be challenging because of the relatively low number of reads obtained for each virus. Targeted amplification and NGS of a small genome region of the virus of interest to determine the prevalence of virus variants within a single wastewater sample is more sensitive and less expensive; use of this approach has been reported for enteroviruses, human mastadenoviruses, and noroviruses (12,18,44). Because the diversity of SARS-CoV-2 is still limited,

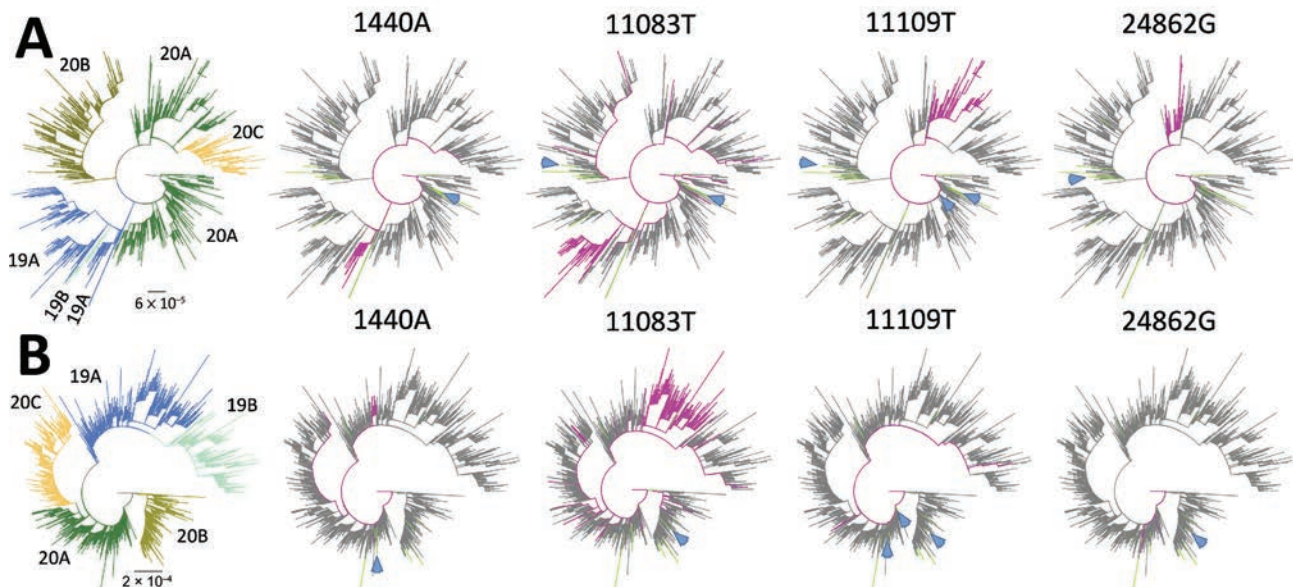


Figure 3. Phylogenetic trees showing 4 low-frequency variants detected in sewage samples in study of severe acute respiratory syndrome coronavirus 2 circulation and diversity through community wastewater sequencing, the Netherlands and Belgium. A) The Netherlands–Belgium subsample; B) global subsample. Patient sequences containing the mutation are shown in magenta. Lines in green indicate sewage samples sequenced in this study. Clades (19A, 19B, 20A, 20B, and 20C) are indicated in colors at the left of the figure. Blue arrows show the consensus sequences (if available) of the sewage samples in which the low-frequency variant was detected. Scale bars indicate the inferred number of nucleotide substitutions per site.

however, this approach would not be useful since no single small piece of the genome can reliably differentiate between clades or lineages. However, we demonstrated that some LFVs and SNPs can be linked to particular clusters or clades within trees without the need for a complete genome. To confidently determine the presence of a particular cluster within a sample, at least 2 LFVs associated with the cluster should be present at substantial levels. Furthermore, variant analysis can also be used to monitor the prevalence of biologically relevant mutations, such as D614G, which has been shown to increase infectivity *in vitro* (45) and might be associated with higher transmission and death rates (46; M. Cortey, unpub. data, <https://www.biorxiv.org/content/10.1101/2020.05.16.099499v1>). Within our dataset, clear temporal changes in the prevalence of LFVs or SNPs in sewage samples that correlated with changes in the clinical dataset were not detected during the first wave.

The combination of whole-genome sequencing of clinical samples with epidemiologic data is vital for public health decision-making (26) because it helps identify clusters of infection, new introductions of virus, and the expansion and decline of circulating strains. Cities with large numbers of visitors are expected to experience several introductions of the virus, whereas the opposite is expected for cities with low numbers of visitors. The use of NGS analysis of sewage samples to evaluate viral diversity within a geographic area and its changes over time can aid in decision-making. For example, in scenarios in which a large increase of viral diversity is detected in sewage, suggesting new introductions of virus, appropriate measures can be taken.

Wastewater can also be used to monitor novel mutations. Our consensus and LFV analyses revealed 57 mutations that were not seen in the global database. These novel mutations might not have been detected for several reasons: they represent technical errors; the mutations did not stay within the population; or the mutations are associated with asymptomatic or mild disease, viruses from animal hosts, enteric shedding, or defective genomes. The presence of defective genomes has previously been suggested for the detection of LFVs that generate stop codons in clinical samples (47). Phenotypic studies could help determine the likelihood and biologic relevance of these novel mutations.

In conclusion, this study illustrates the value of NGS analysis of wastewater to approximate the diversity of SARS-CoV-2 circulating in a community. Sequencing of wastewater samples could be a powerful tool to complement clinical surveillance or could

be used independently in settings in which wide clinical sequencing is unfeasible. In addition, in-depth NGS analysis of wastewater samples can help in assessing changes in viral diversity, which can indicate the emergence of epidemiologically or clinically relevant mutations and thereby aid public health decision-making.

This article was preprinted at <https://www.medrxiv.org/content/10.1101/2020.09.21.20198838v1>.

Acknowledgments

We thank the Water Authorities in the Netherlands (Aa en Maas, Amstel Gooi en Vecht, Delfland, De Dommel, Fryslan, Hollands Noorderkwartier, Stichtse Rijnlanden, Vallei en Veluwe, Evides, Waternet) and Belgium (Aquaflin, De Watergroep) for the provision of the sewage samples. We thank Pelle van der Wal for his help with the Illumina MiSeq runs. We gratefully acknowledge the authors originating and submitting laboratories of the global sequences from the GISAID EpiCoV Database (1), on which this research is based.

This work was supported by the European Union's Horizon H2020 grants VEO (grant no. 874735) and METASTAVA (grant no. 773830), the Erasmus MC foundation, and the Adessium Foundation.

About the Author

Mr. Izquierdo-Lara is a PhD student in the Department of Viroscience, Erasmus University Medical Center, Rotterdam, the Netherlands. His research interests are chronic norovirus infections in immunocompromised patients and virus evolution and emergence.

References

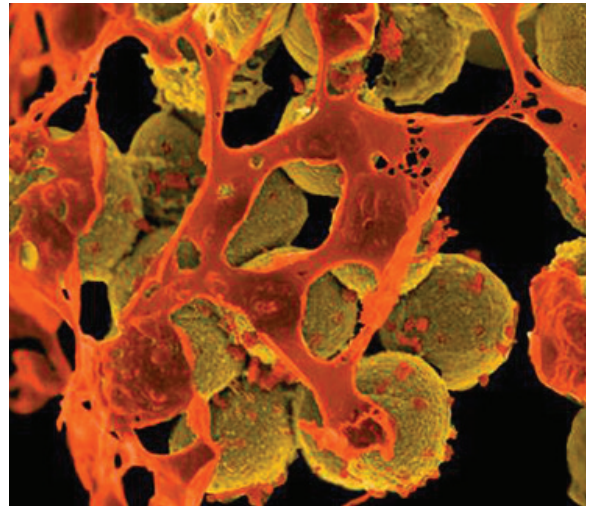
1. Shu Y, McCauley J. GISAID: Global initiative on sharing all influenza data – from vision to reality. *Euro Surveill.* 2017;22:30494. <https://doi.org/10.2807/1560-7917.ES.2017.22.13.30494>
2. Rambaut A, Holmes EC, O'Toole Á, Hill V, McCrone JT, Ruis C, et al. A dynamic nomenclature proposal for SARS-CoV-2 lineages to assist genomic epidemiology. *Nat Microbiol.* 2020;5:1403–7. <https://doi.org/10.1038/s41564-020-0770-5>
3. Hadfield J, Megill C, Bell SM, Huddleston J, Potter B, Callender C, et al. Nextstrain: real-time tracking of pathogen evolution. *Bioinformatics.* 2018;34:4121–3. <https://doi.org/10.1093/bioinformatics/bty407>
4. Lamers MM, Beumer J, van der Vaart J, Knoops K, Puschhof J, Breugem TI, et al. SARS-CoV-2 productively infects human gut enterocytes. *Science.* 2020;369:50–4. <https://doi.org/10.1126/science.abc1669>
5. Xiao F, Tang M, Zheng X, Liu Y, Li X, Shan H. Evidence for gastrointestinal infection of SARS-CoV-2. *Gastroenterology.* 2020;158:1831–1833.e3. <https://doi.org/10.1053/j.gastro.2020.02.055>

6. Xiao F, Sun J, Xu Y, Li F, Huang X, Li H, et al. Infectious SARS-CoV-2 in feces of patient with severe COVID-19. *Emerg Infect Dis*. 2020;26:1920–2. <https://doi.org/10.3201/eid2608.200681>
7. Parasa S, Desai M, Thoguluva Chandrasekar V, Patel HK, Kennedy KF, Roesch T, et al. Prevalence of gastrointestinal symptoms and fecal viral shedding in patients with coronavirus disease 2019: a systematic review and meta-analysis. *JAMA Netw Open*. 2020;3:e2011335. <https://doi.org/10.1001/jamanetworkopen.2020.11335>
8. Jones DL, Baluja MQ, Graham DW, Corbishley A, McDonald JE, Malham SK, et al. Shedding of SARS-CoV-2 in feces and urine and its potential role in person-to-person transmission and the environment-based spread of COVID-19. *Sci Total Environ*. 2020;749:141364. <https://doi.org/10.1016/j.scitotenv.2020.141364>
9. Foladori P, Cutrupi F, Segata N, Manara S, Pinto F, Malpei F, et al. SARS-CoV-2 from faeces to wastewater treatment: what do we know? A review. *Sci Total Environ*. 2020;743:140444. <https://doi.org/10.1016/j.scitotenv.2020.140444>
10. Strubbia S, Phan MVT, Schaeffer J, Koopmans M, Cotten M, Le Guyader FS. Characterization of norovirus and other human enteric viruses in sewage and stool samples through next-generation sequencing. *Food Environ Virol*. 2019;11:400–9. <https://doi.org/10.1007/s12560-019-09402-3>
11. Hellmér M, Paxéus N, Magnus L, Enache L, Arnholm B, Johansson A, et al. Detection of pathogenic viruses in sewage provided early warnings of hepatitis A virus and norovirus outbreaks. *Appl Environ Microbiol*. 2014;80:6771–81. <https://doi.org/10.1128/AEM.01981-14>
12. Bisseux M, Colombet J, Mirand A, Roque-Afonso A-M, Abravanel F, Izopet J, et al. Monitoring human enteric viruses in wastewater and relevance to infections encountered in the clinical setting: a one-year experiment in central France, 2014 to 2015. *Euro Surveill*. 2018;23:17–00237. <https://doi.org/10.2807/1560-7917.ES.2018.23.7.17-00237>
13. Wang W, Xu Y, Gao R, Lu R, Han K, Wu G, et al. Detection of SARS-CoV-2 in different types of clinical specimens. *JAMA*. 2020;323:1843–4. <https://doi.org/10.1001/jama.2020.3786>
14. Medema G, Heijnen L, Elsinga G, Italiaander R, Brouwer A. Presence of SARS-coronavirus-2 RNA in sewage and correlation with reported COVID-19 prevalence in the early stage of the epidemic in the Netherlands. *Environ Sci Technol Lett*. 2020;7:511–6. <https://doi.org/10.1021/acs.estlett.0c00357>
15. Heijnen L, Medema G. Surveillance of influenza A and the pandemic influenza A (H1N1) 2009 in sewage and surface water in the Netherlands. *J Water Health*. 2011;9:434–42. <https://doi.org/10.2166/wh.2011.019>
16. Patel JC, Diop OM, Gardner T, Chavan S, Jorba J, Wassilak SGF, et al. Surveillance to track progress toward polio eradication—worldwide, 2017–2018. *MMWR Morb Mortal Wkly Rep*. 2019;68:312–8. <https://doi.org/10.15585/mmwr.mm6813a4>
17. Suffredini E, Iaconelli M, Equestre M, Valdazo-González B, Ciccaglione AR, Marcantonio C, et al. Genetic diversity among genogroup II noroviruses and progressive emergence of GII.17 in wastewaters in Italy (2011–2016) revealed by next-generation and Sanger sequencing. *Food Environ Virol*. 2018;10:141–50. <https://doi.org/10.1007/s12560-017-9328-y>
18. Fumian TM, Fioretti JM, Lun JH, Dos Santos IAL, White PA, Miagostovich MP. Detection of norovirus epidemic genotypes in raw sewage using next generation sequencing. *Environ Int*. 2019;123:282–91. <https://doi.org/10.1016/j.envint.2018.11.054>
19. Wu F, Zhang J, Xiao A, Gu X, Lee WL, Armas F, et al. SARS-CoV-2 titers in wastewater are higher than expected from clinically confirmed cases. *mSystems*. 2020;5:e00614–20. <https://doi.org/10.1128/mSystems.00614-20>
20. Randazzo W, Truchado P, Cuevas-Ferrando E, Simón P, Allende A, Sánchez G. SARS-CoV-2 RNA in wastewater anticipated COVID-19 occurrence in a low prevalence area. *Water Res*. 2020;181:115942. <https://doi.org/10.1016/j.watres.2020.115942>
21. Wurtzer S, Marechal V, Mouchel JM, Maday Y, Teyssou R, Richard E, et al. Evaluation of lockdown effect on SARS-CoV-2 dynamics through viral genome quantification in waste water, Greater Paris, France, 5 March to 23 April 2020. *Euro Surveill*. 2020;25:2000776. <https://doi.org/10.2807/1560-7917.ES.2020.25.50.2000776>
22. Rimoldi SG, Stefani F, Gigantiello A, Polesello S, Comandatore F, Mileto D, et al. Presence and infectivity of SARS-CoV-2 virus in wastewaters and rivers. *Sci Total Environ*. 2020;744:140911. <https://doi.org/10.1016/j.scitotenv.2020.140911>
23. Nemudryi A, Nemudraia A, Wiegand T, Surya K, Buyukyoruk M, Cicha C, et al. Temporal detection and phylogenetic assessment of SARS-CoV-2 in municipal wastewater. *Cell Rep Med*. 2020;1:100098. <https://doi.org/10.1016/j.xcrm.2020.100098>
24. 2019-novel coronavirus (2019-nCoV) real-time rRT-PCR panel primers and probes [cited 2020 Jul 23]. <https://www.fda.gov/media/134922/download>
25. Corman VM, Landt O, Kaiser M, Molenkamp R, Meijer A, Chu DK, et al. Detection of 2019 novel coronavirus (2019-nCoV) by real-time RT-PCR. *Euro Surveill*. 2020;25:2000045. <https://doi.org/10.2807/1560-7917.ES.2020.25.3.2000045>
26. Oude Munnink BB, Nieuwenhuijse DF, Stein M, O'Toole Á, Haverkate M, Mollers M, et al. Rapid SARS-CoV-2 whole-genome sequencing and analysis for informed public health decision-making in the Netherlands. *Nat Med*. 2020;26:1405–10.
27. Richard M, Kok A, de Meulder D, Bestebroer TM, Lamers MM, Okba NMA, et al. SARS-CoV-2 is transmitted via contact and via the air between ferrets. *Nat Commun*. 2020;11:3496. <https://doi.org/10.1038/s41467-020-17367-2>
28. Martin M. Cutadapt removes adapter sequences from high-throughput sequencing reads. *EMBnet J*. 2011;17:10–2. <https://doi.org/10.14806/ej.17.1.200>
29. Okonechnikov K, Golosova O, Fursov M; UGENE team. Unipro UGENE: a unified bioinformatics toolkit. *Bioinformatics*. 2012;28:1166–7. <https://doi.org/10.1093/bioinformatics/bts091>
30. Oude Munnink BB, Nieuwenhuijse DF, Sikkema RS, Koopmans M. Validating whole genome nanopore sequencing, using Usutu virus as an example. *J Vis Exp*. 2020;157:e60906. <https://doi.org/10.3791/60906>
31. Afgan A, Baker D, Batut B, van den Beek M, Bouvier D, Cech M, et al. The Galaxy platform for accessible, reproducible and collaborative biomedical analyses: 2018 update. *Nucleic Acids Res*. 2018;46(W1):W537–44. <https://doi.org/10.1093/nar/gky379>
32. Chen S, Zhou Y, Chen Y, Gu J. fastp: an ultra-fast all-in-one FASTQ preprocessor. *Bioinformatics*. 2018;34:i884–90. <https://doi.org/10.1093/bioinformatics/bty560>
33. Grubaugh ND, Gangavarapu K, Quick J, Matteson NL, De Jesus JG, Main BJ, et al. An amplicon-based sequencing framework for accurately measuring intrahost virus diversity using PrimalSeq and iVar. *Genome Biol*. 2019;20:8. <https://doi.org/10.1186/s13059-018-1618-7>
34. Wu F, Zhao S, Yu B, Chen Y-M, Wang W, Song Z-G, et al. A new coronavirus associated with human respiratory disease in China. *Nature*. 2020;579:265–9. <https://doi.org/10.1038/s41586-020-2008-3>

35. Farkas K, Hillary LS, Malham SK, McDonald JE, Jones DL. Wastewater and public health: the potential of wastewater surveillance for monitoring COVID-19. *Curr Opin Environ Sci Health*. 2020;17:14–20. <https://doi.org/10.1016/j.coesh.2020.06.001>
36. Michael-Kordatou I, Karaolia P, Fatta-Kassinos D. Sewage analysis as a tool for the COVID-19 pandemic response and management: the urgent need for optimised protocols for SARS-CoV-2 detection and quantification. *J Environ Chem Eng*. 2020;8:104306. <https://doi.org/10.1016/j.jece.2020.104306>
37. Crits-Christoph A, Kantor RS, Olm MR, Whitney ON, Al-Shayeb B, Lou YC, et al. Genome sequencing of sewage detects regionally prevalent SARS-CoV-2 variants. *MBio*. 2021;12:e02703–20. <https://doi.org/10.1128/mBio.02703-20>
38. Mykytyn AZ, Lamers MM, Okba NMA, Breugem TI, Schipper D, van den Doel PB, et al. Susceptibility of rabbits to SARS-CoV-2. *Emerg Microbes Infect*. 2021;10:1–7. <https://doi.org/10.1080/22221751.2020.1868951>
39. Oreshkova N, Molenaar RJ, Vreman S, Harders F, Oude Munnink BB, Hakke-van der Honing RW, et al. SARS-CoV-2 infection in farmed minks, the Netherlands, April and May 2020. *Euro Surveill*. 2020;25:2001005. <https://doi.org/10.2807/1560-7917.ES.2020.25.23.2001005>
40. Halfmann PJ, Hatta M, Chiba S, Maemura T, Fan S, Takeda M, et al. Transmission of SARS-CoV-2 in domestic cats. *N Engl J Med*. 2020;383:592–4. <https://doi.org/10.1056/NEJMc2013400>
41. Schlottau K, Rissmann M, Graaf A, Schön J, Sehl J, Wylezich C, et al. SARS-CoV-2 in fruit bats, ferrets, pigs, and chickens: an experimental transmission study. *Lancet Microbe*. 2020;1:e218–25. [https://doi.org/10.1016/S2666-5247\(20\)30089-6](https://doi.org/10.1016/S2666-5247(20)30089-6)
42. Shi J, Wen Z, Zhong G, Yang H, Wang C, Huang B, et al. Susceptibility of ferrets, cats, dogs, and other domesticated animals to SARS-coronavirus 2. *Science*. 2020;368:1016–20. <https://doi.org/10.1126/science.abb7015>
43. Nieuwenhuijse DF, Oude Munnink BB, Phan MVT, Munk P, Venkatakrishnan S, Aarestrup FM, et al.; Global Sewage Surveillance project consortium. Setting a baseline for global urban virome surveillance in sewage. *Sci Rep*. 2020;10:13748. <https://doi.org/10.1038/s41598-020-69869-0>
44. Lun JH, Crosbie ND, White PA. Genetic diversity and quantification of human mastadenoviruses in wastewater from Sydney and Melbourne, Australia. *Sci Total Environ*. 2019;675:305–12. <https://doi.org/10.1016/j.scitotenv.2019.04.162>
45. Zhang L, Jackson CB, Mou H, Ojha A, Peng H, Quinlan BD, et al. SARS-CoV-2 spike-protein D614G mutation increases virion spike density and infectivity. *Nat Commun*. 2020;11:6013. <https://doi.org/10.1038/s41467-020-19808-4>
46. Toyoshima Y, Nemoto K, Matsumoto S, Nakamura Y, Kiyotani K. SARS-CoV-2 genomic variations associated with mortality rate of COVID-19. *J Hum Genet*. 2020;65:1075–82. <https://doi.org/10.1038/s10038-020-0808-9>
47. Karamitros T, Papadopoulou G, Bousali M, Mexias A, Tsiodras S, Mentis A. SARS-CoV-2 exhibits intra-host genomic plasticity and low-frequency polymorphic quasispecies. *J Clin Virol*. 2020;131:104585. <https://doi.org/10.1016/j.jcv.2020.104585>

Address for correspondence: Miranda de Graaf, Department of Viroscience, Wytemaweg 80, 3015CN, Rotterdam, The Netherlands; email: m.degraaf@erasmusmc.nl

EID Podcast Livestock, Phages, MRSA, and People in Denmark



Methicillin-resistant *Staphylococcus aureus*, better known as MRSA, is often found on human skin. But MRSA can also cause dangerous infections that are resistant to common antimicrobial drugs. Epidemiologists carefully monitor any new mutations or transmission modes that might lead to the spread of this infection.

Approximately 15 years ago, MRSA emerged in livestock. From 2008 to 2018, the proportion of infected pigs in Denmark rocketed from 3.5% to 90%.

What happened, and what does this mean for human health?

In this EID podcast, Dr. Jesper Larsen, a senior researcher at the Statens Serum Institut, describes the spread of MRSA from livestock to humans.

Visit our website to listen:

<https://go.usa.gov/x74Jh>

**EMERGING
INFECTIOUS DISEASES®**

Characteristics and Clinical Implications of Carbapenemase-Producing *Klebsiella pneumoniae* Colonization and Infection, Italy

Marianna Rossi, Liliane Chatenoud, Floriana Gona, Isabella Sala, Giovanni Nattino, Alessia D'Antonio, Daniele Castelli, Teresa Itri, Paola Morelli, Sara Bigoni, Chiara Aldieri, Roberto Martegani, Paolo A. Grossi, Cecilia Del Curto, Stefania Piconi, Sara G. Rimoldi, Paola Brambilla, Paolo Bonfanti, Evelyn Van Hauwermeiren, Massimo Puoti, Gianni Gattuso, Chiara Cerri, Mario C. Raviglione, Daniela M. Cirillo, Alessandra Bandera, Andrea Gori; The KPC-Kp Study Group¹

Medscape **ACTIVITY** EDUCATION

In support of improving patient care, this activity has been planned and implemented by Medscape, LLC and Emerging Infectious Diseases. Medscape, LLC is jointly accredited by the Accreditation Council for Continuing Medical Education (ACCME), the Accreditation Council for Pharmacy Education (ACPE), and the American Nurses Credentialing Center (ANCC), to provide continuing education for the healthcare team.

Medscape, LLC designates this Journal-based CME activity for a maximum of 1.00 **AMA PRA Category 1 Credit(s)**[™]. Physicians should claim only the credit commensurate with the extent of their participation in the activity.

Successful completion of this CME activity, which includes participation in the evaluation component, enables the participant to earn up to 1.0 MOC points in the American Board of Internal Medicine's (ABIM) Maintenance of Certification (MOC) program. Participants will earn MOC points equivalent to the amount of CME credits claimed for the activity. It is the CME activity provider's responsibility to submit participant completion information to ACCME for the purpose of granting ABIM MOC credit.

All other clinicians completing this activity will be issued a certificate of participation. To participate in this journal CME activity: (1) review the learning objectives and author disclosures; (2) study the education content; (3) take the post-test with a 75% minimum passing score and complete the evaluation at <http://www.medscape.org/journal/eid>; and (4) view/print certificate. For CME questions, see page 1550.

Release date: May 22, 2021; Expiration date: May 22, 2022

Learning Objectives

Upon completion of this activity, participants will be able to:

- Describe epidemiology of KPC-Kp and molecular characterization of KPC-Kp strains in colonized and infected inpatients with mild (MI) or serious (SI) infections in Italy, according to a multicenter cohort study of 1,071 patients with KPC-Kp
- Determine clinical characteristics and outcomes of KPC-Kp in colonized and infected inpatients with MI or SI in Italy, according to a multicenter cohort study
- Identify treatment and other clinical implications of KPC-Kp in colonized and infected inpatients with MI or SI in Italy, according to a multicenter cohort study

CME Editor

Amy J. Guinn, BA, MA, Copyeditor, Emerging Infectious Diseases. *Disclosure: Amy J. Guinn, BA, MA, has disclosed no relevant financial relationships.*

CME Author

Laurie Barclay, MD, freelance writer and reviewer, Medscape, LLC. *Disclosure: Laurie Barclay, MD, has disclosed no relevant financial relationships.*

Authors

Disclosures: Disclosures: Marianna Rossi, MD, PhD; Liliane Chatenoud, PhD; Floriana Gona, PhD; Isabella Sala, MS; Giovanni Nattino, PhD; Alessia D'Antonio, MD; Daniele Castelli, MS; Teresa Itri, MSc; Paola Morelli, PhD; Sara Bigoni, MD; Chiara Aldieri, MD; Roberto Martegani, PhD; Paolo A. Grossi, MD, PhD; Cecilia Del Curto, MD; Stefania Piconi, MD; Sara G. Rimoldi, MS; Paola Brambilla, PhD; Evelyn Van Hauwermeiren, MD; Gianni Gattuso, MD; Chiara Cerri, MD; Mario C. Raviglione, MD; Alessandra Bandera, MD, PhD; and Andrea Gori, MD, have disclosed no relevant financial relationships. Paolo Bonfanti, MD, has disclosed the following relevant financial relationships: served as an advisor or consultant for Janssen-Cilag; Gilead Sciences, Inc.; ViiV Healthcare; served as a speaker or a member of a speakers bureau for Gilead Sciences, Inc.; Pfizer Inc. Massimo Puoti, MD, has disclosed the following relevant financial relationships: served as an advisor or consultant for AbbVie Inc.; Merck & Co., Inc.; served as a speaker or a member of a speakers bureau for AbbVie Inc.; Gilead Sciences, Inc.; Merck & Co., Inc.; received grants for clinical research from AbbVie Inc.; Eli Lilly and Company; Gilead Sciences, Inc. Daniela M. Cirillo, MD, PhD, has disclosed the following relevant financial relationships: served as an advisor or consultant for bioMérieux; received grants for clinical research from bioMérieux; DiaSorin.

¹Group collaborators are listed at the end of this article.

Klebsiella pneumoniae carbapenemase-producing *K. pneumoniae* (KPC-*Kp*) has been endemic in Italy since 2013. In a multicenter cohort study, we investigated various aspects of KPC-*Kp* among patients, including 15-day mortality rates and delays in adequate therapy. Most (77%) KPC-*Kp* strains were sequence types ST512 or ST307. During 2017, KPC-*Kp* prevalence was 3.26 cases/1,000 hospitalized patients. Cumulative incidence of KPC-*Kp* acquired >48 hours after hospital admission was 0.68% but varied widely between centers. Among patients with mild infections and noninfected colonized patients, 15-day mortality rates were comparable, but rates were much higher among patients with severe infections. Delays of ≥ 4 days in receiving adequate therapy more frequently occurred among patients with mild infections than those with severe infections, and delays were less common for patients with known previous KPC-*Kp* colonization. Italy urgently needs a concerted surveillance system to control the spread of KPC-*Kp*.

The global emergence and spread of carbapenem-resistant *Enterobacteriaceae* (CRE) pose a major health threat, causing severe illness and high healthcare costs (1). Infections caused by CRE also are associated with high mortality rates because extensive resistance to so-called last-line antimicrobial drugs, such as carbapenems, limit the treatment options (2–5). Only a few antimicrobial drugs, such as colistin, fosfomycin, tigecycline, and ceftazidime/avibactam, are effective against CRE. Moreover, the remaining therapeutic options often have high toxicity profiles, and rates of resistance to these antimicrobial drugs already are increasing (6).

In a 2014 study conducted by the European Survey of Carbapenemase-Producing *Enterobacteriaceae* (EuSCAPE) Working Group, 455 sentinel hospitals in 36 countries submitted clinical isolates (7). Among the 2,703 isolates submitted, 2,301 (85%) were *Klebsiella pneumoniae* and 402 (15%) were *Escherichia coli*, including samples identified as carbapenemase producers among 850 (37%) *K. pneumoniae* and 77 (19%) *E. coli* isolates. Identified carbapenemase-producers included 4 gene families: *K. pneumoniae*

carbapenemase (KPC), New Delhi metallo- β -lactamase, oxacillinase 48-like, and Verona integron-encoded metallo- β -lactamase (7). Positive clinical specimens were found in 1.3 patients/10,000 hospital admissions, but prevalence differed greatly between countries and the highest rates were registered in countries in the Mediterranean and Balkan regions (7). Among these countries, Italy, Greece, and Romania reported the highest percentages of carbapenem resistance. In addition, CRE rates increased from 15% in 2010 to 36% in 2016 (8–10), and CRE became endemic in Greece in 2010 and Italy in 2013 (11). Nevertheless, currently published information is too scant to define the complete picture of KPC *K. pneumoniae* (KPC-*Kp*) epidemiology in both clinical isolates and surveillance screening samples (12).

In this context, we set up a network of 15 hospitals in Lombardy, the most populous region in Italy, and established a cohort of patients affected by KPC-*Kp*. The overarching goal of the KPC-*Kp* Study Group was to identify the challenges of controlling the spread of the bacterium. We describe KPC-*Kp* epidemiology, treatment, and in-hospital mortality rates, along with molecular characterization of KPC-*Kp* strains in colonized and infected inpatients.

Methods

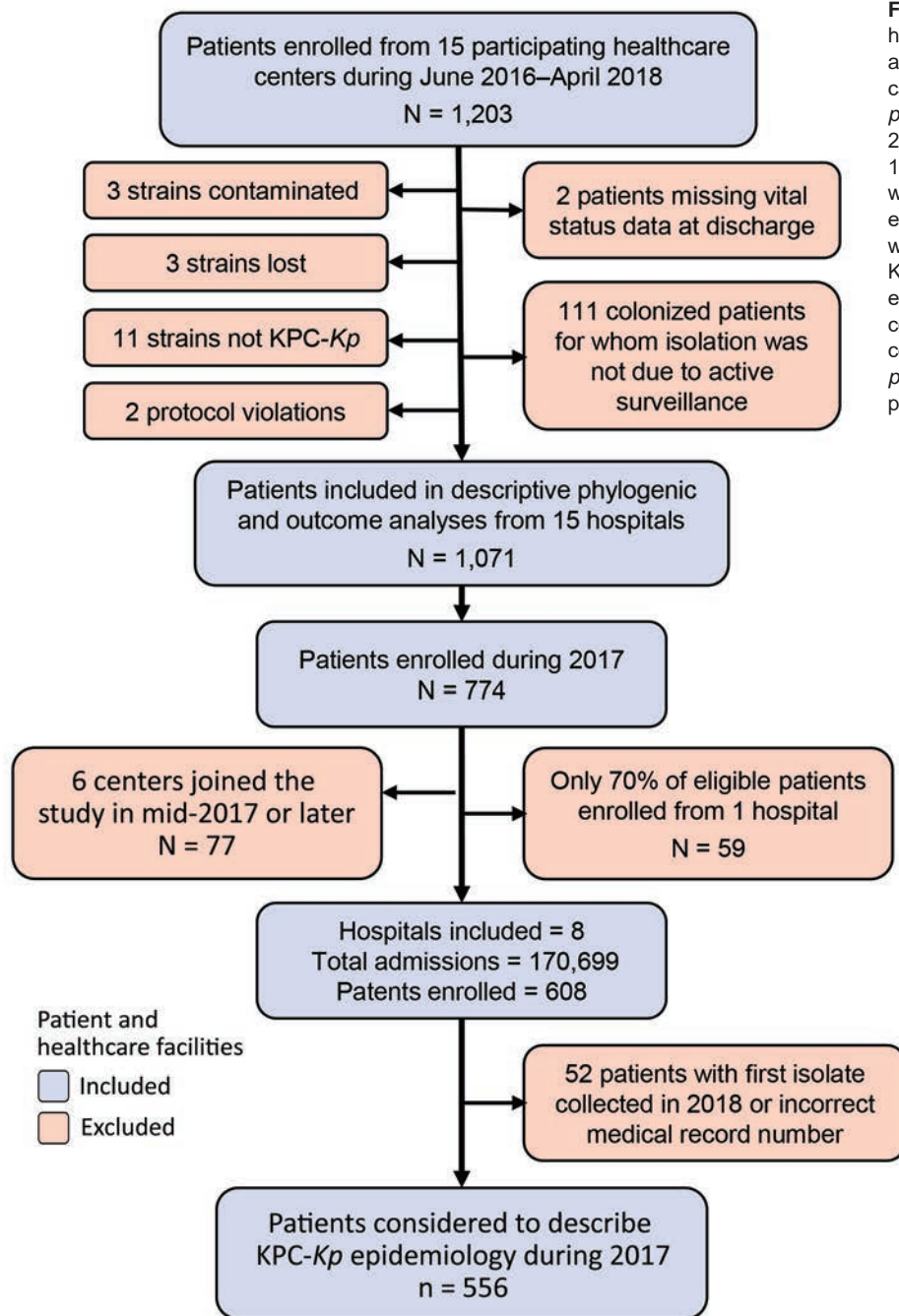
Study Design, Setting, and Patients

We conducted a multicenter cohort study during June 2016–April 2018, which included 15 hospitals in Lombardy (Figure 1; Appendix, <https://wwwnc.cdc.gov/EID/article/27/5/20-3662-App1.pdf>). We asked each enrolled hospital to include data on all consecutively hospitalized adult patients who had ≥ 1 positive KPC-*Kp* isolate during their hospital stay. For patients hospitalized multiple times during the study period, we only considered the first hospitalization. For centers including patients during 2017, the year for which we had a full 12 months of data, we retrieved the administrative datasets of all admitted patients (Figure 1). We merged these data with

Author affiliations: S. Gerardo Hospital, Monza, Italy (M. Rossi, T. Itri, D. Castelli, P. Bonfanti); Istituto di Ricerche Farmacologiche Mario Negri IRCCS, Milan, Italy (L. Chatenoud, I. Sala, G. Nattino, A. D'Antonio); IRCCS San Raffaele Scientific Institute, Milan (F. Gona, C. Del Curto, D.M. Cirillo); Fondazione IRCCS Ca' Granda, Ospedale Maggiore Policlinico, Milan (T. Itri, A. Bandera, A. Gori); Humanitas University, Milan (P. Morelli); Papa Giovanni XXIII Hospital, Bergamo, Italy (S. Bigoni); University of Milan San Paolo Hospital, Milan (C. Aldieri); Busto Arsizio Hospital, Busto Arsizio, Italy (R. Martegani); University of Insubria, ASST Sette

Laghi-Varese, Italy (P.A. Grossi); ASST Fatebenefratelli Sacco, Milan (S. Piconi, S.G. Rimoldi); Clinic of Infectious Diseases of Istituti Ospedalieri of Cremona, Cremona, Italy (P. Brambilla); University of Milan-Bicocca, Milan (P. Bonfanti); University of Brescia and ASST Spedali Civili, Brescia, Italy (E. Van Hauwermeiren); ASST Grande Ospedale Metropolitano Niguarda, Milan (M. Puoti); Carlo Poma Hospital, Mantova, Italy (G. Gattuso); Hospital of Lodi, Lodi, Italy (C. Cerri); University of Milan, Milan (M.C. Raviglione, A. Bandera, A. Gori)

DOI: <https://doi.org/10.3201/eid2705.203662>



those available in the KPC-Kp patient cohort database and used the combined dataset to describe KPC-Kp epidemiology in the hospitalized population.

The study protocol was first approved by the Research Ethics Committee of the coordinating center, Ospedale San Gerardo (Monza, Italy). Informed consent requirement was waived due to the study's observational, noninterventional design. The study protocol was subsequently approved by the ethics committees of the 14 other participating centers. In

accordance with local ethics committee requirements, 3 centers did not waive informed consent. Because this was an observational study, treatment for KPC-Kp infections was at the discretion of the attending physicians and no change to the center-specific surveillance protocol was required.

In all centers, intensive care unit (ICU) patients were tested for CRE at admission and weekly through rectal swab specimens or other surveillance cultures. The same protocol was applied heterogeneously in

hospital wards in which patients are considered to be at higher risk of acquiring CRE, such as hematology, solid organ transplant, and geriatric units (Appendix Table 1). For the other wards, most centers performed surveillance rectal swab specimens at admission on the basis of major risk factors for CRE, such as previous CRE colonization, previous hospitalization during the 12 months before inclusion, or both. Of note, only 3 of the 15 participating centers, B, C, and I (Appendix Table 1), combined the 2 surveillance strategies described for specific wards and patients at higher risk of acquiring CRE.

Patient Classification

Patients were classified according to the most clinically relevant KPC-*Kp* isolate collected from them between hospital admission and discharge. Thus, for patients whose first isolate was attributable to colonization and a subsequent isolate was attributed to an infection, only the second isolate was considered. We used US Centers for Disease Control and Prevention criteria (13) to define diagnosed infection and diagnosis was confirmed by an infectious disease specialist. Infections were classified as KPC-*Kp* bacteremia when a blood culture was positive for a KPC-*Kp* strain with or without KPC-*Kp*-positive cultures from ≥ 1 other site and the patient had clinical signs of systemic inflammatory response syndrome requiring antimicrobial drug treatment. We defined nonbacteremic KPC-*Kp* infections by documented recovery of a KPC-*Kp* isolate from nonblood cultures, such as intra-abdominal wounds, urine, or bronchoalveolar lavage fluid; absence of KPC-*Kp*-positive blood culture during the index hospitalization; and clinical signs of infection.

In line with other studies (14), we classified KPC-*Kp* cases according to infection severity. We classified cases of KPC-*Kp* bloodstream or lower respiratory tract infections, and clinical presentation of septic shock, regardless of infection site, as severe infections. We classified infections from the urinary tract, surgical wounds, or other sites without septic shock as mild infections. We classified all cases identified through active surveillance as colonized when ≥ 1 culture sample grew KPC-*Kp* but the patient did not develop KPC-*Kp* infection during hospitalization.

Data Collection

For patients included in the KPC-*Kp* cohort, data were entered into the web-based case form after pseudonymization of personal data. Data were collected on demographic characteristics, medical history, underlying diseases, previous hospitalization, previous

KPC-*Kp* infection, surgery ≤ 30 days before KPC-*Kp* isolation, invasive procedures ≤ 72 hours before KPC-*Kp* isolation, antimicrobial drug therapy ≤ 30 days before KPC-*Kp* isolation, dates of admission to hospital, and ward of isolation. Date of hospital discharge and patient status at discharge also were collected. The date and ward where the patient was hospitalized when KPC-*Kp* was isolated, the source of isolation, and resistance spectrum also were collected and entered into the web-based case record form. Antimicrobial treatment, including empirical treatment and post-antibiogram treatment regimen, were recorded. Empirical treatment was defined as adequate when it included ≥ 1 antimicrobial drug with in vitro activity against the KPC-*Kp* isolate. Data were collected in a web-based case report form.

For enrolled centers submitting patient data during 2017, we retrieved the clinical record datasets of all admitted patients after pseudonymization of personal information. To verify centers included all eligible patients, we retrieved the total number of patients with ≥ 1 KPC-*Kp*-positive isolate registered in the microbiology laboratory of each center and compared that with the total number of patients included in the cohort (Appendix).

Microbiology and Genomic Analysis

The clinical microbiology laboratory of each of the 15 participating centers performed isolate identification and routine antimicrobial susceptibility testing (Appendix). CRE was defined by using Clinical and Laboratory Standard Institute guidelines (15). All bacterial strains were sent to a central microbiological laboratory at Ospedale San Raffaele for whole-genome sequencing (Appendix).

Statistical Analysis

We estimated the prevalence of KPC-*Kp* in hospitalized patients in the region of Lombardy during 2017, the cumulative incidence of acquired KPC-*Kp* infections among hospitalized patients, and the cumulative incidence of acquired KPC-*Kp* infections occurring >48 hours after hospital admission among hospitalized patients in the same region. We calculated and reported crude estimates for all centers and estimates standardized by age and ward of isolation (Appendix).

To study the role of KPC-*Kp* infection severity on 15-day mortality rates, we considered a multivariable Cox proportional hazard model and the related hazard ratio (HR) estimates and adjusted by center for a random effect and number of days from hospitalization to KPC-*Kp* isolation. Colonized patients

frequently have shorter hospital stays than infected patients. Because a shorter discharge time could affect our results, we performed a sensitivity analysis in which we excluded early-discharge patients. We performed a subgroup analysis to quantify excess mortality hazard due to septic shock among patients with bloodstream infections (Appendix).

We used multivariable mixed logistic regression models and accounted for clustering at the center level to evaluate the association between patient characteristics and delayed or inadequate empirical therapy, which we considered as outcome variables. We adjusted the models for age and type of KPC-*Kp* infection.

Results

Center Characteristics

Among all centers, the median number of annual admissions was 27,600 (interquartile range [IQR] 18,287–40,000). Among 15 enrolled centers, 9 (60%) maintained enrollment over 12 consecutive months; centers had a mean enrollment duration of 13.8 months (Appendix Figure 1).

Patient Baseline Characteristics

Among 1,203 consecutive KPC-*Kp*-positive hospitalized patients found during study, 89.0% (1,071) were considered in the analyses and 11% (132) were excluded for various reasons (Figure 1).

The median age among patients was 72 (IQR 61–80) years, 65% were male, and 35% were female; KPC-*Kp* was isolated from 275 (25.7%) ICU patients (Table 1). Among patients in the study cohort, >90% had ≥ 1 underlying condition, 40% of whom had congestive heart failure, peripheral vascular disease, or chronic renal failure. Severe infections were diagnosed in 221 (20%) patients and mild infections in 109 (10%) patients. Colonized patients $n = 741$, 69.2%), had a median of 6 days between hospitalization and KPC-*Kp* isolation, which was much lower than for patients with severe (median 12 days) or mild (median 11 days) infections. Bloodstream infections accounted for 54% of all infections, and rectal swab samples accounted for 67% of all colonizations (Appendix Figure 2).

Distribution, Phylogeny, and Resistance Mechanisms of KPC-*Kp* Clones

Among the 1,071 patient strains isolated, 82 were from colonized patients included at the end of April 2018; these samples did not arrive at the central laboratory in time for genotyping. Of the 989 strains analyzed, 32 different sequence types (STs) were

identified. The most numerous clones were ST512 in 45% (441), ST307 in 33% (326), ST258 in 7% (71), and ST101 in 6% (57) of isolates (Appendix Table 3). We identified 2 KPC variants, KPC-2 and KPC-3, in 68% of isolates. KPC-2 was absent in ST512 but predominant in ST307 and ST258. Core-genome, single-nucleotide polymorphism (SNP) analysis revealed that ST512 was scattered across all centers, but ST307 was represented in smaller, more localized clusters (Figure 2; Appendix Table 3).

Table 1. Characteristics of patients identified in multicenter surveillance for *Klebsiella pneumoniae* carbapenemase-producing *Klebsiella pneumoniae*, Italy*

Characteristics	KPC- <i>Kp</i> patients, n = 1,071
Sex	
M	694 (64.8)
F	377 (35.2)
Median age (IQR)	72 (61–80)
Ward of isolation	
Intensive care unit	275 (25.7)
Infectious diseases	81 (7.6)
Surgery	149 (13.9)
Geriatrics	47 (4.4)
Oncology	34 (3.2)
Hematology	42 (3.9)
Other medical wards	443 (41.4)
KPC- <i>Kp</i> colonization in previous 12 mo	333 (31.1)
Hospitalization in previous 12 mo	865 (80.8)
Antimicrobial therapy in the 30 d before hospitalization	782 (73.0)
Major surgery in the previous 30 d	262 (24.4)
Underlying conditions†	989 (92.3)
Congestive heart failure	192 (17.9)
Peripheral vascular disease	197 (18.4)
Cerebrovascular disease	205 (19.1)
Chronic lung disease	202 (18.9)
Chronic renal failure	304 (28.4)
Cancer	244 (22.8)
Diabetes	163 (15.2)
Charlson index, median (IQR)	6 (4–8)
Central venous catheter at isolation	414 (38.7)
Urinary catheter at isolation	562 (52.5)
Immunosuppressive therapy	209 (19.5)
Days of hospitalization, median (IQR)	25 (14–45)
KPC- <i>Kp</i> acquisition characteristics‡	
Severe infection	221 (20.6)
Mild infection	109 (10.2)
Colonization _{sur}	741 (69.2)
Median time from hospitalization to isolation of strain, d (IQR)‡	
Severe infection	12 (2–22)
Mild infection	11 (2–25)
Colonization _{sur}	6 (1–17)
Median time from strain isolation to discharge or death, d (IQR)‡	
Severe infection	18 (9–35)
Mild infection	20 (12–35)
Colonization _{sur}	13 (6–22)

*Values are no. (%) except as indicated. IQR, interquartile range; KPC-*Kp*, *Klebsiella pneumoniae* carbapenemase-producing *Klebsiella pneumoniae*.

†Underlying conditions and devices are listed when present in $\geq 10\%$ of patients.

‡Severe infection included bloodstream or lower respiratory tract infection plus septic shock from other sites; Mild infection included infections from other sites; and colonized_{sur} patients were identified through surveillance protocols.

Epidemiology of KPC-Kp

During 2017, the estimated prevalence of KPC-Kp among hospitalized patients in the Lombardy region was 3.26 (95% CI 2.99–3.54) per 1,000 admissions. In the same region, the overall cumulative incidence of KPC-Kp infections was 1.00‰ (95% CI 0.86‰–1.16‰) and the incidence of acquired infections occurring >48 hours after hospital admission was

0.68‰ (95% CI 0.56‰–0.82‰). The proportion of patients infected at admission, considered imported infections, was ≈30% in most centers. We observed marked differences across centers even after standardization by age and ward of isolation, with values ranging from 1.62‰ (95% CI 1.07‰–2.18‰) in center A to 0.21‰ (95% CI 0.02‰–0.40‰) in center B (Appendix Figure 3).

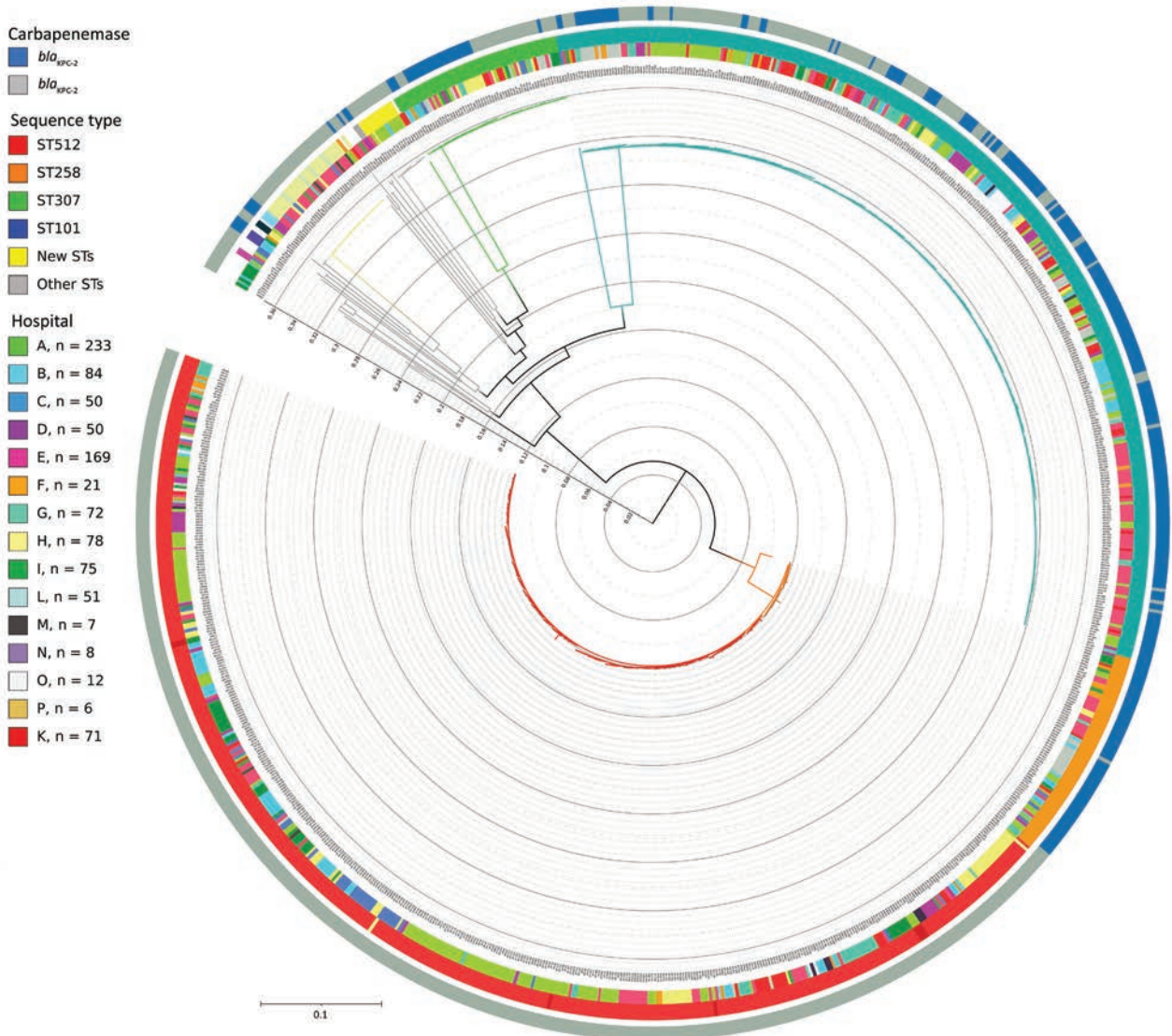


Figure 2. Phylogenetic tree of 989 *Klebsiella pneumoniae* genomes isolated at hospitals participating in the KPC-producing *K. pneumoniae* (KPC-Kp) study, Italy. The key shows the number of isolates included in the study provided by each center; 2 samples (1 from each from hospitals A and I) were excluded because the total quality of the assemblies was not sufficient to have high confidence in the SNPs called through all the genome (total coverage <30). Inner circle shows the KPC-Kp mechanism identified; middle circle shows hospitals from which strains were isolated; and outer circle shows identified STs. The whole genome core single-nucleotide polymorphisms (SNPs) were extracted from the 989 *K. pneumoniae* genome assemblies by using kSNP3.0 (<https://sourceforge.net/projects/ksnp>). Parametric maximum-likelihood estimation (general time-reversible plus gamma distribution plus invariable sites) analysis with 1,000 bootstrap estimates was used to infer the phylogeny. We used IQ-TREE (<http://www.iqtree.org>) to generate the tree and iTOL (<https://itol.embl.de>) to draw the tree. Major STs are represented by branch colors; ST512 and ST307 were the predominant STs. Major branches have bootstrap values >0.75 for branch support. Scale bar indicates nucleotide substitutions per site. KPC, *Klebsiella pneumoniae*-carbapenemase; ST, sequence type.

Patient Outcomes

In-hospital death from all causes was 34% (95% CI 29.2%–39.6%) among KPC-*Kp*-infected patients and 21% (95% CI 17.7%–27.6%) among colonized patients. No differences emerged when we stratified for carbapenem-resistance mechanisms and the most prevalent clones (Appendix Table 4).

Mortality hazards (considering the first 15 days after KPC-*Kp* isolation), were much higher for patients with severe infection than for colonized patients, even after controlling for center, time between hospitalization and isolation, age, ward of isolation, and Charlson index (adjusted HR [aHR] = 1.93, 95% CI 1.40–2.66) (Table 2). In contrast, no excess mortality hazard was noted for patients with mild infections (aHR = 0.75, 95% CI 0.42–1.34) compared with colonized patients.”

When we analyzed the subgroup of patients with bloodstream infections, we found clinical manifestation of septic shock more than doubled the risk for death (HR = 2.71, 95% CI 1.46–5.02). We found comparable results when we excluded from the analysis 343 patients discharged alive before day 15 (data not shown).

Antimicrobial Drug Treatment

On the basis of susceptibility test results, we found that 54% (159/297) of patients infected with KPC-*Kp* received adequate empirical therapy (Appendix Table 5). Empirical treatment was most frequently adequate in patients with KPC-*Kp* colonization during the previous 12 months and in patients with severe infection (Appendix Table 5).

Fewer treatment delays (<4 days, which is considered the maximum acceptable waiting time to receive appropriate antimicrobial treatment) were reported for patients with severe KPC-*Kp* infection

than patients with mild infections (Table 3). Patients reporting KPC-*Kp* colonization during the previous 12 months more frequently received prompt adequate therapy ($p < 0.001$).

Among the 282 KPC-*Kp*-infected patients treated for their infections, 62 (22%) received an in vitro active drug plus carbapenem, but 29 (10%) patients received gentamicin, fosfomycin, or tigecycline monotherapy. The most common drug combination was colistin plus tigecycline plus carbapenem, which most frequently was administered to patients with severe infections. Ceftazidime/avibactam became available in Italy in February 2018, and 26/39 (66%) infected patients included after that date received it: 19/24 (79%) in the severe infection group and 7/15 (47%) in mild infection group (Appendix Table 6).

Discussion

This study provides a detailed picture of KPC-*Kp* burden in an endemic setting and shows that KPC-*Kp* poses a major challenge for Italy's healthcare system. We estimated that 1 of every 1,000 patients admitted to participating hospitals during 2017 had a positive KPC-*Kp* specimen during hospitalization, which is ≈ 10 times the estimated number of CRE infections in Europe (1.3/10,000 hospitalizations) (7). This high rate is at least partly compatible with the heterogeneity in the surveillance protocols adopted by hospitals. Another factor contributing to the high rate of KPC-*Kp* could be the older age of the patient population, most of whom were men >65 years of age. In 2017, the median age of the adult population in Lombardy was 50 years, but the median age for the 170,699 adult patients in our study was 66 years, and 27% were >77 years of age. Of note, the considerable proportion of imported KPC-*Kp* infections, $\approx 30\%$, for most centers, suggests that active surveillance might need to be

Table 2. In-hospital death within 15 days of KPC-*Kp* isolation in a cohort of infected patients and subgroup of patients with bloodstream infections, Italy*

KPC- <i>Kp</i> infections	No.	Died, no. (%)	HR (95% CI)†	p value	HR (95% CI)‡	p value
All patients	1,039	174 (16.7)	NA	NA	NA	NA
Severity of infection§						
Colonized	712	100 (14.0)	Referent	NA	Referent	NA
Mild	109	13 (11.9)	0.71 (0.40–1.27)	0.247	0.75 (0.42–1.34)	0.328
Severe	218	61 (28.0)	1.84 (1.34–2.54)	0.0002	1.93 (1.40–2.66)	<0.0001
Bloodstream infections	176	45 (25.6)	NA	NA	NA	NA
Septic shock at admission						
N	132	25 (18.9)	Referent	NA	Referent	NA
Y	44	20 (45.5)	2.72 (1.50–4.90)	0.0009	2.71 (1.46–5.02)	0.002

*All patients are stratified for severity of infection; the subgroup of patients with bloodstream infection is stratified for septic shock. KPC-*Kp*, *Klebsiella pneumoniae* carbapenemase-producing *Klebsiella pneumoniae*; NA, not applicable.

†Hazard ratio (HR) estimates are from multivariable Cox proportional hazard models, adjusting for center (random effect) and days elapsing from hospitalization to KPC-*Kp* isolation.

‡Multivariable Cox mixed effects model adjusting for center (random effect) and days elapsing from hospitalization to KPC-*Kp* isolation, age, Charlson Index, and whether or not isolates were collected when patient was in the intensive care unit.

§Patients discharged or deceased on the day of KPC-*Kp* isolation were excluded from analyses; 20 patients were discharged, 9 colonized patients died, and 3 colonized patients had severe infections.

Table 3. Association between delay in receiving adequate antimicrobial therapy after KPC-Kp isolation and selected patient characteristics, Italy*

Characteristics	Delay from KPC-Kp isolation to adequate antimicrobial therapy		χ^2 p value	p value†
	<4 d	>4 d		
All	190 (63.9)	107 (36.0)	NA	NA
Age, median (IQR)	68.5 (62–78)	74 (63–81)	0.151	0.285
Charlson Index, median (IQR)	5.0 (4–8)	6.0 (4–8)	0.615	0.439
Intensive care unit admission				
Y	41 (63.1)	24 (36.9)	0.865	0.354
N	149 (64.2)	83 (35.8)		
Previous KPC-Kp colonization during the current hospitalization				
Y	46 (74.2)	16 (25.8)	0.060	0.118
N	144 (61.3)	91 (38.7)		
KPC-Kp colonization in the previous 12 mo				
Y	104 (77.0)	31 (23.0)	<0.001	<0.001
N	86 (53.2)	75 (46.8)		
Hospitalization in the previous 12 mo				
Y	149 (64.5)	82 (35.5)	0.832	0.779
N	41 (63.1)	24 (36.9)		
Antimicrobial therapy in the 30 d before hospitalization				
Y	145 (64.0)	84 (36.0)	0.564	0.627
N	45 (67.2)	22 (32.8)		
Major surgery‡				
Y	48 (53.9)	41 (46.1)	0.018	0.008
N	142 (74.7)	66 (31.7)		
KPC-Kp infection severity§				
Severe	139 (71.5)	55 (28.3)	0.0002	<0.001
Mild	52 (50.0)	52 (50.0)		

*Values are no. (%) except as indicated. Delay determined according to infected patients' resistance profiles; 33 patients were excluded: 17 had follow-up <3 days after isolation and 16 had no data on empirical therapies. IQR, interquartile range; KPC-Kp, *Klebsiella pneumoniae*-carbapenemase producing *Klebsiella pneumoniae*; NA, not applicable.

†Obtained from multivariable mixed logistic model adjusted by center, as random effect; age; and type of KPC-Kp infection, when appropriate.

‡Major surgery includes any invasive operative procedure in which a more extensive resection is performed, including a body cavity is entered, organs are removed, or normal anatomy is altered.

§Severe infection included bloodstream or lower respiratory tract infection plus septic shock from other sites; Mild infection included infections from other sites; and colonized patients were identified through surveillance protocols.

extended to post-acute care, long-term care, or rehabilitation facilities to control the spread of KPC-Kp. As highlighted by a recent report from the European Centre for Disease Prevention and Control (16), standardized actions for CRE containment in Italy must be driven by comprehensive coordinated responses implemented nationally rather than current practice of delegating responsibilities to the regional or hospital level.

In our setting, the KPC-Kp epidemic appears to be driven by the expansion of 3 major *K. pneumoniae* clonal lineages, specifically ST307, ST101, and ST258/ST512. Those epidemic clones have been associated with outbreaks and are reported to have an increased capacity to acquire drug resistance (17–19). Clone ST512 was widely distributed across the centers in our study, confirming its spread in Italy (20). We noted clone ST307 in smaller, scattered clusters but did not note differences in infection severity or death between clones.

We examined the KPC-Kp-associated mortality rate and noted it was highest among patients with severe infections, particularly bloodstream infections with septic shock, which is consistent with previous

research (21–25). We found no excess risk for death among patients with mild infection. KPC-Kp often is found in vulnerable hospital populations at high risk for illness and death (21,26). To estimate the effect of KPC-Kp infection on hospital mortality rates, we compared patients with severe and mild infections with colonized patients. Colonized patients who did not have infectious events during hospitalization represented the best available control group because they were hospitalized in the same hospitals at the same time as KPC-Kp infected cases and are known to have similar clinical characteristics and underlying conditions (27).

Regarding therapeutic approaches, we found the initial empirical selection of antimicrobial drug treatment was more frequently adequate in patients with a known previous KPC-Kp colonization. This result is in line with other published studies reporting that for patients with no history of previous colonization, adequate antimicrobial treatment can only be started once the susceptibility profile has been received, and this delay might lead to unfavorable outcomes (28–31). Thus, in geographic regions with high CRE prevalence, extending rectal swab

specimen surveillance to a broader at-risk hospital population is crucial to reduce time to adequate antimicrobial therapy and, ultimately, to improve patients' outcomes. As previously observed (4,29), a combination of ≥ 2 active agents have been prescribed predominantly in patients with severe infections and at higher risk for death. Of note, we observed a substantial use of colistin despite its unknown efficacy and poor safety profile (mainly related to renal failure), as documented in other studies (32–34). In addition, ceftazidime/avibactam use has increased since 2018, when it became available for routine clinical use in Italy. However, the use of ceftazidime/avibactam in nonbacteremic infections should be discouraged to reduce chances of acquired in vitro resistance (35–37). The wide variety of therapeutic regimens, >30 combinations reported in our centers, confirms the need for multicenter randomized trials to identify the most effective combination and dosage of antimicrobial agents.

The major strengths of our study are the size of the sample and the representation of KPC-*Kp* patients included with homogeneous methodology through an independent network of Lombardy hospitals of different size. The results reveal the multifaceted reality of KPC-*Kp* infection in clinical settings.

The first limitation of our study is that we focused on the most clinically relevant episode for each patient. Therefore, patients who had a colonization followed by an infection were considered and classified according to this second more severe event only. However, in our setting, this subgroup included only 8% of the colonized patients. Second, we limited our attention to KPC-*Kp* strains, ignoring *E. coli* and other carbapenemase, such as oxacillinase 48-like and New Delhi metallo- β -lactamase. Nevertheless, the estimated ratio of *K. pneumoniae* to *E. coli* was 11:1 in Italy (16), and KPC is the only endemic mechanism demonstrating carbapenem resistance (9). Third, despite the inclusion of a large number of infected patients, the multitude of treatment patterns prevented reliable exploration of effects of treatment on clinical outcomes, but the description of this heterogeneity remains one of the findings of this study. Finally, we focused on overall rather than disease-specific mortality rates because we aimed to give a global picture of KPC-*Kp* burden in the Lombardy region. Cause-specific mortality analysis would have required detailed information on the procedures performed before the events occurring during hospitalization, which was beyond the scope of this study.

In conclusion, our study describes KPC-*Kp* in a single region of Italy where KPC-*Kp* has been endemic

since 2013. The KPC-*Kp* epidemic appears to be driven by the expansion of only 3 major clonal lineages. Therefore, the wide heterogeneity in the proportion and incidence of KPC-*Kp* infections are presumably largely influenced by surveillance protocols and hospital policies. Consequently, to reverse this trend, Italy needs a strengthened collaborative surveillance system that includes regional plans and strong, centrally coordinated activities at the national level. Furthermore, the wide range of treatments adopted by healthcare facilities in this study highlights the urgent need to accompany the surveillance system with a concerted, aggressive, and prompt antimicrobial stewardship plan.

KPC-*Kp* Study Group collaborators: Simone Battaglia and Giovanni Lorenzin (IRCCS San Raffaele Scientific Institute, Milan, Italy); Annalisa Cavallero (S. Gerardo de' Tintori Hospital, Monza, Italy); Maddalena Casana and Daria Pocaterra (Humanitas Clinical and Research Centre, Milan); Andrea Cona (San Paolo Hospital, Milan); Antonella D'Arminio Monforte (University of Milan San Paolo Hospital, Milan); Gioconda Brigante and Antonella Carducci (Busto Arsizio Hospital, Busto Arsizio, Italy); Daniela Dalla Gasperina and C. Rovelli (University of Insubria, ASST Sette Laghi-Varese, Italy); Matteo Moro and Paolo Scarpellini (IRCCS San Raffaele Scientific Institute, Milan); Giuliano Rizzardini (ASST Fatebenefratelli Sacco, Milan); Angelo Pan and Alessia Zoncada (Istituti Ospedalieri of Cremona, Cremona, Italy); Marco Franzetti and Alessandro Pandolfo (Ospedale A. Manzoni, Lecco, Italy); Francesco Castelli and Ester Pollastra (University of Brescia and ASST Spedali Civili, Brescia, Italy); Giovanna Travi and Chiara Silvia Vismara (ASST Grande Ospedale Metropolitano Niguarda, Milan); Silvia Garilli (Carlo Poma Hospital, Mantova, Italy); Manuela Piazza and Angelo Regazzetti (Hospital of Lodi, Lodi, Italy); Milena Arghittu and Rosaria Maria Colombo (IRCCS Cà Granda Ospedale Maggiore Policlinico, Milan); Pietro Olivieri (ASST Fatebenefratelli Sacco, Milan); Francesco Petri (University of Milano Bicocca, Monza); and Franca Averara and Francesca Vailati (Papa Giovanni XXIII Hospital, Bergamo, Italy).

Acknowledgments

We thank Igor Monti for IT support and development of web-based case report forms; Joanne Fleming and Judith D. Baggott for their crucial language editing; Alessandro Soave and Matteo Sironi for graphics support; and Ivana Garimoldi for secretarial assistance. We also thank Alessandra Piatti, Danilo Cereda, and Mariella De Biase from Direzione Generale Welfare-Regione Lombardia for their valuable assistance and support on administrative and regulatory procedures during the project.

This work was supported by the Italian Ministry of Health-Lombardy Region (grant no. RF-2011-02351728). The funder had no role in study design, data collection, analysis, interpretation of the results and writing the report.

M.R., L.C., and A.G. designed the study and obtained funding. M.R. supervised the study conduction. L.C. supervised the statistical analysis. T.I. was responsible for conduction of data collection. D.C. was responsible for preparation and storage of all samples. P.M., S.B., C.A., R.M., P.A.G., C.D.C., S.P., S.G.R., P.B., P. Bonfanti, E.V.H., M.P., G.G., and C.C. collected data. F.G. and D.M.C. performed and analyzed the whole genome sequencing of all samples collected. L.C., I.S., and A.D.A. performed statistical data analysis. The paper was written by M.R., L.C., D.M.C., and A.G. and critically revised by G.N., M.C.R., and A.B. All authors reviewed and approved the final version of the manuscript before submission. The KPC-*Kp* Study Group contributed substantially to design the data collection form, to reach a shared infection criteria definition, and to enroll all the patients included in the study.

The de-identified patient data used for the results reported in this article, including data in text, tables, figures, and appendices, will be shared along with the study protocol. Data will be available from 3 months to 5 years after article publication. Data will be available to researchers who provide a methodologically sound proposal to achieve their aims. Proposals should be addressed to marianna.rossi@asst-monza.it. To gain access, data applicants will need to sign a data access agreement.

About the Author

Dr. Rossi is an infectious disease specialist at S. Gerardo Hospital, Monza, Italy. Her primary research interests include antimicrobial resistant organisms, hospital acquired infections and infectious disease surveillance.

References

- van Duin D, Doi Y. The global epidemiology of carbapenemase-producing *Enterobacteriaceae*. *Virulence*. 2017; 8:460-9. <https://doi.org/10.1080/21505594.2016.1222343>
- Nordmann P, Cuzon G, Naas T. The real threat of *Klebsiella pneumoniae* carbapenemase-producing bacteria. *Lancet Infect Dis*. 2009;9:228-36. [https://doi.org/10.1016/S1473-3099\(09\)70054-4](https://doi.org/10.1016/S1473-3099(09)70054-4)
- Gupta N, Limbago BM, Patel JB, Kallen AJ. Carbapenem-resistant *Enterobacteriaceae*: epidemiology and prevention. *Clin Infect Dis*. 2011;53:60-7. <https://doi.org/10.1093/cid/cir202>
- Tumbarello M, Viale P, Viscoli C, Trecarichi EM, Tumietto F, Marchese A, et al. Predictors of mortality in bloodstream infections caused by *Klebsiella pneumoniae* carbapenemase-producing *K. pneumoniae*: importance of combination therapy. *Clin Infect Dis*. 2012;55:943-50. <https://doi.org/10.1093/cid/cis588>
- Stewardson AJ, Marimuthu K, Sengupta S, Allignol A, El-Bouseary M, Carvalho MJ, et al. Effect of carbapenem resistance on outcomes of bloodstream infection caused by *Enterobacteriaceae* in low-income and middle-income countries (PANORAMA): a multinational prospective cohort study. *Lancet Infect Dis*. 2019;19:601-10. [https://doi.org/10.1016/S1473-3099\(18\)30792-8](https://doi.org/10.1016/S1473-3099(18)30792-8)
- van Duin D, Kaye KS, Neuner EA, Bonomo RA. Carbapenem-resistant *Enterobacteriaceae*: a review of treatment and outcomes. *Diagn Microbiol Infect Dis*. 2013;75:115-20. <https://doi.org/10.1016/j.diagmicrobio.2012.11.009>
- Grundmann H, Glasner C, Albiger B, Aanensen DM, Tomlinson CT, Andrasevic AT, et al. European Survey of Carbapenemase-Producing *Enterobacteriaceae* (EuSCAPE) Working Group. Occurrence of carbapenemase-producing *Klebsiella pneumoniae* and *Escherichia coli* in the European survey of carbapenemase-producing *Enterobacteriaceae* (EuSCAPE): a prospective, multinational study. *Lancet Infect Dis*. 2017;2:153-63. [https://doi.org/10.1016/S1473-3099\(16\)30257-2](https://doi.org/10.1016/S1473-3099(16)30257-2)
- European Centre for Disease Prevention and Control. Antimicrobial resistance surveillance in Europe 2011. Annual Report of the European Antimicrobial Resistance Surveillance Network (EARS-Net). Stockholm: The Centre; 2012 [cited 2020 Dec 19]. <https://www.ecdc.europa.eu/en/publications-data/antimicrobial-resistance-surveillance-europe-2011>
- European Centre for Disease Prevention and Control. Antimicrobial resistance surveillance in Europe 2016. Annual Report of the European Antimicrobial Resistance Surveillance Network (EARS-Net). Stockholm: The Centre; 2018 [cited 2020 Dec 19]. <https://www.ecdc.europa.eu/en/publications-data/antimicrobial-resistance-surveillance-europe-2016>
- Higher Institute of Health. Ar-Iss, antibiotic resistance surveillance in Italy: 2012-2016 data [in Italian] [cited 2020 Dec 19]. https://www.epicentro.iss.it/resistenza_antibiotici/dati-2012-2016-ar-iss
- Brolund A, Lagerqvist N, Byfors S, Struelens MJ, Monnet DL, Albiger B, et al.; European Antimicrobial Resistance Genes Surveillance Network EURGen-Net Capacity Survey Group. Worsening epidemiological situation of carbapenemase-producing *Enterobacteriaceae* in Europe, assessment by national experts from 37 countries, July 2018. *Euro Surveill*. 2019;24:24. <https://doi.org/10.2807/1560-7917.ES.2019.24.9.1900123>
- Marimuthu K, Venkatachalam I, Khong WX, Koh TH, Cherng BPZ, Van La M, et al.; Carbapenemase-Producing *Enterobacteriaceae* in Singapore (CaPES) Study Group. Clinical and molecular epidemiology of carbapenem-resistant *Enterobacteriaceae* among adult inpatients in Singapore. *Clin Infect Dis*. 2017;64(suppl_2):S68-75. <https://doi.org/10.1093/cid/cix113>
- Centers for Disease Control and Prevention. CDC/NHSN surveillance definitions for specific types of infections. Atlanta: The Centers; 2014 [cited 2020 Dec 19]. http://www.socinorte.com/wp-content/uploads/2014/06/17pscNosInfDef_current.pdf
- McKinnell JA, Dwyer JP, Talbot GH, Connolly LE, Friedland I, Smith A, et al.; CARE Study Group. Plazomicin for infections caused by carbapenem-resistant *Enterobacteriaceae*. *N Engl J Med*. 2019;380:791-3. <https://doi.org/10.1056/NEJMc1807634>
- Clinical and Laboratory Standards Institute. Performance standards for antimicrobial susceptibility testing;

- twenty-fourth informational supplement. Wayne (PA): The Institute; 2014 [cited 2020 Dec 19]. <https://webstore.ansi.org/Standards/CLSI/CLSIM100S24>
16. European Centre for Disease Prevention and Control. ECDC country visit to Italy to discuss antimicrobial resistance issues. Stockholm: The Centre; 2017 [cited 2020 Dec 19]. <https://www.ecdc.europa.eu/en/publications-data/ecdc-country-visit-italy-discuss-antimicrobial-resistance-issues>
 17. Navon-Venezia S, Kondratyeva K, Carattoli A. *Klebsiella pneumoniae*: a major worldwide source and shuttle for antibiotic resistance. *FEMS Microbiol Rev.* 2017;41:252–75. <https://doi.org/10.1093/femsre/fux013>
 18. Snitkin ES, Zelazny AM, Thomas PJ, Stock F, Henderson DK, Palmore TN, et al.; NISC Comparative Sequencing Program. Tracking a hospital outbreak of carbapenem-resistant *Klebsiella pneumoniae* with whole-genome sequencing. *Sci Transl Med.* 2012;4:148ra116. <https://doi.org/10.1126/scitranslmed.3004129>
 19. Mathers AJ, Peirano G, Pitout JD. The role of epidemic resistance plasmids and international high-risk clones in the spread of multidrug-resistant *Enterobacteriaceae*. *Clin Microbiol Rev.* 2015;28:565–91. <https://doi.org/10.1128/CMR.00116-14>
 20. Conte V, Monaco M, Giani T, D'Ancona F, Moro ML, Arena F, et al.; AR-ISS Study Group on Carbapenemase-Producing *K. pneumoniae*. Molecular epidemiology of KPC-producing *Klebsiella pneumoniae* from invasive infections in Italy: increasing diversity with predominance of the ST512 clade II sublineage. *J Antimicrob Chemother.* 2016;71:3386–91. <https://doi.org/10.1093/jac/dkw337>
 21. Tumbarello M, Treccarichi EM, De Rosa FG, Giannella M, Giacobbe DR, Bassetti M, et al.; ISGRI-SITA (Italian Study Group on Resistant Infections of the Società Italiana Terapia Antinfettiva). Infections caused by KPC-producing *Klebsiella pneumoniae*: differences in therapy and mortality in a multicentre study. *J Antimicrob Chemother.* 2015;70:2133–43. <https://doi.org/10.1093/jac/dkv086>
 22. Daikos GL, Tsaousi S, Tzouveleki LS, Anyfantis I, Psychogiou M, Argyropoulou A, et al. Carbapenemase-producing *Klebsiella pneumoniae* bloodstream infections: lowering mortality by antibiotic combination schemes and the role of carbapenems. *Antimicrob Agents Chemother.* 2014;58:2322–8. <https://doi.org/10.1128/AAC.02166-13>
 23. Patel G, Huprikar S, Factor SH, Jenkins SG, Calfee DP. Outcomes of carbapenem-resistant *Klebsiella pneumoniae* infection and the impact of antimicrobial and adjunctive therapies. *Infect Control Hosp Epidemiol.* 2008;29:1099–106. <https://doi.org/10.1086/592412>
 24. Fraenkel-Wandel Y, Raveh-Brawer D, Wiener-Well Y, Yinnon AM, Assous MV. Mortality due to bla_{KPC} *Klebsiella pneumoniae* bacteraemia. *J Antimicrob Chemother.* 2016;71:1083–7. <https://doi.org/10.1093/jac/dkv414>
 25. Bertolini G, Nattino G, Tascini C, Poole D, Viaggi B, Carrara G, et al.; GiViTI Steering Committee. Mortality attributable to different *Klebsiella* susceptibility patterns and to the coverage of empirical antibiotic therapy: a cohort study on patients admitted to the ICU with infection. *Intensive Care Med.* 2018;44:1709–19. <https://doi.org/10.1007/s00134-018-5360-0>
 26. Hauck C, Cober E, Richter SS, Perez F, Salata RA, Kalayjian RC, et al.; Antibacterial Resistance Leadership Group. Spectrum of excess mortality due to carbapenem-resistant *Klebsiella pneumoniae* infections. *Clin Microbiol Infect.* 2016;22:513–9. <https://doi.org/10.1016/j.cmi.2016.01.023>
 27. Borer A, Saidel-Odes L, Eskira S, Nativ R, Riesenberk K, Livshiz-Riven I, et al. Risk factors for developing clinical infection with carbapenem-resistant *Klebsiella pneumoniae* in hospital patients initially only colonized with carbapenem-resistant *K. pneumoniae*. *Am J Infect Control.* 2012;40:421–5. <https://doi.org/10.1016/j.ajic.2011.05.022>
 28. Shimasaki T, Seekatz A, Bassis C, Rhee Y, Yelin RD, Fogg L, et al.; Centers for Disease Control and Prevention Epicenters Program. Increased relative abundance of *Klebsiella pneumoniae* carbapenemase-producing *Klebsiella pneumoniae* within the gut microbiota is associated with risk of bloodstream infection in long-term acute care hospital patients. *Clin Infect Dis.* 2019;68:2053–9. <https://doi.org/10.1093/cid/ciy796>
 29. Gutiérrez-Gutiérrez B, Salamanca E, de Cueto M, Hsueh PR, Viale P, Paño-Pardo JR, et al.; REIPI/ESGBIS/INCREMENT Investigators. Effect of appropriate combination therapy on mortality of patients with bloodstream infections due to carbapenemase-producing *Enterobacteriaceae* (INCREMENT): a retrospective cohort study. *Lancet Infect Dis.* 2017;17:726–34. [https://doi.org/10.1016/S1473-3099\(17\)30228-1](https://doi.org/10.1016/S1473-3099(17)30228-1)
 30. Cano A, Gutiérrez-Gutiérrez B, Machuca I, Gracia-Ahufinger I, Pérez-Nadales E, Causse M, et al. Risks of infection and mortality among patients colonized with *Klebsiella pneumoniae* carbapenemase-producing *K. pneumoniae*: validation of scores and proposal for management. *Clin Infect Dis.* 2018;66:1204–10. <https://doi.org/10.1093/cid/cix991>
 31. Giannella M, Treccarichi EM, De Rosa FG, Del Bono V, Bassetti M, Lewis RE, et al. Risk factors for carbapenem-resistant *Klebsiella pneumoniae* bloodstream infection among rectal carriers: a prospective observational multicentre study. *Clin Microbiol Infect.* 2014;20:1357–62. <https://doi.org/10.1111/1469-0691.12747>
 32. Giacobbe DR, di Masi A, Leboffe L, Del Bono V, Rossi M, Cappiello D, et al. Hypoalbuminemia as a predictor of acute kidney injury during colistin treatment. *Sci Rep.* 2018;8:11968. <https://doi.org/10.1038/s41598-018-30361-5>
 33. van Duin D, Lok JJ, Earley M, Cober E, Richter SS, Perez F, et al.; Antibacterial Resistance Leadership Group. Colistin versus ceftazidime-avibactam in the treatment of infections due to carbapenem-resistant *Enterobacteriaceae*. *Clin Infect Dis.* 2018;66:163–71. <https://doi.org/10.1093/cid/cix783>
 34. Perez F, Bonomo RA. Carbapenem-resistant *Enterobacteriaceae*: global action required. *Lancet Infect Dis.* 2019;19:561–2. [https://doi.org/10.1016/S1473-3099\(19\)30210-5](https://doi.org/10.1016/S1473-3099(19)30210-5)
 35. Shields RK, Potoski BA, Haidar G, Hao B, Doi Y, Chen L, et al. Clinical outcomes, drug toxicity, and emergence of ceftazidime-avibactam resistance among patients treated for carbapenem-resistant *Enterobacteriaceae* infections. *Clin Infect Dis.* 2016;63:1615–8. <https://doi.org/10.1093/cid/ciw636>
 36. Shields RK, Nguyen MH, Chen L, Press EG, Kreiswirth BN, Clancy CJ. Pneumonia and renal replacement therapy are risk factors for ceftazidime-avibactam treatment failures and resistance among patients with carbapenem-resistant *Enterobacteriaceae* infections. *Antimicrob Agents Chemother.* 2018;62:e02497–17. <https://doi.org/10.1128/AAC.02497-17>
 37. Tumbarello M, Treccarichi EM, Corona A, De Rosa FG, Bassetti M, Mussini C, et al. Efficacy of ceftazidime-avibactam salvage therapy in patients with infections caused by *Klebsiella pneumoniae* carbapenemase-producing *K. pneumoniae*. *Clin Infect Dis.* 2019;68:355–64. <https://doi.org/10.1093/cid/ciy492>

Address for correspondence: Andrea Gori, Infectious Diseases Unit, Department of Internal Medicine, Fondazione IRCCS Ca' Granda Ospedale Maggiore Policlinico, Paviglione Granelli, first floor, Via Sforza 35 Milan 20122, Italy; email: andrea.gori@unimi.it

Engineered NS1 for Sensitive, Specific Zika Virus Diagnosis from Patient Serology

Thai Leong Yap,¹ Shin Yee Hong,¹ Jun Hui Soh, Lekha Ravichandraprabhu, Vanessa W.X. Lim, Hsi-Min Chan, Tommy Z.X. Ong, Ying Ping Chua, Shi En Koh, Huajing Wang, Yee Sin Leo, Jackie Y. Ying, William Sun

Dengue virus (DENV) and Zika virus (ZIKV) belong to the *Flaviviridae* family of viruses spread by *Aedes aegypti* mosquitoes in tropical and subtropical areas. Accurate diagnostic tests to differentiate the 2 infections are necessary for patient management and disease control. Using characterized ZIKV and DENV patient plasma in a blind manner, we validated an ELISA and a rapid immunochromatographic test for ZIKV detection. We engineered the ZIKV nonstructural protein 1 (NS1) for sensitive serologic detection with low cross reactivity against dengue and developed monoclonal antibodies specific for the ZIKV NS1 antigen. As expected, the serologic assays performed better with convalescent than acute plasma samples; the sensitivity ranged from 71% to 88%, depending on the performance of individual tests (IgM/IgG/NS1). Although serologic tests were generally less sensitive with acute samples, our ZIKV NS1 antibodies were able to complement the serologic tests to achieve greater sensitivity for detecting early infections.

Zika virus (ZIKV), a single-stranded RNA virus, belongs to the family *Flaviviridae*. It is transmitted by infected *Aedes* spp. mosquitoes, the same vector that transmits dengue virus (DENV) in tropical and subtropical areas (1–3). Patients infected by ZIKV are often asymptomatic or have mild symptoms similar to those of dengue infections, such as fever, rash, and joint pain (4–6). However, the ZIKV outbreak in Brazil in 2015–2016 has drawn much attention because of

its association with a marked increase in the number of newborns with microcephaly from infected mothers (7–10). Other neurologic diseases, such as Guillain-Barré syndrome, have also been associated with ZIKV infections (7,11,12).

Several molecular- or serologic-based assays have been approved by the US Food and Drug Administration for emergency use to diagnose ZIKV infections (13,14). Nucleic acid testing has shown good specificity in general, but high variations in assay sensitivity have been reported (15). This variability can be the result of complicated experimental setups, genetic variability in different virus strains, or narrow detection window because of low viremia load in ZIKV-infected patients (16,17). Thus, in nucleic acid test-negative cases, complementary assays based on serology testing, such as Zika IgM antibody capture ELISA (MAC-ELISA) and plaque-reduction neutralization test (PRNT), are required to validate the results (18,19). Those secondary tests are not specific because of high cross reactivity with other flaviviruses, further complicating the interpretation of test results (20,21). There is a need to develop a more reliable Zika diagnostic test for outbreak control and improved patient care.

We aimed to develop specific serology tests that could differentiate ZIKV from DENV infections by engineering the ZIKV nonstructural protein 1 (NS1). We established both ELISA and immunochromatographic assays (IAs) for specific and sensitive binding to ZIKV IgM and IgG. In particular, we developed 2 IA assays, in which the engineered antigens were used either as capture (F1 format) or detector (F2 format), resulting in slight difference in sensitivity and specificity. We further assessed assay performance by testing plasma samples collected from patients during acute and convalescent phases of infection.

Author affiliations: Experimental Drug Development Centre, Singapore (T.L. Yap, S.Y. Hong); Institute of Bioengineering and Nanotechnology, Singapore (T.L. Yap, S.Y. Hong, L. Ravichandraprabhu, T.Z.X. Ong, Y.P. Chua, S.E. Koh, H. Wang, W. Sun); NanoBio Lab, Singapore (J.H. Soh, H.-M. Chan, J.Y. Ying); National Centre for Infectious Diseases, Singapore (V.W.X. Lim, Y.S. Leo); Tan Tock Seng Hospital, Singapore (Y.S. Leo); Yong Loo Lin School of Medicine, National University of Singapore (Y.S. Leo, W. Sun).

DOI: <https://doi.org/10.3201/eid2705.190121>

¹These authors contributed equally to this article.

Materials and Methods

Patient Samples and Study Approval

Whole-blood samples were collected with ethylenediaminetetraacetic acid-lined Vacutainer tubes (Becton Dickinson, <http://www.bd.com>) from patients referred to the Communicable Disease Centre, Tan Tock Seng Hospital (TTSH), Singapore. We obtained blood specimens from patients consenting to the study. All patients gave separate written informed consent. The study protocols were approved by the SingHealth Centralized Institutional Review Board (reference no. 2016/2219) and by the National Healthcare Group Domain Specific Review Board (reference no. 2015/00528).

This study included plasma samples obtained from 94 patients with ZIKV who were admitted to the Communicable Disease Centre at TTSH during August 27, 2016–August 14, 2017, and 70 DENV patients admitted during April 29, 2016–March 28, 2017. Samples were collected at 2 phases: acute (1–6 days postonset of symptoms [dpo]) and early convalescent (7–21 dpo). Patients could donate blood samples multiple times during each phase. Only 11/94 (12%) of patients from the ZIKV cohort and 12/70 (17%) of patients from the DENV cohort had traveled within 2 weeks of recruitment. Therefore, we could conclude that most patients were infected from local transmission.

Among the patients with ZIKV, 41 (43.62%) were female and 53 (56.38%) were male (Table 1). These patients were confirmed to be infected with ZIKV according to reverse transcription PCR (RT-PCR) using an adapted protocol (22) performed on plasma and urine samples obtained during their first visits. In addition, all ZIKV patients were tested for dengue NS1 using the SD BIOLINE Dengue Duo rapid test (Abbott, <https://www.globalpointofcare.abbott>); 3 of 94 patients were further confirmed DENV NS1-positive by RT-PCR, indicating a concurrent DENV infection (23). Among the DENV patients, 19 (27.14%) were female and 51 (72.86%) were male. The patients with DENV were tested with hospital routine diagnostics using the SD BIOLINE Dengue Duo rapid test. All NS1-positive samples were confirmed to be dengue positive using the FTD Zika/dengue/chikungunya RT-PCR (Fast Track Diagnostics, <http://www.fast-trackdiagnostics.com>). Dengue serotypes were further determined by FTD dengue differentiation RT-PCR test (Fast Track Diagnostics), according to the manufacturer's instructions (Appendix 1, <https://wwwnc.cdc.gov/EID/article/27/5/19-0121-App1.pdf>).

For the validation tests, we used 70 samples from 62 unique patients with ZIKV (9 patients had >1 sample collected during the time period), and 81 samples from 68 unique patients with DENV (13 patients had >1 sample collected) collected in the acute phase (1–6 dpo). From the early convalescent phase (7–21 dpo), we used 48 samples from 44 unique patients with ZIKV and 70 samples from 53 unique patients with DENV. Samples were randomized and blinded during testing.

During assay optimization, we used a subset of samples from TTSH and a commercial vendor (SeraCare, <https://www.seracare.com>) and designated this combined sample pool as the training set (37 ZIKV samples, 67 DENV samples). TTSH samples have records of the day of collection after onset of symptoms (27 ZIKV samples, 46 DENV samples), whereas this information was not available for the commercial samples (10 ZIKV samples, 21 DENV samples). SeraCare panels 0845-0142 (ZIKV) and 0845-0074 (DENV) were used for training; samples DSC-7, 12, and 20 from SeraCare panel 0845-0051 (DENV) and ZPC-1, -2, -4, and -8 (ZIKV, country of origin Columbia) acquired from Precision Technologies, Singapore (<http://www.pretech.com.sg>) were used for characterization of engineered ZIKV NS1 (Appendix 1).

Results

Engineering Full-Length NS1 Protein for Serologic Assays

We hypothesized that ZIKV NS1 could be used to develop a specific and sensitive serologic test because we were able to generate monoclonal antibodies specific for this antigen without cross-reactivity to NS1 from other flaviviruses. When we first tried to express the full-length ZIKV NS1 protein (GenBank accession

Table 1. Characteristics of patients admitted to Tan Tock Seng Hospital, Singapore, whose blood samples were used for study of Zika diagnosis*

Patient characteristics	Patients with Zika virus	Patients with dengue virus
Total no.	94	70
Sex		
M	53 (56.4)	51 (72.9)
F	41 (43.6)	19 (27.1)
Ethnicity		
Chinese	77 (81.9)	41 (58.6)
Malay	7 (7.4)	5 (7.1)
Indian	5 (5.3)	7 (10.0)
Other	5 (5.3)	17 (24.3)
Median age, y	39	35
Age range, y	14–72	22–60

*Values are no. (%) except as indicated.

no. KX447521.1), we found that it was poorly expressed in our mammalian system. We subsequently constructed various ZIKV NS1 domains fused to different carriers at the N or C terminus. We aimed to optimize the construct with respect to solubility and specific reactivity to ZIKV immune serum samples.

Among the different construct designs, we determined that the His-tagged albumin domain (H, residue 1–197 aa) N terminally fused to the NS1 variants, resulting in H-zWT (NS1 1–352 aa) and H-zD1 (NS1 172–352 aa), showed reasonable solubility (≥ 1 mg per 40–80 mL of culture). Using IgG ELISA, we showed that the 2 constructs had good reactivity to the commercial ZIKV samples (Figure 1, panel A), but H-zD1 showed reactivity to only 1 TTSH ZIKV sample (Figure 1, panel B). We observed that wild-type NS1 (ZIKV WT and DENV WT, obtained from Native Antigen) showed similar reactivity as H-zD1 to these TTSH serum samples (Figure 1, panel B).

Although our full-length ZIKV NS1 was not expressed in soluble form with the thioredoxin (Trx) at the C terminus, we were able to produce 2 soluble forms of C terminal constructs: zD1-Trx (residue 172–352 aa) and zD2-Trx (172–339 aa). We asked whether truncation at the C terminus could differentiate

zD1-Trx from zD2-Trx in DENV IgG cross reactivity. Among the DENV samples from the SeraCare commercial panel 0845_0051 that were available at the time (DSC-7, DSC-12, and DSC-20), we found that DSC-7 showed cross reactivity to the ZIKV WT. We then showed that zD2-Trx has reduced IgG ELISA activity to DSC-7, compared with zD1-Trx (Figure 1, panel C). Although we observed this only with 1 DENV serum sample, we hypothesized that, by altering residues conserved between DENV and ZIKV in the region of 339–352 aa, we could reduce DENV IgG cross reactivity.

We subsequently generated a series of mutants spanning the 339–352 aa region of the H-zWT construct because this format was the most reactive to ZIKV IgG. Of all the mutants, we selected H-zMut1 (V350T, N344D, P341Q) and H-zMut2 (A352D, T351H, S348D, N344K, P341H), for their soluble expression and their ability to reduce DENV cross reactivity without greatly compromising the ZIKV signal in both the ELISA and IA formats. We first showed that H-zMut2 had a greater reduction in reactivity to DSC-7 compared with H-zWT and H-zMut1 in IgG ELISA (Figure 1, panel D). We then further used H-zMut2 as the capture antigen for optimizing the ELISA for

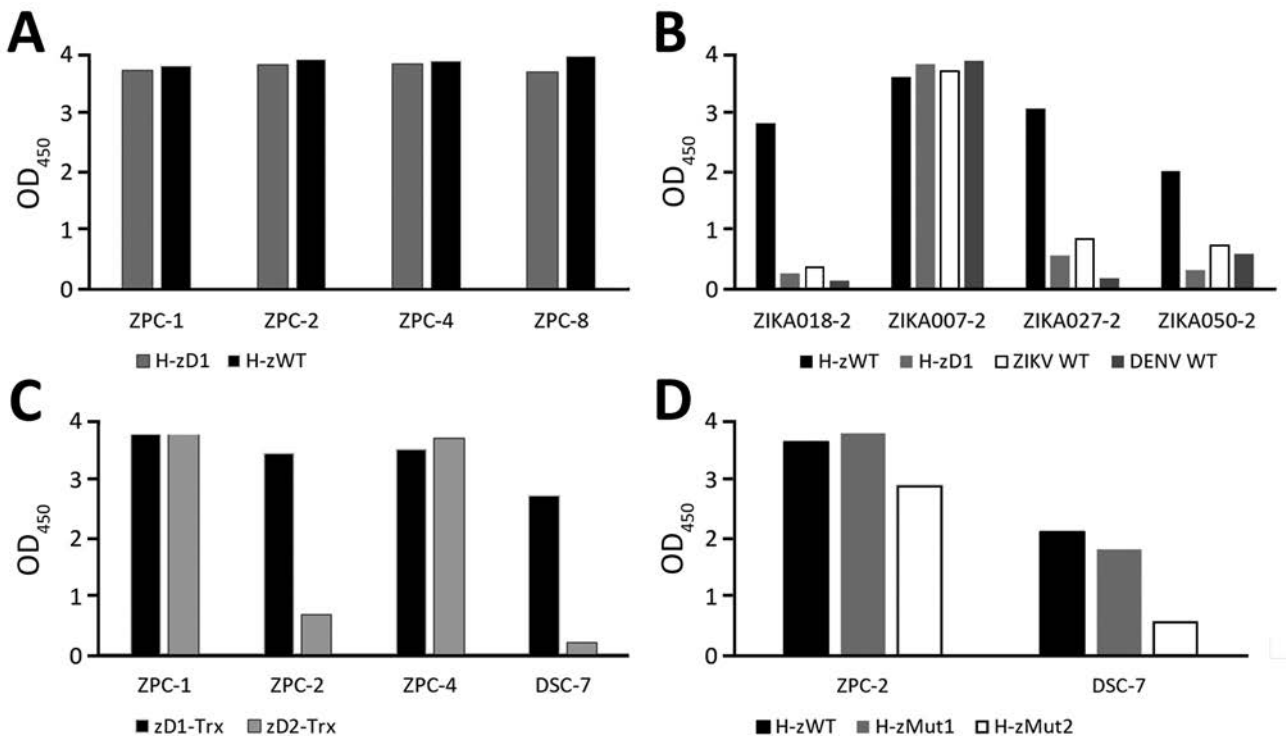


Figure 1. Reactivity of nonstructural protein 1 antigens to ZIKV and DENV plasma in study of Zika diagnosis, Singapore. A) Reactivity of H-zWT and H-zD1 to commercial ZIKV IgG in ELISA format. B) Reactivity of H-zWT, H-zD1, ZIKV WT, and DENV WT to samples from Tan Tock Seng Hospital. C) Comparison of zD1-Trx and zD2-Trx activity to DSC-7. D) comparison of H-zWT, H-zMut1, and H-zMut2 activity to DSC-7. The graphs show mean OD measurements from 2 replicates. DENV, dengue virus; OD, optical density; WT, wild type; ZIKV, Zika virus.

specific binding to IgM and IgG with a collection of plasma samples designated the “training set.” Under the optimized ELISA conditions, H-zMut2 resulted in IgM/IgG detection with sensitivity and specificity >80% (Figure 2, panels A, B; Appendix 1 Table 1).

H-M ut2 ELISA for Blinded Test Evaluation

Upon achieving the desired performance with the training set, we proceeded to evaluate our assay on a larger group of samples in a blinded manner. This validation set consisted of 269 samples collected by TTSH from patients with ZIKV and DENV. Among the 3 engineered antigens, H-zMut2 showed greater detection sensitivity and specificity than ZIKV WT but only slightly lower sensitivity (though higher specificity) compared with H-zWT (Figure 3; Appendix 1 Table 2). In the ELISA test, H-zMut2 showed low sensitivity with acute samples (IgM/IgG 41%/23%) but high specificity (IgM/IgG 100%/97%) (Table 2; Figure 3). The result reflected the low IgG titer during the acute phase of Zika infection, consistent with other studies (Table 2; Figure 3, panels D, E; Appendix 1 Table 2). Compared with H-zMut2, ZIKV WT showed much lower sensitivity (IgM/IgG 3%/14%) (Appendix 1 Table 2). In contrast with the acute samples, H-zMut2 capture antigen showed relatively high sensitivity when tested on convalescent samples (IgM/IgG sensitivity 79%/83%, IgM/IgG specificity 95%/84%) (Table 2; Figure 3), and continued to outperform ZIKV WT (IgM/IgG sensitivity 33%/56%, IgM/IgG specificity 98%/73%) (Appendix 1 Table 2).

Given that the IgM or IgG ELISA with H-zMut2 each detected a different subset of ZIKV samples (Figure 3, panels B, E), combining the IgM/IgG test

results could achieve a greater sensitivity for both acute samples (17% [WT] < 52% [mut2]) and convalescent samples (83% [WT] < 89% [mut2]) (Appendix 1 Table 2). Although H-zWT was more sensitive than ZIKV WT in individual IgM/IgG tests, both antigens showed comparable combined sensitivity (Appendix 1 Table 2). The ZIKV WT, however, was more cross-reactive to DENV IgG (specificity 54% [H-zWT] < 71% [ZIKV WT] < 80% [H-zMut2]).

Engineered NS1 Antigens for Rapid Test Assay

To develop IA that would permit rapid diagnosis of ZIKV infections, we evaluated both candidates, H-zMut1 and H-zMut2, using 2 different assay formats. The first format (F1), similar to the ELISA approach, used the engineered proteins as capture antigens for ZIKV IgM and IgG on 2 independent strips and used a detector antibody conjugated to enzyme for signal amplification (Figure 4). In the second format (F2), the antigens were conjugated to gold nanoparticles and served as a detector for binding patient IgM and IgG that were captured on 2 different spots on the same strip (Figure 5). During the development and optimization of the assays, we found that H-zMut2 showed better sensitivity than H-zMut1 in the F1 format, whereas HzMut1 showed better performance in the F2 format.

When analyzing the training set in the F1 format, H-zMut2 showed greater detection sensitivity and specificity than ZIKV WT (except slightly lower in IgM specificity, 89.6% [H-zMut2] vs. 95.5% [ZIKV WT]) and greater IgG specificity than H-zWT, though with comparable sensitivity (Figure 4; Appendix 1 Table 3). Although H-zWT also showed improved sensitivity compared with ZIKV WT (IgM 49% [WT]

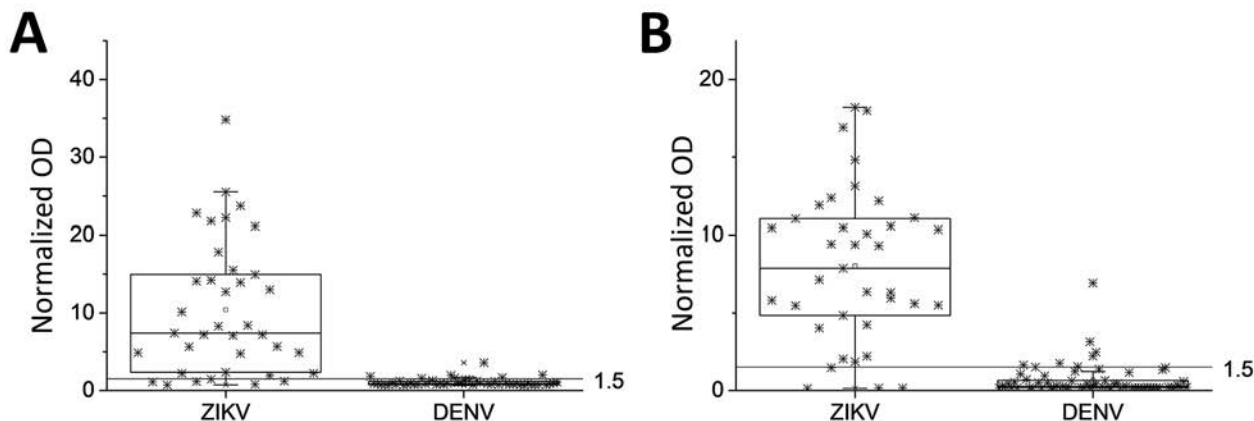


Figure 2. Reactivity of nonstructural protein 1 antigens to ZIKV and DENV plasma in study of Zika diagnosis, Singapore. H-zMut2 ELISA was tested with a training set for binding to IgM (A) and IgG (B). Results are representative of replicates for each sample. Normalized OD >1.5 for plasma or serum sample was determined as positive for ZIKV infection. DENV, dengue virus; OD, optical density; ZIKA, Zika virus.

< 81% [H-zWT]; IgG 70% [WT] < 97% [H-zWT]), it showed lower IgG specificity than H-zMut2 and ZIKV WT (Figure 4; Appendix 1 Table 3).

H-zMut2-F1 and H-zMut1-F2 for Blinded Test Evaluation

When we evaluated the H-zMut2-F1 assay with the validation set in a blinded manner, it showed 51%/95% (IgM) and 44%/93% (IgG) sensitivity/specificity for the acute phase samples (Table 2; Figure 6). In contrast with the acute plasma samples, the F1 assay could achieve >70% test performance for convalescent samples (sensitivity: IgM/IgG 71%/90%; specificity: IgM/IgG 87%/79%). Combining both IgM and IgG tests increased the sensitivity for acute phase samples (69%) without greatly lowering the specificity (89% vs. 95%) (Table 2). Although the combined tests showed no major change in sensitivity with convalescent samples (90%), there was a slight decrease in the specificity (69% [IgM + IgG] <79% [IgG] <87% [IgM]) (Table 2).

When we used H-zMut1 in the F2 format to analyze the validation set, it showed lower sensitivity than HzMut2-F1, noticeably in IgG detection (Table 2). However, when both IgM and IgG tests were

combined, H-zMut1-F2 showed improved sensitivity, 60% for acute samples and 88% for convalescent samples, while maintaining excellent specificity, 96% for acute samples and 84% for convalescent samples (Table 2).

Performance Comparison for F1/F2 IA Format and Commercial Kit

We evaluated a commercially available ZIKV IgM/IgG rapid test kit (GenBody, <http://genbody.co.kr>) with TTSH samples, and compared the results to our F1 and F2 IA formats obtained from the blinded samples test. The GenBody kit used E (envelope) and NS1 antibodies in complex with E/NS1 antigen for detecting ZIKV IgM/IgG. This commercial kit was previously reported to exhibit high sensitivity and specificity for both IgM and IgG (>90%) (24). The GenBody tests did not perform as well as our F1 and F2 IA when applied to the samples from the validation set (Table 3). In particular, the Genbody test showed low sensitivity for IgM (29%) and low specificity for IgG (62%). The combined IgM/IgG test from GenBody showed low specificity (56%) but reasonable sensitivity (79%).

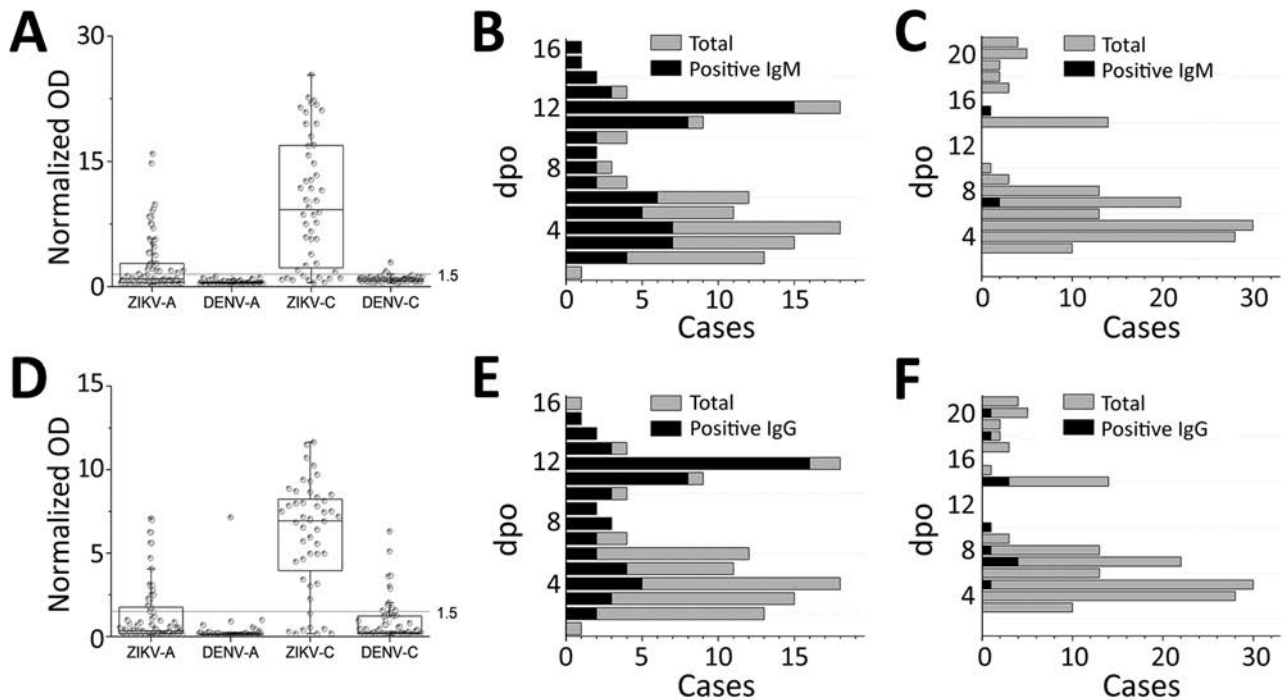


Figure 3. H-zMut2 ELISA for validation set in study of Zika diagnosis, Singapore. A, D) H-zMut2 reactivity to IgM (A) and IgG (D) present in plasma collected during acute and recent convalescent phases (ZIKV-A, n = 70 [1–6 dpo]; ZIKV-C, n = 48 [7–14 dpo]; DENV-A, n = 81 [1–6 dpo]; DENV-B, n = 70 [7–21 dpo]). Plasma samples were blinded and tested with H-zMut2 as the capture antigen. Normalized OD >1.5 for plasma sample was determined as positive for ZIKV infection. Results are representative of 2 replicates for each plasma sample. B, C, E, F) Patient samples for ZIKV (B, E) and DENV (C, F). The plots show distribution of number of plasma cases (x-axis) over number of days post infection (y-axis, dpo) for H-zMut2 ELISA tested with validation set; the number of positive plasma samples (black bar) was shown against the total (gray bar) for each dpo. DENV, dengue virus; dpo, days postonset of symptoms; OD, optical density; ZIKA, Zika virus.

Table 2. Sensitivity and specificity results for validation set in blinded evaluation for study of Zika diagnosis, Singapore*

Phase	Sensitivity, % (95% CI)			Specificity, % (95% CI)		
	ELISA	Lateral flow		ELISA	Lateral flow	
		F1	F2		F1	F2
Acute, 1–6 dpo						
IgM	41.4 (29.8–53.8)	51.4 (39.2–63.6)	50.0 (37.8–62.2)	100.0 (95.5–100.0)	95.1 (87.8–98.6)	97.5 (0.91–1.00)
IgG	22.9 (13.7–34.4)	44.3 (32.4–56.7)	20.0 (11.4–31.3)	98.8 (93.3–100.0)	92.6 (84.6–97.2)	98.8 (0.93–1.00)
IgM/IgG	52.9 (40.6–64.9)	68.6 (56.4–79.1)	60.0 (47.6–71.5)	98.8 (93.3–100.0)	88.9 (80.0–94.8)	96.3 (0.90–0.99)
NS1	41.4 (29.8–53.8)	NP	NP	97.5 (91.4–99.7)	NP	NP
IgM/NS1	55.7 (43.3–67.6)	NP	NP	97.5 (91.4–99.7)	NP	NP
IgG/NS1	61.4 (49.0–72.8)	NP	NP	96.3 (89.6–99.2)	NP	NP
IgM/IgG/NS1	67.1 (54.9–77.9)	NP	NP	96.3 (89.6–99.2)	NP	NP
Convalescent, 7–21 dpo						
IgM	79.2 (65.0–89.5)	70.8 (55.9–83.0)	70.8 (55.9–83.0)	95.7 (88.0–99.1)	87.1 (77.0–93.9)	94.3 (86.0–98.4)
IgG	83.3 (69.8–92.5)	89.6 (77.3–96.5)	79.2 (65.0–89.5)	84.3 (73.6–91.9)	78.6 (67.1–87.5)	90.0 (80.5–95.9)
IgM/IgG	89.6 (77.3–96.5)	89.6 (77.3–96.5)	87.5 (74.8–95.3)	80 (68.7–88.6)	68.6 (56.4–79.1)	84.3 (73.6–91.9)

*ELISA and IA assays were evaluated for the detection of NS1, IgM, and IgG with TTSH plasma samples (ZIKV: n = 70 with 1–6 dpo, and n = 48 with 7–16 dpo; DENV: n = 81 with 1–6 dpo, and n = 70 with 7–21 dpo). Sensitivity and specificity were determined with positive plasmas divided by the total number of respective ZIKV and DENV plasma samples. DENV, dengue virus; dpo, days postonset of symptoms; F1, capture format; F2, detector format; IA, immunochromatographic assay; NP, not performed (NS1 antigen test was not performed in the lateral flow formats because of low sensitivity); NS1, nonstructural protein 1; ZIKV, Zika virus.

Addition of ZIKV NS1 Test to Improve Sensitivity for Acute Phase Samples

Detecting DENV NS1 in serum has been reported to be a suitable method for diagnosing acute DENV infections (25,26). We hypothesized that by detecting NS1 antigen in acute ZIKV-infected plasma, this assay could improve the sensitivity of the IgM/IgG test because ZIKV belongs to the same flavivirus family as DENV. We generated monoclonal antibodies specific against ZIKV NS1 antigen and optimized antibody pairing for quantitative ELISA (Appendix 1 Figure, panel A). Using normal human serum spiked with recombinant ZIKV NS1, we established 0.1 ng/mL as the detection limit in our assay (Appendix 1 Figure, panel B). After testing 45 DENV samples, we set a cutoff above 0.25 ng/mL as being ZIKV NS1 positive (Appendix 1 Figure, panel C).

We next evaluated the performance of our NS1 ELISA by testing the validation set in a blinded fashion. The area under the receiver operating characteristics curve plotted with ZIKV-infected and non-ZIKV-infected samples was 0.715, suggesting that the assay was able to differentiate between these 2 groups of patients with sensitivity of 41% and a specificity of 98% for acute phase samples (Table 2; Figure 7, panel A). We found that the ZIKV NS1 concentration was extremely low or

undetectable in most of the patient samples. Among all the ZIKV-infected acute samples, only 7% had NS1 >1 ng/mL; 34% were in the range of 0.25–1 ng/mL, and 60% of the samples had NS1 level below the detection limit (Figure 7, panels B, C). However, when complementing NS1 antigen detection with either IgM or IgG ELISA, the sensitivity of detection could be improved for acute-phase infections (53% [IgM+IgG] < 56% [IgM+NS1] < 61% [IgG+NS1]) (Table 2). After we combined all 3 tests (NS1/IgM/IgG), the ELISA sensitivity was further improved to 67% while maintaining a high specificity (96%).

Analysis of Acute-Phase Patient Samples

We tested a total of 151 acute-phase samples (70 ZIKV and 81 DENV samples, collected at 1–6 dpo) with ELISA and IA methods. Our data suggested that a combination of 3 immunoassays, NS1, IgM, and IgG, was needed to achieve a reasonable detection sensitivity in the acute phase. Among the 70 acute-phase serum samples, our ELISA tests were able to detect ZIKV infection as early as 2 days after fever onset, through detecting NS1 (7 cases), IgM (4 cases), or IgG (2 cases). The overall detection rate for the 70 acute-phase samples was 41% for NS1 (29 cases), 41% for IgM (29 cases), and 22% for IgG (16 cases). Only 8 of the 70 acute-phase samples were positive for both IgM and IgG. Among the 29 samples positive

Table 3. Sensitivity and specificity comparison between GenBody and in-house IA assays for study of Zika diagnosis, Singapore*

Late phase, 7–16 dpo	Sensitivity, % (95% CI)			Specificity, % (95% CI)		
	GenBody	Lateral flow		GenBody	Lateral flow	
		F1	F2		F1	F2
IgM	28.6 (15.7–44.6)	76.2 (60.5–87.9)	73.8 (58.0–86.1)	97.4 (86.5–99.9)	100.0 (91.0–100.0)	94.9 (82.7–99.4)
IgG	71.4 (55.4–84.3)	85.7 (71.4–94.6)	76.2 (60.5–87.9)	61.5 (44.6–76.6)	79.5 (63.5–90.7)	89.7 (75.8–97.1)
IgM/IgG	78.6 (63.2–89.7)	85.7 (71.4–94.6)	85.7 (71.5–94.6)	56.0 (42.1–74.4)	79.5 (63.5–90.7)	84.6 (69.5–94.1)

*All IA assays were evaluated with TTSH plasma for IgM and IgG test (ZIKV, n = 42; DENV, n = 39, 7–16 dpo, subset of blinded test samples). GenBody strips were tested in a nonblinded approach, and compared with F1 and F2 results that were obtained from the blinded test of the validation set. DENV, dengue virus; dpo, days post onset of symptoms; F1, capture format; F2, detector format; IA, immunochromatographic assay; TTSH, Tan Tock Seng Hospital; ZIKV, Zika virus.

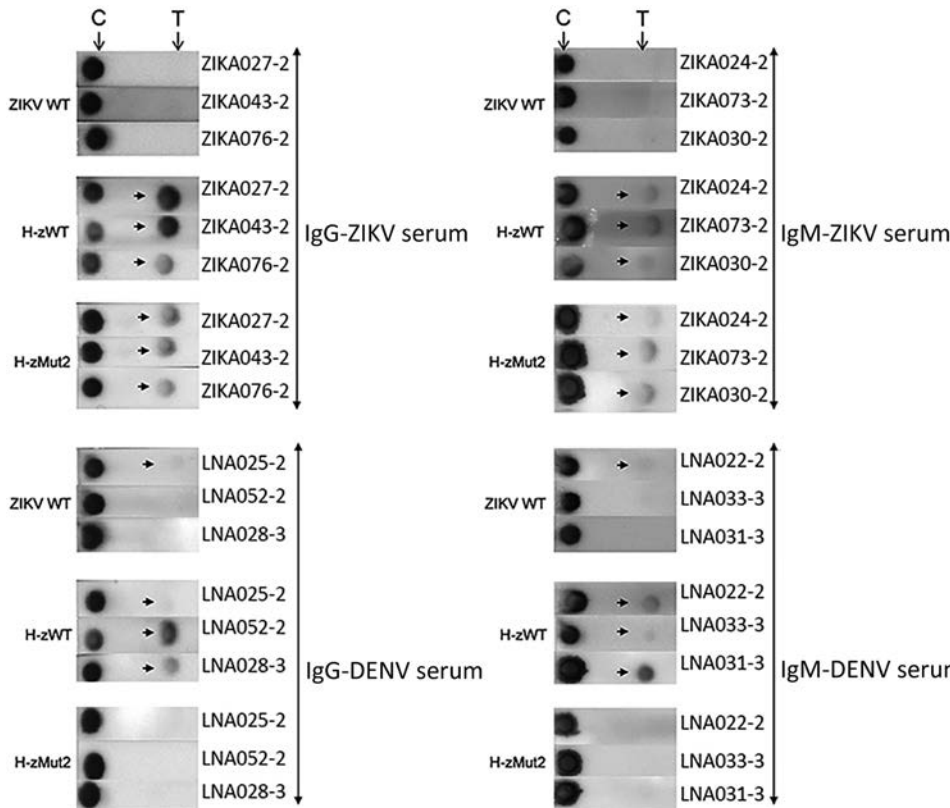


Figure 4. Immunochromatographic assay (IA) of H-zMut2 F1 IA for IgM and IgG detection in study of Zika diagnosis, Singapore. H-zMut2 as capture antigen in the F1 IA format was tested with training set for detecting IgG (left) and IgM (right). Representative strips show a comparison of performance for WT-NS1, H-zWT and H-zMut2. Overall, H-Mut2 showed higher specificity than H-zWT (against DENV plasma, bottom panels), though both H-Mut2 and H-zWT showed greater sensitivity compared to WT-NS1 (against ZIKV plasma, top panels). The arrows indicate positive signals at the test line (T), upstream of the control line (C). DENV, dengue virus; OD, optical density; WT, wild type; ZIKV, Zika virus.

for NS1, 19 were positive for IgM and 2 were positive for IgG. Within the validation set (acute- and convalescent-phase samples, n = 118), 35 patients provided their blood samples at 2 different time points (Appendix 1 Table 4). We observed increased IgM and IgG levels in most of the samples by ELISA, upon disease progression over time (30 of 35 cases). For 28 of these patients, the first collection was in the acute phase and the second in the convalescent phase. We compiled test results and associated information for all patient samples used in this study (Appendix 2, <https://wwwnc.cdc.gov/EID/article/27/5/19-0121-App2.xlsx>).

Discussion

In this study, we engineered ZIKV NS1 mutants for serologic testing in 2 different methods, the ELISA and the IA. We also developed monoclonal antibodies for detecting ZIKV NS1 to complement the serologic tests. A notable feature of our study was the ability to access confirmed ZIKV-infected and DENV-infected samples collected in acute and recent convalescent phases of infection (118 ZIKV samples, 151 DENV samples), which enabled a detailed evaluation and analysis of our assay’s performance.

The ZIKV IgM test was recommended by the Centers for Disease Control and Prevention (CDC) as

part of the diagnostic regimen for symptomatic persons, as well as for nonsymptomatic pregnant women (18). The major drawback for serologic tests, including those authorized by CDC for emergency use, is the high rate of cross-reactivity to DENV-positive samples (21,27). A supplemental PRNT test is thus required to confirm IgM-positive specimens (18,27). Therefore, there is still a need for the development of a rapid, sensitive, and specific serologic test.

Both ZIKV E and NS1 antigens have been used in various serologic assays (21,28,29). In the ELISA format, both CDC and InBios (<https://inbios.com>) IgM kits used a monoclonal antibody that was previously developed against the West Nile virus E antigen. Although the 2 assays showed high positive test agreement (21), some studies demonstrated high false-positive rates with both assays (21,30). To reduce cross-reactivity to native DENV E antigen, either a mutated full-length or a conserved domain have been used (31,32). These capture antigen-based ELISA assays have some drawbacks, such as requiring a competing heterologous antigen to achieve better IgG specificity or showing cross-reactivity to recent convalescent-phase DENV samples obtained within 12 weeks of symptom onset. Good specificity was reported with the use of ZIKV NS1 as capture

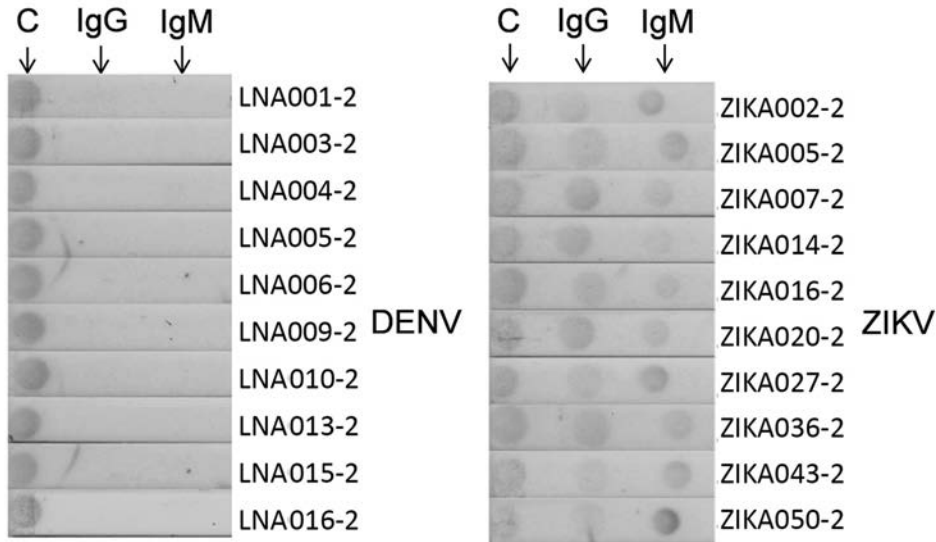


Figure 5. Immunochromatographic assay (IA) of H-zMut1 as detector antigen in the F2 IA for detecting IgM and IgG in study of Zika diagnosis, Singapore. Representative strips showing F2 IA format tested with validation set in blinded manner. Arrows at top indicate test lines. C, control line.

agent for serologic testing, but an evaluation study showed that the assays had low sensitivity (29).

The result of our blinded study indicated that the engineered H-zMut2 is suitable for developing a relatively reliable serologic ZIKV test, especially with convalescent samples (7–16 dpo). In comparison with the serologic assays reported by others, our ELISA tests showed reasonable performance characteristics for convalescent specimens and were relatively easy

to perform. The entire assay can be completed within 90 min for IgM or 30 min for IgG, without the need to use a heterologous competing protein. Our tests also showed low cross-reactivity against recent convalescent-phase DENV samples (7–21 dpo).

We demonstrated the use of an engineered NS1 protein for accurate ZIKV diagnosis in both ELISA and IA approaches. The 2 IA formats were slightly different in test performance with convalescent samples.

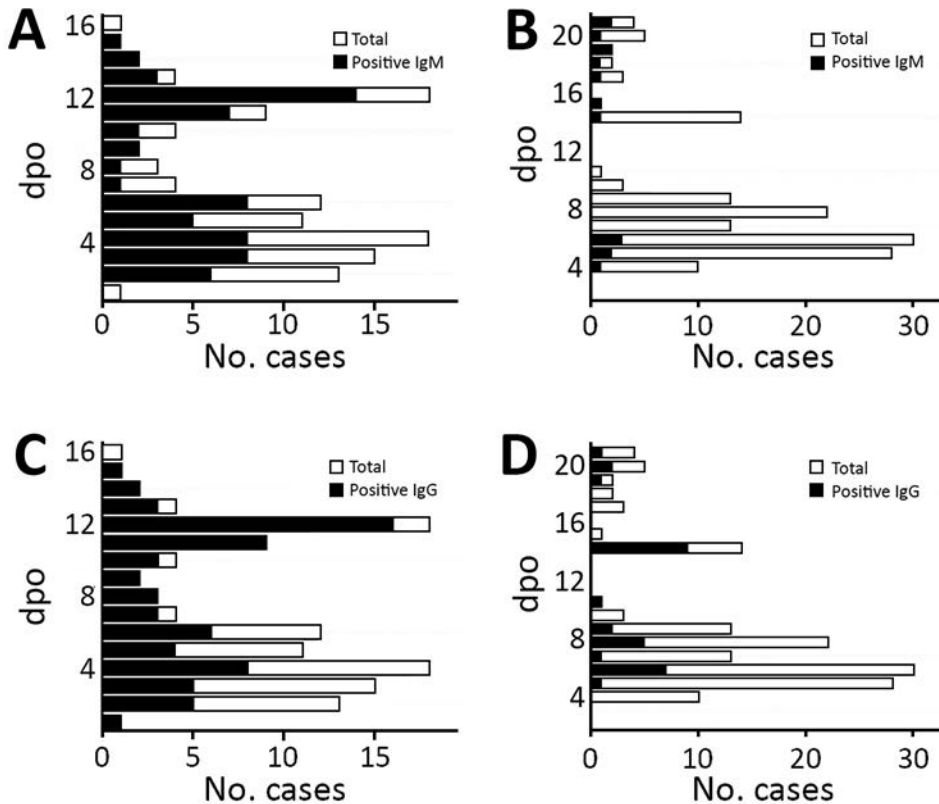


Figure 6. Distribution of number of plasma cases (x-axes) over number of DPO (y-axes) in study of Zika diagnosis, Singapore. F1 immunochromatographic assay format tested with validation set in a blinded manner (Tan Tock Seng Hospital plasma); positive plasma (black) and total plasma cases (gray) over dpo are also shown. A, C) Zika patient samples; B, D) Dengue patient samples. dpo, days postonset of symptoms.

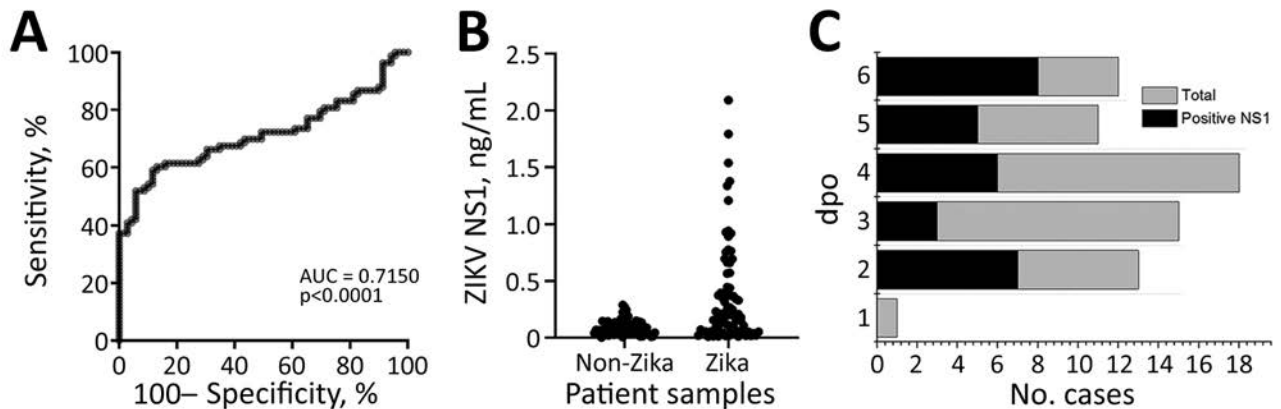


Figure 7. ELISA for ZIKV NS1 detection in study of Zika diagnosis, Singapore. A) Receiver operating characteristics curve analysis showing the performance of C12-C11 sandwich ELISA when tested against ZIKV-infected or non-ZIKV-infected samples. B) ZIKV NS1 quantification in patient samples using in-house antibody pairs. Each dot represents an individual patient sample. C) Distribution of number of plasma cases (x-axis) over dpo (y-axis) for ZIKV NS1 ELISA tested with the validation set; positive plasma (black) and the total plasma cases (gray) at each dpo are also shown. DENV, dengue virus; dpo, days postonset of symptoms; NS1, nonstructural protein 1; ZIKV, Zika virus.

For example, the F1 IA approach showed favorable performance in individual tests (sensitivity/specificity 71%/87% for IgM, 90%/79% for IgG) whereas the F2 IA, albeit conferring lower individual test sensitivity (71% for IgM, 79% for IgG), had improved overall performance with >80% sensitivity and specificity in combined IgM/IgG tests. In addition, we found that our IA assays outperformed the GenBody RDT kit when tested against samples in the validation set.

On the basis of our ZIKV ELISA and IA test performance, we propose that patients being tested in the time window of 7–16 dpo can be evaluated by our IgM/IgG tests as part of the current diagnostic algorithm. These tests would potentially streamline the diagnostic process by reducing the dependency on PRNT. For patients in the acute phase, the combined NS1/IgM/IgG test would be appropriate. Even though the NS1 test by itself was not reliable for diagnosing early ZIKV infections, the inclusion of this test with IgM/IgG improved the overall sensitivity of the assay. Our specificity could be reduced when diagnosing acute ZIKV patients who might have had recent or remote DENV infections; a slight decrease in specificity was observed in the IgG test when comparing DENV convalescent and acute samples. These results indicate that NS1 alone is not sufficient for early diagnosis of ZIKV infection, in contrast to a report by Bosch et al. (33). The discrepancy could be the result of differences in the patients' immune response or in the assay protocols.

In conclusion, we have developed a serologic test based on engineered NS1 mutants for detecting ZIKV IgM/IgG. Coupled with an NS1 antigen detection test,

the combined NS1/IgM/IgG assay showed relatively high sensitivity and specificity and outperformed a commercial kit. Further evaluation using patient samples from different infected regions, ZIKV/DENV strains, and pandemic/epidemiologic records is needed to determine the overall performance of our assays. These assays, in either ELISA or IA format, can potentially be developed for on-site diagnosis to achieve better disease control and improved patient care during outbreaks of ZIKV infections.

Acknowledgments

We thank Luo Dahai (Lee Kong Chian School of Medicine, Singapore) for providing Zika NS1 construct and staff from the Biological Resource Centre, A*STAR, for providing veterinary services.

About the Authors

Dr. Yap is a research scientist at the Experimental Drug Development Centre, Singapore. His research interests include developing diagnostics and therapeutics for infectious diseases. Dr. Hong is a research fellow at the Experimental Drug Development Centre. Her research interests include developing diagnostics and therapeutics for oncology and infectious diseases.

References

1. Fauci AS, Morens DM. Zika virus in the Americas—yet another arbovirus threat. *N Engl J Med*. 2016;374:601–4. <https://doi.org/10.1056/NEJMp1600297>
2. Olson JG, Ksiazek TG, Suhandiman G, Triwibowo V. Zika virus, a cause of fever in Central Java, Indonesia. *Trans*

- R Soc Trop Med Hyg. 1981;75:389–93. [https://doi.org/10.1016/0035-9203\(81\)90100-0](https://doi.org/10.1016/0035-9203(81)90100-0)
3. Marchette NJ, Garcia R, Rudnick A. Isolation of Zika virus from *Aedes aegypti* mosquitoes in Malaysia. *Am J Trop Med Hyg.* 1969;18:411–5. <https://doi.org/10.4269/ajtmh.1969.18.411>
 4. Bearcroft WG. Zika virus infection experimentally induced in a human volunteer. *Trans R Soc Trop Med Hyg.* 1956;50:438–41. [https://doi.org/10.1016/0035-9203\(56\)90090-6](https://doi.org/10.1016/0035-9203(56)90090-6)
 5. Simpson DIH. Zika virus infection in man. *Trans R Soc Trop Med Hyg.* 1964;58:335–7. [https://doi.org/10.1016/0035-9203\(64\)90201-9](https://doi.org/10.1016/0035-9203(64)90201-9)
 6. Duffy MR, Chen T-H, Hancock WT, Powers AM, Kool JL, Lanciotti RS, et al. Zika virus outbreak on Yap Island, Federated States of Micronesia. *N Engl J Med.* 2009;360:2536–43. <https://doi.org/10.1056/NEJMoa0805715>
 7. European Centre for Disease Prevention and Control. Rapid risk assessment: Zika virus epidemic in the Americas: potential association with microcephaly and Guillain-Barré syndrome. Solna, Sweden: The Centre; 2015. p. 1–14.
 8. Rasmussen SA, Jamieson DJ, Honein MA, Petersen LR. Zika virus and birth defects – reviewing the evidence for causality. *N Engl J Med.* 2016;374:1981–7. <https://doi.org/10.1056/NEJMSr1604338>
 9. Cugola FR, Fernandes IR, Russo FB, Freitas BC, Dias JLM, Guimarães KP, et al. The Brazilian Zika virus strain causes birth defects in experimental models. *Nature.* 2016;534:267–71. <https://doi.org/10.1038/nature18296>
 10. Krauer F, Riesen M, Reveiz L, Oladapo OT, Martínez-Vega R, Porgo TV, et al.; WHO Zika Causality Working Group. Zika virus infection as a cause of congenital brain abnormalities and Guillain-Barré syndrome: systematic review. *PLoS Med.* 2017;14:e1002203. <https://doi.org/10.1371/journal.pmed.1002203>
 11. Parra B, Lizarazo J, Jiménez-Arango JA, Zea-Vera AF, González-Manrique G, Vargas J, et al. Guillain-Barré syndrome associated with Zika virus infection in Colombia. *N Engl J Med.* 2016;375:1513–23. <https://doi.org/10.1056/NEJMoa1605564>
 12. Cao-Lormeau VM, Blake A, Mons S, Lastère S, Roche C, Vanhomwegen J, et al. Guillain-Barré Syndrome outbreak associated with Zika virus infection in French Polynesia: a case-control study. *Lancet.* 2016;387:1531–9. [https://doi.org/10.1016/S0140-6736\(16\)00562-6](https://doi.org/10.1016/S0140-6736(16)00562-6)
 13. Landry ML, St. George K. Laboratory diagnosis of Zika virus infection. *Arch Pathol Lab Med.* 2017;141:60–7. <https://doi.org/10.5858/arpa.2016-0406-SA>
 14. US Department of Health and Human Services, US Food and Drug Administration. Emergency use authorizations for medical devices [cited 2018 Dec 1]. <https://www.fda.gov/medicaldevices/safety/emergency-situations/ucm161496.htm>
 15. Bingham AM, Cone M, Mock V, Heberlein-Larson L, Stanek D, Blackmore C, et al. Comparison of test results for Zika virus RNA in urine, serum, and saliva specimens from persons with travel-associated Zika virus disease – Florida, 2016. *MMWR Morb Mortal Wkly Rep.* 2016;65:475–8. <https://doi.org/10.15585/mmwr.mm6518e2>
 16. Corman VM, Rasche A, Baronti C, Aldabbagh S, Cadar D, Reusken CB, et al. Assay optimization for molecular detection of Zika virus. *Bull World Health Organ.* 2016;94:880–92. <https://doi.org/10.2471/BLT.16.175950>
 17. St. George K, Sohi IS, Dufort EM, Dean AB, White JL, Limberger R, et al. Zika virus testing considerations: lessons learned from the first 80 real-time reverse transcription-PCR-positive cases diagnosed in New York state. *J Clin Microbiol.* 2017;55:535–44. <https://doi.org/10.1128/JCM.01232-16>
 18. Centers for Disease Control and Prevention. Testing guidance: new Zika and dengue testing guidance [cited 2018 Dec 1]. <https://www.cdc.gov/zika/hc-providers/testing-guidance.html>
 19. Rabe IB, Staples JE, Villanueva J, Hummel KB, Johnson JA, Rose L, et al.; MTS. Interim guidance for interpretation of Zika virus antibody test results. *MMWR Morb Mortal Wkly Rep.* 2016;65:543–6. <https://doi.org/10.15585/mmwr.mm6521e1>
 20. Calisher CH, Karabatsos N, Dalrymple JM, Shope RE, Porterfield JS, Westaway EG, et al. Antigenic relationships between flaviviruses as determined by cross-neutralization tests with polyclonal antisera. *J Gen Virol.* 1989;70:37–43. <https://doi.org/10.1099/0022-1317-70-1-37>
 21. Granger D, Hilgart H, Misner L, Christensen J, Bistodeau S, Palm J, et al. Serologic testing for Zika virus: comparison of three Zika virus IgM-screening enzyme-linked immunosorbent assays and initial laboratory experiences. *J Clin Microbiol.* 2017;55:2127–36. <https://doi.org/10.1128/JCM.00580-17>
 22. Lanciotti RS, Kosoy OL, Laven JJ, Velez JO, Lambert AJ, Johnson AJ, et al. Genetic and serologic properties of Zika virus associated with an epidemic, Yap State, Micronesia, 2007. *Emerg Infect Dis.* 2008;14:1232–9. <https://doi.org/10.3201/eid1408.080287>
 23. Chia PY, Yew HS, Ho H, Chow A, Sadarangani SP, Chan M, et al. Clinical features of patients with Zika and dengue virus co-infection in Singapore. *J Infect.* 2017;74:611–5. <https://doi.org/10.1016/j.jinf.2017.03.007>
 24. Kim YH, Lee J, Kim Y-E, Chong C-K, Pinchemel Y, Reisdörfer F, et al. Development of a rapid diagnostic test kit to detect IgG/IgM antibody against Zika virus using monoclonal antibodies to the envelope and non-structural protein 1 of the virus. *Korean J Parasitol.* 2018;56:61–70. <https://doi.org/10.3347/kjp.2018.56.1.61>
 25. Hunsperger EA, Yoksan S, Buchy P, Nguyen VC, Sekaran SD, Enria DA, et al. Evaluation of commercially available diagnostic tests for the detection of dengue virus NS1 antigen and anti-dengue virus IgM antibody. *PLoS Negl Trop Dis.* 2014;8:e3171. <https://doi.org/10.1371/journal.pntd.0003171>
 26. Dussart P, Petit L, Labeau B, Bremand L, Leduc A, Moua D, et al. Evaluation of two new commercial tests for the diagnosis of acute dengue virus infection using NS1 antigen detection in human serum. *PLoS Negl Trop Dis.* 2008;2:e280. <https://doi.org/10.1371/journal.pntd.0000280>
 27. Centers for Disease Control and Prevention. Zika MAC-ELISA [cited 2018 Dec 1]. <https://www.cdc.gov/zika/pdfs/zika-mac-elisa-instructions-for-use.pdf>
 28. Balmaseda A, Stettler K, Medialdea-Carrera R, Collado D, Jin X, Zambrana JV, et al. Antibody-based assay discriminates Zika virus infection from other flaviviruses. *Proc Natl Acad Sci U S A.* 2017;114:8384–9. <https://doi.org/10.1073/pnas.1704984114>
 29. Steinhagen K, Probst C, Radzimski C, Schmidt-Chanasit J, Emmerich P, van Esbroeck M, et al. Serodiagnosis of Zika virus (ZIKV) infections by a novel NS1-based ELISA devoid of cross-reactivity with dengue virus antibodies: a multicohort study of assay performance, 2015 to 2016. *Euro Surveill.* 2016;21:30426–41. <https://doi.org/10.2807/1560-7917.ES.2016.21.50.30426>
 30. US Department of Health and Human Services, US Food and Drug Administration. FDA warns health care providers against relying solely on Zika virus serological IgM assay results; reminds them to wait for confirmatory test results before making patient management decisions: FDA safety communication; 2016 [cited 2018 Dec 1]. <http://wayback.archive-it.org/7993/20170722113716/https://www.fda.gov/MedicalDevices/Safety/AlertsandNotices/ucm534515.htm>

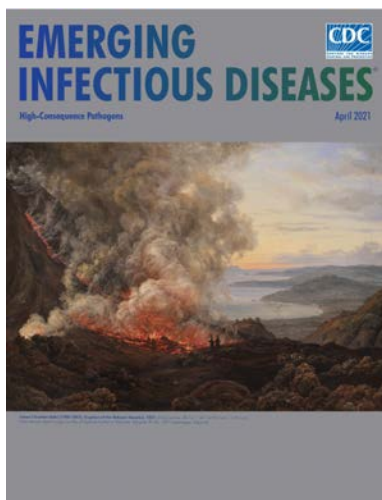
31. Premkumar L, Collins M, Graham S, Liou GA, Lopez CA, Jadi R, et al. Development of envelope protein antigens to serologically differentiate Zika virus infection from dengue virus infection. *J Clin Microbiol*. 2018;56:e01504–17.
32. Rockstroh A, Moges B, Barzon L, Sinigaglia A, Palù G, Kumbukgolla W, et al. Specific detection of dengue and Zika virus antibodies using envelope proteins with mutations in the conserved fusion loop. *Emerg Microbes Infect*. 2017;6:e99. <https://doi.org/10.1038/emi.2017.87>
33. Bosch I, de Puig H, Hiley M, Carré-Camps M, Perdomo-Celis F, Narváez CF, et al. Rapid antigen tests for dengue virus serotypes and Zika virus in patient serum. *Sci Transl Med*. 2017;9:eaan1589. <https://doi.org/10.1126/scitranslmed.aan1589>

Address for correspondence: William Sun, Institute of Bioengineering and Nanotechnology, 31 Biopolis Way, #07-01 Nanos 138669, Singapore; email: wsun@ibn.a-star.edu.sg

April 2021

High-Consequence Pathogens

- Blastomycosis Surveillance in 5 States, United States, 1987–2018
- Reemergence of Human Monkeypox and Declining Population Immunity in the Context of Urbanization, Nigeria, 2017–2020
- Animal Reservoirs and Hosts for Emerging Alphacoronaviruses and Betacoronaviruses
- Difficulties in Differentiating Coronaviruses from Subcellular Structures in Human Tissues by Electron Microscopy
- Characteristics of SARS-CoV-2 Transmission among Meat Processing Workers in Nebraska, USA, and Effectiveness of Risk Mitigation Measures
- Systematic Review of Reported HIV Outbreaks, Pakistan, 2000–2019
- Infections with Tickborne Pathogens after Tick Bite, Austria, 2015–2018
- Emergence of *Burkholderia pseudomallei* Sequence Type 562, Northern Australia
- Histopathological Characterization of Cases of Spontaneous Fatal Feline Severe Fever with Thrombocytopenia Syndrome, Japan
- COVID-19–Associated Pulmonary Aspergillosis, March–August 2020
- Genomic Surveillance of a Globally Circulating Distinct Group W Clonal Complex 11 Meningococcal Variant, New Zealand, 2013–2018
- Rare Norovirus GIV Foodborne Outbreak, Wisconsin, USA



- Persistence of SARS-CoV-2 N-Antibody Response in Healthcare Workers, London, UK
- Analysis of Asymptomatic and Presymptomatic Transmission in SARS-CoV-2 Outbreak, Germany, 2020
- Characteristics and Risk Factors of Hospitalized and Nonhospitalized COVID-19 Patients, Atlanta, Georgia, USA, March–April 2020
- Improving Treatment and Outcomes for Melioidosis in Children, Northern Cambodia, 2009–2018
- Eastern Equine Encephalitis Virus in Mexican Wolf Pups at Zoo, Michigan, USA
- Genomic Analysis of Novel Poxvirus Brazilian Porcupinepox Virus, Brazil, 2019
- Highly Pathogenic Avian Influenza Clade 2.3.4.4 Subtype H5N6 Viruses Isolated from Wild Whooper Swans, Mongolia, 2020
- SARS-CoV-2 Seropositivity among US Marine Recruits Attending Basic Training, United States, Spring–Fall 2020
- Surveillance of COVID-19–Associated Multisystem Inflammatory Syndrome in Children, South Korea
- Low-Level Middle East Respiratory Syndrome Coronavirus among Camel Handlers, Kenya, 2019
- Dynamic Public Perceptions of the Coronavirus Disease Crisis, the Netherlands, 2020
- Evolution of Sequence Type 4821 Clonal Complex Hyperinvasive and Quinolone-Resistant Meningococci
- Epidemiologic and Genomic Reidentification of Yaws, Liberia
- Sexual Contact as Risk Factor for Campylobacter Infection
- Venezuelan Equine Encephalitis Complex Alphavirus in Bats, French Guiana
- Stability of SARS-CoV-2 RNA in Nonsupplemented Saliva
- Experimental SARS-CoV-2 Infection of Bank Voles
- Increased SARS-Cov-2 Testing Capacity with Pooled Saliva Samples

**EMERGING
INFECTIOUS DISEASES**

To revisit the April 2021 issue, go to:
<https://wwwnc.cdc.gov/eid/articles/issue/27/4/table-of-contents>

Global Trends in Norovirus Genotype Distribution among Children with Acute Gastroenteritis

Jennifer L. Cannon, Joseph Bonifacio, Filemon Bucardo, Javier Buesa, Leesa Bruggink, Martin Chi-Wai Chan,¹ Tulio M. Fumian, Sidhartha Giri,² Mark D. Gonzalez, Joanne Hewitt, Jih-Hui Lin, Janet Mans, Christian Muñoz, Chao-Yang Pan, Xiao-Li Pang, Corinna Pietsch, Mustafiz Rahman, Naomi Sakon, Rangaraj Selvarangan, Hannah Browne, Leslie Barclay, Jan Vinjé

Noroviruses are a leading cause of acute gastroenteritis (AGE) among adults and children worldwide. NoroSurv is a global network for norovirus strain surveillance among children <5 years of age with AGE. Participants in 16 countries across 6 continents used standardized protocols for dual typing (genotype and polymerase type) and uploaded 1,325 dual-typed sequences to the NoroSurv web portal during 2016–2020. More than 50% of submitted sequences were GII.4 Sydney[P16] or GII.4 Sydney[P31] strains. Other common strains included GII.2[P16], GII.3[P12], GII.6[P7], and GI.3[P3] viruses. In total, 22 genotypes and 36 dual types, including GII.3 and GII.20 viruses with rarely reported polymerase types, were detected, reflecting high strain diversity. Surveillance data captured in NoroSurv enables the monitoring of trends in norovirus strains associated childhood AGE throughout the world on a near real-time basis.

Globally, noroviruses are associated with ≈20% of acute gastroenteritis (AGE) cases, causing an estimated 685 million episodes and 210,000 deaths each

year (1,2). By 2 years of age, children have probably had ≥1 norovirus infection (3–5). Children in this age group are at risk for severe illness, prolonged symptoms, and infection by multiple strains (3–5). Sporadic illnesses among children might contribute to community transmission and outbreaks among all age groups (6). In countries with successful rotavirus vaccination campaigns, norovirus is now the most common cause of pediatric AGE requiring medical attention (7–9). As of January 2021, vaccines for norovirus are in clinical trials (phase I and II) and developmental stages (10). However, their design is challenging because of the high genetic diversity of noroviruses and incomplete understanding of cross-protective immunity (11). If candidate vaccines are successful at blocking onward transmission events, norovirus vaccination will benefit children and unvaccinated persons across all age groups (12).

Norovirus classification is based on amino acid diversity of the major capsid protein (encoded by

Author affiliations: National Foundation for the Centers for Disease Control and Prevention, Inc., Atlanta, Georgia, USA (J.L. Cannon, H. Browne); Research Institute for Tropical Medicine, Manila, the Philippines (J. Bonifacio); National Autonomous University of Nicaragua, León, Nicaragua (F. Bucardo); University of Valencia, Valencia, Spain (J. Buesa); Peter Doherty Institute for Infection and Immunity, Melbourne, Victoria, Australia (L. Bruggink); Chinese University of Hong Kong, Hong Kong, China (M.C.-W. Chan); Instituto Oswaldo Cruz, Rio de Janeiro, Brazil (T.M. Fumian); Christian Medical College, Vellore, India (S. Giri); Children's Healthcare of Atlanta, Atlanta (M.D. Gonzalez); Institute of Environmental Science and Research, Porirua, New Zealand (J. Hewitt); Taiwan Centers for Disease Control, Taipei, Taiwan (J.-H. Lin); University of Pretoria, Pretoria, South Africa (J. Mans); University of Antofagasta, Antofagasta, Chile (C. Muñoz);

California Department of Public Health, Richmond, California, USA (C.-Y. Pan); Alberta Precision Laboratory, Edmonton, Alberta, Canada (X.-L. Pang); Leipzig University Hospital, Leipzig, Germany (C. Pietsch); International Centre for Diarrhoeal Disease Research, Bangladesh, Dhaka, Bangladesh (M. Rahman); Osaka Institute of Public Health, Osaka, Japan (N. Sakon); Children's Mercy Hospitals and Clinics, Kansas City, Missouri, USA (R. Selvarangan); Centers for Disease Control and Prevention, Atlanta (L. Barclay, J. Vinjé)

DOI: <https://doi.org/10.3201/eid2705.204756>

¹Current affiliation: Food and Health Bureau, Hong Kong.

²Current affiliation: Ministry of Health & Family Welfare, Bhubaneswar, India.

open reading frame [ORF] 2), which is also the primary neutralization site for antibodies produced after norovirus infection or vaccination (13–15). Noroviruses are classified into 10 genogroups, GI–GX, and ≥ 48 genotypes: 9 genotypes in the GI genogroup, 26 in GII, 3 in GIII, 2 in GIV, 2 in GV, 2 in GVI, 1 in GVII, 1 in GVIII, 1 in GIX, and 1 in GX (16). ORF1 encodes the viral nonstructural proteins including the polymerase, which is classified into ≥ 60 polymerase types (P-types) (16). Much about the evolutionary role of recombination among noroviruses, which occurs primarily at the ORF1/ORF2 junction, remains unknown (17–19). Norovirus classification was recently updated to include typing of the polymerase region (16). This dual typing strategy considers the genotype encoding the major capsid protein and the P-type encoding the polymerase region (16). A short genomic region spanning the 3' end of the polymerase gene through the 5' end of the capsid gene is the basis for sequence-based dual typing (20).

Genogroup II genotype 4 (GII.4) viruses have been the most frequently detected noroviruses globally since the mid-1990s, before which GII.3 viruses were dominant (13,21,22). New GII.4 variants regularly emerge and spread across the globe and often contribute to increased illness and death, especially in healthcare settings (23–25). During 2002–2012, new GII.4 variants with antigenically distinct capsid epitopes, which enable the viruses to escape neutralizing antibodies, emerged and replaced previous variants every 2–3 years (15). These changes indicate that norovirus vaccines might need to be updated regularly. Despite recent recombination events resulting in the global spread of GII.4 Sydney viruses with a novel P16 polymerase, no new variant causing widespread infections has emerged since 2012 (20,26,27). Although GII.4 strains are the most common strains detected among all age groups, non-GII.4 strains, such as GII.2, GII.3, and GII.6 viruses, are common causes of sporadic cases and illness in young children (6,28–32). Rare strains (4) and GII.4 variants can circulate, especially among children, for years before spreading globally among all age groups (33,34). Consequently, children might be an important reservoir for emerging norovirus strains against which little or no population immunity exists.

NoroSurv (<https://www.norosurv.org>), which is maintained by the Centers for Disease Control and Prevention (Atlanta, Georgia, USA), is a global pediatric norovirus strain surveillance network for children <5 years of age with medically attended AGE and can only be accessed by registered NoroSurv laboratories. Surveillance of norovirus strains infecting children is

crucial for monitoring the emergence of new or rare strains and for developing vaccines that protect against the most common strains.

Methods

NoroSurv

All but 2 participating hospitals and medical centers collected norovirus-positive stool samples from children with AGE; 2 sites in Nicaragua and Australia obtained only samples from symptomatic children in community-based studies. Staff at hospitals, medical centers, universities, and reference laboratories processed and typed the samples. Each laboratory uploaded norovirus sequences; patient demographic data (e.g., deidentified patient age and sex); and information on sample type, collection date, and setting to the password-protected NoroSurv web portal. All laboratories used a standardized protocol for norovirus dual typing that comprised screening by genotype-specific real-time reverse transcription PCR (RT-PCR), conventional RT-PCR, and Sanger sequencing of RT-PCR products (20). Raw DNA chromatogram files or nucleotide sequences were automatically typed by NoroSurv using the most recent reference sequences and classification for noroviruses (16). Ethics approval by the New Zealand component of this study was granted by the Health and Disability Ethics Committee, New Zealand (approval no. 19/CEN/96).

Data Analysis

We analyzed NoroSurv data associated with samples collected during September 1, 2016–August 31, 2020. We excluded samples from children ≥ 5 years of age, from asymptomatic patients, or that had missing or low-quality dual typing information. We downloaded sequences and associated data from NoroSurv; we then aggregated, cleaned, analyzed, and visualized the data using R software (The R Project, <https://www.r-project.org>). After downloading the sequences from NoroSurv as fasta files, we checked the quality of the submitted sequences using Bioconductor (<http://bioconductor.org>) packages in R. When discrepancies existed between the manually entered and autotyped information, we conducted phylogenetic analysis to confirm the correct type; we updated NoroSurv records accordingly.

Results

A total of 1,325 dual-typed norovirus sequences collected during September 2016–August 2020 from

children <5 years of age with AGE were submitted to NoroSurv. Sequences were received from 19 sites in 16 countries in Africa (South Africa, $n = 13$), Asia (Bangladesh, $n = 32$; Hong Kong, China, $n = 326$; India, $n = 36$; Japan, $n = 89$; the Philippines, $n = 132$; and Taiwan, $n = 19$), Oceania (Australia, $n = 71$; New Zealand, $n = 54$), Europe (Germany, $n = 111$ and Spain, $n = 44$), North and Central America (Canada, $n = 90$; Nicaragua, $n = 78$; and the United States, $n = 173$), and South America (Brazil, $n = 14$ and Chile, $n = 43$) (Figure 1). Each country submitted a median of 63 sequences (range 13–326); 48% of sequences were from countries in Asia. We excluded 62 of the 1,387 NoroSurv sequences: 11 that could not be typed because of poor sequence quality or missing fasta files; 7 with sample collection dates before September 1, 2016; 31 from children ≥ 5 years of age; and 13 from asymptomatic children.

To compare genotype distribution over time, we defined seasons as September 1–August 31; these periods reflected the seasonality reported for noroviruses, with peak cases often occurring during the cooler months: October–March in the Northern Hemisphere and April–September in the Southern Hemisphere (35). During the pilot phase (September 1, 2016–August 31, 2018), a total of 382 sequences were submitted (144 in 2016–2017 and 238 in 2017–2018). During the first 2 official years of NoroSurv, 600 sequences were submitted in the 2018–2019 season and 343 in 2019–2020 season. The number of submissions peaked

between the months of October and May (Figure 2), coinciding with cooler months in the Northern Hemisphere. However, only 15% (195/1,325) of sequences were submitted by Southern Hemisphere countries; for this reason, analyzing trends in the Southern Hemisphere was difficult. Many sample collection sites in the Philippines were equatorial and had norovirus cases year-round. The number of submitted sequences declined in 2020, coinciding with the emergence of the coronavirus disease pandemic (Figure 2).

Throughout the study period, GII.4 Sydney was the most common genotype on all 6 continents and was detected in 52% (687/1,325) of sequences, peaking at 62% (213/343) in 2019–2020 (Figure 2; Appendix Table 1, <https://wwwnc.cdc.gov/EID/article/27/5/20-4756-App1.pdf>). The GII.3 (190; 14%), GII.2 (149; 11%), and GII.6 (64; 5%) genotypes comprised 30% of sequences (Figure 2; Appendix Table 1). GI.3 was the most frequently detected GI genotype, accounting for 55% (50/91) of all GI viruses and 4% of all NoroSurv sequences. The remaining 14% (185/1,325) of sequences were composed of 17 other genotypes: GI.1, GI.2, GI.4, GI.5, GI.6, GI.7, GI.9, GII.1, GII.4 Hong Kong, GII.4 untypable, GII.7, GII.8, GII.12, GII.13, GII.14, GII.17, and GII.20 (Appendix Table 1). We detected 687 GII.4 Sydney viruses associated with 3 P-types: P16 (399; 58%), P31 (280; 41%), and P4 (8; 1%). The proportions of each genotype varied by year (Figure 2; Appendix Table 1) and country (Appendix Tables 2–17). The most



Figure 1. Countries participating in NoroSurv, September 2016–August 2020. Shades of blue and size of circles indicate the number of genetic sequences included from each country.

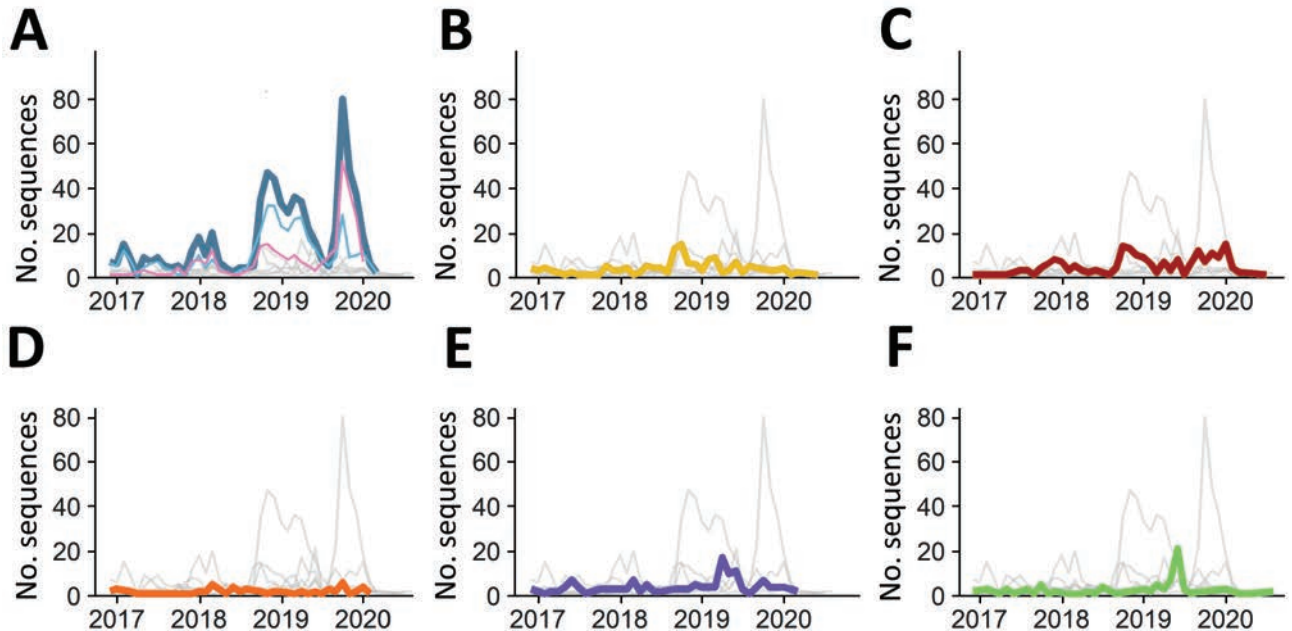


Figure 2. Global genotype distribution of norovirus sequences catalogued in NoroSurv during September 2016–August 2020. A) Dark blue line indicates all GII.4 Sydney viruses; light blue indicates GII.4 Sydney[P16] and pink indicates GII.4 Sydney[P31]; B) yellow indicates GII.2 viruses; C) red indicates GII.3 viruses; D) orange indicates GII.6 viruses; E) purple indicates other GII viruses; F) green indicates GI viruses. Gray lines overlay the distributions of other pictured genotypes to enable comparisons.

common P-type among the 190 detected GII.3 viruses was P12 (146; 77%) (Figure 3; Appendix Table 1). We detected 149 GII.2 viruses, most (148; 99%) of which were P16. All 64 GII.6 viruses were P7 (Figure 3; Appendix Table 1).

The 5 most frequently detected dual types were GII.4 Sydney[P16], GII.4 Sydney[P31], GII.2[P16], GII.3[P12], and GII.6[P7]. In total, 22% (288/1,325) of sequences were composed of 31 other dual types, each accounting for <5% of all sequences (Figure 3; Appendix Table 1). The 10 most frequently detected dual types included GII.12[P16], GII.4 untypeable[P4], GI.[P3], GII.3[P21], and GII.3[P16] (Figure 3). We found that the 23 GII.4 untypeable[P4] viruses detected in Chile, 4 in the United States, 3 in Australia, 1 in Germany, 1 in New Zealand, and 4 in Spain (1 P4 and 3 P31) formed a GII.4 Sydney subclade. This subclade exceeded the >2% designated cutoff for percent nucleotide differences between these strains and the closest GII.4 Sydney reference sequence (GenBank accession no. KX354134, mean nucleotide percent difference = 2.2%, SD = 0.3%). Several genotypes were associated with ≥ 2 P-types. For example, GII.3 viruses were associated with P12, P21, P16, P30, and PNA3; GI.3 viruses were associated with P3, P13, and P10; and GII.13 viruses were associated with P16 and P21 (Figure 3; Appendix Table 1). We also detected dual types rarely reported in literature, including GII.3[PNA3]

in South Africa; GII.20[P20] and GII.20[P7] in New Zealand; and GII.3[P30] in Hong Kong, Canada, and Spain (Appendix Tables 5, 8, 11, 14, 15).

During the 2019–2020 season, 65% (138/213) of GII.4 Sydney viruses had a P31 polymerase, compared with only 28% (89/314) in the previous season (Figure 2; Appendix Table 1). This dual type was most common (115; 81%) in Hong Kong (Appendix Table 8). In total, sites in Hong Kong submitted 25% (326/1,325) of all NoroSurv sequences, including 46% (159/343) in 2019–2020. In Japan, South Africa, and Taiwan, GII.4 Sydney[P31] viruses were also more common than GII.4 Sydney[P16] viruses (Appendix Tables 10, 14, 16). In the 12 remaining countries, GII.4 Sydney[P16] viruses were either more than or as common as GII.4 Sydney[P31] viruses (Appendix Tables 2–7, 9, 11–13, 15, 17).

GII.4 Sydney viruses were the most common virus in all but 3 countries: GII.3[P12] viruses were most common in New Zealand (26/54; 48%) and Taiwan (7/19; 37%) and GII.4 untypeable[P4] viruses were most common in Chile (23/43; 53%) (Figure 3; Appendix Tables 6, 11, 16). Norovirus strain diversity was high in many countries, with >10 strains detected in 7 countries: 18 each in the Philippines and the United States, 16 in Spain, 15 in Germany, 13 in Hong Kong, and 12 each in Australia and New Zealand (Appendix Tables 2, 7, 8, 11, 13, 15, 17).

Discussion

We used NoroSurv data to monitor global trends in norovirus genotypes causing sporadic AGE in children <5 years of age. These children would probably benefit most from norovirus vaccines and are a critical group for evaluating future vaccine effectiveness. Although the number of sequences submitted from different countries varied during 2016–2020 on NoroSurv, the overall surveillance from 16 countries across 6 continents identified common genotypes around the world. Standardized protocols for dual typing across all NoroSurv sites enabled global comparisons, surveillance, and detection of recombinant strains.

During 2016–2020, NoroSurv documented 22 genotypes of norovirus causing illness in young children. GII.4 Sydney viruses, which globally are the

most common among all age groups (13,26), comprised >50% of all NoroSurv sequences. GII.2, GII.3, and GII.6 viruses, which are leading causes of childhood norovirus infections but less common among adults, were also frequently detected (6,28,30–32). One study found that among children with sporadic AGE, GII.6 viruses were second most common after GII.4; however, GII.13 viruses were the second most common cause of norovirus outbreaks in adults (6). Although ≈5% of reported norovirus outbreaks in the United States are caused by GII.3 viruses (17,20), we found they comprised nearly 23% of sporadic cases among children. Thus, GII.2, GII.3, and GII.6 viruses appear to be major causes of AGE in children but might be less transmissible to adults. This lack of transmissibility might be caused by virus-specific properties or long-term immunity in adults after childhood infection. Norovirus vaccines in development focus on the major capsid protein, which is also the genomic region used for genotyping (14,16). Vaccine candidates should protect against a broad diversity of genotypes and be easily adapted to emerging genotypes or GII.4 variants. Noroviruses contribute substantially to the prevalence of diarrheal disease among children (1), causing more severe illness and death in resource-limited countries (30,36). Childhood vaccination might reduce norovirus prevalence among children. If vaccination prevents transmission, then it also might reduce infections among all age groups (6,12).

GII.4 Sydney viruses, primarily associated with P31 and P16 polymerases, were responsible for most norovirus cases during 2012–2019 (33,34). Recombination at the ORF1/ORF2 junction is a common occurrence among noroviruses and contributes to norovirus evolution, although the exact mechanism is poorly understood (17–19). Acquisition of a novel P16 polymerase did not result in emergence of a novel GII.4 variant or substantial changes to the antigenic region of the capsid (17,37,38). However, changes to the polymerase or other nonstructural proteins might have increased the replicative or transmission fitness of GII.4 viruses (17,18,26).

Overall, 36 dual types were detected in NoroSurv and several genotypes were associated with >1 P-type. GII.3 viruses were primarily associated with P12, but many had P21, P16, and the rare P30 and PNA3 polymerases, indicating a high propensity for recombination among GII.3 strains. Other rarely detected strains included GII.20[P20] and GII.20[P7]. Several rare and novel norovirus genotypes have been detected only in children (4), suggesting differences in children's and adults' susceptibility to certain strains.

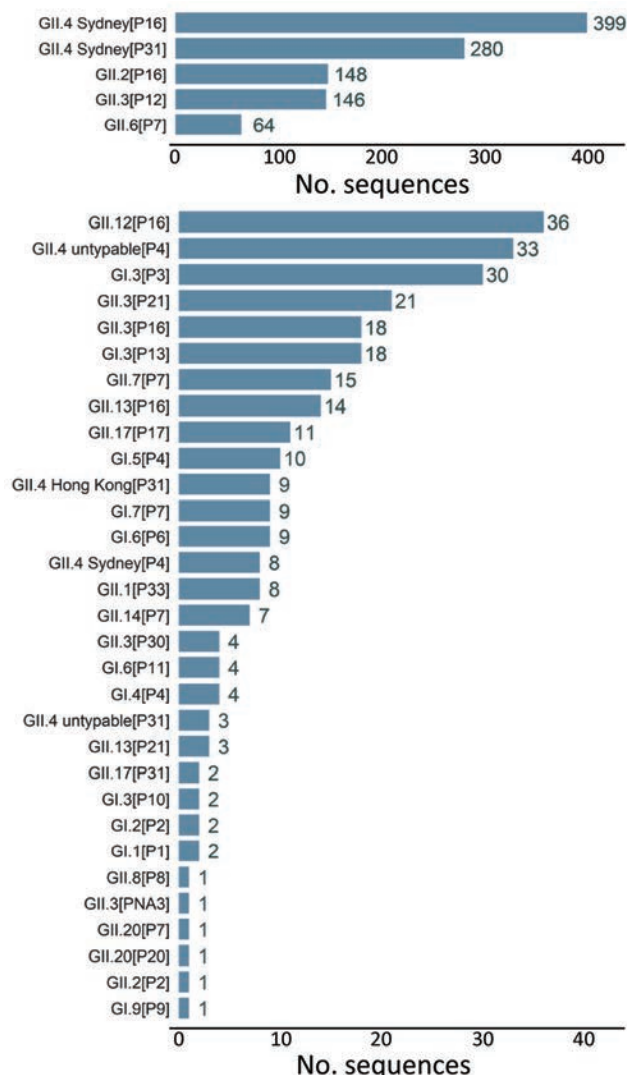


Figure 3. Distribution of dual typed sequences in NoroSurv, 2016–2020. Numbers to the right of bars indicate the number of sequences detected for each dual type.

We identified a subcluster of GII.4 Sydney (GII.4 untypable) viruses in 6 countries spanning 4 continents during 2017–2019. Complete ORF2 sequences for this strain are needed to analyze possible changes in the antigenic region of the capsid, which could enable viruses to escape antibody neutralization. If such changes exist, or if strains within this subcluster continue to evolve and spread globally, a new GII.4 variant could emerge. A recent study reported that GII.4 variants can begin to circulate, especially among children, for up to 9 years before emerging globally (33). Low-level circulation enables accumulation of mutations and emergence of new strains (18,38) and access to niches in the host environment, thereby promoting spread (33); thus, children might be a reservoir for the recombination and evolution of noroviruses. This concern highlights the necessity of norovirus surveillance among children.

NoroSurv complements NoroNet (34), a well-established global network for norovirus surveillance that has illuminated global trends in norovirus strain diversity, recombination, and evolution, including tracking the emergence of novel GII.4 variants. NoroSurv sequences are derived from sporadic cases among children, whereas NoroNet includes sequences from outbreaks and sporadic cases in adults and children. NoroSurv requires standardized protocols for dual typing (20) across all sites to ensure global comparability. However, NoroNet, which was established in 1999, has a much longer history than NoroSurv. Because the importance of dual typing was not well recognized at the time NoroNet was established, many of its sequences are derived from either the polymerase or capsid genes, but not both. In addition, the NoroSurv web portal incorporates a unique automatic typing tool and an internal dashboard of all data by location. In 2021, we plan to make the dashboard publicly available for near real-time data on global trends in sporadic norovirus infections in children.

NoroSurv is a passive surveillance system comprised of voluntary submissions from participating laboratories. As a result, its data do not necessarily correlate with national surveillance records. Furthermore, the number of sequences submitted from each country varies; this number depends in part on the availability of resources such as time and laboratory capacity. Low-income countries are currently underrepresented in NoroSurv, as are countries in Africa and Central America. However, a recent review of norovirus genotypes detected in 8 low-income and 21 low-to-middle income countries showed that GII.4 viruses were the most common genotype, with

substantial proportions of GII.3 and GII.6 viruses; in addition, GI.3 viruses were the most commonly detected GI viruses (30). Trends in the genotype distribution of noroviruses in these countries resembled the global trends illuminated in NoroSurv. In future years, NoroSurv aims to expand of the number of countries, sites, and submissions.

The 2019–20 norovirus season coincided with the emergence of the coronavirus disease pandemic, which has limited the capacity and resources for norovirus surveillance. In addition, it is unknown whether the global lockdowns, including school and daycare closures; physical distancing; and heightened hygiene awareness and practices such as handwashing, disinfection, and wearing of face masks (39), will reduce norovirus transmission among children. When settings prone to norovirus outbreaks (e.g., childcare facilities and schools) return to prepandemic capacities, norovirus cases might increase, especially if the use of alcohol-based hand sanitizers, which have limited efficacy against noroviruses (40), are substituted for handwashing in these settings. Although submissions to NoroSurv declined during February–August 2020, users might upload sequences retrospectively. As a result, data for the 2019–2020 season might not fully reflect global trends.

NoroSurv enables the near real-time detection of global norovirus genotype trends and diversity among children <5 years of age with AGE. Our findings support previous research indicating that although some overlap exists between the genotypes detected in children and adults, genotypes such as GII.2, GII.3, and GII.6 are more common among children. Childhood norovirus vaccination will probably reduce the prevalence of norovirus associated AGE among children and interrupt community transmission among all age groups (12). As such, researchers should ensure that candidate vaccines are protective against strains commonly seen in children or produce sufficient cross-protective immunity against those strains. Surveillance of rare genotypes, recombinant strains, and potentially new GII.4 variants can better predict the emergence of new strains, guiding potentially updated vaccine formulation. Sequencing larger regions of the genome, particularly the major capsid gene, can help identify antigenic changes that might enable the virus to escape antibody neutralization, which provides important information for predicting strain emergence and updating vaccine formulations. The continued expansion of the NoroSurv network to include countries with geographic and economic diversity will enhance our understanding of norovirus infections

among children worldwide. NoroSurv surveillance will inform efforts to develop and adapt norovirus vaccine candidates; it will also aid in the evaluation of future vaccine efficacy by documenting baseline global strain diversity of noroviruses in children.

Acknowledgments

We thank the NoroSurv international laboratory teams involved in sample collection, sequence analysis, and reporting, which includes Mary Ann Igoy, C. Eures Iyar Oasin, and Mayan Lumandas at the Research Institute for Tropical Medicine; Noemi Navarro-Lleó at the University of Valencia; Lin-yao Zhang at the Chinese University of Hong Kong; K. Maheswari at Christian Medical College; Margarita Lay at the Universidad de Antofagasta; Gary McAucliffe and Terri Swager at LabPLUS; Dawn Croucher at the Institute of Environmental Science and Research; Shu-Chun Chiu at the Taiwan Centers for Disease Control; Nicola Page at the South Africa National Institute for Communicable Diseases; Thalia Huynh, Tasha Padilla, Christine Morales, and Debra Wadford at the California Department of Public Health; Kanti Pabbaraju at Alberta Precision Laboratory; Mohammad Enayet Hossain at the International Centre for Diarrhoeal Disease Research, Bangladesh; and Ferdaus Hassan, Dithi Banerjee, Chris Harrison, and Mary Moffat at Children's Mercy Hospitals and Clinics.

About the Author

Dr. Cannon is a microbiologist in the Division of Viral Diseases, National Centers for Immunization and Respiratory Diseases, Centers for Disease Control and Prevention in Atlanta, Georgia, USA. Her primary research interests include global and national trends in norovirus strains causing diarrheal illness in children and adults; trends in norovirus evolution and recombination; and virus detection, inactivation, and survival on food and environmental surfaces.

References

- Ahmed SM, Hall AJ, Robinson AE, Verhoef L, Premkumar P, Parashar UD, et al. Global prevalence of norovirus in cases of gastroenteritis: a systematic review and meta-analysis. *Lancet Infect Dis*. 2014;14:725–30. [https://doi.org/10.1016/S1473-3099\(14\)70767-4](https://doi.org/10.1016/S1473-3099(14)70767-4)
- Pires SM, Fischer-Walker CL, Lanata CF, Devleeschauwer B, Hall AJ, Kirk MD, et al. Aetiology-specific estimates of the global and regional incidence and mortality of diarrhoeal diseases commonly transmitted through food. *PLoS One*. 2015;10:e0142927. <https://doi.org/10.1371/journal.pone.0142927>
- Cannon JL, Lopman BA, Payne DC, Vinjé J. Birth cohort studies assessing norovirus infection and immunity in young children: a review. *Clin Infect Dis*. 2019;69:357–65. <https://doi.org/10.1093/cid/ciy985>
- Chhabra P, Rouhani S, Browne H, Yori PP, Salas MS, Olortegui MP, et al. Homotypic and heterotypic protection and risk of re-infection following natural norovirus infection in a highly endemic setting. *Clin Infect Dis*. 2020;72:222–9. PubMed <https://doi.org/10.1093/cid/ciaa019>
- Shioda K, Kambhampati A, Hall AJ, Lopman BA. Global age distribution of pediatric norovirus cases. *Vaccine*. 2015;33:4065–8. <https://doi.org/10.1016/j.vaccine.2015.05.051>
- Parikh MP, Vandekar S, Moore C, Thomas L, Britt N, Piya B, et al. Temporal and genotypic associations of sporadic norovirus gastroenteritis and reported norovirus outbreaks in middle Tennessee, 2012–2016. *Clin Infect Dis*. 2020;71:2398–404. <https://doi.org/10.1093/cid/ciz1106>
- Bucardo F, Reyes Y, Svensson L, Nordgren J. Predominance of norovirus and sapovirus in Nicaragua after implementation of universal rotavirus vaccination. *PLoS One*. 2014;9:e98201. <https://doi.org/10.1371/journal.pone.0098201>
- Payne DC, Vinjé J, Szilagyi PG, Edwards KM, Staat MA, Weinberg GA, et al. Norovirus and medically attended gastroenteritis in U.S. children. *N Engl J Med*. 2013;368:1121–30. <https://doi.org/10.1056/NEJMsa1206589>
- Velasquez DE, Parashar U, Jiang B. Decreased performance of live attenuated, oral rotavirus vaccines in low-income settings: causes and contributing factors. *Expert Rev Vaccines*. 2018;17:145–61. <https://doi.org/10.1080/14760584.2018.1418665>
- Cates JE, Vinjé J, Parashar U, Hall AJ. Recent advances in human norovirus research and implications for candidate vaccines. *Expert Rev Vaccines*. 2020;19:539–48. <https://doi.org/10.1080/14760584.2020.1777860>
- Ramani S, Estes MK, Atmar RL. Correlates of protection against norovirus infection and disease – where are we now, where do we go? *PLoS Pathog*. 2016;12:e1005334. <https://doi.org/10.1371/journal.ppat.1005334>
- Steele MK, Remais JV, Gambhir M, Glasser JW, Handel A, Parashar UD, et al. Targeting pediatric versus elderly populations for norovirus vaccines: a model-based analysis of mass vaccination options. *Epidemics*. 2016;17:42–9. <https://doi.org/10.1016/j.epidem.2016.10.006>
- Green KY. *Caliciviridae*: the noroviruses. In: Knipe MM, Howley PM, editors. *Fields virology*. 6th ed. Philadelphia (PA): Lippincott, Williams, Wilkins; 2013. p. 582–608.
- Lindesmith LC, McDaniel JR, Changela A, Verardi R, Kerr SA, Costantini V, et al. Sera antibody repertoire analyses reveal mechanisms of broad and pandemic strain neutralizing responses after human norovirus vaccination. *Immunity*. 2019;50:1530–1541.e8. <https://doi.org/10.1016/j.immuni.2019.05.007>
- Mallory ML, Lindesmith LC, Graham RL, Baric RS. GII.4 human norovirus: surveying the antigenic landscape. *Viruses*. 2019;11:177. <https://doi.org/10.3390/v11020177>
- Chhabra P, de Graaf M, Parra GI, Chan MC, Green K, Martella V, et al. Updated classification of norovirus genogroups and genotypes [Erratum in: *J Gen Virol*. 2020;101:893]. *J Gen Virol*. 2019;100:1393–406.
- Barclay L, Cannon JL, Wikswo ME, Phillips AR, Browne H, Montmayeur AM, et al. Emerging novel GII.16 noroviruses associated with multiple capsid genotypes. *Viruses*. 2019;11:535. <https://doi.org/10.3390/v11060535>
- Eden JS, Tanaka MM, Boni MF, Rawlinson WD, White PA. Recombination within the pandemic norovirus GII.4 lineage. *J Virol*. 2013;87:6270–82. <https://doi.org/10.1128/JVI.03464-12>
- Ludwig-Begall LF, Mauroy A, Thiry E. Norovirus recombinants: recurrent in the field, recalcitrant in the lab –

- a scoping review of recombination and recombinant types of noroviruses. *J Gen Virol*. 2018;99:970–88. <https://doi.org/10.1099/jgv.0.001103>
20. Cannon JL, Barclay L, Collins NR, Wikswo ME, Castro CJ, Magaña LC, et al. Genetic and epidemiologic trends of norovirus outbreaks in the United States from 2013 to 2016 demonstrated emergence of novel GII.4 recombinant viruses. [Erratum in: *J Clin Microbiol*. 2017;57:e00695–19]. *J Clin Microbiol*. 2017;55:2208–21. <https://doi.org/10.1128/JCM.00455-17>
 21. Bok K, Abente EJ, Realpe-Quintero M, Mitra T, Sosnovtsev SV, Kapikian AZ, et al. Evolutionary dynamics of GII.4 noroviruses over a 34-year period. *J Virol*. 2009;83:11890–901. <https://doi.org/10.1128/JVI.00864-09>
 22. Hoa Tran TN, Trainor E, Nakagomi T, Cunliffe NA, Nakagomi O. Molecular epidemiology of noroviruses associated with acute sporadic gastroenteritis in children: global distribution of genogroups, genotypes and GII.4 variants. *J Clin Virol*. 2013;56:185–93. <https://doi.org/10.1016/j.jcv.2012.11.011>
 23. Burke RM, Shah MP, Wikswo ME, Barclay L, Kambhampati A, Marsh Z, et al. The norovirus epidemiologic triad: predictors of severe outcomes in US norovirus outbreaks, 2009–2016. *J Infect Dis*. 2019;219:1364–72. <https://doi.org/10.1093/infdis/jiy569>
 24. Desai R, Hembree CD, Handel A, Matthews JE, Dickey BW, McDonald S, et al. Severe outcomes are associated with genogroup 2 genotype 4 norovirus outbreaks: a systematic literature review. *Clin Infect Dis*. 2012;55:189–93. <https://doi.org/10.1093/cid/cis372>
 25. Siebenga JJ, Vennema H, Zheng DP, Vinjé J, Lee BE, Pang XL, et al. Norovirus illness is a global problem: emergence and spread of norovirus GII.4 variants, 2001–2007. *J Infect Dis*. 2009;200:802–12. <https://doi.org/10.1086/605127>
 26. Ruis C, Roy S, Brown JR, Allen DJ, Goldstein RA, Breuer J. The emerging GII.P16–GII.4 Sydney 2012 norovirus lineage is circulating worldwide, arose by late-2014 and contains polymerase changes that may increase virus transmission. *PLoS One*. 2017;12:e0179572. <https://doi.org/10.1371/journal.pone.0179572>
 27. Matsushima Y, Shimizu T, Ishikawa M, Komane A, Okabe N, Ryo A, et al. Complete genome sequence of a recombinant GII.P16–GII.4 norovirus detected in Kawasaki City, Japan, in 2016. *Genome Announc*. 2016;4:e01099–16. <https://doi.org/10.1128/genomeA.01099-16>
 28. Boon D, Mahar JE, Abente EJ, Kirkwood CD, Purcell RH, Kapikian AZ, et al. Comparative evolution of GII.3 and GII.4 norovirus over a 31-year period. *J Virol*. 2011;85:8656–66. <https://doi.org/10.1128/JVI.00472-11>
 29. Bucardo F, Reyes Y, Becker-Dreps S, Bowman N, Gruber JF, Vinjé J, et al. Pediatric norovirus GII.4 infections in Nicaragua, 1999–2015. *Infect Genet Evol*. 2017;55:305–12. <https://doi.org/10.1016/j.meegid.2017.10.001>
 30. Mans J. Norovirus infections and disease in lower-middle and low-income countries, 1997–2018. *Viruses*. 2019;11:341. <https://doi.org/10.3390/v11040341>
 31. Niendorf S, Jacobsen S, Faber M, Eis-Hübinger AM, Hofmann J, Zimmermann O, et al. Steep rise in norovirus cases and emergence of a new recombinant strain GII.P16–GII.2, Germany, winter 2016. *Euro Surveill*. 2017;22:30447. <https://doi.org/10.2807/1560-7917.ES.2017.22.4.30447>
 32. Sakon N, Yamazaki K, Nakata K, Kanbayashi D, Yoda T, Mantani M, et al. Impact of genotype-specific herd immunity on the circulatory dynamism of norovirus: a 10-year longitudinal study of viral acute gastroenteritis. *J Infect Dis*. 2015;211:879–88. <https://doi.org/10.1093/infdis/jiu496>
 33. Ruis C, Lindesmith LC, Mallory ML, Brewer-Jensen PD, Bryant JM, Costantini V, et al. Preadaptation of pandemic GII.4 noroviruses in unsampled virus reservoirs years before emergence. *Virus Evol*. 2020;6:veaa067. <https://doi.org/10.1093/ve/veaa067>
 34. van Beek J, de Graaf M, Al-Hello H, Allen DJ, Ambert-Balay K, Botteldoorn N, et al.; NoroNet. Molecular surveillance of norovirus, 2005–16: an epidemiological analysis of data collected from the NoroNet network. *Lancet Infect Dis*. 2018;18:545–53. [https://doi.org/10.1016/S1473-3099\(18\)30059-8](https://doi.org/10.1016/S1473-3099(18)30059-8)
 35. Ahmed SM, Lopman BA, Levy K. A systematic review and meta-analysis of the global seasonality of norovirus. *PLoS One*. 2013;8:e75922. <https://doi.org/10.1371/journal.pone.0075922>
 36. Riera-Montes M, O’Ryan M, Verstraeten T. Norovirus and rotavirus disease severity in children: systematic review and meta-analysis. *Pediatr Infect Dis J*. 2018;37:501–5. <https://doi.org/10.1097/INF.0000000000001824>
 37. Lun JH, Hewitt J, Yan GJH, Enosi Tuipulotu D, Rawlinson WD, White PA. Recombinant GII.P16/GII.4 Sydney 2012 was the dominant norovirus identified in Australia and New Zealand in 2017. *Viruses*. 2018;10:548. <https://doi.org/10.3390/v10100548>
 38. Tohma K, Lepore CJ, Gao Y, Ford-Siltz LA, Parra GI. Population genomics of GII.4 noroviruses reveal complex diversification and new antigenic sites involved in the emergence of pandemic strains. *MBio*. 2019;10:e02202–19. <https://doi.org/10.1128/mBio.02202-19>
 39. Chu DK, Akl EA, Duda S, Solo K, Yaacoub S, Schünemann HJ, et al.; COVID-19 Systematic Urgent Review Group Effort (SURGE) study authors. Physical distancing, face masks, and eye protection to prevent person-to-person transmission of SARS-CoV-2 and COVID-19: a systematic review and meta-analysis. *Lancet*. 2020;395:1973–87. [https://doi.org/10.1016/S0140-6736\(20\)31142-9](https://doi.org/10.1016/S0140-6736(20)31142-9)
 40. Park GW, Collins N, Barclay L, Hu L, Prasad BV, Lopman BA, et al. Strain-specific virolysis patterns of human noroviruses in response to alcohols. *PLoS One*. 2016;11:e0157787. <https://doi.org/10.1371/journal.pone.0157787>

Address for correspondence: Jan Vinjé, Centers for Disease Control and Prevention, 1600 Clifton Rd NE, Mailstop H18-7, Atlanta, GA 30329-4027, USA; email: jvinje@cdc.gov

Genetic Evidence and Host Immune Response in Persons Reinfected with SARS-CoV-2, Brazil

Natalia Fintelman-Rodrigues, Aline P.D. da Silva, Monique Cristina dos Santos, Felipe B. Saraiva, Marcelo A. Ferreira, João Gesto, Danielle A.S. Rodrigues, André M. Vale, Isaclaudia G. de Azevedo, Vinícius C. Soares, Hui Jiang, Hongdong Tan, Diogo A. Tschoeke, Carolina Q. Sacramento, Fernando A. Bozza, Carlos M. Morel, Patrícia T. Bozza, Thiago Moreno L. Souza

The dynamics underlying severe acute respiratory syndrome coronavirus 2 (SARS-CoV-2) reinfection remain poorly understood. We identified a small cluster of patients in Brazil who experienced 2 episodes of coronavirus disease (COVID-19) in March and late May 2020. In the first episode, patients manifested an enhanced innate response compared with healthy persons, but neutralizing humoral immunity was not fully achieved. The second episode was associated with different SARS-CoV-2 strains, higher viral loads, and clinical symptoms. Our finding that persons with mild COVID-19 may have controlled SARS-CoV-2 replication without developing detectable humoral immunity suggests that reinfection is more frequent than supposed, but this hypothesis is not well documented.

Confirmed cases of severe acute respiratory syndrome coronavirus 2 (SARS-CoV-2) have surpassed 110 million, along with 2.5 million deaths by 2019 coronavirus disease (COVID-19) (1). New waves of the pandemics in different Northern and Southern Hemisphere countries provide evidence that herd immunity might not have been fully achieved and that new variants could escape the response to natural infection (2,3).

Although there is evidence of the generation of B and T memory cells to SARS-CoV-2 proteins after

infection (4,5), it has also been documented that neutralizing seroconversion is heterogeneous among the population (6). Even for those who seroconvert, the sustainability of the immune response, as judged by IgG level, might decay after the primary exposure to coronaviruses (7–9). Cases of reinfection by SARS-CoV-2 can be associated with the absence of neutralizing serologic titers, diminishment of immunoglobulin titers after primo-infection, or viral polymorphisms to escape the host SARS-CoV-2 immune response (10–16).

To better understand the dynamics of the immune and virological responses in mild cases of COVID-19 that might predispose patients to reinfection, we continuously followed up with patients for potential exposure to SARS-CoV-2. For 2 patients, reinfection was documented. The National Review Board of Brazil approved the study protocol (Comissão Nacional de Ética em Pesquisa [CONEP] 30650420.4.1001.0008), and informed consent was obtained from all participants or patients' representatives.

Materials and Methods

Ethics and Study Population

During March–December 2020, the COVID-19 research task force screened a group of 30 participants weekly, independent of any symptoms, for SARS-CoV-2 detection by RT-PCR in nasopharyngeal swab specimens. If any of these participants exhibited positive results, or members of their households experienced signs or symptoms of COVID-19, they were invited to participate in the study and follow-up. At baseline and follow-up, we collected plasma, serum, and nasopharyngeal swab samples biweekly or at longer intervals if the patient was unavailable (Table). Households were included upon their request to be tested for SARS-CoV-2. Among

Author affiliations: Fundação Oswaldo Cruz (Fiocruz), Rio de Janeiro, Brazil (N. Fintelman-Rodrigues, A.P.D. da Silva, M.C. dos Santos, F.B. Saraiva, M.A. Ferreira, J. Gesto, I.G. de Azevedo, V.C. Soares, C.Q. Sacramento, F.A. Bozza, C.M. Morel, P.T. Bozza, T.M.L. Souza); Universidade Federal do Rio de Janeiro, Rio de Janeiro (D.A.S. Rodrigues, A.M. Vale, V.C. Soares, D.A. Tschoeke); MGI Tech Co., Ltd., Shenzhen, China (H. Jiang, H. Tan); D'Or Institute for Research and Education (F.A. Bozza)

DOI: <https://doi.org/10.3201/eid2705.204912>

the participants, 4 exhibited >1 episode of mild self-limiting COVID-19 with positive RT-PCR. For comparison, we included age-matched controls from the same group of participants and city in which the patients lived, Rio de Janeiro, Brazil. Controls were composed of 5 persons negative for SARS-CoV-2 throughout the investigated period.

Measurement of Serum SARS-CoV-2 Antibodies and Plasma Cytokine Levels

For quantitative analysis of SARS-CoV-2 spike protein IgM, IgA, and IgG antibodies, we performed the S-UFRJ test developed at Universidade Federal do Rio de Janeiro (R.G.F. Alvim et al., unpub. data, <https://doi.org/10.1101/2020.07.13.20152884>) (Appendix, <https://wwwnc.cdc.gov/EID/article/27/5/20-4912-App1.pdf>).

We collected plasma samples in tubes containing EDTA. We used commercial ELISA kits from R&D Systems (<https://www.rndsystems.com>) to measure cytokines and chemokine (Appendix).

Molecular Diagnosis

To determine serum titers to block SARS-CoV-2 infection, we performed miniaturized plaque-reduction neutralization test (PRNT) (Appendix). SARS-CoV-2 RNA has been detected in accordance with the US Centers for Disease Control and Prevention (CDC) recommendation (17). We used the standard curve method for virus quantification, using synthetic RNA for gene N (Microbiologics, <https://www.microbiologics.com>). We compared cycle thresholds (C_t) for the target gene to those obtained with different cell amounts (10^7 – 10^2), for reaction calibration (Appendix).

Genomic Analysis

We extracted total viral RNA from nasopharyngeal swabs using QIAamp Viral RNA (QIAGEN, <https://www.qiagen.com>), with minor modifications (18) (Appendix). We performed an amplicon-based enrichment strategy using the ATOplex SARS-CoV-2 Full-Length Genome Panel version 1.0 (MGI Tech Co., <https://en.mgi-tech.com>; donated by the vendor). Single-stranded circular DNA library pools were converted to DNA nanoballs by rolling circle amplification and submitted to pair-end sequencing (100 nt) on the MGISEQ-2000 platform (recently named DNBSEQ-G400; MGI Tech Co. Ltd.).

We quality-scored, filtered, trimmed, and assembled genomic sequences in contigs through a validated workflow for SARS-CoV-2 (19). Genomes were aligned with MAFFT (20) or ClustalW (21), and phylogenies were constructed with MEGA version

7.0 (22,23), using the Jukes-Cantor model for maximum-likelihood estimates by applying neighbor-joining and BioNJ algorithms (24), or by MrBayes version 3.2.7 (<http://nbisweden.github.io/MrBayes>) (25,26) with a relaxed clock model with a priori model testing using the gamma rates and invariant sites nucleotide substitution model, selected by jModelTest version 1.6 <http://darwin.uvigo.es/software/jmodeltest.htm>. We visualized and edited the tree with FigTree version 1.4.2 (<http://tree.bio.ed.ac.uk>). We determined SARS-CoV-2 clades using the Nextclade software, beta version 0.14 (<https://clades.nextstrain.org>). To categorize mutations and polymorphisms, we aligned the SARS-CoV-2 reference genome Wuhan-Hu-1 (GISAID EPI_ISL no. 402125; <https://www.gisaid.org>) to our sequences. The original sequences used in this work are publicly available on <https://nextstrain.org/ncov>: GISAID EPI_ISL nos. 636737, 636834–636838. The dataset included in the analysis contained representative sequences of the emerging clades associated with our sequences, 19A and 20B, as well as sequences from the genome 20A as a negative control (Appendix Table 1).

Results

Among the households of the COVID-19 research task force, a 54-year-old man (patient A) requested an RT-PCR test for SARS-CoV-2 on March 23 because of a recurrent headache on the prior 2 days. He also had previous contact with a symptomatic co-worker returning from travel who refused to be tested. Patient A had a detectable viral load (C_t 27.41) of $\approx 10^5$ copies/mL in nasopharyngeal swab samples (Table). Although patient B, a 57-year-old woman with a previous history of discoid lupus erythematosus, was in self-isolation, she was tested because of close contact with patient A. She tested positive for COVID-19 on March 24; her nasopharyngeal swab sample C_t was ≈ 36.31 ($\approx 10^3$ copies/mL) (Table). Two days afterward, she experienced diarrhea (Table).

Patient B shares a household with patients C and D, a married couple, both 34 years old. Patients C and D were not in social isolation because of their work duties. Although patient C was asymptomatic, he displayed a C_t of 35.71 (10^3 copies/mL) on March 25 (Table). Patient D was negative by molecular testing on March 26, but 1 week later, she had a detectable viral load (C_t 36.01, 10^3 copies/mL) and reported diarrhea in the following days (Table). On March 27, all 4 patients experienced an increase of inflammatory mediators (interleukin [IL] 6, IL-8, and tumor necrosis factor α) and regulatory (IL-10) and chemotactic (C-X-C motif chemokine ligand 10) and antiviral

(interferon γ) signals, relative to healthy SARS-CoV-2-negative controls (Figure 1). Although cytokine response was consistent with the resolution of the infection, the anti-SARS-CoV-2 neutralizing humoral response was not detected in late March 2020 (Table; Appendix Figure 2).

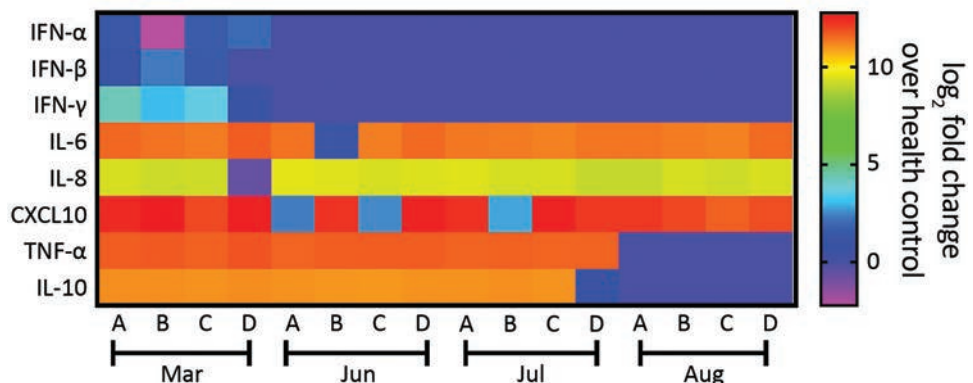
For patients B and C, we were able to obtain a full-length SARS-CoV-2 genome (Table). Complete genome sequencing, with Phred quality score >30 , composed of 140,000–20,000,000 reads and 100-fold to 10,000-fold coverage, argues against a false-positive RT-PCR result (Appendix Table 2, first column). For patients A and D, the samples were insufficient for sequencing. In March 2020, patients B was infected with emerging SARS-CoV-2 clade 19A and patient C with SARS-CoV-2 clade 20B, (Table; Figure 2; Appendix Figure 3). The detection of the 2 distinct lineages indicates that patients B and C were infected independently and did not transmit the virus to each other (Table; Figure 2; Appendix Figure 3). These distinct lineages were co-circulating in Brazil in March 2020 when multiple introductions of the SARS-CoV-2 occurred (27). Emerging clade 19A is associated with imported cases in Brazil, because of its proximity to the Wuhan-01 sequence (Figure 2; Appendix Figure 3). Indeed, detection of clade 19A in the sample from Patient B is consistent with household transmission from patient A, and his contact with the symptomatic traveler. Patient C, a police officer, was frequently exposed to various probable sources of contamination; he was infected with an emerging clade 20B virus, the most prevalent variant in Brazil, during December 2020 (Figure 2; Appendix Figure 3). All patients recovered from a mild COVID-19 episode and were retested in the first half of April, when they had negative RT-PCR results.

In the last week of May 2020, when COVID-19 cases in Rio de Janeiro were at the peak of the first wave of the pandemic (28), these 4 patients reported more signs and symptoms of SARS-CoV-2 infection than in March (Table). During the second episode, they experienced fever and cough, along with fatigue, headache, body ache, anosmia, and ageusia. Real-time RT-PCR revealed higher viral loads in the nasopharyngeal swab samples than at the time of the first infection: C_t of 21.76 ($\approx 10^7$ copies/mL) for patient A, 21.84 ($\approx 10^7$ copies/mL) for patient B, 26.38 ($\approx 10^5$ copies/mL) for patient C, and 16.87 ($\approx 10^9$ copies/mL) for patient D (Table).

On June 3, a week after the second episode, we detected SARS-CoV-2 immunoglobulins in patients A and B, but they had low to no neutralizing activity (Table; Appendix Figure 2). These serologic samples from June indicate that the first episode of COVID-19 was not followed by a sustained neutralizing humoral response, as judged by 90% PRNT ($PRNT_{90}$) titers (Table). Because signals of a humoral effector memory were inconsistent after the first episode of COVID-19 (Table), we could speculate that the enhanced production of interferons and proinflammatory mediators led to resolution of the primo-infection (Figure 1). During the second episode of COVID-19, most of the cytokine levels were still higher than in healthy volunteers (Figure 1).

On July 9, forty days after the episode of reinfection, all patients had detectable immunoglobulin levels and their lowest $PRNT_{90}$ results (Table; Appendix Figure 2), declining thereafter by August 10 (Table; Appendix Figure 2). In July, patients' tests continuously showed upregulated pro-inflammatory markers (Figure 1), which are consistent with an enhanced

Figure 1. Heatmap showing the profile of innate immune response from patients who experienced 2 episodes of severe acute respiratory syndrome coronavirus 2 (SARS-CoV-2) infection, Brazil, 2020. We measured the mediators of innate immunity by ELISA for patients A–D. For comparison, these molecules were also quantified in the plasma from 5 healthy donors negative for SARS-CoV-2. The heatmap displays the \log_2 ratio of the fold-change from the plasma



of the patients over the healthy volunteers. The means \pm standard error of the means for the healthy volunteers were the following: IFN- α = 20.4 ± 4.7 pg/mL; IFN- β = 26.0 ± 3.9 pg/mL; IFN- γ = 27.8 ± 7.8 pg/mL; IL-6 = 13.4 ± 1.7 pg/mL; IL-8 = 137 ± 21.6 pg/mL; IL-10 = 165.4 ± 40.7 pg/mL; TNF- α = 33.8 ± 11.5 pg/mL; and CXCL-10 = 61.0 ± 27.3 pg/mL. CXCL, C-X-C motif chemokine ligand; IFN, interferon; IL, interleukin; TNF, tumor necrosis factor.

Table. Characteristics of patients reinfected with severe acute respiratory syndrome coronavirus 2, Brazil, 2020*

Characteristic	Patient A	Patient B	Patient C	Patient D
Primo-infection				
Sex	M	F	M	F
Age, y	54	57	34	34
Concurrent conditions	None	Discoid lupus erythematosus	None	None
Date of symptom onset	March 21	March 26	Asymptomatic	March 31
Symptoms	Headache	Mild diarrhea	No	Mild diarrhea
N1 RT-PCR, log ₁₀ copies/mL	5.12	3.21	3.83	3.01
Date conducted	March 23	March 24	March 24	April 2
RNP RT-PCR (internal control), C _t	26.5	26.66	27.41	28.48
Serology†	IgM, IgA, IgG detected	IgM, IgA, IgG detected	IgM, IgA, IgG detected	IgM, IgA, IgG detected
PRNT ₉₀ /25 uL‡	<1:4	<1:4	<1:4	<1:4
Sequencing ID	Not enough sample	Emerging clade 19A EPI_ISL_636834	Emerging clade 20B EPI_ISL_636836	Not enough sample NA
Second infection				
Date of onset illness	May 25	May 26	May 27	May 30
Symptoms	Fever, dry cough, tiredness, body ache, anosmia, ageusia	Fever, diarrhea, headache, body ache, anosmia, ageusia	Fever, nausea, tiredness, headache, body ache	Dry cough, diarrhea, tiredness, headache, body ache, anosmia, ageusia
RT-PCR, log ₁₀ copies/mL	7.31	7.42	5.18	9.61
Date conducted	May 29	May 29	May 29	May 29
RNP RT-PCR internal control	24.6	27.06	28.12	24.5
Serology results‡	IgM, IgA, IgG detected	IgM, IgA, IgG detected	IgM, IgA, IgG undetectable	IgM, IgA, IgG undetectable
PRNT ₉₀ /25 uL‡	1:16	<1:4	<1:4	<1:4
Sequencing Accession ID	Emerging clade 20B EPI_ISL_636737	Emerging clade 20B EPI_ISL_636835	Emerging clade 20B EPI_ISL_636837	Emerging clade 20B EPI_ISL_636838
Follow-up				
Serology§	IgM, IgA, IgG detected	IgM, IgA, IgG detected	IgM, IgA, IgG detected	IgM, IgA, IgG detected
PRNT ₉₀ /25 uL§	1:128	1:32	1:64	1:64
Serology results¶	IgM, IgA, IgG detected	IgM, IgA, IgG detected	IgM, IgA, IgG detected	IgM, IgA, IgG detected
PRNT ₉₀ /25 uL	1:64	1:16	1:8	1:8

*N1, nucleocapsid gene; NA, not available; PRNT₉₀, 90% plaque-reduction neutralization test; RNP, human RNase P gene; RT-PCR, reverse transcription PCR.

†Tests conducted March 27.

‡Tests conducted June 3.

§Tests conducted July 9.

¶Tests conducted August 10.

response to a second SARS-CoV-2 exposure. In August, the markers of inflammation and regulatory responses, tumor necrosis factor α and IL-10, decreased compared with levels from previous months (Figure 1).

In the second episode, we fully sequenced the SARS-CoV-2 genome from all patients (Table; Figure 2; Appendix Table 2, Figure 3). SARS-CoV-2 sequences from the reinfection clustered together, suggesting a household transmission for patients A–D (Figure 2; Appendix Figure 3). The emerging genotype 20B, which was the main variant circulating in Brazil since May 2020, was detected in all samples from the second episode (Figure 2; Table; Appendix Figure 3). For patient B, the first episode was associated with the emerging clade 19A and the second with 20B (Figure 2; Appendix Figure 3). Two episodes provoked by genetically distinct lineages support the possibility of reinfection.

Although both episodes in patient C were associated with clade 20B, they clustered apart on the

phylogeny with significant statistical support: by 86% of bootstrap using maximum likelihood (Figure 2) and by Bayesian inference (Appendix Figure 3). Genetic markers in the SARS-CoV-2 genome were different in the patient’s 2 episodes of COVID-19 (Appendix Table 2). The genomes diverge at the genes encoding the nonstructural protein (NSP) 3, 3C-like proteinase, and exonuclease (Appendix Table 2). In addition to the genetic variations, poor development of anti-SARS-CoV-2 serology between the 2 episodes of infection points suggests a reinfection scenario.

Discussion

Seasonal human coronaviruses may cause reinfection, as documented for the past 35 years (8,29). Of note, in veterinary medicine, domestic mammals also have coronavirus reinfection (30). Adaptive, memory-generating immunity to coronaviruses is heterogeneously sustainable in mammals, and some events of infection are controlled at the level of the

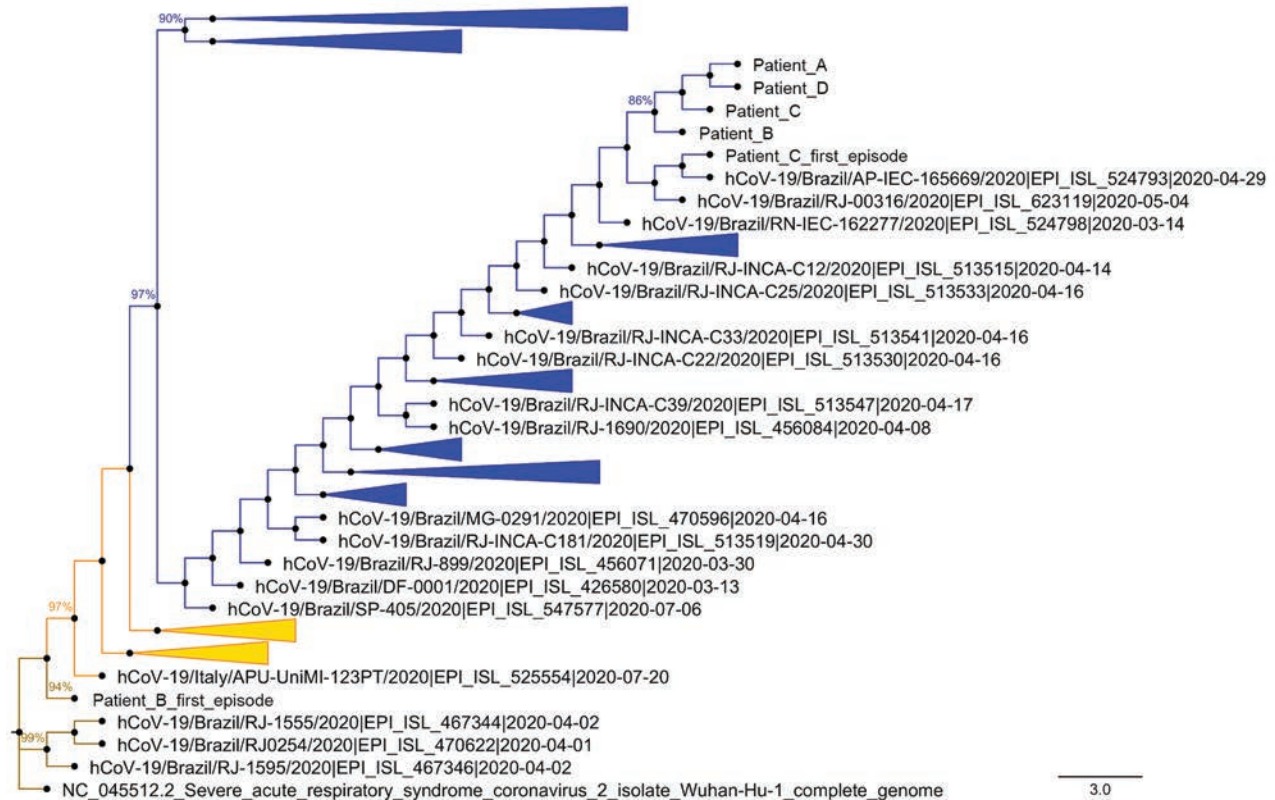


Figure 2. Phylogenetic analysis of severe acute respiratory syndrome coronavirus 2 genomes from reinfected patients, Brazil, 2020. Representative genomes deposited in GISAID (Appendix Table 1, Figure 3, <https://wwwnc.cdc.gov/EID/article/27/5/20-4912-App1.pdf>) were compared with sequences from virus genomes found in the respiratory samples from the first infection of patients B and C, and the second infection of patients A–D. A condensed phylogenetic tree rooted by reference genome Wuhan-Hu-1 (EPI_ISL_402125) was created with 1,000 bootstraps. Initial trees for the heuristic search were obtained automatically by applying neighbor-joining and BioNJ algorithms to a matrix of pairwise distances estimated using the Jukes-Cantor model (24), and then selecting the topology with a superior log-likelihood value. The tree with the highest log likelihood (−46487.36) is shown. The final dataset included a total of 29,920 positions. Evolutionary analyses were conducted in MEGA version 7.0 (22,23). Evolutionary history was inferred using the maximum-likelihood method and Jukes-Cantor model. Brown represents the emerging clade 19A, orange the clade 20A, and blue the clade 20B. Scale bar indicates substitutions per site. hCoV, human coronavirus.

innate immunity (31–33). We fully documented reinfection in 2 genetically unrelated persons in Rio de Janeiro, Brazil, describing patients who sought care twice in a 2-month interval who received clinical and laboratory diagnosis of COVID-19. Virus polymorphisms from the primary and second episodes and negative RT-PCR between the events strengthen the argument toward reinfection. Neutralizing anti-SARS-CoV-2 titers were not detected during the first episode, nor at the baseline of the second episode, suggesting that patients were still vulnerable after the primary episode.

SARS-CoV-2 reinfection has been associated with new variants that overcome the immune response to natural infection, short-lasting humoral response, and a limited or absent neutralizing immunity after the primo-infection (10–13). The patients in Brazil described in this study are similar to cases in the United

States and Ecuador (10,13), in which reinfection was associated with more symptoms. Antibody-dependent enhancement or exposure to higher amounts of the virus could be the reason for the change from asymptomatic or oligosymptomatic to syndromic. In our study, primary and second infections were caused by a strain carrying the D614G mutation in the spike protein, which has been associated with higher replication efficiency (34). We did not detect other contemporaneous changes in the spike protein, such as 69/70 deletion, K417N, E484K, N501Y, P681H, or the 17 unique mutations of the P1 variant, which precluded association with more virulent strains (35). Beyond the spike protein, we detected the V125F change in the NSP14 protein; V125F is a nonconservative mutation that might increase the volume in the loop between β -sheets number 5 and 6, which could affect its methyltransferase activity (36).

The V125F mutation is unlikely to increase virulence in a second episode. On the other hand, changes in NSP6 protein (37) and open reading frame 6 mRNA (S. Sarif Hassan et al., unpub. data, <https://doi.org/10.1101/2020.11.06.372227>) might result in viral evasion from innate immunity.

The primary infections of patients B and C were associated with emerging clades 19A and 20B, indicating that the 2 cohabitants were infected independently. Indeed, while 1 patient was in social isolation, the others were working outside in the community. The cocirculation of these clades of SARS-CoV-2 is consistent with the COVID-19 databases in GISAID and the multiple introductions of the new coronavirus in Brazil (27). In the following months, emerging clade 20B was identified as the most prevalent genotype, representing 60% of the deposited genomes on GISAID. The detection of clade 20B on the second episode of COVID-19, by the end of May, is associated with the peak of the pandemic in Rio de Janeiro, Brazil (28).

Distinct clades of SARS-CoV-2 were found in the primary and secondary respiratory samples from patient B, supporting the notion of reinfection. For patient C, both the first and second detections of SARS-CoV-2 were associated with clade 20B. Although viral persistence could be imagined in this scenario, SARS-CoV-2 genomic sequences from the first and second episodes do not cluster together in the same branch, as they did for an immunocompromised patient that shed SARS-CoV-2 for 150 days (38). Thus, phylogeny does not support the interpretation of persistence, by different methods. By branching apart, SARS-CoV-2 genomes associated with patient C strengthen the chances of a relevant degree of variation (39), indicating the direction of reinfection. In the documented case of SARS-CoV-2 and human coronavirus NL63 reinfection, different episodes were genetically associated with similar viral clades or strains (40). Whereas the detection of 2 episodes of SARS-CoV-2 infection from patient C was separated by >60 days, prolonged virus shedding in the nasopharyngeal swab specimens from mild cases lasted for 22–46 days (41), which is further evidence against persistence.

Results of SARS-CoV-2 reinfection affirm that immune rechallenge may be necessary to achieve humoral protection and underscore that sustainability of the immune response may be heterogeneous. We documented that these patients with mild COVID-19 displayed an innate immune response composed of pro-inflammatory and regulatory signals. Although cytokine storm has been associated with severe COVID-19 (42), we interpret that in the case of our

patients, the innate immune response might have led to infection resolution (43). Another possibility, not explored in detail here, is that cellular-mediated immunity could have contributed to the mild clinical outcome (2,4,44). The natural history of mild COVID-19 described for these patients might also be representative of many persons exposed to the first wave of the pandemic, leading to the hypothesis that they would also be susceptible to other episodes of SARS-CoV-2 infections, even without the challenge being imposed by new variants.

We determined, on the basis of 6 years of surveillance and follow-up of human coronavirus reinfections, that initial exposure was insufficient to elicit a protective immune response, imposing limited pressure on selection on new seasonal coronavirus variants (40). Similarly, our data on a small cluster of patients recapitulate this natural history of reinfection, which may also occur for SARS-CoV-2.

Acknowledgments

We thank Carmen Beatriz Wagner and Giacoia Gripp for assessments related to the Biosafety Level 3 facility and Marco Alberto Medeiros for assessments related to the sequencing platform. We thank Gonzalo Bello, Dumith Chequer Bou-Habib, Willian Provance, and Fabiano Thompson for insightful discussions. We greatly appreciated the MGI, a partner in the implementation of next-generation sequencing through collaborations with Oswaldo Cruz Foundation, especially for challenging samples of COVID-19.

Author contributions: F.A.B. and P.T.B. conducted clinical surveillance. N.F.R. and F.A.B. enrolled patients in the study. N.F.R., C.Q.S., D.R., I.G.A., V.C.S. performed immunologic assessments. N.F.R., A.P.D.S., M.C.S., F.B.S., M.A.F., J.G., H.J., and H.T. performed sequencing. A.P.D.S., M.C.S., and D.A.T. were responsible for bioinformatics. F.A.B., P.T.B., C.M.M., T.M.L.S. handled study coordination. N.F.R., P.T.B., A.M.V., and T.M.L.S. prepared and revised the manuscript. All authors revised and approved the manuscript.

About the Author

Dr. Fintelman-Rodrigues is based at the Laboratory of Immunopharmacology, Instituto Oswaldo Cruz (IOC), Fundação Oswaldo Cruz (Fiocruz), Rio de Janeiro, Brazil.

References

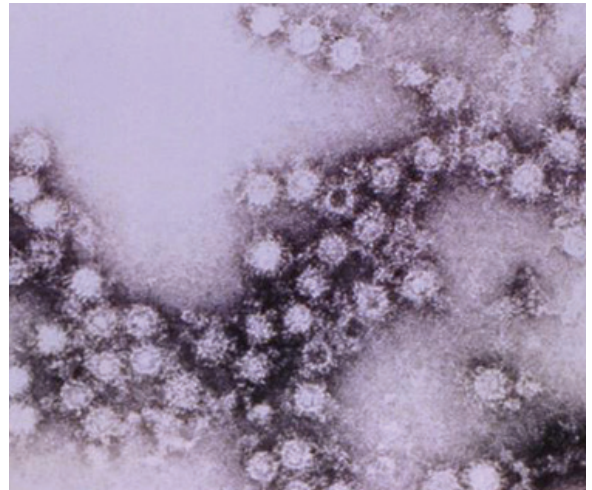
1. World Health Organization. Coronavirus disease (COVID-19) dashboard. 2020 [cited 2020 Nov 12]. <https://covid19.who.int/>
2. Rodda LB, Netland J, Shehata L, Pruner KB, Morawski PA, Thouvenel C, et al. Functional SARS-CoV-2-specific immune

- memory persists after mild COVID-19. *Cell*. 2021;184:169-83. <https://doi.org/10.1016/j.cell.2020.11.029> <https://doi.org/10.1101/2020.08.11.20171843>
3. Centers for Disease Control and Prevention. Cases, data, and surveillance. 2020 [cited 2021 Feb 12]. <https://www.cdc.gov/coronavirus/2019-ncov/cases-updates/variant-surveillance/variant-info.html>
 4. Hartley GE, Edwards ESJ, Aui PM, Varese N, Stojanovic S, McMahon J, et al. Rapid generation of durable B cell memory to SARS-CoV-2 spike and nucleocapsid proteins in COVID-19 and convalescence. *Sci Immunol*. 2020;5:eabf8891. <https://doi.org/10.1126/sciimmunol.abf8891>
 5. Le Bert N, Tan AT, Kunasegaran K, Tham CYL, Hafezi M, Chia A, et al. SARS-CoV-2-specific T cell immunity in cases of COVID-19 and SARS, and uninfected controls. *Nature*. 2020;584:457-62. <https://doi.org/10.1038/s41586-020-2550-z>
 6. Ripperger TJ, Uhrlaub JL, Watanabe M, Wong R, Castaneda Y, Pizzato HA, et al. Detection, prevalence, and duration of humoral responses to SARS-CoV-2 under conditions of limited population exposure. *Immunity*. 2020;53:925-33. <https://doi.org/10.1101/2020.08.14.20174490>
 7. Hueston L, Kok J, Guibone A, McDonald D, Hone G, Goodwin J, et al. The antibody response to SARS-CoV-2 infection. *Open Forum Infect Dis*. 2020;7:a387. <https://doi.org/10.1093/ofid/ofaa387>
 8. Edridge AWD, Kaczorowska J, Hoste ACR, Bakker M, Klein M, Loens K, et al. Seasonal coronavirus protective immunity is short-lasting. *Nat Med*. 2020;26:1691-3. <https://doi.org/10.1038/s41591-020-1083-1>
 9. Dan JM, Mateus J, Kato Y, Hastie KM, Yu ED, Faliti CE, et al. Immunological memory to SARS-CoV-2 assessed for up to 8 months after infection. *Science*. 2021;371:eabf4063. <https://doi.org/10.1126/science.abf4063>
 10. Tillett RL, Sevinsky JR, Hartley PD, Kerwin H, Crawford N, Gorzalski A, et al. Genomic evidence for reinfection with SARS-CoV-2: a case study. *Lancet Infect Dis*. 2021;21:52-8. [https://doi.org/10.1016/S1473-3099\(20\)30764-7](https://doi.org/10.1016/S1473-3099(20)30764-7)
 11. To KK-W, Hung IF-N, Ip JD, Chu AW-H, Chan W-M, Tam AR, et al. Coronavirus disease 2019 (COVID-19) reinfection by a phylogenetically distinct severe acute respiratory syndrome coronavirus 2 strain confirmed by whole genome sequencing. *Clin Infect Dis*. 2020 Aug 25 [Epub ahead of print]. <https://doi.org/10.1093/cid/ciaa1275> <https://doi.org/10.1093/cid/ciaa1275>
 12. Van Elslande J, Vermeersch P, Vandervoort K, Wawina-Bokalanga T, Vanmechelen B, Wollants E, et al. Symptomatic SARS-CoV-2 reinfection by a phylogenetically distinct strain. *Clin Infect Dis*. 2020 Sep 5 [Epub ahead of print]. <https://doi.org/10.1093/cid/ciaa1330> <https://doi.org/10.1093/cid/ciaa1330>
 13. Prado-Vivar B, Becerra-Wong M, Guadalupe JJ, Marquez S, Gutierrez B, Rojas-Silva P, et al. COVID-19 reinfection by a phylogenetically distinct SARS-CoV-2 variant, first confirmed event in South America. SSRN. 2020 September 9 [cited 2021 Mar 19]. <https://doi.org/10.2139/ssrn.3686174>
 14. Mulder M, van der Vegt DSJM, Oude Munnink BB, GeurtsvanKessel CH, van de Bovenkamp J, Sikkema RS, et al. Reinfection of severe acute respiratory syndrome coronavirus 2 in an immunocompromised patient: a case report. *Clin Infect Dis*. 2020 Oct 9 [Epub ahead of print]. <https://doi.org/10.1093/cid/ciaa1538> <https://doi.org/10.1093/cid/ciaa1538>
 15. Selhorst P, Van Ierssel S, Michiels J, Mariën J, Bartholomeeusen K, Dirinck E, et al. Symptomatic SARS-CoV-2 reinfection of a health care worker in a Belgian nosocomial outbreak despite primary neutralizing antibody response. *Clin Infect Dis*. 2020 Dec 14 [Epub ahead of print]. <https://doi.org/10.1093/cid/ciaa1850> <https://doi.org/10.1093/cid/ciaa1850>
 16. Larson D, Brodnyak SL, Voegtly LJ, Cer RZ, Glang LA, Malagon FJ, et al. A case of early reinfection with severe acute respiratory syndrome coronavirus 2 (SARS-CoV-2). *Clin Infect Dis*. 2020 Sep 19 [Epub ahead of print]. <https://doi.org/10.1093/cid/ciaa1436> <https://doi.org/10.1093/cid/ciaa1436>
 17. Centers for Disease Control and Prevention. Research use only 2019-novel coronavirus (2019-nCoV) real-time RT-PCR primers and probes. 2020 [cited 2020 Nov 11]. <https://www.cdc.gov/coronavirus/2019-ncov/lab/rt-pcr-panel-primer-probes.html>
 18. Metsky HC, Matranga CB, Wohl S, Schaffner SF, Freije CA, Winnicki SM, et al. Zika virus evolution and spread in the Americas. *Nature*. 2017;546:411-5. <https://doi.org/10.1038/nature22402>
 19. Cleemput S, Dumon W, Fonseca V, Abdool Karim W, Giovanetti M, Alcantara LC, et al. Genome Detective coronavirus typing tool for rapid identification and characterization of novel coronavirus genomes. *Bioinformatics*. 2020;36:3552-5. <https://doi.org/10.1093/bioinformatics/btaa145>
 20. Katoh K, Kuma K, Toh H, Miyata T. MAFFT version 5: improvement in accuracy of multiple sequence alignment. *Nucleic Acids Res*. 2005;33:511-8. <https://doi.org/10.1093/nar/gki198>
 21. Larkin MA, Blackshields G, Brown NP, Chenna R, McGettigan PA, McWilliam H, et al. Clustal W and Clustal X version 2.0. *Bioinformatics*. 2007;23:2947-8. <https://doi.org/10.1093/bioinformatics/btm404>
 22. Kumar S, Stecher G, Li M, Knyaz C, Tamura K. MEGA X: Molecular Evolutionary Genetics Analysis across computing platforms. *Mol Biol Evol*. 2018;35:1547-9. <https://doi.org/10.1093/molbev/msy096>
 23. Felsenstein J. Confidence limits on phylogenies: an approach using the bootstrap. *Evolution*. 1985;39:783-91. <https://doi.org/10.1111/j.1558-5646.1985.tb00420.x>
 24. Jukes TH, Cantor CR. Evolution of protein molecules. In: Mammalian protein metabolism. Vol. III. Munro HN, editor. New York: Academic Press; 1969. p. 21-132.
 25. Huelsenbeck JP, Ronquist F. MRBAYES: Bayesian inference of phylogenetic trees. *Bioinformatics*. 2001;17:754-5. <https://doi.org/10.1093/bioinformatics/17.8.754>
 26. Ronquist F, Huelsenbeck JP. MrBayes 3: Bayesian phylogenetic inference under mixed models. *Bioinformatics*. 2003;19:1572-4. <https://doi.org/10.1093/bioinformatics/btg180>
 27. Candido DS, Claro IM, de Jesus JG, Souza WM, Moreira FRR, Dellicour S, et al.; Brazil-UK Centre for Arbovirus Discovery, Diagnosis, Genomics and Epidemiology (CADDE) Genomic Network. Evolution and epidemic spread of SARS-CoV-2 in Brazil. *Science*. 2020;369:1255-60. <https://doi.org/10.1126/science.abd2161>
 28. Secretaria de Saúde do Estado do Rio de Janeiro. Covid-19 monitoring panel in the Rio de Janeiro State [in Portuguese]. 2020 [cited 2020 Nov 24]. <http://painel.saude.rj.gov.br/monitoramento/covid19.html#>
 29. Kiyuka PK, Agoti CN, Munywoki PK, Njeru R, Bett A, Otieno JR, et al. Human coronavirus NL63 molecular epidemiology and evolutionary patterns in rural coastal Kenya. *J Infect Dis*. 2018;217:1728-39. <https://academic.oup.com/jid/article/217/11/1728/4948258>
 30. Decaro N, Martella V, Saif LJ, Buonavoglia C. COVID-19 from veterinary medicine and one health perspectives: what animal coronaviruses have taught us. *Res Vet Sci*. 2020;131:21-3. <https://doi.org/10.1016/j.rvsc.2020.04.009>

31. Neeland MR, Bannister S, Clifford V, Dohle K, Mulholland K, Sutton P, et al. Innate cell profiles during the acute and convalescent phase of SARS-CoV-2 infection in children. *Nat Commun.* 2021;12:1084. <https://doi.org/10.1038/s41467-021-21414-x>
32. Tay MZ, Poh CM, Rénia L, MacAry PA, Ng LFP. The trinity of COVID-19: immunity, inflammation and intervention. *Nat Rev Immunol.* 2020;20:363–74. <https://doi.org/10.1038/s41577-020-0311-8>
33. Sallenne J-M, Guillot L. Innate immune signaling and proteolytic pathways in the resolution or exacerbation of SARS-CoV-2 in COVID-19: key therapeutic targets? *Front Immunol.* 2020;11:1229. <https://doi.org/10.3389/fimmu.2020.01229>
34. Groves DC, Rowland-Jones SL, Angyal A. The D614G mutations in the SARS-CoV-2 spike protein: Implications for viral infectivity, disease severity and vaccine design. *Biochem Biophys Res Commun.* 2021;538:104–7. <https://doi.org/10.1016/j.bbrc.2020.10.109>
35. Centers for Disease Control and Prevention. Emerging SARS-CoV-2 variants. 2020 [cited 2021 Feb 12]. <https://www.cdc.gov/coronavirus/2019-ncov/more/science-and-research/scientific-brief-emerging-variants.html>
36. Krafcikova P, Silhan J, Nencka R, Boura E. Structural analysis of the SARS-CoV-2 methyltransferase complex involved in RNA cap creation bound to sinefungin. *Nat Commun.* 2020;11:3717. <https://doi.org/10.1038/s41467-020-17495-9>
37. Cottam EM, Whelband MC, Wileman T. Coronavirus NSP6 restricts autophagosome expansion. *Autophagy.* 2014;10:1426–41. <https://doi.org/10.4161/auto.29309>
38. Choi B, Choudhary MC, Regan J, Sparks JA, Padera RF, Qiu X, et al. Persistence and evolution of SARS-CoV-2 in an immunocompromised host. *N Engl J Med.* 2020;383:2291–3.
39. Koyama T, Platt D, Parida L. Variant analysis of SARS-CoV-2 genomes. *Bull World Health Organ.* 2020;98:495–504. <https://doi.org/10.2471/BLT.20.253591>
40. Kiyuka PK, Agoti CN, Munywoki PK, Njeru R, Bett A, Otieno JR, et al. Human coronavirus NL63 molecular epidemiology and evolutionary patterns in rural coastal Kenya. *J Infect Dis.* 2018;217:1728–39. <https://doi.org/10.1093/infdis/jiy098>
41. Sun J, Xiao J, Sun R, Tang X, Liang C, Lin H, et al. Prolonged persistence of SARS-CoV-2 RNA in body fluids. *Emerg Infect Dis.* 2020;26:1834–8. <https://doi.org/10.3201/eid2608.201097>
42. de la Rica R, Borges M, Gonzalez-Freire M. COVID-19: in the eye of the cytokine storm. *Front Immunol.* 2020;11:558898. <https://doi.org/10.3389/fimmu.2020.558898>
43. Arunachalam PS, Wimmers F, Mok CKP, Perera RAPM, Scott M, Hagan T, et al. Systems biological assessment of immunity to mild versus severe COVID-19 infection in humans. *Science.* 2020;369:1210–20. <https://doi.org/10.1126/science.abc6261>
44. Sekine T, Perez-Potti A, Rivera-Ballesteros O, Strålin K, Gorin J-B, Olsson A, et al.; Karolinska COVID-19 Study Group. Robust T cell immunity in convalescent individuals with asymptomatic or mild COVID-19. *Cell.* 2020;183:158–168.e14. <https://doi.org/10.1016/j.cell.2020.08.017>

Address for correspondence: Thiago Moreno Lopes e Souza, Fundação Oswaldo Cruz (Fiocruz), Centro de Desenvolvimento Tecnológico em Saúde (CDTS), Instituto Oswaldo Cruz (IOC), Pavilhão Osório de Almeida, sala 16, Av. Brasil 4365, Mangueiras, Rio de Janeiro, RJ, CEP 21060340, Brazil; email: tmoreno@cdts.fiocruz.br

EID Podcast Enterovirus D68 and Acute Flaccid Myelitis, 2020



Around 2014, a mysterious, polio-like illness emerged in California and Colorado. Acute flaccid myelitis (AFM) primarily infects children, and if untreated, can lead to paralysis and respiratory failure. Despite extensive surveillance and research campaigns, the true cause of this debilitating disease remains unknown.

New research has shed light on a possible connection between AFM and a pathogen called enterovirus D68.

In this EID podcast, Dr. Sarah Kidd, a medical epidemiologist at CDC, and Sarah Gregory discuss what is known—and unknown—about AFM.

Visit our website to listen:

<https://go.usa.gov/x7CkY>

**EMERGING
INFECTIOUS DISEASES®**

COVID-19–Associated Mold Infection in Critically Ill Patients, Chile

Ricardo Rabagliati, Nicolás Rodríguez, Carolina Núñez, Alvaro Huete, Sebastian Bravo, Patricia Garcia

Patients with severe coronavirus disease (COVID-19) may have COVID-19–associated invasive mold infection (CAIMI) develop. We report 16 cases of CAIMI among 146 nonimmunocompromised patients with severe COVID-19 at an academic hospital in Santiago, Chile. These rates correspond to a CAIMI incidence of 11%; the mortality rate for these patients was 31.2%.

Invasive mold infection is a serious complication described in patients with severe viral pneumonia (1). Centers in Europe, China, and the United States have reported cases of fungal superinfections among patients with severe coronavirus disease (COVID-19). Aspergillosis is the main reported etiology; incidences range from 7.7% to 27.7% (2–8). Recently, the European Confederation on Medical Mycology and the International Society on Human and Animal Mycology published the diagnostic criteria for COVID-19–associated invasive pulmonary aspergillosis (CAPA), on the basis of histology, microbiology, imaging reports, and clinical factors (9).

We retrospectively identified adults admitted to the intensive care unit (ICU) at Hospital Clínico of UC-CHRISTUS Health Network in Santiago, Chile, during May 18–July 18, 2020 for COVID-19–associated invasive mold infection (CAIMI). We diagnosed CAIMI on the basis of respiratory failure, refractory fever, lung infiltrates, positive mold culture, positive galactomannan from serum, bronchoalveolar lavage (BAL), or a combination of these. The study was approved by the hospital's institutional review board (ID no. 190320003, July 15, 2020).

We recorded clinical and microbiological data, imaging reports, treatments, and survival outcome. A thoracic radiologist (A.H.) reviewed chest radiographs and computed tomography (CT) scans, and

we calculated a chest radiograph severity score (10). We confirmed fungal identification by matrix-assisted laser desorption/ionization time-of-flight mass spectrometry or sequencing.

Of the 856 COVID-19 patients admitted, 146 (17.1%) were hospitalized in the ICU and 16 (11%) received a diagnosis of CAIMI (Appendix Table, <https://wwwnc.cdc.gov/EID/article/27/5/20-4412-App1.pdf>). Median age of the 16 patients was 65 (range 30–89) years; 10 (62.5%) were male. Nine (56.3%) had hypertension, 4 (25%) asthma/COPD, 4 (25%) diabetes, and 3 (18.8%) obesity; none were immunocompromised. Median Acute Physiology and Chronic Health Evaluation (APACHE-II) score was 8 (range 4–20), and the median worst PaO₂/FiO₂ for each patient was 124 (range 57–476). Fourteen patients (87.5%) required invasive mechanical ventilation. In 12 cases (75%), prone position was applied for an average of 5 (range 2–19) days. All patients received antimicrobial drug therapy, 15 (93.8%) received corticosteroids, and 3 (18.8%) received tocilizumab.

We diagnosed CAIMI a mean of 18.5 (range 1–47) days after a positive COVID-19 test, at 14.5 (range 0–28) days after ICU admission, and at 12.5 (range 0–28) days after invasive mechanical ventilation was initiated. We performed BAL in 4 cases (25%); during bronchoscopy, we observed no ulcerative lesions in tracheobronchial mucosa. We diagnosed bacterial infection in 7 patients (43.8%). We obtained mold mycological evidence by fungal culture in 9 cases (56.3%) and galactomannan in 8 cases (50%); cultures came from tracheal aspirate in 7 cases and BAL in 2 (cases 15 and 16; Appendix Table). In 7 cases only 1 mold grew; in 2 cases >1 mold grew (cases 2 and 14). We identified a total of 12 molds: 9 (75%) *Aspergillus* spp. (4 *A. niger*, 2 *A. fumigatus*, 2 *A. terreus*, 1 *A. lentulus*), 2 (16.7%) *Rhizopus* spp. (1 *R. microsporus*, 1 *R. stolonifera*), and 1 (8.3%) *Scedosporium* spp. In relation to positive galactomannan, 6 cases (37.5%) were obtained from serum (index 1.29 [0.75–3.61]) and 2 (12.5%) from BAL (index 4.63 [3.65–5.6]).

Author affiliation: Pontificia Universidad Católica de Chile School of Medicine, Santiago, Chile

DOI: <https://doi.org/10.3201/eid2705.204412>

All patients had chest radiographs, and 15 (93.7%) had CT. The mean radiologic score (10) at admission was 5 (range 3–6). Follow-up CT interpretation was challenging because of the presence of extensive viral pneumonia infiltrates. Findings included cavitation (case 11), nodules (case 16), cavitated nodule (case 15), pleural effusion (cases 3 and 14), pulmonary embolism (cases 4, 7, 11, 14, and 16), organizing pneumonia (cases 5 and 12), pneumothorax and bullas (cases 8 and 13) and preexisting airway disease (case 2). The mucormycosis patient (case 15) also had cerebral involvement shown by magnetic resonance imaging (Appendix Table).

Applying CAPA diagnostic criteria (9) to cases 1–13, we found 7 probable and 6 possible cases of CAPA. For the co-infection and non-*Aspergillus* identification cases, the CAPA criteria do not apply. Case 14 was in a previously healthy person who had *Aspergillus* and mucorales co-infection without other fungal foci. Case 15 was a proven disseminated mucorales infection, according to European Organization for Research and Treatment of Cancer/Invasive Fungal Infections Cooperative Group and the National Institute of Allergy and Infectious Diseases Mycoses Study Group criteria (11), in a man with uncontrolled diabetes (glycated hemoglobin 8.8%) who had *R. microsporus* identified in the airway and in an acute thoracic skin lesion, along with brain involvement suggested by cranial MRI. Case 16 involved 2 concurrent conditions and the fungal disease was limited to respiratory system. Considering the 16 CAIMI cases, we observed an incidence of 11% in patients with severe COVID-19 (6.8% aspergillosis, 0.7% mucormycosis, 0.7% aspergillosis/mucormycosis, and 0.7% scedosporiosis). Thirteen (81.3%) patients received antifungal therapy at standard doses: 10 (76.9%) received voriconazole, 2 (15.4%) liposomal amphotericin B, and 1 (7.7%) isavuconazole. We obtained therapeutic drug monitoring in 9 patients receiving voriconazole therapy (median 3.9 mg/L; range 0.1–7.2 mg/L). Eleven (68.8%) patients survived.

The 6.8% CAPA rate shown in our series is below the lower range reported previously (2–7). However, our retrospective design is a limitation for the real incidence calculations. Regarding the other molds identified, we have previously reported mucorales as the second most frequent identified mold in our center (12), which is also the case in this report.

Diagnoses beyond aspergillosis, such as mucormycosis and scedosporiosis, add to a previously reported pulmonary fusariosis in an immunocompetent patient (13) and contribute to the knowledge of the epidemiology of fungal superinfections in

severe COVID-19. Similarly, Garg et al. reported cases of mucormycosis in patients with severe COVID-19 (3 rhino-orbital, 3 pulmonary, 1 gastric, and 1 disseminated mucormycosis), with a mortality rate of 87.5% (14).

The classic predisposing underlying conditions associated with mold disease were absent in our cases. In fact, all patients were apparently immunocompetent, and the most relevant underlying conditions were the frequent conditions described in severe COVID-19 cases (5). Critically ill patients with COVID-19 have characteristics that could predispose them to fungal colonization and further invasive infection; these factors include severe hypoxia, broad-spectrum antibiotic drugs plus high corticosteroid doses, prolonged ICU length of stay, long intubation period, and airway/lung damage and infarction areas.

As previously reported (4), in our clinical series, 2 patients survived despite not receiving antifungal therapy. The explanation of this observation is not clearly understood. These patients could have had spontaneous mold clearance, favored at least in 1 case by less severe underlying conditions, lower steroid doses, not receiving tocilizumab, or minor lung injury. These cases might also have not been truly invasive infections but rather colonization, which illustrates the diagnostic difficulties in this field.

The certainty of CAIMI diagnosis is one of the main challenges in the COVID-19 scenario. Serum galactomannan is included in the CAPA diagnostic criteria (9), but this value has low sensitivity among patients without neutropenia (15). Another problem to consider is restrictions on performing BAL and bronchial or lung biopsy because of infection control policies and the conditions of severely ill patients. In our opinion, for CAIMI diagnostic criteria, it seems necessary to consider other factors, including host variables associated with the lung injury secondary to viral infection, bacterial superinfection, corticosteroids, thromboembolic disease, and others, that could favor a rapid and inadvertent progression from mold airway colonization to invasive infection.

In conclusion, we highlight the need for clinicians to have a high level of suspicion of mold infection in the list of possible superinfections among patients with severe COVID-19. In addition, CAIMI diagnostic criteria should include non-*Aspergillus* mold infections.

Acknowledgments

The authors thank Tamara González Villarroel for her excellent work in fungi identification in the microbiology laboratory.

About the Author

Dr. Rabagliati is an infectious diseases specialist professor at Pontificia Universidad Católica de Chile with clinical practice at Hospital Clínico Red de Salud UC-CHRISTUS, Santiago, Chile. His primary research interest is in fungal infection and immunocompromised patients.

References

- Schauwvlieghe AFAD, Rijnders BJA, Philips N, Verwijns R, Vanderbeke L, Van Tienen C, et al.; Dutch-Belgian Mycosis Study Group. Invasive aspergillosis in patients admitted to the intensive care unit with severe influenza: a retrospective cohort study. *Lancet Respir Med*. 2018;6:782-92. [https://doi.org/10.1016/S2213-2600\(18\)30274-1](https://doi.org/10.1016/S2213-2600(18)30274-1)
- Hughes S, Troise O, Donaldson H, Mughal N, Moore LSP. Bacterial and fungal coinfection among hospitalized patients with COVID-19: a retrospective cohort study in a UK secondary-care setting. *Clin Microbiol Infect*. 2020;26:1395-9. <https://doi.org/10.1016/j.cmi.2020.06.025>
- Wang J, Yang Q, Zhang P, Sheng J, Zhou J, Qu T. Clinical characteristics of invasive pulmonary aspergillosis in patients with COVID-19 in Zhejiang, China: a retrospective case series. *Crit Care*. 2020;24:299. <https://doi.org/10.1186/s13054-020-03046-7>
- Alanio A, Dellièrè S, Fodil S, Bretagne S, Mégarbane B. Prevalence of putative invasive pulmonary aspergillosis in critically ill patients with COVID-19. *Lancet Respir Med*. 2020;8:e48-9. [https://doi.org/10.1016/S2213-2600\(20\)30237-X](https://doi.org/10.1016/S2213-2600(20)30237-X)
- Koehler P, Cornely OA, Böttiger BW, Dusse F, Eichenauer DA, Fuchs F, et al. COVID-19 associated pulmonary aspergillosis. *Mycoses*. 2020;63:528-34. <https://doi.org/10.1111/myc.13096>
- Rutsaert L, Steinfors N, Van Hunsel T, Bomans P, Naesens R, Mertes H, et al. COVID-19-associated invasive pulmonary aspergillosis. *Ann Intensive Care*. 2020;10:71. <https://doi.org/10.1186/s13613-020-00686-4>
- Bartoletti M, Pascale R, Cricca M, Rinaldi M, Maccaro A, Busini L, et al.; PREDICO study group. Epidemiology of invasive pulmonary aspergillosis among COVID-19 intubated patients: a prospective study. *Clin Infect Dis*. 2020 July 28 [Epub ahead of print]. <https://doi.org/10.1093/cid/ciaa1065>
- Marr KA, Platt A, Tornheim JA, Zhang SX, Datta K, Cardozo C, et al. Aspergillosis complicating severe coronavirus disease. *Emerg Infect Dis*. 2021;27:18-25. <https://doi.org/10.3201/eid2701.202896>
- Koehler P, Bassetti M, Chakrabarti A, Chen SCA, Colombo AL, Hoenigl M, et al. Defining and managing COVID-19-associated pulmonary aspergillosis: the 2020 ECMM/ISHAM consensus criteria for research and clinical guidance. *Lancet Infect Dis*. 2020 Dec 14 [Epub ahead of print]. [https://doi.org/10.1016/S1473-3099\(20\)30847-1](https://doi.org/10.1016/S1473-3099(20)30847-1)
- Toussie D, Voutsinas N, Finkelstein M, Cedillo MA, Manna S, Maron SZ, et al. Clinical and chest radiography features determine patient outcomes in young and middle-aged adults with COVID-19. *Radiology*. 2020;297:E197-206. <https://doi.org/10.1148/radiol.2020201754>
- De Pauw B, Walsh TJ, Donnelly JP, Stevens DA, Edwards JE, Calandra T, et al.; European Organization for Research and Treatment of Cancer/Invasive Fungal Infections Cooperative Group; National Institute of Allergy and Infectious Diseases Mycoses Study Group (EORTC/MSG) Consensus Group. Revised definitions of invasive fungal disease from the European Organization for Research and Treatment of Cancer/Invasive Fungal Infections Cooperative Group and the National Institute of Allergy and Infectious Diseases Mycoses Study Group (EORTC/MSG) Consensus Group. *Clin Infect Dis*. 2008;46:1813-21. <https://doi.org/10.1086/588660>
- Valenzuela P, Legarraga P, Rabagliati R. Epidemiology of invasive fungal disease by filamentous fungi in the period 2005 to 2015, in a university hospital in Santiago, Chile [in Spanish]. *Rev Chilena Infectol*. 2019;36:732-41. <https://doi.org/10.4067/S0716-10182019000600732>
- Poignon C, Blaize M, Vezinet C, Lampros A, Monsel A, Fekkar A. Invasive pulmonary fusariosis in an immunocompetent critically ill patient with severe COVID-19. *Clin Microbiol Infect*. 2020;26:1582-4. <https://doi.org/10.1016/j.cmi.2020.06.026>
- Garg D, Muthu V, Sehgal IS, Ramachandran R, Kaur H, Bhalla A, et al. Coronavirus disease (Covid-19) associated mucormycosis (CAM): case report and systematic review of literature. *Mycopathologia*. 2021 Feb 5 [Epub ahead of print]. <https://doi.org/10.1007/s11046-021-00528-2>
- Dobias R, Jaworska P, Tomaskova H, Kanova M, Lyskova P, Vrba Z, et al. Diagnostic value of serum galactomannan, (1,3)- β -d-glucan, and *Aspergillus fumigatus*-specific IgA and IgG assays for invasive pulmonary aspergillosis in non-neutropenic patients. *Mycoses*. 2018;61:576-86. <https://doi.org/10.1111/myc.12765>

Address for correspondence: Ricardo Rabagliati, Hospital Clínico Red de Salud UC-CHRISTUS, Marcoleta 367, Santiago, Chile; email: rabagli@med.puc.cl

Multisystem Inflammatory Syndrome in Children, Chile, May–August 2020

Carmen Niño-Taravilla, Hugo Otaola-Arca, Natalie Lara-Aguilera, Yuri Zuleta-Morales, Paula Ortiz-Fritz

We describe 26 children with multisystem inflammatory syndrome associated with coronavirus disease in the pediatric intensive care unit of Roberto del Río Hospital (Santiago, Chile). In total, 10 (38.5%) children required mechanical ventilation; 13 (50.0%) required inotropic support. In addition, 18 (69.2%) patients had echocardiographic abnormalities. No patients died.

On March 11, 2020, the World Health Organization declared a coronavirus disease (COVID-19) pandemic. Acute respiratory failure is the most common complication of COVID-19 in adults (1); as of February 2021, COVID-19 has been associated with 2.4 million deaths according to the World Health Organization (<https://www.who.int/publications/m/item/weekly-epidemiological-update---23-february-2021>). Most children and adolescents with COVID-19 have mild disease that does not require medical intervention (2).

In April 2020, a total of 8 previously healthy children with hyperinflammatory shock in the United Kingdom tested positive for antibodies against severe acute respiratory syndrome coronavirus 2 (SARS-CoV-2), the causative agent of COVID-19 (3). Consequently, the Royal College of Pediatrics and Child Health proposed the diagnosis of multisystem inflammatory syndrome associated with COVID-19 in children (MIS-C), defined as a persistent fever, inflammation, and evidence of organ dysfunction, after the exclusion of any other microbial cause, with or without PCR confirmation of SARS-CoV-2 infection (4). On May 14, 2020, the US Centers for Disease Control and Prevention issued an advisory for

MIS-C; the same day, the World Health Organization also issued a report with a case definition of MIS-C (<https://emergency.cdc.gov/han/2020/han00432.asp>). Researchers have since reported similar cases in the United States (5) and Europe (6–9). The signs and symptoms of MIS-C can resemble Kawasaki disease, toxic shock syndrome, hemophagocytic lymphohistiocytosis, and macrophage activation syndrome (10).

Few publications on COVID-19 in children (11) and MIS-C (12) have reviewed cases in Latin America. We describe the clinical characteristics, treatment, and results of a cohort of children admitted to the pediatric intensive care unit (PICU) with MIS-C in a tertiary hospital in Chile.

The Study

We analyzed patients with MIS-C treated in the PICU of Roberto del Río Hospital (Santiago, Chile) during May 11–August 30, 2020 (Figure). We used the case definition of MIS-C proposed by the Ministry of Public Health of Chile (13).

We collected demographic data, medical history, clinical symptoms, and physical examination findings, as well as results of imaging, cardiac, and laboratory tests conducted during the patient's stay in the emergency room and PICU. We also analyzed data on treatment, complications, outcome, and length of PICU and total hospital stay. The institutional ethics committee of Roberto del Río Hospital approved the study protocol. We described categorical variables with absolute frequencies and percentages; we described continuous variables with medians and IQRs.

Of the 33 patients with SARS-CoV-2 who were hospitalized in the PICU during the study period, 26 met the definition for MIS-C. In total, 16 (61.5%) of these 26 patients met the criteria for Kawasaki disease. The median age was 6.5 years (IQR 2–10.5 years); 15 (57.7%) patients were male. Only 1 patient had a chronic underlying condition (Table 1, <https://wwwnc.cdc.gov/EID/article/27/5/20-4591-T1.htm>) (14).

Author affiliations: Clínica INDISA, Santiago, Chile (C. Niño-Taravilla); Hospital Roberto del Río, Santiago (C. Niño-Taravilla, N. Lara-Aguilera, Y. Zuleta-Morales, P. Ortiz-Fritz); Clínica Alemana de Santiago, Santiago (H. Otaola-Arca)

DOI: <https://doi.org/10.3201/eid2705.204591>

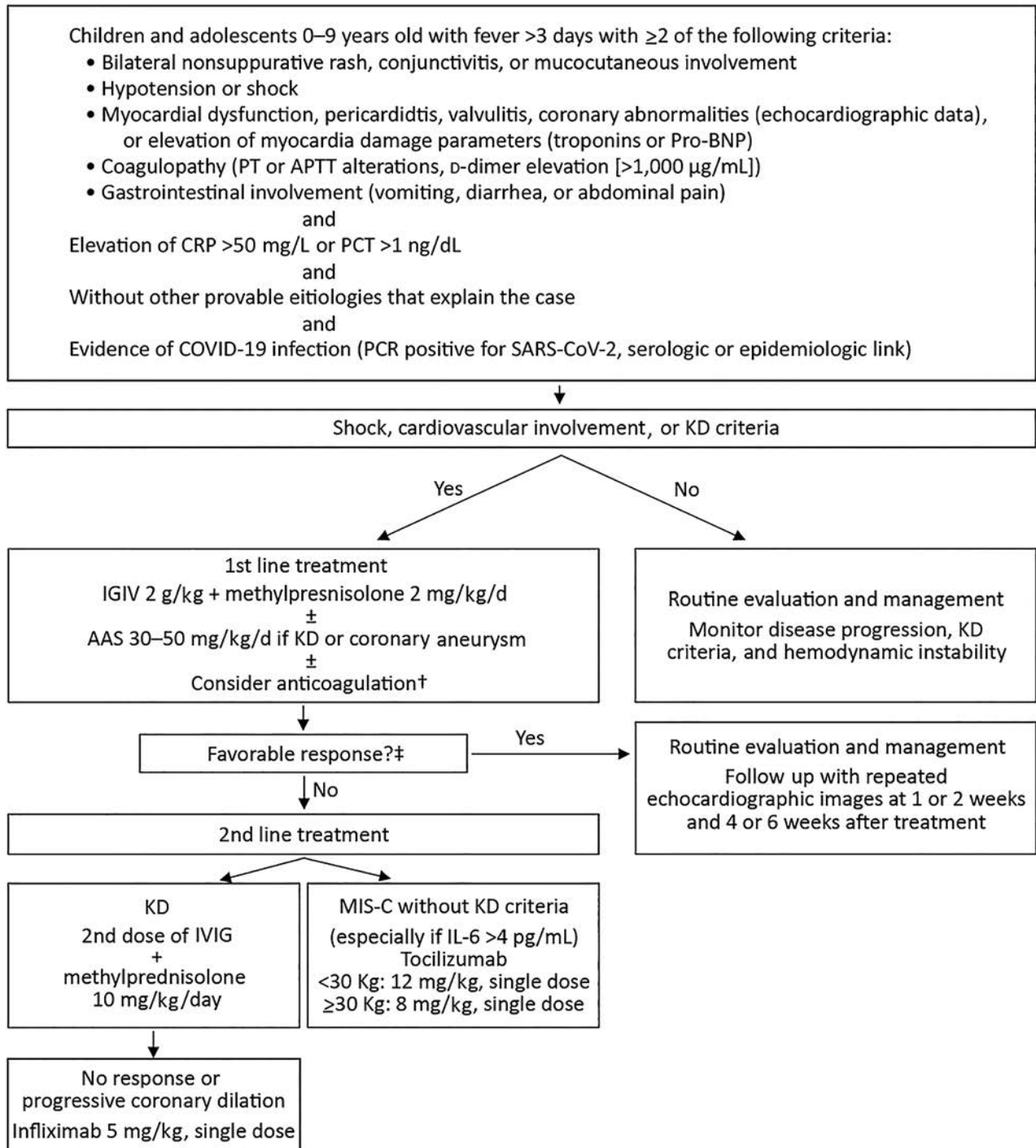


Figure. Treatment algorithm for children with multisystem inflammatory syndrome associated with COVID-19, Chile, May–August 2020. †Prophylactic anticoagulation was considered if D-dimer was $>1,000 \text{ ng/dL}$ or progressively increasing; treatment was 1 mg/kg/d of low molecular weight heparin (Enoxaparin). When thrombosis was suspected or confirmed, the dose was increased to 1 mg/kg every 12 hours and adjusted with anti-Xa factor activity. ‡Favorable response was considered absence of fever for 48 hours, hemodynamic stability, and improvement of inflammatory parameters. AAS, acetylsalicylic acid; APTT, activated partial thromboplastin time; COVID-19, coronavirus disease; CRP, C-reactive protein; IVIG, intravenous immunoglobulin; KD, Kawasaki disease; MIS-C, pediatric inflammatory multisystem syndrome temporally associated with coronavirus disease; PCT, procalcitonin; pro-BNP, pro-brain natriuretic peptide; PT, prothrombin time; SARS-CoV-2, severe acute respiratory syndrome coronavirus 2.

In total, 22 (84.6%) patients tested positive for SARS-CoV-2 infection, 7 (26.9%) by reverse transcription PCR and 15 (57.6%) by serologic assay. The other 4 (15.3%) patients tested negative for SARS-CoV-2 but had a COVID-19 exposure. The most frequent symptoms were fever (26, 100%), shock (24, 92.3%), abdominal pain (17, 65.4%), diarrhea (16, 61.5%), vomiting (12, 46.2%), rash (16, 61.5%), and conjunctivitis (15, 57.7%) (Table 1).

We also collected data on laboratory test values (Table 2), critical care interventions, treatments, and outcomes (Table 1). Ten (38.5%) patients required mechanical ventilation for a median duration of 4 days (IQR 2.5–5 days). Only 1 (3.8%) patient met the criteria for acute respiratory distress syndrome; that patient had an oxygenation index of 25. Half (13, 50.0%) of the patients required vasoactive drugs. We used high-flow hemofiltration as salvage therapy for refractory shock in 1 patient. No patients required extracorporeal membrane oxygenation (ECMO). In total, 20 (76.9%) patients received intravenous immunoglobulin; 2 (9.1%) received a second dose. We treated 23 (88.5%) patients with corticosteroids; 1 (3.8%) required a larger dose (Figure). We prescribed immunomodulatory agents for 4 (15.4%) patients: tocilizumab for 3 patients and infliximab for 1.

In total, 18 (69.2%) patients had echocardiographic abnormalities (Table 1), including 5 (19.2%) patients who met the criteria for Kawasaki disease with coronary artery abnormalities. The median duration of PICU stay was 5 days (IQR 2–7 days). None of the patients died.

Conclusions

We describe 26 MIS-C patients in the PICU of Roberto del Río Hospital in Chile. In this hospital, the maximum incidence of MIS-C occurred ≈4 weeks after the peak of COVID-19 cases in adults, as described in the literature (5–9).

The median age of the cohort in our study was 6.5 years, lower than usually reported for patients with MIS-C (8–9 years) (5); 2 patients were neonates. Slightly more than half (61.5%) of patients met criteria for typical or atypical Kawasaki disease.

Nearly all (84.6%) patients had laboratory-confirmed SARS-CoV-2 infection. However, whereas many (57.6%) had antibodies against SARS-CoV-2, only 7 (26.9%) tested positive by PCR. These findings suggest that MIS-C might be caused by a hyper-inflammatory response after asymptomatic SARS-CoV-2 infection, rather than direct cell injury from active viral replication. Although the syndrome’s pathophysiology has been correlated with the cytokine storm described in adults with severe COVID-19 (13), the mechanisms of MIS-C remain unclear.

We observed clinical manifestations similar to those described internationally (5–9). In this cohort, the most frequent manifestation was fever with gastrointestinal symptoms (65.4%), in agreement with findings described in the literature (8).

Similar to previous reports (5–9), our results showed almost all patients had cardiovascular involvement: 92% had shock and 50% required vasoactive support. Although Roberto del Río Hospital is a

Table 2. Laboratory test values of 26 children with multisystem inflammatory syndrome associated with coronavirus disease, Chile, May–August 2020*

Test	Median value (IQR)		Reference range
	Emergency department	Intensive care unit	
Leukocytes, mm ³	10,540.0 (7,400.0–15,900.0)	NA	4,500–11,000
Lymphocytes, mm ³	1,080.0 (732.5–2,579.5)	560.5 (409.5–943.0)	1,500–4,000
Platelets, mm ³	175,000.0 (96,000.0–232,000.0)	82,000.0 (40,000.0–111,250.0)	150,000–400,000
Albumin, g/dL	3.1 (2.9–3.4)	2.2 (2.0–2.8)	3.4–5.4
Troponins, ng/mL†	NA	0.1 (0.0–1.8)	<0.034
Creatine phosphokinase, U/L	133.5 (55.5–234.0)	100.0 (162.5–220.5)	32–294
Creatinine kinase-MB, U/L	2.2 (1.1–11.9)	3.3 (1.2–13.4)	<12
C-reactive protein, mg/L	134.0 (94.0–300.5)	198.5 (121.5–302.8)	<5
Procalcitonin, ng/mL‡	NA	13.0 (2.39–38.0)	<0.5
Ferritin, ng/mL	206.5 (91.5–368.8)	567.0 (304.5–1000.0)	15–150
Triglycerides, mg/dL	175.5 (103.0–244.5)	205.5 (151.5–316.0)	<75
Lactate dehydrogenase, U/L	288.0 (257.0–357.0)	285.5 (261–328.3)	105–333
Glutamic oxaloacetic transaminase, U/L	45.0 (32.0–66.0)	51.0 (36.5–66.0)	0–40
Fibrinogen, mg/mL	457.0 (375.0–513.0)	447.0 (353.25–509.0)	200–400
D-dimer, ng/mL	1,700.0 (730.0–3,500.0)	2,900.0 (1,670.0–3,950.0)	<500
Creatinine, mg/dL	0.6 (0.4–1.2)	0.8 (0.5–1.5)	Varies‡
Type B natriuretic pro-peptide, pg/mL§	NA	1,749.0 (255.8–4,722.8)	<125
Interleukin 6, g/mL¶	NA	322.0 (95.5–621.8)	<3.4

*Emergency department indicates value at admission; intensive care unit value indicates most severe value. IQR, interquartile range; NA, not available.

†Troponins and procalcitonin were only measured in the intensive care unit.

‡Creatine reference ranges: <1 mo, 0.3–1.0 mg/dL; 1–12 mo, 0.2–0.4 mg/dL; 1–12 y, 0.3–0.7 mg/dL; >12 y, 0.5–1.1 mg/dL.

§Only determined in 6 patients.

¶Only determined in 10 patients.

national reference center for ECMO, none of the patients in this cohort required extracorporeal supportive treatment; in contrast, Radia et al. (15) found that 4% of patients with MIS-C needed ECMO. This difference might be attributable to early immunotherapy.

Approximately two thirds (69.2%) of patients had echocardiographic abnormalities. The most frequent (26.9%) anomaly was left ventricular dysfunction with or without pericardial effusion. In all affected patients, cardiac function recovered before discharge from the PICU. Only 5 (19.2%) of our patients had coronary abnormalities: 4 had a coronary dilatation (Z-score of ≈ 2.5 –2.8) and 1 had a medium coronary aneurysm (Z-score of 6). The frequency of coronary involvement is also consistent with previous reports (5–9).

We treated nearly all children with intravenous immunoglobulin (76.9%) or corticosteroids (88.5%). Treatment seemed to improve symptoms and decrease inflammatory responses, similar to findings in Europe and the United States (5–9). According to our treatment protocol, we administered tocilizumab to 3 (11.7%) children; we administered infliximab to 1 (3.8%) child with a medium coronary aneurysm. The main limitations of this study are small sample size and descriptive, nonrandomized design.

In conclusion, we described 26 children with MIS-C in Chile. Our findings were similar to those reported in other countries. Most patients had echocardiographic abnormalities, and half required vasoactive drug support. We administered immunomodulatory therapy to most patients. Clinical trials and long-term follow-up are needed to elucidate the mechanisms of various treatments and potential sequelae of this condition.

Acknowledgments

We thank all the health professionals in the pediatric intensive care unit of Roberto del Río Hospital (Santiago, Chile). We also thank the COVID-19 Committee of Roberto del Río Hospital.

About the Author

Dr. Niño-Taravilla is a pediatric intensivist at the PICU of Hospital Roberto del Río and Clínica Indisa in Santiago, Chile. Her research interests include sepsis and viral infection.

References

1. Fu L, Wang B, Yuan T, Chen X, Ao Y, Fitzpatrick T, et al. Clinical characteristics of coronavirus disease 2019 (COVID-19) in China: a systematic review and meta-analysis. *J Infect.* 2020;80:656–65. <https://doi.org/10.1016/j.jinf.2020.03.041>
2. Ludvigsson JF. Systematic review of COVID-19 in children shows milder cases and a better prognosis than adults. *Acta Paediatr.* 2020;109:1088–95. <https://doi.org/10.1111/apa.15270>
3. Riphagen S, Gomez X, Gonzalez-Martinez C, Wilkinson N, Theocharis P. Hyperinflammatory shock in children during COVID-19 pandemic. *Lancet.* 2020;395:1607–8. [https://doi.org/10.1016/S0140-6736\(20\)31094-1](https://doi.org/10.1016/S0140-6736(20)31094-1)
4. Royal College of Paediatrics and Child Health. Guidance: paediatric multisystem inflammatory syndrome temporally associated with COVID-19. 2020 [cited 2020 Aug 30]. <https://www.rcpch.ac.uk/sites/default/files/2020-05/COVID-19-Paediatric-multisystem-%20inflammatory%20syndrome-20200501.pdf>
5. Feldstein LR, Rose EB, Horwitz SM, Collins JP, Newhams MM, Son MBF, et al.; Overcoming COVID-19 Investigators; CDC COVID-19 Response Team. Multisystem inflammatory syndrome in U.S. children and adolescents. *N Engl J Med.* 2020;383:334–46. PubMed <https://doi.org/10.1056/NEJMoa2021680>
6. Verdoni L, Mazza A, Gervasoni A, Martelli L, Ruggeri M, Ciuffreda M, et al. An outbreak of severe Kawasaki-like disease at the Italian epicentre of the SARS-CoV-2 epidemic: an observational cohort study. *Lancet.* 2020;395:1771–8. PubMed [https://doi.org/10.1016/S0140-6736\(20\)31103-X](https://doi.org/10.1016/S0140-6736(20)31103-X)
7. Toubiana J, Poirault C, Corsia A, Bajolle F, Fourgeaud J, Angoulvant F, et al. Kawasaki-like multisystem inflammatory syndrome in children during the covid-19 pandemic in Paris, France: prospective observational study. *BMJ.* 2020;369:m2094. PubMed <https://doi.org/10.1136/bmj.m2094>
8. Cabrero-Hernández M, García-Salido A, Leoz-Gordillo I, Alonso-Cadenas JA, Gochi-Valdovinos A, González Brabin A, et al. Severe SARS-CoV-2 infection in children with suspected acute abdomen: a case series from a tertiary hospital in Spain. *Pediatr Infect Dis J.* 2020;39:e195–8. <https://doi.org/10.1097/INF.0000000000002777>
9. Whittaker E, Bamford A, Kenny J, Kafrou M, Jones CE, Shah P, et al.; PIMS-TS Study Group and EUCLIDS and PERFORM Consortia. Clinical characteristics of 58 children with a pediatric inflammatory multisystem syndrome temporally associated with SARS-CoV-2. *JAMA.* 2020;324:259–69. <https://doi.org/10.1001/jama.2020.10369>
10. Nakra NA, Blumberg DA, Herrera-Guerra A, Lakshminrusimha S. Multi-system inflammatory syndrome in children (MIS-C) following SARS-CoV-2 infection: review of clinical presentation, hypothetical pathogenesis, and proposed management. *Children (Basel).* 2020;7:69. <https://doi.org/10.3390/children7070069>
11. Prata-Barbosa A, Lima-Setta F, Santos GRD, Lanziotti VS, de Castro REV, de Souza DC, et al.; Brazilian Research Network in Pediatric Intensive Care, (BRnet-PIC). Pediatric patients with COVID-19 admitted to intensive care units in Brazil: a prospective multicenter study. *J Pediatr (Rio J).* 2020;96:582–92. <https://doi.org/10.1016/j.jped.2020.07.002>
12. Torres JP, Izquierdo G, Acuña M, Pavez D, Reyes F, Fritis A, et al. Multisystem inflammatory syndrome in children (MIS-C): report of the clinical and epidemiological characteristics of cases in Santiago de Chile during the SARS-CoV-2 pandemic. *Int J Infect Dis.* 2020;100:75–81. <https://doi.org/10.1016/j.ijid.2020.08.062>
13. Ministerio de Salud. Protocolo Síndrome Inflamatorio Multisistémico en niños, niñas y adolescentes con SARS-CoV-2. 2020 [cited 2021 March 4]. <https://www.minsal.cl/wp-content/uploads/2020/07/Si%CC%81ndromeInflamatorio-Multisiste%CC%81mico.pdf>

14. McCrindle BW, Rowley AH, Newburger JW, Burns JC, Bolger AF, Gewitz M, et al; American Heart Association Rheumatic Fever, Endocarditis, and Kawasaki Disease Committee of the Council on Cardiovascular Disease in the Young; Council on Cardiovascular and Stroke Nursing; Council on Cardiovascular Surgery and Anesthesia; and Council on Epidemiology and Prevention. Diagnosis, treatment, and long-term management of Kawasaki disease: a scientific statement for health professionals from the American Heart Association. *Circulation*. 2017;135:e927-99. <https://doi.org/10.1161/CIR.0000000000000484>
15. Radia T, Williams N, Agrawal P, Harman K, Weale J, Cook J, et al. Multi-system inflammatory syndrome in children & adolescents (MIS-C): a systematic review of clinical features and presentation. *Paediatr Respir Rev*. 2020 Aug 11 [Epub ahead of print]. <https://doi.org/10.1016/j.prrv.2020.08.001>

Address for correspondence: Carmen Niño-Taravilla, Pediatric Intensive Care Unit, Roberto del Rio Children Hospital, Av. Profesor Zañartu 1085, Independencia, Región Metropolitana, Chile; email: carmen.nino@hotmail.com



@CDC_EIDjournal

Want to stay updated on the latest news in *Emerging Infectious Diseases*? Let us connect you to the world of global health. Discover groundbreaking research studies, pictures, podcasts, and more by following us on Twitter at @CDC_EIDjournal.

Prescribing Antimicrobial Drugs for Acute Gastroenteritis, Primary Care, Australia, 2013–2018

Wen-Qiang He, Martyn D. Kirk, John Hall, Bette Liu

Medscape **ACTIVITY** EDUCATION

In support of improving patient care, this activity has been planned and implemented by Medscape, LLC and Emerging Infectious Diseases. Medscape, LLC is jointly accredited by the Accreditation Council for Continuing Medical Education (ACCME), the Accreditation Council for Pharmacy Education (ACPE), and the American Nurses Credentialing Center (ANCC), to provide continuing education for the healthcare team.

Medscape, LLC designates this Journal-based CME activity for a maximum of 1.00 **AMA PRA Category 1 Credit(s)**[™]. Physicians should claim only the credit commensurate with the extent of their participation in the activity.

Successful completion of this CME activity, which includes participation in the evaluation component, enables the participant to earn up to 1.0 MOC points in the American Board of Internal Medicine's (ABIM) Maintenance of Certification (MOC) program. Participants will earn MOC points equivalent to the amount of CME credits claimed for the activity. It is the CME activity provider's responsibility to submit participant completion information to ACCME for the purpose of granting ABIM MOC credit.

All other clinicians completing this activity will be issued a certificate of participation. To participate in this journal CME activity: (1) review the learning objectives and author disclosures; (2) study the education content; (3) take the post-test with a 75% minimum passing score and complete the evaluation at <http://www.medscape.org/journal/eid>; and (4) view/print certificate. For CME questions, see page 1551.

Release date: May 26, 2021; Expiration date: May 26, 2022

Learning Objectives

Upon completion of this activity, participants will be able to:

- Distinguish the rate of antibiotic prescriptions for AGE in the current study
- Assess variables associated with higher rates of antibiotic prescriptions for AGE
- Analyze trends in antibiotic prescribing for AGE
- Identify the most common antibiotic class prescribed in cases of AGE

CME Editor

P. Lynne Stockton Taylor, VMD, MS, ELS(D), Technical Writer/Editor, Emerging Infectious Diseases. *Disclosure: P. Lynne Stockton Taylor, VMD, MS, ELS(D), has disclosed no relevant financial relationships.*

CME Author

Charles P. Vega, MD, Health Sciences Clinical Professor of Family Medicine, University of California, Irvine School of Medicine, Irvine, California. *Disclosure: Charles P. Vega, MD, has disclosed the following relevant financial relationships: served as an advisor or consultant for GlaxoSmithKline.*

Authors

Disclosures: Wen-Qiang He, PhD; Martyn David Kirk, BAppSci, MAppEpid, PhD; John Hall, MBBS, MTPH, PhD; and Bette Liu, MBBS, MPH, DPhil, have disclosed no relevant financial relationships..

Author affiliations: University of New South Wales, Sydney, New South Wales, Australia (W.-Q. He, H. Hall, B. Liu); Australian National University, Canberra, Australian Capital Territory, Australia (M.D. Kirk)

DOI: <https://doi.org/10.3201/eid2705.203692>

During 2013–2018, antimicrobial drugs were prescribed for 6.8% of cases of acute gastroenteritis encountered in general practice in Australia, including 35.7% of *Salmonella* infections and 54.1% of *Campylobacter* infections. During that time, prescriptions for acute gastroenteritis decreased by 2.0%. Managing infectious gastroenteritis in general practice will require greater antimicrobial stewardship.

Worldwide every year, acute gastroenteritis causes a loss of ≈89.5 million disability-adjusted life-years and 1.45 million deaths (1). In 2010, an estimated 16.6 million persons in Australia (population 22 million [2]) were affected, and ≈1.1 million of these persons sought care at a general practice (3,4). The most common cause of acute gastroenteritis is viral infection; therefore, antimicrobial drugs are not routinely recommended (5–7). Even for some common bacterial causes of acute gastroenteritis (e.g., nontyphoidal *Salmonella* and *Campylobacter* infections), antimicrobial therapy is not required for most patients because these infections are usually self-limiting (8).

Overuse of antimicrobial drugs for treating upper respiratory tract infections (mostly caused by viruses) has been well described (9,10) but not as much for acute gastroenteritis (11). Knowing the extent and pattern of antimicrobial drug use for acute gastroenteritis can help determine whether interventions to improve antimicrobial drug use for this specific clinical scenario are warranted.

We examined prescription of antimicrobial drugs for acute gastroenteritis in primary care practice in Australia during 2013–2018. The study was approved by the MedicineInsight Independent External Data Governance Committee (reference no. 2019-030; December 23, 2019) and the University of New South Wales Human Research Ethics Committee (no. HC190886).

The Study

We extracted clinical encounters for cases (including multiple episodes/patient) of acute gastroenteritis, nontyphoidal *Salmonella* infection, and *Campylobacter* infection recorded by MedicineInsight, a national primary healthcare database in Australia (<https://www.nps.org.au/medicine-insight>) during 2013–2018 and examined whether an antimicrobial drug was prescribed on the day of diagnosis (Appendix, <https://wwwnc.cdc.gov/EID/article/27/5/20-3692-App1.pdf>). Antimicrobial drugs were prescribed for 6.8% (6,652/98,496) of cases of acute gastroenteritis, including 35.7% (391/1,096) cases of nontyphoidal *Salmonella* infection and 54.1% (1,066/1,969) cases of *Campylobacter* infection.

Antimicrobial drug prescriptions for acute gastroenteritis increased with patient age (<10 years, 3.8%; ≥65 years, 13.7%) (Table 1). Antimicrobial drugs were more likely to be prescribed for those with than without the following: fever or no temperature measurement, a requested fecal sample test, underlying conditions, or a record of bacterial or parasitic infection. Antimicrobial drugs were less likely to be prescribed for those with a record of viral infection. Prescribing also differed by practice remoteness; prescribing was higher in practices in more remote areas than in cities. During the study period, the trend toward antimicrobial drug prescribing decreased from 7.8% to 5.8% ($p < 0.001$). Similar findings were observed for children <10 years of age (Appendix Table 1).

The greatest reductions in antimicrobial drug prescriptions were found for those ≥65 years of age (2.8% absolute reduction from 13.4% to 10.6% ($p = 0.049$)). The next greatest reductions were for those 30–49 years of age (2.4% absolute reduction from 8.3% to 5.9%; $p = 0.006$), 10–29 years (from 6.7% to 4.8%; $p < 0.001$), and <10 years (from 4.8% to 3.0%; $p = 0.03$) (Figure 1).

For patients with nontyphoidal *Salmonella* infection (Appendix Table 2), prescriptions for antimicrobial drugs were more likely for those 30–49 than those <10 years of age (41.7% vs. 34.1%; $p = 0.02$) and in practices in outer regional or remote areas than in cities. Trend analysis of antimicrobial drug prescriptions for patients with nontyphoidal *Salmonella* infection suggested a significant reduction; absolute reduction was 11.4% (from 42.1% in 2013 to 30.7% in 2018; $p = 0.01$). For patients with *Campylobacter* infection (Appendix Table 3), antimicrobial drugs were more likely to be prescribed for female than male patients (56.8% vs. 51.7%; $p = 0.02$). We observed no significant reduction in antimicrobial drug prescriptions for patients with *Campylobacter* infection (55.8% to 57.1%; $p = 0.81$).

Of the 6,652 acute gastroenteritis cases for which antimicrobial drugs were prescribed, a reason was recorded for 42.9% (2,854/6,652), including 80.4% (2,295/2,854) for acute gastroenteritis, 1.1% (30/2,854) for other gastrointestinal illnesses, 5.7% (162/2,854) for respiratory tract infections, 1.8% (50/2,854) for urinary tract infections, and 11.1% (317/2,854) for other reasons. Of the 6,652 acute gastroenteritis cases for which antimicrobial drugs were prescribed, 7,159 prescriptions were written: 1 for 92.9% (6,179/6,652) of cases and ≥2 (range 2–5) for 7.1% (473/6,652). The predominant class of drug prescribed for acute gastroenteritis

was nitroimidazoles (41.6% of total; Table 2), of which metronidazole accounted for the most prescriptions (24.7% of total; Appendix Table 4).

Prescriptions of cephalosporins, quinolones, and nitroimidazoles decreased significantly over the study period (Figure 2). The greatest reduction was for nitroimidazoles (absolute reduction from 3.9% to 2.3%; $p = 0.001$), followed by quinolones (1.3% to 0.8%; $p = 0.02$) and cephalosporins (0.7% to 0.5%; $p = 0.049$). However, prescriptions of macrolides increased significantly (0.6% to 1.0%; $p = 0.01$).

For the 391 cases of nontyphoidal *Salmonella* infection, a total of 418 prescriptions were written: 1 for 93.1% (364/391) and 2 for 6.9% (27/391). No dominant antimicrobial drugs were prescribed for patients with nontyphoidal *Salmonella*; most commonly prescribed were quinolones (30.4% of total; Table 2). For 1,066 cases of *Campylobacter* infection, 1,165 prescriptions were written: 1 for 91.0% (970/1,066) and ≥ 2 (range 2–4) for 9.0% (96/1,066). The predominant antimicrobial drugs prescribed for *Campylobacter* infections were macrolides (70.9%

Table 1. Proportion of cases of acute gastroenteritis for which antimicrobial drugs were prescribed overall and according to various characteristics, Australia, 2013–2018

Characteristic	No. prescriptions/no. cases (%)	Adjusted odds ratio (95% CI)	p value*
Overall	6,652/98,496 (6.8)		
Age, y			
<10	762/20,130 (3.8)	Referent	
10–29	1,774/30,695 (5.8)	1.56 (1.42–1.71)	<0.001
30–49	2,065/29,315 (7.0)	1.87 (1.71–2.05)	<0.001
50–64	1,093/11,369 (9.6)	2.46 (2.21–2.73)	<0.001
≥ 65	958/6,987 (13.7)	3.27 (2.88–3.71)	<0.001
Sex			
M	3,098/47,892 (6.5)	Referent	
F	3,554/50,604 (7.0)	1.02 (0.97–1.08)	0.41
Aboriginal or Torres Strait Islander			
No	5,076/74,978 (6.8)	Referent	
Yes	145/2,516 (5.8)	0.98 (0.82–1.17)	0.82
Unknown	1,431/21,002 (6.8)		
Concession card holder			
No	3,447/56,841 (6.1)	Referent	
Yes	1,820/22,177 (8.2)	1.04 (0.97–1.12)	0.31
Unknown	1,385/19,478 (7.1)		
Fever, temperature $>38.5^{\circ}\text{C}$			
No	1,748/30,312 (5.8)	Referent	
Yes	71/566 (12.5)	2.75 (2.09–3.60)	<0.001
Not recorded	4,833/67,618 (7.1)	1.14 (1.07–1.21)	<0.001
Fecal sample test requested			
No	4,832/86,085 (5.6)	Referent	
Yes	1,820/12,411 (14.7)	2.75 (2.58–2.92)	<0.001
Etiology			
Not recorded	5,820/79,799 (7.3)	Referent	
Viral	342/17,896 (1.9)	0.30 (0.27–0.34)	<0.001
Bacterial	483/790 (61.1)	19.49 (16.66–22.80)	<0.001
Parasitic	7/11 (63.6)	24.12 (6.22–93.59)	<0.001
Underlying conditions†			
No	5,314/85,970 (6.2)	Referent	
Yes	1,338/12,526 (10.7)	1.09 (1.00–1.19)	0.04
No visits to general practitioner in past year			
0–7	5,000/74,630 (6.7)	Referent	
8–14	950/14,332 (6.6)	1.02 (0.94–1.10)	0.60
≥ 15	702/9,534 (7.4)	0.95 (0.86–1.04)	0.28
Remoteness of practice			
Major city	4,421/69,557 (6.4)	Referent	
Inner regional	1,172/16,438 (7.1)	0.97 (0.90–1.04)	0.35
Outer regional or remote	1,059/12,501 (8.5)	1.21 (1.12–1.30)	<0.001
Year of diagnosis			
2013	1,238/15,845 (7.8)	Referent	
2014	1,258/16,681 (7.5)	0.92 (0.84–1.00)	0.046
2015	1,165/16,912 (6.9)	0.84 (0.77–0.92)	<0.001
2016	1,143/17,613 (6.5)	0.77 (0.71–0.84)	<0.001
2017	1,008/16,995 (5.9)	0.71 (0.65–0.78)	<0.001
2018	840/14,450 (5.8)	0.71 (0.65–0.78)	<0.001

*Adjusted for all variables listed in the table.

†Any medical history of diabetes mellitus, arthritis, or chronic kidney disease.

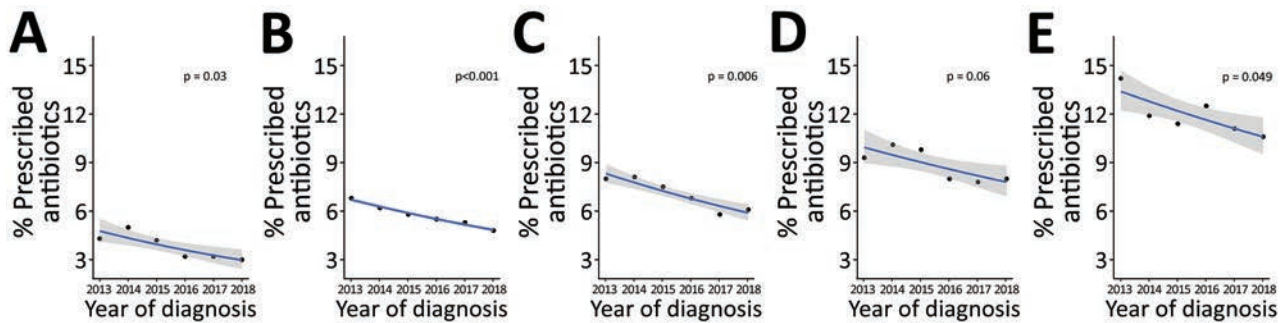


Figure 1. Proportion of acute gastroenteritis cases for which antimicrobial drugs were prescribed, by year of diagnosis and patient age, Australia, 2013–2018. A) <10 y; B) 10–29 y; C) 30–49 y; D) 50–64 y; E) ≥65 y.

of total; Table 2), of which most were azithromycin (44.4% of total; Appendix Table 4).

Conclusions

In this large study of patient clinical encounters in general practices in Australia, we found that antimicrobial drugs were prescribed for 6.8% of all cases of acute gastroenteritis but for 35.7% of nontyphoidal *Salmonella* infections and 54.1% of *Campylobacter* infections. Over the 6-year study period, the absolute proportion of cases for which antimicrobial drugs were prescribed for acute gastroenteritis decreased by 2%.

Of the few studies reporting on how often antimicrobial drugs are prescribed for acute gastroenteritis, estimates range from 8.5% of 2,089 cases in a sentinel

surveillance sample from primary care in Switzerland in 2014 (12) to 65% in a survey of 237 physicians in China in 2012 (13). Our results were most similar to the estimates reported from the Switzerland study, which also found that antimicrobial drugs were more likely to be prescribed for older patients and those with fever (12).

In Australia, treatment guidelines recommend that empirical prescription of antimicrobial drugs is of no benefit for acute gastroenteritis and is indicated only for patients with manifestations of severe disease, those who are immunocompromised, returned travelers of all ages, or children in whom systemic bacterial infection is suspected (7). Our results suggest that general practitioners are more likely to

Table 2. Classes of antimicrobial drugs prescribed for cases of acute gastroenteritis, nontyphoidal *Salmonella* infection, and *Campylobacter* infection, Australia, 2013–2018

Case type, drug class	No. prescriptions	Proportion of total prescriptions, %
Acute gastroenteritis, 7,159 cases		
Nitroimidazoles	2980	41.6
Quinolones	1059	14.8
Penicillins	901	12.6
Macrolides	799	11.1
Cephalosporins	561	7.8
Sulfonamides and trimethoprim	445	6.2
Tetracyclines	295	4.1
Amphenicols	109	1.5
Nontyphoidal <i>Salmonella</i> infection, 418 cases		
Quinolones	127	30.4
Macrolides	105	25.1
Penicillins	88	21.0
Sulfonamides and trimethoprim	59	14.1
Nitroimidazoles	21	5.0
Cephalosporins	13	3.1
Tetracyclines	4	1.0
Amphenicols	1	0.2
<i>Campylobacter</i> infection, 1,165 cases		
Macrolides	826	70.9
Quinolones	243	20.9
Nitroimidazoles	58	5.0
Tetracyclines	12	1.0
Penicillins	10	0.9
Cephalosporins	8	0.7
Sulfonamides and trimethoprim	5	0.4
Amphenicols	3	0.3

*Ten prescriptions for acute gastroenteritis are not shown: 7 for nitrofurantoin, 2 for tobramycin and 1 for methenamine.

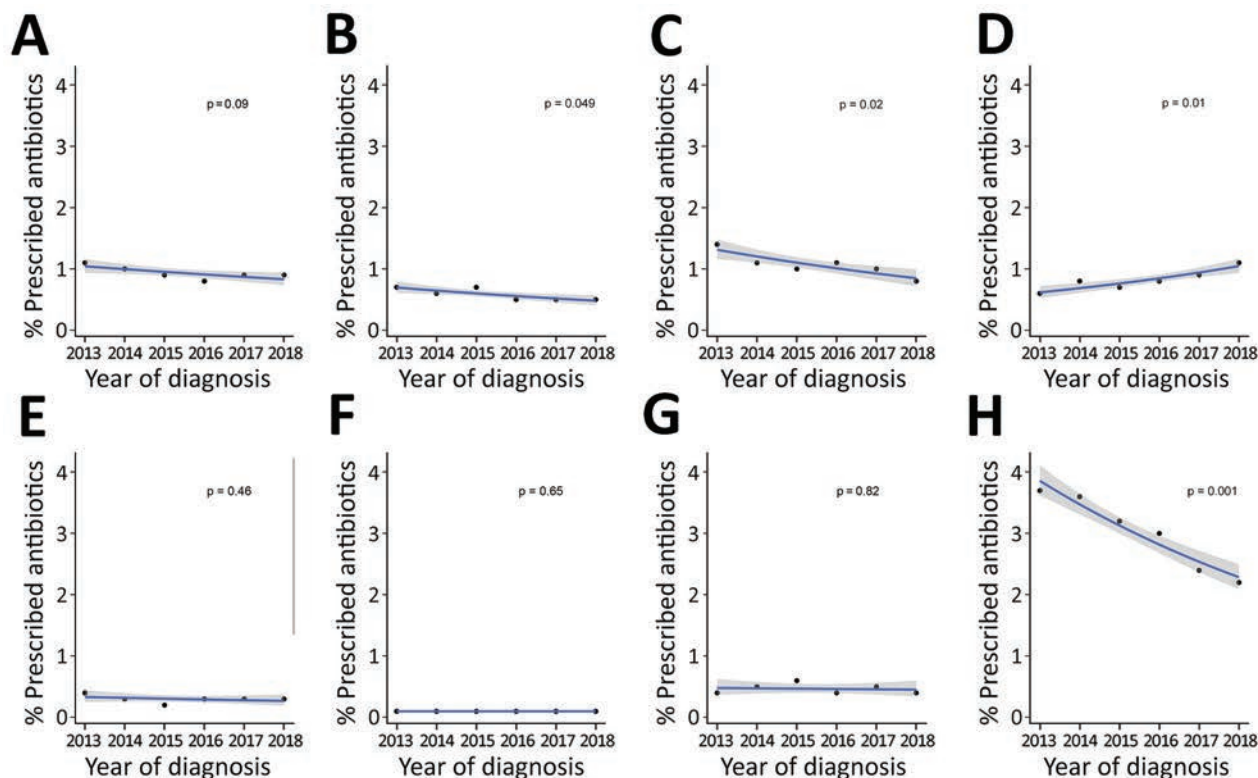


Figure 2. Trend in antimicrobial drug prescriptions for cases of acute gastroenteritis, by year and antimicrobial therapeutic class, Australia, 2013–2018. Ten prescriptions acute gastroenteritis are not shown: 7 for nitrofurantoin, 2 for tobramycin, and 1 for methenamine. A) Penicillins; B) cephalosporins; C) quinolones; D) macrolides; E) tetracyclines; F) amphenicols; G) sulfonamides and trimethoprim; H) nitroimidazoles.

adhere to guidelines and that antimicrobial drugs are more likely to be prescribed for patients who are older, those with underlying conditions, and those with systemic symptoms (e.g., fever). However, the substantial numbers of patients without these indications for whom antimicrobial drugs were still prescribed suggests overuse of antimicrobial drugs for acute gastroenteritis.

Reassuringly, we did find reduced antimicrobial drug prescriptions for acute gastroenteritis during the 6-year study period. This finding is consistent with that of an earlier study that used the same dataset and found an overall reduction in the proportion of patients for whom systemic antimicrobial drugs were prescribed: from 31.7% in 2015 to 26% in 2017 (14). This reduction has been attributed to a series of antimicrobial stewardship programs implemented during 2009–2014, which included educational and advertising campaigns aimed at general practitioners and consumers (15). Our results suggest that these antimicrobial stewardship programs may have reduced antimicrobial drug prescriptions for acute gastroenteritis.

Given the estimated 1.1 million cases of acute gastroenteritis seen in general practices in Australia

annually (3), we estimate that nationwide $\approx 74,000$ antimicrobial drugs are prescribed for acute gastroenteritis every year. Because most of these drugs are probably unnecessary, our findings highlight the need for greater antimicrobial stewardship to support management of infectious gastroenteritis in primary care.

Acknowledgement

We thank the MedicineWise MedicineInsight for providing the data for this study. We are grateful to the general practices and general practitioners who participate in MedicineInsight and the patients who allowed the use of de-identified information for MedicineInsight.

This work was supported by the funding from School of Public Health and Community Medicine, University of New South Wales (grant no. SPF02 to WQH). B.L. and M.D.K. were funded by fellowships funded by the National Health and Medical Research Council.

Data and more information may be obtained from MedicineWise MedicineInsight (<https://www.nps.org.au/medicine-insight>).

About the Author

Dr. He is a postdoctoral research fellow at the School of Population Health, University of New South Wales. He has research interests in infections and reproductive health as well as large-scale prospective cohorts and data-linkage studies.

References

- Hay SI, Abajobir AA, Abate KH, Abbafati C, Abbas KM, Abd-Allah F, et al.; GBD 2016 DALYs and HALE Collaborators. Global, regional, and national disability-adjusted life-years (DALYs) for 333 diseases and injuries and healthy life expectancy (HALE) for 195 countries and territories, 1990-2016: a systematic analysis for the Global Burden of Disease Study 2016. *Lancet*. 2017;390:1260-344. [https://doi.org/10.1016/S0140-6736\(17\)32130-X](https://doi.org/10.1016/S0140-6736(17)32130-X)
- Gibney KB, O'Toole J, Sinclair M, Leder K. Disease burden of selected gastrointestinal pathogens in Australia, 2010. *Int J Infect Dis*. 2014;28:176-85.
- Britt H. BEACH—bettering the evaluation and care of health: a continuous national study of general practice activity. *Commun Dis Intell Q Rep*. 2003;27:391-3.
- Chen Y, Ford L, Hall G, Dobbins T, Kirk M. Healthcare utilization and lost productivity due to infectious gastroenteritis, results from a national cross-sectional survey Australia 2008-2009. *Epidemiol Infect*. 2016;144:241-6. <https://doi.org/10.1017/S0950268815001375>
- Graves NS. Acute gastroenteritis. *Prim Care*. 2013;40:727-41. <https://doi.org/10.1016/j.pop.2013.05.006>
- Hall G, Kirk MD, Becker N, Gregory JE, Unicomb L, Millard G, et al.; OzFoodNet Working Group. Estimating foodborne gastroenteritis, Australia. *Emerg Infect Dis*. 2005;11:1257-64. <https://doi.org/10.3201/eid1108.041367>
- Therapeutic Guidelines: acute infectious diarrhoea [cited 2020 Mar 28]. https://tgldcdp.tg.org.au/viewTopic?topicfile=acute-gastroenteritis&guidelineName=Antibiotic#toc_d1e47
- Zollner-Schwetzel I, Krause R. Therapy of acute gastroenteritis: role of antibiotics. *Clin Microbiol Infect*. 2015;21:744-9. <https://doi.org/10.1016/j.cmi.2015.03.002>
- McCullough AR, Pollack AJ, Plejdrup Hansen M, Glasziou PP, Looke DF, Britt HC, et al. Antibiotics for acute respiratory infections in general practice: comparison of prescribing rates with guideline recommendations. *Med J Aust*. 2017;207:65-9. <https://doi.org/10.5694/mja16.01042>
- Linder JA, Stafford RS. Antibiotic treatment of adults with sore throat by community primary care physicians: a national survey, 1989-1999. *JAMA*. 2001;286:1181-6. <https://doi.org/10.1001/jama.286.10.1181>
- He WQ, Kirk MD, Sintchenko V, Hall JJ, Liu B. Antibiotic use associated with confirmed influenza, pertussis, and nontyphoidal *Salmonella* infections. *Microb Drug Resist*. 2020;26:1482-90. <https://doi.org/10.1089/mdr.2020.0017>
- Schmutz C, Bless PJ, Mäusezahl D, Jost M, Mäusezahl-Feuz M; Swiss Sentinel Surveillance Network. Acute gastroenteritis in primary care: a longitudinal study in the Swiss Sentinel Surveillance Network, Sentinella. *Infection*. 2017;45:811-24. <https://doi.org/10.1007/s15010-017-1049-5>
- Ke B, Ran L, Wu S, Deng X, Ke C, Feng Z, et al. Survey of physician diagnostic and treatment practices for patients with acute diarrhea in Guangdong province, China. *Foodborne Pathog Dis*. 2012;9:47-53. <https://doi.org/10.1089/fpd.2011.0964>
- Australian Commission on Safety and Quality in Health Care. AURA 2019: third Australian report on antimicrobial use and resistance in human health [cited 2020 Mar 28]. <https://www.safetyandquality.gov.au/publications-and-resources/resource-library/aura-2019-third-australian-report-antimicrobial-use-and-resistance-human-health>
- Wu J, Taylor D, Ovchinnikova L, Heaney A, Morgan T, Dartnell J, et al. Relationship between antimicrobial-resistance programs and antibiotic dispensing for upper respiratory tract infection: an analysis of Australian data between 2004 and 2015. *J Int Med Res*. 2018;46:1326-38. <https://doi.org/10.1177/0300060517740813>

Address for correspondence: Wen-Qiang He, Rm 210, Samuels Bldg, School of Population Health, UNSW, Samuel Terry Ave, Sydney, NSW 2052, Australia; email: wen-qiang.he@unsw.edu.au

Epidemiology of Confirmed COVID-19 Deaths in Adults, England, March–December 2020

Alison E. Brown, Ellen Heinsbroek, Meaghan M. Kall, Hester Allen, Kazim Beebeejaun, Paula Blomquist, Ines Campos-Matos, Colin N.J. Campbell, Hamish Mohammed, Katy Sinka, Theresa Lamagni, Nicholas Phin, the PHE COVID-19 Mortality Working Group,¹ Gavin Dabrera

Of the 58,186 coronavirus deaths among adults in England during March–December 2020, 77% occurred in hospitals, 93% were in patients ≥ 60 years, and 91% occurred within 28 days of positive specimen. Cumulative mortality rates were highest among persons of Black, Asian, other, or mixed ethnicities and in socioeconomically deprived areas.

Reliable ascertainment and description of mortality rates is vital in monitoring the public health response to coronavirus disease (COVID-19). Disparities between population subgroups provide critical insights into which groups are most affected, directly informing the public response. In England, COVID-19 was first detected on January 30, 2020; the first COVID-19 death occurred on March 2, 2020. We describe trends in COVID-19 mortality rates by age group, sex, ethnicity, residential region and socioeconomic deprivation, time from positive specimen date to death, and place of death during the first 9 months after the first known COVID-19 death in England.

The Study

Public Health England (PHE) receives daily reports of the date of death, the date the specimen is taken for COVID-19 testing, and laboratory results for adults ≥ 18 years of age from 3 sources: hospital trusts using the COVID-19 Patient Notification System; local PHE Health Protection Teams (for nonhospital settings); and the National Health Service Demographic Batch Service, which matches of all laboratory-confirmed COVID-19 cases against registered deaths records. Data from each source were combined daily into a single dataset, the COVID-19 Specific Mortality Surveillance System (COSMOSS) (1).

COSMOSS data are matched using a unique patient identifier (National Health Service number) to death registrations from the Office for National Statistics (2) to ascertain setting and cause of death. The data are then matched to Hospital Episode Statistics to identify ethnicity and to area-level data to categorize relative socioeconomic deprivation based on Indices for Multiple Deprivation (IMD) (3). Data are deduplicated daily so that 1 record reported from the multiple data sources is retained for each decedent.

COSMOSS COVID-19 deaths are defined as any death occurring within 60 days of a date on which a positive specimen was taken for COVID-19, or any death for which COVID-19 is listed on the death registration (codes U0.71 or U0.72 from the International Classification of Diseases, 10th Revision, Clinical Modification) (2). Cumulative mortality rates (deaths/100,000 population) were calculated using denominator data from Office for National Statistics population estimates (4).

By December 3, 2020, a total of 58,186 COVID-19 deaths in adults had been reported to PHE, yielding a crude mortality rate of 132 deaths/100,000 population. An additional 31 deaths among children (persons < 18 years of age) were reported.

Social distancing measures were announced nationally on March 23, 2020, 3 weeks after the first death. The number of COVID-19 deaths peaked on April 8, ≈ 2 weeks after social distancing began (Figure 1, 2), gradually fell to lower levels that were sustained throughout summer, and then increased in late September.

Overall, 93% (54,282) of deaths in adults occurred in persons ≥ 60 years of age, and 57% (32,970)

Author affiliation: Public Health England, London, UK

DOI: <https://doi.org/10.3201/eid2705.203524>

¹Members of the PHE COVID-19 Mortality Working Group are listed at the end of this article.

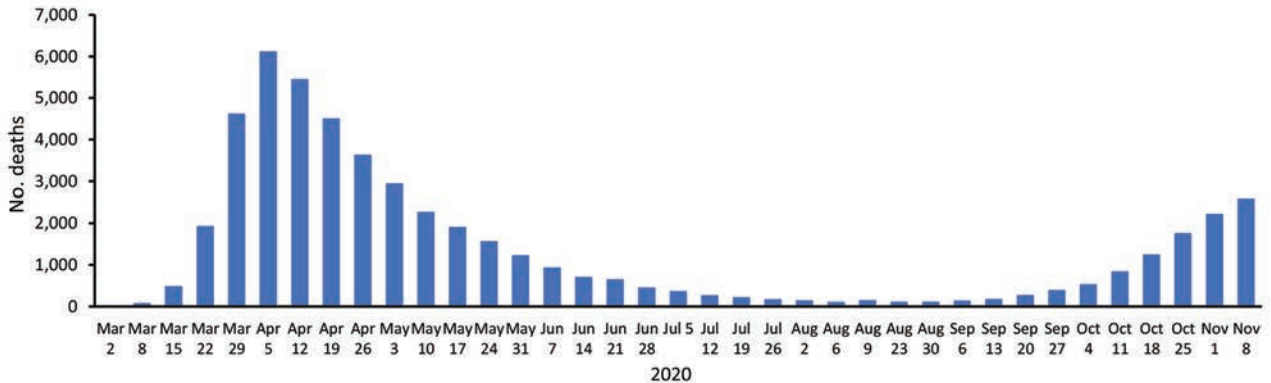


Figure 1. Deaths occurring within 60 days of a laboratory-confirmed coronavirus disease (COVID-19) diagnosis or with COVID-19 on the death registration certificate, by date of death, England, UK, March 2–December 3, 2020.

occurred in men (Table); 64% of those 18–59 years of age were men. The cumulative mortality rate was 410 deaths/100,000 population among persons ≥60 years of age, >30 times more than persons 18–59 years of age (13 deaths/100,000 population) (Table). During March 2–December 3, 2020, a total of 0.50% of men and 0.34% of women >60 years of age died, compared with 0.02% of men and 0.01% of women of working age. Irrespective of age, cumulative mortality was highest in men, Black persons, Asian persons, persons of other or mixed ethnic groups, and persons in socioeconomically deprived areas (Table).

Place of death was available for 86% (50,227) of decedents. Overall, 77% of deaths occurred in hospitals, 18% in residential care homes, and the remainder elsewhere (e.g., home, hospices, and

other communal establishments). The median time from specimen date to death was 8 days (interquartile range 4–15 days); 91% (53,000) died within 28 days of the specimen date. Of those dying in hospital, 96% died within 28 days of the specimen date, compared with 86% in residential care homes and 84% elsewhere.

When we compared first 4.5 month period with the second, the demographic profile of decedents did not change substantially by sex (57% vs. 57% were men), ethnicity (87% vs. 89% White), place of death (77% vs. 78% hospital), or time to death (91% vs. 91% within 28 days of specimen date). However, region of death became less London-focused (Figure 2), and the proportion of deaths occurring in the most deprived residential quintile rose from 24% to 30%.

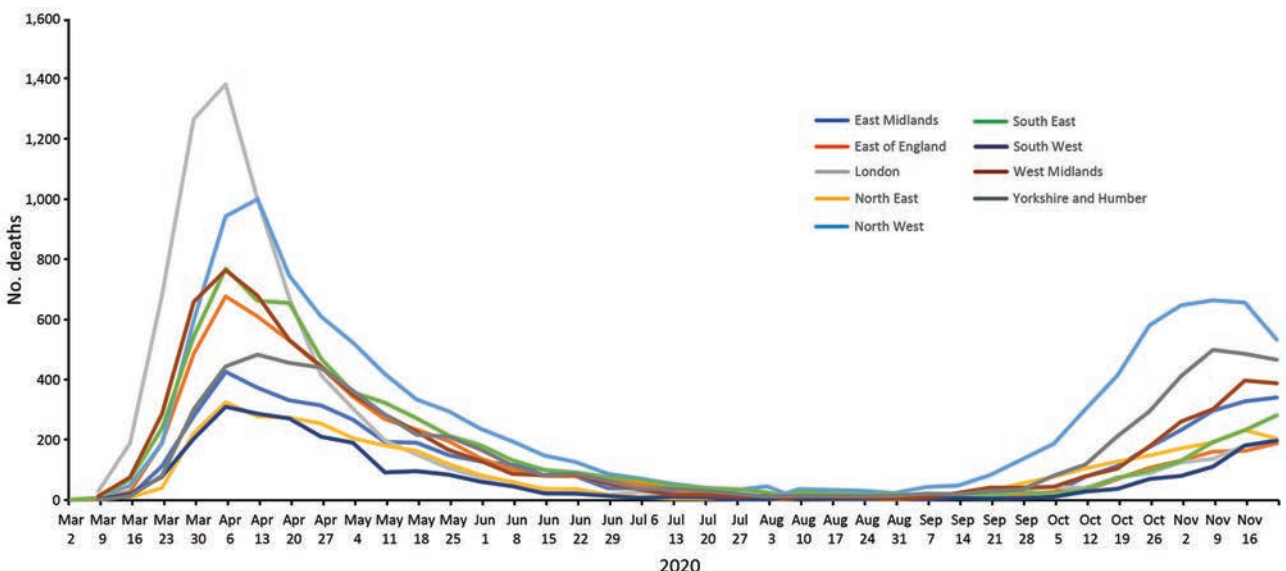


Figure 2. Region-specific coronavirus disease cumulative mortality rate (deaths/100,000 population), by week of death, England, UK, March 2–December 3, 2020.

Table. Coronavirus disease cumulative mortality rates among adults, by age group, sex, region, ethnicity, and residence-based socioeconomic deprivation score, England, UK, March 2–December 3, 2020*

Characteristic	Age group, y					
	18–59			≥60		
	No. cumulative deaths	Population†	Cumulative mortality rate‡	No. cumulative deaths	Population†	Cumulative mortality rate‡
Sex						
F	1,406	15,399,252	9.1	23,809	7,081,746	336
M	2,497	15,399,681	16.2	30,473	6,141,881	496
Region						
London	868	5,266,170	16.5	6,959	1,437,281	484
South East	368	4,554,266	8.1	6,399	2,217,002	289
East of England	371	3,313,330	11.2	5,332	1,646,457	324
West Midlands	479	3,059,310	15.7	6,696	1,405,816	476
Yorkshire and Humber	399	2,854,445	14.0	6,494	1,324,798	490
East Midlands	299	2,486,593	12.0	4,844	1,201,199	403
North West	727	3,803,145	19.1	10,708	1,765,241	607
North East	182	1,377,087	13.2	3,652	686,963	532
South West	156	2,797,918	5.6	2,777	1,568,870	177
Ethnicity						
White	2,625	25,429,023	10.3	48,054	12,384,629	388
Black or Black British	407	1,299,892	31.3	1,523	202,902	751
Asian or Asian British	561	2,920,985	19.2	3,163	510,845	619
Mixed	56	750,086	7.5	241	66,357	363
Other	187	398,948	46.9	866	58,894	1,470
IMD score						
1 (most deprived)	1,299	6,214,331	20.9	13,633	1,934,761	705
2	985	6,414,752	15.4	11,601	2,314,652	501
3	651	5,925,517	11.0	10,226	2,777,687	368
4	537	5,619,071	9.6	9,824	2,965,692	331
5 (least deprived)	377	5,263,233	7.2	8,577	3,020,639	284
Total*	3,904	30,798,933	12.7	54,282	13,223,627	410

*IMD, Indices for Multiple Deprivation.

†Deaths with missing information are excluded: 476 for region, 503 for ethnicity, and 476 for IMD. Population denominator is from 2018 except for IMD.

‡For IMD (3), population denominator is 20–59 and ≥60 year age groups only, and is from 2017.

§Deaths/100,000 population.

Conclusions

In the 9-month period after the first COVID-19 death in England, ~58,000 adults died of COVID-19 (5). COVID-19 deaths disproportionately affected specific adults; 9 of 10 occurred among those ≥60 years of age. Men, Black persons, Asian persons, persons of other or mixed ethnic groups, and residents in deprived areas also experienced higher cumulative mortality rates compared with White persons and persons in less deprived areas. Almost 1 of 10 persons died >28 days after their specimen date, and 1 of 4 persons died outside hospital.

This comprehensive epidemiologic overview of COVID-19 deaths in England directly informs the pandemic response, including vaccination strategy, and highlights inequalities between populations that require redress (6,7). Previous reports focused on subsets of deaths, primary-care records, or both. However, our results are consistent with other studies in the United Kingdom (A.B. Docherty et al., unpub. data, <https://doi.org/10.1101/2020.04.23.20076042>; The OpenSAFELY Collaborative et al., unpub. data, <https://doi.org/10.1101/2020.05.06.20092999>) that show older age is associated with higher COVID-19 mortality rates (8).

The increased rates in older age groups might be attributable to physiologic factors, such as immune senescence (9), which, combined with other factors, can increase the risk for acquiring COVID-19 (e.g., frequently receiving healthcare) and complications (e.g., underlying conditions). The higher mortality rates among Black persons, Asian persons, persons of other or mixed ethnic groups, and persons in more deprived areas are probably influenced by factors that reduce capacity to maintain social distancing, including occupation, use of public transportation, crowded or multigenerational housing, and higher rates of chronic conditions (6).

The cumulative mortality rate of 132 deaths/100,000 population in our study is consistent with reports from other countries in Western Europe (10). However, meaningful comparisons of COVID-19 mortality rates are limited by differing levels of pandemic activity, definitions for COVID-19 deaths, and methods of reporting.

No international standard exists for defining COVID-19 deaths. Some countries exclude deaths occurring >28 days after specimen date; the absence of a time cutoff increases the risk that unrelated deaths are misclassified as COVID-19. Furthermore, daily monitoring

of deaths within 28 days might be used as a proxy for underlying incidence and a pragmatic alternative to death registrations that can be delayed. However, we estimate that a 28-day cutoff excludes $\approx 9\%$ of COVID-19 deaths (1). In England, 2 metrics are produced: all deaths within 28 days of specimen date, and all deaths within 60 days of specimen date or with COVID-19 listed on the death certificate (1). These definitions were selected after rigorous sensitivity analyses relating to cause of death (1). A global consensus on defining COVID-19 deaths is needed urgently.

The PHE mortality reporting system (COSMOSS) was developed rapidly, is comprehensive, and captures deaths daily in all settings (1). However, our definition excludes those who died of COVID-19 without having a test and for whom no death registration certificate is yet available. This exclusion is likely most relevant at the start of the epidemic, when tests were only undertaken at hospital admission; we estimate $\approx 20\%$ of deaths occurred outside of hospitals. Finally, increasing evidence indicates that long-term health problems can occur after COVID-19, but the impact on COVID-19 mortality is unknown.

Further analyses using multivariate models are underway and will better measure the clinical and demographic risk factors for COVID-19 deaths. Furthering understanding of the characteristics of those who die and the context in which they are living is the only way we can reduce COVID-19 mortality overall and address the factors that are driving the inequalities observed across England.

PHE COVID-19 mortality working group (in alphabetical order): Hannah Charles, Jayne Evans, Sarah Foulkes, Sema Mandal, Elizabeth Marchant, Olisaeloka Nsonwu, Anne-Marie O'Connell, Rebecca Russell, Ruth Simmons, Julia Stowe, Simon Thelwall, and Kate Twohig.

Acknowledgments

We thank Myer Glickman and Nalyni Shanmugathan.

This work was undertaken as a core function of work at Public Health England, and no financial support was provided.

About the Author

Dr. Brown is an HIV epidemiologist at Public Health England.

References

1. Public Health England. PHE data series on deaths in people with COVID-19: technical summary – 12 August update [cited 2020 Dec 17]. <https://www.gov.uk/government/publications/phe-data-series-on-deaths-in-people-with-covid-19-technical-summary>
2. Office of National Statistics. Deaths involving COVID-19, England and Wales, provisional [cited 2020 Dec 17]. <https://www.ons.gov.uk/peoplepopulationandcommunity/birthsdeathsandmarriages/deaths/datasets/weeklyprovisional-figuresondeathsregisteredinenglandandwales>
3. Ministry of Housing, Communities, and Local Government. English indices of deprivation, 26 September 2019 [cited 2020 Dec 17]. <https://www.gov.uk/government/statistics/english-indices-of-deprivation-2019>
4. Office of National Statistics. Population estimates 2018 [cited 2020 Dec 17]. <https://www.ons.gov.uk/peoplepopulationandcommunity/populationandmigration/populationestimates>
5. Public Health England. Weekly COVID-19 surveillance report published [cited 2020 Dec 17]. https://assets.publishing.service.gov.uk/government/uploads/system/uploads/attachment_data/file/901803/Weekly_COVID19_Surveillance_Report_week_29_FINAL.pdf
6. Public Health England. Beyond the data: understanding the impact of COVID-19 on BAME groups. June 2020 [cited 2020 Dec 17]. https://assets.publishing.service.gov.uk/government/uploads/system/uploads/attachment_data/file/892376/COVID_stakeholder_engagement_synthesis_beyond_the_data.pdf
7. Public Health England. Disparities in the risk and outcomes of COVID-19. June 2020 [cited 2020 Dec 17]. https://assets.publishing.service.gov.uk/government/uploads/system/uploads/attachment_data/file/892085/disparities_review.pdf
8. Kluge HHP. Older people are at highest risk from COVID-19, but all must act to prevent community spread. April 2, 2020 [cited 2020 Jul 17]. <http://www.euro.who.int/en/health-topics/health-emergencies/coronavirus-covid-19/statements/statement-older-people-are-at-highest-risk-from-covid-19,-but-all-must-act-to-prevent-community-spread>
9. Koff WC, Williams MA. COVID-19 and immunity in aging populations – a new research agenda. *N Engl J Med.* 2020;383:804–5. <https://doi.org/10.1056/NEJMp2006761>
10. European Centre for Disease Prevention and Control. COVID-19 country overviews [cited 2020 Dec 17]. <https://covid19-country-overviews.ecdc.europa.eu>

Address for correspondence: Dr. Alison Brown, Public Health England, National Infection Service, 61 Colindale Ave, London NW9 5EQ, UK; email: alison.brown@phe.gov.uk

Longevity of Middle East Respiratory Syndrome Coronavirus Antibody Responses in Humans, Saudi Arabia

Abeer N. Alshukairi,¹ Jincun Zhao,¹ Maha A. Al-Mozaini, Yanqun Wang, Ashraf Dada, Salim A. Baharoon, Sara Alfaraj, Waleed A. Ahmed, Mushira A. Enani, Fatehi E. Elzein, Nazik Eltayeb, Laila Layqah, Aiman El-Saed, Husam A. Bahauden, Abdul Haseeb, Sherif A. El-Kafrawy, Ahmed M. Hassan, Najlaa A. Siddiq, Ibtihaj Alsharif, Isamel Qushmaq, Esam I. Azhar,² Stanley Perlman,² Ziad A. Memish²

Understanding the immune response to Middle East respiratory syndrome coronavirus (MERS-CoV) is crucial for disease prevention and vaccine development. We studied the antibody responses in 48 human MERS-CoV infection survivors who had variable disease severity in Saudi Arabia. MERS-CoV-specific neutralizing antibodies were detected for 6 years postinfection.

Three novel human coronaviruses have caused different worldwide outbreaks that had variable disease severity and geographic distribution: severe acute respiratory syndrome coronavirus (SARS-CoV) during 2003; Middle East respiratory syndrome (MERS) coronavirus (MERS-CoV) during 2012; and severe acute respiratory syndrome coronavirus 2 (SARS-CoV-2), which caused coronavirus disease starting in 2019 (1). Understanding the immune response to coronavi-

rus infections is crucial for vaccine development and disease prevention (2). Recurrent MERS-CoV infection has not been described in humans. However, longitudinal studies in seropositive camels detected recurrent infections and intermittent shedding of RNA (3).

A limited number of studies have evaluated the longevity of MERS antibody responses. Payne et al. described persistence of MERS-CoV neutralizing antibodies for ≥ 34 months postinfection in 6 (86%) of 7 survivors (4). Choe et al. showed that patients who had severe disease had robust MERS-CoV neutralizing antibody titers for 1 year, and patients who had mild disease had waning antibody response over time (5). We assessed antibody responses in 48 MERS survivors who had variable disease severity and duration ≤ 6 years postinfection.

The Study

We recruited 48 MERS survivors from 5 hospitals in Jeddah and Riyadh, Saudi Arabia. All participants who agreed to participate provided consent. The study was approved by the institutional research boards of the hospitals involved. All MERS cases were diagnosed on the basis of positive reverse transcription PCR results. Disease severity was divided into 3 categories: mild infection (asymptomatic and upper respiratory tract infection), moderate infection (pneumonia not requiring intubation and ventilation), and severe infection (pneumonia requiring intubation and ventilation in the intensive care unit). Blood samples were collected for serologic testing from survivors in various hospitals at a single time point, except for 1 patient (case-patient 45; Table) who provided samples at 4 and 6 years postinfection. On the basis of date of

Author affiliations: King Faisal Specialist Hospital and Research Center, Jeddah, Saudi Arabia (A.N. Alshukairi, A. Dada, N.A. Siddiq, I. Qushmaq); First Affiliated Hospital of Guangzhou Medical University, Guangzhou, China (J. Zhao, Y. Wang); King Faisal Specialist Hospital and Research Center, Riyadh, Saudi Arabia (M.A. Al-Mozaini, I. Alsharif); King Abdulaziz Medical City, Riyadh (S.A. Baharoon, A. El-Saed); Prince Mohammed Bin Abdulaziz Hospital, Riyadh (S. Alfaraj); Security Forces Hospital, Makkah, Saudi Arabia (W.A. Ahmed); King Fahad Medical City, Riyadh (M.A. Enani); Prince Sultan Military Medical City, Riyadh (F.E. Elzein, N. Eltayeb); King Abdullah International Medical Research Center, Riyadh (L. Layqah); King Saud bin Abdulaziz University for Health Sciences, Jeddah (H.A. Bahauden); Umm Al Qura University, Makkah, Saudi Arabia (A. Haseeb); King Abdulaziz University, Jeddah (S.A. El-Kafrawy, A.M. Hassan); King Fahd Medical Research Center, Jeddah (E.F. Azhar); University of Iowa, Iowa City, Iowa, USA (S. Perlman); King Saud Medical City, Riyadh (Z.A. Memish); Al-Faisal University, Riyadh (Z.A. Memish)

DOI: <https://doi.org/10.3201/eid2705.204056>

¹These authors contributed equally to this article.

²These senior authors contributed equally to this article.

diagnosis, MERS-CoV antibody responses were measured 2–6 years postinfection.

An ELISA was performed for 45/49 samples. Microneutralization assays were performed for 43/49 samples in China and 6/49 samples in Saudi Arabia. A total of 43/49 samples were collected 2–5 years postinfection, and 6/49 samples were collected 6 years postinfection. A commercial MERS-CoV

S1ELISA Kit (Euroimmun, <https://www.euroimmun.com>) was used to measure human IgG titers against the MERS-CoV spike protein as described (6). Samples with an optical density ≥ 1.1 were considered positive, those < 0.8 negative, and those 0.8–1.1 borderline. A MERS-CoV focus reduction neutralization test (modified microneutralization assay) and a MERS-CoV microneutralization test were performed

Table. Clinical and serologic findings for 48 patients 2–6 y after infection with Middle East respiratory syndrome coronavirus, Saudi Arabia*

Patient ID	Age, y/sex	Time, y between serologic analysis and infection	Diagnosis	Disease or condition	Illness grade	ELISA result	ELISA titer	NT titer	NT result
46	34/F	6	AS	Healthy	Mild	–	0.0	<20	–
47	41/M	6	AS	Healthy	Mild	–	0.02	40	+
48	41/F	6	PN	Healthy	Moderate	–	0.76	320	+
45	42/M	6	PN	Healthy	Moderate	–	0.75	80	+
43	56/M	6	SPN	Healthy	Severe	–	3.0	80	+
44	38/F	6	SPN	Pregnant, thyroid disease	Severe	+	2.4	80	+
1	52/F	5	URTI	HPT, thyroid disease	Mild	–	0.1	<20	–
2	43/F	5	URTI	Healthy	Mild	–	0.3	42	+
15	35/M	5	PN	DM, hyperlipidemia	Moderate	B	0.8	30	+
33	39/F	4	URTI	Healthy	Mild	–	0.7	28	–
7	49/M	4	URTI	DM, HPT, BA, IHD, ESRD	Mild	+	1.5	104	+
34	42/F	4	URTI	HPT	Mild	+	1.9	144	+
40	28/F	4	URTI	Healthy	Mild	NP	NP	40	+
41	32/F	4	AS	Healthy	Mild	NP	NP	41	+
31	33/M	4	URTI	Healthy	Mild	–	0.5	34	+
32	45/F	4	URTI	Healthy	Mild	B	0.9	44	+
3	45/M	4	PN	Smoker	Moderate	+	1.1	48	+
5	61/M	4	PN	DM, HPT, IHD	Moderate	+	2.9	160	+
25	28/M	4	PN	Healthy	Moderate	+	2.5	315	+
42	47/M	4	PN	Healthy	Moderate	NP	NP	351	+
45	42/M	4	PN	Healthy	Moderate	NP	NP	162	+
29	58/M	3	URTI	Healthy	Mild	–	0.1	45	+
23	28/M	3	URTI	Healthy	Mild	–	0.1	42	+
8	47/M	3	URTI	HPT, hyperlipidemia	Mild	+	2.5	320	+
18	55/M	3	URTI	DM	Mild	+	3.4	648	+
20	34/M	3	URTI	Healthy	Mild	–	0.6	81	+
26	39/M	3	URTI	Healthy	Mild	–	0.6	75	+
35	63/M	3	URTI	DM	Mild	+	2.5	501	+
37	61/M	3	URTI	DM, HPT	Mild	+	1.2	81	+
14	32/F	3	AS	Healthy	Mild	–	0.1	45	+
39	34/M	3	URTI	Healthy	Mild	+	1.2	31	+
9	36/F	3	URTI	Healthy	Mild	–	0.2	32	+
6	74/M	3	URTI	DM, lipid	Mild	–	0.1	<20	–
10	46/F	3	AS	Healthy	Mild	–	0.1	20	–
11	47/F	3	AS	Grave's disease	Mild	–	0.1	20	–
12	33/F	3	AS	Healthy	Mild	–	0.3	20	–
17	54/F	3	URTI	HPT, thyroid disease	Mild	+	4.3	<20	–
27	29/M	3	URTI	Healthy	Mild	–	0.1	<20	–
30	41/F	3	URTI	Healthy	Mild	–	0.2	<20	–
4	41/M	3	PN	Stroke	Moderate	+	3.4	446	+
19	50/M	3	PN	Healthy	Moderate	+	3.7	315	+
24	54/M	3	PN	DM, HPT, myocarditis	Moderate	+	2.4	398	+
22	57/M	3	PN	Asthma	Moderate	+	1.9	41	+
16	62/F	3	SPN	Asthma, hyperlipidemia	Severe	+	2.6	416	+
21	34/F	3	SPN	Healthy	Severe	+	2.4	375	+
28	38/M	3	SPN	Healthy	Severe	+	1.8	117	+
13	59/M	3	SPN	Healthy	Severe	–	0.1	20	–
36	64/M	2	URTI	Healthy	Mild	+	2.5	160	+
38	34/M	2	URTI	Healthy	Mild	–	0.3	27	+

*AS, asymptomatic; B, borderline; BA, bronchial asthma; DM, diabetes mellitus; ESRD, end-stage renal disease; HPT, hypertension; IHD, ischemic heart disease; NP, not performed; NT, neutralization test; PN, pneumonia; SPN, severe pneumonia (patients were in intensive care unit and required intubation and ventilation); URTI, upper respiratory tract infection; –, negative; +, positive.

in certified Biosafety Level 3 laboratories in Guangzhou, China, and Jeddah, Saudi Arabia, as described (7,8). The cutoff value for a positive neutralization assay result was 1:20 (Appendix, <https://wwwnc.cdc.gov/EID/article/27/5/20-4056-App1.pdf>). We used reference MERS-CoV isolates (GenBank accession nos. EMC/2012 in Guangzhou and KF958702 in Jeddah).

We presented continuous variables as median and interquartile range (IQR). We used Kruskal-Wallis, Mann-Whitney, Jonckheere-Terpstra, Fisher exact, and Gamma tests to study the differences between variables. All *p* values were 2-tailed, and *p* values <0.05 were considered significant. We used SPSS Statistics 25.0 (IBM Corp., <https://www.ibm.com>) for all statistical analyses.

Of 49 specimens, 28 (57.1%) were collected from MERS convalescent patients at 2–3 years postinfection, 12 (24.5%) at 4 years postinfection, and 9 (18.4%) at 5–6 years postinfection. Of 49 specimens, 31 (63.3%) were collected from MERS convalescent patients who had mild disease, 12 (24.5%) from those who had moderate disease, and 6 (12.2%) from those who had severe disease (Table). We found that 38/49 specimens had neutralizing antibodies (median [IQR] titer 45 [29–161]). Of these 38 samples, 12 (31%) were negative by ELISA. Ten of these 12 samples were collected from survivors who had mild illness (Table).

The percentage of samples that had positive neutralizing antibodies was 20/28 (71.4%) at 2–3 years, 11/12 (91.7%) at 4 years, and 7/9 (77.6%) at 5–6 years postinfection (*p* = 0.405 for any difference and 0.349 for trend) (Table). The median (IQR) titer

of neutralizing antibodies was 45 (20–319) at 2–3 years, 76 (40–162) at 4 years, and 42 (23–80) at 5–6 years postinfection (*p* = 0.499 for any difference and 0.755 for trend) (Figure, panel A).

Positive neutralizing antibodies were found in 21 (67.7%) of 31 survivors who had mild disease, 12 (100.0%) of 12 survivors who had moderate disease, and 5 (83.3%) of 6 survivors who had severe disease (*p* = 0.054 for any difference and *p* = 0.035 for trend) (Table). The median (IQR) titer of neutralizing antibodies was 40 (20–81) for survivors who had mild disease, 239 (56–343) for survivors who had moderate disease, and 99 (65–385) for survivors who had severe disease, respectively (*p* = 0.004 for any difference and *p* = 0.002 for trend).

Survivors who had mild, moderate, and severe disease had the following median (IQR) titers for neutralizing antibodies: 37 (20–81), 357 (110–434), and 246 (44–406) at 2–3 years postinfection (*p* = 0.109 for any difference and *p* = 0.053 for trend); 41 (34–104) and 162 (104–333) (mild or moderate disease only) at 4 years postinfection (*p* = 0.010); and 28 (15–42), 80 (30–320), and 80 (80–80) at 5–6 years postinfection (*p* = 0.130 for any difference and *p* = 0.065 for trend) (Figure, panel B). We found no major decrease in neutralizing antibody titers over 6 years (Figure, panel A). Survivors who had moderate and severe disease had higher titers than survivors who had mild disease over 6 years (Figure, panel B).

Conclusions

At 6 years postinfection, we detected antibody responses in 100% of MERS survivors who had severe

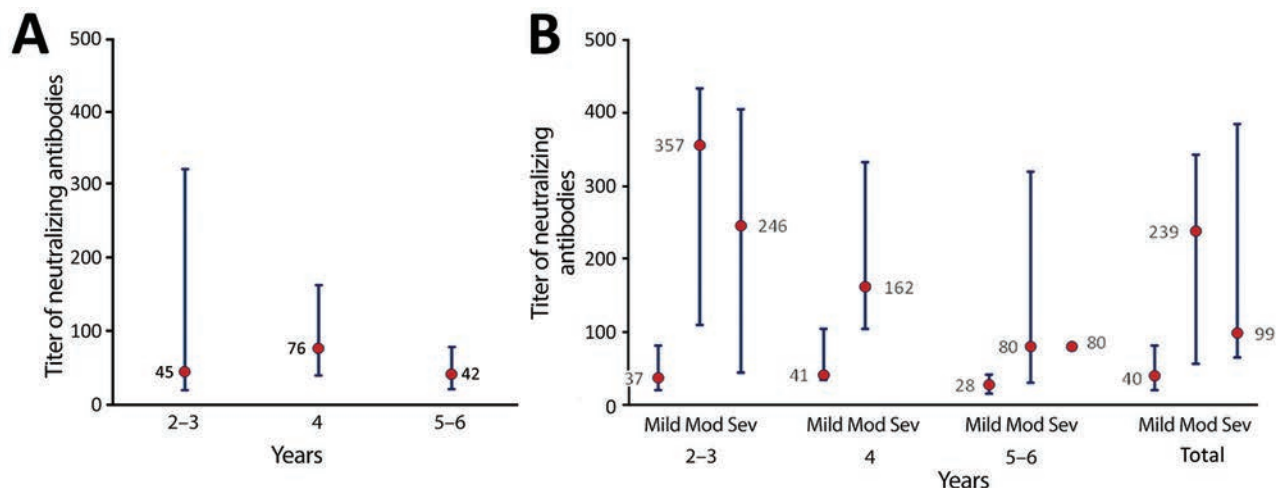


Figure. Neutralization antibody titers in Middle East respiratory syndrome (MERS) convalescent-phase serum samples measured 2–6 years postinfection, Saudi Arabia. Three groups (patients who had mild, moderate, or severe MERS) were enrolled in this study, and serum samples were collected for neutralizing antibody detection (median focus reduction neutralization test titer) at the indicated times after recovery. The cutoff value was 1:20. Median titers of neutralizing antibody (red dots) and interquartile range (blue bars) were measured according to years postinfection (panel A) and disease severity (panel B). There was no major decrease in neutralizing antibodies over 6 years postinfection. Survivors who had moderate and severe disease had higher neutralizing antibody titers than survivors who had mild disease. Mod, moderate; Sev, severe.

or moderate disease and in 50% of survivors who had mild disease, demonstrating durability of the MERS-CoV-specific antibody response. Because we did not measure MERS-CoV-specific T lymphocyte responses, the number of MERS survivors who had detectable immune responses was probably underestimated. T-cell responses were detected in several MERS survivors who had negative antibody responses at 6 months postinfection (9). The results are consistent with those of previous studies, which the association between disease severity and decrease of antibody response in MERS survivors over time (10). Similar results were described after the SARS epidemic. SARS survivors had persistent antibody responses for 3 years postinfection, and a decrease by 6 years postinfection (11,12). However, a recent study indicated that low levels of SARS-CoV-specific antibody could be detected in some survivors at 12 years postinfection (X. Guo et al., Sun Yat-sen University, pers. comm., 2020 Jan 1).

In this study, we performed ELISA and neutralizing antibody assays for all cases. Although cases of severe disease showed good concordance between the 2 assays, some cases of mild or moderate disease had a negative ELISA result and a positive neutralizing test result. Similar results were observed in camel workers who had asymptomatic MERS-CoV infections, most of whom who had negative ELISA results but detectable neutralizing antibody titers (13). Negative ELISA results might reflect either insensitivity of the assay or high cutoff values established by the manufacturer to minimize the rate of false-positive results. In either instance, these results suggest that negative ELISA results should be read with caution in some settings.

A limitation of our study was the small number of cases of moderate or severe disease and a lack of serial samples for nearly all patients. It will also be useful to determine whether levels of antibody would be protective if MERS-CoV reinfection occurred. In conclusion, we showed that virus-specific neutralizing antibodies are detectable in most MERS survivors for ≥ 6 years, consistent with durable immunity against the virus.

Acknowledgments

We thank all the patients for participating in the study and the late Sheikh Ibraheem Ahmed Azhar for providing reagents and supplies.

This study was supported by grants from the National Institutes of Health, USA (PO1 AI060699) and the National Science and Technology Project (81772191).

S.M.F organized data; A.N.A. designed the study, collected data, and wrote the manuscript; S.P. designed the study, analyzed data, and reviewed the manuscript; Z.A.M. investigated study sites and reviewed the manuscript; J.Z., M.A.A., E.I.A., A.D., Y.W., I.A., A.M.H., and S.A.E. performed experiments; S.A.B, S.A., W.A.A., M.A.E., F.E.E., N.E.M., L.L., and HAB investigated sites; N.A.S. and I.Q. provided samples; and A.E.S. and A.H. analyzed data.

About the Author

Dr. Alshukairi is an infectious diseases consultant at the King Faisal Specialist Hospital and Research Center, Jeddah, Saudi Arabia. Her primary research interest is immune responses against human coronaviruses, including MERS-CoV and SARS-CoV-2.

References

1. Perlman S. Another decade, another coronavirus. *N Engl J Med.* 2020;382:760–2. <https://doi.org/10.1056/NEJMe2001126>
2. Sariol A, Perlman S. Lessons for COVID-19 immunity from other coronavirus infections. *Immunity.* 2020;53:248–63. <https://doi.org/10.1016/j.immuni.2020.07.005>
3. Ali MA, Shehata MM, Goma MR, Kandeil A, El-Shesheny R, Kayed AS, et al. Systematic, active surveillance for Middle East respiratory syndrome coronavirus in camels in Egypt. *Emerg Microbes Infect.* 2017;6:e1. <https://doi.org/10.1038/emi.2016.130>
4. Payne DC, Iblan I, Rha B, Alqasrawi S, Haddadin A, Al Nsour M, et al. Persistence of antibodies against Middle East respiratory syndrome coronavirus. *Emerg Infect Dis.* 2016;22:1824–6. <https://doi.org/10.3201/eid2210.160706>
5. Choe PG, Perera RA, Park WB, Song KH, Bang JH, Kim ES, et al. MERS-CoV antibody responses 1 year after symptom onset, South Korea, 2015. *Emerg Infect Dis.* 2017;23:1079–84. <https://doi.org/10.3201/eid2307.170310>
6. Drosten C, Meyer B, Müller MA, Corman VM, Al-Masri M, Hossain R, et al. Transmission of MERS-coronavirus in household contacts. *N Engl J Med.* 2014;371:828–35. <https://doi.org/10.1056/NEJMoa1405858>
7. Wang Y, Zhang L, Sang L, Ye F, Ruan S, Zhong B, et al. Kinetics of viral load and antibody response in relation to COVID-19 severity. *J Clin Invest.* 2020;130:5235–44. <https://doi.org/10.1172/JCI138759>
8. Muthumani K, Falzarano D, Reuschel EL, Tingey C, Flingai S, Villarreal DO, et al. A synthetic consensus anti-spike protein DNA vaccine induces protective immunity against Middle East respiratory syndrome coronavirus in nonhuman primates. *Sci Transl Med.* 2015;7:301ra132. <https://doi.org/10.1126/scitranslmed.aac7462>
9. Zhao J, Alshukairi AN, Baharoon SA, Ahmed WA, Bokhari AA, Nehdi AM, et al. Recovery from the Middle East respiratory syndrome is associated with antibody and T-cell responses. *Sci Immunol.* 2017;2:eaan5393. <https://doi.org/10.1126/sciimmunol.aan5393>
10. Alshukairi AN, Khalid I, Ahmed WA, Dada AM, Bayumi DT, Malic LS, et al. Antibody response and disease severity in healthcare worker MERS survivors. *Emerg Infect Dis.* 2016;22:1113. <https://doi.org/10.3201/eid2206.160010>

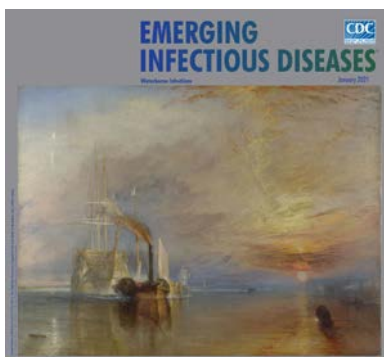
11. Wu LP, Wang NC, Chang YH, Tian XY, Na DY, Zhang LY, et al. Duration of antibody responses after severe acute respiratory syndrome. *Emerg Infect Dis.* 2007;13:1562–4. <https://doi.org/10.3201/eid1310.070576>
12. Tang F, Quan Y, Xin ZT, Wrarmert J, Ma MJ, Lv H, et al. Lack of peripheral memory B cell responses in recovered patients with severe acute respiratory syndrome: a six-year follow-up study. *J Immunol.* 2011;186:7264–8. <https://doi.org/10.4049/jimmunol.0903490>
13. Alshukairi AN, Zheng J, Zhao J, Nehdi A, Baharoon SA, Layqah L, et al. High prevalence of MERS-CoV infection in camel workers in Saudi Arabia. *MBio.* 2018;9:e01985–18. <https://doi.org/10.1128/mBio.01985-18>

Address for correspondence: Abeer N. Alshukairi, Adult Infectious Diseases Section, Department of Medicine, King Faisal Specialist Hospital and Research Center, Jeddah, PO Box 40047, Jeddah 21499, Saudi Arabia; email: abeer.alshukairi@gmail.com

January 2021

Waterborne Infections

- Impact of Human Papillomavirus Vaccination, Rwanda and Bhutan
- Nosocomial Coronavirus Disease Outbreak Containment, Hanoi, Vietnam, March–April 2020
- Aspergillosis Complicating Severe Coronavirus Disease
- Rising Ethnic Inequalities in Acute Rheumatic Fever and Rheumatic Heart Disease, New Zealand, 2000–2018
- Differential Yellow Fever Susceptibility in New World Nonhuman Primates, Comparison with Humans, and Implications for Surveillance
- Comparative Omics Analysis of Historic and Recent Isolates of *Bordetella pertussis* and Effects of Genome Rearrangements on Evolution
- Hospitalization for Invasive Pneumococcal Diseases in Young Children Before Use of 13-Valent Pneumococcal Conjugate
- Human Diversity of Killer Cell Immunoglobulin-Like Receptors and Human Leukocyte Antigen Class I Alleles and Ebola Virus Disease Outcomes
- IgG Seroconversion and Pathophysiology in Severe Acute Respiratory Syndrome Coronavirus 2 Infection
- Hannibal's Ophthalmia—A New Answer to an Ancient Question



- Recency-Weighted Statistical Modeling Approach to Attribute Illnesses Caused by 4 Pathogens to Food Sources Using Outbreak Data, United States
- Estimate of Burden and Direct Healthcare Cost of Infectious Waterborne Disease in the United States
- Post-13-Valent Pneumococcal Conjugate Vaccine Dynamics in Young Children of Serotypes Included in Candidate Extended-Spectrum Conjugate Vaccines
- Precise Species Identification by Whole-Genome Sequencing of *Enterobacter* Bloodstream Infection
- Delineating and Analyzing Locality-Level Determinants of Cholera, Haiti
- Viral Metagenomic Analysis of Cerebrospinal Fluid from Patients with Acute Central Nervous System Infections of Unknown Origin, Vietnam
- Severe Human Bocavirus-Associated Pneumonia in Adults at a Referral Hospital, Seoul, South Korea
- Performance of Nucleic Acid Amplification Tests for Detection of Severe Acute Respiratory Syndrome Coronavirus 2 in Prospectively Pooled Specimens
- Susceptibility of Domestic Swine to Experimental Infection with Severe Acute Respiratory Syndrome Coronavirus 2
- Cellular Immunity in COVID-19 Convalescents with PCR-Confirmed Infection but with Undetectable SARS-CoV-2-Specific IgG
- Estimating the Force of Infection for Dengue Virus Using Repeated Serosurveys, Ouagadougou, Burkina Faso
- Attribution of Illnesses Transmitted by Food and Water to Comprehensive Transmission Pathways Using Structured Expert Judgment, United States
- Intrafamilial Exposure to SARS-CoV-2 Associated with Cellular Immune Response without Seroconversion, France
- Invasive Fusariosis in Nonneutropenic Patients, Spain, 2000–2015

**EMERGING
INFECTIOUS DISEASES**

To revisit the January 2021 issue, go to:

<https://wwwnc.cdc.gov/eid/articles/issue/27/1/table-of-contents>

Racial and Ethnic Disparities in Incidence of SARS-CoV-2 Infection, 22 US States and DC, January 1–October 1, 2020

NaTasha D. Hollis,¹ Wen Li,¹ Miriam E. Van Dyke, Gibril J. Njie, Heather M. Scobie, Erin M. Parker, Ana Penman-Aguilar,² Kristie E.N. Clarke²

We examined disparities in cumulative incidence of severe acute respiratory syndrome coronavirus 2 by race/ethnicity, age, and sex in the United States during January 1–October 1, 2020. Hispanic/Latino and non-Hispanic Black, American Indian/Alaskan Native, and Native Hawaiian/other Pacific Islander persons had a substantially higher incidence of infection than non-Hispanic White persons.

Health disparities among racial/ethnic minority groups in the United States are closely related to structural inequities in social determinants of health. Some racial/ethnic minority groups have disproportionate rates of underlying conditions that increase the risk for severe illness from coronavirus disease (COVID-19) (1,2). Certain groups are overrepresented in occupations that require public contact, have crowded conditions, or are unamenable to telework, increasing the risk for exposure to severe acute respiratory infection coronavirus 2 (SARS-CoV-2), the virus that causes COVID-19 (3,4). Structural inequities in housing, education, wealth, and healthcare access also increase disparities in infection and COVID-related illness and death (5–8).

We conducted an intersectional analysis by race/ethnicity, age, and sex to identify disparities in SARS-CoV-2 incidence using data from multiple US jurisdictions. Monitoring these disparities is critical for guiding action to reduce health inequities.

Author affiliations: Centers for Disease Control and Prevention, Atlanta, Georgia, USA (N.D. Hollis, W. Li, M.E. Van Dyke, G.J. Njie, H.M. Scobie, E.M. Parker, A. Penman-Aguilar, K.E.N. Clarke); Commissioned Corps of the US Public Health Service, Atlanta (N.D. Hollis, H.M. Scobie, E. Parker, K.E.N. Clarke)

DOI: <https://doi.org/10.3201/eid2705.204523>

The Study

We analyzed SARS-CoV-2 infections reported to the Centers for Disease Control and Prevention (<https://data.cdc.gov/browse?tags=covid-19>) by jurisdictional health departments. To minimize information bias, we included only jurisdictions reporting $\geq 30\%$ of cases (<https://protect-public.hhs.gov>) and $\geq 70\%$ completeness of race/ethnicity data of cases during January 1–October 1, 2020. We analyzed data on race/ethnicity, age, and sex in 1,751,627 cases from 22 US states and the District of Columbia (Table).

We determined cumulative incidence of infection per 100,000 population and cumulative incidence ratios (CIRs) with 95% CIs by race/ethnicity, age, and sex. Patients were grouped as Hispanic or Latino (Hispanic), non-Hispanic American Indian or Alaska Native (AIAN), non-Hispanic Black or African American (Black), non-Hispanic Asian (Asian), non-Hispanic Native Hawaiian or other Pacific Islander (NHOPI), non-Hispanic White (White), or non-Hispanic of multiple races (multiple race). Of Hispanic persons in this sample, 53.8% identified as White, 33.2% as persons of multiple or other races, 1.7% as Black, 0.2% as Asian, and 0.2% as NHOPI; 10.5% of Hispanic persons were of unknown race. We used population denominators from the 2019 US Census (Annual County Resident Population Estimates by Age, Sex, Race, and Hispanic Origin, <https://www.census.gov/programs-surveys/popest/technical-documentation/file-layouts.html>). We considered CIR 95% CIs excluding 1.0 to be significant. We assessed differences in rates by sex after adjusting for race/ethnicity and age using Analysis of Variance. We conducted statistical analyses using R version 4.0.0 (9). This study was conducted in

¹These first authors contributed equally to this article.

²These senior authors contributed equally to this article..

Table. Incidence of severe acute respiratory syndrome coronavirus 2 infections by sex, race/ethnicity, and age group, 22 US states and District of Columbia, January 1–October 1, 2020*

Characteristic	No. (%), n = 1,751,627†	Cumulative incidence (95% CI)‡§	Cumulative incidence ratio (95% CI)§
Sex			
F	898,970 (51.7)	1,734 (1,730–1,737)	Referent
M	841,487 (48.3)	1,672 (1,668–1,675)	0.96 (0.96–0.97)
Race and ethnicity¶			
Non-Hispanic White	657,437 (47.7)	935 (933–938)	Referent
Non-Hispanic Black	225,477 (16.4)	1,974 (1,965–1,982)	2.11 (2.10–2.12)
Non-Hispanic Asian	33,703 (2.4)	874 (865–884)	0.93 (0.92–0.95)
Non-Hispanic multiple races	22,650 (1.6)	957 (944–969)	1.02 (1.01–1.04)
Non-Hispanic American Indian or Alaska Native	19,259 (1.4)	2,274 (2,242–2,306)	2.43 (2.40–2.47)
Non-Hispanic Native Hawaiian or other Pacific Islander	7,226 (0.5)	2,693 (2,631–2,755)	2.88 (2.81–2.95)
Hispanic or Latino	375,418 (27.3)	2,860 (2,850–2,869)	3.06 (3.05–3.07)
Non-Hispanic other	36,104 (2.6)	NA	NA
Age group, y			
<19	191,303 (11.5)	774 (770–777)	0.33 (0.33–0.34)
20–34	473,627 (28.4)	2,316 (2,310–2,323)	Referent
35–44	270,405 (16.2)	2,146 (2,138–2,154)	0.93 (0.92–0.93)
45–54	258,400 (15.5)	2,060 (2,052–2,068)	0.89 (0.89–0.89)
55–64	216,848 (13.0)	1,591 (1,584–1,597)	0.69 (0.68–0.69)
65–74	128,348 (7.7)	1,220 (1,213–1,226)	0.53 (0.52–0.53)
75–84	74,539 (4.5)	1,366 (1,356–1,376)	0.59 (0.59–0.59)
>85	51,472 (3.1)	2,283 (2,263–2,303)	0.99 (0.98–0.99)

*Data from District of Columbia and 22 US states: Alaska, Arkansas, Florida, Hawaii, Iowa, Kansas, Massachusetts, Maine, Michigan, Minnesota, Mississippi, Montana, Nebraska, New Hampshire, New Mexico, Nevada, Ohio, Oregon, Tennessee, Utah, Vermont, and Wisconsin. Data from Data Collation and Integration for Public Health Event Responses platform (<https://data.cdc.gov/browse?tags=covid-19>). NA, not available.

†Missing sex data for 11,170 persons; race/ethnicity data for 374,353 persons; and age data for 86,685 persons (not included in percentage calculations).

‡Cases per 100,000 persons. Population denominators from 2019 US Census (Annual County Resident Population Estimates by Age, Sex, Race, and Hispanic Origin, <https://www.census.gov/programs-surveys/popest/technical-documentation/file-layouts.html>).

§Calculated using a normal approximation (Xu J, Kockanek KD, Murphy SL, Tejada-Vera B. Deaths: final data for 2007. National Center for Health Statistics. 2010 [cited 2020 Oct 16]. https://www.cdc.gov/nchs/data/nvsr/nvsr58/nvsr58_19.pdf).

¶No measures were calculated for 36,104 Non-Hispanic persons of other races because of lack of population denominator information from US Census Bureau.

accordance with applicable federal law and Centers for Disease Control and Prevention policy [45 Code of Federal Regulations part 46.102(1)(2)].

We found that most racial/ethnic minority groups had significantly higher cumulative incidence of SARS-CoV-2 than did White persons (Table). Cumulative incidence ranged from 874 (95% CI 865–884)/100,000 population in Asian persons to 2,860 (95% CI 2,850–2,869)/100,000 population in Hispanic persons. CIRs were significantly higher among Black (2.11), AIAN (2.43), NHOPI (2.88), and Hispanic persons (3.06) compared with White persons; the CIR was nominally but significantly different for multiple race (1.02) and Asian persons (0.93). Cumulative incidence for men compared with women, when adjusted for both race/ethnicity and age, was similar ($p = 0.982$; data not shown).

Cumulative incidence of SARS-CoV-2 was significantly higher among most racial/ethnic minority groups than among White persons of the same age group (Figure 1; Appendix Table 1, <https://wwwnc.cdc.gov/EID/article/27/5/20-4523-App1.pdf>). Among Asian persons <45 or ≥75 years of age, CIRs were lower (0.53–0.95) than among White persons. Among multiple race persons, results varied by age: CIRs were significantly lower among those <19 years of age (CIR 0.54,

95% CI 0.52–0.56) and 20–34 years of age (CIR 0.88, 95% CI 0.86–0.90) but »4–6 times higher among those ≥75 years of age. Black, AIAN, NHOPI (except for persons aged ≥85), and Hispanic persons had CIRs of 1.45–3.83 by age group.

We found differences in infection rates by sex within various racial/ethnic and age groups (CIRs 0.64–1.30) (Figure 2; Appendix Table 2). Overall, cumulative incidence among men in all racial/ethnic groups was significantly lower than among women (CIRs 0.85–0.97), with an exception among Asian men (CIR 1.05). Men who were Black and ≥65 years of age, multiple race and 65–74 years of age, and Hispanic or White and 55–84 years of age had a higher cumulative incidence than women. Among NHOPI and AIAN persons, cumulative incidence was significantly lower than for White persons only for men 20–44 years of age.

Conclusions

Among >1.75 million persons with SARS-CoV-2 in 23 US jurisdictions during January 1–October 1, 2020, persons from most racial/ethnic minority groups had higher cumulative incidence than White persons. Hispanic persons had a 3.1-fold higher incidence and Black, AIAN, and NHOPI persons a >2-fold higher

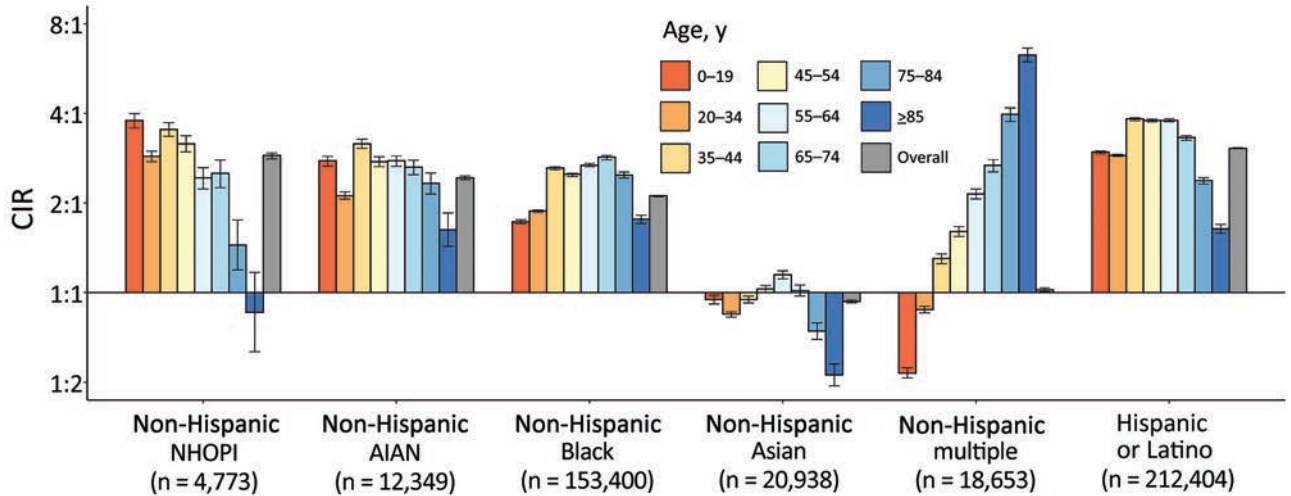


Figure 1. CIRs of severe acute respiratory syndrome coronavirus 2 among persons of different racial/ethnic groups compared with non-Hispanic White persons, 22 US states and the District of Columbia, January 1–October 1, 2020. Ratios are displayed on binary logarithmic scale; error bars indicate 95% CIs (Appendix Table 1, <https://wwwnc.cdc.gov/EID/article/27/5/20-4523-App1.pdf>). CIRs are displayed on binary logarithmic scale; error bars indicate 95% CIs. CIRs with error bars not crossing the origin (1:1) are significant ($p < 0.05$). AIAN, American Indian or Alaska Native; CIR, cumulative incidence ratio; NHOPI, Native Hawaiian or other Pacific Islander.

incidence of SARS-CoV-2 than did White persons. Racial/ethnic disparities varied by age group. Sex differences in cumulative incidence within racial/ethnic groups were less pronounced than disparities between racial/ethnic groups.

We found the highest incidence of infection among Hispanic persons, similar to findings of studies examining SARS-CoV-2 positivity rates in more limited US geographic areas (6,10–12). We also found high incidence among NHOPI persons. Previous analyses

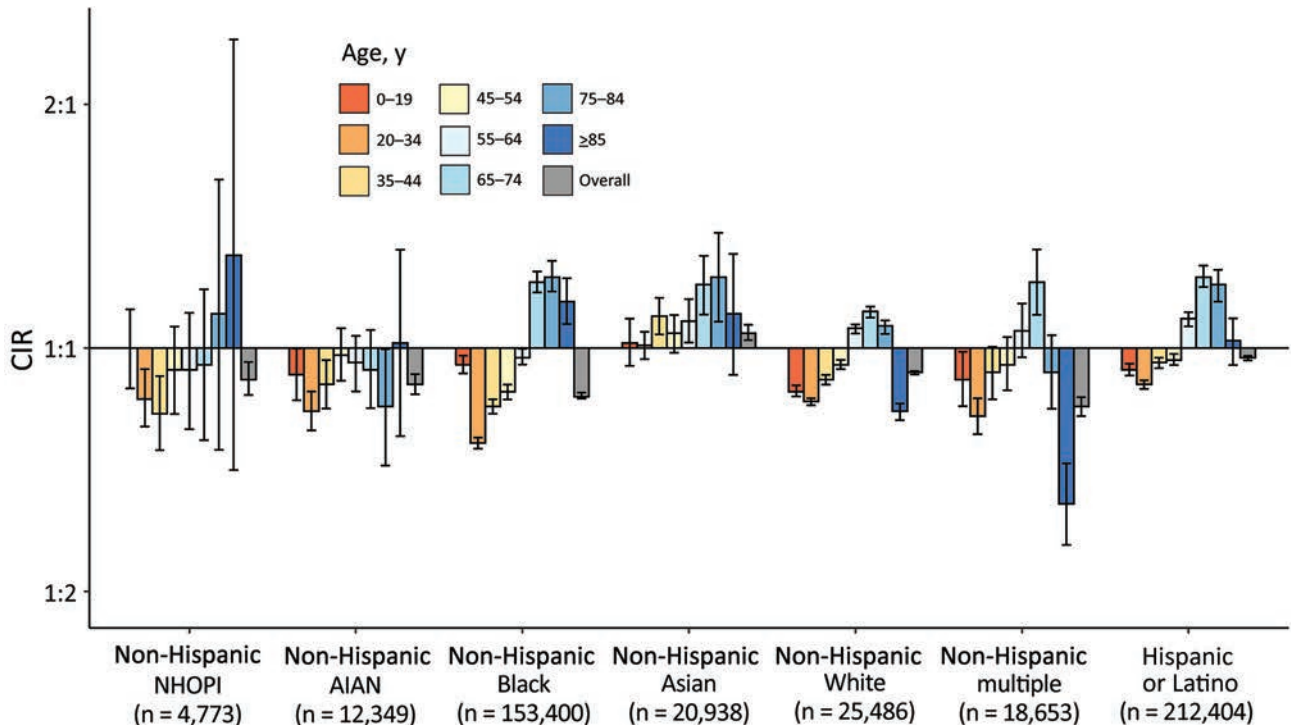


Figure 2. CIRs of severe acute respiratory syndrome coronavirus 2 for male sex, compared with female sex, 22 US states and District of Columbia, January 1–October 1, 2020. Ratios are displayed on binary logarithmic scale; error bars indicate 95% CIs (Appendix Table 2, <https://wwwnc.cdc.gov/EID/article/27/5/20-4523-App1.pdf>). CIRs are displayed on binary logarithmic scale; error bars indicate 95% CIs. CIRs with error bars not crossing the origin (1:1) are significant ($p < 0.05$). AIAN, American Indian or Alaska Native; CIR, cumulative incidence ratio; NHOPI, Native Hawaiian or other Pacific Islander.

have rarely disaggregated NHOPI persons, preventing detection of disparities. Although previous studies have shown higher rates of severe COVID-19 illness among men, we observed lower infection rates among men overall (1,13).

Social determinants of health drive racial/ethnic disparities in disease incidence (3–8). For example, members of some racial/ethnic groups are overrepresented in the essential workforce and more likely to live in multigenerational or high-density housing, increasing the risk for SARS-CoV-2 exposure (<https://www.cdc.gov/coronavirus/2019-ncov/community/health-equity/racial-ethnic-disparities/index.html>). Outbreaks in some occupational settings have had racial/ethnic disparities in infection (3,8). Employers, community organizations, healthcare systems, public health agencies, and governments can act to reduce racial/ethnic disparities in COVID-19 incidence by implementing flexible, nonpunitive leave policies (e.g., paid sick leave); equitable access to testing and screening programs, personal protective equipment, and vaccines; and policies that encourage physical distancing (14). In addition, public health officials can tailor COVID-19 prevention messaging to the languages and cultures of various racial/ethnic groups. Multisectoral partnerships could support COVID-19 mitigation strategies through initiatives that provide spaces for isolation or self-quarantine, safe transportation, free or reduced-cost broadband internet, and housing resources (14).

One limitation of this study is that underreporting to the Centers for Disease Control and Prevention database, which documented 78% of cases in selected jurisdictions, probably caused underestimates in calculated incidence. Second, selected jurisdictions comprise 31% of the US population; in these jurisdictions, NHOPI, White, AIAN, and multiple race persons are overrepresented and Asian, Hispanic, and Black persons underrepresented (Appendix Table 3). As a result, our findings are not nationally representative or generalizable. Third, we excluded persons of unknown race/ethnicity (24%) from incidence calculations. Among persons of unknown race/ethnicity, 33% specified race but not ethnicity; minority racial groups were overrepresented (Appendix Table 4). Fourth, cases among racial/ethnic minority groups might be underreported because of disparities in testing access (15). The third and fourth issues probably resulted in underestimation of racial/ethnic disparities. Finally, aggregation of NHOPI and Asian persons in ≥ 2 jurisdictions probably resulted in underestimating incidence among NHOPI persons and overestimating among Asian persons.

In summary, documenting population-based racial/ethnic disparities in SARS-CoV-2 infection rates and how disparities vary by age and sex informs the development and implementation of equitable policies and intervention strategies. Strategies should prioritize collection and analysis of data relating to health equity and focus on mitigating disproportionate risks of exposure related to social determinants of health.

Acknowledgments

We thank Jayme Coyle for providing technical assistance and data visualization support. We also thank all COVID-19 response personnel at the Centers for Disease Control and Prevention for data collection, reporting, and guidance during the COVID-19 pandemic.

About the Author

Dr. Hollis is an epidemiologist in the National Center on Birth Defects and Developmental Disabilities, Centers for Disease Control and Prevention in Atlanta, Georgia, USA. Her research interests include improving health and well-being and decreasing disparities among vulnerable populations.

References

- Garg S, Kim L, Whitaker M, O'Halloran A, Cummings C, Holstein R, et al. Hospitalization rates and characteristics of patients hospitalized with laboratory-confirmed coronavirus disease 2019—COVID-NET, 14 states, March 1–30, 2020. *MMWR Morb Mortal Wkly Rep.* 2020;69:458–64. <https://doi.org/10.15585/mmwr.mm6915e3>
- Raifman MA, Raifman JR. Disparities in the population at risk of severe illness from COVID-19 by race/ethnicity and income. *Am J Prev Med.* 2020;59:137–9. <https://doi.org/10.1016/j.amepre.2020.04.003>
- Bui DP, McCaffrey K, Friedrichs M, LaCross N, Lewis NM, Sage K, et al. Racial and ethnic disparities among COVID-19 cases in workplace outbreaks by industry sector—Utah, March 6–June 5, 2020. *MMWR Morb Mortal Wkly Rep.* 2020;69:1133–8. <https://doi.org/10.15585/mmwr.mm6933e3>
- Hawkins D. Differential occupational risk for COVID-19 and other infection exposure according to race and ethnicity. *A J Ind Med.* 2020;15:15. PubMed <https://doi.org/10.1002/ajim.23145>
- Cordes J, Castro MC. Spatial analysis of COVID-19 clusters and contextual factors in New York City [Erratum in: *Spat Spatio-Temporal Epidemiol.* 2020;36:100399]. *Spat Spatio-Temporal Epidemiol.* 2020;34:100355. <https://doi.org/10.1016/j.sste.2020.100355>
- Rodriguez-Diaz CE, Guilamo-Ramos V, Mena L, Hall E, Honermann B, Crowley JS, et al. Risk for COVID-19 infection and death among Latinos in the United States: examining heterogeneity in transmission dynamics. *Ann Epidemiol.* 2020;52:46–53.e2. <https://doi.org/10.1016/j.annepidem.2020.07.007>
- Rodriguez-Lonebear D, Barceló NE, Akee R, Carroll SR. American Indian reservations and COVID-19: correlates

- of early infection rates in the pandemic. *J Public Health Manag Pract.* 2020;26:371–7. <https://doi.org/10.1097/PHH.0000000000001206>
8. Waltenburg MA, Victoroff T, Rose CE, Butterfield M, Jervis RH, Fedak KM, et al.; COVID-19 Response Team. Update: COVID-19 among workers in meat and poultry processing facilities – United States, April–May 2020. *MMWR Morb Mortal Wkly Rep.* 2020;69:887–92. <https://doi.org/10.15585/mmwr.mm6927e2>
 9. R Core Team. R: a language and environment for statistical computing. Vienna (Austria): R Foundation for Statistical Computing; 2020.
 10. Martinez DA, Hinson JS, Klein EY, Irvin NA, Saheed M, Page KR, et al. SARS-CoV-2 positivity rate for Latinos in the Baltimore–Washington, DC region. *JAMA.* 2020;324:392–5. <https://doi.org/10.1001/jama.2020.11374>
 11. Millett GA, Jones AT, Benkeser D, Baral S, Mercer L, Beyrer C, et al. Assessing differential impacts of COVID-19 on black communities. *Ann Epidemiol.* 2020;47:37–44. <https://doi.org/10.1016/j.annepidem.2020.05.003>
 12. Moore JT, Ricaldi JN, Rose CE, Fuld J, Parise M, Kang GJ, et al.; COVID-19 State, Tribal, Local, and Territorial Response Team. Disparities in incidence of COVID-19 among under-represented racial/ethnic groups in counties identified as hotspots during June 5–18, 2020 – 22 states, February–June 2020. *MMWR Morb Mortal Wkly Rep.* 2020;69:1122–6. <https://doi.org/10.15585/mmwr.mm6933e1>
 13. Hsu HE, Ashe EM, Silverstein M, Hofman M, Lange SJ, Razzaghi H, et al. Race/ethnicity, underlying medical conditions, homelessness, and hospitalization status of adult patients with COVID-19 at an urban safety-net medical center – Boston, Massachusetts, 2020. *MMWR Morb Mortal Wkly Rep.* 2020;69:864–9. <https://doi.org/10.15585/mmwr.mm6927a3>
 14. Centers for Disease Control and Prevention. Coronavirus disease 2019 (COVID-19): what we can do. 2020 [cited 2020 Sep 15]. <https://www.cdc.gov/coronavirus/2019-ncov/community/health-equity/what-we-can-do.html>
 15. Rader B, Astley CM, Sy KTL, Sewalk K, Hswen Y, Brownstein JS, et al. Geographic access to United States SARS-CoV-2 testing sites highlights healthcare disparities and may bias transmission estimates. *J Travel Med.* 2020;27:taaa076. <https://doi.org/10.1093/jtm/taaa076>
- Address for correspondence: NaTasha Hollis, Centers for Disease Control and Prevention, 4470 Buford Highway NE, Mailstop S106-4, Atlanta, GA 30341, USA; email: iym7@cdc.gov

EID Podcast: Two Ways of Tracking *C. difficile* in Switzerland

Science wields many different tools in the pursuit of public health. These tools can work together to capture a detailed picture of disease. However, many tools accomplish similar tasks, often leaving policymakers wondering, when it comes to disease surveillance, what is the best tool for the job?

Different tests are currently used to diagnose *Clostridioides difficile*, a dangerous bacterium found in hospitals around the world. As rates of this infection surge globally, researchers need to be able to compare statistics from different hospitals, regions, and countries.

In this EID podcast, Sarah Tschudin-Sutter, a professor of infectious disease epidemiology at the University Hospital - Basel in Switzerland, discusses using 2 tests for *C. difficile* infection in Europe.

Visit our website to listen:
<https://go.usa.gov/xGEuz>

**EMERGING
INFECTIOUS DISEASES**

Emergence of Toscana Virus, Romania, 2017–2018

Corneliu P. Popescu,¹ Ani I. Cotar,¹ Sorin Dinu, Mihaela Zaharia, Gratiela Tardei, Emanoil Ceausu, Daniela Badescu, Simona Ruta, Cornelia S. Ceianu, Simin A. Florescu

We describe a series of severe neuroinvasive infections caused by Toscana virus, identified by real-time reverse transcription PCR testing, in 8 hospitalized patients in Bucharest, Romania, during the summer seasons of 2017 and 2018. Of 8 patients, 5 died. Sequencing showed that the circulating virus belonged to lineage A.

Toscana phlebovirus (TOSV; genus *Phlebovirus*, family *Phenuiviridae*) is transmitted by sand flies. Three genetic lineages (A, B, and C) with different geographic distribution have been described to date. TOSV is the only sand fly-transmitted virus causing neuroinvasive disease in humans and the most prevalent arthropodborne virus in the Mediterranean area; however, it remains a neglected pathogen and is seldom included in the diagnostic algorithm for central nervous system (CNS) infections (1–4).

An increased number of acute viral CNS infections were reported during the summer and fall seasons during 2016–2018 in Romania. Many of them, including severe cases, were confirmed as West Nile virus (WNV) infections; additional cases were caused by herpes and enteroviruses infections (5). Nevertheless, several severe cases, diagnosed mainly in elderly patients, remained without a known etiology. We describe the evidence of TOSV involvement in these neuroinvasive infections in patients admitted to a

tertiary-care facility (Dr. Victor Babes Clinical Hospital of Infectious Diseases, Bucharest, Romania).

The Study

We tested 31 adult patients (18 in 2017 and 13 in 2018) with neurologic manifestations; all tested negative by cerebrospinal fluid nucleic acid testing for WNV, herpesviruses, and enteroviruses. Seven confirmed cases and 1 probable case of TOSV neuroinvasive disease were identified by real-time reverse transcription PCR (rRT-PCR); cycle threshold values ranged from 34.61 to 41.18.

All cases were characterized by progression to severe illness (encephalitis in 7 cases and meningoencephalitis in 1 case). Cerebrospinal fluid (CSF) was analyzed after lumbar puncture in all patients. Computed tomography of the brain was performed in 7 cases, and cerebral magnetic resonance imaging was performed in 1 case.

Median age of patients was 77.75 years (range 68–91 years); 5 were men, and 3 were women. Underlying conditions were recorded in all patients, most frequently hypertension (5 cases), diabetes mellitus and ischemic heart disease (3 cases), and stroke sequelae and congestive heart failure (2 cases). Five patients died, 2 recovered with sequelae, and 1 had complete recovery.

Although this is a retrospective study, informed consent was obtained from each patient included in the study as part of the routine hospital activity. Demographic data, clinical features, diagnostics and outcome of patients are summarized in Appendix Table (<https://wwwnc.cdc.gov/EID/article/27/5/204598-App1.pdf>).

In all patients TOSV RNA was detected by using a TaqMan assay. Standard nested PCRs for large and medium segments were negative for all tested samples. In the 7 confirmed cases, both CSF and serum samples collected 1–4 days after illness onset were

Author affiliations: Dr. Victor Babes Clinical Hospital of Infectious and Tropical Diseases, Bucharest, Romania (C.P. Popescu, M. Zaharia, G. Tardei, E. Ceausu, S.A. Florescu); European Society of Clinical Microbiology and Infectious Diseases Study Group for Infectious Diseases of the Brain, Basel, Switzerland (C.P. Popescu, M. Zaharia); Carol Davila University of Medicine and Pharmacy, Bucharest (C.P. Popescu, M. Zaharia, S. Ruta, S.A. Florescu); Cantacuzino National Medico–Military Institute for Research and Development, Bucharest (A.I. Cotar, S. Dinu, D. Badescu, C.S. Ceianu); Stefan S. Nicolau Institute of Virology, Bucharest (S. Ruta)

DOI: <https://doi.org/10.3201/eid2705.204598>

¹These authors contributed equally to this article.

positive and the rRT-PCR amplicons were sequenced. In the probable case, only the serum sample was positive, but no sequence could be obtained. Urine samples collected on day 3 after illness onset in 2 patients were also positive by rRT-PCR.

On the basis of the short sequence of the small genomic segment derived from our patient samples, we determined that the virus belongs to genetic lineage A. The sequences were deposited in the European Nucleotide Archive (accession nos. LR735597–603) (Figure)

The serologic tests performed poorly in these patients; IgM was detected in only 1 patient by indirect immunofluorescence test at the lowest dilution

of 1:10. In 2 convalescent patients, seroconversion for IgG was found in samples collected 28 days apart by indirect immunofluorescence test in 1 patient and by immunoblotting in both patients.

Conclusions

We describe 8 cases of CNS infections with TOSV, all in elderly patients, 7 of whom were residents of the city of Bucharest and 1 of the surrounding county (Ilfov). The onset dates ranged from June 17–September 1, overlapping the transmission period of WNV in the Bucharest area. Simultaneous occurrence of cases of vectorborne WNV and TOSV CNS infections were previously reported in southeastern Europe

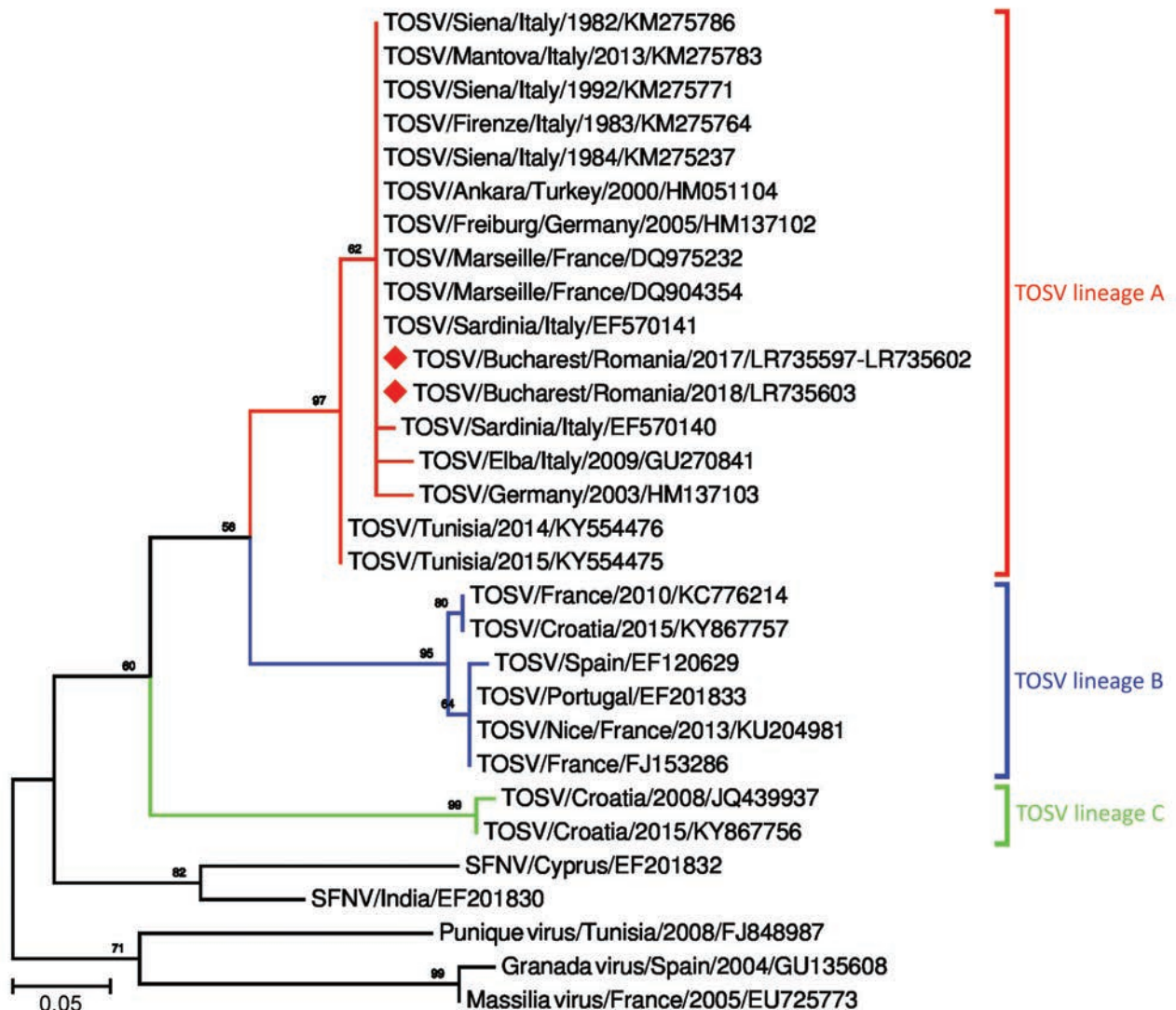


Figure. Phylogenetic tree of TOSV identified in 8 patients, Bucharest and surrounding area, Romania, 2017–2018, and reference sequences. Red diamonds indicate sequence obtained in this study; the other sequences included in the analysis were retrieved from GenBank. Numbers at nodes represent bootstrap percentages (values <50% are not shown). Phylogenetic relatedness was inferred from a 111-nt sequence of nucleocapsid gene, small segment (positions 1392–1502, numbering according to GenBank accession no. NC_006318.1) by using the neighbor-joining, Kimura 2-parameter method and 1,000 bootstrap replicates. SFNS, sandfly fever Naples virus; TOSV, Toscana virus.

(6). Progression to severe illness might be linked to older age, and this observation might be biased by the selection of cases referred to a tertiary-care hospital with an intensive care unit. TOSV has been previously associated with human neurologic infections, ranging from mild disease to severe cases, both in the autochthonous population and in travelers, but with a low mortality rate (1,7,8). A case of severe meningoencephalitis was previously reported in a brother and sister, both of whom recovered but had neurologic sequelae (9). Other neurologic manifestations such as Guillain-Barré syndrome, polymyeloradiculopathy, hydrocephalus, change of personality, or hearing loss have been described (4).

In our study, the diagnosis relied on rRT-PCR detection of the viral RNA, followed by amplicon sequencing, because very few samples showed serologic reactivity. Negative results obtained when the samples were tested by using standard nested PCRs for large and medium genes can be explained by the low viral load, as indicated by the high cycle threshold values (34.61–41.18) in rRT-PCR tests. Viral RNA was detected only in serum and CSF samples collected during the first 1–4 days after illness onset; urine proved to be a valuable specimen for molecular diagnosis, as previously reported (10).

The reason for the poor performance of serologic assays in our case series is not clear but might be related to the patients' immune status. An enzyme immunoassay test did not demonstrate high sensitivity, as previously reported, and the average percentage agreement between the commercial assays we used was low (57.8%), an observation also made by other researchers (10,11). On the other hand, all of our patients had an abrupt onset of symptoms, including rapid progression and hospitalization (median 2.4 days from onset, range 1–5 days). Sampling took place very early after illness onset, when antibodies levels are low and difficult to detect, possibly before seroconversion. The rapid death of 5 of the 8 patients precluded longitudinal antibody testing. In these cases, detection of TOSV RNA by using rRT-PCR, now the reference standard for TOSV diagnosis (2), was of paramount importance.

Genetic analysis based on a highly conserved 111-nt sequence showed that the circulating virus in Romania belonged to lineage A. This lineage has been described in Italy and southern France, in northern Africa (Tunisia), and in central and northern Anatolia (Turkey), but to our knowledge had never before recorded in southeastern Europe. Lineage B genotype has been reported in Spain, France, Portugal, Croatia, Morocco, and Turkey (4). A new

genetic lineage of TOSV (lineage C) has been detected in Croatia, where it was co-circulating with lineage B TOSV (12). A novel variant of TOSV most closely related to lineage C has been detected in Greece (7,13). Other co-circulation of different lineages has been reported France and Turkey (lineages A and B) (4,6). No differences have been observed in the clinical picture or disease severity associated with these TOSV genotypes (1,4).

The emergence of TOSV in an urban area in southeastern Romania warrants attention to the sand fly vector. During 1939–1952, according to clinical records, sand fly viruses causing sandfly fever (i.e., 3-day fever or pappataci fever), transmitted by *Phlebotomus papatasi* sandflies, were thought to be circulating in southern Romania, with outbreaks occurring during the summer months. Bucharest and the surrounding Ilfov County area were thought to have been affected during 1944–1946 (14).

No recent data on sand flies are available for urban Bucharest and its surrounding area. During recent years, the distribution of some *Phlebotomus* sand fly species harboring TOSV was updated for Romania, including *P. perfiliewi*, *P. neglectus*, *P. sergenti*, but not *P. perniciosus* (15). Given that only a handful of severe cases were diagnosed at a tertiary-care hospital, the real magnitude of TOSV human infections and those of affected areas are unknown and warrant further study.

Acknowledgments

The authors acknowledge valuable advice regarding laboratory diagnosis of Toscana virus, kindly offered by Remy Charrel.

The laboratory component of this work was supported by National Research Council/Advisory Council for Research Development and Innovation-Executive Unit for the Financing of Higher Education, Research, Development and Innovation (project no. PN-III-P1.2-PCCDI-2017-0005/2018, as part of National Research-Development and Innovation Plan III).

About the Author

Dr. Popescu, is an assistant professor in the Virology Department of Carol Davila University of Medicine and Pharmacy, head of the Infectious and Tropical Diseases Department of Dr. Victor Babes Clinical Hospital of Infectious and Tropical Diseases, and a member of the European Society of Clinical Microbiology and Infectious Diseases Study Group for Infectious Diseases of the Brain. His current research focuses on viral infections of the central nervous system.

References

- Charrel RN, Bichaud L, de Lamballerie X. Emergence of Toscana virus in the Mediterranean area. *World J Virol.* 2012;1:135–41. <https://doi.org/10.5501/wjv.v1.i5.135>
- Charrel RN, Berenger JM, Laroche M, Ayhan N, Bitam I, Delaunay P, et al. Neglected vector-borne bacterial diseases and arboviruses in the Mediterranean area. *New Microbes New Infect.* 2018;26:S31–6. <https://doi.org/10.1016/j.nmni.2018.08.015>
- Barzon L. Ongoing and emerging arbovirus threats in Europe. *J Clin Virol.* 2018;107:38–47. <https://doi.org/10.1016/j.jcv.2018.08.007>
- Ayhan N, Charrel RN. An update on Toscana virus distribution, genetics, medical and diagnostic aspects. *Clin Microbiol Infect.* 2020;26:1017–23. <https://doi.org/10.1016/j.cmi.2019.12.015>
- Popescu CP, Florescu SA, Cotar AI, Badescu D, Ceianu CS, Zaharia M, et al. Re-emergence of severe West Nile virus neuroinvasive disease in humans in Romania, 2012 to 2017 – implications for travel medicine. *Travel Med Infect Dis.* 2018;22:30–5. <https://doi.org/10.1016/j.tmaid.2018.03.001>
- Erdem H, Ergunay K, Yilmaz A, Naz H, Akata F, Inan AS, et al. Emergence and co-infections of West Nile virus and Toscana virus in Eastern Thrace, Turkey. *Clin Microbiol Infect.* 2014;20:319–25. <https://doi.org/10.1111/1469-0691.12310>
- Papa A, Paraforou T, Papakonstantinou I, Pagdatoglou K, Kontana A, Koukoubani T. Severe encephalitis caused by Toscana virus, Greece. *Emerg Infect Dis.* 2014;20:1417–9. <https://doi.org/10.3201/eid2008.140248>
- Dupouey J, Bichaud L, Ninove L, Zandotti C, Thirion-Perrier L, de Lamballerie X, et al. Toscana virus infections: a case series from France. *J Infect.* 2014;68:290–5. <https://doi.org/10.1016/j.jinf.2013.11.006>
- Baldelli F, Ciufolini MG, Francisci D, Marchi A, Venturi G, Fiorentini C, et al. Unusual presentation of life-threatening Toscana virus meningoencephalitis. *Clin Infect Dis.* 2004;38:515–20. <https://doi.org/10.1086/381201>
- Ergunay K, Ayhan N, Charrel RN. Novel and emergent sandfly-borne phleboviruses in Asia Minor: a systematic review. *Rev Med Virol.* 2017;27:27. <https://doi.org/10.1002/rmv.1898>
- Ergunay K, Litzba N, Lo MM, Aydoğan S, Saygan MB, Us D, et al. Performance of various commercial assays for the detection of Toscana virus antibodies. *Vector Borne Zoonotic Dis.* 2011;11:781–7. <https://doi.org/10.1089/vbz.2010.0224>
- Ayhan N, Alten B, Ivovic V, Martinkovic F, Kasap OE, Ozbel Y, et al. Cocirculation of two lineages of Toscana virus in Croatia. *Front Public Health.* 2017;5:336. <https://doi.org/10.3389/fpubh.2017.00336>
- Papa A. Emerging arboviruses of medical importance in the Mediterranean region. *J Clin Virol.* 2019;115:5–10. <https://doi.org/10.1016/j.jcv.2019.03.007>
- Lupașcu G, Agvriloaei P, Costin ME, Zelig M, Radvov G, Feodorovici S, et al. Contributions to the study of pappataci fever [in Romanian]. *Rev Stiint Med.* 1956;8:265–9.
- Cazan CD, Păstrav IR, Ionică AM, Oguz G, Erisoz Kasap O, Dvorak V, et al. Updates on the distribution and diversity of sand flies (Diptera: Psychodidae) in Romania. *Parasit Vectors.* 2019;12:247. <https://doi.org/10.1186/s13071-019-3507-7>

Address for correspondence: Corneliu Petru Popescu, Carol Davila University of Medicine and Pharmacy, Dr. Victor Babes Clinical Hospital of Infectious and Tropical Diseases, Sos Mihai Bravu 281, Sector 3, Bucharest, Romania; email: cornel160@yahoo.com

EID Podcast Telework during Epidemic Respiratory Illness



The COVID-19 pandemic has caused us to reevaluate what “work” should look like. Across the world, people have converted closets to offices, kitchen tables to desks, and curtains to videoconference back-grounds. Many employees cannot help but wonder if these changes will become a new normal.

During outbreaks of influenza, corona-viruses, and other respiratory diseases, telework is a tool to promote social distancing and prevent the spread of disease. As more people telework than ever before, employers are considering the ramifications of remote work on employees’ use of sick days, paid leave, and attendance.

In this EID podcast, Dr. Faruque Ahmed, an epidemiologist at CDC, discusses the economic impact of telework.

Visit our website to listen:
<https://go.usa.gov/xfcM>

**EMERGING
INFECTIOUS DISEASES®**

SARS CoV-2 Serial Interval Variation, Montana, USA, March 1–July 31, 2020

Isaiah G. Reed, Ethan S. Walker, Erin L. Landguth

We report mean severe acute respiratory syndrome coronavirus 2 serial intervals for Montana, USA, from 583 transmission pairs; infectors' symptom onset dates occurred during March 1–July 31, 2020. Our estimate was 5.68 (95% CI 5.27–6.08) days, SD 4.77 (95% CI 4.33–5.19) days. Subperiod estimates varied temporally by nonpharmaceutical intervention type and fluctuating incidence.

In support of efforts in response to the emergence of severe acute respiratory syndrome coronavirus 2 (SARS-CoV-2), the pathogen causing novel coronavirus disease (COVID-19), the scientific community has attempted to predict its transmission trends, often through disease modeling. However, disease-specific parameter estimates for SARS-CoV-2 vary greatly. These parameters include the serial interval (SI), or the duration between onset of symptoms in connected primary and secondary cases, which is crucial in estimating epidemic reproduction numbers (R_0) and assessing the effects of nonpharmaceutical interventions (NPIs) on transmission (1). Recent studies report SARS-CoV-2 SIs ranging from 2.97 to 7.5 days, with estimates representing primarily densely populated and urban settings (Table 1; Figure 1). The rural United States was relatively untouched in early epidemic waves, but major outbreaks followed in subsequent waves, so it is unknown whether rural- and urban-based transmission differ. Our objective was to report and compare SARS-CoV-2 SI values for Montana, USA, a primarily rural population, with other global and urban estimates. The study was defined as a public health surveillance activity by the University of Montana Institutional Review Board.

Author affiliations: Montana Department of Public Health and Human Services, Helena, Montana, USA (I.G. Reed); University of Montana, Missoula, Montana, USA (E.S. Walker, E.L. Landguth)

DOI: <https://doi.org/10.3201/eid2705.204663>

The Study

We acquired COVID-19 data, reported by local health jurisdictions, from the Montana Department of Public Health and Human Services; we obtained 45,102 case records as of November 15, 2020. We examined a subset of cases with symptom onset dates during March 1–July 31, 2020 ($n = 4,793$), as well as secondary cases resulting from primary infections during that period, regardless of onset date. We selected this period because all reported cases were PCR positive, all NPI stages were represented (pre-shelter-in-place [pre-SIP], shelter-in-place [SIP], and reopening phase 1 and phase 2), and the proportion of identifiable transmission chains among cases was relatively high (March–June 39%–44%; July 11%) compared with later periods (August–November 0%–2%).

We assessed the records to identify all epidemiologic links. We defined links as cases having contact with another reported case, when viral infection through accepted modes of transmission was plausible. Linked records ($n = 1,005$) were organized into pairs and designated as primary or secondary cases. When appropriate, cases were listed as primaries for multiple secondary cases; however, cases were limited to 1 secondary designation. For some secondary cases, 1 specific primary was not clearly defined. To estimate a serial range in these situations, we assigned upper and lower bounds using the shortest and longest SIs from all possible primaries. We excluded records when we could not determine an epidemiologic link or transmission direction. We identified 583 pairs, with 466 primary and 583 secondary cases.

We gave temporal markers to pairs on the basis of the primary case's symptom onset date, consistent with forward-looking SIs (2), and grouped them by the corresponding statewide NPI: pre-SIP, March 1–27; SIP, March 28–April 25; phase 1, April 26–May 31; phase 2 (June), June 1–30; and phase 2 (July), July 1–31. We divided phase 2 into 2 subperiods to account for changing incidence trends.

Table 1. Published mean serial interval estimates for severe acute respiratory syndrome coronavirus 2, 2020*

Publication†	Study location, dates (all in 2020 except as indicated)	No. cases (pairs)	SI mean (95% CI)	SI SD (95% CI)	SI estimate method
This study	Montana, USA, Mar 1–Jul 31	4,793 (583)	5.68 (5.27–6.08)	4.77 (4.33–5.19)	Forward
Prete et al. (13)‡	Brazil, Feb 25–Mar 19	NA (65)	2.97	3.29	Other
Talmoudi et al. (14)‡	Tunisia, Feb 29–May 5	NA (491)	5.30 (4.66–5.95)	0.26 (0.23–0.30)	Other
Lavezzo et al. (15)	Vo', Italy, Feb 21–Mar 7	81 (41)	7.2 (5.9–9.6)	NA	Other
Aghaali et al. (16)	Qom, Iran, Feb 20–Mar 8	88 (37)	4.55	3.30	Forward
You et al. (17)‡	China (OHP), as of Mar 31	14,828 (198)	4.60	5.55	Intrinsic
Ali et al. (1)‡	China (OHP), Jan 9–Feb 13	9,120 (677)	5.1 (4.7–5.5)	5.3 (5.0–5.6)	Forward
Zhang et al. (18)	China (OHP), Jan 19–Feb 17	8,579 (35)	5.1 (1.3–11.6)	NA	Forward
Du et al. (10)‡	China (OHP), Jan 21–Feb 8	752 (468)	3.96 (3.53–4.39)	4.75 (4.46–5.07)	Backward
Liao et al. (19)	China (CTGCH), Jan 7–Mar 20	46 (12)	6.50 (2.45–17.38)	NA	Forward
Zhao et al. (20)	Hong Kong, Jan 16–Feb 15	56 (21)	4.9 (3.6–6.2)	4.4 (2.9–8.3)	Other
Chan et al. (21)	Hong Kong, Jan 23–Apr 6	915 (47)	6.5 (0–18)	4.7	Unknown
Bi et al. (22)	Shenzhen, China, Jan 14–Feb 9	391 (48)	6.3 (5.2–7.6)	4.2 (3.1–5.3)	Other
Wang et al. (23)	Shenzhen, China, Jan 19–Feb 22	417 (27)	5.9 (3.9–9.6)	4.8 (3.1–10.1)	Other
Ganyani et al. (24)‡	Tianjin, China, Jan 14–Feb 27	135 (NA)	3.95 (–4.47 to 12.51)	4.24 (4.03–4.95)	Other
Tindale et al. (25)	Tianjin, China, Jan 21–Feb 22	135 (72)	4.31 (2.91–5.72)	0.716	Forward
Li et al. (26)	Wuhan, China, as of Jan 22	425 (6)	7.5 (5.3–19.0)	3.4	Other
Ganyani et al. (24)‡	Singapore, Jan 21–Feb 26	91 (NA)	5.21 (–3.35 to 13.94)	4.32 (4.06–5.58)	Other
Tindale et al. (25)	Singapore, Jan 23–Feb 26	93 (56)	4.17 (2.44–5.89)	0.882	Forward
Ki et al. (27)	South Korea, Jan 10–Feb 10	28 (12)	6.6 (3–15)	NA	Unknown
Mettler et al. (12)‡	South Korea, Jan 20–Jun 30	5,201 (102)	3.43 (2.62–4.24)	NA	Forward
Chun et al. (28)‡	South Korea, Jan 23–Mar 31	9,887 (69)	3.18 (2.22–4.24)	0.75 (0.47–1.03)	Forward
Son et al. (29)	Busan, South Korea, Feb 21–Mar 24	108 (28)	5.54 (4.08–7.01)	3.90 (2.47–5.32)	Other
Nishiura et al. (30)	Meta-analysis, 2019 Dec 21–2020 Feb 12	NA (28)	4.7 (3.7–6.0)	2.9 (1.9–4.9)	Other
He et al. (11)‡	Meta-analysis, Jan 21–Feb 12	NA (77)	5.8 (4.8–6.8)	NA	Other

*All articles published during 2020 except this study. CTGCH, Chongqing Three Gorges Central Hospital; NA, not available; OHP, outside Hubei Province; SARS-CoV-2, severe acute respiratory syndrome coronavirus 2; SI, serial interval.

†See References and Appendix (<https://wwwnc.cdc.gov/EID/article/27/5/20-4663-App1.pdf>) for full publication information.

‡Study included negative-valued serial interval pairs in the estimate.

We analyzed data using R version 3.6.2 and the EpiEstim package (3,4). Complying with EpiEstim functional requirements, we assigned pairs with a zero-valued SI an upper bound of 1 day, with lower bounds unchanged ($n = 52$ pairs). No negative-valued SIs were identified. We excluded pairs with a SI >2 incubation periods (>28 days). We determined that a gamma distribution was most appropriate using the R0 package *est.GT* function (5). Next, we used EpiEstim *estimate_R*, with case-pair and daily incidence data, to perform a Bayesian estimation of the SI gamma distribution using Markov chain Monte Carlo specified for the joint posterior sample of possible SI values (6,7).

Montana's overall mean SI estimate was 5.68 (95% CI 5.27–6.08) days (SD 4.77 [95% CI 4.33–5.19] days) (Figure 2). Pre-SIP provided the longest subperiod estimate, 6.84 (95% CI 5.84–7.87) days. The SI shortened during SIP, to 5.54 (95% CI 3.34–8.26) days, and again during phase 1, to 5.26 (95% CI 3.64–7.21) days. However, the SI lengthened during phase 2 (June) to 6.23 (95% CI 5.59–6.85) days, almost reaching pre-SIP levels. Phase 2 (July) demonstrated a sharp reduction to the shortest SI observed, 4.42 (95% CI 3.92–4.93) days. Sensitivity analyses of NPI impact delays resulted in altered subperiod estimates, especially

for phase 1 relative to other subperiods (Table 2). Additional sensitivity analyses, comparing forward- and backward-looking SIs, produced vastly dissimilar point estimates and trends.

Conclusions

Analysis of SARS-CoV-2 transmission in Montana during March 1–July 31, 2020, identified a mean SI of 5.68 (95% CI 5.27–6.08) days, falling within the bounds of 16 of 24 published estimates from more urbanized settings across the globe (Table 1; Figure 1). However, an aggregate estimate derived from data spanning multiple outbreak stages may not accurately describe Montana-based transmission because changing contact patterns and environmental influences may cause variation (1,2). Temporal analyses suggest that NPIs influenced transmission patterns, as demonstrated by Montana's epidemic curve and fluctuating SI values (Figure 2). Ali found that SIs shorten as stricter NPIs are applied (1,8), which our subperiod estimates mostly support. However, phase 2 (July) contradicts the premise, with the shortest subperiod SI and a less restrictive NPI (Table 2). Furthermore, when accounting for NPI impact delays, the alignment falters during phase 2. This difference may occur because Ali did not assess additional epidemic

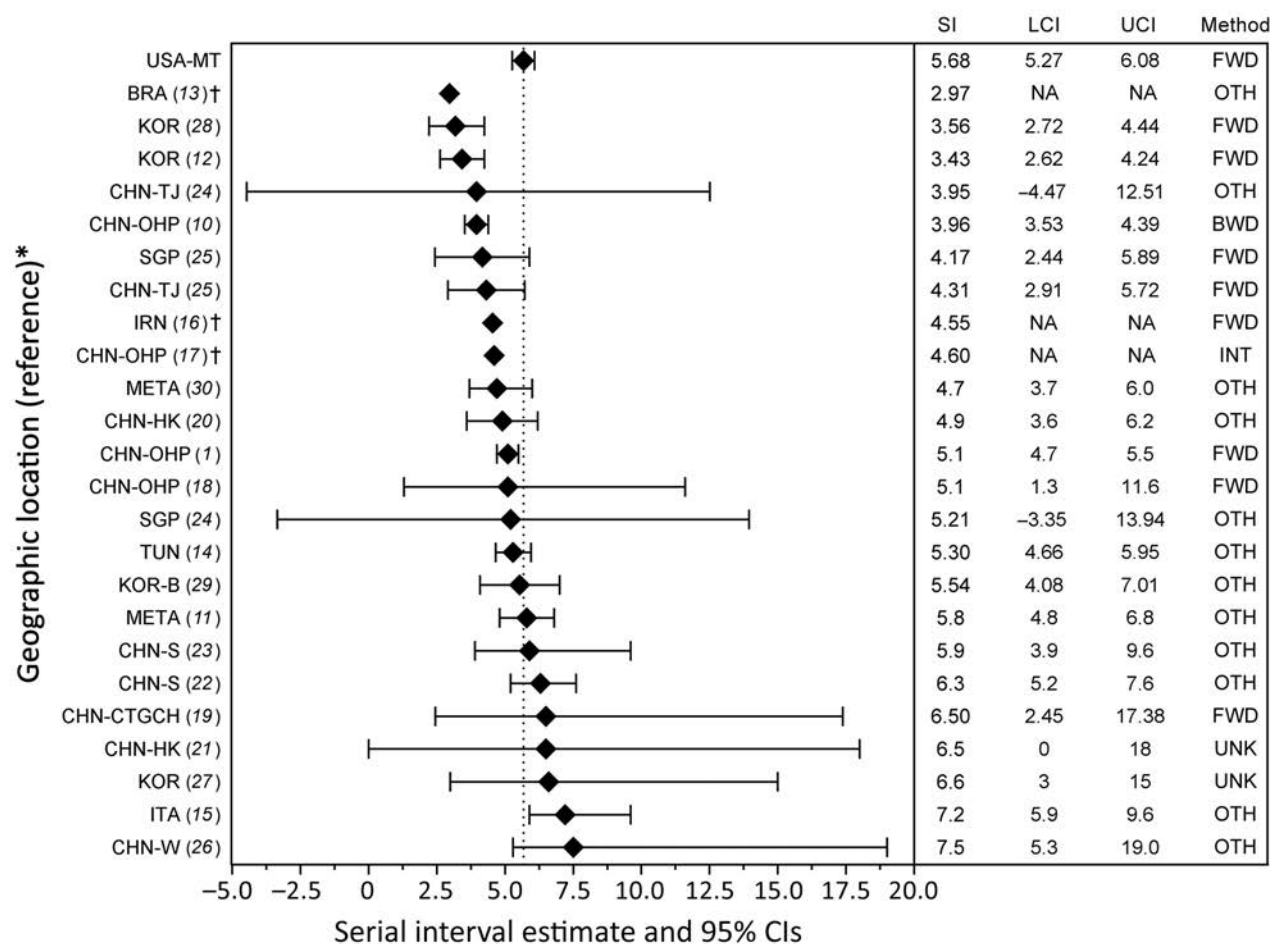


Figure 1. Published mean serial interval estimates for severe acute respiratory syndrome coronavirus 2. *See References and Appendix (<https://wwwnc.cdc.gov/EID/article/27/5/20-4663-App1.pdf>) for full study information. †These studies did not report CIs. Only point estimates are given. BRA, Brazil; BWD, backward; CHN-CTGCH, China–Chongqing Three Gorges Central Hospital; CHN-HK, China–Hong Kong; CHN-OHP, China–outside Hubei Province; CHN-S, China–Shenzhen; CHN-TJ, China–Tianjin; CHN-W, China–Wuhan; FWD, forward; INT, intrinsic; IRN, Iran; ITA, Italy; KOR, South Korea; KOR-B, South Korea–Busan; LCI, lower confidence interval; META, meta-analysis; NA, data not available; OTH, other; SGP, Singapore; TUN, Tunisia; UCI, upper confidence interval; UNK, unknown; USA-MT, United States–Montana.

waves, which complicates direct NPI comparisons (1). Park agreed with Ali, while also offering a mathematical proof for the relationship between epidemic growth rates, calculated from incidence data, and forward-looking SIs (2,9). Park showed that as growth rates increase, forward SIs lengthen, and that when incidence decreases (either over time or because of external factors) forward SIs shorten (2). This better describes Montana's incidence and our subperiod estimates, with NPIs providing context (Figure 2). Increased incidence and longer SIs during pre-SIP and phase 2 (June) stem from nonexistent and relaxed NPIs, whereas decreased incidence and shorter SIs during SIP and phase 2 (July) likely result from stricter NPIs and increased

compliance with public health recommendations (e.g., mask wearing and social distancing). Additional data describing social compliance would benefit this interpretation.

The first limitation of this study is that the proportion of cases with identifiable transmission chains was lower during July than in previous periods. Despite this limitation, we felt it was necessary to report an SI for a period experiencing sizable incidence fluctuations. In addition, whereas others have reported negative-valued SIs among 1.2%–14.46% of infector–infectee pairs (10–14), we failed to identify any within our data. This difference could be caused by multiple factors, including incorrectly reported symptom onset dates,

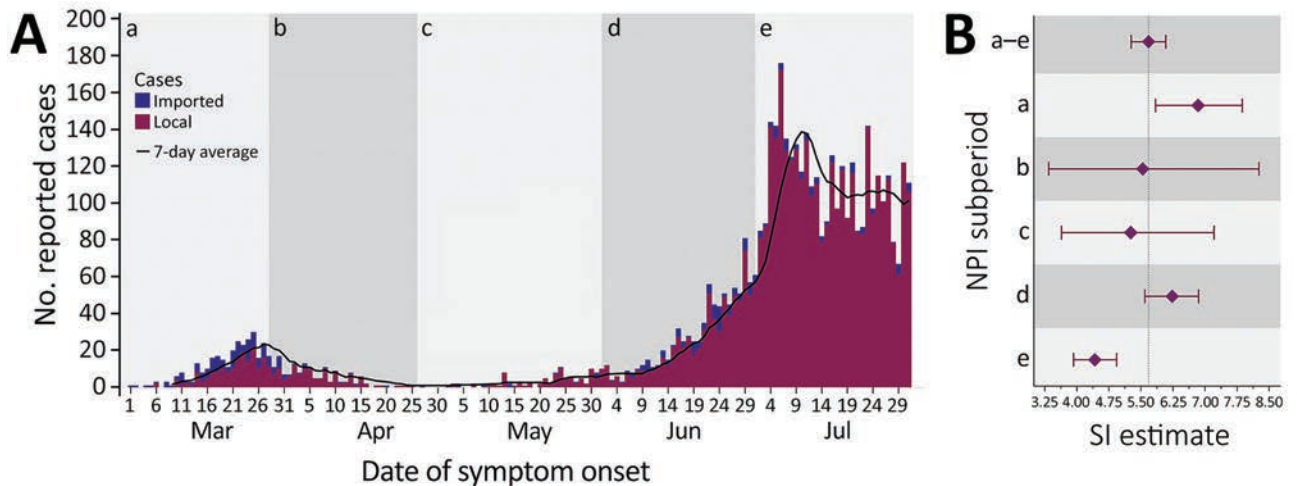


Figure 2. Reported COVID-19 cases and SARS-CoV-2 SI estimates by NPI subperiod, Montana, USA, March 1–July 31, 2020. A) COVID-19 cases, by date of symptom onset. Total cases, 4,793; total pairs, 583. For subperiod pair totals, see the Forward section of Table 2. B) SI estimates and 95% CIs (error bars). Overall mean SI was 5.68 (95% CI 5.27–6.08) days, overall SD 4.77 (95% CI 4.33–5.19) days. For subperiod SI and SD estimates, see the Forward section of Table 2. SI estimates are forward-looking and are based on the symptom onset date of the primary case in the infector–infectee pair. NPI subperiods: a) Pre-SIP, March 1–27, no NPIs in place; no. cases, 285. b) SIP, March 28–April 25, statewide stay-at-home order instituted and all nonessential businesses closed; no. cases, 168. c) Phase 1, April 26–May 31, statewide stay-at-home order lifted and limited business types allowed to open with reduced capacity; no. cases, 99. d) Phase 2 (June), June 1–30, all business types allowed to open under less restrictive capacity regulations; no. cases, 824. e) Phase 2 (July), July 1–31, all business types allowed to open under less restrictive capacity regulations; no. cases, 3,417. Black line is the average number of cases for the preceding 7 days. Imported case: COVID-19 case linked to out-of-state OR out-of-county transmission; local case: nonimported COVID-19 case linked to in-state AND in-county transmission. COVID-19, coronavirus disease 2019; SARS-CoV-2, severe acute respiratory syndrome coronavirus 2; SI, serial interval; SIP, shelter-in-place.

misidentified transmission direction between pairs, or both. However, the absence of negative SIs was not unique to our study; 14 of 24 published SI estimates did not include negative-valued pairs (Table 1).

Furthermore, to include pairs with a zero-valued SI, our study required changing their upper range. A sensitivity analysis of the adjustment showed minimal impact to the resulting estimate, whereas another sensitivity analysis, examining zero-valued pairs' exclusion, returned a substantially elevated estimate. These analyses indicate that non-traditional SIs play key roles in generation time, SI, and R_0 studies, especially for SARS-CoV-2, and that inclusive methods should be used when possible.

Our study offers evidence that rural-based SARS-CoV-2 SI estimates are consistent with those describing transmission occurring in urban settings. Furthermore, temporal variations in incidence, which can be caused by NPIs, must be considered when assessing SI distributions and other transmission measures. More period-based analyses of varying NPIs and their effects on transmission dynamics would help corroborate these findings.

Acknowledgments

We thank Montana's local county and tribal health jurisdictions for their dedication and commitment in responding to the COVID-19 pandemic and for collecting the data used in this study. We also thank the Montana Department of Public Health and Human Services, Communicable Disease Epidemiology Section, for allowing us access to the state's COVID-19 case investigation data; the authors of the serial interval publications referenced in this paper who kindly responded to our inquiries concerning their studies; as well as Todd Harwell, Curtis Noonan, Erin Semmens, Jeffrey Shaman, Scott Whittenburg, Laura Williamson, and the anonymous reviewers for offering feedback on the manuscript.

This research was supported by the National Institute of General Medical Sciences of the National Institutes of Health (NIH), United States (award no. P20GM130418) and Montana state special revenue funds.

About the Author

Mr. Reed is an epidemiologist with the Office of Epidemiology and Scientific Support at the Montana Department of Public Health and Human Services, where

Table 2. Sensitivity analyses: forward and backward severe acute respiratory syndrome coronavirus 2 serial interval estimates by nonpharmaceutical intervention subperiod and length of intervention effects delay*

SI estimate method	NPI subperiod	Measure	Sensitivity analysis scenarios†		
			No delay	1-week delay	2-week delay
Forward: onset of primary case	Pre-shelter-in-place, Mar 1–27	No. pairs	95	105	113
		Mean SI (95% CI)	6.84 (5.84–7.87)	6.83 (5.67–8.07)	6.66 (5.61–7.80)
		SD (95% CI)	5.56 (4.45–6.80)	5.78 (4.48–7.24)	5.61 (4.50–6.84)
	Shelter-in-place, Mar 28–Apr 25	No. pairs	20	10	3
		Mean SI (95% CI)	5.54 (3.34–8.26)	4.08 (2.61–5.85)	2.46 (1.24–4.10)
		SD (95% CI)	5.30 (2.69–8.76)	2.83 (1.47–4.66)	1.52 (0.38–3.38)
	Reopening, phase 1, Apr 26–May 31	No. pairs	25	64	114
		Mean SI (95% CI)	5.26 (3.64–7.21)	7.45 (6.02–9.02)	7.10 (6.08–8.16)
		SD (95% CI)	4.74 (2.86–7.09)	6.24 (4.70–8.03)	5.82 (4.77–6.99)
	Reopening, phase 2, Jun 1–30	No. pairs	248	296	289
		Mean SI (95% CI)	6.23 (5.59–6.85)	5.39 (4.88–5.94)	5.08 (4.56–5.59)
		SD (95% CI)	5.32 (4.61–6.05)	4.59 (4.01–5.21)	4.32 (3.75–4.94)
	Reopening, phase 2, Jul 1–31	No. pairs	195	117	76
		Mean SI (95% CI)	4.42 (3.92–4.93)	4.20 (3.65–4.78)	3.98 (3.36–4.67)
		SD (95% CI)	3.51 (2.97–4.06)	3.20 (2.65–3.80)	2.90 (2.29–3.60)
Backward: onset of secondary case	Pre-shelter-in-place, Mar 1–27	No. pairs	61	89	105
		Mean SI (95% CI)	4.82 (3.88–5.84)	5.83 (4.86–6.82)	6.48 (5.55–7.51)
		SD (95% CI)	3.84 (2.88–4.93)	4.91 (3.86–6.08)	5.50 (4.44–6.63)
	Shelter-in-place, Mar 28–Apr 25	No. pairs	54	26	11
		Mean SI (95% CI)	8.57 (6.77–10.58)	9.03 (6.73–11.66)	7.58 (4.29–11.83)
		SD (95% CI)	6.95 (5.10–8.99)	6.52 (4.28–9.22)	6.21 (2.91–10.73)
	Reopening, phase 1, Apr 26–May 31	No. pairs	19	30	62
		Mean SI (95% CI)	3.79 (2.46–5.37)	4.95 (3.53–6.60)	4.57 (3.64–5.60)
		SD (95% CI)	3.10 (1.70–4.90)	4.41 (2.78–6.43)	3.73 (2.72–4.90)
	Reopening, phase 2, Jun 1–30	No. pairs	202	280	310
		Mean SI (95% CI)	5.38 (4.72–6.08)	5.14 (4.64–5.67)	5.22 (4.73–5.77)
		SD (95% CI)	4.59 (3.86–5.41)	4.31 (3.77–4.90)	4.38 (3.85–4.97)
	Reopening, phase 2, Jul 1–31	No. pairs	233	161	106
		Mean SI (95% CI)	5.43 (4.85–6.05)	5.82 (5.12–6.56)	6.45 (5.37–7.57)
		SD (95% CI)	4.52 (3.90–5.17)	4.88 (4.14–5.70)	5.41 (4.35–6.64)

*NPI, nonpharmaceutical intervention; SI, serial interval.

†Serial interval estimation methods and delay scenarios contain dissimilar pair totals because of their temporal differences (forward pairs, n) no delay: 583; 1-week delay: 592; 2-week delay: 595; (backward pairs, n) no delay: 569; 1-week delay: 586; 2-week delay: 594.

he manages the state's hospital discharge data and public health data visualization systems. His primary research interests include infectious disease modeling, vectorborne disease, and global health.

References

- Ali ST, Wang L, Lau EHY, Xu XK, Du Z, Wu Y, et al. Serial interval of SARS-CoV-2 was shortened over time by nonpharmaceutical interventions. *Science*. 2020;369:1106–9. <https://doi.org/10.1126/science.abc9004>
- Park SW, Sun K, Champredon D, Li M, Bolker BM, Earn DJD, et al. Forward-looking serial intervals correctly link epidemic growth to reproduction numbers. *Proc Natl Acad Sci U S A*. 2021;118:e2011548118. <https://doi.org/10.1073/pnas.2011548118>
- R Core Team. R: A language and environment for statistical computing. Vienna: R Foundation for Statistical Computing; 2019 [cited 2021 Feb 11]. <https://www.R-project.org>
- Cori A. EpiEstim: estimate time varying reproduction numbers from epidemic curves. R package version 2.2–1; 2019 [cited 2021 Feb 11]. <https://CRAN.R-project.org/package=EpiEstim>
- Boelle P, Obadia T. R₀: estimation of R⁰ and real-time reproduction number from epidemics. R package version 1.2–6; 2015 [cited 2021 Feb 11]. <https://CRAN.R-project.org/package=R0>
- Reich NG, Lessler J, Cummings DAT, Brookmeyer R. Estimating incubation period distributions with coarse data. *Stat Med*. 2009;28:2769–84. <https://doi.org/10.1002/sim.3659>
- Thompson RN, Stockwin JE, van Gaalen RD, Polonsky JA, Kamvar ZN, Demarsh PA, et al. Improved inference of time-varying reproduction numbers during infectious disease outbreaks. *Epidemics*. 2019;29:100356. <https://doi.org/10.1016/j.epidem.2019.100356>
- Griffin J, Casey M, Collins Á, Hunt K, McEvoy D, Byrne A, et al. Rapid review of available evidence on the serial interval and generation time of COVID-19. *BMJ Open*. 2020;10:e040263. <https://doi.org/10.1136/bmjopen-2020-040263>
- Ma J, Dushoff J, Bolker BM, Earn DJD. Estimating initial epidemic growth rates. *Bull Math Biol*. 2014;76:245–60. <https://doi.org/10.1007/s11538-013-9918-2>
- Du Z, Xu X, Wu Y, Wang L, Cowling BJ, Meyers LA. Serial interval of COVID-19 among publicly reported confirmed cases. *Emerg Infect Dis*. 2020;26:1341–3. <https://doi.org/10.3201/eid2606.200357>
- He X, Lau EHY, Wu P, Deng X, Wang J, Hao X, et al. Temporal dynamics in viral shedding and transmissibility of COVID-19. *Nat Med*. 2020;26:672–5. <https://doi.org/10.1038/s41591-020-0869-5>
- Mettler SK, Kim J, Maathuis MH. Diagnostic serial interval as a novel indicator for contact tracing effectiveness exemplified with the SARS-CoV-2/COVID-19 outbreak in South Korea.

Int J Infect Dis. 2020;99:346–51. <https://doi.org/10.1016/j.ijid.2020.07.068>

13. Prete CA, Buss L, Dighe A, Porto VB, da Silva Candido D, Ghilardi F, et al. Serial interval distribution of SARS-CoV-2 infection in Brazil. *J Travel Med.* 2021;28:taaa115. <https://doi.org/10.1093/jtm/taaa115>
14. Talmoudi K, Safer M, Letaief H, Hchaichi A, Harizi C, Dhaouadi S, et al. Estimating transmission dynamics and serial interval of the first wave of COVID-19 infections under

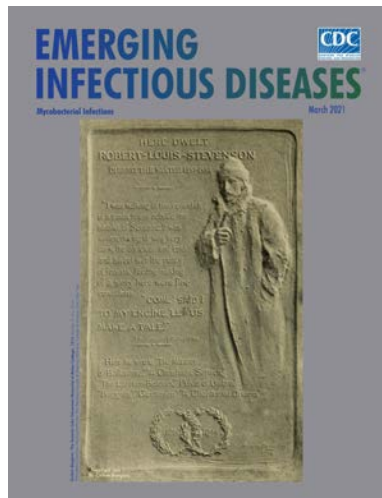
different control measures: a statistical analysis in Tunisia from February 29 to May 5, 2020. *BMC Infect Dis.* 2020;20:914. <https://doi.org/10.1186/s12879-020-05577-4>

Address for correspondence: Isaiah G. Reed, Montana Department of Public Health and Human Services, 1400 Broadway, Rm A113, PO Box 202951, Helena, MT 59620-2951, USA; email: isaiah.reed@mt.gov

March 2021

Mycobacterial Infections

- Parallels and Mutual Lessons in Tuberculosis and COVID-19 Transmission, Prevention, and Control
- Genomic Evidence of In-Flight Transmission of SARS-CoV-2 Despite Predeparture Testing
- Evaluation of National Event-Based Surveillance, Nigeria, 2016–2018
- Clinical Features and Comparison of Kingella and Non-Kingella Endocarditis in Children, Israel
- Use of US Public Health Travel Restrictions during COVID-19 Outbreak on Diamond Princess Ship, Japan, February–April 2020
- Systematic Review of Pooling Sputum as an Efficient Method for Xpert MTB/RIF Tuberculosis
- Testing during COVID-19 Pandemic Decentralized Care for Rifampicin-Resistant Tuberculosis, Western Cape, South Africa
- Transmission of Antimicrobial-Resistant *Staphylococcus aureus* Clonal Complex 9 between Pigs and Humans, United States
- Epidemiology and Clinical Course of First Wave Coronavirus Disease Cases, Faroe Islands Oral Human Papillomavirus Infection in Children during the First 6 Years of Life, Finland
- Clusters of Drug-Resistant Mycobacterium tuberculosis Detected by Whole-Genome Sequence Analysis of Nationwide Sample, Thailand, 2014–2017



- Population-Based Geospatial and Molecular Epidemiologic Study of Tuberculosis Transmission Dynamics, Botswana, 2012–2016
- Extrapulmonary Nontuberculous Mycobacteria Infections in Hospitalized Patients, United States, 2010–2014
- Genomic Characterization of hlyF-positive Shiga Toxin-Producing *Escherichia coli*, Italy and the Netherlands, 2000–2019
- Isolate-Based Surveillance of *Bordetella pertussis*, Austria, 2018–2020
- Decline of Tuberculosis Burden in Vietnam Measured by Consecutive National Surveys, 2007–2017
- Foodborne Origin and Local and Global Spread of *Staphylococcus saprophyticus* Causing Human Urinary Tract Infections
- Prevalence of SARS-CoV-2 Antibodies in First Responders and Public Safety Personnel, New York City, New York, USA, May–July 2020
- Local and Travel-Associated Transmission of Tuberculosis at Central Western Border of Brazil, 2014–2017
- Antibody Responses 8 Months after Asymptomatic or Mild SARS-CoV-2 Infection
- Lung Pathology of Mutually Exclusive Co-infection with SARS-CoV-2 and *Streptococcus pneumoniae*
- Daily Forecasting of Regional Epidemics of Coronavirus Disease with Bayesian Uncertainty
- Quantification, United States Fluconazole-Resistant *Candida glabrata* Bloodstream Isolates, South Korea, 2008–2018
- Excess All-Cause Deaths during Coronavirus Disease Pandemic, Japan, January–May 2020
- Mycoplasma genitalium and Other Reproductive Tract Infections in Pregnant Women, Papua New Guinea, 2015–2017
- Effectiveness of Preventive Therapy for Persons Exposed at Home to Drug-Resistant Tuberculosis, Karachi, Pakistan
- Familial Clusters of Coronavirus Disease in 10 Prefectures, Japan, February–May 2020

**EMERGING
INFECTIOUS DISEASES**

To revisit the March 2021 issue, go to:
<https://wwwnc.cdc.gov/eid/articles/issue/27/3/table-of-contents>

Introduction of ORF3a-Q57H SARS-CoV-2 Variant Causing Fourth Epidemic Wave of COVID-19, Hong Kong, China

Daniel K.W. Chu,¹ Kenrie P.Y. Hui,¹ Haogao Gu, Ronald L.W. Ko, Pavithra Krishnan, Daisy Y.M. Ng, Gigi Y.Z. Liu, Carrie K.C. Wan, Man-Chun Cheung, Ka-Chun Ng, John M. Nicholls, Dominic N.C. Tsang, Malik Peiris, Michael C.W. Chan, Leo L.M. Poon

We describe an introduction of clade GH severe acute respiratory syndrome coronavirus 2 causing a fourth wave of coronavirus disease in Hong Kong. The virus has an ORF3a-Q57H mutation, causing truncation of ORF3b. This virus evades induction of cytokine, chemokine, and interferon-stimulated gene expression in primary human respiratory cells.

Hong Kong, China, has had 4 waves of coronavirus disease (COVID-19) outbreaks since the emergence of severe acute respiratory syndrome coronavirus 2 (SARS-CoV-2) in December 2019. By February 1, 2021, Hong Kong had recorded 10,453 reverse transcription PCR (RT-PCR)-confirmed COVID-19 cases, and many of those occurred during the last 2 waves. The third wave occurred during late June to early September 2020 and was caused by a single introduction of GISAID (<https://platform.gisaid.org>) clade GR virus (1). The fourth wave began in early November 2020 and was caused by a newly introduced GISAID clade GH SARS-CoV-2 (1). We describe the origin of a clade GH virus causing the fourth epidemic wave in Hong Kong.

The Study

Before our investigation, epidemiologic investigations in early October 2020 revealed 2 local COVID-19 clusters associated with bar/building X or hotel C (Appendix Figure 1, <https://wwwnc.cdc.gov/EID/>

article/27/5/21-0015-App1.pdf), both of which are located in the same district of Hong Kong. The bar/building X cluster had 15 RT-PCR-confirmed COVID-19 cases (patients BB1–BB15), and the hotel C cluster had 9 RT-PCR-confirmed cases (patients C1–C9) (Figure 1).

To determine whether the 2 clusters were epidemiologically linked, we sequenced near full-length genomes from all available samples, including respiratory samples from patients BB1–BB13 and patients C1–C9, by using a previously described protocol (2,3). We found the viral genomes were highly similar (sequence identity $\geq 99.98\%$) (Appendix Figure 2). All sequences belonged to clade GH, which was not found in local COVID-19 cases during the third wave (1). Our results indicate that this newly introduced clade GH virus was circulating in the local community ≈ 1 month before the beginning of the fourth epidemic wave in Hong Kong.

We also noted 4 imported cases (patients A1–A4) in a nearby hotel (hotel A), which is ≈ 350 m walking distance from bar/building X and hotel C, during late September to early October 2020 (Figure 1; Appendix Table 1). Patients A1–A3 traveled from Nepal to Hong Kong on the same direct flight and had their mandatory quarantine in hotel A during September 9–20, 2020 (Appendix). Of note, 2 additional RT-PCR-confirmed cases, patients B1 and B2, traveled on the same flight as patients A1–A3 (Figure 1). B1 and B2 were unrelated to patients A1–A3 and had their mandatory quarantine in hotel B, which is in another district of Hong Kong. Our sequencing results indicate that the viral genomes of these 5 cases are identical or almost identical to those from the 2 local clusters (Appendix

Author affiliations: The University of Hong Kong, Hong Kong, China (D.K.W. Chu, K.P.Y. Hui, H. Gu, R.L.W. Ko, P. Krishnan, D.Y.M. Ng, G.Y.Z. Liu, C.K.C. Wan, M.-C. Cheung, K.-C. Ng, J.M. Nicholls, M. Peiris, M.C.W. Chan, L.L.M. Poon); Department of Health, Hong Kong (D.N.C. Tsang)

DOI: <https://doi.org/10.3201/eid2705.210015>

¹These first authors contributed equally to this article.

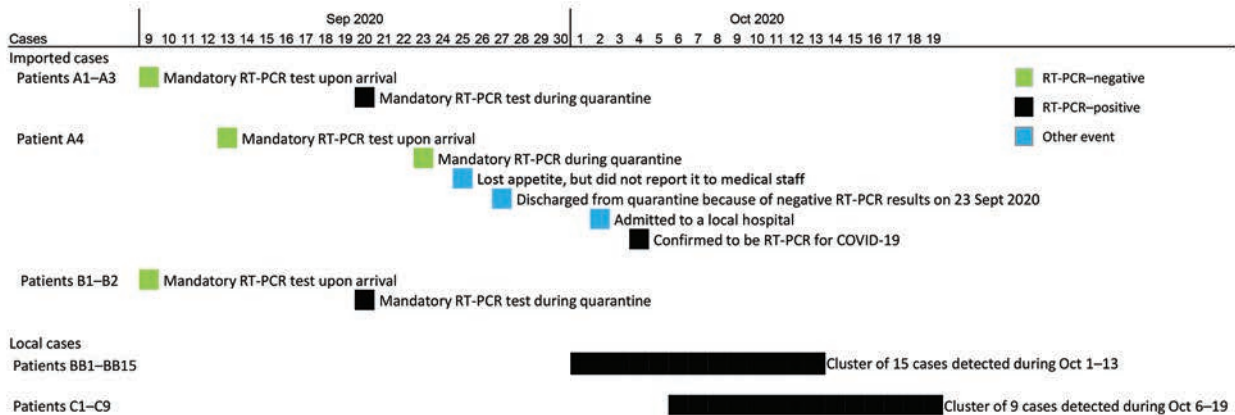


Figure 1. Timeline of COVID-19 cases during fourth epidemic, September 9–October 19, 2020, Hong Kong, China. Asymptomatic cases occurred in patients A1–A3, B1, B2, BB4, BB12, BB13, BB15, C3, C4, C7, and C9. Symptomatic cases occurred among patients A4, BB1–BB3, BB5–BB11, BB14, C1, C2, C5, C6, and C8. COVID-19, coronavirus disease; RT-PCR, reverse transcription PCR.

Figure 2). Although it is not known whether in-flight transmission occurred among patients A1–A3 and B1 and B2 (2), our results suggest that the fourth COVID-19 epidemic wave in Hong Kong was introduced from Nepal, and the deduced sequences are closely related to sequences from Nepal (Appendix Figure 2).

Patient A4, who was quarantined in hotel A during September 13–27, 2020, also traveled from Nepal to Hong Kong on a separate flight. The viral genome of case A4 is identical or closely related to sequences from patients A1–A3 and B1 and B2. Patient A4 had consecutive negative RT-PCR results upon arrival and on day 12 during quarantine (Figure 1). Patient A4 might have acquired SARS-CoV-2 in Nepal and had a long incubation period. Alternatively, A4 might have acquired the infection while quarantined in hotel A. We do not know how this virus was introduced into the local community. However, patient A4 finished the mandatory quarantine on September 27 and started to interact with the local community 7 days before testing positive for SARS-CoV-2. Patient A4 might have had opportunities to introduce the clade GH virus into the local community, but we cannot exclude the possibility that this virus was introduced in hotel A via an unnoticed transmission chain or chains.

Our full genome analysis revealed that the wave 4 virus has several nonsilent mutations associated with host adaptation (4–6; B. Zhou et al., unpub. data, <https://doi.org/10.1101/2020.10.27.357558>), including mutations in the RNA-dependent RNA polymerase (RdRp[L323P]), Spike(D614G), open reading frame 3a (ORF3a[Q57H]), ORF3b(E14*), and nucleocapsid (N[S194L]) proteins. The ORF3a(Q57H) mutation leads a major truncation of ORF3b protein, ORF3b(E14*) (6). Because the ORF3b protein is

reported to be a potent interferon antagonist (6), we isolated the virus from patient A2 and conducted phenotypic characterizations using ex vivo human organ cultures and human airway organoids (7,8). We noted that this wave 4 virus contains a Spike(D614G) mutation that is associated with enhanced virus replication and transmission (B. Zhou et al., unpub. data). To differentiate the effect of Spike(D614G) and ORF3a(Q57H) mutations in our assays, we included viruses isolated from epidemic waves 1 and 3 as controls. The wave 1 virus we studied did not have these 2 mutations; the wave 3 virus had the Spike(D614G) but not the ORF3a(Q57H) mutation (Table). Our sequence data are available from GISAID (accession nos. EPI_ISL_760031–58).

We first studied the virus replication kinetics by using human bronchus and lung ex vivo cultures (Appendix Figure 3). In bronchus tissues, the wave 4 virus had a replication rate comparable to the wave 1 virus, but it had a lower replication rate than the wave 1 virus in lung tissues at 48 h, 72 h, and 96 h and a lower area under the curve. By contrast, the wave 3 virus had a slightly higher replication rate than the wave 1 virus in human bronchus, but not in human lung ex vivo cultures (Appendix Figure 3, panel A). Immunohistochemical staining analyses confirmed these observations (Appendix Figure 3, panel B). We found the wave 3 virus, not the wave 4 virus, might have marginally better replication competence than the wave 1 virus.

We previously demonstrated that the wave 1 virus is not a potent proinflammatory cytokine and chemokine inducer in infected human cells (7). To determine whether the ORF3a(Q57H) would affect this phenotype, we tested these viruses in human

Table. Amino acid differences between severe acute respiratory syndrome coronavirus 2 variants in 3 waves of coronavirus disease, Hong Kong, China*

Genome category	Amino acid position	Wave 1 virus	Wave 3 virus	Wave 4 virus
		VM20001061	Case 4533	Patient A2
ORF1A/1AB				
NSP2	141	M	V	M
NSP3	85	A	V	A
	238	V	V	L
RdRp	453	V	I	V
	1,179	A	A	V
	323	P	L	L
EndoRNase	231	A	V	A
Spike				
Spike	12	S	F	S
	25	L	P	P
	367	F	V	V
	614	D	G	G
	680	Q	R	R
	1,002	E	Q	Q
ORF3a				
ORF3a	57	Q	Q	H
	227	T	T	I
ORF3b	14	E	E	STOP
ORF8				
ORF8	62	L	V	V
	84	S	L	L
Nucleocapsid				
Nucleocapsid	12	A	G	A
	194	S	S	L
	203	R	K	R
	204	G	R	G
ORF9b				
ORF9b	9	H	D	H

*Bold text indicates position where isolated differs from the other isolates. A, alanine; D, aspartic acid; E, envelope; F, phenylalanine; G, glycine; H, histidine; I, isoleucine; L, leucine; M, membrane; NSP, nonstructural protein; ORF, open reading frame; P, proline; Q, glutamine; R, arginine; S, spike; STOP, stop codon; T, threonine; V, valine.

respiratory organoid cultures. We extracted RNA from infected organoids at 48 h post infection and tested the RNA samples in RT-PCR assays for a range of innate immune response genes. The viral RNA in

organoids infected by the wave 3 or 4 virus was ≈ 1 log unit lower than the one infected by the wave 1 virus ($p < 0.05$; Figure 2). The cytokine, chemokine, and interferon-stimulated gene mRNA levels induced by

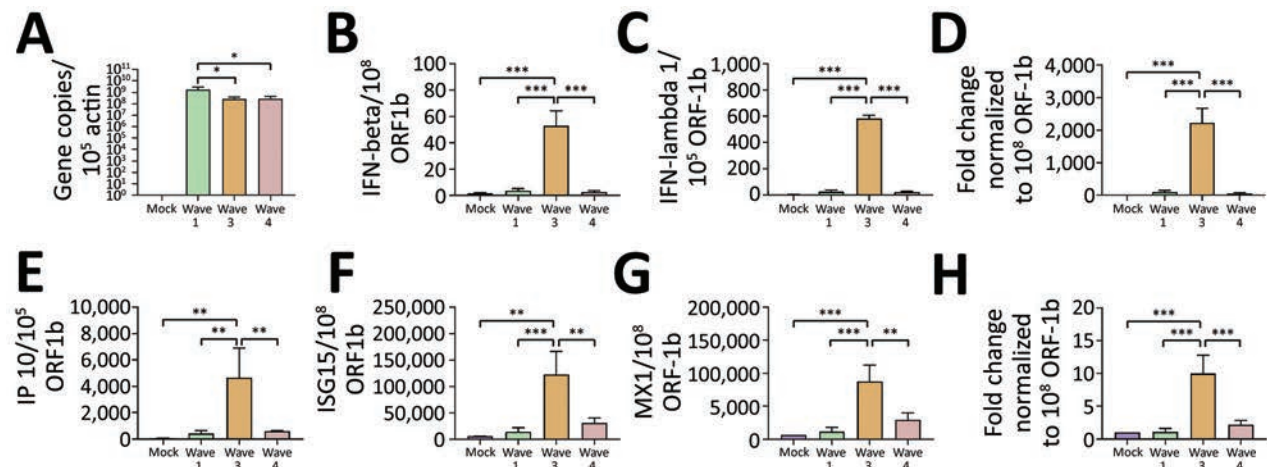


Figure 2. Innate immune responses in human airway organs experimentally infected with SARS-CoV-2 viruses from COVID-19 epidemic waves 1, 3, and 4, Hong Kong, China. A) ORF1b; B) IFN-β; C) IFN-λ 1; D) IFN-λ 2/3; E) IP-10; F) ISG15; G) MX1; H) MDA5. Messenger RNA expression of viral genes in human airway air-liquid interface organoids (n = 4; multiplicity of infection = 2) from the apical side at 48 h post infection. Mock samples were not infected. The gene expression of infected cells was first normalized with β-actin and further normalized with ORF1b gene. The gene expression of mock-infected cells was presented after normalization with β-actin. The differences were compared using 1-way ANOVA followed by a Tukey multiple-comparison test. Means and SD error bars are as shown. *p < 0.05; **p < 0.01; ***p < 0.001. COVID-19, coronavirus disease; IFN, interferon; IP-10, interferon gamma-induced protein-10; ISG15, interferon stimulated gene 15; MDA5, melanoma differentiation-associated protein 5; MX1, interferon-induced GTP binding protein 1; ORF, open reading frame; SARS-CoV-2, severe acute respiratory syndrome coronavirus 2.

the wave 4 virus were low and were only similar to the wave 1 virus. In addition, gene expressions in cells infected by the wave 3 virus were much higher than those caused by the wave 1 virus. Interferon gamma-induced protein-10 measurement of these cultures corroborated our observations (Appendix Figure 4).

Despite the major ORF3b deletion, our results demonstrate that the wave 4 virus does not have an enhanced ability to replicate *ex vivo* and retains potent innate immune evasion capacity in our experimental models. We noted that the wave 3 virus replicates slightly better than isolates from wave 1 and 4, and it can induce higher innate immune responses. The wave 3 virus has several unique mutations not found in the other 2 viruses (Table). Many of these mutations are in the ORF1ab or N gene. Although not within the scope of this study, further characterization of mutations found in the wave 3 virus via reverse genetics (9) might help explain our observations.

Conclusion

In summary, we found the virus causing the fourth COVID-19 epidemic wave in Hong Kong does not have enhanced replication kinetics and is not a potent cytokine or chemokine inducer. However, our work highlights the need for stringent COVID-19 control policy in quarantine settings.

Acknowledgments

We gratefully acknowledge the staff from the originating laboratories responsible for obtaining the specimens and from the submitting laboratories where the genome data were generated and shared via GISAID (Appendix Table 2). We thank the following for providing technical support: Rachel H.H. Ching and John C.W. Ho from the School of Public Health, the University of Hong Kong; Kevin Fung from the Pathology Department of the University of Hong Kong; and colleagues from the Centre for PanorOmic Sciences of the University of Hong Kong.

This work is supported by grants from the National Institute of Allergy and Infectious Diseases (contract no. HHSN272201400006C), Research Grant Council of Hong Kong (no. T11-712/19-N), and the Health and Medical Research Fund (grant nos. COVID190205 and COVID190202).

About the Author

Dr. Chu is a research assistant professor at The University of Hong Kong, Hong Kong. His interests focus on diagnostic virology, molecular diagnostics, and virus evolution.

References

1. Siu GK, Lee LK, Leung KS, Leung JS, Ng TT, Chan CT, et al. Will a new clade of SARS-CoV-2 imported into the community spark a fourth wave of the COVID-19 outbreak in Hong Kong? *Emerg Microbes Infect.* 2020;9:2497-500. <https://doi.org/10.1080/22221751.2020.1851146>
2. Choi EM, Chu DKW, Cheng PKC, Tsang DNC, Peiris M, Bausch DG, et al. In-flight transmission of SARS-CoV-2. *Emerg Infect Dis.* 2020;26:2713-6. <https://doi.org/10.3201/eid2611.203254>
3. Sit THC, Brackman CJ, Ip SM, Tam KWS, Law PYT, To EMW, et al. Infection of dogs with SARS-CoV-2. *Nature.* 2020;586:776-8. <https://doi.org/10.1038/s41586-020-2334-5>
4. Garvin MR, Prates EI, Pavicic M, Jones P, Amos BK, Geiger A, et al. Potentially adaptive SARS-CoV-2 mutations discovered with novel spatiotemporal and explainable AI models. *Genome Biol.* 2020;21:304. <https://doi.org/10.1186/s13059-020-02191-0>
5. Xia H, Cao Z, Xie X, Zhang X, Chen JY, Wang H, et al. Evasion of type I interferon by SARS-CoV-2. *Cell Rep.* 2020;33:108234. <https://doi.org/10.1016/j.celrep.2020.108234>
6. Lam JY, Yuen CK, Ip JD, Wong WM, To KK, Yuen KY, et al. Loss of orf3b in the circulating SARS-CoV-2 strains. *Emerg Microbes Infect.* 2020;9:2685-96. <https://doi.org/10.1080/22221751.2020.1852892>
7. Hui KPY, Cheung MC, Perera RAPM, Ng KC, Bui CHT, Ho JCW, et al. Tropism, replication competence, and innate immune responses of the coronavirus SARS-CoV-2 in human respiratory tract and conjunctiva: an analysis in ex-vivo and in-vitro cultures. *Lancet Respir Med.* 2020;8:687-95. [https://doi.org/10.1016/S2213-2600\(20\)30193-4](https://doi.org/10.1016/S2213-2600(20)30193-4)
8. Hui KPY, Ching RHH, Chan SKH, Nicholls JM, Sachs N, Clevers H, et al. Tropism, replication competence, and innate immune responses of influenza virus: an analysis of human airway organoids and ex-vivo bronchus cultures. *Lancet Respir Med.* 2018;6:846-54. [https://doi.org/10.1016/S2213-2600\(18\)30236-4](https://doi.org/10.1016/S2213-2600(18)30236-4)
9. Thi Nhu Thao T, Labrousseau F, Ebert N, V'kovski P, Stalder H, Portmann J, et al. Rapid reconstruction of SARS-CoV-2 using a synthetic genomics platform. *Nature.* 2020;582:561-5. <https://doi.org/10.1038/s41586-020-2294-9>

Addresses for correspondence: Michael Chan or Leo Poon, School of Public Health, G/F Patrick Manson Building (North Wing), University of Hong Kong, 7 Sassoon Road, Pokfulam, Hong Kong, China; email: mchan@hku.hk or llmpoon@hku.hk

Detecting Rapid Spread of SARS-CoV-2 Variants, France, January 26–February 16, 2021

Stéphanie Haim-Boukobza, Bénédicte Roquebert, Sabine Trombert-Paolantoni, Emmanuel Lecorche, Laura Verdurme, Vincent Foulongne, Christian Selinger, Yannis Michalakis, Mircea T. Sofonea,¹ Samuel Alizon¹

Variants of severe acute respiratory syndrome coronavirus 2 raise concerns regarding the control of coronavirus disease epidemics. We analyzed 40,000 specific reverse transcription PCR tests performed on positive samples during January 26–February 16, 2021, in France. We found high transmission advantage of variants and more advanced spread than anticipated.

Since the end of 2020, at least 3 strains, or “variants,” of severe acute respiratory syndrome coronavirus 2 (SARS-CoV-2) bearing a high number of mutations have been associated with rapid epidemic spread in the United Kingdom (lineage B.1.1.7) (1), South Africa (lineage B.1.351) (2), and Brazil (lineage P.1) (3). Because of their increased transmissibility (4; E. Volz et al., unpub. data, <https://www.medrxiv.org/content/10.1101/2020.12.30.20249034v2>; A.S. Walker et al., unpub. data, <https://www.medrxiv.org/content/10.1101/2021.01.13.21249721v1>) and potential ability to evade host immunity (5; S. Cele et al., unpub. data, <https://www.medrxiv.org/content/10.1101/2021.01.26.21250224v1>), monitoring these variants is crucial in the context of mass vaccination.

In France, beginning February 5, 2021, every sample that tested SARS-CoV-2–positive by reverse transcription PCR (RT-PCR) underwent an additional variant-specific RT-PCR with probes targeting the $\Delta 69-70$ deletion and the N501Y mutation, both in the spike glycoprotein. Both targets are present in lineage B.1.1.7. For lineages B.1.351 and P.1, only the N501Y mutation is present. If only the $\Delta 69-70$

deletion is detected, the infection might be caused by another variant or by a wild-type strain with a deletion. Finally, if neither target is detected, the infection is considered to be caused by a wild-type strain. These tests are cheaper and easier to implement than full-genome sequencing, which enables their rapid deployment on a wide scale. We report the results of this testing program.

The Study

RT-PCR testing for SARS-CoV-2 strains was conducted using 2 assays, VirSNIp SARS-CoV-2 Spike del+501 (TIB Molbiol, <https://www.tib-molbiol.de>) and ID SARS-CoV-2/UK/SA Variant Triplex (ID Solutions, <https://www.id-solutions.fr>), which target the $\Delta 69-70$ deletion and N501Y mutation. We performed tests on 42,229 positive samples collected during January 26–February 16, 2021, from 40,777 persons from 12 regions in France. Most samples came from the general population, and 3,323 (7.9%) samples came from hospitals. For the 1,397 patients for whom multiple tests were performed, only the first test was considered. We only included data from persons 5–80 years of age to minimize the weight of preschool children and persons living in aged-care facilities in our analysis. Finally, we removed persons whose age or testing region was unknown. This study was approved by the Institutional Review Board of the CHU of Montpellier and is registered at ClinicalTrials.gov (identifier NCT04738331).

Overall, we analyzed 35,208 SARS-CoV-2–positive samples from the same number of persons (Appendix 1 Table 1, <https://wwwnc.cdc.gov/EID/article/27/5/21-0397-App1.xlsx>). Results of 6,702 (19%) variant-specific RT-PCR tests were uninterpretable, mainly because of an insufficient amplification of the control, which targets the SARS-CoV-2

Author affiliations: Cerba Laboratory, Saint Ouen L'Aumône, France (S. Haim-Boukobza, B. Roquebert, S. Trombert-Paolantoni, E. Lecorche, L. Verdurme); CHU de Montpellier, Montpellier, France (V. Foulongne); IRD, Montpellier (C. Selinger); CNRS, Montpellier (Y. Michalakis, S. Alizon); Université de Montpellier, Montpellier (M.T. Sofonea)

DOI: <https://doi.org/10.3201/eid2705.210397>

¹These authors contributed equally to this article.

N gene. These results were treated as missing in the analyses. Given that most of the variants were B.1.1.7 (Appendix 2 Figure 1, <https://wwwnc.cdc.gov/EID/article/27/5/21-0397-App2.pdf>), we grouped all samples bearing the N501Y mutation into a broader class of variant-positive.

We used a generalized linear model (GLM) to analyze the binary strain variable (with values wild-type or variant). The covariates were the patient’s age, the RT-PCR kit used for variant detection, the sampling date, and the geographic region from which the sample originated (Appendix 2). By using a type-II analysis of variance, we found that all covariates except the type of RT-PCR kit to be significant (Table 1). In particular, the proportion of variants increased with date and decreased with age (Appendix 2 Figure 2) and hospital origin.

To investigate the temporal trends, we fitted a logistic growth model to the fitted values of an analogous GLM only on the data from general population samples (Appendix 2). Assuming that variations in frequencies are driven by transmission advantages, we found that variants have a 50% (95% CI 37%–64%) transmission advantage over wild-type strains (Figure 1).

The analysis of variance already showed that variant frequency varied across regions (Table 1). We performed the logistic growth fit at the local level for regions for which adequate data was available (Figure 2). The growth advantage of the variant was more pronounced in some regions. In Ile-de-France, more than half of infections already appeared to be caused by the variants by February 16, whereas in other regions, such as Burgundy, this proportion would not be reached until March 2021. However, some regions were less well represented in this analysis, which could affect local estimates.

Finally, we investigated the correlation between the increase in variant frequency among positive tests in a region and the temporal reproduction number, denoted R_t in that same region. R_t was estimated from coronavirus disease intensive care unit admission data by using the EpiEstim method (6) with a serial interval from Nishiura et al. (7), as described in Reyné et al. (unpub. data, <https://www.medrxiv.org/content/10.1101/2020.12.05.20244376v1>) (Appendix 2). We used the Spearman rank correlation test and found a positive but nonsignificant trend ($\rho = 0.50$; $p = 0.09$) (Appendix 2 Figure 3).

Conclusions

We used 2 variant-specific RT-PCR tests to detect the fraction of infections caused by SARS-CoV-2

Table 1. Risk for variant detection estimated using the general linear model in study of rapid spread of severe acute respiratory syndrome coronavirus 2 variants, France, January 26–February 16, 2021*

Covariate	OR	2.5% CI	97.5% CI
Date, per day	1.07	1.03	1.11
Age, per year	0.993	0.992	0.995
Kit 2	0.94	0.93	1.16
Nonhospital location	1.25	1.13	1.39

*For categorical variables, reference values are the other kit (1) and the hospital setting. Bold indicates statistical significance. OR, odds ratio.

lineages B.1.1.7, B.351, and P.1 in regions in France during January 25–February 16, 2021. We did not find any significant difference between the 2 specific RT-PCR kits used, suggesting that similar data collected in France could be pooled. Our results have several practical implications.

In general, we found that many infections screened were caused by variants, especially B.1.1.7, and the trend increased over time. On the basis of our estimates, by February 16, 2021, more than half of SARS-CoV-2 infections in France could have been caused by variants, although with pronounced spatial heterogeneity. In a conservative scenario, where all uninterpretable tests were assumed to be caused by the wild type, most infections would have been caused by variants by the end of week 7 of 2021, and the estimated variants transmission advantage was 36% (95% CI 26%–48%) (Appendix 2 Figure 4).

Variant-positive samples originated from significantly younger patients, which is consistent with an earlier report (E. Volz et al., unpub. data) but contrasts with Davies et al. (4). Our analysis did not enable us to discriminate between epidemiologic effects (e.g., if variants’ transmission chains were seeded in different populations than the wild types), sampling biases, or biologic effects. Additional data

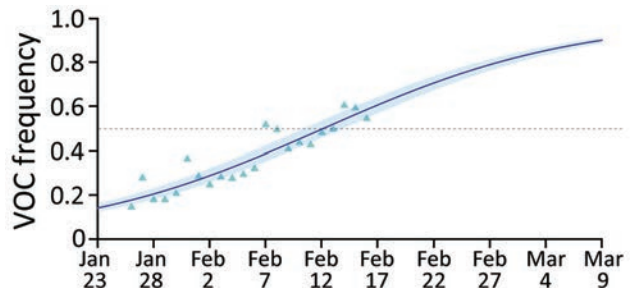


Figure 1. Estimated variants frequency kinetics in study of rapid spread of severe acute respiratory syndrome coronavirus 2 spread, France, January 26–February 16, 2021. Triangles indicate the general linear model–fitted values, line indicates output of the logistic growth model estimation, and shading indicates 95% CIs. Overall estimated transmission advantage of the variants (with respect to the wild-type reproduction number) is 50 (95% CI 38%–64%) (Appendix 2, <https://wwwnc.cdc.gov/EID/article/27/5/21-0397-App2.pdf>). VOC, variant of concern.

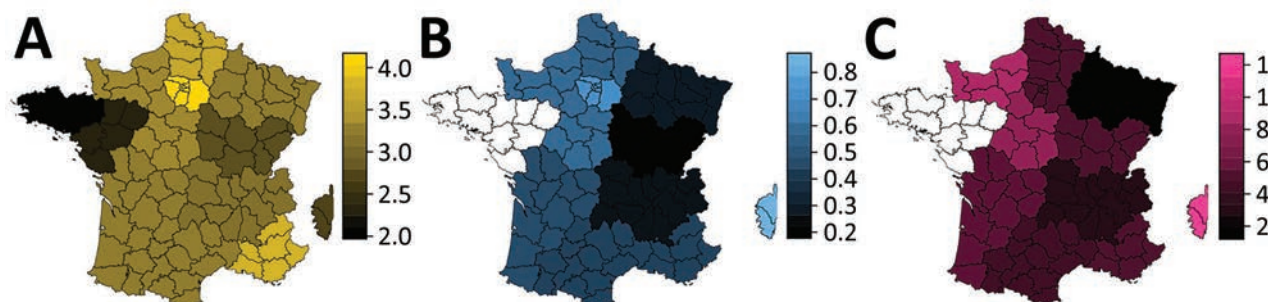


Figure 2. Regions of France in study of rapid spread of SARS-CoV-2 variants, January 26–February 16, 2021. For each region, we show the \log_{10} of the number of tests analyzed (A), the estimated total variant frequency by February 16, 2021 (B), and the estimated percentage transmission advantage (of the variant strains relative to the wild-type strain) (C). Additional details in Appendix 2 Figure 5 (<https://wwwnc.cdc.gov/EID/article/27/5/21-0397-App2.pdf>).

from RT-PCR amplification cycles could provide useful insights. Finally, earlier reports have found variant proportion to be associated with higher basic reproduction number (4; E. Volz et al., unpub. data). We found such a trend among regions in France, but it is not statistically significant.

A limitation of this study is that, in spite of its intensity, the sampling was performed retrospectively, which could generate biases if, for instance, transmission chains associated with variants were increasingly sampled. However, we found that samples that originated in hospitals were associated with a lower variant detection. Because testing in the general population is usually performed a week after infection and hospital admissions occur ≈ 2 weeks after infection (M.T. Sofonea et al., unpub. data, <https://www.medrxiv.org/content/10.1101/2020.05.22.20110593v1>), we expect hospital data would reflect an older state of the epidemic than screening data. RT-PCR does not have the resolution of full-genome sequencing, and other variants of concern could be underestimated or missed with this approach. However, the time scale considered and the relatively slow evolutionary rate of SARS-CoV-2 make this approach appropriate to monitor variant spread. Furthermore, next-generation sequencing performed on 48 samples showed a strong consistency with the specific RT-PCR tests (Cohen κ of 1 for the TIB Molbiol test and 0.87 or 0.88 for the ID Solutions test depending on the variant; data not shown).

These results illustrate that variant-specific RT-PCRs are an option for SARS-CoV-2 epidemic monitoring because of their affordability and rapid deployment. They also demonstrate that SARS-CoV-2 variants spread in France was faster than anticipated (L.D. Domenico et al., unpub. data, <https://www.medrxiv.org/content/10.1101/2021.02.14.21251708v1>), which stresses the importance of swift public health responses.

This article was preprinted at <https://www.medrxiv.org/content/10.1101/2021.02.17.251927>.

Acknowledgments

We thank the ETE modelling team and Florence Débarre for discussion.

Funding was provided by the CNRS, the IRD, the ANR, and the Région Occitanie (PHYEPI grant).

About the Author

Dr. Haim-Boukobza is a virologist and head of the Department of Infectious Disease at Cerba Laboratory, Saint Ouen L'Aumône, France. Her primary research interests are viral hepatitis, human papillomaviruses, and HIV, with additional interests in gut and vaginal microbiomes.

References

1. Rambaut A, Loman N, Pybus O, Barclay W, Barrett J, Carabelli A, et al. Preliminary genomic characterisation of an emergent SARS-CoV-2 lineage in the UK defined by a novel set of spike mutations. *Virological*. 2021 [cited 2020 Dec 9]. <https://virological.org/t/preliminary-genomic-characterisation-of-an-emergent-sars-cov-2-lineage-in-the-uk-defined-by-a-novel-set-of-spike-mutations/563>
2. Tegally H, Wilkinson E, Giovanetti M, Iranzadeh A, Fonseca V, Giandhari J, et al. Emergence of a SARS-CoV-2 variant of concern with mutations in spike glycoprotein. *Nature*. 2021; Epub ahead of print. <https://doi.org/10.1038/s41586-021-03402-9>
3. Faria NR, Claro IM, Candido D, Moyses Franco L, Andrade PS, Coletti TM, et al. Genomic characterisation of an emergent SARS-CoV-2 lineage in Manaus: preliminary findings. *Virological*. 2021 [cited 2021 Jan 12]. <https://virological.org/t/genomic-characterisation-of-an-emergent-sars-cov-2-lineage-in-manau-preliminary-findings/586>
4. Davies NG, Abbott S, Barnard RC, Jarvis CI, Kucharski AJ, Munday J, et al. Estimated transmissibility and severity of novel SARS-CoV-2 variant of concern 202012/01 in England. *Science*. 2021 Mar 3 [Epub ahead of print]. <https://doi.org/10.1126/science.abg3055>

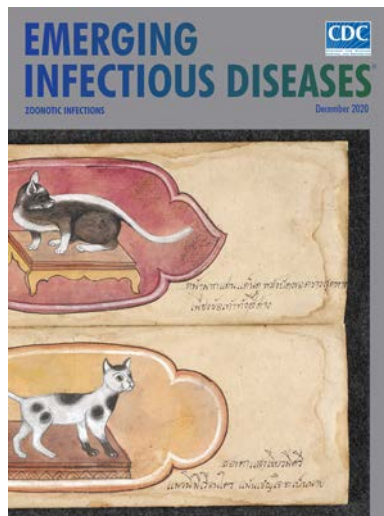
5. Thomson EC, Rosen LE, Shepherd JG, Spreafico R, da Silva Filipe A, Wojcechowskyj JA, et al.; ISARIC4C Investigators; COVID-19 Genomics UK (COG-UK) Consortium. Circulating SARS-CoV-2 spike N439K variants maintain fitness while evading antibody-mediated immunity. *Cell*. 2021; 184:1171–1187.e20. <https://doi.org/10.1016/j.cell.2021.01.037>
6. Cori A, Ferguson NM, Fraser C, Cauchemez S. A new framework and software to estimate time-varying reproduction numbers during epidemics. *Am J Epidemiol*. 2013;178:1505–12. <https://doi.org/10.1093/aje/kwt133>
7. Nishiura H, Linton NM, Akhmetzhanov AR. Serial interval of novel coronavirus (COVID-19) infections. *Int J Infect Dis*. 2020;93:284–6. <https://doi.org/10.1016/j.ijid.2020.02.060>

Address for correspondence: Samuel Alizon, MIVEGEC, CNRS, IRD, Université de Montpellier, 911 av. Agropolis, 34394 Montpellier CEDEX 5, France; email: samuel.alizon@cnrs.fr

December 2020

Zoonotic Infections

- Outbreak of Anthrax Associated with Handling and Eating Meat from a Cow, Uganda, 2018
- *Mycoplasma bovis* Infections in Free-Ranging Pronghorn, Wyoming, USA
- Control and Prevention of Anthrax, Texas, 2019
- Animal Rabies Surveillance, China, 2004–2018
- Small Particle Aerosol Exposure of African Green Monkeys to MERS-CoV as a Model for Highly Pathogenic Coronavirus Infection
- Coronavirus Disease Model to Inform Transmission-Reducing Measures and Health System Preparedness, Australia
- Genomic Epidemiology of Severe Acute Respiratory Syndrome Coronavirus 2, Colombia
- SARS-CoV-2 Seroprevalence among Healthcare, First Response, and Public Safety Personnel, Detroit Metropolitan Area, Michigan, USA, May–June 2020
- Flight-Associated Transmission of Severe Acute Respiratory Syndrome Coronavirus 2 Corroborated by Whole-Genome Sequencing
- Risk for Hepatitis E Virus Transmission by Solvent/Detergent-Treated Plasma
- Game Animal Density, Climate, and Tick-Borne Encephalitis in Finland, 2007–2017
- Trends in Population Dynamics of *Escherichia coli* Sequence Type 131, Calgary, Alberta, Canada 2006–2016. Peirano et al. 2907
- Outbreak of Haff Disease along the Yangtze River, Anhui Province, China, 2016
- Outbreaks of H5N6 Highly Pathogenic Avian Influenza (H5N6) Virus Subclade 2.3.4.4h in Swans, Xinjiang, Western China, 2020
- Differential Tropism of SARS-CoV and SARS-CoV-2 in Bat Cells
- Highly Pathogenic Avian Influenza A(H7N3) Virus in Poultry, United States, 2020
- Sensitive Detection of SARS-CoV-2-Specific Antibodies in Dried Blood Spot Samples
- Antibody Profiles According to Mild or Severe SARS-CoV-2 Infection, Atlanta, Georgia, USA, 2020
- Experimental Infection of Cattle with SARS-CoV-2
- Susceptibility of Raccoon Dogs for Experimental SARS-CoV-2 Infection
- Coyotes as Reservoirs for *Onchocerca lupi*, United States, 2015–2018
- Direct Transmission of Severe Fever with Thrombocytopenia Syndrome Virus from Domestic Cat to Veterinary Personnel
- Endovascular Infection with *Kingella kingae* Complicated by Septic Arthritis in Immunocompromised Adult Patient
- Lymphocytic Choriomeningitis Virus Infections and Seroprevalence, Southern Iraq
- Range Expansion of Bombali Virus in *Mops condylurus* Bats, Kenya
- Novel Rickettsia Species Infecting Dogs, United States
- Detection and Characterization of Bat Sarbecovirus Phylogenetically Related to SARS-CoV-2, Japan
- Equine-Like H3 Avian Influenza Viruses in Wild Birds, Chile
- Clinical and Multimodal Imaging Findings and Risk Factors for Ocular Involvement in a Presumed Waterborne Toxoplasmosis Outbreak, Brazil
- Tuberculosis among Children and Adolescents at HIV Treatment Centers in Sub-Saharan Africa
- Human-Pathogenic Kasokero Virus in Field-Collected Ticks
- Characterization and Source Investigation of Multidrug-Resistant *Salmonella Anatum* from a Sustained Outbreak, Taiwan
- Human Monocytic Ehrlichiosis, Mexico City, Mexico
- Hantavirus Cardiopulmonary Syndrome in Canada



**EMERGING
INFECTIOUS DISEASES**

To revisit the December 2020 issue, go to:
<https://wwwnc.cdc.gov/eid/articles/issue/26/12/table-of-contents>

Detecting COVID-19 Clusters at High Spatiotemporal Resolution, New York City, New York, USA, June–July 2020

Sharon K. Greene, Eric R. Peterson, Dominique Balan,
Lucretia Jones, Gretchen M. Culp, Annie D. Fine, Martin Kulldorff

A surveillance system that uses census tract resolution and the SaTScan prospective space-time scan statistic detected clusters of increasing severe acute respiratory syndrome coronavirus 2 test percent positivity in New York City, NY, USA. Clusters included one in which patients attended the same social gathering and another that led to targeted testing and outreach.

Spatiotemporal analysis of high-resolution coronavirus disease (COVID-19) data can help health officials monitor disease spread and target interventions (1,2). Publicly available data have been used to detect COVID-19 spatiotemporal clusters at county and daily resolution levels across the United States (3; R. Amin et al., unpub. data, <https://doi.org/10.1101/2020.05.22.20110155>) and spatial clusters at ZIP code resolution in New York City (NYC), New York, USA (4).

For routine surveillance, the NYC Department of Health and Mental Hygiene (DOHMH) uses the case-only space-time permutation scan statistic (5) in SaTScan (<https://www.satscan.org>) to detect new outbreaks in the context of minimal or stable citywide incidence of reportable diseases (6) (e.g., Legionnaires' disease [7] and salmonellosis [8]). Given wide testing variability, case-only analyses could be poorly suited for COVID-19 monitoring because true differences in disease rates across space and time would be indistinguishable from changing testing rates. We sought to detect in near real-time—regardless whether overall transmission was increasing, decreasing, or steady—newly emerging or re-emerging hotspots (i.e., areas

where COVID-19 diagnoses, adjusted for the number of persons tested, were increasing or not decreasing as quickly relative to elsewhere in the city).

The Study

Clinical and commercial laboratories are required to report all severe acute respiratory syndrome coronavirus 2 (SARS-CoV-2) molecular test results (positive, negative, indeterminate) for New York state residents to the New York State Electronic Clinical Laboratory Reporting System (9). For NYC residents, this reporting system transmits reports to DOHMH. Laboratory reports include specimen collection date and patient demographics, including residential address, which we geocoded by census tract. Patient symptoms and illness onset date, if any, are obtained through interviews, although not all patients are interviewed.

To detect emerging clusters, the space-time scan statistic uses a cylinder in which the circular base covers a geographic area and the height corresponds to time (10). This cylinder is moved, or scanned, over space and time to cover different areas and periods. At each position, the number of cases inside the cylinder is compared with the expected count under the null hypothesis of no clusters by using a likelihood function, and the position with the maximum likelihood is the primary candidate for a cluster. The statistical significance of this cluster is then evaluated, adjusting for the multiple testing inherent in the many cylinder positions evaluated.

To quickly detect emerging hotspots, prospective analyses are conducted daily (11). To adjust for the multiple testing stemming from daily analyses, recurrence intervals are used instead of p values (12). A recurrence interval of D days means that under the null hypothesis, if we conduct the analysis repeatedly

Author affiliations: New York City Department of Health and Mental Hygiene, Long Island City, New York, USA (S.K. Greene, E.R. Peterson, D. Balan, L. Jones, G.M. Culp, A.D. Fine); Harvard Medical School, Boston, Massachusetts, USA (M. Kulldorff)

DOI: <https://doi.org/10.3201/eid2705.203583>

over D days, then the expected number of clusters of the same or larger magnitude is 1.

The space-time scan statistic can be used with different probability models; we used the Poisson model (10), adjusting not for population size (which would fail to account for changing testing rates) but rather for persons tested. Because the goal was to detect newly emerging hotspots rather than areas with consistently high percent positivity, we further adjusted analyses

nonparametrically for purely geographic variations that were consistent over time. Fitting a log-linear function, we also adjusted for citywide temporal trends in percent positivity because the goal was to detect local hotspots rather than general citywide trends. For each day and location, the expected count was calculated as the number of persons tested × temporal trend function × a location-specific constant to ensure that, summed over all days in the study period, the location

Table 1. Input file specifications for SARS-CoV-2 test percent positivity cluster detection analyses in New York City, NY, USA, June–July 2020*

Feature	Selection	Notes
Geographic aggregation	Census tract (defined by using US Census 2010 boundaries) of residential address at time of report	With less aggregated data, the more precisely areas with elevated rates can be identified. New York City has 2,165 census tracts located on land. If geocoding is not feasible, then ZIP code could be used but with a loss of spatial precision.
Case file	Unique persons reported with a positive result for a molecular amplification detection (PCR) test for SARS-CoV-2 RNA in a clinical specimen. Retain specimen collection date of first positive test.	Confirmed COVID-19 cases (https://cdn.ymaws.com/www.cste.org/resource/resmgr/2020ps/Interim-20-ID-01_COVID-19.pdf)
Population file	Unique persons reported with a molecular amplification detection (PCR) test for SARS-CoV-2 RNA in a clinical specimen. For persons who ever tested positive, retain specimen collection date of first positive test. Otherwise, retain most recent specimen collection date. For a given census tract and date, if no specimens were collected, then include in file as having 0 population.	Necessary to control for spatial and temporal variability in testing access. A census-based population denominator would not control for variable testing uptake because the number of persons tested is not necessarily proportional to population size.
Omissions from input files	Residents of long-term care facilities, correctional facilities, facilities housing people with developmental disabilities, or homeless shelters; persons whose home address matches selected providers or facilities; persons diagnosed in the 14 d before a more recent case residing in the same building identification number from geocoding; persons with COVID-19 illness onset (where available from patient interview) ≥14 d before specimen collection.	To focus on detecting recent community-based transmission, exclude residents of congregate settings because building-level clusters are detected by using other methods (13), persons whose listed home address is not a residence, >1 case/building, and patients whose diagnosis was made long after illness onset.
Date of interest for analysis	Specimen collection date	Defining reportable disease clusters according to when patients became ill is preferred, although a large proportion of COVID-19 infections are asymptomatic. Specimen collection date is the earliest date available for the study population of persons tested.
Study period	21 d for analysis to support prioritization of case investigations; since June 1, 2020, for analysis to support place-based resource allocation	Defining a study period ≥3 times the maximum temporal window helps with statistical power. Extending the study period further may decrease the accuracy of the log-linear temporal trend adjustment but might be of interest for detecting more prolonged clusters. If citywide percent positivity reaches an inflection point (e.g., begins to increase again after a period of decrease), the study period would need to be either temporarily shortened and reset after that inflection point to preserve suitability of a log-linear temporal trend adjustment or a nonparametric temporal trend adjustment could be used. For a longer temporal window, June 1, 2020, was selected as the earliest date when citywide percent positivity trend seemed stable without an inflection point. After 63 d elapsed from June 1, 2020, switched to 63-d rolling study period until next inflection point was reached.
Lag for data accrual	3 d	Given lags between specimen collection and report, exclude very incomplete data at end of study period when estimating the temporal trend. Three days is the minimum lag possible to preserve a timely analysis while allowing for at least some data to be reported, geocoded, and analyzed before open of business.

*The prospective Poisson-based space-time scan statistic was used. COVID-19, coronavirus disease; SARS-CoV-2, severe acute respiratory syndrome coronavirus 2.

Table 2. Spatiotemporal clusters of SARS-CoV-2 test percent positivity prospectively detected and prompting public health action, New York City, NY, USA, June–July 2020*

Maximum temporal window applied, d	Specimen collection date range	Detection date†	Radius, km	Observed cases	Relative risk	Recurrence interval, d	SARS-CoV-2 positivity within cluster, %	Median age (range), y	Notes
7	Jun 17–19	Jun 22	0.6	6	4.0	1	2.2	40 (28–58)	Low recurrence interval; epidemiologic linkage of a gathering identified
21	Jul 5–12	Jul 15	0.6	20	3.4	55	8.9	34 (4–87)	Cluster contributed to selection of area for geographically targeted testing, outreach, and education

*SARS-CoV-2, severe acute respiratory syndrome coronavirus 2.

†To account for data accrual lags, a 3-d delay was imposed between the end of the SaTScan (<https://www.satscan.org>) study period and the detection date.

has the same number of observed and expected cases. To prioritize quickly emerging clusters to identify epidemiologic linkages, we used a short maximum temporal window of 7 days. To detect sustained clusters to inform place-based resource allocation, starting July 15, we also ran secondary analyses with a maximum temporal window of 21 days.

We developed SAS code (SAS Institute, <https://www.sas.com>; <https://github.com/CityOfNewYork/communicable-disease-surveillance-nycdohmh>) to generate daily input and parameter files (Table 1; Appendix

Table, <https://wwwnc.cdc.gov/EID/article/27/5/20-3583-App1.pdf>). The SAS code then invoked SaTScan in batch mode, read analysis results back into SAS for further processing, output files to secured folders (including patient line lists with demographics and map and time-trend visualizations), and sent an investigator notification email.

We launched the system on June 11, 2020, and 2 clusters detected by July 31 prompted public health action (Table 2). First, on June 22, in the context of waning case counts citywide, the only cluster

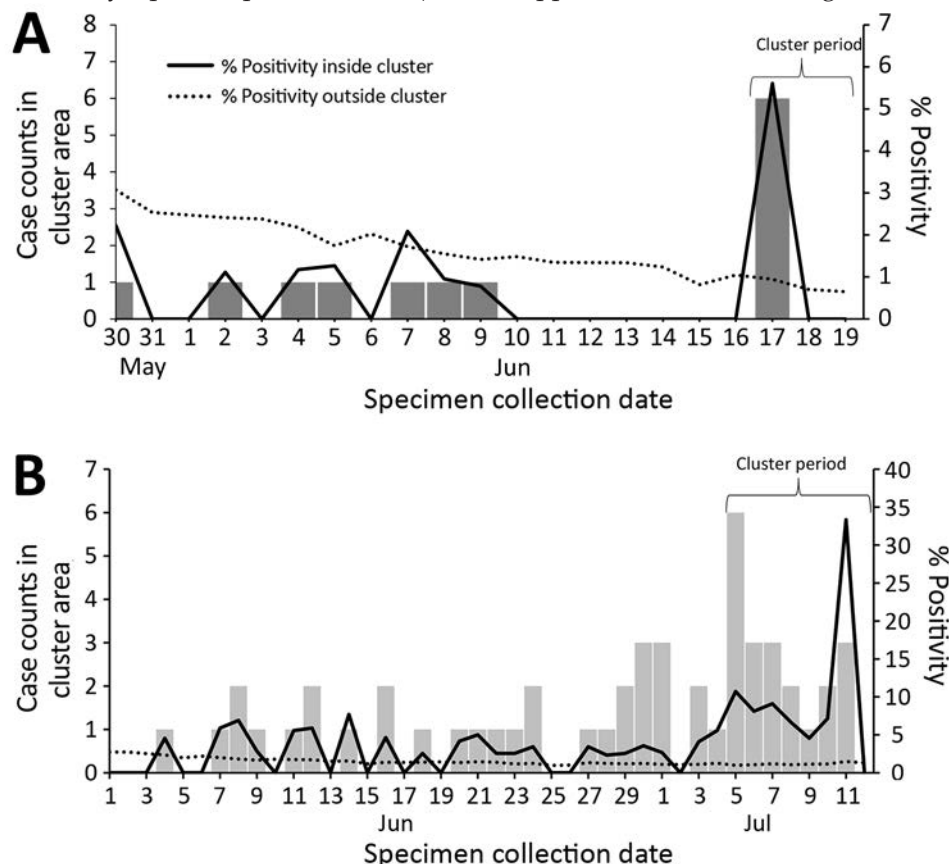


Figure. Cluster case counts and severe acute respiratory syndrome coronavirus 2 test percent positivity inside and outside cluster area for selected clusters detected in New York City, NY, USA, 2020. A) Cluster detected on June 22, 2020, in 5 census tracts in which patients reported common attendance at a social gathering; B) cluster detected on July 15, 2020, in 7 census tracts, contributing to the selection of 1 area for targeted testing and outreach.

detected was of 6 patients residing in a 0.6-km radius, all with specimens collected on June 17 (Figure, panel A). Consequently, DOHMH staff interviewed patients to collect and compare potential common exposures, such as attending the same event or visiting the same location. On June 23, a DOHMH surveillance investigator (D.B.) determined that 2 patients had attended the same gathering, where recommended social distancing practices had not been observed. In response, DOHMH launched an effort to limit further transmission, including testing, contact tracing, community engagement, and health education emphasizing the importance of isolation and quarantine. No other epidemiologic linkages were identified after attempts to investigate ≈ 65 additional clusters detected through July 2020. Second, detection of a sustained cluster on July 15 (lasting >1 week) with a high percent positivity (Figure, panel B) contributed to geographically targeted testing, outreach, and education, as part of NYC's hyper-local plan to prevent COVID-19 transmission (14).

Conclusions

COVID-19 community clusters detected by SaTScan prompted localized public education, testing, and community engagement (15). In addition, prioritizing interviews of patients in clusters can identify epidemiologic linkages and opportunities for interrupting further transmission, as is done for other reportable diseases (6–8). Identification of only 1 linkage in this study could be attributable to changing cluster investigation protocols, low patient response rates, or transmission occurring diffusely in small gatherings. Because all patients are referred for contact tracing, DOHMH discontinued reactively interviewing cluster patients for linkages and instead used clusters to proactively target resources.

The first limitation in this study was timeliness. Analyses were based on specimen collection date; however, given delays in testing availability and care seeking, these dates did not necessarily represent recent infections. Timeliness was further limited by delays from specimen collection to laboratory testing and reporting. Clusters dominated by asymptomatic patients or patients with illness onset >14 days before diagnosis may not require intervention because positive PCR results indicate presence of viral RNA but not necessarily viable virus. The second limitation involved the need to geocode for spatial precision. Of unique NYC residents for whom a specimen was collected for SARS-CoV-2 RNA PCR testing during June–July 2020, residential

address was not geocodable for $\approx 3\%$ of residents, so they were excluded. Third, although recurrence interval thresholds can be used to prioritize responding to clusters (6), COVID-19 cluster interpretation can be more complex. Other characteristics for prioritizing COVID-19 clusters, besides statistical significance, include percent positivity, relative risk, case count, epidemic curve trajectory, radius, demographics, and persistence. Prioritization can differ by response activity (e.g., establishing new testing sites, conducting outreach) and how quickly resources can be reallocated. Deciding when and where to initiate interventions in response to COVID-19 clusters cannot be fully automated and requires epidemiologic interpretation.

In summary, our COVID-19 early detection system highlighted areas warranting a rapid response. Targeted, place-based approaches for education and outreach efforts and for localized high transmission warnings could better protect persons at high risk for severe illness and death.

Acknowledgments

We thank all staff members of the DOHMH Incident Command System Surveillance and Epidemiology Section for processing, cleaning, and managing input data; for conducting patient interviews and cluster investigations; and for logistical support. We also thank the NYC Test and Trace Corps for their assistance in managing the cases and contacts included in and identified by cluster investigations.

S.K.G. and E.R.P. were supported by the Public Health Emergency Preparedness Cooperative Agreement (grant NU90TP922035-01), funded by the Centers for Disease Control and Prevention (CDC). M.K. was supported by the SaTScan Enhancements Project, managed by the Fund for Public Health in New York City and funded by the CDC Foundation, CDC ELC CARES (grant NU50CK000517-01-09), Alfred P. Sloan Foundation, and Open Society Foundations.

About the Author

Dr. Greene is the director of the Data Analysis Unit at the Bureau of Communicable Disease of the NYC DOHMH, Long Island City, New York. Her research interests include infectious disease epidemiology and applied surveillance methods for outbreak detection.

References

1. De Ridder D, Sandoval J, Vuilleumier N, Stringhini S, Spechbach H, Joost S, et al. Geospatial digital monitoring of COVID-19 cases at high spatiotemporal resolution. *Lancet*

- Digit Health. 2020;2:e393–4. [https://doi.org/10.1016/S2589-7500\(20\)30139-4](https://doi.org/10.1016/S2589-7500(20)30139-4)
2. Furuse Y, Sando E, Tsuchiya N, Miyahara R, Yasuda I, Ko YK, et al. Clusters of coronavirus disease in communities, Japan, January–April 2020. *Emerg Infect Dis*. 2020;26:2176–9. <https://doi.org/10.3201/eid2609.202272>
 3. Hohl A, Delmelle EM, Desjardins MR, Lan Y. Daily surveillance of COVID-19 using the prospective space-time scan statistic in the United States. *Spat Spatio-Temporal Epidemiol*. 2020;34:100354. <https://doi.org/10.1016/j.sste.2020.100354>
 4. Cordes J, Castro MC. Spatial analysis of COVID-19 clusters and contextual factors in New York City. *Spat Spatio-Temporal Epidemiol*. 2020;34:100355. <https://doi.org/10.1016/j.sste.2020.100355>
 5. Kulldorff M, Heffernan R, Hartman J, Assunção R, Mostashari F. A space-time permutation scan statistic for disease outbreak detection. *PLoS Med*. 2005;2:e59. <https://doi.org/10.1371/journal.pmed.0020059>
 6. Greene SK, Peterson ER, Kapell D, Fine AD, Kulldorff M. Daily reportable disease spatiotemporal cluster detection, New York City, New York, USA, 2014–2015. *Emerg Infect Dis*. 2016;22:1808–12. <https://doi.org/10.3201/eid2210.160097>
 7. Weiss D, Boyd C, Rakeman JL, Greene SK, Fitzhenry R, McProud T, et al.; South Bronx Legionnaires' Disease Investigation Team. A large community outbreak of Legionnaires' disease associated with a cooling tower in New York City, 2015. *Public Health Rep*. 2017;132:241–50. <https://doi.org/10.1177/0033354916689620>
 8. Latash J, Greene SK, Stavinsky F, Li S, McConnell JA, Novak J, et al. Salmonellosis outbreak detected by automated spatiotemporal analysis—New York City, May–June 2019. *MMWR Morb Mortal Wkly Rep*. 2020;69:815–9. <https://doi.org/10.15585/mmwr.mm6926a2>
 9. New York State Department of Health. Health advisory: reporting requirements for all laboratory results for SARS-CoV-2, including all molecular, antigen, and serological tests (including “rapid” tests) and ensuring complete reporting of patient demographics [cited 2020 Jun 24]. https://coronavirus.health.ny.gov/system/files/documents/2020/04/doh_covid19_reportingtestresults_rev_043020.pdf
 10. Kulldorff M, Athas WF, Feurer EJ, Miller BA, Key CR. Evaluating cluster alarms: a space-time scan statistic and brain cancer in Los Alamos, New Mexico. *Am J Public Health*. 1998;88:1377–80. <https://doi.org/10.2105/AJPH.88.9.1377>
 11. Kulldorff M. Prospective time-periodic geographical disease surveillance using a scan statistic. *J R Stat Soc Ser A Stat Soc*. 2001;164:61–72. <https://doi.org/10.1111/1467-985X.00186>
 12. Kleinman K, Lazarus R, Platt R. A generalized linear mixed models approach for detecting incident clusters of disease in small areas, with an application to biological terrorism. *Am J Epidemiol*. 2004;159:217–24. <https://doi.org/10.1093/aje/kwh029>
 13. Levin-Rector A, Nivin B, Yeung A, Fine AD, Greene SK. Building-level analyses to prospectively detect influenza outbreaks in long-term care facilities: New York City, 2013–2014. *Am J Infect Control*. 2015;43:839–43. <https://doi.org/10.1016/j.ajic.2015.03.037>
 14. NYC Health + Hospitals. Mayor de Blasio expands hyper-local testing response in Sunset Park, Brooklyn [cited 2020 Nov 27]. <https://www.nychealthandhospitals.org/pressrelease/mayor-de-blasio-expands-hyper-local-testing-response-in-sunset-park>
 15. Stack L, Goldstein J. How a virus surge among Orthodox Jews became a crisis for New York. <https://www.nytimes.com/2020/10/08/nyregion/orthodox-jews-queens-brooklyn-closures.html>

Address for correspondence: Sharon K. Greene, New York City Department of Health and Mental Hygiene, 42-09 28th St, CN 22A, WS 06-154, Long Island City, NY 11101, USA; email: sgrune4@health.nyc.gov

Evaluating Differences in Whole Blood, Serum, and Urine Screening Tests for Zika Virus, Puerto Rico, USA, 2016

Asher Y. Rosinger,¹ Samantha M. Olson,¹ Sascha R. Ellington, Janice Perez-Padilla, Regina M. Simeone, Caitlin S. Pedati, Betsy A. Schroeder, Gilberto A. Santiago, Freddy A. Medina, Jorge L. Muñoz-Jordán, Laura E. Adams, Romeo R. Galang, Miguel Valencia-Prado, Sonia Bakkour, Candimar Colón, Mary Goodwin, Dana Meaney-Delman, Jennifer S. Read, Lyle R. Petersen, Denise J. Jamieson, Carmen C. Deseda, Margaret A. Honein, Brenda Rivera-García, Carrie K. Shapiro-Mendoza

We evaluated nucleic acid amplification testing (NAAT) for Zika virus on whole-blood specimens compared with NAAT on serum and urine specimens among asymptomatic pregnant women during the 2015–2016 Puerto Rico Zika outbreak. Using NAAT, more infections were detected in serum and urine than in whole blood specimens.

Zika virus (ZIKV) infection during pregnancy can cause severe brain and eye malformations and is associated with neurodevelopmental abnormalities in affected infants (1). Currently, ZIKV testing with concurrent dengue virus (DENV) testing is recommended for pregnant women who have symptoms

and travel to areas with active DENV and risk for ZIKV transmission (2–4).

Many specimens can be tested for ZIKV, including blood, urine, cerebrospinal fluid, and delivery specimens (e.g., amniotic fluid, placenta) (1). Uncertainty still exists about the optimal specimens and tests to detect infection and the duration of detection for each specimen (4,5). Several reports suggest higher sensitivity of nucleic acid amplification testing (NAAT) on whole-blood and urine specimens compared with serum specimens (6–10). However, these studies were small or conducted among nonpregnant or symptomatic populations. Since the 2015–2016 Zika outbreak in the Americas, new whole-blood molecular and serologic assays have been approved, but limited data exist on the sensitivity of NAAT for the detection of ZIKV in whole-blood specimens among pregnant women. In addition, ZIKV detection might be transient during pregnancy, and absence of a positive test does not indicate lack of infection (11). Therefore, we compared ZIKV NAAT results in whole blood specimens to those in serum and urine specimens among asymptomatic pregnant women living in Puerto Rico during the 2015–2016 Zika outbreak.

The Study

From October 1–November 4, 2016, ≈2–3 months after the peak of the Puerto Rico Zika outbreak (12), the Puerto Rico Department of Health recruited pregnant women during routine prenatal care visits at 7 clinical sites to provide serum, urine, and

Author affiliations: The Pennsylvania State University, State College, Pennsylvania, USA (A.Y. Rosinger); Centers for Disease Control and Prevention, Atlanta, Georgia, USA (A.Y. Rosinger, S.M. Olson, S.R. Ellington, R.M. Simeone, C.S. Pedati, B.A. Schroeder, R.R. Galang, M. Goodwin, D. Meaney-Delman, D.J. Jamieson, M.A. Honein, C.K. Shapiro-Mendoza); G²S Corporation, San Antonio, Texas, USA (S.M. Olson); Centers for Disease Control and Prevention, San Juan, Puerto Rico, USA (J. Perez-Padilla, G.A. Santiago, F.A. Medina, J.L. Muñoz-Jordán, L.E. Adams, C. Colón, J.S. Read); Iowa Department of Public Health, Des Moines, Iowa, USA (C.S. Pedati); Pennsylvania Department of Health, Harrisburg, Pennsylvania, USA (B.A. Schroeder); Puerto Rico Department of Health, San Juan (M. Valencia-Prado, C.C. Deseda, B. Rivera-García); Vitalant Research Institute, San Francisco, California, USA (S. Bakkour); University of Vermont Medical Center and Vermont Department of Health, Burlington, Vermont, USA (J.S. Read); Centers for Disease Control and Prevention, Fort Collins, Colorado, USA (L.R. Petersen); Emory University School of Medicine, Atlanta (D.J. Jamieson)

DOI: <https://doi.org/10.3201/eid2705.203960>

¹These authors contributed equally to this article.

Table 1. Demographic characteristics among 514 asymptomatic pregnant women, Puerto Rico, USA, October 1–November 4, 2016*

Characteristics	Results
Median age, y (range)	25 (15–43)
Trimester of pregnancy at specimen collection†	
1st trimester: <14 weeks gestation	170 (33)
2nd trimester: 14–27 weeks gestation	187 (36)
3rd trimester: >28 weeks gestation	156 (30)

*Values are no. (%) except as indicated.

†Data regarding trimester at time of specimen collection was missing for 1 pregnant woman.

whole-blood specimens. Women provided verbal consent, and information was collected on demographic and clinical characteristics. Women with any laboratory evidence of ZIKV infection during pregnancy before recruitment or with any reported clinically compatible symptoms, including fever, rash, headache, eye pain, myalgia, or arthralgia, ≤ 7 days before specimen collection were excluded. This study was deemed nonresearch and exempt from institutional review board review.

At collection, specimens were refrigerated at 4°C, transported to the Centers for Disease Control and Prevention (CDC; San Juan, PR, USA) within 12 hours of collection, and stored according to Food and Drug Administration and CDC guidelines (13). For each specimen, 200 μ L was tested by the Trioplex real-time reverse transcription PCR (rRT-PCR), by using previously described methods (13,14), including primer pairs specific to ZIKV, DENV, and chikungunya virus (CHIKV). According to surveillance systems in Puerto Rico, DENV and CHIKV circulation were minimal, and no confirmed cases were reported during the study period.

CDC (Fort Collins, CO, USA) performed quality-control testing by singleplex NAAT (13,14) on all ZIKV-positive specimens. In addition, whole-blood specimens were tested by the Hologic Aptima assay (Hologic, <https://www.hologic.com>) at Vitalant Research Institute (San Francisco, CA, USA) (8). Be-

cause results of quality-control testing were consistent and did not change findings, we report Trioplex assay results only.

We also tested serum specimens by the Zika virus IgM capture ELISA (Zika MAC-ELISA) (15). We used a positive-to-negative optical density ratio of ≥ 3 to determine sample positivity, suggesting previous ZIKV infection (15).

Among 514 pregnant women, all were asymptomatic during specimen collection; 14 were symptomatic 8–187 days before collection. The median age was 25 (range 15–43) years; specimen collection was evenly distributed by trimester of pregnancy (Table 1). Of the 1,521 specimens collected, all tested negative for DENV and CHIKV by Trioplex NAAT. Overall, 69 (13%) pregnant women tested positive for ZIKV by NAAT or IgM in ≥ 1 specimen (Table 2). A total of 24 (5%) participants tested positive for ZIKV by serum, urine, or whole-blood NAAT and had negative IgM results, whereas 41 (8%) participants had positive IgM and negative NAAT results. Only 4 (1%) participants had positive NAAT and IgM results, and 1 (<1%) woman was positive by NAAT on all specimens and IgM.

Among 28 women who tested positive by NAAT, 8 were by whole blood, 10 by urine, and 20 by serum (Figure). Among the 8 women with NAAT-positive whole-blood specimens, none were positive by only whole blood; 5 tested positive by serum NAAT, 2 by

Table 2. Number of positive tests for Zika virus among 514 asymptomatic pregnant women tested by specimen type and assay, Puerto Rico, USA, October 1–November 4, 2016*

Category	NAAT		IgM
	No. positive tests/no. tested (%)	Median C _t value (range)	No. positive tests/no. tested (%)
Specimen type			
Serum	20/509† (4)	37.2 (29.8–37.9)	45/508‡ (9)
Urine	10/503§ (2)	37.4 (36.2–37.9)	
Whole blood	8/507¶ (2)	34.2 (29.8–36.7)	
Total positive tests among pregnant women by test type#	28/514 (5)		45/508 (9)
Total positive tests among pregnant women by any test or specimen type#	69/514 (13)		

*C_t values were not compared across specimen types. IgM was performed only on serum specimens. C_t, cycle threshold; NAAT, nucleic acid amplification testing.

†5 serum specimens from asymptomatic women were unable to be provided for Trioplex NAAT.

‡6 serum specimens from asymptomatic women were unable to be provided or were inconclusive for Zika virus IgM testing.

§11 urine specimens from asymptomatic women were unable to be provided for Trioplex NAAT.

¶7 whole blood specimens from asymptomatic women were unable to be provided for Trioplex NAAT.

#The denominator includes pregnant women who were missing a test type.

urine NAAT, and 1 by urine and serum NAAT and IgM. Serum NAAT identified 13 positive results not detected by NAAT in another specimen, and urine NAAT identified 6 positive results not otherwise detected (Figure).

Conclusions

This study provides information about laboratory testing to maximize detection of ZIKV infection among asymptomatic pregnant women. In this small sample of ZIKV NAAT-positive asymptomatic pregnant women, no additional ZIKV-positive cases were identified by whole-blood NAAT beyond those identified through tests of other samples. This finding contrasts with other studies that note prolonged detection, higher viral load, and greater sensitivity of whole-blood NAAT versus NAAT on other specimens (6,8–10). Unlike previous studies that tested mostly symptomatic persons (6,10,11) we restricted our analysis to asymptomatic pregnant women.

All asymptomatic ZIKV-positive women had detectable ZIKV in NAAT of urine or serum samples in our study. Although previous studies detected ZIKV RNA in urine more frequently than in serum (5,7), we found that ZIKV RNA was detected in serum more frequently than in urine; 64% (18/28) tested positive by serum NAAT and negative by urine NAAT. However, serum and urine NAAT together are critical because urine alone identified only 21% (6/28) of pregnant women with a positive NAAT result.

This large study comparing NAAT for ZIKV on serum, urine, and whole-blood specimens is unique in that the study population is among asymptomatic pregnant women. Although studies have mentioned lack of overlap between different specimens tested by NAAT (7,10) and whole blood yielding fewer positive results in symptomatic persons (14), in this study NAAT on whole-blood specimens yielded fewer positive results than NAAT on serum or urine specimens among asymptomatic pregnant women. Because ZIKV-associated birth defects have been noted among asymptomatic pregnant women (1), identification of ZIKV infection is critical, especially when the virus is circulating in a community. Timely identification enables appropriate counseling and clinical management.

Our detection of acute ZIKV infections by NAAT is likely low because the study occurred 2–3 months after the peak of the Puerto Rico outbreak (12), and false-negative results in pregnant women are possible (11). Further, ZIKV RNA-positive results have been reported days or months after symptom onset or first

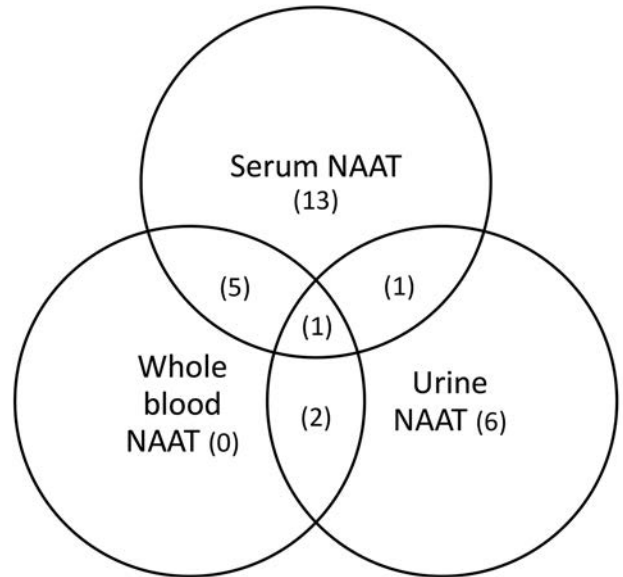


Figure. Comparison of positive NAAT results by specimen type for Zika virus infection among asymptomatic pregnant women, Puerto Rico, USA, October 1–November 4, 2016. NAAT, nucleic acid amplification testing.

positive test (6,9), and other cases were reported in Puerto Rico during the study period. Our analysis was among asymptomatic pregnant women, and we could not determine infection onset or whether infection occurred at all. False-positive results were also possible, but samples tested by singleplex NAAT revealed similar results, and results were independently validated in multiple laboratories.

These findings support CDC guidance to perform NAAT on asymptomatic pregnant women during outbreaks when ZIKV is widely circulating (3,4). Identification of infections among pregnant women who reside in or travel to areas at risk for ZIKV infection is critical for prenatal and postnatal counseling and clinical management (2,4). Although our understanding of viral persistence in various specimens is growing and the percentage positive in this study was small, NAAT of urine contributed to additional diagnoses, and NAAT on serum and urine combined yielded more positive results compared with whole-blood testing among asymptomatic pregnant women. Timely and accurate prenatal screening and notification of infection can optimize pregnancy and infant care during Zika outbreaks.

Acknowledgments

We thank Michael P. Busch, Van T. Tong, and Suzanne M. Gilboa.

About the Author

Dr. Rosinger is the Ann Atherton Hertzler Early Career Professor in Global Health in the Departments of Biobehavioral Health and Anthropology at Pennsylvania State University. His primary research interests are the health consequences of water insecurity. Ms. Olson is an epidemiologist in the Influenza Division, National Center for Immunization and Respiratory Diseases, Centers for Disease Control and Prevention. Her research has spanned Zika virus infection during pregnancy, influenza, and SARS-CoV-2.

References

- Musso D, Ko AI, Baud D. Zika virus infection – after the pandemic. *N Engl J Med*. 2019;381:1444–57. <https://doi.org/10.1056/NEJMr1808246>
- Centers for Disease Control and Prevention. Testing guidance: new Zika and dengue testing guidance (updated November 2019) [cited 2020 Jul 14]. <https://www.cdc.gov/zika/hc-providers/testing-guidance.html>
- Sharp TM, Fischer M, Muñoz-Jordán JL, Paz-Bailey G, Staples JE, Gregory CJ, et al. Dengue and Zika virus diagnostic testing for patients with a clinically compatible illness and risk for infection with both viruses. *MMWR Recomm Rep*. 2019;68:1–10. <https://doi.org/10.15585/mmwr.rr6801a1>
- Oduyebo T, Polen KD, Walke HT, Reagan-Steiner S, Lathrop E, Rabe IB, et al. Update: interim guidance for health care providers caring for pregnant women with possible Zika virus exposure – United States (including U.S. territories), July 2017. *MMWR Morb Mortal Wkly Rep*. 2017;66:781–93. <https://doi.org/10.15585/mmwr.mm6629e1>
- Chua A, Prat I, Nuebling CM, Wood D, Moussy F. Update on Zika diagnostic tests and WHO's related activities. *PLoS Negl Trop Dis*. 2017;11:e0005269. <https://doi.org/10.1371/journal.pntd.0005269>
- Lustig Y, Mendelson E, Paran N, Melamed S, Schwartz E. Detection of Zika virus RNA in whole blood of imported Zika virus disease cases up to 2 months after symptom onset, Israel, December 2015 to April 2016. *Euro Surveill*. 2016; 21:30269. <https://doi.org/10.2807/1560-7917.ES.2016.21.26.30269>
- George KS, Sohi IS, Dufort EM, Dean AB, White JL, Limberger R, et al. Zika virus testing considerations: lessons learned from the first eighty real-time RT-PCR-positive cases diagnosed in New York State. *J Clin Microbiol*. 2017;55:535–44. <https://doi.org/10.1128/JCM.01232-16>
- Stone M, Bakkour S, Lanteri MC, Brambilla D, Simmons G, Bruhn R, et al.; NHLBI Recipient Epidemiology Donor Evaluation Study REDS-III Program. Zika virus RNA and IgM persistence in blood compartments and body fluids: a prospective observational study. *Lancet Infect Dis*. 2020;20:1446–56. [https://doi.org/10.1016/S1473-3099\(19\)30708-X](https://doi.org/10.1016/S1473-3099(19)30708-X)
- Mansuy JM, Mengelle C, Pasquier C, Chapuy-Regaud S, Delobel P, Martin-Blondel G, et al. Zika virus infection and prolonged viremia in whole-blood specimens. *Emerg Infect Dis*. 2017;23:863–5. <https://doi.org/10.3201/eid2305.161631>
- Voermans JJC, Pas SD, van der Linden A, GeurtsvanKessel C, Koopmans M, van der Eijk A, et al. Whole-blood testing for diagnosis of acute Zika virus infections in routine diagnostic setting. *Emerg Infect Dis*. 2019;25:1394–6. <https://doi.org/10.3201/eid2507.182000>
- Schaub B, Vouga M, Najioullah F, Gueneret M, Monthieux A, Harte C, et al. Analysis of blood from Zika virus-infected fetuses: a prospective case series. [Erratum in: *Lancet Infect Dis*. 2017;17:362]. *Lancet Infect Dis*. 2017;17:520–7. [10.1016/S1473-3099\(17\)30102-0](https://doi.org/10.1016/S1473-3099(17)30102-0) [https://doi.org/10.1016/S1473-3099\(17\)30102-0](https://doi.org/10.1016/S1473-3099(17)30102-0)
- Hills SL, Fischer M, Petersen LR. Epidemiology of Zika virus infection. *J Infect Dis*. 2017;216(suppl_10):S868–74. <https://doi.org/10.1093/infdis/jix434>
- US Food and Drug Administration. Trioplex real-time RT-PCR assay. 2017 Apr 6 [cited 2020 Jun 24]. <https://www.fda.gov/media/123606/download>
- Santiago GA, Vázquez J, Courtney S, Matías KY, Andersen LE, Colón C, et al. Performance of the Trioplex real-time RT-PCR assay for detection of Zika, dengue, and chikungunya viruses. *Nat Commun*. 2018;9:1391. <https://doi.org/10.1038/s41467-018-03772-1>
- US Food and Drug Administration. Zika MAC-ELISA [cited 2020 Jun 24]. <https://www.fda.gov/downloads/MedicalDevices/Safety/EmergencySituations/UCM488044.pdf>

Address for correspondence: Samantha M. Olson, Centers for Disease Control and Prevention, 1600 Clifton Rd NE, Mailstop H24-7, Atlanta, GA 30329-4027, USA; email: ylz8@cdc.gov

Whole-Genome Sequencing of Shiga Toxin–Producing *Escherichia coli* OX18 from a Fatal Hemolytic Uremic Syndrome Case

Kenichi Lee, Atsushi Iguchi, Kazuhiro Uda, Sohshi Matsumura, Isao Miyairi, Kenji Ishikura, Makoto Ohnishi, Junji Seto, Kanako Ishikawa, Noriko Konishi, Hiromi Obata, Ichiro Furukawa, Hiromi Nagaoka, Hirotaka Morinushi, Natsuki Hama, Ryohei Nomoto, Hiroshi Nakajima, Hideaki Kariya, Mitsuhiro Hamasaki, Sunao Iyoda

We report a fatal case of hemolytic uremic syndrome with urinary tract infection in Japan caused by Shiga toxin–producing *Escherichia coli*. We genotypically identified the isolate as OX18:H2. Whole-genome sequencing revealed 3 potentially pathogenic lineages (OX18:H2, H19, and H34) that have been continuously isolated in Japan.

Shiga toxin–producing *Escherichia coli* (STEC) is a consequential foodborne pathogen worldwide. The most prevalent STEC O serogroups—O157, O26, O111, O103, O121, O145, and O45—cause severe symptoms, including bloody diarrhea and hemolytic uremic syndrome (HUS). These STECs usually carry the locus of enterocyte effacement (LEE) region, which is required for intimate bacterial adherence to host epithelial cells (1). However,

LEE-negative STEC serotypes, including O104:H4 and O113:H21, can also cause outbreaks or severe cases (2,3). Although most severe cases develop from intestinal tract infections, HUS cases related to urinary tract infections have been reported (4). We report a fatal case of HUS in Japan caused by a LEE-negative strain identified as OX18:H2.

The Case

In 2017, an 8-year-old girl in Japan was hospitalized for a urinary tract *E. coli* infection, which was treated with ceftazidime. Two days after hospitalization, she became unconscious. Laboratory results revealed anemia (hemoglobin 10.5 g/dL) with schistocytes; low platelet count ($3.8 \times 10^4/\mu\text{L}$); and elevated creatinine (1.38 mg/dL), total bilirubin (1.7 mg/dL), and lactate dehydrogenase (1,848 U/L). Magnetic resonance imaging of her head showed hyperintensity in the basal ganglia and thalamus, suggesting edema and necrosis. From the urine sample, we isolated a LEE-negative STEC (strain JNE170426) carrying the Shiga toxin 2 gene (*stx2*). On the basis of these findings we diagnosed her condition as HUS with urinary tract infection. We performed intravenous high-dose methylprednisolone therapy, plasma exchange, and hemodialysis for HUS encephalopathy and renal failure, but after 12 days of intensive therapy, she died of HUS encephalopathy.

The isolated STEC did not show agglutination against commercial O1–O188 antisera (Denka Company Ltd., <https://www.denka.co.jp>; Statens Serum Institut, <https://en.ssi.dk>). However, comprehensive PCR-based O serogrouping (5) revealed that the isolate was classified into OX18, an atypical O serogroup originally identified from a nonpathogenic *E. coli* strain from

Author affiliations: National Institute of Infectious Diseases, Tokyo, Japan (K. Lee, M. Ohnishi, S. Iyoda); University of Miyazaki, Miyazaki, Japan (A. Iguchi); National Center for Child Health and Development, Tokyo (K. Uda, S. Matsumura, I. Miyairi, K. Ishikura); Tokyo Metropolitan Children's Medical Center, Tokyo (K. Uda); Kanagawa Children's Medical Center, Kanagawa, Japan (S. Matsumura); Kitasato University School of Medicine, Tokyo (K. Ishikura); Yamagata Prefectural Institute of Public Health, Yamagata, Japan (J. Seto); Ibaraki Prefectural Institute of Public Health, Ibaraki, Japan (K. Ishikawa); Tokyo Metropolitan Institute of Public Health, Tokyo (N. Konishi, H. Obata); Kanagawa Prefectural Institute of Public Health, Kanagawa (I. Furukawa); Shizuoka Institute of Environment and Hygiene, Shizuoka, Japan (H. Nagaoka, H. Morinushi); Kobe Institute of Health, Hyogo, Japan (N. Hama, R. Nomoto); Okayama Prefectural Institute for Environmental Science and Public Health, Okayama, Japan (H. Nakajima, H. Kariya); Fukuoka Institute of Health and Environmental Sciences, Fukuoka, Japan (M. Hamasaki)

DOI: <https://doi.org/10.3201/eid2705.204162>

a healthy sow (6). Using OX18-specific PCR screening of O-untypable STEC isolates obtained during 2007–2019 by the National Institute of Infectious Diseases in Japan, we found 25 additional STEC OX18 isolates (Table). To characterize these isolates, we performed whole-genome sequencing (WGS) using MiSeq (Illumina, <https://www.illumina.com>). WGS results were analyzed as described elsewhere (7,8) with slight modification. We used BactSNP version 1.0.2 (<http://platanus.bio.titech.ac.jp/bactsnp>) (9) and Gubbins version 2.4.1 (<https://sanger-pathogens.github.io>) (10) for core genome SNP extraction. Public database strains used for the phylogenetic analysis are shown in Appendix Table 1 (<https://wwwnc.cdc.gov/EID/article/27/5/20-4162-App1.pdf>). We deposited draft genome sequences and short-read sequencing data into the DDBJ/National Center for Biotechnology Information/European Nucleotide Archive database (BioProject accession no. PRJDB10421; Sequence Read Archive accession no. DRA010812).

In silico analysis revealed that none of the STEC OX18 isolates carried LEE; we classified them into 5 H-genotypes: H2 (n = 2), H8 (n = 1), H19 (n = 20), H28 (n = 1), and H34 (n = 2) (Table). Core-genome SNP phylogeny revealed that OX18 isolates with the same H-types formed closely related groups (Table; Figure). Isolates from patients belonged to OX18:H2, H19, and H34; isolates belonging to OX18:H8 and H28 were obtained from asymptomatic carriers. The

OX18 isolate from the case-patient who died of HUS (strain JNE170426) belonged to H2 and carried *stx2a* and several virulence genes, including STEC autoagglutination adhesin (*saa*), subtilase toxin (*sub*), enterohemolysin (*ehx*), and serine protease (*espP*) (Appendix Table 2). These regions showed high similarity (>99%) to a large plasmid of STEC O104:H21 strain CFSAN002236 (11). Therefore, these virulence factors are likely to be encoded in similar plasmids.

On the other hand, the other OX18:H2 isolate (strain JNE133347) from an asymptomatic carrier did not carry the virulence genes described above but carried genes for Shiga toxin 2e (*stx2e*), heat-stable enterotoxin (*st*), and Pap fimbriae (*pap*). Of note, the other isolates obtained from HUS belonged to OX18:H19 and were phylogenetically close to OX18:H2 (Figure). The OX18:H19 lineage showed a similar virulence profile to the OX18:H2 isolate from the fatal HUS case, and carried *saa*, *sub*, *ehx*, and *espP* virulence genes on plasmid-like elements. All bovine isolates in our study were grouped into this serotype. OX18:H19 isolates from humans and bovines could not be distinguished by their lineages, suggesting that cattle can be a reservoir for that lineage. We identified OX18:H34 in isolates that carried *pap* as an adhesin from a patient with bloody diarrhea and from swine. The other isolates, from asymptomatic carriers, we classified into H8 and H28. The OX18:H8 isolate carried *saa*, *sub*, *ehx*, and *espP*

Table. OX18 isolates used in study of whole-genome sequencing of Shiga toxin-producing *Escherichia coli* OX18 from a fatal hemolytic uremic syndrome case, Japan*

Strain	Year isolated	Source	Symptoms	H genotype	Phylogenetic group	MLST	stx subtype		Accession no.	
							stx1	stx2	Draft genome	Short reads
JNE101081	2010	Human	BD	H34	E	9185	1a	ND	BNCS00000000	SAMD00244533
JNE130471	NA	Swine	NA	H34	E	9185	1a	ND	BNCT00000000	SAMD00244534
JNE130573	2012	Human	D	H19	B1	205	ND	2a	BNCU00000000	SAMD00244535
JNE133347	2012	Human	AC	H2	B1	9397	ND	2e	BNCV00000000	SAMD00244536
JNE150598	2015	Human	BD	H19	B1	205	ND	2a	BNCW00000000	SAMD00244537
JNE151350	2015	Human	AC	H19	B1	205	ND	2d	BNCX00000000	SAMD00244538
JNE170426	2017	Human	HUS, death	H2	B1	847	ND	2a	BNCY00000000	SAMD00244539
JNE180342	2018	Human	AC	H8	B1	Novel	1a	2d	BNCZ00000000	SAMD00244540
JNE181771	2018	Human	HUS	H19	B1	205	ND	2a	BNDA00000000	SAMD00244541
JNE182474	2018	Human	BD	H19	B1	205	ND	2a	BNDB00000000	SAMD00244542
JNE182523	NA	Human	NA	H19	B1	205	ND	2a	BNDK00000000	SAMD00244543
JNE191031	2019	Human	BD	H19	B1	205	ND	2a	BNDL00000000	SAMD00244544
JNE192124	2019	Human	AC	H19	B1	205	ND	2a	BNDE00000000	SAMD00244545
JNE192333	2019	Human	AC	H28	B1	1056	1d	ND	BNDF00000000	SAMD00244546
A140161	2010	Cattle	NA	H19	B1	205	ND	2a	BNDG00000000	SAMD00244547
A140164	2010	Cattle	NA	H19	B1	205	ND	2a	BNDH00000000	SAMD00244548
A140165	2010	Cattle	NA	H19	B1	205	ND	2a	BNDI00000000	SAMD00244549
A140286	2012	Cattle	NA	H19	B1	205	ND	2a	BNDJ00000000	SAMD00244550
A140453	2010	Cattle	NA	H19	B1	Novel	1a	2a	BNDK00000000	SAMD00244551
A140462	2010	Cattle	NA	H19	B1	205	1a	ND	BNDL00000000	SAMD00244552
A140486	2014	Cattle	NA	H19	B1	205	ND	2ax2†	BNDM00000000	SAMD00244553
A150011	2014	Cattle	NA	H19	B1	205	ND	2ax2†	BNDN00000000	SAMD00244554
A150026	2014	Cattle	NA	H19	B1	205	ND	2ax2†	BNDQ00000000	SAMD00244555
A150037	2015	Cattle	NA	H19	B1	205	ND	2ax2†	BNDP00000000	SAMD00244556
A150038	2015	Cattle	NA	H19	B1	205	ND	2ax2†	BNDQ00000000	SAMD00244557
A150039	2015	Cattle	NA	H19	B1	205	ND	2ax2†	BNDR00000000	SAMD00244558

*AC, asymptomatic carrier; BD, bloody diarrhea; D, diarrhea; HUS, hemolytic uremic syndrome; NA, not available; ND, not detected.

†2ax2, two copies of *stx2a* were detected.

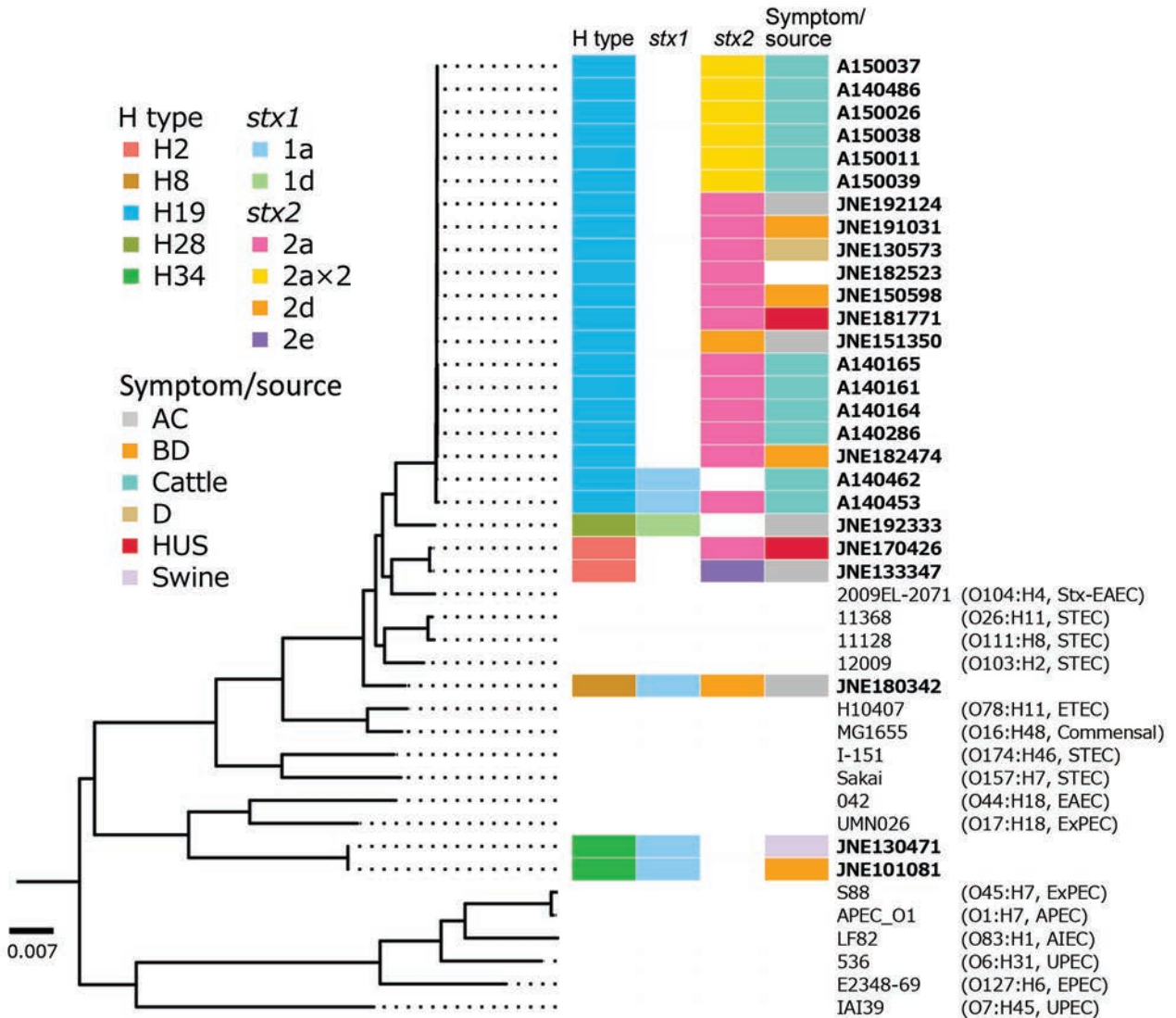


Figure. Maximum-likelihood phylogeny of STEC OX18 from a patient in Japan and other *Escherichia coli* strains. Isolate identifications of STEC OX18 are shown in bold. Colored boxes indicate collection countries, *stx* profiles, and symptoms of human carrier or source of the STEC OX18 isolates, as shown in the keys. Serotype and pathotype information of non-OX18 *E. coli* strains are shown in parentheses. The tree is rooted by *E. fergusonii* ATCC35469. AC, asymptomatic carrier; BD, bloody diarrhea; D, diarrhea; HUS, hemolytic uremic syndrome; STEC, Shiga toxin-producing *E. coli*; Stx, Shiga toxin. APEC, avian pathogenic *E. coli*; AIEC, adherent/invasive *E. coli*; EAEC, enteroaggregative *E. coli*; EPEC, enteropathogenic *E. coli*; ExPEC, extraintestinal pathogenic *E. coli*; UPEC, uropathogenic *E. coli*. Scale bar indicates number of substitutions per site.

on plasmid-like elements, similar to the H19 lineage. Meanwhile, the OX18:H28 isolate did not carry adherence factors known in pathogenic *E. coli*, including LEE genes, *saa*, *pap*, *aggR*, *afaD*, F4, F6, F17, F18, or F41.

Among LEE-negative STEC isolates, *saa*-positive STEC has often been reported in patients with severe symptoms (2,3). WGS analyses of *saa*-positive STEC O104:H21 and O113:H21 revealed that they carry a large plasmid (>100 kb) with several virulence genes, including *saa* and *sub*. Because the draft genomes of *saa*-positive OX18:H2 and H19 showed

high similarity to the plasmid, it is plausible that they carry a similar large plasmid. The source or natural reservoir of these lineages was unclear. However, some OX18:H19 isolates have been obtained from cattle, suggesting that cattle or fecally contaminated foods can be a source of the infection. In addition to these lineages, OX18:H34 was found to cause severe symptoms in humans. We were unable to elucidate the pathogenesis and natural reservoir of the lineage because of the small sample size of our study; further studies are required.

Conclusion

In this study, we report a HUS case with urinary tract infection caused by a STEC belonging to the emerging O serogroup OX18. Our retrospective survey revealed that the novel pathogenic STECs OX18:H2, H19, and H34 have been continually isolated from humans and cattle. However, commercial antisera cannot identify these lineages. Elucidating the transmission routes and natural reservoirs of the bacteria is essential to control infection. DNA-based serotyping methods, including Og/Hg typing (6,12,13) and whole-genome sequencing (7,14,15), would be helpful for identification and surveillance of these potentially pathogenic lineages.

Acknowledgments

We are grateful to Saomi Ozawa, Yukie Nakajima, Ayumi Takemoto, and Yu Takizawa for technical assistance and WGS analyses. We are also grateful to Mai Sato, Koichi Kamei, Masaya Kubota, Naho Nishimura, and Satoshi Nakagawa for supporting clinical practice.

STEC isolates were kindly provided by the Department of Microbiology at the Miyagi Prefectural Institute of Public Health and Environment, the Gunma Prefectural Institute of Public Health and Environmental Sciences, the Kagawa Prefectural Research Institute for Environmental Sciences and Public Health, and the Fukuoka City Institute of Health and Environment.

This work was partially supported by the Research Program on Emerging and Re-emerging Infectious Diseases from the Japan Agency for Medical Research and Development (AMED) (grant number: JP20fk0108065), JSPS KAKENHI (18K15156 and 20K07506), and grants-in-aid from the Ministry of Health, Labour, and Welfare of Japan (JPMH20HA1009).

About the author

Dr. Lee is a senior researcher in the Department of Bacteriology I, National Institute of Infectious Diseases in Tokyo. His primary research interests are the genomics and pathogenesis of Shiga toxin-producing *Escherichia coli*.

References

1. Stevens MP, Frankel GM. The locus of enterocyte effacement and associated virulence factors of enterohemorrhagic *Escherichia coli*. *Microbiol Spectr*. 2014;2:EHEC-0007-2013.
2. Frank C, Werber D, Cramer JP, Askar M, Faber M, an der Heiden M, et al. HUS Investigation Team. Epidemic profile of Shiga-toxin-producing *Escherichia coli* O104:H4 outbreak in Germany. *N Engl J Med*. 2011;365:1771–80. <https://doi.org/10.1056/NEJMoa1106483>
3. Paton AW, Woodrow MC, Doyle RM, Lanser JA, Paton JC. Molecular characterization of a Shiga toxigenic *Escherichia coli* O113:H21 strain lacking *eae* responsible for a cluster of cases of hemolytic-uremic syndrome. *J Clin Microbiol*. 1999;37:3357–61. <https://doi.org/10.1128/JCM.37.10.3357-3361.1999>
4. Schifferli A, von Vigier RO, Fontana M, Sparta G, Schmid H, Bianchetti MG, et al.; Swiss Pediatric Surveillance Unit. Hemolytic-uremic syndrome in Switzerland: a nationwide surveillance 1997–2003. *Eur J Pediatr*. 2010;169:591–8. <https://doi.org/10.1007/s00431-009-1079-9>
5. Iguchi A, Nishii H, Seto K, Mitobe J, Lee K, Konishi N, et al. Additional Og-typing PCR techniques targeting *E. coli*-novel and Shigella-unique O-antigen biosynthesis gene clusters. *J Clin Microbiol*. 2020;58:e01493–20. <https://doi.org/10.1128/JCM.01493-20>
6. DebRoy C, Fratamico PM, Yan X, Baranzoni G, Liu Y, Needleman DS, et al. Comparison of O-antigen gene clusters of all O-serogroups of *Escherichia coli* and proposal for adopting a new nomenclature for O-typing. *PLoS One*. 2016;11:e0147434-e.
7. Lee K, Izumiya H, Iyoda S, Ohnishi M. Effective surveillance using multilocus variable-number tandem-repeat analysis and whole-genome sequencing for enterohemorrhagic *Escherichia coli* O157. *Appl Environ Microbiol*. 2019;85:e00728–19. <https://doi.org/10.1128/AEM.00728-19>
8. Kimata K, Lee K, Watahiki M, Isobe J, Ohnishi M, Iyoda S. Global distribution of epidemic-related Shiga toxin 2 encoding phages among enteroaggregative *Escherichia coli*. *Sci Rep*. 2020;10:11738. <https://doi.org/10.1038/s41598-020-68462-9>
9. Yoshimura D, Kajitani R, Gotoh Y, Katahira K, Okuno M, Ogura Y, et al. Evaluation of SNP calling methods for closely related bacterial isolates and a novel high-accuracy pipeline: BactSNP. *Microb Genom*. 2019;5:e000261. <https://doi.org/10.1099/mgen.0.000261>
10. Croucher NJ, Page AJ, Connor TR, Delaney AJ, Keane JA, Bentley SD, et al. Rapid phylogenetic analysis of large samples of recombinant bacterial whole genome sequences using Gubbins. *Nucleic Acids Res*. 2015;43:e15. <https://doi.org/10.1093/nar/gku1196>
11. Gonzalez-Escalona N, McFarland MA, Rump LV, Payne J, Andrzejewski D, Brown EW, et al. Draft genome sequences of two O104:H21 *Escherichia coli* isolates causing hemorrhagic colitis during a 1994 Montana outbreak provide insight into their pathogenicity. *Genome Announc*. 2013;1:e00805–13. <https://doi.org/10.1128/genomeA.00805-13>
12. Banjo M, Iguchi A, Seto K, Kikuchi T, Harada T, Scheutz F, et al.; Pathogenic *E. coli* Working Group in Japan. *Escherichia coli* H-genotyping PCR: a complete and practical platform for molecular H typing. *J Clin Microbiol*. 2018;56:e00190–18. <https://doi.org/10.1128/JCM.00190-18>
13. Iguchi A, Iyoda S, Seto K, Nishii H, Ohnishi M, Mekata H, et al. Six novel O genotypes from Shiga toxin-producing *Escherichia coli*. *Front Microbiol*. 2016;7:765. <https://doi.org/10.3389/fmicb.2016.00765>
14. Lee K, Morita-Ishihara T, Iyoda S, Ogura Y, Hayashi T, Sekizuka T, et al.; EHEC Working Group in Japan. A geographically widespread outbreak investigation and development of a rapid screening method using whole genome sequences of enterohemorrhagic *Escherichia coli* O121. *Front Microbiol*. 2017;8:701. <https://doi.org/10.3389/fmicb.2017.00701>
15. Holmes A, Allison L, Ward M, Dallman TJ, Clark R, Fawkes A, et al. Utility of whole-genome sequencing of *Escherichia coli* O157 for outbreak detection and epidemiological surveillance. *J Clin Microbiol*. 2015;53:3565–73. <https://doi.org/10.1128/JCM.01066-15>

Address for correspondence: Kenichi Lee, Department of Bacteriology I, National Institute of Infectious Diseases, 1-23-1, Toyama, Shinjuku, Tokyo, 1628640, Japan; email: leek@niid.go.jp

Coordinated Response to Imported Vaccine-Derived Poliovirus Infection, Barcelona, Spain, 2019–2020

Dolores Álamo-Junquera, Julieta Politi, Pere Simón, Romina Dieli-Crimi, Ricardo Pujol Borrell, Roger Colobran, Monica Martínez-Gallo, Magda Campins, Andrés Antón, Juliana Esperalba, Cristina Andrés, María Gema Codina, Eva Polverino, M. Rosa Narciso, Emilia Molinero, Cristina Rius

In 2019, the Public Health Agency of Barcelona, Spain, was notified of a vaccine-derived poliovirus infection. The patient had an underlying common variable immunodeficiency and no signs of acute flaccid paralysis. We describe the ongoing coordinated response to contain the infection, which included compassionate-use treatment with pocapavir.

In the nearly 30 years since the inception of the Global Polio Eradication Initiative (GPEI) by the World Health Organization (WHO), polio eradication efforts have decreased the number of wild poliovirus (WPV) cases by more than 99%, from 350,000 worldwide in 1988 to only 143 reported cases in 2019 (1). The trivalent Sabin vaccine (oral polio vaccine [OPV]), chosen for the eradication program, results in a temporary intestinal infection in immunocompetent persons. These vaccine-derived strains can revert to being neurovirulent after vaccination, especially in immunocompromised patients, leading to vaccine-associated paralytic poliomyelitis or chronic poliovirus infection (2).

The Polio Eradication and Endgame Strategic Plan 2013–2018 established by the GPEI proposed introducing inactivated polio vaccine (IPV) into routine

childhood vaccination and eventually removing OPV from global use (3). This transition began in 2016 with the replacement of trivalent OPV with bivalent OPV types 1 and 3 (4).

After WHO declared a Public Health Emergency of International Concern regarding WPV in 2014 (5), worldwide eradication of indigenous WPV serotype 2 was declared in 2015 (6). Worldwide eradication of WPV serotype 3 was achieved in 2019, after the last case of WPV serotype 3 was reported in Nigeria in 2012 (7). Nonetheless, endemic transmission of WPV serotype 1 continues to cause cases in Afghanistan and Pakistan (9).

In Spain, the last endemic case of WPV occurred in 1988, which prompted improvement in polio vaccination coverage and replacement of OPV with IPV in 2004. Although the WHO's European Region has been certified polio-free since 2002, the risk for imported cases of WPV or vaccine-derived polioviruses (VDPVs) from other countries still exists.

Primary immunodeficiencies are a heterogeneous group of disorders with a substantial hereditary component. In patients with primary immunodeficiencies, the immune response to microbial pathogens is defective, leading to higher susceptibility to infections, which can then become chronic (9). These patients can become infected by immunization if they receive live vaccines (10), and these infections can pose a risk to immunodeficient contacts and potentially jeopardize the success of the GPEI (11).

Case Report

In May 2019, the Public Health Agency of Barcelona (PHAB) was notified about a poliovirus infection in an asymptomatic person with a primary immunodeficiency, identified through ongoing nonpolio

Author affiliations: Public Health Agency of Barcelona, Barcelona, Spain. (D. Álamo-Junquera, J. Politi, P. Simón, E. Molinero, C. Rius); Parc de Salut Mar, Barcelona (J. Politi); Hospital Universitari Vall d'Hebron, Barcelona (R. Dieli-Crimi, R. Pujol Borrell, R. Colobran, M. Martínez-Gallo, M. Campins, A. Antón, J. Esperalba, M. Gema Codina, E. Polverino); Universitat Autònoma de Barcelona, Barcelona (R. Colobran, M. Martínez-Gallo, M. Campins, A. Antón, J. Esperalba, M. Gema Codina); Institut Català de la Salut, Barcelona (M.R. Narciso); Centro de Investigación Biomédica en Red de Epidemiología y Salud Pública, Barcelona (C. Rius)

DOI: <https://doi.org/10.3201/eid2705.204675>

enterovirus surveillance at Vall d'Hebron Hospital (Barcelona), which conducted VP1 sequencing of all detected enteroviruses (Figure). The patient, a 26-year-old man, tested positive for enterovirus (identified as poliovirus types 1 and 3) in a pharyngeal swab specimen. His medical history included a common variable immunodeficiency that had been diagnosed in 2012 and treated with intravenous immunoglobulin-replacement therapy.

Born in Pakistan, the patient had lived in Barcelona since 2010, and the household included 4 family members (parents, partner, and child). He was a cook at a local restaurant. The patient was adequately vaccinated with 3 polio vaccine doses in 1993 in Pakistan (probably trivalent OPV) and 1 dose of IPV in 2015 in Barcelona. His child was correctly vaccinated with IPV, in accordance with the vaccine schedule of Catalonia, of which Barcelona is the capital. His parents reported previous vaccination with 3 OPV doses in Pakistan. His partner recalled receiving their most recent OPV dose in February 2017 before leaving Pakistan for Barcelona; they had also received 3 doses of OPV as a child in Pakistan.

Neither the patient nor his 4 household members reported recent travel to polio-endemic areas. However, they recalled receiving visits by relatives and friends who frequently traveled to Pakistan.

After the notification, a public health nurse visited the patient and his family to collect epidemiologic

information and stool samples and to explain how to prevent transmission. National public health authorities also were notified.

The patient's stool samples were positive for poliovirus types 1 and 3. The grade of divergence to the parent Sabin strain (2.7% for type 1 and 1.5% for type 3) was consistent with a 2-year reproduction time. A recovered respiratory sample collected from the patient in January 2019 also tested positive for both strains. In contrast, the stool samples of the 4 household members tested negative for poliovirus.

To coordinate the epidemiologic investigation and determine future actions, PHAB convened all the healthcare professionals involved in the patient's follow-up, including primary-care clinicians and hospital specialists. Polio immunization coverage in the patient's surrounding community was confirmed to be >95%, and environmental samples did not show any evidence of circulation in the community. Contact tracing, beyond family members, included work contacts, healthcare personnel, and other patients. A total of 59 persons exposed were vaccinated with IPV. In addition, a contact-precautions alert was added to the patient's electronic medical record. Because he worked as a food handler, and given the possibility of a long excretion period, PHAB authorized a medical leave and suggested a reorientation of his professional career.

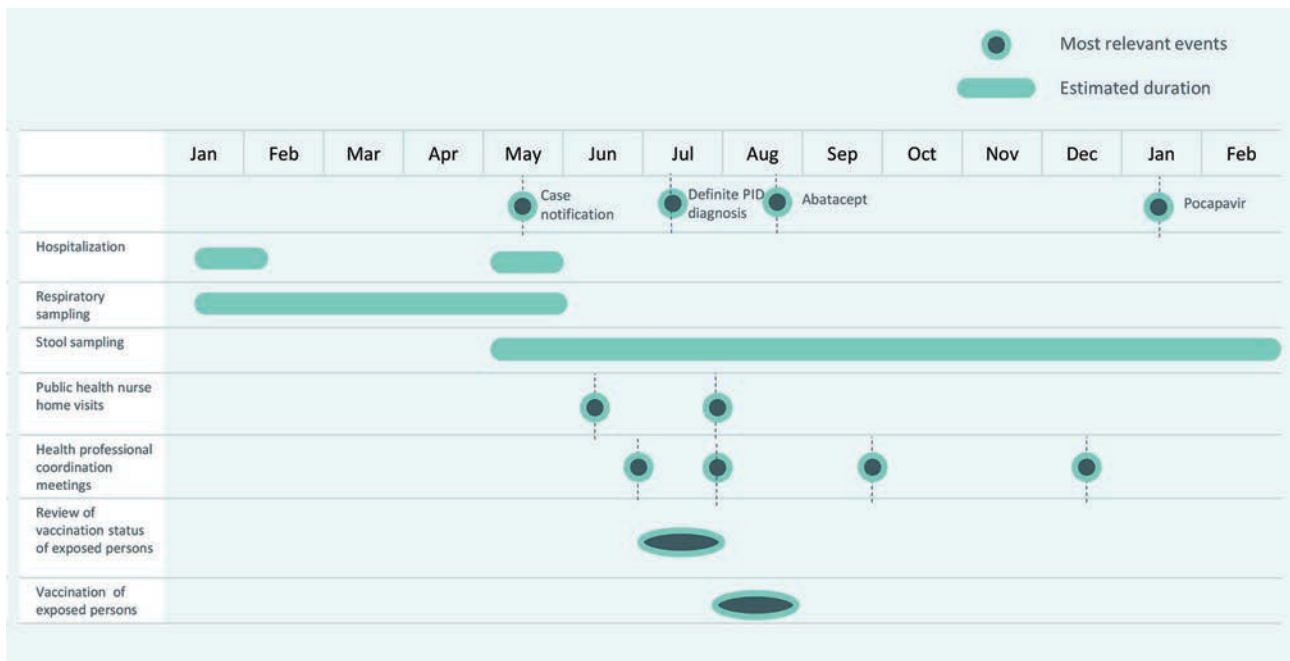


Figure. Timeline of public health actions in response to an imported vaccine-derived poliovirus infection, Barcelona, Spain, 2019–2020. PID, primary immunodeficiency.

Further testing of the patient was indicated after the first meeting. Massive parallel sequencing identified a mutation supporting the diagnosis of CTLA-4 deficiency, a dominant monogenic disease, specifically an autoimmune lymphoproliferative syndrome, type V, which is treatable. Abatacept (a recombinant soluble form of CTLA-4) was started in August 2019 and resulted in substantial clinical improvement. Specific treatment with pocapavir (authorized for compassionate use) was provided by ViroDefense Inc. (Chevy Chase, MD, USA) and was started in January 2020.

To date, the patient's poliovirus excretion is monitored by monthly stool samples and pharyngeal swab specimens every 6 months. Although the most recent pharyngeal swab specimens was negative, stool samples remain intermittently positive. Stool samples provided by household members every 6 months continue to be negative. No onward transmission has been identified.

Conclusions

We report a chronic vaccine-derived poliovirus excretion in a person with a primary immunodeficiency who was living in a polio-free country. Immunodeficient patients have a high risk for becoming chronic primary immunodeficiency carriers and face an increased risk for VDPV complications. In a nonendemic area, the most likely infection source is secondary exposure to vaccine-related strains imported by persons vaccinated in countries that have ongoing vaccination with OPV.

Because patients with antibody deficiency are susceptible to vaccine-associated paralytic poliomyelitis, OPV and other live vaccines are contraindicated in such persons. However, the diagnosis of an antibody deficiency often is delayed, making this recommendation challenging.

The grade of divergence to the parent Sabin strain is estimated to occur at a rate of 1.1% per year for the capsid protein (VP1) region, which for this case is consistent with a 2-year excretion. This finding, along with the OPV vaccination of the patient's partner in 2017, supports secondary exposure to be the most likely source of infection.

In a polio-free country, the occurrence of vaccine-derived carriers is infrequent. However, persons with immunodeficiency-related VDPV infection can maintain prolonged excretions while remaining asymptomatic (12). Detection of asymptomatic poliovirus infections entails difficulties, as in the case we have described. Physicians treating patients with primary immunodeficiency might encourage their

screening by including serial stool samples for all newly identified patients with primary immunodeficiency. Results from stool specimen screening should be included in a global poliovirus surveillance reporting system (13).

Antivirals represent a potential means to manage immunodeficiency-related VDPV excretors and the risk their conditions represent to eradication efforts (14). Currently, pocapavir is being considered for use in poliovirus-excreting patients with primary immunodeficiency on a compassionate-use basis (15). The case-patient we describe has been treated with pocapavir, although viral excretion remained active at the time of this report. Further research is needed to identify effective antiviral drugs. In conclusion, in certified polio-free countries, clinical and virologic surveillance guidelines must address asymptomatic poliovirus carriers and the need for screening in immunocompromised persons.

About the Author

Dr. Álamo-Junquera is a public health technical officer at the Epidemiology Service of the Public Health Agency of Barcelona, Spain. Her main research interests are surveillance, prevention, and control of infectious diseases.

References

1. Global Polio Eradication Initiative. Global wild poliovirus 2014–2019 [cited 2021 Jan 10]. <https://polioeradication.org/wp-content/uploads/2020/01/Weekly-GPEI-Polio-Analyses-wpv-20191231.pdf>
2. Dunn G, Klapsa D, Wilton T, Stone L, Minor PD, Martin J. Twenty-eight years of poliovirus replication in an immunodeficient individual: impact on the Global Polio Eradication Initiative. *PLoS Pathog*. 2015;11:e1005114. <https://doi.org/10.1371/journal.ppat.1005114>
3. Li L, Ivanova O, Driss N, Tiongco-Recto M, da Silva R, Shahmahmoodi S, et al. Poliovirus excretion among persons with primary immune deficiency disorders: summary of a seven-country study series. *J Infect Dis*. 2014;210(Suppl 1):S368–72. <https://doi.org/10.1093/infdis/jiu065>
4. Duintjer Tebbens RJ, Hampton LM, Thompson KM. Implementation of coordinated global serotype 2 oral poliovirus vaccine cessation: risks of potential non-synchronous cessation. *BMC Infect Dis*. 2016;16:231. <https://doi.org/10.1186/s12879-016-1536-9>
5. World Health Organization. WHO statement on the meeting of the International Health Regulations Emergency Committee concerning the international spread of wild poliovirus [cited 2020 Feb 15]. <https://www.who.int/mediacentre/news/statements/2014/polio-20140505/en/#.XkeU7O5-dMM.mendeley>
6. Global Polio Eradication Initiative. Global eradication of wild poliovirus type 2 declared [cited 2020 Nov 15]. <https://polioeradication.org/news-post/global-eradication-of-wild-poliovirus-type-2-declared>
7. World Health Organization. Poliomyelitis [cited 2020 Nov 15]. <https://www.who.int/news-room/fact-sheets/detail/poliomyelitis>

8. Makoni M. Africa eradicates wild polio. *Lancet Microbe*. 2020;1:e243. [https://doi.org/10.1016/S2666-5247\(20\)30152-X](https://doi.org/10.1016/S2666-5247(20)30152-X)
9. Picard C, Al-Herz W, Bousfiha A, Casanova JL, Chatila T, Conley ME, et al. Primary immunodeficiency diseases: an update on the classification from the International Union of Immunological Societies Expert Committee for Primary Immunodeficiency 2015. *J Clin Immunol*. 2015;35:696–726. <https://doi.org/10.1007/s10875-015-0201-1>
10. Eibl MM, Wolf HM. Vaccination in patients with primary immune deficiency, secondary immune deficiency and autoimmunity with immune regulatory abnormalities. *Immunotherapy*. 2015;7:1273–92. <https://doi.org/10.2217/IMT.15.74>
11. Shaghghi M, Shahmahmoodi S, Abolhassani H, Soleyman-Jahi S, Parvaneh L, Mahmoudi S, et al. Vaccine-derived polioviruses and children with primary immunodeficiency, Iran, 1995–2014. *Emerg Infect Dis*. 2016;22:1712–9. <https://doi.org/10.3201/eid2210.151071>
12. Macklin G, Liao Y, Takane M, Dooling K, Gilmour S, Mach O, et al.; iDVPV Working Group. Prolonged excretion of poliovirus among individuals with primary immunodeficiency disorder: an analysis of the World Health Organization registry. *Front Immunol*. 2017;8:1103. <https://doi.org/10.3389/fimmu.2017.01103>
13. Global Polio Eradication Initiative. Guidelines for implementing poliovirus surveillance among patients with primary immunodeficiency disorders (PIDs) [cited 2020 Nov 15]. <https://polioeradication.org/wp-content/uploads/2020/12/Guidelines-for-Implementing-PID-Suveillance-3.3-20201215.pdf>
14. Duintjer Tebbens RJ, Pallansch MA, Thompson KM. Modeling the prevalence of immunodeficiency-associated long-term vaccine-derived poliovirus excretors and the potential benefits of antiviral drugs. *BMC Infect Dis*. 2015;15:379. <https://doi.org/10.1186/s12879-015-1115-5>
15. Aghamohammadi A, Abolhassani H, Kutukculer N, Wassilak SG, Pallansch MA, Kluglein S, et al.; JMF Centers Network Investigators and Study Collaborators. Patients with primary immunodeficiencies are a reservoir of poliovirus and a risk to polio eradication. *Front Immunol*. 2017;8:685. <https://doi.org/10.3389/fimmu.2017.00685>

Address for correspondence: Dolores Álamo-Junquera, Epidemiology Service, Public Health Agency of Barcelona, Barcelona, Spain. Pl. de Lesseps, 1, 08023 Barcelona, Spain; email: lola.alamo@gmail.com

prions *Plasmodium knowlesi* cholera tularemia
Eptesicus fuscus syncytium *Klebsiella*
 Kaposi *Leptospira* sapovirus yaws *Rickettsia*
Vibrio vulnificus Quinine variola *Campylobacter* *Acinetobacter*
 Chagas disease rotavirus Lyssavirus *Aspergillus*
 botulism *Escherichia coli* *Babesia* hemozoin
 syphilis knemidocoptic mange *Bordetella* *Leishmaniasis*
Naegleria fowleri Ehrlichia *Leishmaniasis*
 Anopheles *Bordetella* rabies
 Verona integrin vaccination *Artemisinin* Dengue Zika virus
 Herpesvirus *Artemisinin* *Dengue* *Shigella*
 Borna disease virus Ebola *Franciscella tularensis* typhus *Rickettsia*
 orf *Coxiella burnetii* kobuvirus *Candida* Q fever
Orientia tsutsugamushi Bocavirus chimera *Brucella*
 Norovirus tuberculosis quarantine Mange tetanus
 Malaria measles *Borrelia* Leprosy influenza
 Chikungunya pertactin *Borrelia* Leprosy influenza
 Calcivirus quarantine Peste des petits ruminants
 melioidosis Diphtheria *O'nyong-nyong virus* *Pseudoterranova azarasi*
 pertussis Merkel cells *Ignatzschineria* Glanders *Yersinia*
 featured **EMERGING**
 monthly in **INFECTIOUS DISEASES** <http://wwwnc.cdc.gov/eid/articles/etymologia>

Intersecting Paths of Emerging and Reemerging Infectious Diseases

Tais M. Wilson, Christopher D. Paddock, Sarah Reagan-Steiner, Julu Bhatnagar, Roosecelis B. Martines, Andrea L. Wiens, Michael Madsen, Kenneth K. Komatsu, Heather Venkat, Sherif R. Zaki

Author affiliations: Universidade de Brasília, Brasília, Brazil (T.M. Wilson); Centers for Disease Control and Prevention, Atlanta, Georgia, USA (T.M. Wilson, C.D. Paddock, S. Reagan-Steiner, J. Bhatnagar, R.B. Martines, H. Venkat, S.R. Zaki); Pinal County Office of the Medical Examiner, Florence, Arizona, USA (A.L. Wiens); Coconino County Health and Human Services Medical Examiner's Office, Flagstaff, Arizona, USA (M. Madsen); Arizona Department of Health Services, Phoenix, Arizona, USA (K.K. Komatsu, H. Venkat)

DOI: <https://doi.org/10.3201/eid2705.204779>

Severe acute respiratory syndrome coronavirus 2 (SARS-CoV-2) shares common clinicopathologic features with other severe pulmonary illnesses. Hantavirus pulmonary syndrome was diagnosed in 2 patients in Arizona, USA, suspected of dying from infection with SARS-CoV-2. Differential diagnoses and possible co-infections should be considered for cases of respiratory distress during the SARS-CoV-2 pandemic.

Severe acute respiratory syndrome coronavirus 2 (SARS-CoV-2), the virus that causes coronavirus disease (COVID-19), emerged in Wuhan, China, during December 2019 and spread rapidly to other parts of China and the world (1). However, the clinical and pathologic features of COVID-19 are also found for other respiratory disease, such as hantavirus pulmonary syndrome (HPS). In 1993, a hantavirus (*Sin Nombre virus*) and its rodent reservoir (*Peromyscus maniculatus* deer mouse) were identified as the causative agent and vertebrate reservoir responsible for an outbreak of severe pulmonary illness, named HPS, in the Four Corners region in the southwestern United States (2–4).

Soon after the emergence and recognition of COVID-19 in the United States in early 2020, the Infectious Diseases Pathology Branch, Division of High-Consequence Pathogens and Pathology, National Center for Emerging and Zoonotic Infectious Diseases, Centers for Disease Control and Prevention initiated diagnostic testing of fixed tissue specimens from deceased persons who had suspected or confirmed SARS-CoV-2 infection (5,6). During

May 2020, Infectious Diseases Pathology Branch received tissues from an 11-year-old child (patient 1) from Arizona, who died after a brief illness culminating in severe respiratory distress. Histopathological findings included diffuse alveolar damage with rare hyaline membranes, intraalveolar edema, leukocytosis with a left shift (Figure, panel A), interstitial pneumonitis and immunoblasts in the red pulp and periarteriolar sheaths of the spleen (Figure, panel B). RNA extracted from formalin-fixed, paraffin-embedded trachea and lung tissues was positive for SARS-CoV-2 by conventional reverse transcription PCR (RT-PCR) and sequencing of positive amplicons. However, evaluation for SARS-CoV-2 by using an immunohistochemical (IHC) assay (5) showed negative results.

Subsequently, embalmed lung tissues were received from the child's mother, a 25-year-old woman (patient 2) who died 2 days before the child after a brief illness characterized by progressive shortness of breath, cough, abdominal pain, fever, and hemoptysis. Histopathologic findings for the lungs of patient 2 resembled those identified for patient 1 (Figure, panels C, D), but there was no evidence of SARS-CoV-2 in the lung tissues by RT-PCR. Because clinicopathologic features were characteristic of HPS, we performed IHC assay for hantavirus. IHC showed typical punctate granular staining of hantaviral antigens in pulmonary and glomerular capillaries, characteristic of HPS (4) (Figure, panels E, F). IHC evaluation of lung and kidney tissues of patient 1 for hantavirus showed a similar pattern, confirming the infection in both patients (Figure, panel A, right side).

The clinicopathologic and IHC findings indicate that both patients died from HPS. Although SARS-CoV-2 RNA was detected by RT-PCR in patient 1, it was not the probable underlying cause of death. This scenario provides an essential reminder that previously recognized, nonendemic infectious diseases that clinically resemble COVID-19 continue to occur during the pandemic, in a manner similar to other clinicopathologic mimics described previously during other pandemic diseases (7).

Consideration of alternative diagnoses of diseases that precipitate acute respiratory distress syndrome and co-infections remains crucial for diagnosing and treating of critically ill patients, as well as accurately determining causes of death. For HPS, triage tools such as peripheral blood smear review and identifying 4 of 5 findings (thrombocytopenia, hemoconcentration, granulocytic left shift, absence of toxic changes, and >10% immunoblasts) can be used

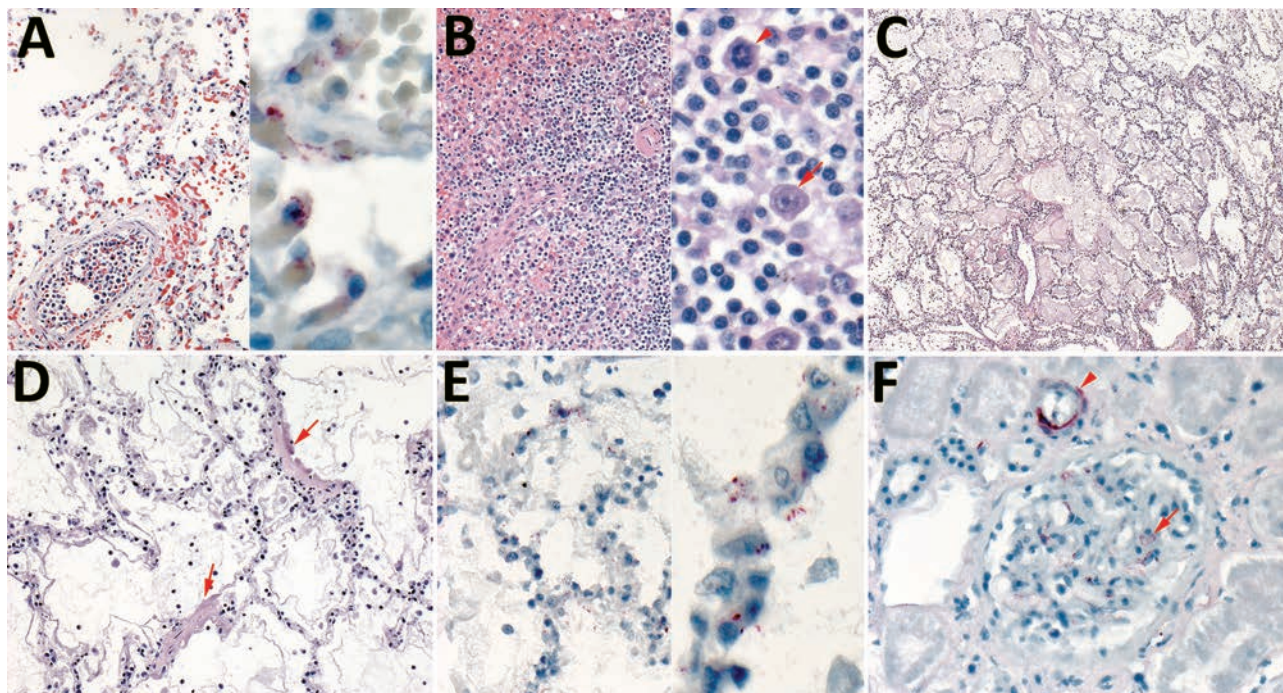


Figure. Histopathologic and immunohistochemical characteristics of fatal hantavirus pulmonary syndrome in 2 patients, Arizona, USA, 2020. A) Patient 1 lung tissue, showing intravascular leukocytosis with left shift (left, original magnification $\times 50$) and hantavirus antigen immunostaining (red) in pulmonary microvasculature (right, original magnification $\times 158$). B) Patient 1 spleen tissue, showing immunoblast proliferation in the red pulp and periarteriolar sheaths (left, original magnification $\times 50$) and immunoblasts with high nuclear to cytoplasmic ratio, vesicular and prominent nucleoli (arrows) and mitosis (arrowhead) (right, original magnification $\times 158$). C) Patient 2 lung tissue, showing severe intraalveolar edema (original magnification $\times 12.5$). D) Patient 2 lung tissue, showing interstitial pneumonitis with hyaline membranes (arrows) (original magnification $\times 50$). E) Patient 2 lung tissue, showing hantavirus antigen immunostaining (red) in pulmonary microvasculature (left, original magnification $\times 50$; right, original magnification $\times 158$). F) Patient 2 kidney tissue, showing hantavirus antigen immunostaining (red) in glomerular capillaries (arrowhead) and interstitial vessel (arrow) (original magnification $\times 100$).

to diagnose the disease rapidly and presumptively in the clinical setting (8,9). Communication and partnerships of local, state, and federal public health officials and healthcare professionals, including clinicians, infectious disease specialists, pathologists, and medical examiners, are essential during these challenging times of the SARS-CoV-2 pandemic.

This study was supported by the Coordenação de Aperfeiçoamento de Pessoal de Nível Superior Brazil (Finance Code 001; doctoral scholarship for T.M.W.).

About the Author

Ms. Wilson is a guest researcher, as part of a doctoral scholarship from the Capes-PrInt Program, in the Division of High-Consequence Pathogens and Pathology, National Center for Emerging and Zoonotic Infectious Diseases, Centers for Disease Control and Prevention, Atlanta, GA. Her research interests include investigative and comparative pathology and pathogenesis of zoonotic and human infectious diseases.

References

1. Zhu N, Zhang D, Wang W, Li X, Yang B, Song J, et al.; China Novel Coronavirus Investigating and Research Team. A novel coronavirus from patients with pneumonia in China, 2019. *N Engl J Med.* 2020;382:727-33. <https://doi.org/10.1056/NEJMoa2001017>
2. Duchin JS, Koster FT, Peters CJ, Simpson GL, Tempest B, Zaki SR, et al.; The Hantavirus Study Group. Hantavirus pulmonary syndrome: a clinical description of 17 patients with a newly recognized disease. *N Engl J Med.* 1994;330:949-55. <https://doi.org/10.1056/NEJM199404073301401>
3. Nichol ST, Spiropoulou CF, Morzunov S, Rollin PE, Ksiazek TG, Feldmann H, et al. Genetic identification of a hantavirus associated with an outbreak of acute respiratory illness. *Science.* 1993;262:914-7. <https://doi.org/10.1126/science.8235615>
4. Zaki SR, Greer PW, Coffield LM, Goldsmith CS, Nolte KB, Foucar K, et al. Hantavirus pulmonary syndrome: pathogenesis of an emerging infectious disease. *Am J Pathol.* 1995;146:552-79.
5. Martines RB, Ritter JM, Matkovic E, Gary J, Bollweg BC, Bullock H, et al.; COVID-19 Pathology Working Group. Pathology and pathogenesis of SARS-CoV-2 associated with fatal coronavirus disease, United States. *Emerg Infect Dis.* 2020;26:2005-15. <https://doi.org/10.3201/eid2609.202095>

6. Centers for Disease Control and Prevention. Collection and submission of postmortem specimens from deceased persons with known or suspected COVID-19, November 2020 (Interim Guidance) [cited 2020 Oct 21]. <https://www.cdc.gov/coronavirus/2019-ncov/hcp/guidance-postmortem-specimens.html>
7. Blau DM, Denison AM, Bhatnagar J, DeLeon-Carnes M, Drew C, Paddock C, et al.; Infectious Diseases Pathology Branch Working Group. Fatal infectious diseases during pandemic (H1N1) 2009 outbreak. *Emerg Infect Dis*. 2011;17:2069–70. <https://doi.org/10.3201/eid1711.110429>
8. Koster F, Foucar K, Hjelle B, Scott A, Chong YY, Larson R, et al. Rapid presumptive diagnosis of hantavirus cardiopulmonary syndrome by peripheral blood smear review. *Am J Clin Pathol*. 2001;116:665–72. <https://doi.org/10.1309/CNWF-DC72-QYMR-M8DA>
9. Dvorscak L, Czuchlewski DR. Successful triage of suspected hantavirus cardiopulmonary syndrome by peripheral blood smear review: a decade of experience in an endemic region. *Am J Clin Pathol*. 2014;142:196–201. <https://doi.org/10.1309/AJCPNFVWG46NUHED>

Address for correspondence: Sherif R. Zaki, Centers for Disease Control and Prevention, 1600 Clifton Rd NE, Mailstop H18-SB, Atlanta, GA 30329-4027, USA; e-mail: szaki@cdc.gov

Novel Mutation of SARS-CoV-2, Vietnam, July 2020

Hoang Vu Mai Phuong,¹ Trinh Son Tung,¹ Ung Thi Hong Trang, Nguyen Le Khanh Hang, Nguyen Vu Son, Pham thi Hien, Le thi Thanh, Vuong Duc Cuong, Ton That Thanh, Nguyen thi Thanh Nhan, Tran Nhu Duong, Ngu Duy Nghia, Tran Anh Tu, Marc Choisy, Maia A. Rabaa, H. Rogier van Doorn, Dang Duc Anh, Le Quynh Mai

Author affiliations: National Institute of Hygiene and Epidemiology, Hanoi, Vietnam (H.V.M. Phuong, U.T.H. Trang, N.L.K. Hang, N.V. Son, P. thi Hien, L. thi Thanh, V.D. Cuong, T.N. Duong, N.D. Nghia, T.A. Tu, D.D. Anh, L.Q. Mai); Oxford University Clinical Research Unit, Hanoi (T.S. Tung, H.R. van Doorn); Centre for Disease Control and Prevention, Danang, Vietnam (T.T. Thanh, N. thi T. Nhan); Oxford University Clinical Research Unit, Ho Chi Minh City, Vietnam (M. Choisy, M.A. Rabaa); University of Oxford, Oxford, UK (M. Choisy, M.A. Rabaa, H.R. van Doorn)

DOI: <https://doi.org/10.3201/eid2705.210013>

¹These authors equally contributed to this work.

A cluster of severe acute respiratory syndrome coronavirus 2 infections in Danang, Vietnam, began July 25, 2020, and resulted in 551 confirmed cases and 35 deaths as of February 2021. We analyzed 26 sequences from this cluster and identified a novel shared mutation in nonstructural protein 9, suggesting a single introduction into Vietnam.

Vietnam experienced 2 clusters of severe acute respiratory syndrome coronavirus 2 (SARS-CoV-2) infections during January 23–April 15, 2020 (270 cases, 163/270 imported) (1–4). After 99 days without community transmission, a cluster of SARS-CoV-2 infections of unknown origin was detected in Danang; it was found in Danang General Hospital on July 25 in a 57-year-old male patient (DN001) experiencing pneumonia who had no travel history. During a subsequent round of contact tracing, 14 additional SARS-CoV-2-positive cases were detected both in the community (n = 3) and Danang hospitals (n = 11). Vietnam then initiated large-scale contact tracing and quarantining. A total of 551 confirmed cases were reported from 15 cities and provinces across the country; 540 (98%) either were related to major hospitals in Danang or were in patients who had visited Danang during July 25–September 3. This cluster included 35 COVID-19 fatalities, most (32) hospital-acquired and associated with concurrent conditions or old age (2,5). Danang General Hospital, the epicenter of the outbreak, reported 246 cases among inpatients, caregivers, and health-care workers. Strict prevention measures of contact tracing, quarantine, and isolation were again implemented nationally, and the outbreak was successfully contained. We describe the molecular epidemiology of this cluster.

We performed sequencing of 26 nasopharyngeal or throat swab specimens that were sent to the National Institute of Hygiene and Epidemiology (Hanoi, Vietnam) for diagnostics; all were positive for SARS-CoV-2 and had cycle threshold value <30 by real-time reverse transcription PCR (6–8). Of those specimens, 18 were collected from patients in hospitals and communities in Danang and the rest from outside Danang: Ha Nam (1), Quang Nam (1), Thanh Hoa (1), Hanoi (2), Lang Son (2), and Hai Duong (1). We uploaded sequences to the GISAID database (<https://www.gisaid.org>; accession nos. 759869–91 and 766029–31).

All 26 sequences belonged to lineage B.1.1 and clustered together in the global tree, with the exception of DN013 (Figure 1, panel A). DN013 contains an additional single-nucleotide polymorphism

(SNP), C835T, that is also present in sequences from India and that artifactually clusters with those sequences in the global tree (Figure 1, panel A). A

novel SNP at position 12772 (A>C) was found in all 26 sequences; it represents a nonsynonymous mutation in nonstructural protein 9 resulting in a leucine

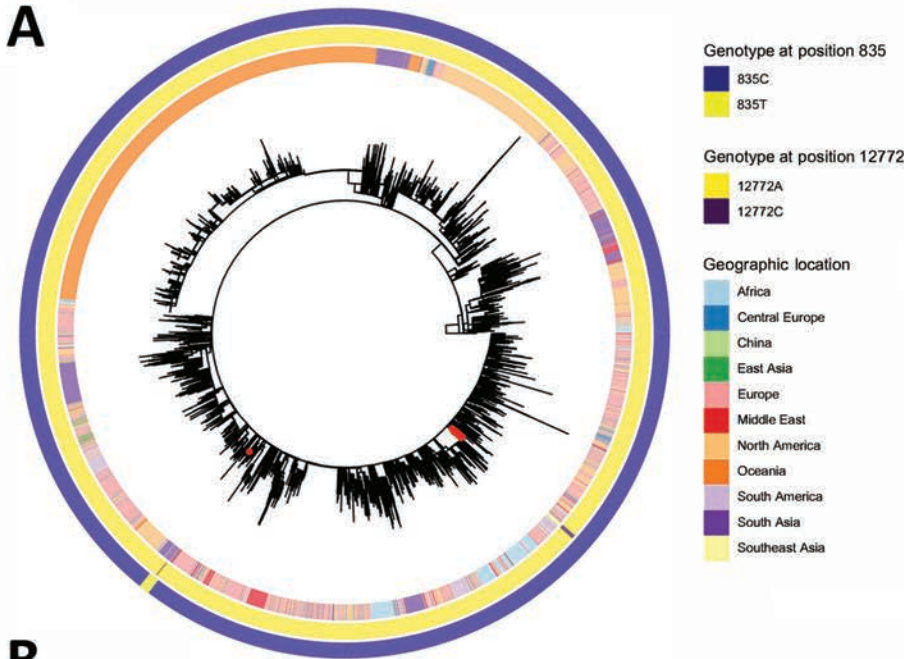
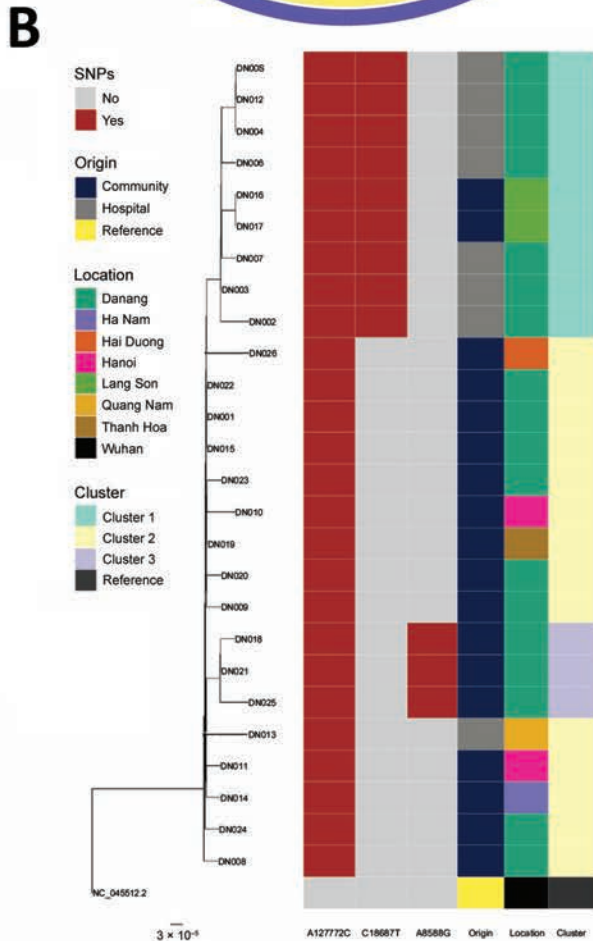


Figure. Maximum likelihood phylogenetic trees of SARS-CoV-2 B.1.1 lineage sequences globally and sequences from Danang, Vietnam. A) Global maximum-likelihood phylogenetic tree of SARS-CoV-2 B.1.1 lineage. The phylogeny was inferred with the general time-reversible plus frequencies model using 1,000 bootstrap replicates. Red dots represent viruses from the Danang cluster. The outer ring shows lineage as determined using Pangolin (<https://github.com/cov-lineages/pangolin/releases/tag/v2.3.0>), and the inner ring shows the geographic location of collection. B) Maximum-likelihood phylogenetic tree built from 26 Danang-related SARS-CoV-2 sequences (represented by DN plus a 3-digit number); the Wuhan strain genome (GenBank accession no. NC_045512.2) is an outgroup. Columns to the right show the nucleotide variation in 3 locations on the SARS-CoV-2 genome that define phylogenetic clusters in the Danang cluster with their origin, the location the patients were found, and the cluster of the sequence. The ModelFinder Plus option Hasegawa-Kishino-Yano substitution model, including modelling of amino acid frequencies was the best model for these samples. Scale bar indicates substitutions per site. SARS-CoV-2, severe acute respiratory syndrome coronavirus 2.



to phenylalanine change at amino acid site 4169 in open reading frame 1ab. This SNP was not reported in any other sequences collected globally and has no known associations with virulence or transmissibility. Sequences further clustered into 3 groups based on additional SNPs: cluster 1, a hospital cluster from the 2 largest hospitals in Danang (n = 9); cluster 2, a simultaneously detected community cluster within the center of Danang (n = 14); and cluster 3, a community cluster in the Son Tra district of Danang, detected August 6–8 (n = 3).

A synonymous mutation, C18687T, defines cluster 1 (Figure 1, panel B). Cases belonging to cluster 1 were mostly hospital-related (inpatients, caregivers, and workers). This mutation was later also found in 2 sequences (DN016 and DN017) from Lang Son Province in patients who had recently traveled to Danang but were not linked to the hospitals. Sample size and availability of clinical metadata are limited and therefore no conclusions about transmission route and associations with severity can be drawn.

Cluster 2 is a community cluster detected in the center of Danang and among epidemiologically linked cases across the country (Hai Duong, Ha Nam, Thanh Hoa, Quang Nam); sequences carry only the unique A12772C mutation associated with this outbreak. This cluster also contains case-patient DN013, with the additional C835T SNP. An epidemiologic link between the index patient, DN001 (cluster 1), and cases of cluster 2 has not been confirmed.

Cluster 3 is defined by an additional mutation, A8588G (K2775E in open reading frame 1ab), which was found in cases DN021, DN018, and DN025. Neither of these mutations was found among B.1.1 sequences in the GISAID database.

The nonsynonymous A12772C mutation that all sequences shared, which acted as a biomarker to determine the relatedness of cases found within and outside of Danang, was not found in the GISAID database or elsewhere. This finding suggests that a single introduction of SARS-CoV-2 of unknown origin with potential undetected circulation in the community before detection in case DN001 was responsible for this cluster.

The lack of community cases found in Vietnam for 99 days before this cluster, the observed high level of nucleotide identity (99.96% minimum, 99.97% median), and the presence of a unique shared mutation indicate that this virus was unlikely to have been circulating undetected in the community since April 2020 or that this outbreak was caused by multiple importations. Given the very low circulation of SARS-CoV-2

and restricted entry, contact tracing and quarantining of contacts on the basis of exposure rather than symptoms remain effective measures to prevent and contain circulation of SARS-CoV-2 in Vietnam.

Acknowledgments

We thank the Centre for Disease Control and Prevention of Danang for support.

About the Author

Dr. Hoang is head of the virology department at the National Institute of Hygiene and Epidemiology, Hanoi, Vietnam. Her research interest is the molecular epidemiology of emerging infectious diseases. Mr. Trinh is a researcher at Oxford University Clinical Research Unit, Hanoi. His work focuses on building and exploring next-generation sequencing and viral infections by using bioinformatics, biostatistics, and modelling.

References

1. Minister of Health Vietnam. COVID-19 respiratory infections website [in Vietnamese]. 2021 [cited 2021 Feb 10]. <https://ncov.moh.gov.vn>
2. World Health Organization. Viet Nam COVID-19 situation report #7 situation summary. Recent / upcoming events and priorities. 2020 [cited 2021 Feb 23].
3. Pham QT, Rabaa MA, Duong HL, Dang QT, Tran DQ, Quach HL, et al.; OUCRU COVID-19 Research Group. The first 100 days of severe acute respiratory syndrome coronavirus 2 (SARS-CoV-2) control in Vietnam. *Clin Infect Dis.* 2020;ciaa1130. <https://doi.org/10.1093/cid/ciaa1130>
4. Le TQM, Takemura T, Moi ML, Nabeshima T, Nguyen LKH, Hoang VMP, et al. Severe acute respiratory syndrome coronavirus 2 shedding by travelers, Vietnam, 2020. *Emerg Infect Dis.* 2020;26:1624–6. <https://doi.org/10.3201/eid2607.200591>
5. World Health Organization. Viet Nam COVID-19 situation report # 6 situation summary. Recent/upcoming events and priorities. 2020 [cited 2021 Feb 23]. <https://www.who.int/docs/default-source/wpro---documents/countries/viet-nam/covid-19/vnm-moh-who-19sitrep6.pdf>
6. Nguyen LT, Schmidt HA, von Haeseler A, Minh BQ. IQ-TREE: a fast and effective stochastic algorithm for estimating maximum-likelihood phylogenies. *Mol Biol Evol.* 2015;32:268–74. <https://doi.org/10.1093/molbev/msu300>
7. Moshiri N. ViralMSA: Massively scalable reference-guided multiple sequence alignment of viral genomes. *Bioinformatics.* 2020;btaa743. <https://doi.org/10.1093/bioinformatics/btaa743>
8. World Health Organization. TIB MOLBIOL RT-PCR test kits and VirSNiP mutation assays strain surveillance. 2020 [cited 2021 Feb 23]. <https://www.tib-molbiol.de/covid-19/unknown>

Address for correspondence: Le Quynh Mai, National Institute of Hygiene and Epidemiology, Hanoi 10000, Vietnam; email: lom9@hotmail.com or ltqm@nihe.org.vn

Genomic Evidence of SARS-CoV-2 Reinfection Involving E484K Spike Mutation, Brazil

Carolina Kymie Vasques Nonaka, Marília Miranda Franco, Tiago Gräf, Camila Araújo de Lorenzo Barcia, Renata Naves de Ávila Mendonça, Karoline Almeida Felix de Sousa, Leila Machado Costa Neiva, Vagner Fosenca, Ana Verena Almeida Mendes, Renato Santana de Aguiar, Marta Giovanetti, Bruno Solano de Freitas Souza

Author affiliations: D'Or Institute for Research and Education (IDOR), São Rafael Hospital Center for Biotechnology and Cell Therapy, Salvador, Brazil (C.K. Vasques Nonaka, B. Solano de Freitas Souza); São Rafael Hospital Department of Infectology, Salvador (M.M. Franco, C. Araújo de Lorenzo Barcia, R. Naves de Ávila Mendonça, K. Almeida Felix de Sousa, A. Verena Almeida Mendes); Fundação Oswaldo Cruz, Gonçalo Moniz Institute, Salvador (T. Gräf); Coordenação Geral dos Laboratórios de Saúde Pública/Ministério da Saúde, Brasília, Brazil (V. Fosenca); University of KwaZulu-Natal College of Health Sciences, Durban, South Africa (V. Fosenca); Universidade Federal de Minas Gerais Instituto de Ciências Biológicas, Belo Horizonte, Brazil (V. Fosenca, R.S. de Aguiar, M. Giovanetti); Fundação Oswaldo Cruz Instituto Oswaldo Cruz, Rio de Janeiro (M. Giovanetti); University Campus Bio-Medico of Rome Unit of Medical Statistics and Molecular Epidemiology, Rome, Italy (M. Giovanetti)

DOI: <https://doi.org/10.3201/eid2705.210191>

Uncertainty remains about how long the protective immune responses against severe acute respiratory syndrome coronavirus 2 persists, and suspected reinfection in recovered patients has been reported. We describe a case of reinfection from distinct virus lineages in Brazil harboring the E484K mutation, a variant associated with escape from neutralizing antibodies.

Viral evolution might favor reinfections (1), and the recently described spike mutations, particularly in the receptor binding domain in severe acute respiratory syndrome coronavirus 2 (SARS-CoV-2) lineages circulating in the United Kingdom, South Africa, and most recently in Brazil (A. Rambaut et al., unpub. data, <https://virological.org/t/preliminary-genomic-characterisation-of-an-emergent-sars-cov-2-lineage-in-the-uk-defined-by-a-novel-set-of-spike-mutations/563>; H. Tegally et al., unpub. data, <https://doi.org/10.1101/2020.12.21.20248640>; C.M. Voloch et al., unpub. data, <https://doi.org/10.1101/2020.12.23.20248598>), have raised concern on their potential impact in infectivity, immune escape, and reinfection. We report a case of reinfection from distinct SARS-CoV-2 lineages in Brazil harboring the E484K mutation, a variant associated with escape from neutralizing antibodies (2; A.J. Greaney, unpub. data, <https://doi.org/10.1101/2020.12.31.425021>; Z. Liu, unpub. data, <https://doi.org/10.1101/2020.11.06.372037>).

A 45-year-old woman residing in Salvador (Bahia State, northeast Brazil) with no underlying conditions had symptoms of viral infection on 2 occasions (May 26, 2020, and October 26, 2020). In the first episode, the patient had diarrhea, myalgia, asthenia, andodynophagia for ≈ 7 days. She took 40 mg prednisone for 5 days and returned to normal activities 21 days later, after resolution of symptoms without sequelae or complaints. In the second episode, which was symptomatically more severe in terms of intensity and duration, the patient had headache, malaise, diarrhea, cough, and sore throat that evolved to myalgia and ageusia, muscle fatigue, insomnia, mild dyspnea on exertion, and shortness of breath. In both episodes, however, disease was classified as mild, and she was treated at home, not requiring hospitalization.

The patient was a healthcare executive. Identified workplace exposure included frequent meetings with coronavirus disease (COVID-19) frontline physicians and healthcare teams. Also, before the second episode, she attended a meeting with a group of physicians, one of whom had COVID-19 diagnosed in the days following.

On both occasions, viral RNA was extracted from nasopharyngeal swab specimens and tested for SARS-CoV-2 by multiplex real-time reverse transcription PCR (rRT-PCR) Allplex SARS-CoV-2 assay (Seegene, <https://www.seegene.com>). Both times, results of rRT-PCR tests targeting 3 genes (N, E, and RdRp) were positive for SARS-CoV-2 (Figure, panel A). Cycle threshold values of N, E, and RdRp targets were 25, 26, and 27 in the first episode and 21, 12, and 17 in the second episode, respectively. In the second episode, the patient had a high viral load (presumed because of low cycle threshold values detected). Four weeks after the patient tested positive by rRT-PCR in the second episode, an IgG test against S1 protein by chemiluminescence (VITROS, Ortho Clinical Diagnostics, <https://www.orthoclinicaldiagnostics.com>) yielded a positive result. We then sequenced swab specimens by using PGM Ion Torrent (ThermoFisher, <https://www.thermofisher.com>), according to the manufacturer's instructions. A total of 1,405,009 mapped reads for sample A (from the

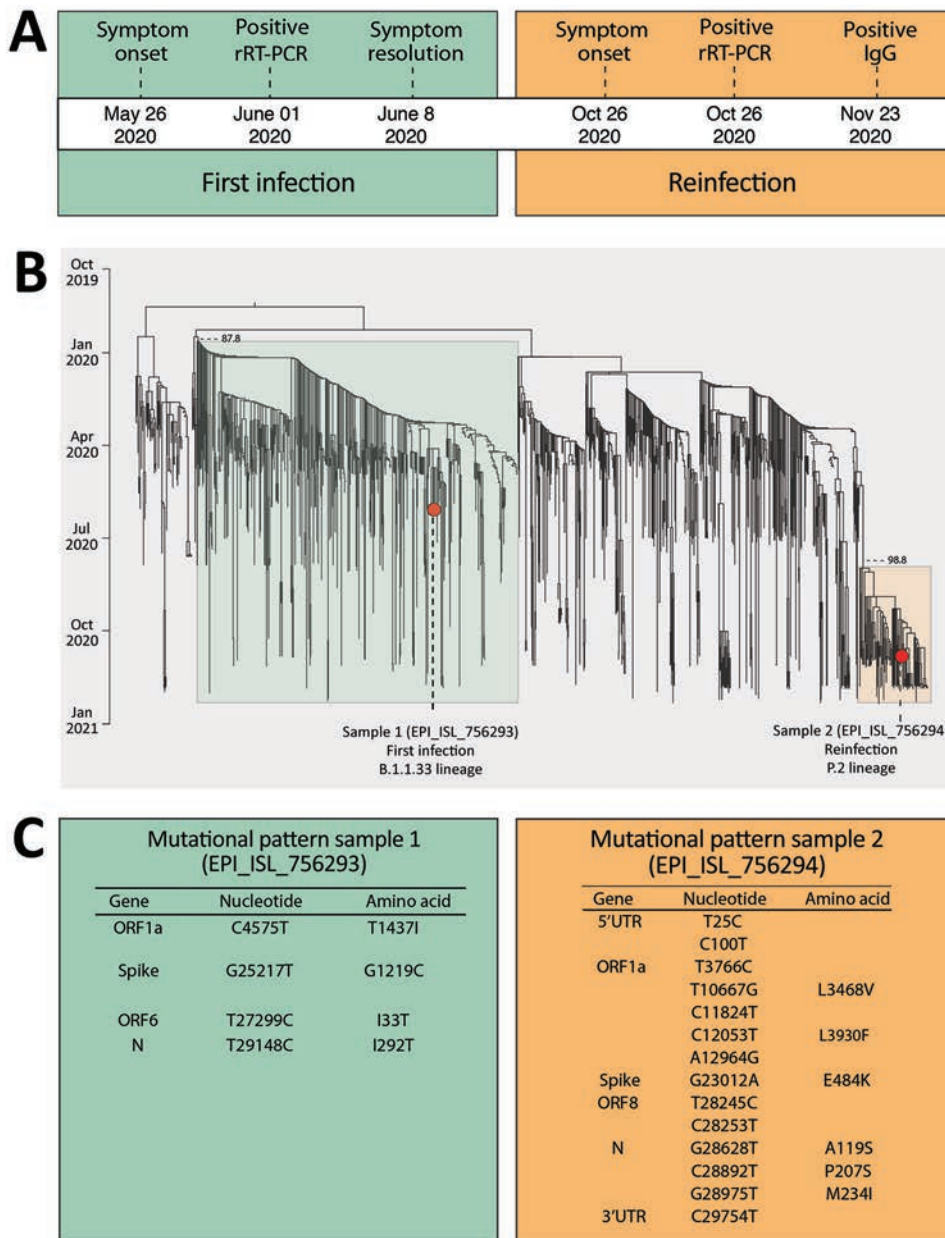


Figure. Molecular characterization of a severe acute respiratory syndrome coronavirus 2 reinfection case in Salvador, Bahia State, northeast Brazil. A) Timeline of symptom onset and molecular and serologic diagnosis. B) Time-scaled maximum-likelihood phylogenetic tree, including the new genomes (GISAID accession nos. EPI_ISL_756293 and EPI_ISL_756294; <https://www.gisaid.org>) recovered from a 45-year-old woman residing in Salvador and full-length viral genomes from Brazil available through GISAID as of January 14, 2021 (Appendix Table, <https://wwwnc.cdc.gov/EID/article/27/5/21-0191-App1.xlsx>). New genomes are highlighted with red circles. Branch support (SH-aLTR >0.8) is shown at key nodes. C) Mutational pattern of the 2 isolates obtained from the same patient within a 147-day interval. Only unique mutations and lineage defining mutations for B.1.1.33 and P.2 are shown. ORF, open reading frame; rRT-PCR, real-time reverse transcription PCR; UTR, untranslated region.

first episode) and 2,570,182 reads for sample B (from the second episode) were obtained, resulting in a sequencing mean depth >1,000× for both samples and a coverage of >99%.

We further assessed the distinct viral origin of the 2 infections by phylogenetic inference, comparing the 2 new isolates (GISAID accession nos. EPI_ISL_756293 and EPI_ISL_756294; <https://www.gisaid.org>) with all SARS-CoV-2 genomes from Brazil available through GISAID as of January 14, 2021. Only genomes >29,000 bp and <1% of ambiguities were retrieved (n = 1,164). Sequences were aligned by using MAFFT (3) and submitted to IQ-TREE for

maximum-likelihood phylogenetic analysis (4). We inferred time-scaled trees by using TreeTime (5).

Comparison of the phylogenetic profiles of the 2 new sequences with contemporaneous sequences from Brazil (Appendix Table, <https://wwwnc.cdc.gov/EID/article/27/5/21-0191-App1.xlsx>) clearly demonstrated that the 2 COVID-19 episodes, separated by a 147-day interval, were indeed caused by different SARS-CoV-2 lineages, confirming reinfection (Figure, panel B). In the first episode, the lineage B.1.1.33 was detected, whereas lineage P.2 (an alias for B.1.1.28.2) was detected in the second infection (Figure, panel B), according to the Pangolin lineage

classification (<https://github.com/hCoV-2019/pangolin> [accessed 2021 Jan 11]). Further, we identified several mutations distinguishing the 2 genomes (Figure, panel C), 2 of which were in the SARS-CoV-2 spike glycoprotein. In the first infection, the retrieved genome had the S:G1219C mutation, whereas the mutation S:E484K was observed in the second infection.

This reinfection case aligns with another reinfection recently described in Brazil in which a first infection with the B.1.1.33 lineage was followed by a second one with the P.2 lineage (P.C. Resende et al., unpub. data, <https://virological.org/t/spike-e484k-mutation-in-the-first-sars-cov-2-reinfection-case-confirmed-in-brazil-2020/584>). The E484K mutation, located in the viral receptor binding domain, has been emerging independently in several SARS-CoV-2 variants, and its monitoring is of pivotal importance in the current stage of the pandemic. At least 3 main lineages harbor E484K: B.1.351, first identified in South Africa and widespread worldwide (H. Tegally et al.); P.1, recently described in Manaus, Brazil, which harbors a constellation of new mutations (including N501Y) (N.R. Faria et al., unpub. data, <https://virological.org/t/genomic-characterisation-of-an-emergent-sars-cov-2-lineage-in-manau-preliminary-findings/586>); and P.2, also described in Brazil (C.M. Voloch et al.) and already detected in the United Kingdom, United States, Canada, and Argentina (<https://cov-lineages.org/lineages.html>). Our report of SARS-CoV-2 reinfection with a E484K variant corroborates *in vitro* and *in silico* studies that estimated the potential of lineages carrying this mutation to escape from neutralizing antibodies (3; Z. Liu et al.) and highlights the importance of genomic surveillance to detect and monitor the emergence of new viral lineages with possible implications for public health policies and immunization strategies.

Acknowledgments

We thank the personnel from Health Surveillance System from the São Rafael Hospital that helped with samples, sources, epidemiological data collection. We also would like to thank all the authors who have kindly deposited and shared genome data on GISAID. A table with genome sequence acknowledgments is available at <https://github.com/genomicsurveillance/SARS-CoV-2-surveillance>.

This research was approved by the São Rafael Hospital Ethics Review Committee (approval no. 41528620.1.0000.0048).

This work was supported by INOVA Fiocruz, Serrapilheira Institute, and D'Or Institute for Research and Education. M.G. is supported by Fundação de Amparo à Pesquisa do Estado do Rio de Janeiro.

Author contributions include conception and design: C.K.V.N., A.V.A.M., R.S.A., B.S.F.S.; investigations: C.K.V.N., M.M.F., T.G., C.A.L.B., R.N.A.M., K.A.F.S., A.V.A.M., R.S.A., M.G., and B.S.F.S.; data curation: C.K.V.N., T.G., M.G., and B.S.F.S.; formal analysis: C.K.V.N., T.G., M.G., V.F., and B.S.F.S.; manuscript writing: C.K.V.N., T.G., M.G., and B.S.F.S.; manuscript revision: C.K.V.N., M.M.F., T.G., A.V.A.M., R.S.A., M.G., and B.S.F.S.; and resources: B.S.F.S. and R.S.A.

About the Author

Dr. Nonaka is a researcher at the Biotechnology and Cell Therapy Centre of São Rafael Hospital, Salvador, Brazil. Her research focuses on the implementation of next-generation sequencing techniques to track the spread of emerging and reemerging viral pathogens and to identify novel disease biomarkers.

References

1. Tillett RL, Sevinsky JR, Hartley PD, Kerwin H, Crawford N, Gorzalski A, et al. Genomic evidence for reinfection with SARS-CoV-2: a case study. *Lancet Infect Dis*. 2021;21:52-8. [https://doi.org/10.1016/S1473-3099\(20\)30764-7](https://doi.org/10.1016/S1473-3099(20)30764-7)
2. Weisblum Y, Schmidt F, Zhang F, DaSilva J, Poston D, Lorenzi JC, et al. Escape from neutralizing antibodies by SARS-CoV-2 spike protein variants. *eLife*. 2020;9:3-10. <https://doi.org/10.7554/eLife.61312>
3. Nakamura T, Yamada KD, Tomii K, Katoh K. Parallelization of MAFFT for large-scale multiple sequence alignments. *Bioinformatics*. 2018;34:2490-2. <https://doi.org/10.1093/bioinformatics/bty121>
4. Nguyen L-T, Schmidt HA, von Haeseler A, Minh BQ. IQ-TREE: a fast and effective stochastic algorithm for estimating maximum-likelihood phylogenies. *Mol Biol Evol*. 2015;32:268-74. <https://doi.org/10.1093/molbev/msu300>
5. Sagulenko P, Puller V, Neher RA. TreeTime: Maximum-likelihood phylodynamic analysis. *Virus Evol*. 2018;4:vex042. <https://doi.org/10.1093/ve/vex042>

Address for correspondence: Bruno S.F. Souza, Instituto Gonçalo Moniz, Fundação Oswaldo Cruz, Rua Waldemar Falcão, 121, Candeal, Salvador, Bahia, CEP 40296-710, Brazil; email: bruno.solano@fiocruz.br; or Marta Giovanetti, Reference Laboratory of Flavivirus, Oswaldo Cruz Institute (Fundação Oswaldo Cruz-RJ), Av. Brasil, 4365, Manguinhos, Rio de Janeiro, RJ, CEP 21040-360, Brazil; email: giovanetti.marta@gmail.com

Upper Respiratory Infections in Schools and Childcare Centers Reopening after COVID-19 Dismissals, Hong Kong

Min Whui Fong, Nancy H.L. Leung, Benjamin J. Cowling, Peng Wu

Author affiliations: WHO Collaborating Centre for Infectious Disease Epidemiology and Control, University of Hong Kong, Hong Kong, China (M.W. Fong, N.H.L. Leung, B.J. Cowling, P. Wu); Laboratory of Data Discovery for Health Limited, Hong Kong (B.J. Cowling, P. Wu)

DOI: <https://doi.org/10.3201/eid2705.210277>

A large number of common cold outbreaks in Hong Kong schools and childcare centers during October–November 2020 led to territorywide school dismissals. Increased susceptibility to rhinoviruses during prolonged school closures and dismissals for coronavirus disease and varying effectiveness of nonpharmaceutical interventions may have heightened transmission of cold-causing viruses after school attendance resumed.

Many countries implemented school closures and dismissals in 2020 as a public health measure to reduce spread of coronavirus disease (COVID-19), caused by severe acute respiratory syndrome coronavirus 2 (SARS-CoV-2). In Hong Kong, schools were dismissed after the Lunar New Year holiday in late January 2020 and remained dismissed until late May; during early July–late September, schools were dismissed again in response to a surge in cases of COVID-19 (Figure, panel A). During the dismissal periods, most school campuses remained open to staff but lessons were delivered online. Here, we report a large number of outbreaks of acute upper respiratory tract infections (URTIs), likely rhinovirus infections, that were identified during October–November 2020 in reopened primary schools, secondary schools, kindergartens, childcare centers, and nursery schools in Hong Kong; these outbreaks led to further territorywide school dismissals for younger children.

In the last week of October 2020, the Hong Kong Centre for Health Protection began receiving reports of URTI outbreaks in kindergartens, childcare centers, nursery schools, and primary schools. Outbreaks of URTIs in schools continued to increase rapidly in the following weeks (Figure, panel A). A school URTI

outbreak was defined as ≥ 3 students in the same class each developing ≥ 2 symptoms of respiratory tract infection within 4 days (Table). Various measures were implemented in response to these URTI outbreaks. Initially, schools with outbreaks were advised to dismiss affected classes for ≥ 3 days; this guideline was expanded to dismissal of entire schools for ≥ 7 days beginning November 18. SARS-CoV-2 testing was also conducted for students in affected classes and all staff in these schools.

Territorywide school dismissals took effect beginning November 14. Kindergartens, childcare centers, and nursery schools were dismissed first, for 2 weeks, because most outbreaks had occurred in this age group (1); primary grades 1–3 were dismissed beginning November 23. In total, 482 outbreaks were reported during October 25–November 28, including 308 (63.9%) outbreaks in primary schools, 149 (30.9%) in kindergartens, childcare centers, and nursery schools, and 25 (5.2%) in secondary schools (2). There were 81 larger outbreaks involving ≥ 20 persons (3), equal to the total number of 2017–2019 outbreaks of the same scale for URTIs (Figure, panel B), and influenza-like illnesses and influenza (Figure, panel C). Laboratory testing suggested that rhinoviruses or enteroviruses were the likely pathogens, and no SARS-CoV-2 or influenza viruses were detected (1). It is very unusual for schools to be closed or dismissed in response to outbreaks of common colds. In this particular circumstance, one rationale for dismissing students was to spare the public health laboratory resources needed to test the many samples from school outbreaks for SARS-CoV-2, despite the very low risk of in-school transmission (4).

From cross-sectional surveys conducted in February and March 2020, we reported that 75% of school-aged children did not have contact with persons outside their own household when schools were dismissed (5). Indicators of respiratory virus activity, such as rates of consultation for influenza-like illnesses and detection of influenza viruses in respiratory specimens, remained extremely low throughout 2020 (6). However, population susceptibility to rhinoviruses and other respiratory viruses, including influenza viruses, might have been increasing over time because persons were likely less exposed to the viruses when intense social distancing measures, including school dismissals, were implemented in response to the COVID-19 pandemic. This would have increased transmission potential when schools resumed. In England in September 2020, ≈ 2 weeks after full reopening of

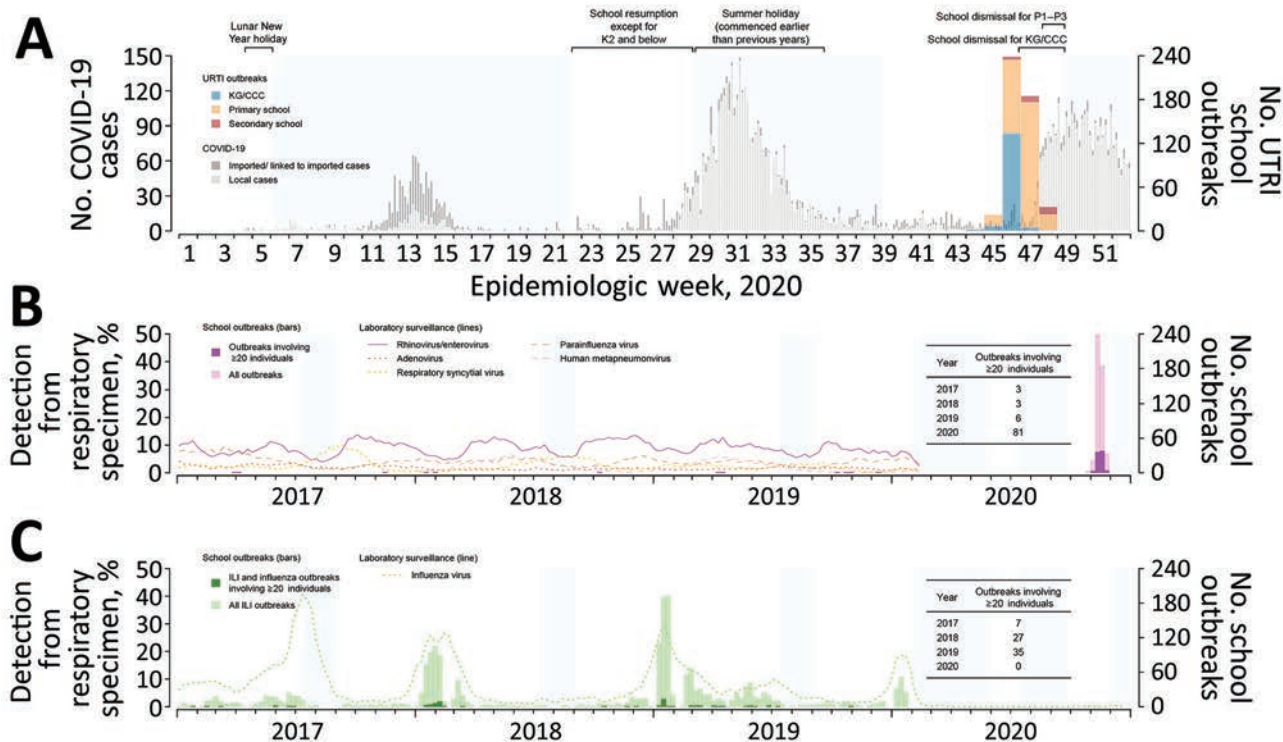


Figure. Respiratory illness outbreaks in primary and secondary schools, kindergartens, childcare centers, and nursery schools in Hong Kong. A) Weekly number of outbreaks of upper respiratory tract infection in schools reported during October 25–November 28, 2020, overlaid on the epidemic curve of daily COVID-19 case numbers in Hong Kong, by date of reporting. B) Weekly numbers of outbreaks of upper respiratory tract infection in schools during weeks 44–48 of 2020 and school outbreaks involving ≥ 20 persons reported during 2017–2020. Lines indicate detection rates of rhinovirus/enterovirus and other viruses in respiratory specimens collected for laboratory surveillance. C) Weekly numbers of outbreaks of influenza-like illness and influenza in schools reported during 2017–2020. Dotted line indicates detection of influenza virus in respiratory specimens collected for laboratory surveillance. Durations of territorywide regular school breaks (summer holiday) during 2017–2019 and school dismissals implemented in response to COVID-19 in 2020 are shaded in blue. ILI, influenza-like-illness; UTRI, upper respiratory tract infection; KG/CCC, kindergartens, child-care centers, and nursery schools; K2, kindergarten year 2 (4–5 years of age); P1–P3, primary school years 1–3 (6–9 years of age)

schools following prolonged dismissals, a substantial increase in the detection of rhinoviruses among adults was recorded (7), possibly driven by transmission among children.

URTI outbreaks caused by the respiratory viruses responsible for common colds (i.e., other than influenza viruses) occurred in Hong Kong schools despite a wide range of infection control measures being in place. Staff and students wore face masks at all times; lunch hours were cancelled, desks were spaced out, and group activities were limited (4). Although in gen-

eral transmission modes may be similar for different respiratory viruses, how much each mode contributes to transmission of a specific virus remains unclear; therefore, the effectiveness of certain nonpharmaceutical interventions might differ between viruses (8). For example, face masks were shown to be efficacious in blocking the release of coronaviruses and influenza viruses, but not rhinoviruses, in exhaled breath (9). In addition, enveloped viruses (e.g., coronaviruses and influenza viruses) are less resistant to lipophilic disinfectants than nonenveloped viruses (e.g., rhinoviruses) (10). This difference might have played a role in URTI outbreaks in Hong Kong related to rhinoviruses but not influenza viruses, even though individual persons and schools had practiced frequent cleaning and disinfection. Our findings highlight the increased risk posed by common cold viruses in locations where schools have been closed or dismissed for extended periods during the COVID-19 pandemic.

Table. Symptoms reported in 81 upper respiratory tract infection outbreaks involving ≥ 20 persons in schools, kindergartens, childcare centers, and nursery schools, Hong Kong, October–November 2020

Symptoms	No. (%) outbreaks
Cough, runny nose, fever, and sore throat	49 (60.5)
Cough, runny nose, and sore throat	27 (33.3)
Cough, runny nose, and fever	1 (1.2)
Cough and runny nose	4 (4.9)

This project was supported by the Health and Medical Research Fund, Food and Health Bureau, Government of the Hong Kong Special Administrative Region (grant no. COVID190118).

B.J.C. consults for Roche and Sanofi Pasteur. The authors report no other potential conflicts of interest.

About the Author

Ms. Fong is a research postgraduate student at the School of Public Health, University of Hong Kong. Her research interests are the transmission and control of respiratory viruses among children, particularly in school settings.

References

1. Government of the Hong Kong Special Administrative Region. Media session (2020 November 12) [cited 2020 Dec 23]. <https://isd.wecast.hk/vod/?id=11384>
2. Government of the Hong Kong Special Administrative Region. Media session (2020 November 20) [cited 2020 Dec 23]. <https://isd.wecast.hk/vod/?id=11436>
3. Centre for Health Protection. Press releases [cited 2020 Dec 23]. <https://www.chp.gov.hk/en/media/116/index.html>
4. Fong MW, Cowling BJ, Leung GM, Wu P. Letter to the editor: COVID-19 cases among school-aged children and school-based measures in Hong Kong, July 2020. *Euro Surveill.* 2020;25:2001671. PubMed <https://doi.org/10.2807/1560-7917.ES.2020.25.37.2001671>
5. Cowling BJ, Ali ST, Ng TWY, Tsang TK, Li JCM, Fong MW, et al. Impact assessment of non-pharmaceutical interventions against coronavirus disease 2019 and influenza in Hong Kong: an observational study. *Lancet Public Health.* 2020;5:e279–88. [https://doi.org/10.1016/S2468-2667\(20\)30090-6](https://doi.org/10.1016/S2468-2667(20)30090-6)
6. Centre for Health Protection. Flu express. 2020 Dec 20–26 [cited 2021 Jan 19]. https://www.chp.gov.hk/files/pdf/flu-express_week52_31_12_2020_eng.pdf
7. Poole S, Brendish NJ, Tanner AR, Clark TW. Physical distancing in schools for SARS-CoV-2 and the resurgence of rhinovirus. *Lancet Respir Med.* 2020;8:e92–3. [https://doi.org/10.1016/S2213-2600\(20\)30502-6](https://doi.org/10.1016/S2213-2600(20)30502-6)
8. Leung NHL. Transmissibility and transmission of respiratory viruses. *Nat Rev Microbiol.* 2021;22:1–18. <https://doi.org/10.1038/s41579-021-00535-6>
9. Leung NHL, Chu DKW, Shiu EYC, Chan KH, McDevitt JJ, Hau BJP, et al. Respiratory virus shedding in exhaled breath and efficacy of face masks. *Nat Med.* 2020;26:676–80. <https://doi.org/10.1038/s41591-020-0843-2>
10. Lin Q, Lim JYC, Xue K, Yew PYM, Owh C, Chee PL, et al. Sanitizing agents for virus inactivation and disinfection. *VIEW.* 2020;1:e16. <https://doi.org/10.1002/viw2.16>

Address for correspondence: Benjamin J Cowling, School of Public Health, Li Ka Shing Faculty of Medicine, University of Hong Kong, 21 Sassoon Rd, Pokfulam, Hong Kong; email: bcowling@hku.hk

Risk for International Importations of Variant SARS-CoV-2 Originating in the United Kingdom

Zhanwei Du,¹ Lin Wang,¹ Bingyi Yang, Sheikh Taslim Ali, Tim K. Tsang, Songwei Shan, Peng Wu, Eric H.Y. Lau, Benjamin J. Cowling, Lauren Ancel Meyers

Author affiliations: WHO Collaborating Centre for Infectious Disease Epidemiology and Control, University of Hong Kong, Hong Kong, China (Z. Du, B. Yang, S.T. Ali, T.K. Tsang, S. Shan, P. Wu, E.H.Y. Lau, B.J. Cowling); Laboratory of Data Discovery for Health, Hong Kong (Z. Du, S.T. Ali, S. Shan, P. Wu, E.H.Y. Lau, B.J. Cowling); University of Cambridge, Cambridge, UK (L. Wang); The University of Texas at Austin, Austin, Texas, USA (L.A. Meyers); Santa Fe Institute, Santa Fe, New Mexico, USA (L.A. Meyers)

DOI: <https://doi.org/10.3201/eid2705.210050>

A fast-spreading severe acute respiratory syndrome coronavirus 2 variant identified in the United Kingdom in December 2020 has raised international alarm. We analyzed data from 15 countries and estimated that the chance that this variant was imported into these countries by travelers from the United Kingdom by December 7 is >50%.

The United Kingdom has detected a variant of severe acute respiratory syndrome coronavirus 2 (SARS-CoV-2), the causative agent coronavirus disease (COVID-19), from samples initially collected in Kent on September 20 and London on September 21, 2020 (1). The variant was associated with increased transmissibility and includes deletions at amino acid sites 69 and 70 of the spike protein (2). In mid-December, the UK government tightened measures in London and southeastern England to mitigate transmission of the fast-spreading virus variant (3). On January 5, 2021, England initiated a national lockdown that included closing all schools and nonessential businesses until mid-February (4). By December 20, restrictions for travelers from the United Kingdom had been implemented by ≈40 countries (5). The new variant (501Y) has subsequently been reported worldwide, including in the United States (6), Spain, Sweden, and France, and might be spreading without detection in countries with limited virus sequencing capacity (5).

Using data from 15 countries, we estimated the probability that travelers from the United Kingdom

¹These first authors contributed equally to this article.

introduced this 501Y variant into each of the countries and estimated the extent of local transmission. Our estimations were based on the changing proportion of infections caused by the 501Y variant identified in the United Kingdom (2) and population mobility from the United Kingdom to each country, determined from Facebook Data for Good (<https://dataforgood.fb.com>). The highest risk for importation

from September 22 through December 7, 2020, was in Ireland. By October 22 (a month after the variant was first detected in the United Kingdom), the chance that 10 of the 15 countries would receive 1 imported case from the United Kingdom was at least 50% (Figure), except for Romania, Portugal, Cyprus, India, and the United States, although by November 1, this risk threshold was exceeded for all of these countries.

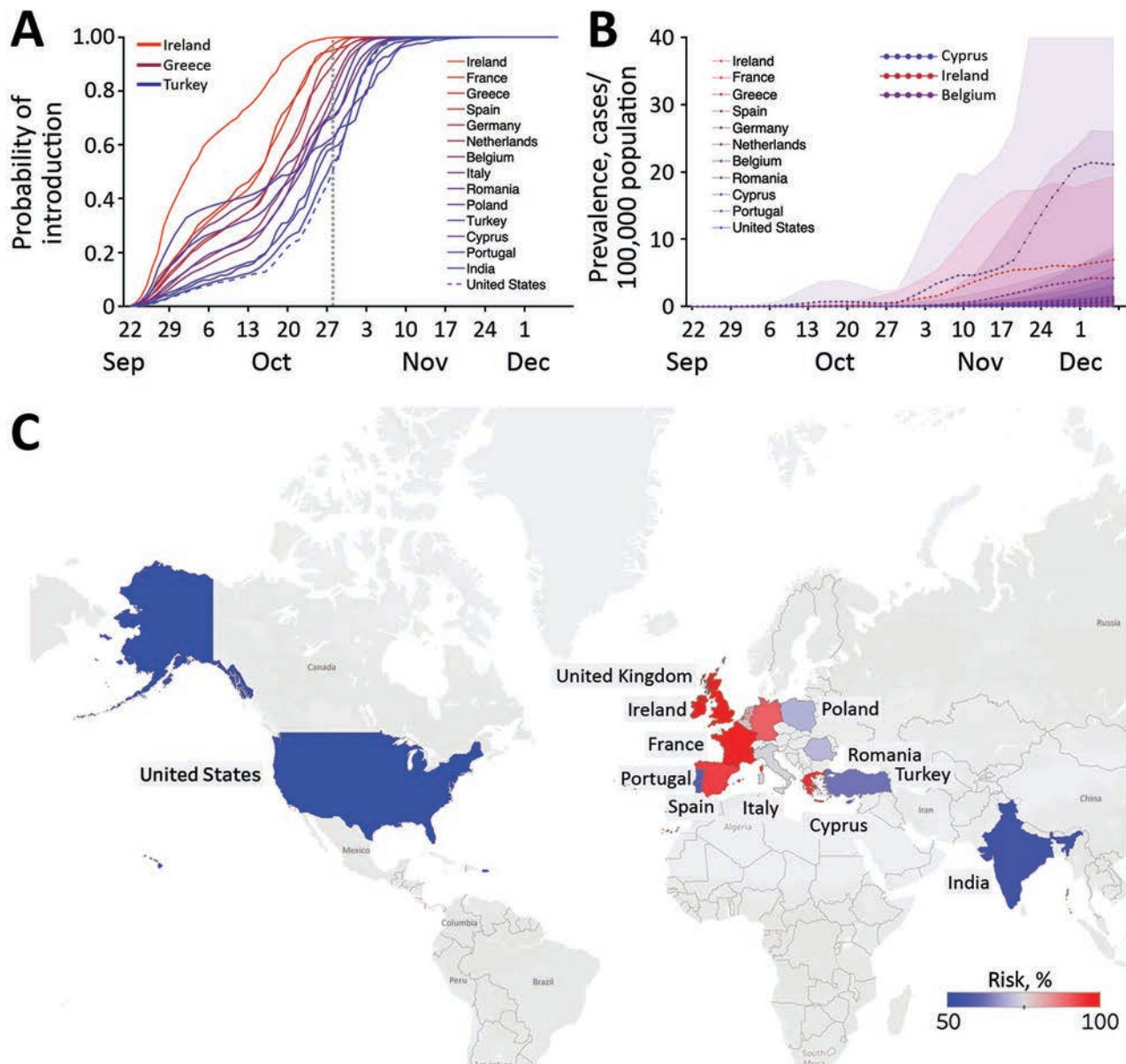


Figure. Estimated risks for introduction of the 501Y variant of severe acute respiratory syndrome coronavirus 2 (SARS-CoV-2) from the United Kingdom to 15 other countries before December 7, 2020. A) Probability that ≥ 1 person infected with this SARS-CoV-2 variant arrived at the target country from the United Kingdom by the date indicated on the x-axis, based on Facebook mobility data (<https://dataforgood.fb.com>). The dotted gray vertical line indicates October 28, 2020, the date when the introduction risk for the United States surpassed 50%; line colors correspond to the relative risk for importations as of that date. B) Estimated daily prevalence of the 501Y variant of SARS-CoV-2 in 11 countries between September 22 and December 7, 2020, assuming that the variant is σ , which means 50% more transmissible than the 501N variant (11). Points and bands indicate means and SDs based on 100 simulations. C) Probability of ≥ 1 variant importation by October 28, 2020. Grey indicates countries/regions where mobility data were not available.

Using COVID-19 hospital admission data, we further estimated the local prevalence of the 501Y variant in 11 of the 15 countries, assuming that the 501Y variant is 50% more transmissible than the circulating 501N strain (Figure). The variant seems to have ascended fastest in Ireland before slowing in mid-November and is expected to be spreading rapidly in many of the other countries. As of December 7, the expected prevalence of the variant and the expected proportion of coronavirus disease cases were highest in Cyprus (prevalence 13 cases, 95% CI 0–79 cases/100,000 population; proportion 6% of cases, 95% CI 0–38% of cases) (Figure; Appendix Figures 1, 2, <https://wwwnc.cdc.gov/EID/article/27/5/21-0050-App1.pdf>).

These projections suggest that countries with substantial population movement from the United Kingdom were likely to harbor cases of the 501Y variant by late October 2020. Our conclusions were based on several key assumptions. The mobility data, which include ≈ 3 million trips from the United Kingdom to the 15 countries we analyzed, might be demographically biased by the user profile of Facebook, a major social media company with ≈ 2.8 billion monthly active users in the fourth quarter of 2020 (7). We assume that all introductions during this early period occurred via asymptomatic travelers from the United Kingdom and ignore possible importations from other countries or by symptomatic case-patients traveling to seek healthcare. A sensitivity analysis suggests that these assumptions may cause a downward bias in the estimated rates of global expansion (Appendix Figure 3). Furthermore, we assume a 10-day lag between infection and hospitalization on the basis of estimates from the United States (8) and Europe (9) and estimate the daily prevalence of the 501Y variant by using the method introduced in (2), under the assumptions that the 2 variants (501Y and 501N) share the same natural history (2) and symptomatic proportion (10,11). Should future studies reveal substantial epidemiologic differences between the variant and wildtype, then these estimates can be readily updated by using the full equations provided in (2).

This article was preprinted at <https://www.ncbi.nlm.nih.gov/pmc/articles/PMC7814837>

Financial support was provided by the Health and Medical Research Fund, Food and Health Bureau, Government of the Hong Kong Special Administrative Region (grant no. COVID190118), the US National Institutes of Health (grant no. R01 AI151176), and Centers for Disease Control and Prevention COVID Supplement (grant no. U01IP001136).

About the Author

Dr. Du is a research assistant professor in the School of Public Health, Li Ka Shing Faculty of Medicine, The University of Hong Kong, Hong Kong Special Administrative Region, China. He develops mathematical models to elucidate the transmission dynamics, surveillance, and control of infectious diseases.

References

1. Kupferschmidt K. Mutant coronavirus in the United Kingdom sets off alarms, but its importance remains unclear. 2020 Dec 20 [cited 2021 Jan 2]. <https://www.sciencemag.org/news/2020/12/mutant-coronavirus-united-kingdom-sets-alarms-its-importance-remains-unclear>
2. Leung K, Shum MHH, Leung GM, Lam TTY, Wu JT. Early transmissibility assessment of the N501Y mutant strains of SARS-CoV-2 in the United Kingdom, October to November 2020. *Euro Surveill.* 2021;26:2002106. <https://doi.org/10.2807/1560-7917.ES.2020.26.1.2002106>
3. Kupferschmidt K. Fast-spreading U.K. virus variant raises alarms. *Science.* 2021;371:9–10. <https://doi.org/10.1126/science.371.6524.9>
4. Clark N, Dathan M. National lockdown – Boris Johnson orders nation to stay at home until middle of February as 13.5m Brits get Covid jab. 2021 Jan 5 [cited 2021 Jan 7]. <https://www.thesun.co.uk/news/politics/13648237/national-lockdown-stay-home-boris-johnson-announcement>
5. BBC News. Coronavirus: Cases of new variant appear worldwide. 2020 Dec 26 [cited 2021 Jan 2]. <https://www.bbc.com/news/world-europe-55452262>
6. Centers for Disease Control and Prevention. Emerging SARS-CoV-2 variants. 2020 Dec 29 [cited 2021 Jan 2]. <https://www.cdc.gov/coronavirus/2019-ncov/more/science-and-research/scientific-brief-emerging-variants.html>
7. Statista. Number of monthly active Facebook users worldwide as of 4th quarter 2020 [cited 2021 Mar 20]. <https://www.statista.com/statistics/264810/number-of-monthly-active-facebook-users-worldwide>
8. Aleta A, Martín-Corral D, Pastore y Piontti A, Ajelli M, Litvinova M, Chinazzi M, et al. Modelling the impact of testing, contact tracing and household quarantine on second waves of COVID-19. *Nat Hum Behav.* 2020;4:964–71. <https://doi.org/10.1038/s41562-020-0931-9>
9. International Severe Acute Respiratory and Emerging Infections Consortium (ISARIC). COVID-19 report: 19 [cited 2021 Feb 1]. https://media.tghn.org/medialibrary/2020/05/ISARIC_Data_Platform_COVID-19_Report_19MAY20.pdf
10. King's College London. No evidence of change in symptoms from new coronavirus variant. King's College London. 2021 Feb 1 [cited 2021 Mar 3]. <https://www.kcl.ac.uk/news/no-evidence-change-symptoms-new-coronavirus-variant>
11. Davies NG, Abbott S, Barnard RC, Jarvis CI, Kucharski AJ, Munday JD, et al.; CMMID COVID-19 Working Group; COVID-19 Genomics UK (COG-UK) Consortium. Estimated transmissibility and impact of SARS-CoV-2 lineage B.1.1.7 in England. *Science.* 2021 Mar 3 [Epub ahead of print]. <https://doi.org/10.1126/science.abg3055>

Address for correspondence: Lauren Ancel Meyers, Department of Integrative Biology, The University of Texas at Austin, 2415 Speedway #C0930, Austin, TX 78712, USA; email: laurenmeyers@austin.utexas.edu

Severe Case of Rickettsiosis Identified by Metagenomic Sequencing, China

Zhongqiu Teng,¹ Yan Shi,¹ Yao Peng,¹ Huayi Zhang, Xia Luo, Xinchang Lun, Lianxu Xia, Yuanhai You, Zhenpeng Li, Wen Zhang, Ying Zhang, Shicun Dong, Wentao Guo, Biao Kan, Bo Pang, Jianguo Xu, Aiping Qin

Author affiliations: National Institute for Communicable Disease Control and Prevention, Chinese Center for Disease Control and Prevention, Beijing, China (Z. Teng, Y. Peng, X. Luo, X. Lun, L. Xia, Y. You, Z. Li, W. Zhang, B. Kan, B. Pang, J. Xu, A. Qin); Qinghai Center for Disease Control and Prevention, Xining, China (Y. Shi, H. Zhang, S. Dong); Baotou Medical College, Baotou, China (Y. Zhang); Institute of Endemic Diseases of Qinghai, Xining (W. Guo)

DOI: <https://doi.org/10.3201/eid2705.203265>

A case of *Rickettsia sibirica* subspecies *sibirica* BJ-90 infection in China was identified by metagenomic analysis of an eschar biopsy specimen and confirmed by nested PCR. Seroprevalence of spotted fever group *Rickettsia* was $\approx 17.4\%$ among the local population. This report highlights the threat of rickettsioses to public health in the Qinghai–Tibet Plateau.

Rickettsia, mainly transmitted by ticks, are a group of obligate gram-negative bacteria that cause mild to life-threatening rickettsioses. Two main groups of *Rickettsia* have been described on the basis of genetic differences and pathology, spotted fever group (SFG) and typhus group (TG). In China, 5 members of SFG have been identified in human cases (1–4), and 7 kinds of *Rickettsia* have been detected from ticks or animals in the Qinghai–Tibet Plateau, including *R. heilongjiangensis*, *R. raoultii*, *R. slovaca*, and *R. sibirica*, which are known to be pathogenic to humans (5–7). However, clinical cases have not been reported. Thus, rickettsioses are probably neglected by local physicians and public health officers. We report a severe case of *R. sibirica* subspecies *sibirica* BJ-90 infection in this region.

A 50-year-old herdsman from Zhamashi, Qinghai Province, China, was hospitalized on July 13, 2018, because of intensive intermittent headache, anorexia, and chest tightness. On his fifth day of sheep shearing (designated as day 1), a blood-fed tick had been found on his head. The tick was removed by hand but its mouth parts remained in the man's scalp. The next

day, he became ill with fever, myalgia, itchiness, and asthenia. On day 5, his symptoms intensified and included severe intermittent headaches, which lasted for ≈ 10 minutes at each onset; high fever, up to 39.5°C ; and fatigue, palpitation, nausea, and vomiting. Erythematous rashes appeared on his trunk, all 4 limbs, and the area behind the ears. Because signs of neurologic dysfunction, including confusion, drowsiness, and delirium appeared, he sought care at Qilian County Hospital on day 9, where he was treated for infectious endocarditis for 3 days before transfer to Qinghai State Hospital. During his visit at the Qinghai State Hospital, he was conscious and alert. Erythematous macules were observed over his trunk, elbow, and lower limbs. A $1.5 \times 1.1 \text{ cm}^2$ black eschar was visible at his right posterior occipital bone area; no tenderness was reported (Appendix Figure 1, <https://wwwnc.cdc.gov/EID/article/27/5/20-3265-App1.pdf>). The eschar was surgically excised on day 16. No lymphadenopathy was found.

Alterations of the patient's blood biochemistry included increased neutrophils (88.5% [reference 45%–75%]); decreased lymphocytes (9.3% [reference 20%–50%]), eosinophils (0% [reference 0.4%–8%]), and monocytes (1.9% [reference 3%–10%]); elevated creatine kinase-MB (42 U/L [reference 0–25 U/L]) and lactate dehydrogenase (445 U/L [reference 110–245 U/L]); and highly increased C-reactive protein (97.1 mg/dL [reference 0–5 mg/dL]), procalcitonin (0.433 ng/dL [reference 0–0.046 ng/dL]), D-dimers (12.28 $\mu\text{g}/\text{mL}$ [reference 0–1.5 $\mu\text{g}/\text{mL}$]), fibrinogen degradation products (25 $\mu\text{g}/\text{mL}$ [reference 0–5 $\mu\text{g}/\text{mL}$]), and β -microglobulin (4.5 $\mu\text{g}/\text{mL}$ [reference 0.8–1.8 $\mu\text{g}/\text{mL}$]). The patient was prescribed levofloxacin lactate (0.5 g/d for 6 d). His symptoms subsided, and he was discharged on day 20.

On the basis of tick-bite history and the triad clinical characteristics (fever, rash, and eschar), nested PCR targeting the rickettsial citrate synthase conserved gene (*gltA*) was performed by using the eschar DNA as a template (Appendix). The 547-bp amplicon sequence shared 100% identity to *R. sibirica* 246, *R. sibirica* subsp. *sibirica* BJ-90, and *R. sibirica* subsp. *mongolitimonae* HA-91. The eschar DNA was sequenced by next-generation sequencing (BGI Genomics, <https://www.bgi.com>). A total of 21.6 Gb clean data were recovered from the high-throughput sequencing. Human reads (accounting for 99.9%) were filtered out. The remaining reads were mapped on the genome of *R. sibirica* 246 (GenBank accession no. AABW0100000). Rickettsial unique reads ($n = 266$) were analyzed against Refseq (<https://www.ncbi.nlm.nih.gov/refseq>; taxid 766). Most (226/266 [85%])

¹These authors contributed equally to this article.

Table. Homology of 266 identified rickettsial unique reads shared by *Rickettsia* species, China*

% Identity	No. reads			
	BJ-90	<i>R. sibirica</i> 246†	HA-91‡	<i>R. heilongjiangensis</i> ‡
100	226	213	153	48
99	25	35	76	65
98	6	9	19	46
1–97	9	9	17	102
0	0	0	1	5

*BJ-90, *R. sibirica* subsp. *sibirica* BJ-90; HA-91, *R. sibirica* subsp. *mongolitimoniae* HA-91.

†No significant difference ($p = 0.35$) compared with BJ-90 by Wilcoxon ranked nonparametric test.

‡Significant difference ($p < 0.05$) compared with BJ-90 by Wilcoxon ranked nonparametric test.

reads were 100% identical to *R. sibirica* subsp. *sibirica* BJ-90, whereas 213/266 (80%) were identical to *R. sibirica* 246, indicating that the *Rickettsia* was closest to *R. sibirica* subsp. *sibirica* BJ-90 (Table; Appendix Figure 2). Partial sequences of outer membrane protein A, outer membrane protein B, 17 kDa lipoprotein, surface cell antigen 1, and surface cell antigen 4 were amplified with specific primers. Phylogenetic trees showed that the Qinghai sequences clustered with *R. sibirica* subsp. *sibirica* BJ-90 (Figure; Appendix Figure 3). On the basis of next-generation sequencing data

and PCR results, we concluded that the causative agent of the patient's infection is closely related to *R. sibirica* subsp. *sibirica* BJ-90.

We evaluated serum samples from the patient and persons from his surrounding community. Antibodies against *R. rickettsii* (SFG) and *R. typhi* (TG) were determined by indirect immunofluorescence assay. IgG titers of the patient's paired serum samples on day 13 (1:128) and day 167 (1:4,096) against SFG were increased by ≥ 4 -fold, suggesting a recent infection with SFG. Approximately 17.4% (4/23) of the serum

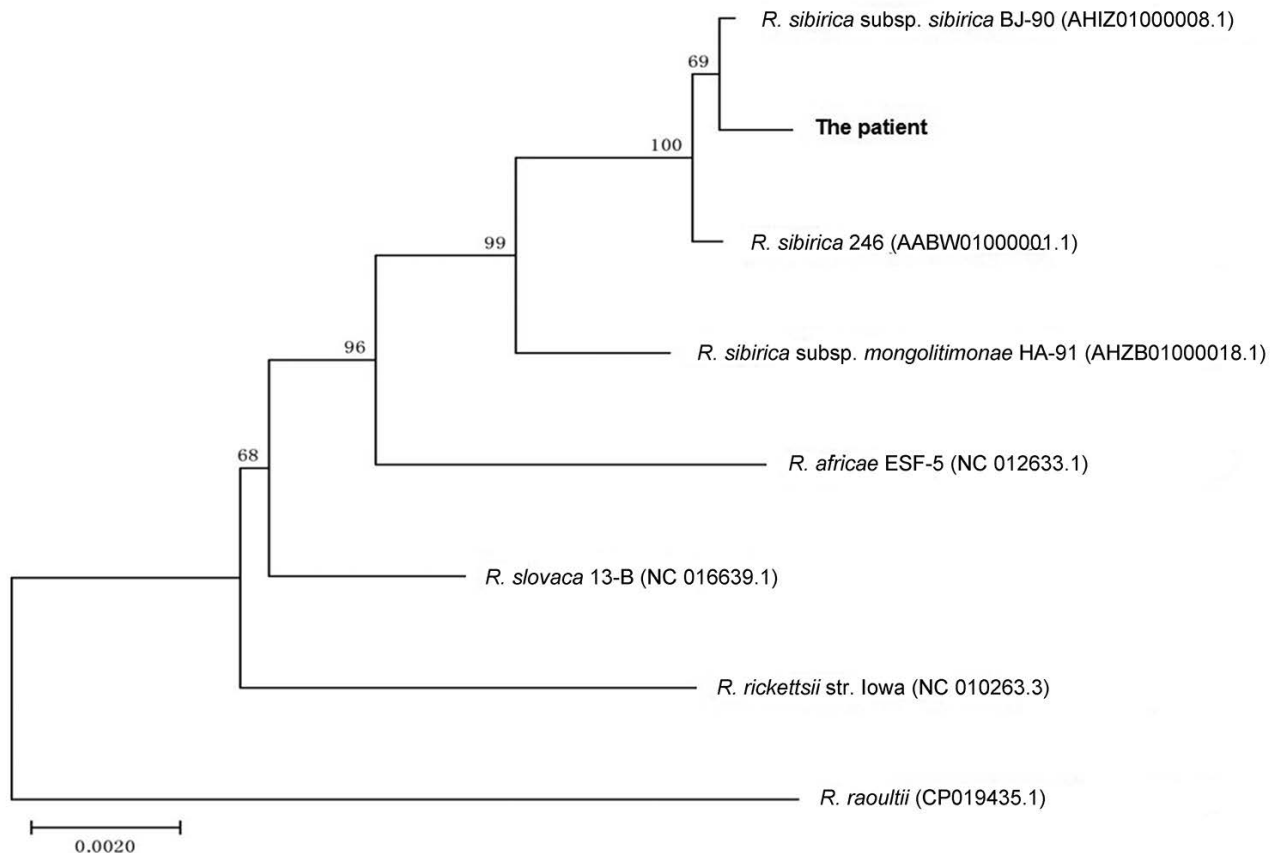


Figure. Phylogenetic analysis of concatenated nucleotide sequences from *Rickettsia* species collected in 2018 from eschar DNA from a patient in Qinghai Tibet Plateau, China (boldface), and reference sequences. A phylogenetic tree was constructed on the basis of the concatenated partial *gltA*, *ompA*, *ompB*, 17 kDa, *sca1*, and *sca4* nucleotide sequences by using the neighbor-joining method with 1,000 bootstrap replicates. Numbers >70 indicate the bootstrapping value. GenBank accession numbers listed in Appendix Table 3 (<https://wwwnc.cdc.gov/EID/article/27/5/20-3265-App1.pdf>). Scale bar represents nucleotide substitutions.

samples from the local community were positive for SFG, and 4.3% (1/23) were positive for TG (Appendix Table 1), indicating a high seroprevalence of SFG and co-circulation of TG in the region.

Because of the treating physicians' unawareness of the prevalence of rickettsioses, the patient's illness was misdiagnosed and incorrectly treated. In light of the fatal cases of *R. sibirica* subsp. *sibirica* infection recently documented in Russia and China (8–10), our report highlights the risk for rickettsial diseases among the public in the Qinghai–Tibet Plateau region and the urgent need for a large-scale seroepidemiologic survey.

Acknowledgments

We thank Pierre Rivaller for analyzing the metagenomic sequences and reviewing this manuscript.

This study was supported by the National Science and Technology Major Projects on Infectious Disease Control and prevention (grant no. 2018ZX10714-002) and Development of Capacity for Pathogen Detection (grant no. 13103110200015003) from the National Institute for Communicable Disease Control and Prevention at the China Centers for Disease Control and Prevention.

About the Author

Dr. Teng is a research associate at the National Institute for Communicable Disease Control and Prevention, China Centers for Disease Control and Prevention. His research interests include the detection and isolation of rickettsia and the epidemiology of rickettsioses.

References

1. Merhej V, Angelakis E, Socolovschi C, Raoult D. Genotyping, evolution and epidemiological findings of *Rickettsia* species. *Infect Genet Evol.* 2014;25:122–37.
2. Fang LQ, Liu K, Li XL, Liang S, Yang Y, Yao HW, et al. Emerging tick-borne infections in mainland China: an increasing public health threat. *Lancet Infect Dis.* 2015; 15:1467–79. [https://doi.org/10.1016/S1473-3099\(15\)00177-2](https://doi.org/10.1016/S1473-3099(15)00177-2)
3. Li J, Hu W, Wu T, Li HB, Hu W, Sun Y, et al. Japanese spotted fever in eastern China, 2013. *Emerg Infect Dis.* 2018;24:2107–9. <https://doi.org/10.3201/eid2411.170264>
4. Abdad MY, Abou Abdallah R, Fournier PE, Stenos J, Vasoo S. A concise review of the epidemiology and diagnostics of rickettsioses: *Rickettsia* and *Orientia* spp. *J Clin Microbiol.* 2018;56:e01728-17. <https://doi.org/10.1128/JCM.01728-17>
5. Han R, Yang J, Niu Q, Liu Z, Chen Z, Kan W, et al. Molecular prevalence of spotted fever group rickettsiae in ticks from Qinghai Province, northwestern China. *Infection, genetics and evolution: journal of molecular epidemiology and evolutionary genetics in infectious diseases.* *Infect Genet Evol.* 2018;57:1–7.
6. Ying L, Zeng-kui L, Gang C, Ming K, Dao-xin L, Yan-ming Z. Identification and phylogenetic analysis of spotted fever group *Rickettsia* isolated from Qinghai province [in Chinese]. *Chin J Vet Sci.* 2014;34:1956–61.
7. Jian Y, Li J, Adjou Moumouni PF, Zhang X, Tumwebaze MA, Wang G, et al. Human spotted fever group *Rickettsia* infecting Yaks (*Bos grunniens*) in the Qinghai-Tibetan Plateau area. *Pathogens.* 2020;9:E249. <https://doi.org/10.3390/pathogens9040249>
8. Li H, Fu XY, Jiang JF, Liu RX, Li R, Zheng YC, et al. Severe illness caused by *Rickettsia sibirica* subspecies *sibirica* BJ-90 infection, China. *Emerg Microbes Infect.* 2017;6:e107. <https://doi.org/10.1038/emi.2017.95>
9. Rudakov N, Samoylenko I, Shtrek S, Igolkina Y, Rar V, Zhirakovskaia E, et al. A fatal case of tick-borne rickettsiosis caused by mixed *Rickettsia sibirica* subsp. *sibirica* and “*Candidatus Rickettsia tarasevichiae*” infection in Russia. *Ticks Tick Borne Dis.* 2019;10:101278. <https://doi.org/10.1016/j.ttbdis.2019.101278>
10. Jia N, Jiang JF, Huo QB, Jiang BG, Cao WC. *Rickettsia sibirica* subspecies *sibirica* BJ-90 as a cause of human disease. *N Engl J Med.* 2013;369:1176–8. <https://doi.org/10.1056/NEJMc1303625>

Address for correspondence: Aiping Qin, State Key Laboratory of Infectious Diseases Prevention and Control, National Institute for Communicable Disease Control and Prevention, Chinese Center for Disease Control and Prevention, 155 Changbai Rd, Changping, Beijing 102206, China; email: qinaiping@icdc.cn

Eosinophilic Meningitis and Intraocular Infection Caused by *Dirofilaria* sp. Genotype Hongkong

Aruna S. Jyotsna, Kollencheri Puthenveetil Vinayan, Lalitha Biswas, Sujithra Haridas, Arun G. Roy, Paramal Suresh, Anil Kumar

Author affiliation: Amrita Institute of Medical Sciences, Amrita Viswa Vidyapeetham Cochin, India

DOI: <https://doi.org/10.3201/eid2705.203599>

Eosinophilic meningitis caused by human dirofilial infection is rare. We report a case of eosinophilic meningitis and concomitant intraocular dirofilial infection in India. Sequencing of the mitochondrial genome identified the worm as *Dirofilaria* sp. genotype Hongkong, a close relative of *D. repens* nematodes.

Dirofilariasis is a group of mosquito-borne parasitoses. The most prevalent *Dirofilaria* species causing infection are *D. immitis* and *D. repens* nematodes (1). Dogs are the definitive hosts in the life cycle, in which microfilariaemia is observed. Humans are aberrant hosts, and the worms usually remain infertile (1,2). Human dirofilariasis is reported mostly as 1 worm in the subconjunctival or subcutaneous spaces. Surgical extraction of the worm constitutes definitive therapy. These worms are rarely observed inside the eye (1,2). Identification of the worm by using morphologic features is difficult because a large number of *Dirofilaria* species have similar features.

Diagnosis of eosinophilic meningitis is based mainly on clinical features and microscopic identification of eosinophils in the central nervous system. Helminthic infections, such as angiostrongylosis, baylisascariasis, and gnathostomiasis, are most commonly implicated in eosinophilic meningitis (3). We report a rare case of eosinophilic meningitis and concomitant intraocular dirofilarial infection. Sequencing of the mitochondrial genome of the extracted worm identified it as *Dirofilaria* sp. genotype Hongkong, a close relative of *D. repens* (4).

A 17-year-old woman came to our institute in Kochi, India, because of acute onset of severe headache, irritability, visual blurring, and diplopia, after 3 weeks of intermittent fever. She had meningeal signs, bilateral lateral rectus palsy, and papilledema. Peripheral eosinophilia (14.2%) was observed. Magnetic resonance imaging of the brain (Appendix Figure 1, <https://wwwnc.cdc.gov/EID/article/27/5/20-3599-App1.pdf>) showed diffuse leptomeningeal enhancement. Cerebrospinal fluid showed lymphocytic pleocytosis (1,040 cells/ μ L), major eosinophilia (37%), and protein and glucose levels within reference ranges.

A live worm was detected in the anterior chamber of her left eye (Figure, panel A), confirmed by slit lamp examination (Figure, panel B; Video, <https://wwwnc.cdc.gov/EID/article/27/5/20-3599-V1.htm>). The lens showed cataractous changes. Indirect ophthalmoscopy showed inflammatory changes in retinal pigment epithelium, suggestive of a migratory tract. Serologic analysis for helminthic antibodies was not conducted because serologic testing was not available. A white, thread-like worm (length \approx 15 mm) was extracted after the worm was paralyzed by injection of lignocaine into the anterior chamber of the eye (Figure, panel C).

Because a PCR was available, histopathologic analysis was not conducted. Morphologic features or sex could not be determined. The worm specimen was subjected to multiplex PCR for *D. repens* and *D. immitis* using an equimolar combination of general and species-specific primers: *Diro_12S_F* (5'-GTTCCAGAATAATCGGCTA-3'), *Diro_12S_R* (5'-ATTGACGGATGGTTTGTACC-3'), *D. immitis_F* (5'-TTTTTACTTTTTTGGTAATG-3'), and *D. repens_R* (5'-AAAAGCAACACAAATAAAA-3'). The cytochrome c oxidase subunit 1 (COX1) region was amplified by using primers *Fil_COX1F* (5'-GCTTTRTCTTTTTGGKTTACTTTT-3') and *Fil_COX1R* (5'-TAGTRTCATAAAAAGAAGTATTA-3') (5).

Although the specimen was identified as a *D. repens* worm, Sanger sequencing of the COX1 and 12S rDNA PCR products was performed by using the Big-Dye Terminator v3.1 Cycle Sequencing Kit (Applied Biosystems, <https://www.thermofisher.com>) and the Genetic Analyzer 3130XL (Applied Biosystems). Sequences of 12S rRNA and COX1 genes obtained were deposited in GenBank (accession nos. MT984272 and MT984209).

Phylogenetic analysis of the 12S rRNA (MT984272) and COX1 (MT984209) sequences obtained from the

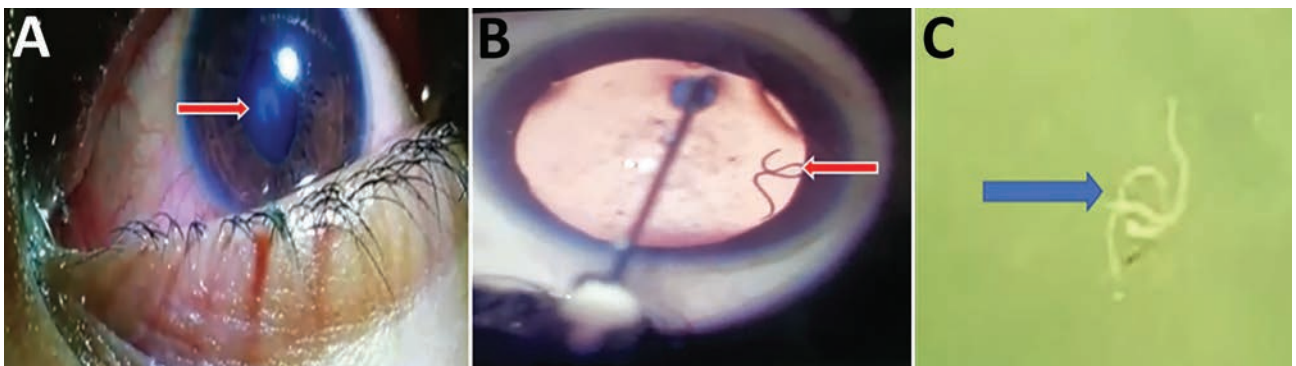


Figure. Eosinophilic meningitis and intraocular infection caused by *Dirofilaria* sp. genotype Hongkong in a patient in Kochi, India. A) Organism (arrow) in the left eye of patient during routine clinical examination. The organism caused an abnormal shape of the pupil. B) Live worm (arrow) in anterior chamber of the left eye. This image was obtained while lignocaine was being injected. C) Gross specimen of the worm (arrow) after extraction. Worm is in saline in a Petri dish.

isolate was performed by using the maximum-likelihood method with 1,000 bootstrap replications and MEGA X version 7 (<https://www.megasoftware.net>). Both the 12S rRNA and the COX1 sequences obtained from the human isolate were in the same cluster with *Dirofilaria* sp. genotype Hongkong and were separated from other *Dirofilaria* species (5,6) (Appendix Figure 2). Peripheral blood smears were negative for microfilaria. Symptoms of the patient resolved slowly after worm extraction and initiation of treatment with steroids.

Migrating worms in humans might cause a variety of clinical problems, which could be caused by mechanical effects or immune responses. Intraocular parasites might induce severe damage to various structures in the eye. Literature on eosinophilic meningitis and concomitant ocular parasites is limited. Clinical manifestations of eosinophilic meningitis are usually attributed to the severe inflammatory response incited by migrating worms, even though they are rarely demonstrated in vivo. Eosinophilic meningitis caused by *Angiostrongylus cantonensis* worms has been frequently reported in the Asia-Pacific region (7). *Dirofilaria* infection rarely results in eosinophilic meningitis (1,2).

Poppert et al. reported a case of *D. repens* infection, which was subsequently identified as *Dirofilaria* sp. genotype Hongkong, which caused subcutaneous infection and concomitant eosinophilic meningoencephalitis in a traveler returning from Kerala, India, and Sri Lanka to Germany (8). Subconjunctival infection with *Dirofilaria* sp. genotype Hongkong has also been reported in a patient returning to Austria after a 7-week stay in India (9). A recent study from Kerala, India, suggested that most of *D. repens* infections reported from southern India have the *Dirofilaria* sp. Hongkong genotype (10).

Demonstration of a live, intraocular worm and its subsequent identification as *Dirofilaria* sp. genotype Hongkong by using sequencing added a new dimension to this case of eosinophilic meningitis. Infection with the *Dirofilaria* sp. Hongkong genotype, blood eosinophilia, and eosinophilic meningitis are the 3 strikingly similar features between our case-patient and Poppert et al. (8), suggesting that *Dirofilaria* sp. genotype Hongkong might induce a more systemic eosinophilic reaction than *D. repens*.

Sequencing using panfilarial primers might help characterize most filarial species. Such an approach might clarify the etiopathogenesis of eosinophilic meningitis, leading to newer therapeutic and preventive strategies.

About the Author

Dr. Jyotsna is a resident in pediatric neurology at Amrita Institute of Medical Sciences and Research Centre, Kochi, Kerala, India. Her primary research interest is neurologic manifestations of infectious diseases.

References

- Genchi C, Rinaldi L, Mortarino M, Genchi M, Cringoli G. Climate and *Dirofilaria* infection in Europe. *Vet Parasitol*. 2009;163:286-92. <https://doi.org/10.1016/j.vetpar.2009.03.026>
- Simón F, Siles-Lucas M, Morchón R, González-Miguel J, Mellado I, Carretón E, et al. Human and animal dirofilariasis: the emergence of a zoonotic mosaic. *Clin Microbiol Rev*. 2012;25:507-44. <https://doi.org/10.1128/CMR.00012-12>
- Graeff-Teixeira C, da Silva AC, Yoshimura K. Update on eosinophilic meningoencephalitis and its clinical relevance. *Clin Microbiol Rev*. 2009;22:322-48. <https://doi.org/10.1128/CMR.00044-08>
- To KK, Wong SS, Poon RW, Trendell-Smith NJ, Ngan AH, Lam JW, et al. A novel *Dirofilaria* species causing human and canine infections in Hong Kong. *J Clin Microbiol*. 2012;50:3534-41. <https://doi.org/10.1128/JCM.01590-12>
- Gioia G, Lecová L, Genchi M, Ferri E, Genchi C, Mortarino M. Highly sensitive multiplex PCR for simultaneous detection and discrimination of *Dirofilaria immitis* and *Dirofilaria repens* in canine peripheral blood. *Vet Parasitol*. 2010;172:160-3. <https://doi.org/10.1016/j.vetpar.2010.04.027>
- To KK, Wong SS, Poon RW, Trendell-Smith NJ, Ngan AH, Lam JW, et al. A novel *Dirofilaria* species causing human and canine infections in Hong Kong. *J Clin Microbiol*. 2012;50:3534-41. <https://doi.org/10.1128/JCM.01590-12>
- Wang QP, Wu ZD, Wei J, Owen RL, Lun ZR. Human *Angiostrongylus cantonensis*: an update. *Eur J Clin Microbiol Infect Dis*. 2012;31:389-95. <https://doi.org/10.1007/s10096-011-1328-5>
- Poppert S, Hodapp M, Krueger A, Hegasy G, Niesen WD, Kern WV, et al. *Dirofilaria repens* infection and concomitant meningoencephalitis. *Emerg Infect Dis*. 2009;15:1844-6. <https://doi.org/10.3201/eid1511.090936>
- Winkler S, Pollreisz A, Georgopoulos M, Bagò-Horvath Z, Auer H, To KK, et al. *Candidatus* *Dirofilaria hongkongensis* as causative agent of human ocular filariasis after travel to India. *Emerg Infect Dis*. 2017;23:1428-31. <https://doi.org/10.3201/eid2308.170423>
- Pradeep RK, Nimisha M, Pakideery V, Johns J, Chandy G, Nair S, et al. Whether *Dirofilaria repens* parasites from south India belong to zoonotic *Candidatus* *Dirofilaria hongkongensis* (*Dirofilaria* sp. *hongkongensis*)? *Infect Genet Evol*. 2019;67:121-5. <https://doi.org/10.1016/j.meegid.2018.10.019>

Address for correspondence: Kollencheri P. Vinayan, Department of Pediatric Neurology, Amrita Institute of Medical Sciences and Research Centre, Ponnakkara, Edapally, Kochi 682041 India; email: vinayankp@aims.amrita.edu

COVID-19 Co-infection with *Legionella pneumophila* in 2 Tertiary-Care Hospitals, Germany

Hedda L. Verhasselt, Jan Buer, Jutta Dedy, Renate Ziegler, Joerg Steinmann, Frank Herbstreit, Thorsten Brenner, Peter-Michael Rath

Author affiliations: University of Duisburg-Essen, Essen, Germany (H.L. Verhasselt, J. Buer, J. Dedy, F. Herbstreit, T. Brenner, P.-M. Rath); Paracelsus Medical University, Nuremberg, Germany (R. Ziegler, J. Steinmann)

DOI: <https://doi.org/10.3201/eid2705.203388>

We describe screening results for detection of co-infections with *Legionella pneumophila* in patients infected with severe acute respiratory syndrome coronavirus 2. In total, 93 patients were tested; 1 was positive (1.1%) for *L. pneumophila* serogroup 1. Co-infections with *L. pneumophila* occur in coronavirus disease patients and should not be missed.

Severe acute respiratory syndrome coronavirus 2 (SARS-CoV-2) infection, which causes coronavirus disease (COVID-19), is characterized by severe respiratory distress, fever, and cough. High death rates, especially in older persons and those with underlying health conditions, have been described (1). According to World Health Organization guidelines and public health agencies, persons with cardiovascular disease, chronic respiratory disease, diabetes, and cancer are considered to be at increased risk for severe COVID-19. Moreover, the risk of becoming severely ill increases with age ≥ 60 years (<https://www.who.int/publications/m/item/covid-19-and-ncds>).

Groups at risk are largely the same for COVID-19 and Legionnaires' disease (LD), a severe and potentially fatal pneumonia caused by *Legionella* spp. These bacteria are found in many environments, including complex building water systems. In Europe and North America, *Legionella* spp. account for $\approx 1\%$ – 16% of all community-acquired pneumonias that require hospitalization (2); in 2017, the overall notification rate was 1.8/100,000 population for the European Union/European Economic Area (European Centre for Disease Prevention and Control, <https://www.ecdc.europa.eu/en/publications-data/legionnaires-disease-annual-epidemiological-report-2017>). *L. pneumophila* is responsible for $>90\%$ of LD cases; specifically, serogroup 1 causes 70%–80% of LD cases in the United States and Europe (3). Currently, the Centers for Disease Control and Prevention and the

European Society of Clinical Microbiology and Infectious Diseases Study Group for Legionella Infections give warning of increased risk for *Legionella* spp. infections resulting from stagnant or standing water in plumbing systems after the temporary shutdown of buildings and reductions in normal water use (4,5). A single person with SARS-CoV-2 revealed *L. pneumophila* co-infection in the context of travel (6). This case underlines the importance of making differential diagnoses during the COVID-19 pandemic by diagnostic microbiology to identify other infectious microorganisms causing similar symptoms.

In this retrospective analysis, we evaluated the co-occurrence of infections with *L. pneumophila* in patients infected with SARS-CoV-2. We performed urine antigen tests for detection of *L. pneumophila* serogroup 1 (BinaxNOW Legionella; Abbott Rapid Diagnostics Germany GmbH, <https://www.de.abbott>). We analyzed urine samples from 93 patients from 2 tertiary-care hospitals in Germany: University Hospital Essen, Essen, and General Hospital Nürnberg, Nuremberg. This retrospective study was approved by the Ethics Committee of the Medical Faculty at the University of Duisburg-Essen, Germany (approval no. 20-9335-BO).

The cohort was mostly male (71.0%) and had a mean age of 65 years; 90% had symptoms of pneumonia (Table). All were hospitalized, and 38.7% received mechanical ventilation. More than one third of the cohort had ≥ 2 underlying conditions and reflected the groups at risk for infection with *Legionella* spp.

We detected 1 *L. pneumophila* serogroup 1 antigen in the entire cohort (1.1%). The patient with *L. pneumophila* serogroup 1 co-infection was a 41-year-old man with severe acute respiratory deficiency syndrome and bronchial asthma as underlying disease; he initially came to the hospital with fever, cough, and dyspnea and had no recent travel history. Before admission to the University Hospital, he was treated with azithromycin and ceftriaxone for 4 days, until a switch to levofloxacin on day 1 after first diagnosis of LD in the referral hospital. In the University Hospital, urine antigen test was still positive, and detection of *Legionella* spp. DNA from bronchoalveolar fluid revealed a PCR cycle threshold value of 34 (ampliCube Respiratory Panel 1; Mikrogen Diagnostic, <https://www.mikrogen.de>), which was assessed as negative. To exclude a false-positive antigen test result, we retested this specific urine sample after boiling for 5 min and centrifugation (5 min at $12,000 \times g$), which yielded a positive result again (7). As of July 2020, the patient was still critically ill, receiving mechanical ventilation and intravenous levofloxacin (500 mg 2 \times /d; day 6 of levofloxacin treatment).

Table. Demographics and underlying conditions of patients with COVID-19 examined for *Legionella pneumophila* urine antigen, Germany

Characteristic	Value
Total	93 (100.0)
Negative for <i>L. pneumophila</i> serogroup 1 antigen	92 (98.9)
Positive for <i>L. pneumophila</i> serogroup 1 antigen	1 (1.1)
Average time between admission and <i>Legionella</i> antigen test processing	2.6 d (mean), 1 d (median)
Legionella-specific culture† performed/positive	18 (19.4)/0
Legionella nonspecific culture performed/positive	35 (37.6)/11 (31.4)
Multiplex PCR‡ performed/positive	31 (33.3)/5 (16.1)
Clinical symptoms typical for COVID-19§	60 (90.0)
Hospitalized	93 (100)
Transferred from other hospital	35 (37.6)
Treated in intensive care unit	40 (43.0)
Mean age, years	65
Sex	
M	66 (71.0)
F	27 (29.0)
Invasive mechanical ventilation	36 (38.7)
Extracorporeal membrane oxygenation	17 (18.3)
Mortality	30 (32.3)
Underlying conditions	
Cardiovascular disease	50 (53.8)
Diabetes	28 (30.1)
Chronic respiratory disease	13 (14.0)
Cancer	10 (11.0)
Other: rheumatism, Parkinson's disease	17 (18.3)
Addictions: alcohol, nicotine	7 (7.5)
Solid organ transplantation: lung	1 (1.1)
None	15 (16.1)
1 underlying condition	55 (59.1)
2 underlying conditions	29 (31.2)
>2 underlying conditions	7 (7.5)

*Values are no. (%) except as indicated.

†Legionella BMPA selective agar (Thermo Scientific, <https://www.thermofisher.com>).

‡Unyvero P50 pneumonia application (Curetis GmbH, <https://curetis.com>) or ampliCube Respiratory Panel 1 (Mikrogen Diagnostic, <https://www.mikrogen.de>).

§Data available for 67 patients.

Xing et al. reported *L. pneumophila*, detected by indirect immunofluorescence in 20% of COVID-19 patients, as the second most prevalent bacterium causing respiratory disease (Q. Xing et al., unpub. data, <https://www.medrxiv.org/content/10.1101/2020.02.29.20027698v2>). However, cross-reactivity of indirect immunofluorescence tests with other bacterial species has been described. Antibody titers without follow-up should be interpreted with caution because antibodies can be generated even after mild infections and can persist over years.

In view of epidemiologic data, detection of only *L. pneumophila* serogroup 1 antigen in urine is a suitable diagnostic approach for outpatient-acquired and travel-associated pneumonia, with varying sensitivity and specificity (8). The false-negative rate of this diagnostic approach is low because antigen excretion starts 24 hours after first symptoms and generally persists for weeks, and in rare cases even months (9); positive urine antigen tests can be found after initiation of antimicrobial drug treatment. However, pre-test probability of *L. pneumophila* pneumonia should be reasonably high to have clinical utility (10).

The findings from our small cohort study in 2 geographically distinct areas in Germany indicate that co-infections with *L. pneumophila* serogroup 1 can occur in patients with COVID-19. Clinicians treating patients positive for SARS-CoV-2 should be aware of possible co-infections with *L. pneumophila* and should use appropriate diagnostic approaches.

About the Author

Dr. Verhasselt is a research associate and laboratory head of the serology section of the Institute of Medical Microbiology at University Hospital Essen, University of Duisburg-Essen, Essen, Germany. Her primary research interests are diagnosis and therapy of fungal infections and antifungal susceptibility testing.

References

- Guan WJ, Ni ZY, Hu Y, Liang WH, Ou CQ, He JX, et al.; China Medical Treatment Expert Group for Covid-19. Clinical characteristics of coronavirus disease 2019 in China. *N Engl J Med.* 2020;382:1708–20. <https://doi.org/10.1056/NEJMoa2002032>

2. Muder RR, Yu VL, Fang GD. Community-acquired Legionnaires' disease. *Semin Respir Infect.* 1989;4:32-9.
3. Fields BS, Benson RF, Besser RE. Legionella and Legionnaires' disease: 25 years of investigation. *Clin Microbiol Rev.* 2002;15:506-26. <https://doi.org/10.1128/CMR.15.3.506-526.2002>
4. Centers for Disease Control and Prevention. Guidance for reopening buildings after prolonged shutdown or reduced operation; 2019 [cited 2020 Jul 19]. <https://www.cdc.gov/coronavirus/2019-ncov/php/building-water-system.html>
5. ESCMID Study Group for Legionella Infections. ESGLI Guidance for managing Legionella in building water systems during the COVID-19 pandemic. 2020 [cited 2020 Dec 15]. <https://www.pwtag.org/esgli-guidance-managing-legionella-building-water-systems-covid-19-pandemic>
6. Arashiro T, Nakamura S, Asami T, Mikuni H, Fujiwara E, Sakamoto S, et al. SARS-CoV-2 and legionella co-infection in a person returning from a Nile cruise. *J Travel Med.* 2020;27:taaa053. <https://doi.org/10.1093/jtm/taaa053>
7. Rota MC, Fontana S, Montaña-Remacha C, Scaturro M, Caporali MG, Vullo V, et al. Legionnaires' disease pseudoepidemic due to falsely positive urine antigen test results. *J Clin Microbiol.* 2014;52:2279-80. <https://doi.org/10.1128/JCM.00493-14>
8. Pierre DM, Baron J, Yu VL, Stout JE. Diagnostic testing for Legionnaires' disease. *Ann Clin Microbiol Antimicrob.* 2017;16:59. <https://doi.org/10.1186/s12941-017-0229-6>
9. Kohler RB, Winn WC Jr, Wheat LJ. Onset and duration of urinary antigen excretion in Legionnaires disease. *J Clin Microbiol.* 1984;20:605-7. <https://doi.org/10.1128/JCM.20.4.605-607.1984>
10. Dionne M, Hatchette T, Forward K. Clinical utility of a *Legionella pneumophila* urinary antigen test in a large university teaching hospital. *Can J Infect Dis.* 2003;14:85-8. <https://doi.org/10.1155/2003/642159>

Address for correspondence: Hedda Luise Verhasselt, Institute of Medical Microbiology, University Hospital Essen, Virchowstr 179, 45147 Essen, Germany; email: hedda-luise.verhasselt@uk-essen.de

Temporal Variations in Respiratory Syncytial Virus Epidemics, by Virus Subtype, 4 Countries

Lisa Staaedegaard, Adam Meijer, Ana Paula Rodrigues, Sue Huang, Cheryl Cohen, Clarisse Demont, Jojanneke van Summeren, Saverio Caini, John Paget

Author affiliations: Netherlands Institute for Health Services Research (Nivel), Utrecht, the Netherlands (L. Staaedegaard, J. van Summeren, S. Caini, J. Paget); National Institute for Public Health and the Environment (RIVM), Bilthoven, the Netherlands (A. Meijer); Instituto Nacional de Saúde Doutor Ricardo Jorge, Lisbon, Portugal (A.P. Rodrigues); Institute of Environmental Science and Research Limited, Upper Hutt, New Zealand (S. Huang); National Institute for Communicable Diseases, Johannesburg, South Africa (C. Cohen); University of Witwatersrand, Johannesburg (C. Cohen); Sanofi Pasteur, Lyon, France (C. Demont)

DOI: <https://doi.org/10.3201/eid2705.204615>

Temporal variation of respiratory syncytial virus (RSV) epidemics was recently reported to be determined by the dominant RSV subtype. However, when we repeated the analysis for 4 countries in the Northern and Southern Hemispheres, the dominant subtype did not seem to affect temporal variation of RSV epidemics.

Respiratory syncytial virus (RSV) is responsible for most acute lower respiratory tract infections in young children worldwide (1) and accounts for a substantial burden among older adults (2). Although it is generally accepted that RSV epidemics in temperate climates occur in winter, some temporal variation epidemics remains unexplained (3).

Recently, Yu et al. conducted a study among children (<13 years of age) with pneumonia at the Beijing Children's Hospital (Beijing, China) during July 2007-June 2015 and reported that temporal variation is partly explained by seasonal differences in virus subtype dominance (4). To define the timing of RSV seasonality, they used a regression model and 10% threshold method previously described (3). They found that onset and peak of seasons occurred \approx 3-5 weeks earlier and that duration was \approx 6 weeks longer when RSV subtype A (RSV-A) was dominant than when subtype B (RSV-B) was dominant. These results, if generalizable, would have major implications for the

epidemiology of RSV surveillance programs and healthcare planning.

We examined whether similar patterns in the dominant RSV subtype and timing of RSV epidemics were found in the Northern and Southern Hemispheres by using a large dataset from the Global Epidemiology of RSV in the Community and Hospitalised Care study (<https://www.nivel.nl/en/geri>). We included in our analysis only countries with a temperate climate. For Northern Hemisphere countries, seasons were defined as week 27 through week 26 of the next calendar year; for Southern Hemisphere countries, seasons were defined as week 1 through 52 of the same calendar year. We included seasons if ≥ 50 RSV cases with subtyped information available (diagnosed by PCR) had been reported. We included persons of all ages; the Beijing study included only children < 13 years of age. In addition, the case definitions for each study did not entirely overlap. In defining the start, duration, and peak of the RSV seasons, we followed a similar approach as Yu et al. (i.e., 10% threshold [4]). We defined the onset week of

an epidemic as the first of 2 consecutive weeks in which the percentage of specimens testing positive exceeded 10%. The offset week was determined as the second week of the last 2 consecutive weeks when this threshold was breached (3).

We explored the relationship between the timing of an epidemic and the dominant RSV subtype ($> 50\%$ of cases) by calculating the mean start, end, and duration of the seasons according to virus subtype. We applied a regression analysis with robust SEs to account for the potential clustering of individual country results.

We included weekly subtyped RSV data from the Northern (Netherlands and Portugal) and Southern (New Zealand and South Africa) Hemispheres; surveillance systems for those countries are described elsewhere (5–8). We analyzed 24 seasons (5,189 cases), of which RSV-A was dominant for 14 (Table). A dominant RSV-A or RSV-B season was determined by using the 50% cutoff; this percentage was frequently close to 50%. For example, the proportion of persons with an RSV-A–positive test result was 51%–85% (Figure). All differences in timing were not significant;

Table. Summary of seasonal metrics of respiratory syncytial virus epidemics, defined by 10% positivity threshold, by season and country*

Location, season	Start, calendar wk	End, calendar wk	Duration, wk	Peak, calendar wk	No. cases	No. subtyped cases	Subtype A, %	Dominant subtype
Northern Hemisphere								
The Netherlands								
2009–10	49	8	12	3	100	100	44	B
2010–11	4	7	4	6	82	82	68	A
2011–12	51	4	6	51	53	53	36	B
2012–13	51	5	7	2	60	60	75	A
2013–14	3	8	6	4	72	72	44	B
2014–15	6	13	8	9	73	73	37	B
2015–16	51	5	7	2	110	110	35	B
2016–17	47	2	8	51	123	123	70	A
2017–18	47	52	7	51	75	75	17	B
Average	52	6	7	3	83	83	47	B
Portugal								
2012–13	50	1	4	50	94	80	78	A
2013–14	52	3	4	52	298	103	70	A
2014–15	44	18	27	51	412	38	13	B
2015–16	47	13	19	51	646	99	63	A
2016–17	45	12	20	4	682	91	55	A
2017–18	44	15	24	5	1,084	142	51	A
2018–19	44	18	27	10	1,662	101	27	B
Average	47	11	18	2	697	93	51	A
Southern Hemisphere								
New Zealand								
2012	18	37	20	26	880	152	85	A
2013	15	32	18	27	1,238	367	21	B
2014	24	34	11	27	1,406	409	65	A
2015	13	32	20	24	1,430	295	58	A
2016	12	32	21	26	1,020	185	66	A
Average	16	33	18	26	1,195	282	52	A
South Africa								
2016	8	28	21	17	750	675	59	A
2017	7	30	24	16	848	825	33	B
2018	6	26	21	15	922	879	60	A
Average	7	28	22	16	840	793	51	A

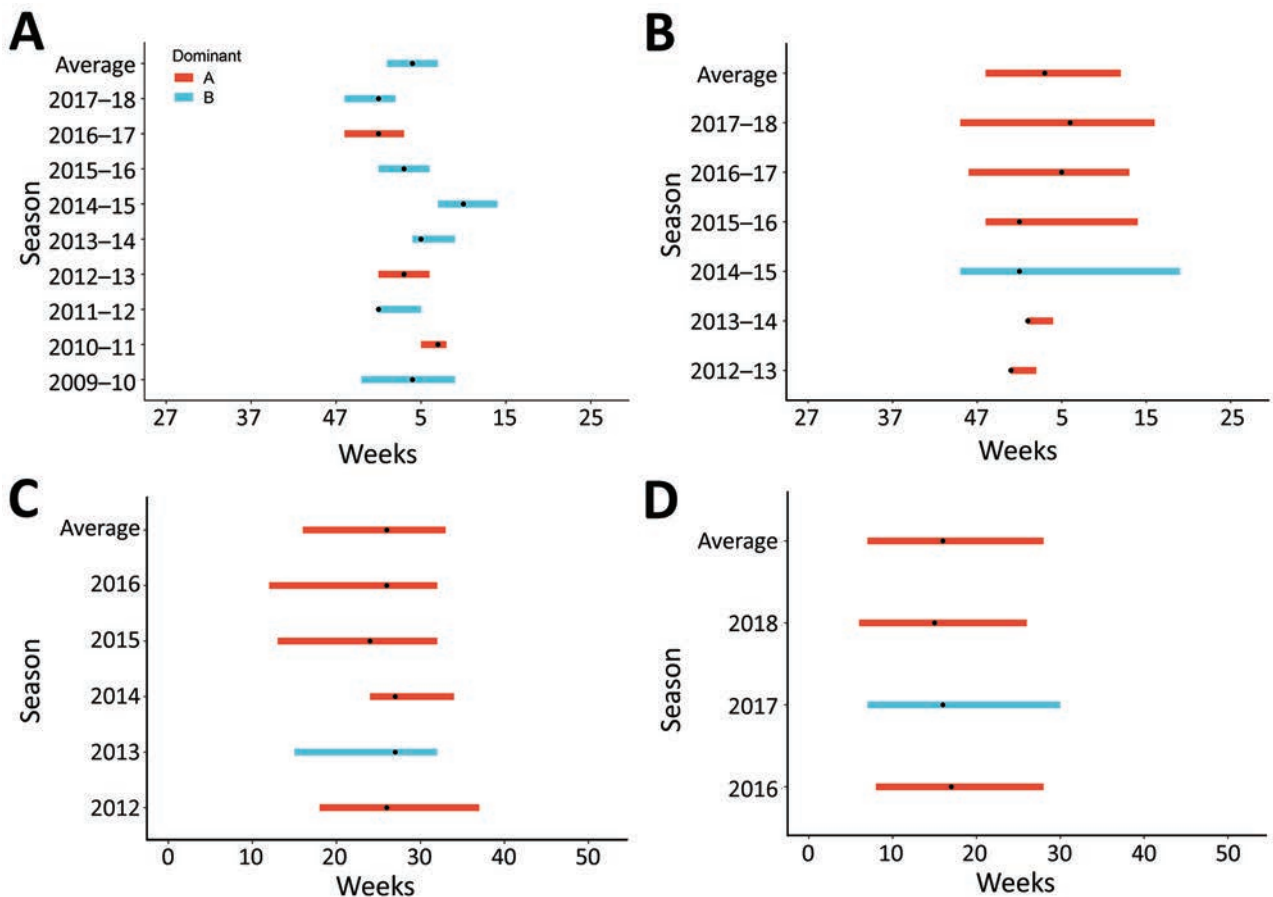


Figure. Temporal variation in respiratory syncytial virus, defined by using 10% positivity threshold, by dominant virus subtype, country, and season. A) The Netherlands; B) Portugal; C) New Zealand; D) South Africa. Black dots indicate the peak (highest percentage of cases testing positive) of the season.

RSV-A-dominant seasons started 2 weeks earlier ($p = 0.3$), ended 2 weeks earlier ($p = 0.3$), and peaked 2 weeks earlier ($p = 0.2$) than RSV-B-dominant seasons. Mean durations were 14.5 weeks for RSV-A-dominant seasons and 14.9 weeks for RSV-B-dominant seasons ($p = 0.9$).

We found no significant difference in the effect of the dominant RSV subtype on temporal variation of RSV epidemics. We did not find the earlier start and longer duration of RSV-A-dominant seasons described by Yu et al. when we used similar methods for the countries included in our analysis. Although the national datasets and dataset used by Yu et al. differ from those that we used in several ways (e.g., case definition and age categories), we believe that these differences do not preclude conducting temporal comparisons of this type.

One limitation of our analysis and that of Yu et al. is the definition of a dominant season. Small differences in virus subtype distribution potentially

have a major effect on the results, especially when case numbers are lower in included seasons. An example is the 2016-17 season in Portugal, when RSV-A prevailed but was responsible for only 142 (51%) cases. That finding was similar to that described by Yu et al. for the 2013-14 season, which experienced an almost equal number of cases caused by RSV-A ($n = 35$) and RSV-B ($n = 33$). This limitation substantially reduces conclusions that can be drawn from this type of analysis, and we advocate a more stringent definition of an RSV dominant subtype per season (e.g., >70% threshold) for future analyses, thereby ensuring that differences in subtype distribution are real. We recommend that countries monitor RSV subtypes so that our findings can be validated with more data because a temporal variation in RSV epidemics caused by this subtype would have a major effect on the epidemiology of RSV, surveillance programs, and healthcare planning at the local level.

Acknowledgments

We thank Anne Teirlinck, Gé Donker, Mariëtte Hooiveld, Janneke Hendriksen, the general practitioners, and the patients who contributed to the virologic part of the national sentinel surveillance for influenza-like illness and acute respiratory infection. We also thank Peter Spreeuwenberg for his statistical advice.

This study was funded by Sanofi Pasteur and AstraZeneca.

L.S., A.M., A.P.R., S.H., C.C., J.S., and S.C. declare no competing interests. J.P. declares that Nivel has received unrestricted research grants from the World Health Organization, Sanofi Pasteur, and the Foundation for Influenza Epidemiology. C.D. is an employee of Sanofi Pasteur and may hold shares or stock options in the company.

About the Author

Ms. Staaedegaard is an epidemiologist working at the Netherlands Institute for Health Services Research in the Netherlands. Her main research interests include the epidemiology of infectious diseases, with a current focus on respiratory infections.

References

1. Shi T, McAllister DA, O'Brien KL, Simoes EAF, Madhi SA, Gessner BD, et al.; RSV Global Epidemiology Network. Global, regional, and national disease burden estimates of acute lower respiratory infections due to respiratory syncytial virus in young children in 2015: a systematic review and modelling study. *Lancet*. 2017;390:946–58. [https://doi.org/10.1016/S0140-6736\(17\)30938-8](https://doi.org/10.1016/S0140-6736(17)30938-8)
2. Shi T, Denouel A, Tietjen AK, Campbell I, Moran E, Li X, et al. Global disease burden estimates of respiratory syncytial virus-associated acute respiratory infection in older adults in 2015: a systematic review and meta-analysis. *J Infect Dis*. 2020;222:S577–83.
3. Haynes AK, Prill MM, Iwane MK, Gerber SJ; Centers for Disease Control and Prevention (CDC). Respiratory syncytial virus—United States, July 2012–June 2014. *MMWR Morb Mortal Wkly Rep*. 2014;63:1133–6.
4. Yu J, Liu C, Xiao Y, Xiang Z, Zhou H, Chen L, et al. Respiratory syncytial virus seasonality, Beijing, China, 2007–2015. *Emerg Infect Dis*. 2019;25:1127–35. <https://doi.org/10.3201/eid2506.180532>
5. Vos LM, Teirlinck AC, Lozano JE, Vega T, Donker GA, Hoepelman AI, et al. Use of the moving epidemic method (MEM) to assess national surveillance data for respiratory syncytial virus (RSV) in the Netherlands, 2005 to 2017. *Euro Surveill*. 2019;24. <https://doi.org/10.2807/1560-7917.ES.2019.24.20.1800469>
6. Sáez-López E, Pechirra P, Costa I, Cristóvão P, Conde P, Machado A, et al. Performance of surveillance case definitions for respiratory syncytial virus infections through the sentinel influenza surveillance system, Portugal, 2010 to 2018. *Euro Surveill*. 2019;24. <https://doi.org/10.2807/1560-7917.ES.2019.24.45.1900140>
7. Prasad N, Newbern EC, Trenholme AA, Wood T, Thompson MG, Aminisani N, et al. Respiratory syncytial

virus hospitalisations among young children: a data linkage study. *Epidemiol Infect*. 2019;147:e246.

<https://doi.org/10.1017/S0950268819001377>

8. Rha B, Dahl RM, Moyes J, Binder AM, Tempia S, Walaza S, et al. Performance of surveillance case definitions in detecting respiratory syncytial virus infection among young children hospitalized with severe respiratory illness—South Africa, 2009–2014. *J Pediatric Infect Dis Soc*. 2019;8:325–33. <https://doi.org/10.1093/jpids/piy055>

Address for correspondence: Lisa Staaedegaard, Nivel, Otterstraat 118, 3513 CR Utrecht, the Netherlands; email: l.staaedegaard@nivel.nl

Novel SARS-CoV-2 Variant Derived from Clade 19B, France

Slim Fourati, Jean-Winoc Decousser, Souraya Khouider, Melissa N'Debi, Vanessa Demontant, Elisabeth Trawinski, Aurélie Gurgeon, Christine Gangloff, Grégory Destras, Antonin Bal, Laurence Josset, Alexandre Soulier, Yannick Costa, Guillaume Gricourt, Bruno Lina, Raphaël Lepeule, Jean-Michel Pawlotsky, Christophe Rodriguez

Author affiliations: Institut Mondor de Recherche Biomédicale, Université Paris-Est, Créteil, France; (S. Fourati, S. Khouider, A. Gurgeon, A. Soulier, J.-M. Pawlotsky, C. Rodriguez); Hôpital Henri Mondor, Créteil (J.-W. Decousser, M. N'Debi, V. Demontant, E. Trawinski, G. Gricourt, R. Lepeule, C. Rodriguez); Hôpital Albert Chenevier, Créteil (C. Gangloff); Université de Lyon, France (G. Destras, A. Bal, L. Josset, B. Lina); Grand Hôpital de l'Est Francilien, Jossigny, France (Y. Costa)

DOI: <https://doi.org/10.3201/eid2705.210324>

We report a novel severe acute respiratory syndrome coronavirus 2 variant derived from clade 19B (HMN.19B variant or Henri Mondor variant). This variant is characterized by the presence of 18 amino acid substitutions, including 7–8 substitutions in the spike protein and 2 deletions. These variants actively circulate in different regions of France.

During fall 2020, new severe acute respiratory syndrome coronavirus 2 (SARS-CoV-2) variants, some of which have become variants of concern, progressively replaced the original strains in regions

Table. Amino acid changes within the spike protein sequence of the HMN.19B variant in France compared with the reference sequence of the international GISAID database (GenBank accession no. NC_045512.2), in comparison with other recently identified SARS-CoV-2 variants*

<i>Spike protein sequence</i>				
<i>HMN.19B</i> (<i>Henri Mondor variant</i>)	20I/501Y.V1 (UK variant)	20H/501Y.V2 (South African variant)	P1 20J/501Y.V3 (Brazilian variant)	CAL.20C (Californian variant) S13I
L18F		L18F	L18F T20N P26S	
	Del69/70	D80A	D138Y	
	Del144		R190S	W152C
		D215G Del 242–244 R246I K417N	K417T	
L452R		E484K	E484K	L452R
N501Y	N501Y A570D	N501Y	N501Y	
A653V H655Y Q677H†			H655Y	
	P681H	A701V		
	T716I			
D796Y	S982A		T1027I	
	D1118H			
G1219V				

*Bold type indicates amino acid changes observed in ≥ 1 of the recent variants.

†Inconstantly detected, recently found in the genome of the "Midwest" variant (Q677H variant) observed in Ohio (USA) in December 2020 and January 2021.

where they were first identified. We report a new SARS-CoV-2 variant of interest derived from clade 19B (tentatively named HMN.19B variant, or Henri Mondor variant) that is actively circulating in France.

On January 21, 2021, a hospital administrative assistant receiving long-term treatment with anti-tumor necrosis factor- α (adalimumab) for ankylosing spondylitis sought treatment for headache, fatigue, and rhinitis suggestive of coronavirus disease (COVID-19). SARS-CoV-2 RNA was confirmed by reverse transcription PCR (RT-PCR). Her partner (household contact), along with 2 nurses from the same occupational health unit sharing their locker room with the administrative assistant, sought treatment for symptoms suggestive of COVID-19 during January 21–23. Virus was confirmed in all instances by RT-PCR.

The slightly immunocompromised administrative assistant and her immunocompetent partner reported a history of symptomatic COVID-19 infection in early October 2020, confirmed in both cases by a positive RT-PCR result. However, both patients tested negative for SARS-CoV-2 protein N antibody

in January 2021. One of the 2 infected nurses had received a first dose of COVID-19 vaccine (Pfizer-BioNTech, <https://www.pfizer.com>) 11 days before her positive RT-PCR result. All 4 patients experienced mild COVID-19 and did not require hospitalization.

Full-length genome sequencing revealed that the 4 cluster members were infected with a new phylogenetic variant stemming from clade 19B, tentatively called HMN.19B variant or Henri Mondor variant (Appendix, <https://wwwnc.cdc.gov/EID/article/27/5/21-0324-App1.pdf>). Compared with the reference sequence (GenBank accession no. NC_045512.2) from the international GISAID database (<https://www.gisaid.org>), variant HMN.19B carries 25 nt substitutions, with a high ratio of non-synonymous ($n = 18$) to synonymous ($n = 7$) mutations, 2 deletions, and a high number of amino acid substitutions within the spike protein ($n = 8$) at key positions: spike substitutions in comparison with other recently emerged variants (Table) and all mutations (Figure).

In the 4 weeks after its first detection, our laboratory, which maintains 1 of the 4 national SARS CoV-2

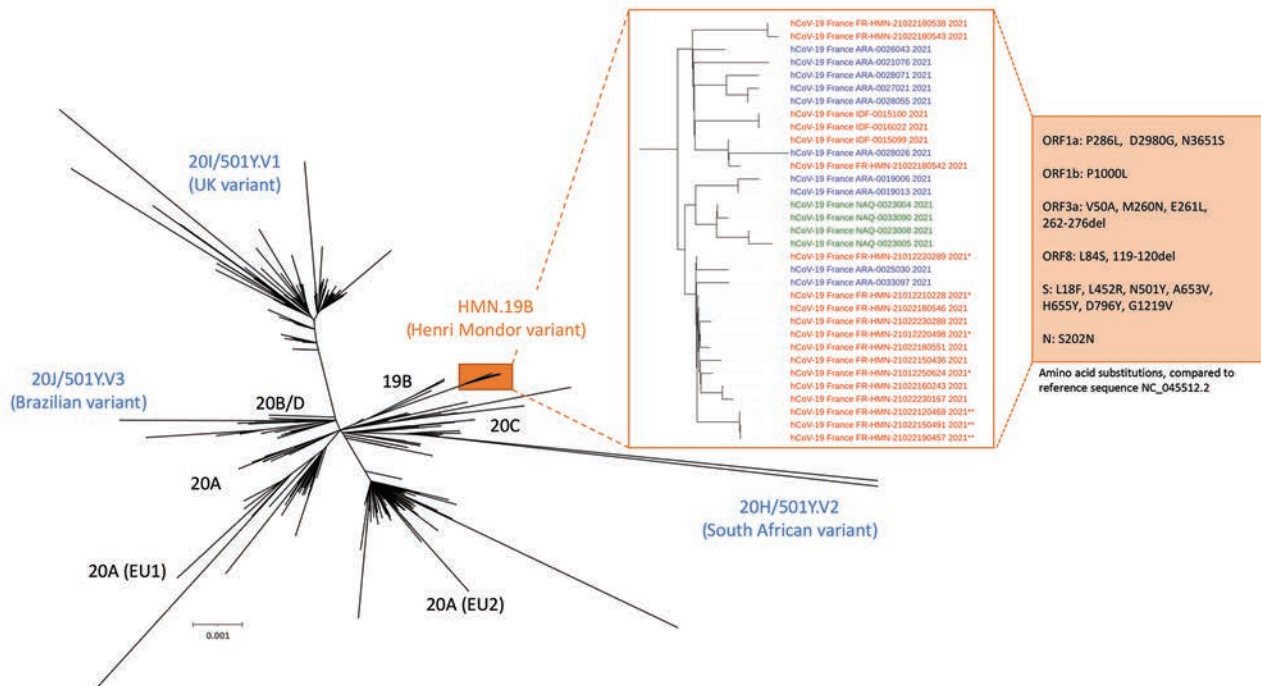


Figure. Phylogenetic tree built with sequences from the 33 patients infected with the new HMN.19B or Henri Mondor variant and from 1,537 SARS-CoV-2-infected patients in France sampled during January 18–February 23, 2021, sequenced in 9 successive series. Phylogeny was performed after full-length genome alignment with Muscle 3.8.31 (maximum-likelihood model general time-reversible plus invariant sites model, 1,000 bootstrap replicates) by means of IQ-Tree 1.3.11.1 and iTOL. The HMN.19B (Henri Mondor) variant cluster is considerably different from all the others, with a 99% bootstrap value. HMN.19B sequences are colored according to the geographic origin of the patients: red, greater Paris area (IDF or HMN); blue, southeast France (ARA); green, southwest France (NAQ). *Original cluster in an occupational health unit; **cluster in the hematology department of our institution. Amino-acid substitutions and deletions detected in all sequences are described in the orange box. ARA, Auvergne-Rhône-Alpes; HMN, Henri Mondor; IDF, Ile-de-France; NAQ, Nouvelle-Aquitaine.

sequencing surveillance platforms in France, found the HMN.19B variant in 12 patients from the greater Paris area (Figure). These patients were 1 prison administration staff member from northeast of the Paris area, tested February 9 during a prison screening campaign; 3 epidemiologically related subjects from a cluster in the hematology department of our hospital (an asymptomatic nursing student tested February 12, his mentor nurse tested February 14, and a hospitalized patient tested February 15); and 8 epidemiologically unrelated cases found positive for SARS-CoV-2 RNA during February 3–23 in different hospitals in the greater Paris area (GISAID identification numbers in Appendix Table).

During the same period, the National Reference Center for Respiratory Viral Infections (Lyon, France) identified 17 additional patients infected with closely related viruses, which carried ≥ 7 similar substitutions in spike (some were lacking Q677H in spike [Figure]). Three patients were from the greater Paris area, 10 from southeastern France, and 4 from southwestern France (Figure).

We identified a new, previously undescribed variant of SARS-CoV-2 (HMN.19B or Henri Mondor variant) within a cluster of hospital staff in Paris. This variant stems from an older SARS-CoV-2 clade, 19B, which emerged in late 2019 but have been rarely detected since early 2020, overtaken by clades 20A, 20B, and 20C, which harbor the D614G substitution believed to improve viral transmission (1). The HMN.19B variant is characterized by the presence of 2 deletions and 18 amino acid substitutions over the entire sequence, including 8 substitutions within the spike protein, some of which are common with other recently described variants, a finding in keeping with the ongoing evolutionary convergence of SARS-CoV-2 variants. The acquisition of spike substitutions, including N501Y and L452R, has been suggested to enhance the interaction of spike with the angiotensin-converting enzyme 2 viral receptor. The resulting substantial fitness acquisition could explain the reappearance of clade 19B (2; Yang et al., unpub. data, <https://doi.org/10.1101/2020.12.29.42469>).

New variants with several spike mutations (20I/501Y.V1) have been associated with increased transmissibility. Whether HMN.19B will be less susceptible to protection by natural, therapeutic, or vaccine-induced immune responses remains to be determined. Several of its spike substitutions (N501Y, L452R, and H655Y) have been shown to require higher levels of neutralizing antibodies to be controlled, both in vitro and in vivo (3,4; Liu et al., unpub. data, <https://doi.org/10.1101/2020.11.06.372037>).

In conclusion, we report a new SARS-CoV-2 variant circulating in France. Our results emphasize the need for careful molecular surveillance of SARS-CoV-2 evolution to track emergence of any new variant of interest with potential epidemiologic or pathologic consequences.

Acknowledgments

We thank Martine Valette and Quentin Semanas for their help and commitment.

About the Author

Dr. Fourati is a researcher at University of East Paris, Créteil, France. He is also a clinical virologist in the Department of Microbiology, Henri Mondor Hospital, Créteil, France. His primary research interests include viral evolution and adaptation, and viral hepatitis and respiratory viruses including SARS CoV-2.

References

1. Korber B, Fischer WM, Gnanakaran S, Yoon H, Theiler J, Abfalterer W, et al.; Sheffield COVID-19 Genomics Group. Tracking changes in SARS-CoV-2 spike: evidence that D614G increases infectivity of the COVID-19 virus. *Cell*. 2020;182:812–827.e19. <https://doi.org/10.1016/j.cell.2020.06.043>
2. Weisblum Y, Schmidt F, Zhang F, DaSilva J, Poston D, Lorenzi JC, et al. Escape from neutralizing antibodies by SARS-CoV-2 spike protein variants. *eLife*. 2020;9:e61312. <https://doi.org/10.7554/eLife.61312>
3. Choi B, Choudhary MC, Regan J, Sparks JA, Padera RF, Qiu X, et al. Persistence and evolution of SARS-CoV-2 in an immunocompromised host. *N Engl J Med*. 2020;383:2291–3. <https://doi.org/10.1056/NEJMc2031364>
4. Baum A, Fulton BO, Wloga E, Copin R, Pascal KE, Russo V, et al. Antibody cocktail to SARS-CoV-2 spike protein prevents rapid mutational escape seen with individual antibodies. *Science*. 2020;369:1014–8. <https://doi.org/10.1126/science.abd0831>

Address for correspondence: Slim Fourati, Virology Department, Henri Mondor Hospital, 51 Av. du Maréchal de Lattre de Tassigny, 94010 Créteil, France; email: slim.fourati@aphp.fr

Undocumented Migrants Reintroducing COVID-19, Yunnan Province, China

Meiling Zhang,¹ Jienan Zhou,¹ Senquan Jia, Xiaonan Zhao, Yaoyao Chen, Yanhong Sun, Zhaosheng Liu, Xiaofang Zhou, Duo Li, Chunrui Luo, Yong Zhang, Violet Magoma Onsongo, Yong Shao, Xiaoqing Fu

Author affiliations: Yunnan Provincial Center for Disease Control and Prevention, Kunming, China (M.L. Zhang, J.N. Zhou, S.Q. Jia, X.N. Zhao, Y.Y. Chen, Y.H. Sun, Z.S. Liu, X.F. Zhou, D. Li, C.R. Luo, Y. Zhang, X.Q. Fu); Kunming Institute of Zoology, Kunming (V.M. Onsongo, Y. Shao)

DOI: <https://doi.org/10.3201/eid2705.204944>

To limit the spread of severe acute respiratory syndrome coronavirus 2, the government of China has been monitoring infected travelers and minimizing cold-chain contamination. However, other factors might contribute to recurring outbreaks. We analyze the role of undocumented migrants as potential transmitters of severe acute respiratory syndrome coronavirus 2 in China.

China's efforts to suppress coronavirus disease (COVID-19), the illness caused by severe acute respiratory syndrome coronavirus 2 (SARS-CoV-2), rely on rigorous quarantine measures. These measures contributed to a decline in COVID-19 cases; no new locally acquired cases were reported in China on March 18, 2020 (http://www.nhc.gov.cn/xcs/yqtb/list_gzbd_10.shtml). As a result, the focus of epidemic control and prevention work has shifted from local to imported cases of COVID-19. Although viral spread has been contained by mandates minimizing travel and cold-chain contamination (1), recurring COVID-19 outbreaks might be caused by other factors and pathways. On September 14, 2020, the discovery of 2 SARS-CoV-2-infected undocumented migrants from Myanmar prompted large-scale testing of >280,000 persons in Ruili, Yunnan Province, China (Figure).

On March 31, 2020, the Yunnan Provincial Leading Group for COVID-19 Epidemic Response published Notice No. 15 (http://www.yn.gov.cn/zttg/yqfk/zcfk/202004/t20200401_201604.html), which outlined strict measures to prevent COVID-19 importation from land and water ports. This notice discouraged citizens of adjacent countries from entering Yunnan Province; if entry was required, then those

¹These authors contributed equally to this article.

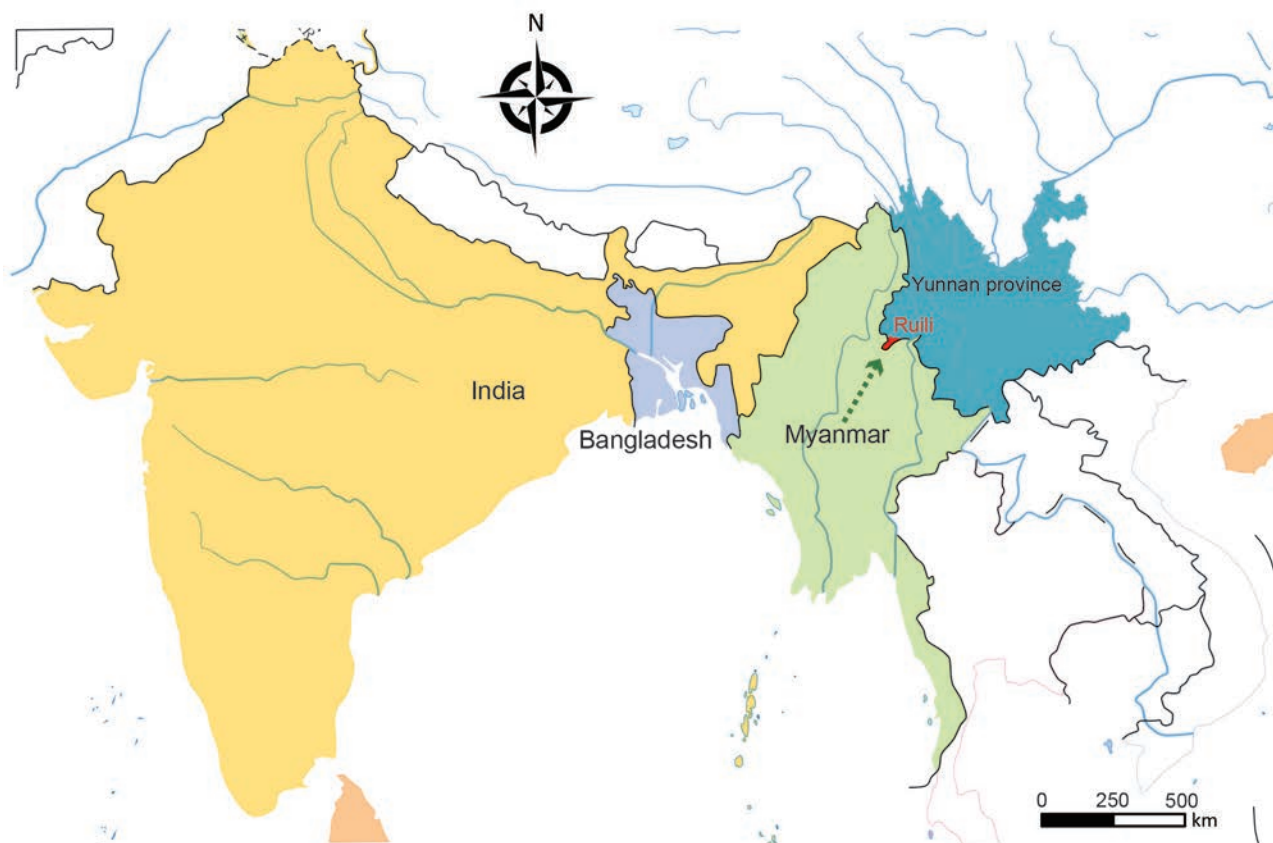


Figure. Ruili, Yunnan Province, China, in relation to neighboring countries. Map from <http://bzdt.ch.mnr.gov.cn>. Arrow indicates direction of migration.

citizens should enter Yunnan Province via 1 of 19 official land ports (Appendix Table 1, <https://wwwnc.cdc.gov/EID/article/27/5/20-4944-App1.pdf>). Before continuing their travels, these persons needed to undergo 14 days of quarantine and test negative for SARS-CoV-2 by nucleic acid amplification test. On September 3, 2020, two undocumented migrants with no history of rejection at any official port crossed the Ruili River from Nankan (Myanmar) to Ruili.

Patient 1, who had lost her senses of smell and taste for 1 week before diagnosis, received a COVID-19 diagnosis on September 12, 2020, ending a 139-day period in which no new cases had been reported in Yunnan Province. In Myanmar, she had not had contact with any known COVID-19 patient. Officials identified 201 close contacts of patient 1 in Yunnan Province; these contacts were then tested for SARS-CoV-2. All contacts tested negative except the person who had entered China with patient 1. Because of the 9-day delay between entry and diagnosis, whether community transmission had occurred was unknown.

To evaluate potential spread, we undertook a large-scale SARS-CoV-2 screening campaign of

>280,000 citizens and legal migrants in Ruili during September 15–19, 2020. We did not detect any cases of community transmission, possibly because of patient 1's low viral load; she had a mild case of COVID-19, with normal lung physiology and an N-gene cycle threshold of 37.41, suggesting a low level of infectiousness (2) (Appendix Figure 1). Patient 1 also wore a mask in public, potentially hindering COVID-19 transmission. In addition, patient 2 did not spend much time in public, further reducing potential for transmission. Although this event did not cause community spread of SARS-CoV-2 in Ruili, it highlights the need to curb undocumented immigration to prevent recurring outbreaks of COVID-19. This need is especially relevant in Yunnan Province, which shares a 4,060-km border with Myanmar, Laos, and Vietnam. The border spans 8 cities and 25 counties of China.

To evaluate potential variations in SARS-CoV-2 sequences for the 2 cases, we conducted whole-genome sequencing (3) of high-quality reads mapped to a reference sequence from Wuhan (GenBank accession no. MN908947.3). We deposited consensus sequences in GISAID (<https://www.gisaid.org>) under accession

nos. EPI_ISL_632934 and EPI_ISL_632935. Sequence alignment analyses (4) revealed that the 2 SARS-CoV-2 sequences from Ruili shared 13 mutations: C241T, C3037T, G11083T, C14408T, G18756T, C18877T, C22444T, A23403G, G25494T, G25563T, C26735T, C28854T, and G29737C (Appendix Figure 2) (5,6). According to the Pangolin COVID-19 Lineage Assigner (7), 9 of these mutations (i.e., C241T, C3037T, C14408T, C18877T, C22444T, A23403G, G25563T, C26735T, and C28854T) indicate membership in the B.1.36 clade of SARS-CoV-2. Further phylogenetic analyses supported this conclusion (Appendix Table 2, Figure 3). Compared with sequences from earlier COVID-19 outbreaks in Beijing Xinfadi Market (1,8), Dalian (9), and Qingdao, the Ruili sequences had 7 previously unreported mutations (Appendix Figure 2, panel B) (5). The Ruili cases were not associated with the mentioned outbreaks and were probably imported.

Although the SARS-CoV-2-infected migrants did not cause a COVID-19 outbreak, the event illustrates a transmission pathway distinct from air travel and cold-chain food transmission (1). The International Health Regulations and World Health Organization encourage open borders and suggest that COVID-19 control measures be applied only in limited circumstances (10). In 2020, official land ports in Yunnan Province did not close for the COVID-19 pandemic. Because of the long international border, epidemic control remains challenging in this province. Governments should control illegal immigration to avoid future reintroductions of COVID-19. Regional guidelines for COVID-19 control and prevention should strengthen surveillance of undocumented movement across borders, especially from neighboring countries with high rates of infection.

Acknowledgments

We are grateful to the health workers who contributed to this epidemiologic survey. We thank the staff at Ruili People's Hospital for sample collection and transportation.

About the Author

Dr. Zhang is a supervising technician at Yunnan Provincial Center for Disease Control and Prevention, Kunming,

China. Her research interests include viral genomics research associated with infectious diseases.

References

1. Pang X, Ren L, Wu S, Ma W, Yang J, Di L, et al. Cold-chain food contamination as the possible origin of Covid-19 resurgence in Beijing. *Natl Sci Rev*. 2020;7:1861–4. <https://doi.org/10.1093/nsr/nwaa264>
2. Choi B, Choudhary MC, Regan J, Sparks JA, Padera RF, Qiu X, et al. Persistence and evolution of SARS-CoV-2 in an immunocompromised host. *N Engl J Med*. 2020;383:2291–3. <https://doi.org/10.1056/NEJMc2031364>
3. Paden CR, Tao Y, Queen K, Zhang J, Li Y, Uehara A, et al. Rapid, sensitive, full-genome sequencing of severe acute respiratory syndrome coronavirus 2. *Emerg Infect Dis*. 2020;26:2401–5. <https://doi.org/10.3201/eid2610.201800>
4. Katoh K, Misawa K, Kuma K, Miyata T. MAFFT: a novel method for rapid multiple sequence alignment based on fast Fourier transform. *Nucleic Acids Res*. 2002;30:3059–66. <https://doi.org/10.1093/nar/gkf436>
5. Mercatelli D, Giorgi FM. Geographic and genomic distribution of SARS-CoV-2 mutations. *Front Microbiol*. 2020;11:1800. <https://doi.org/10.3389/fmicb.2020.01800>
6. Rahimi A, Mirzazadeh A, Tavakolpour S. Genetics and genomics of SARS-CoV-2: a review of the literature with the special focus on genetic diversity and SARS-CoV-2 genome detection. *Genomics*. 2021;113:1221–32. <https://doi.org/10.1016/j.ygeno.2020.09.059>
7. Rambaut A, Holmes EC, O'Toole A, Hill V, McCrone JT, Ruis C, et al. A dynamic nomenclature proposal for SARS-CoV-2 lineages to assist genomic epidemiology. *Nat Microbiol*. 2020;5:1403–7. <https://doi.org/10.1038/s41564-020-0770-5>
8. Wenjie T, Peihua N, Xiang Z, Yang P, Yong Z, Lijuan C, et al. Reemergent cases of COVID-19 – Xinfadi Wholesales Market, Beijing Municipality, China, June 11, 2020. *China CDC Weekly*. 2020;2:502–4. <https://doi.org/10.46234/ccdcw2020.132>
9. Zhao X, Mao L, Zhang J, Zhang Y, Song Y, Bo Z, et al. Reemergent cases of COVID-19 – Dalian City, Liaoning Province, China, July 22, 2020. *China CDC Weekly*. 2020;2:658–60. <https://doi.org/10.46234/ccdcw2020.182>
10. Ferhani A, Rushton S. The International Health Regulations, COVID-19, and bordering practices: who gets in, what gets out, and who gets rescued? *Contemp Secur Policy*. 2020;41:458–77. <https://doi.org/10.1080/13523260.2020.1771955>

Address for correspondence: Meiling Zhang, Yunnan Center for Disease Control and Prevention, 158 Dongsi St, Xishan District, Kunming 650022, China; email: meilingz2011@163.com; Yong Shao, Kunming Institute of Zoology, 17 Longxin Rd, Panlong District, Kunming 650203, China; email: shaoyong@mail.kiz.ac.cn

Correction: Vol. 27, No. 3

The order of the authors was incorrect for Drug-Resistant Tuberculosis in Pet Ring-Tailed Lemur, Madagascar (M. LaFleur et al.). The article has been corrected online (https://wwwnc.cdc.gov/eid/article/27/3/20-2924_article).

Apollo's Arrow: The Profound and Enduring Impact of Coronavirus on the Way We Live

Nicholas A. Christakis; Little, Brown Spark/Hachette Audio, New York, NY, USA, 2020; ISBN-10: 0316628212/ ISBN-13: 978-031662821 (hardcover); ISBN-13: 9780316628204 (paperback); ISBN-13: 9780316628228 (e-book); ISBN-13: 9781549160738 (audiobook); Pages: 384; Price: \$29 (hardcover); \$18.99 (paperback); \$14.99 (e-book); \$25.98 (audiobook)

DOI: <https://doi.org/10.3201/eid2705.210381>

In 1969, misplaced optimism led some to proclaim it time to “close the book on infectious diseases”; this prediction has been shattered by the emergence and reemergence of various human pathogens (1). *Apollo's Arrow: The Profound and Enduring Impact of Coronavirus on the Way We Live* by Nicholas A. Christakis provides a real-time account of events that began in December 2019 when doctors confirmed the first cases of a disease caused by a pathogen later named severe acute respiratory syndrome coronavirus 2 (SARS-CoV-2). Christakis, a physician, epidemiologist, and sociologist at Yale University, unravels how and why the emergence of SARS-CoV-2 cascaded into a human catastrophe.

In the first 7 chapters of this well-researched and well-referenced book, focusing on events in the United States, Christakis describes the evolution of the coronavirus disease (COVID-19) pandemic and interprets these events in historical, human, and societal contexts. In Chapter 1, he uses epidemiological investigations of early cases to describe the onset of the pandemic. Christakis notes the unfortunate timing of the virus emerging during the leadup to the Lunar New Year celebration, when >3 billion trips are made within China and, while worldwide travel continued unabated, how the first confirmed COVID-19 case-patient was identified in the United States.

Christakis describes how using whole-genome sequencing to map SARS-CoV-2 variants spurred research and vaccine development. Contrasting the novel virus with previous human coronaviruses, Christakis uses analyses of social interactions to highlight the importance of host variation in superspreading. He writes: “SARS-CoV-2 has a positive mismatch period; this allows for asymptomatic transmission and makes traditional public health responses... very difficult.”

Christakis cites analogous examples of mask-wearing mandates in California during the 1918 Spanish flu pandemic to compare societal responses

then and now. He illuminates how, despite the many social controversies around COVID-19 response, Americans overall have adopted social distancing measures with generosity, cooperation, and ingenuity. He also writes about the sacrifices made by healthcare and custodial workers who risked their lives during the first wave of COVID-19. Yet, Christakis reminds us that this personal altruism occurred while leaders even in wealthy countries failed to fully provide necessary protective equipment (2).

The book shines in its epidemiological and clinical observations and in descriptions of disproportionate illness and death among subpopulations in the United States. For example, Christakis highlights outbreaks of COVID-19 in meat processing plants with horrific working conditions. At other times he seems overly optimistic, such as when he suggests that a lasting impact of COVID-19 may be “respect for science and expertise, even when it leads to people taking actions they would rather avoid.” Christakis highlights the successful implementation of COVID-19 control measures in China and New Zealand and notes the United States' ability to spend trillions of dollars on mitigation measures, including vaccine development.

Apollo's Arrow balances the gloom of the pandemic period with insights from the past, accounts of hands-on patient care, and population-level observations. We were also delighted with the author's engaging narration in the audiobook. This book will interest anyone questioning why, despite impressive advances in biological sciences, COVID-19 has evolved into an unimaginable global catastrophe, resulting in >119.6 million reported illnesses and >2.6 million deaths by mid-March 2021 (3).

References

1. Cohen ML. Changing patterns of infectious disease. *Nature*. 2000;406:762-7. <https://doi.org/10.1038/35021206>
2. Nguyen LH, Drew DA, Graham MS, Joshi AD, Guo CG, Ma W, et al.; Coronavirus Pandemic Epidemiology Consortium. Risk of COVID-19 among front-line health-care workers and the general community: a prospective cohort study. *Lancet Public Health*. 2020;5:e475-83. [https://doi.org/10.1016/S2468-2667\(20\)30164-X](https://doi.org/10.1016/S2468-2667(20)30164-X)
3. World Health Organization. WHO coronavirus (COVID-19) dashboard [cited 2021 Mar 15] <https://covid19.who.int>

Nkuchia M. M'ikanatha, Christopher E. Carr

Author affiliations: Pennsylvania Department of Health, Harrisburg, Pennsylvania, USA (N.M. M'ikanatha); Georgia Institute of Technology, Atlanta, Georgia, USA (C.E. Carr)

Address for correspondence: Nkuchia M. M'ikanatha, Department of Health, Division of Infectious Disease Epidemiology, Health and Welfare Building, 7th and Forster St, Rm 933, Harrisburg, Pennsylvania 17120, USA; email: nmikanatha@pa.gov



Ambika Devi (1971–), *Handwashing Is Important*, 2020. Natural pigments on handmade paper, 7.5. in x 7.5 in/19.1 cm x 19.1 cm. Digital image used with permission from Dastkar, Kisan Haat Andheria Modh, Anuvrat Marg, New Delhi 110074, India.

Ancient Methods Deliver a Current Message

Byron Breedlove

In March 2020, the World Health Organization classified the coronavirus disease (COVID-19) outbreak as a pandemic. According to data from the WHO Coronavirus (COVID-19) Dashboard (April 12, 2021), approximately 137,000,000 confirmed cases of COVID-19, including approximately 2,930,000

confirmed deaths, have been documented in 223 countries. Actual numbers of cases and deaths are larger because of challenges with testing and determining causes of death.

The UN Educational, Scientific and Cultural Organization (UNESCO) notes that the culture sector, which includes more than 30 million people globally, has been hit hard by the coronavirus pandemic. Nonetheless, artists everywhere have responded to the pandemic; many are not only depicting

Author affiliation: Centers for Disease Control and Prevention, Atlanta, Georgia, USA

DOI: <https://doi.org/10.3201/eid2705.AC2705>

their experiences and circumstances but are also promoting public health practices that can aid in reducing the spread of COVID-19, such as washing hands and wearing masks.

Journalist Sudha G. Tilak writes that “India’s folk artists have long used traditional art for social messaging” and that since the start of the COVID-19 pandemic, “a number of those artists have released works that reinforce and promote those basic public health practices.” Tilak also quotes Laila Tyabji, chairperson of Dastkar, a private nonprofit organization that supports traditional craftspeople in India, who said, “Though many fear the impact of COVID-19 may be the end of craftspeople, it is their creativity and resilience that could save them.” For context, WHO Coronavirus Dashboard data (April 12, 2021) indicate that India ranks second among the world’s countries in cumulative total of confirmed cases of COVID-19 and fourth in confirmed deaths.

This month’s cover image is a modern example of a traditional art genre known as Madhubani by Indian artist Ambika Devi, from the village of Rashidpur in the Madhubani district of Bihar, an ancient city now divided between India and Nepal. Devi has been practicing Madhubani art since she was 12 years old. She learned its techniques from her mother, Leela Devi, who in turn, learned them from her mother. Devi, considered a master of this art form, has won multiple awards for her work—including the President of India’s National Handicrafts Award for her contributions to art (2009), the Crafts Council of India’s Kamala Award for Excellence in Craftsmanship (2018), the Sanmaan Award for Excellence in Handicrafts by the Crafts Council of Telangana (2019), and Jasthi Ramaiah Award for Excellence in Craft by the Craft Council of Telangana (2021).

For centuries, Madhubani has been practiced in the northern corner of India and adjoining parts of Terai in southern Nepal. Madhubani artisans use natural dyes and pigments created from various leaves, berries, and tree bark, fresh turmeric, soot, and even cow dung. Using twigs, brushes, nib pens, and their fingers, the artists create colorful intricate works filled with geometrical patterns on paper, canvas, fabric, walls, and other surfaces.

In this work, an example of the Katchni (line style) of Madhubani, Devi limits her palette to red and black pigments on a light background. She shows a mother and children washing hands by a pump—an everyday scene that could be from many village squares. Devi’s initial steps involve painstakingly drawing complex patterns on a blank surface. Next, she meticulously fills in the shapes and

forms with pigments or dyes and uses double lines to set off the foreground from the background and to add depth. The various stripes, textures, fringes, brocades, jewelry, and other details of the mother’s clothing create a kaleidoscopic array of shapes that dominates the painting. An older child is shown washing her hands near her watchful mother who holds a younger child. All three are wearing face masks as protection from COVID-19, and Devi’s use of an ancient craft to depict this very modern behavior does not seem in the least incongruous.

Since the start of the COVID-19 pandemic, people everywhere have been adjusting to social distancing and mask wearing. Hospitals are being overwhelmed by admissions and healthcare professionals working to exhaustion. The evidence confirming that wearing masks is an effective nonpharmacologic way to reduce the spread of COVID-19 continues to grow. Devi’s painting relies on traditional artistic methods to provide a glimpse of life in her village during this pandemic and to deliver a contemporary message, gently reminding viewers of ways to protect their health and the health of others.

Bibliography

1. Anand SN. Madhubani comes alive [cited 2021 March 9]. <https://www.thehindu.com/features/metroplus/madhubani-comes-alive/article5448003.ece>
2. Brooks JT, Butler JC. Effectiveness of mask wearing to control community spread of SARS-CoV-2. *JAMA*. 2021;325:998-9. <https://doi.org/10.1001/jama.2021.1505>
3. Centers for Disease Control and Prevention. Guidance for wearing masks. Help slow the spread of COVID-19 [cited 2021 March 16]. <https://www.cdc.gov/coronavirus/2019-nCoV/prevent-getting-sick/cloth-face-cover-guidance.html>
4. Crafts Council of India. Kamala Award for Excellence in Craftsmanship 2018 Smt. Ambika Devi [cited 2021 March 9]. <https://www.craftscouncilofindia.in/kamala-award-for-excellence-in-craftsmanship-2018-2>
5. Thakur U. Madhubani painting. New Delhi, India: Abhinav Publications; 2003. p 11-12; 63-65.
6. Tilak SG. Gods in face masks: India’s folk artists take on Covid-19, May 2020 [cited 2021 Mar 9]. <https://www.bbc.com/news/world-asia-india-52464028>
7. UN News. . Culture in crisis: arts fighting to survive COVID-19 impact [cited 2021 Mar 9]. <https://news.un.org/en/story/2020/12/1080572>
8. World Health Organization. Coronavirus disease (COVID-19) pandemic. Numbers at a glance [cited 2021 Mar 9]. <https://www.who.int/emergencies/diseases/novel-coronavirus-2019>
9. World Health Organization. WHO coronavirus (COVID-19) dashboard [cited 2021 Mar 9]. <https://covid19.who.int>

Address for correspondence: Byron Breedlove, EID Journal, Centers for Disease Control and Prevention, 1600 Clifton Rd NE, Mailstop H116-2, Atlanta, GA 30329-4027, USA; email: wbb1@cdc.gov

EMERGING INFECTIOUS DISEASES®

UPCOMING ISSUE

- Pertactin-Deficient *Bordetella pertussis*, Vaccine-Driven Evolution, and Reemergence of Pertussis
- Seroprevalence of SARS-CoV-2 IgG antibodies in Juba, South Sudan
- Molecular Epidemiology and Evolutionary Trajectory of Emerging Echovirus 30, Europe
- Macrolide-Resistant *Mycoplasma pneumoniae* Infections in Children
- Precision Tracing of Household Dengue Spread Using Inter- and Intra-Host Viral Variation Data, Kamphaeng Phet, Thailand
- Association between Birth Region and Time to Tuberculosis Diagnosis among Non-US-Born Persons Entering the United States
- Molecular Characterization and Antimicrobial Resistance in *Neisseria gonorrhoeae*, Nunavut Region of Inuit Nunangat, Canada, 2018–2019
- Cutaneous Leishmaniasis Caused by an Unknown *Leishmania* Strain in the Subgenus *Leishmania* (*Leishmania*), Arizona, USA
- Reemergence of Scabies in Germany Driven by Adolescents and Young Adults, 2009–2018
- Epidemiologic Evidence for Airborne Transmission of SARS-CoV-2 during Church Singing, Australia, 2020
- Rapid Detection of SARS-CoV-2 Variants of Concern, Including B.1.1.28/P.1, in British Columbia, Canada
- Brucellosis Outbreak Traced to Commercially Sold Camel Milk through Whole-Genome Sequencing, Israel
- Seroepidemiologic Survey of Crimean-Congo Hemorrhagic Fever Virus in Logging Communities, Myanmar
- Role of *Anopheles stephensi* in Malaria Outbreak, Djibouti, 2019
- Changing Molecular Epidemiology of Hepatitis A Virus Infection, United States, 1996–2019
- Evidence of *Oropouche orthobunyavirus* Infection, Colombia, 2017
- Highly Pathogenic Avian Influenza A(H5N8) Virus in Swans, China, 2020
- Multisystem Inflammatory Syndrome in Adults after Mild SARS-CoV-2 Infection, Japan
- Rapid Antigen Test for Postmortem Evaluation of SARS-CoV-2 Carriage
- Novel Incursion of Highly Pathogenic Avian Influenza A(H5N8) Virus, the Netherlands, October 2020

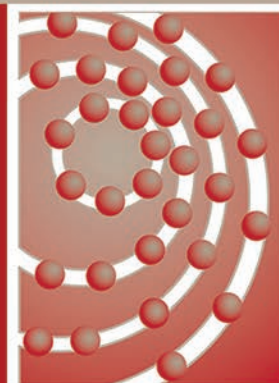
Complete list of articles in the June issue at <http://www.cdc.gov/eid/upcoming.htm>

SAVE the DATE

11th International Conference on Emerging Infectious Diseases



Atlanta • March 6–9, 2022 iceid.org



ICEID
2022

Earning CME Credit

To obtain credit, you should first read the journal article. After reading the article, you should be able to answer the following, related, multiple-choice questions. To complete the questions (with a minimum 75% passing score) and earn continuing medical education (CME) credit, please go to <http://www.medscape.org/journal/eid>. Credit cannot be obtained for tests completed on paper, although you may use the worksheet below to keep a record of your answers.

You must be a registered user on <http://www.medscape.org>. If you are not registered on <http://www.medscape.org>, please click on the "Register" link on the right hand side of the website.

Only one answer is correct for each question. Once you successfully answer all post-test questions, you will be able to view and/or print your certificate. For questions regarding this activity, contact the accredited provider, CME@medscape.net. For technical assistance, contact CME@medscape.net. American Medical Association's Physician's Recognition Award (AMA PRA) credits are accepted in the US as evidence of participation in CME activities. For further information on this award, please go to <https://www.ama-assn.org>. The AMA has determined that physicians not licensed in the US who participate in this CME activity are eligible for AMA PRA Category 1 Credits™. Through agreements that the AMA has made with agencies in some countries, AMA PRA credit may be acceptable as evidence of participation in CME activities. If you are not licensed in the US, please complete the questions online, print the AMA PRA CME credit certificate, and present it to your national medical association for review.

Article Title

Characteristics and Clinical Implications of Carbapenemase-Producing *Klebsiella pneumoniae* Colonization and Infection, Italy

CME Questions

1. Your patient is a 69-year-old man hospitalized with *Klebsiella pneumoniae* carbapenemase-producing (KPC-Kp) infection. According to the multicenter cohort study of 1071 patients with KPC-Kp from Italy, which of the following statements about epidemiology of KPC-Kp and molecular characterization of KPC-Kp strains in colonized and infected inpatients with mild (MI) or serious (SI) infections is correct?

- A. During 2017, KPC-Kp prevalence was 1.26/1000 hospitalized patients
- B. Cumulative incidence of hospital-acquired KPC-Kp infections (within 48 hours of admission) was similar among all centers studied
- C. Clones ST512 and ST307 accounted for 77% of all strains
- D. 6 KPC variants were identified

2. According to the multicenter cohort study from Italy, which of the following statements about clinical characteristics and outcomes of KPC-Kp in colonized and infected inpatients with MI or SI is correct?

- A. 15-day mortality was significantly higher in MI than in noninfected colonized patients and 25% higher in SI than in MI

- B. Delays ≥ 4 days in receiving adequate treatment were more common in SI than in MI
- C. Half of the study cohort had ≥ 1 comorbidity; 10% had congestive heart failure (CHF), peripheral vascular disease (PVD), or chronic kidney failure (CKF)
- D. All-cause in-hospital mortality was 34% in patients with KPC-Kp infection and 21% in patients with colonization

3. According to the multicenter cohort study from Italy, which of the following statements about treatment and other clinical implications of KPC-Kp in colonized and infected inpatients with MI or SI is correct?

- A. Marked variability in proportion and incidence of KPC-Kp infections may reflect surveillance protocols and hospital policies, mandating a strengthened collaborative surveillance system
- B. Treatments were standardized across centers
- C. 80% of all patients received ceftazidime-avibactam (CAZ-AVI)
- D. Susceptibility tests showed adequate empirical therapy (≥ 1 drug with in vitro activity against the KPC-Kp isolate) in 86% of patients

Earning CME Credit

To obtain credit, you should first read the journal article. After reading the article, you should be able to answer the following, related, multiple-choice questions. To complete the questions (with a minimum 75% passing score) and earn continuing medical education (CME) credit, please go to <http://www.medscape.org/journal/eid>. Credit cannot be obtained for tests completed on paper, although you may use the worksheet below to keep a record of your answers.

You must be a registered user on <http://www.medscape.org>. If you are not registered on <http://www.medscape.org>, please click on the “Register” link on the right hand side of the website.

Only one answer is correct for each question. Once you successfully answer all post-test questions, you will be able to view and/or print your certificate. For questions regarding this activity, contact the accredited provider, CME@medscape.net. For technical assistance, contact CME@medscape.net. American Medical Association’s Physician’s Recognition Award (AMA PRA) credits are accepted in the US as evidence of participation in CME activities. For further information on this award, please go to <https://www.ama-assn.org>. The AMA has determined that physicians not licensed in the US who participate in this CME activity are eligible for AMA PRA Category 1 Credits™. Through agreements that the AMA has made with agencies in some countries, AMA PRA credit may be acceptable as evidence of participation in CME activities. If you are not licensed in the US, please complete the questions online, print the AMA PRA CME credit certificate, and present it to your national medical association for review.

Article Title

Prescribing Antimicrobial Drugs for Acute Gastroenteritis, Primary Care, Australia, 2013–2018

CME Questions

1. What was the overall approximate rate of antibiotic prescriptions for acute gastroenteritis (AGE) in the current study?

- A. 0.2%
- B. 7%
- C. 22%
- D. 63%

2. Antibiotic prescriptions were associated with which of the following patient characteristics in the current study?

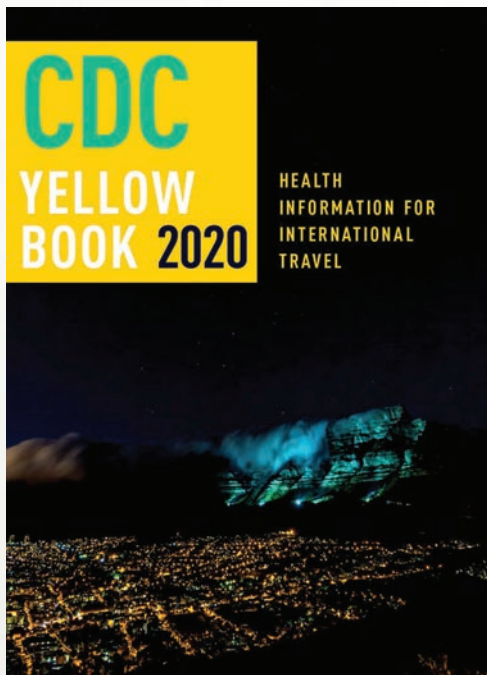
- A. Younger age and living in urban areas
- B. Older age and living in urban areas
- C. Younger age and living in rural areas
- D. Older age and living in rural areas

3. Which of the following trends was noted in antibiotic prescribing for AGE in the current study?

- A. There was a gradual decrease in the rate of antibiotic prescribing for AGE
- B. The rate of antibiotic prescriptions for AGE was fairly static over time
- C. There was a gradual increase in the rate of antibiotic prescribing for AGE
- D. The rate of antibiotic prescriptions for AGE increased the most among older adults

4. Which of the following drug classes was most prescribed for AGE in the current study?

- A. Nitroimidazoles
- B. Cephalosporins
- C. Fluoroquinolones
- D. Macrolides



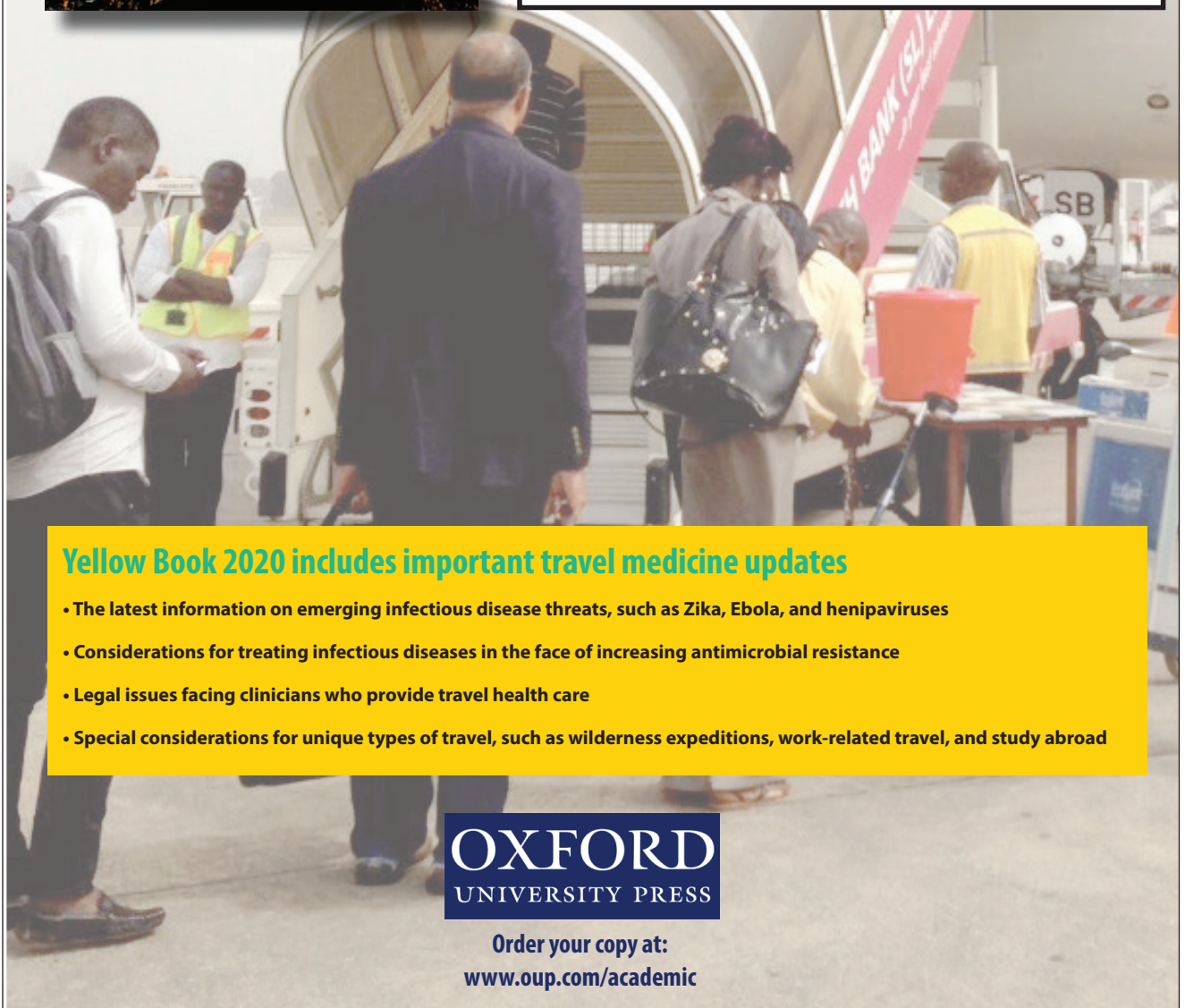
Available Now

Yellow Book 2020

The fully revised and updated CDC Yellow Book 2020: Health Information for International Travel codifies the US government's most current health guidelines and information for clinicians advising international travelers, including pretravel vaccine recommendations, destination-specific health advice, and easy-to-reference maps, tables, and charts.

ISBN: 978-0-19-006597-3 | \$115.00 | May 2019 | Hardback | 720 pages

ISBN: 978-0-19-092893-3 | \$55.00 | May 2019 | Paperback | 687 pages



Yellow Book 2020 includes important travel medicine updates

- The latest information on emerging infectious disease threats, such as Zika, Ebola, and henipaviruses
- Considerations for treating infectious diseases in the face of increasing antimicrobial resistance
- Legal issues facing clinicians who provide travel health care
- Special considerations for unique types of travel, such as wilderness expeditions, work-related travel, and study abroad

OXFORD
UNIVERSITY PRESS

Order your copy at:
www.oup.com/academic